Functional genomics in *Candida albicans*: Tackling drug resistance and morphology

By Elias Epp

Department of Biology
McGill University, Montréal

June 2011

A thesis submitted to McGill University in partial fulfillment of the requirement of the degree of Doctor in Philosophy

Table of Contents

Acknowledgments

First and foremost, I would like to thank my supervisor, Dr. Malcolm Whiteway. Taking on a new graduate student from over-seas based on the student's CV that says 'playing Didgeridoo' under the 'other activities' section was a brave move. I am extremely glad that you dared doing this, Malcolm, because the time I have spent in this lab has truly been marvelous. The teaching and research environment of the lab, together with the endless resources, the patient and extremely experienced staff, as well as your guidance and willingness to provide students scientific freedom are just the tip of the iceberg of what I got to appreciate here. Attending several international scientific conferences, teaching the Yeast Genetics Course at Cold Spring Harbor, writing post-peer reviewed evaluations for Faculty 1000 Biology, and the chance to serve on Animal Care Committee's provided additional extra-curriculum opportunities that have rounded up my overall experience during the PhD program. I fail to express how grateful I am for making this experience so rich and positive.

I would also like to extend my gratitude to current and past members of the lab, especially Doreen, Josée, Anne, Zully, Daniel, Cule, André, Jean-Sébastien, Adnane, Hugo, Pierre, Chris, Jaideep and Nina for help on many occasions when I needed a protocol, was looking for reagents or simply wanted to discuss science. As well, a big thanks to our collaborators and co-authors, which have always been open to discussions and feedbacks. Working in a team has made such a difference.

Thanks also to members of my supervisory committee who have always been supportive of my plans and provided constructive feedback. Thanks to McGill University for granting me several awards (CIHR systems biology fellowship, Carpenter fellowship, travel grants).

Finally, I would like to express my thanks to my family and friends who have constantly supported me despite the big distance from home. It's tremendously relieving to know that there is a place one can always return to while travelling the world and spending years abroad. The one person who has started and continues this journey with me deserves special thanks. Vilä herzlichä Dank, Schätzi.

Abstract

The human fungal pathogen *Candida albicans* is a diploid organism that lacks a complete sexual cycle, thus making functional genetics challenging. Consequently, linking a function to a gene often relies on predictions from other model organisms. In this thesis, I have explored different genetic strategies to address two important aspects of the biology of *C. albicans*, drug resistance and morphology, which are associated with virulence. Using a reverse genetics approach based on the model *Saccharomyces cerevisiae*, I first identify and validate a new drug target in *C. albicans*. Next, I use forward genetics screening directly in the pathogen to identify genes regulating morphology by showing that the Arp2/3 complex is required for the yeast-to-hyphae switch as well as virulence. Lastly, I follow up on the Arp2/3 complex and demonstrate how this fungus can be used to study some unique cell biological aspects regarding actin dynamics and endocytosis. Collectively, this thesis illustrates how various genomic techniques can be applied to understand different aspects of this human fungal pathogen.

Résumé

La levure pathogène *Candida albicans* est un organisme diploïde n'ayant pas de cycle sexuel complet, ce qui rend difficile la génétique fonctionnelle. Par conséquence, la liaison d'un gène à une fonction repose souvent sur des prévisions à partir d'autres organismes modèles. Dans cette thèse, j'ai exploré différentes stratégies génétiques afin d'étudier deux aspects importants de la biologie de *C. albicans*, la résistance aux médicaments et la morphologie, qui est associée à la virulence. Avec l'aide d'une approche de génétique inverse basée sur l'organisme modèle *Saccharomyces cerevisiae*, j'ai d'abord identifié et validé une nouvelle cible thérapeutique chez *C. albicans*. Ensuite, j'ai utilisé la génétique directe de *C. albicans* pour identifier des gènes qui régulent sa morphologie. Ceci m'a permis de montrer que le complexe Arp2/3 est requis pour la formation des hyphes ainsi que la virulence. Enfin, je me suis concentré sur le complexe Arp2/3 et j'ai démontré que cette levure peut être utilisée pour étudier certains aspects unique de sa biologiques cellulaire, en particulier, la dynamique de l'actine et l'endocytose. Collectivement, cette thèse montre comment diverses techniques de génétique et de génomique peuvent être appliquées afin de comprendre différents aspects de ce pathogène fongique humain.

Contribution of authors

Chapter II.
Jansen G., Lee A.Y., Epp E., Fredette A., Surprenant J., Harcus D., Scott M., Tan E., Nishimura T., Whiteway M., Hallett M. and Thomas D.Y. (2009) Chemogenomic profiling predicts antifungal synergies. Molecular Systems Biology 5:338

G.J. conceived and performed experiments, analyzed data and wrote the paper
A.L.Y. conceived, performed and analyzed all bioinformatics work, wrote the paper
E.E. performed all work related to *C. albicans*
A.F., J.S., D.H., M.S., E.T., T.N. performed the screen with the yeast deletion library
M.W., M.H., D.Y.T. oversaw the work

Chapter III.
Epp E., Vanier G., Harcus D., Lee A.Y., Jansen G., Hallett H., Sheppard D.C., Thomas D.Y., Munro C.M., Mullick A. and Whiteway M. (2010) Reverse Genetics in *Candida albicans* Predicts ARF Cycling Is Essential for Drug Resistance and Virulence. PLoS Pathogens 5;6(2):e1000753

E.E. conceived and performed all experiments, analyzed data and wrote the paper
G.V. assisted with the *A. fumigatus* experiment
D.H., A.Y.L, G.J. contributed with discussions
S.D.C., D.Y.T, C.M.M., A.M., M.W. oversaw the work

Chapter IV.2.
Epp E., Walther A., Lépine G., Leon Z., Mullick A., Raymond M., Wendland J. and Whiteway M. (2010) Forward genetics in *Candida albicans* that reveals the Arp2/3 complex is required for hyphal formation, but not endocytosis. Molecular Microbiology 75(5), 1182–1198

E.E. conceived and performed all experiments, except the time-lapse experiment, analyzed the data and wrote the paper
A.W. performed the time-lapse experiment
Z.L. assisted with the mouse study
G.L. assisted with the *UAU1* transposon technique
M.R., J.W., M.W. oversaw the work

Chapter V.2.
Epp E., Nazarova E., Douglas L.M., Konopka J.B., Vogel J., Whiteway M. (manuscript in preparation) Actin dynamics and endocytosis in the absence of Arp2/3 in *Candida albicans*

E.E. conceived and performed all experiments, except the EM study, analyzed the data and wrote the paper
E.N. assisted with confocal microscopy studies
D.M.L. performed the EM study
J.B.K., J.V., M.W. oversaw the work

List of Figures

Abbreviations

5-FC	5-flucytosine
5-FU	5-fluorouracil
ABPs	actin binding proteins
ADP	adenosine diphosphate
AmB	amphotericin B
ARF	ADP-ribosylation factor
ARF GAP	ADP-ribosylation factor GTPase activating effector protein
ARG GEF	ADP-ribosylation factor guanyl-nucleotide exchange factors
ATP	adenosine triphosphate
CA	cytochalasin A
cAMP	cyclic adenosine monophosphate
CLSI	clinical and laboratory standards institute
CME	clathrin-mediated endocytosis
ESCRT	endosomal sorting complex required for transport
F-actin	filamentous actin
FCZ	fluconazole
FDA	food and drug administration
FUDP	5-fluorouridine diphosphate
FUMP	5-fluorouridine monophosphate
FUTP	5-fluorouridine triphosphate
G-actin	globular actin
GAP	GTPase activating effector protein
GEF	guanyl-nucleotide exchange factors
GTP	guanosine-5'-triphosphate
Lat-A	latrunculin-A
LY	lucifer yellow
MAPK	mitogen activated protein kinase
MAPKK	MAPK kinase
MAPKKK	MAPKK kinase
MFC	minimum fungicidal concentration
MIC	minimal inhibitory concentration
NPFs	nucleation-promoting factors
ORF	open reading frame
PKA	protein kinase A
ROC	receiver-operating characteristic curve
SCPR	search, capture, pull, and release
SGA	synthetic genetic analysis
SIN	septation initiation network
uPRTase	uridine monophosphate pyrophosphorylase

Presentation

In this manuscript-based thesis, I have investigated different functional genomic approaches in *Candida albicans*, addressing two important aspects of *C. albican's* biology, drug resistance and morphology.

In chapter I, I will introduce the protagonist of my thesis, the human fungal pathogen *C. albicans,* and provide an overview of why we should study *C. albicans*, currently available therapy options and their limitations, as well as functional genomic methods to study gene function. This leads to the first two publications (chapter II, published in Molecular Systems Biology, PMID: 20029371, and chapter III, published in PLoS Pathogens, PMID: 20140196), where we used reverse genetics based on the model *Saccharomyces cerevisiae* to identify new drug targets. Following this, I will outline limitations of this strategy and provide a forward genetic approach to perform functional genomics directly in the pathogen, which leads to chapter IV (published in Molecular Microbiology, PMID: 20141603). In this publication, I focus on the morphology aspect of *C. albicans*, and link one gene in particular, *ARP2*, to this trait. Following up on these observations, I will provide an extension on *ARP2* and present in a first draft version (chapter V.2) the cell biological function of the Arp2/3 complex in regards to actin dynamics and endocytosis.

Overall, my thesis has a strong focus on functional genomics, starting with reverse genetics that addresses drug resistance, continuing with forward genetics looking at morphology, and finally extending on one of the hits resulting from forward genetic screening to understand some unique aspects of the biology of *C. albicans*, thus providing an example that studying this fungus is not only important because of its pathogenic capacity, but also because it serves as a useful model organism for cell biology. Finally, in the last chapter (chapter VI), I will reflect on some of our main findings and provide my views what these results mean.

Appendix A provides additional co-authored publications as well as evaluations for Faculty 1000 Biology (F1000) that were produced during the course of my Ph.D. work, but were not directly aligned with the main chapters presented here. I thus felt that

mentioning the 5 co-authored publications and 6 F1000 evaluations in the appendix was appropriate.

CHAPTER I

I. Introduction

The name “fungi” can invoke unpleasant associations and memories in many people, as fungal species are notoriously involved in processes such as decaying wood, spoiling food, attacking crops, annoyingly decorating our apartments on walls or ceilings, and causing various infections in humans, ranging from rather harmless toenail infections to more serious lung or blood-stream infections that often lead to death. On the other side, the ecosystem wouldn’t work as we know it without the estimated 1.5 million existing fungal species. Together with bacteria, fungi decompose organic material and release carbon, nitrogen and phosphorous, so that plants and animals can reuse them for growth. As well, fungi are important as mutualists, forming beneficial relationships with plants in the form of mycorrhizae, with cyanobacteria in the form of lichens, or with animals such as grazing mammals, where fungi provide services in breaking down plant material in the gut. Human economy also heavily depends on fungi, as they are used to produce wine, beer, bread, antibiotics, and more recently bioethanol as fuel for our cars. Finally, fungi frequently serve as important model organisms to study molecular genetics of eukaryotes, because some fungi, like the budding yeast *Saccharomyces cerevisiae*, are easily cultured and genetically manipulated. Scientists make use of these advantages to gain insights into Parkinson’s disease and other human diseases by examining homologous genes in *S. cerevisiae* [1]. Thus, while fungi can cause disease and dramatically threaten human health, their benefits to humans as well as the entire ecosystem as a whole clearly outweigh the negative aspects. Studying fungi is therefore a fascinating area and certainly provides a rich resource to understand processes essential for life.

I.1. A brief introduction to *Candida albicans*

The first mention of an oral fungal infection is credited to Hippocrates (4th century BC)[2], but it was not until 1665 when Pepys described this infection as "thrush" (a milky-white lesion in the mouth, on lips and in the throat) [3,4]. In 1839 Langenbeck was the first to recognize that thrush was caused by a fungus [5], and Wilkinson in 1849 and Mayer in 1862 observed that this fungus can grow in different growth forms that can cause other types of infections, like vaginal thrush, cutaneous and systemic infections [6,7]. Robin in 1847 was the first to use the word "*albicans*" (from Latin, "albus" meaning "to whiten")[8], and in 1923 Berkhout proposed the generic name should be *Candida* (derived from the Latin phrase *toga candida*, which was used to describe a white robe worn by candidates of the Roman Senate) [2,9]. In 1954 the Eighth Botanical Congress officially adopted the taxonomic name *Candida albicans* [2], and the following half-century saw an expansion of studies in the areas of taxonomy, biochemistry and microscopy with the first report on molecular biological approaches published in 1981 [10].

Today, we distinguish among more than 160 different *Candida* species [11]. Approximately 65% of all these species are unable to grow at 37°C and are therefore not considered pathogenic [12], but exist as environmental saprophytes [13]. Among all potentially pathogenic *Candida* species, *C. albicans* is the most often isolated from the human host, accounting for over half (62%) of all isolates, followed by *C. glabrata* (17 %), *C. parapsilosis* (9%), *C. tropicalis* (4%), *C. krusei* (3%) and other *Candida* species that together account for less than 10% of all isolates [14,15]. *Candida* spp. remain the most common human fungal pathogen isolated in intensive care units, accounting for 42% of all fungal infections. However, besides infections caused by *Candida* spp., other fungi are also frequently isolated in human patients. Among the most prominent of those are *Aspergillus* spp., e.g. *A. fumigatus,* and *Crytococcus* spp. like *C. neoformans* [16].

We understand today that *C. albicans* colonization is established early in life, possibly as early as birth when passing through the birth canal [17], and consequently

over 50% of one-month-old infants have associated *C. albicans* [18]. In general, the interaction between *C. albicans* and the human host is benign with the fungus growing as a commensal on the skin, the mouth, the throat, the gastrointestinal tract and lower female reproductive tract in about 70% of the healthy human population [19,20]. In other cases, *C. albicans* can cause disease, generally referred to as candidiasis, that we can divide into two broad categories, mucosal and systemic. Mucosal candidiasis can result after mucosal insults, such as poor oral hygiene, burn injury to the skin or a surgical procedure. These cases of candidiasis are usually not life-threatening and, although unpleasant, can typically be treated successfully with existing drugs. Systemic candidiasis, also referred to as candidemia, however, is much more serious. In these cases, *C. albicans* breaches the mucosal membrane and enters the blood stream, which leads to a disseminated disease where *C. albicans* can infect virtually every organ [21].

Although *C. albicans* infections were described centuries ago, we observed a tremendous increase in fungal infections during the 20th and 21st centuries. For instance, the annual number of fungal infections increased by 207% between 1979 and 2000 in the United States alone [22]. One reason for this increase lies probably in improved detection methods. More importantly, however, this increase can be attributed to other medical advances, particularly the management of cancer with chemotherapy, management of organ transplantation with potent immunosuppressive drugs and the development of antibacterial drugs [23]. In other cases, the long-term usage of vascular catheters and prosthetic devices has formed an artificial niche for the pathogen. The increased number of people infected with the human immune deficiency virus (HIV) over the last few decades as well as the increasing number of people older than 60 years has resulted in an even larger group of susceptible patients since the transition of a commensal *C. albicans* to the pathogenic form is often facilitated by a weakened immune system of the host.

Having described what *C. albicans* is and why it can become a problem in certain patient populations, I am now going to summarize existing treatment options against fungal infections with a focus on *C. albicans* in particular.

I.2. Treatment options against fungal infections

Candida is the fourth leading cause of nosocomial, i.e. hospital derived, infections worldwide and can be acquired as early as 72 hours after hospitalization [24,25]. Generally, treating patients suffering from candidiasis is hampered by the fact that the immune system of these individuals is already compromised. Treating such patients has always been challenging, but was significantly improved in the 1950's when the first antifungal agent, nystatin, was isolated from a soil fungus [26]. Over the next 60 years, antifungal drug development has continued, and today we have several classes of antifungal drugs that are used in the clinic to treat fungal infections. The next section describes these agents and groups them into 4 categories according to their mode of action.

I.2.1. The polyenes

The class of polyenes includes several hundred different drugs, but the most commonly used ones are nystatin and Amphotericin B deoxycholate (AmB), which was discovered in 1954 and today marketed as Fungizone® by X-Gen pharmaceuticals [27,28]. Polyenes are isolated from soil dwelling fungi of the genus *Streptomyces*. While nyastin is usually restricted to treating mucosal *Candida* infections due to solubility issues, AmB has been used to treat all kinds of fungal infections and has the broadest spectrum of currently available antifungal drugs [28]. AmB is active against all three major human fungal pathogens, i.e. *Candidia* spp., *Cryptococcus* spp. and *A. fumigatus*. Because of this wide-spectrum activity, together with the fact that clinical resistance is still rare (s. chapter I.3.1.), AmB has been a gold standard in the treatment of fungal infections for over 4 decades.

Polyenes have an amphipathic nature, i.e. one part of the molecule is hydrophilic and charged, and another side is hydrophobic and uncharged [29]. Through this property, polyenes target ergosterol, a major lipid in fungal plasma membranes. Through binding to ergosterol, AmB creates a pore that allows ions and other cellular constituents to diffuse across the membrane, ultimately leading to fungal cell death [30,31]. This fungicidal, i.e.

lethal to fungal cells, property of AmB has further contributed to its clinical success, especially in cases where a rapid response is needed [29].

The main disadvantage of polyenes is host toxicity, as they cannot only bind to lipids present in fungi, but also to cholesterol-containing membranes present in human cells. This has considerable disadvantages to the human host, including nephrotoxicity, anemia, anaphylaxis as well as infusion-related reactions that can occur in approximately 70-90% of patients [32,33]. For these reasons, lipid formulations have been developed for AmB, which partially solve the solubility and toxicity issues. Lipid formulations can be used for intravenous delivery and are often superior compared to treatment options relying on other classes of drugs [34]. Three lipid formulations of AmB are currently available, and include AmBisome® (AmBi, liposomal amphotericin B from Gilead Sciences Inc.), Abelcet® (ABLC, amphotericin B lipid complex from Enzon Pharmaceuticals Inc.), and Amphocil/Amphotec® (ABCD, amphotericin B colloidal dispersion from Three River Pharmaceuticals Inc.) [28].

I.2.2. Flucytosine

Flucytosine, namely 5-flucytosine (5-FC), which is marketed as Ancobon® and distributed by Valeant pharmaceuticals Intl., was originally discovered in 1957 for its antitumor activity [28]; only four years later was its antifungal property recognized [35]. 5-FC is active against *Candida spp., Cryptococcus spp.* and has also been used to treat chromoblastomycosis (infections caused by *Fonsecaea* spp., *Phialophora* spp. and *Cladosporium* spp.), but is ineffective against filamentous fungi such as *A. fumigatus* [36,37,38]. 5-FC is rarely used as a single agent, but is commonly used in combination with other drugs, particularly AmB, because when used as monotherapy, 5-FC is only fungistatic (causing arrest of fungal cell growth). Another reason why combination therapy is preferred over monotherapy is because fungal cells rapidly develop resistance against 5-FC (s. chapter I.3.1.) [28].

5-FC targets the process of nucleic acid synthesis. 5-FC is first rapidly converted into 5-fluorouracil (5-FU) by the enzyme cytosine deaminase [39]. 5-FU then exerts its

activity by two mechanisms. The first mechanism includes the conversion of 5-FU into 5-fluorouridine triphosphate (FUTP) through the enzymes 5-fluorouridine monophosphate (FUMP) and 5-fluorouridine diphosphate (FUDP) [39]. FUTP is then incorporated into fungal RNA, thus disturbing the amino acid pool and inhibiting protein synthesis. The second mechanism of action of 5-FU is through its conversion into 5-fluorodeoxyuridine monophosphate (FdUMP) by the enzyme uridine monophosphate pyrophosphorylase [39]. FdUMP acts as a potent inhibitor of thymidylate synthase, a key enzyme involved in DNA synthesis and nuclear division [40]. Therefore, 5-FC interferes with pyrimidine metabolism as well as protein synthesis [41].

Although mammalian cells can also metabolize 5-FC, effects are minimized because mammalian cells lack the enzyme cytosine deaminase [29]. The most common adverse events in patients undergoing 5-FC therapy are symptoms such as nausea, vomiting, diarrhea, abdominal discomfort, as well as hepatotoxicity, which can occur in up to 41% of patients [28].

I.2.3. The azoles

The class of azole drugs is one of the major groups of antifungals used in clinics. Ketoconazole is the first azole derivative that was approved in 1981 by the Food and Drug Administration (FDA) for clinical use [42], and was followed by the first generation triazole, fluconazole (FCZ), in 1990 [43]. FCZ was developed by Pfizer and has several advantages over ketoconazole. For instance, in contrast to ketoconazole, FCZ is highly water soluble, can be administered intravenously to seriously ill patients, is relatively safe even at high doses, and, due to its favourable serum half-life, allows once-daily dosing [44]. Based on these positive pharmacokinetic properties, FCZ rapidly became the first choice for the treatment of a number of fungal infections and has been studied extensively in clinical settings [45]. Today, FCZ is approved for treating mucosal and systemic candidiasis as well as cryptococcal meningitis. However, the enthusiasm for FCZ has been hampered because of its limited spectrum of activity against emerging fungal pathogens. For example, FCZ doesn't show any significant activity against

filamentous fungi like *A. fumigatus*. Another shortcoming of FCZ is the emergence of drug resistance, particularly in *Candida* spp. [29]. Due to these limitations of first-generation azoles like FCZ, second-generation triazoles have been developed in the past 10 years and are used today in the clinics [46]. Voriconazole and posaconazole, two of these second-generation azoles, are active against a wider range of fungal pathogens, including *A. fumigatus,* and show enhanced activity against *Candida* spp. [28,47].

Azoles target the fungal specific ergosterol biosynthesis pathway. The ergosterol pathway can be divided into an early pathway, producing squalene from acetate, and a late pathway that produces ergosterol starting from squalene [48]. All azoles block the late pathway by inhibiting the product of the *ERG11* gene, the P450-dependent enzyme lanosterol 14-α-demethylase. Inhibiting this enzyme results in the accumulation of toxic methylated sterols, which are then incorporated into the plasma membrane, thus replacing ergosterol. This in turn results in altered membrane fluidity as well as altered activity of membrane bound enzymes, such as chitin synthase [49]. The net effect of azole action is inhibition of fungal growth and replication.

The main disadvantage in regards to treating *Candida* infections is that azoles like FCZ only inhibit fungal growth, i.e. they are fungistatic and not fungicidal. This can often lead to the accumulation of drug resistance (s. chapter I.3.1.). Nevertheless, due to its long track record, its low costs, excellent bioavailability and tolerable adverse events like nausea, vomiting and diarrhea, FCZ is still used extensively in the clinic, and remains the antifungal of choice against mucosal candidiasis like oropharyngeal or esophageal infections [28,50].

I.2.4. The echinocandins

The echinocandins are the newest class of antifungals and consist of 3 FDA-approved agents, caspofungin (marketed as Cancidas® and developed by Merck & Co.), micafungin (brand name Mycamine® and developed by Astellas Pharma), and anidulafungin (also known as Eraxis® and developed by Pfizer Inc.). Although caspofungin was first reported in 1989, it took another decade until it was approved in

2001 for treatment of invasive fungal infections [51,52]. Micafungin and anidulafungin were approved in 2005 and 2006, respectively. All three echinocandins are marketed as semisynthetic lipopeptides that have been chemically modified from natural products of fungi; caspofungin from pneumocandin B of *Glarea lozoyensis*, anidulafungin from echinocandin B_0 from *A. nidulans* and micafungin from the hexapeptide FR901370 from *Coleophoma empedri*. Due to its short history of clinical use, extensive clinical data of echinocandins remain limited. Currently, echinocandins are approved for treating infections caused by several *Candida* spp., including *C. albicans*, as well as *A. fumigatus*, but don't show any significant activity against *Cryptococcus* infections [28,29].

All echinocandins target the cell wall of fungal cells by inhibiting the enzyme β-glucan synthetase, which is involved in the synthesis of the major cell wall polysaccharide, β-1,3-glucan [53]. *FKS1*, which encodes for the β-glucan synthetase, is the direct target of echinocandins. Given that mammalian cells lack cell walls, echinocandin action is fungal specific, and results in fungicidal interactions against most *Candida* spp., but fungistatic interactions against the majority of *Aspergillus* spp. [54,55,56].

Although echinocandins are generally well tolerated, echinocandin therapy can infrequently result in liver function abnormalities. A more serious disadvantage of echinocandins, however, is that there is no generic formulation currently available, which makes this antifungal therapy more expensive compared to other antifungals like FCZ.

Having summarized the 4 main classes of clinically available antifungals, I am now going to talk about limitations of each of these classes by looking at mechanisms of drug resistance with a focus on azoles in particular.

I.3. Antifungal drug resistance

I.3.1. General considerations

Despite several clinically approved classes of antifungals, no single drug treatment option is suitable for all existing fungal infections. Physicians have to take into account factors such as the underlying characteristics of the patient, the site of infection, identity of fungal species and so on, in order to maximize chances of clinical success. One way to help choose the appropriate therapy is determining the susceptibility of the pathogen to various compounds *in vitro*. This is usually done by standardized testing methods, such as the reference methods from the Clinical and Laboratory Standards Institute (CLSI) [57,58]. Other testing methods exist as well and include the use of calometric dyes such as XTT, or E-test strips [59,60]. The goal of these standardized methods is to determine the minimal inhibitory concentration (MIC) of a particular drug *in vitro*. The MIC is defined as 80% growth inhibition compared to the control at 48 hours. MIC values are then used to predict how a strain will behave clinically, for instance whether a pathogen will be susceptible or drug resistant.

In general, there are two different types of drug resistance. Intrinsic resistance refers to resistance that arose in a strain before it encountered a drug, while secondary or acquired resistance refers to a strain that became drug resistant while being exposed to the drug. Elucidating the mechanism of intrinsic resistance is challenging, because strain differences unrelated to the resistance may confound the analysis. On the other hand, resistance mechanisms related to acquired resistance are easier to identify and characterize. In these cases, comparing matched sets of susceptible and resistant clinical isolates has often been very useful in pinpointing to molecular mechanisms of acquired resistance [29].

Besides these two broad distinctions of intrinsic and acquired resistance, there are several other types of resistance. For example, stable resistance refers to a strain that maintains resistance once the drug pressure is released. This type of resistance has been encountered in clinical isolates of AIDS patients who have been receiving azole drugs for extended periods [61]. Transient resistance, on the other hand, refers to a strain that looses its resistance in the absence of the drug. Examples of transient resistance come from clinical isolates from bone marrow patients who have been receiving high doses of drugs for a short period [62]. Finally, the phenomenon of drug tolerance can also be considered as one form of resistance. Tolerance is defined as the ability of a strain to

survive at drug concentrations above the MIC value [63]. Tolerance can become particularly important in cases where a drug acts fungistatically as in the case with most azoles, but can be overcome when a fungistatic drug is converted into a fungicidal agent. For instance, when the fungistatic drug FCZ was combined with cyclosporine A, an inhibitor of calcineurin activity, and directed against *C. albicans*, cell viability decreased more than 99.9% after 24 hours compared to robust growth when either drug was used alone [64]. Although progress has been made to understand on the molecular level how the calcineurin pathway contributes to drug resistance, as yet we don't completely understand the significance of this pathway in clinical settings [65].

I.3.2. Molecular mechanisms of drug resistance

Clinical drug resistance has been reported for all 4 major classes of drugs. However, the frequency of developing antifungal resistance varies greatly between these 4 classes. For instance, resistance to AmB is still rare despite extensive use over several decades. The exact rate of AmB resistance remains unknown, and although AmB resistance has been observed in clinical isolates as well as in laboratory strains, the mechanism of AmB resistance remains elusive [66,67]. In some cases, AmB resistance has been linked to a significant reduction of ergosterol in the plasma membrane, thus leading to drug resistance because the target of AmB is reduced or even absent [68]. Resistance to 5-FC, on the other side, is very common. Known resistance mechanisms include decreased transport into the cell via the enzyme cytosine permease, alterations of metabolic enzymes (cytosine deaminase and uridine monophosphate pyrophosphorylase, uPRTase), as well as increased production of competitive pyrimidines. Mutations in the enzyme uPRTase seem to be the most commonly encountered event leading to 5-FC resistance in clinical isolates [69,70,71].

Probably the most-studied and best-understood mechanisms of drug resistance come from the use of azole drugs. Azole resistance is likely a consequence of extensive clinical use. Another reason why we frequently observe azole resistance is because azoles

are generally fungistatic. At least 4 different types of azole resistance mechanisms have been described.

The first one is facilitated by enhanced ATP-dependent efflux where the cell actively pumps the drug out of the cell. In such azole resistant isolates, genes encoding transporters containing the ATP binding cassette (ABC) have been found to be upregulated compared to susceptible isolates. Genes that encode for such ABC transporters were first identified in *C. albicans* as *CDR1* (standing for "*Candida* drug resistance 1") and *CDR2*, but have now also been characterized in *C. glabrata*, *C. tropicalis* and in *C. neoformans* [72]. There are at least two possibilities for how *CDR1* and *CDR2* can become upregulated in drug resistant *C. albicans* isolates. The first results when a region within the coding sequence of *CDR1* is mutated, leading to increased transcription initiation and mRNA stability [73]. The second results from the hyperactivation of *TAC1*, a transcription factor that regulates *CDR1* expression. Two mutations in particular, N972D and N977D**,** have been shown to cause hyperactivity of *TAC1,* leading to drug resistance in clinical isolates of *C. albicans* [74,75].

A second mechanism causing azole resistance is through the process of passive diffusion, where the cell uses the proton gradient across the plasma membrane to pump drugs out of the cell. This mechanism has been observed in several *Candida* spp., including *C. albicans*, *C. tropicalis* and *C. dubliniensis* and has been linked to one gene in particular, *MDR1* (multidrug resistance 1) [76]. *MDR1*-mediated resistance to one azole often leads to cross-resistance to other azoles, as evidenced by *C. tropicalis* isolates that were first treated with FCZ and then became resistant to another azole, itraconazole [77]. The problem of cross-resistance is increasingly becoming an issue even in other *Candida* spp. [78,79]. Moreover, acquired resistance based on *MDR1* is usually maintained even when the drug pressure is released [29]. However, despite its clinical significance, *MDR1* was shown to efflux only one clinically important compound, FCZ [80]. The mechanism behind *MDR1*-coupled drug resistance has recently been elucidated by microarray studies. Comparing transcriptional profiles of a drug resistant clinical isolate and its susceptible parent strain, it was shown that *MDR1* overexpression correlates with *MRR1* overexpression [81]. *MRR1* is a transcription factor controlling

MDR1 activity, and when *MRR1* mutations, such as P683S or G997V were introduced in susceptible strains they became drug resistant.

A third mechanism of azole resistance includes the alteration of the drug target itself, *ERG11*, and has been observed in all three major human fungal pathogens, *C. albicans*, *A. fumigatus* and *C. neoformans*. Drug target alteration can occur in at least two different ways; either by overexpressing *ERG11* or by mutating *ERG11* so that drugs are less actively binding to it. Drug resistance based on mutations in *ERG11* have been reported either as a single mutation or as multiple mutations within *ERG11*. Several research groups have independently identified mutations in the same functional region of *ERG11*, suggesting that there might be some "hot-spots" for development of azole resistance [47]. Once a cell has acquired an *ERG11* allele with such a resistance mutation, it is possible that the other allele also acquires this mutation through the process of gene conversion [82,83]. Fortunately, some of the second-generation triazoles, like posaconazole, have been shown to be more insensitive to mutations within *ERG11*, as was reported in a recent publication where up to 5 of these mutations were required to decrease sensitivity to posaconazole in *C. albcians* isolates [84].

Finally, a fourth mechanism leading to azole resistance is alteration of the ergosterol biosynthetic pathway. There are two ways this can happen. The first is by deletion of *ERG3*, which leads to high levels of azole resistance in laboratory strains of *C. albicans* when tested *in vitro* [29,68]. *ERG3* encodes for the Δ5,6-desaturase and, in the absence of azole drugs, converts episterol into non-toxic ergosta-5,7,24(28) trienol [53]. However, when *ERG11* is inhibited by azoles, 14-methyl intermediates accumulate and are converted by *ERG3* into toxic sterols like 14-methylergosta-8,24(28)-dien-3,6-diol [85,86]. Consequently, when *ERG3* is deleted there is less accumulation of such toxic sterols. Instead, *erg3* mutants treated with azoles exhibit an accumulation of the less toxic metabolite 14a-methylfecosterol, which still allows growth. Curiously, however, this type of drug resistance has only been observed *in vitro,* but has not been confirmed through *in vivo* experiments [87]. The second mechanism of altered ergosterol biosynthesis is the upregulation of ergosterol genes, which leads to increased ergosterol content in the plasma membrane. This mechanism has been linked to the transcription factor *UPC2* [88,89]. Two recent studies have demonstrated that hyperactivation of

UPC2 resulted in upregulation of not only ergosterol genes, including *ERG11*, but also other targets such as *CDR1* and *MDR1* in drug resistant clinical isolates in *C. albicans*. Introducing this *UPC2* mutation (G648D) into susceptible strains conferred drug resistance [90,91].

Resistance to the newest class of antifungals, the echinocandins, has also been described, despite the fact that all echinocandins have been in the clinic for less than a decade. However, the frequency of echinocandin resistance remains low. Clinical echinocandin resistance has been described for *C. albicans* and *C. parapsilosis*, while in *A. fumigatus* resistance could be engineered in a laboratory strain [92,93,94]. All mutations associated with echinocandin resistance have so far been shown to lie in the gene encoding the enzyme β-glucan synthetase, *FKS1*, the target of the echinocandins.

Having summarized limitations of existing antifungals, I am now going to talk about genomic approaches that help us identify gene functions in *C. albicans.*

I.4. Functional genomics in *C. albicans* - how to link a function to a gene?

I.4.1. *Saccharomyces cerevisiae* as a surrogate model

Before the genome sequence of *C. albicans* became available, functional genomics heavily relied on reverse genetic approaches, making use of surrogate models to study gene functions in *C. albicans*. For instance, many genes in *C. albicans* were initially identified by experiments where a cloned DNA sequence conferred the ability to complement a mutation in *S. cerevisiae*. Other genes have initially been identified by cloning experiments on the basis of their ability to interfere with a process in *S. cerevisiae* or even to confer new properties [reviewed in: 95]. The main reason why research in *C. albicans* has heavily relied on *S. cerevisiae* as a model is because functional genomic approaches are well advanced in the budding yeast. For instance, in

1996 *S. cerevisiae* became the first eukaryote whose genome was completely sequenced, it is also the first eukaryote where nearly every non-essential gene has been systematically deleted and the first eukaryote that was expression-profiled [96,97,98]. More recently, whole-genome sets of tagged proteins have become available to allow systematic cellular localization studies, whole-genome protein-protein interaction networks have been constructed either by coimmunoprecipitation or the two-hybrid method [99,100,101], and the SGA method (synthetic genetic analysis) has provided a tremendous amount of information regarding genetic interactions [102,103].

Another reason why budding yeast has frequently served as surrogate model is that although budding yeast diverged from *C. albicans* about 140-841 million years ago, these two fungal species are sufficiently similar so that the sophisticated technologies developed in *S. cerevisiae* have helped in studying gene function in *C. albicans*. Progress on understanding processes such as cell-cycle progression, signal transduction, mating, metabolism and cell-wall biosynthesis have all been accelerated in *C. albicans* based on information already available in *S. cerevisiae* [95]. Even aspects of fungal virulence and drug target discovery can be studied by relying on *S. cerevisiae* despite the fact that the budding yeast is usually not pathogenic. For instance, initial studies showing that *S. cerevisiae* can switch from the normal budding-yeast morphology to the pseudo-hyphal form prompted similar studies in *C. albicans*. These initial studies have formed the basis that led to the paradigm that morphological switching is important for virulence in *C. albicans* (s. chapter IV.1.4) [104,105,106]. Consequently, researchers identified and characterized signalling pathways that are involved in the morphological transition in the pathogen [107,108]. Another example is the discovery that budding yeast adheres to polystyrene and forms biofilms [109]. Many fungal pathogens, including *C. albicans*, form biofilms on implanted prosthetic devices, such as catheters, that are very hard to treat because they are often resistant to drug treatment [110].

Finally, budding yeast was successfully used as a model to study aspects of drug resistance and to elucidate the mode of action of antifungals. For instance, studying *S. cerevisiae* has helped to determine various resistance mechanisms related to FCZ, and has led to the identification of *FKS1*, the target of echinocandins [111,112,113,114].

More recently, chemical genetics has emerged as a complementary approach to study gene functions and the mode of action of bioactive compounds [reviewed in: 115]. The idea behind chemical genetics is that compounds can either activate or inactivate a specific gene or a group of genes, thus providing functional information on the targeted gene(s) without the need to genetically manipulate it.

Probably the most useful tool for functional genetic studies in budding yeast, both in terms of classical genetics and chemical genetics, is the construction of a *S. cerevisiae* deletion collection, which contains precise start-to-end deletions of all known genes [116]. In this collection, every mutant contains two unique barcodes, which allows pooling all mutants into one mixture and treating it with a drug. The effect of drug treatment on each mutant can then be analyzed by quantitative detection based on microarrays, where PCR-amplified barcodes of all mutants in the drug sample are compared to PCR-amplified barcodes of the control sample. This collection has been used extensively to probe gene functions, particularly in terms of antifungal drug response [115].

I.4.2. Limitations of *S. cerevisiae* as a surrogate model

Budding yeast and *C. albicans* have roughly the same number of genes, which is currently annotated with around 6000 open reading frames (ORFs) in both species; 6051 for *C. albicans* and 5797 in *S. cerevisiae* (not counting dubious ORFs) [117,118]. While the majority (4905 or 74%) of genes in budding yeast have been experimentally characterized, and almost all genes (5860, 95%) in the *C. albicans* genome have been manually annotated [119], there are only 1357 genes (22%) for which we possess functional experimental evidence in *C. albicans* (not counting the roughly 2000 genes that have been detected based on high-resolution tiling arrays or RNA-sequencing) [120,121]. The importance of characterizing the remaining genes in *C. albicans*, as opposed to simply relying on functional predictions based on homology, is evidenced by the fact that 774 genes are specific to *C. albicans* [122]. Another strong argument to experimentally study gene functions directly in the pathogen comes from a series of

recent studies. One such example is rewiring, or 'reprogramming', which refers to the reorganization of transcriptional networks between species, and has been shown to occur either through the addition or removal of upstream transcription factor binding motifs and/or through the substitution in the identity of the transcription factors involved in regulation of a particular process [119,123]. There are a number of well-documented events of rewiring that took place since *S. cerevisae* and *C. albicans* last shared a common ancestor. For example, while the transcription factor *GAL4* is involved in galactose metabolism in budding yeast, the *GAL4* homolog in *C. albicans* is not involved in this process, but instead regulates glycolysis [124]. Another example is ribosomal gene regulation, which is mediated by Rap1 in *S. cerevisiae*, but Tbf1 in *C. albicans* [125]. Yet other examples illustrating rewiring in the two fungal species include the regulation of the mating type locus, stress responses, as well as hypoxic and filamentation regulatory programs [126,127,128].

Other differences between budding yeast and *C. albicans* include that meiosis has not been observed in *C. albicans*, despite the presence of many homologous *S. cerevisiae* meiotic genes and the fact that *C. albicans* can mate. Instead, genetic recombination has been suggested to occur through a parasexual cycle in *C. albicans*, where mated tetraploid strains undergo random chromosomal loss that generates diploid strains with a shuffled combination of all chromosomes [129]. Another difference between the two species is that *C. albicans* translates the CUG codon into serine instead of leucine, while *S. cerevisiae* uses the 'standard' codon translation to convert messenger RNA into polypeptide sequences [130]. Finally, there are some important morphological differences between the two species. While *S. cerevisiae* primarily grows as budding yeast, *C. albicans* is considered a polymorphic fungus that can grow as a yeast, elongate into pseudo-hyphal or true hyphal structures, form chlamydospores or grow in the mating-competent opaque form [131].

Taken together, while *S. cerevisiae* has been an invaluable surrogate model to study gene function in *C. albicans* for many decades, some limitations are becoming apparent and urge the development of similar genetic tools to study gene function directly

in the pathogen. The next section provides a summary of currently available tools to study such functions in the pathogen.

I.4.2. Overview of available genetic tools in *C. albicans*

Functional analysis of the *C. albicans* genome was significantly sped up once the genome of this pathogen was sequenced in 2004 [132]. Over the course of the next several years, an international consortium generated a genome annotation, which was done by comparative genomics, i.e. comparing the *C. albicans* sequence to already annotated genomes, and a sequence assembly was established [124,133]. Recently, the availability of an even larger number of sequenced genomes from pathogenic and non-pathogenic fungal species has allowed a refinement of gene annotation and ORFs [134]. Different groups have now also started to experimentally validate the sequence information of the *C. albicans* genome using methods such as high resolution tiling arrays and RNA-sequencing [120,121].

While researchers have adapted some of the genomic tools developed in other systems for use in *C. albicans* even before an annotated genome was available, the number of tools has increased significantly with the genome annotation at hand. For instance, based on methods first developed in *S. cerevisiae, Schizosaccharomyces pombe* (fission yeast) and *Pichia pastoris*, protocols for transformation using recombinant DNA and PCR products, auxotrophic and dominant markers based on antibiotic resistance, inducible promoters, fluorescent reporter constructs, as well as epitope-tagging plasmids have been developed for *C. albicans* [reviewed in: 135,136]. While these techniques are providing a resource for functional genomics in the pathogen, these reverse-genetic methods are inherently biased in that one relies on information derived from surrogate models. A solution to this is provided by forward genetics, which allows investigators to ask specific questions directly in the organism of choice. The advantage of forward genetics is that this approach assigns gene function without *a priori* knowledge of the underlying genetic material. Forward genetics, however, is challenging in *C. albicans* due to the lack of meiosis and its constitutively diploid genome, which necessitates that two

copies of a gene of interest have to be inactivated in order to have a complete knock out genotype. Nevertheless, some forward genetic techniques have been developed in *C. albicans*. The most popular one is transcriptional profiling based on microarrays [137]. Many groups, including our own, have developed microarray platforms and analyzed various biological processes on a genome-wide scale [138]. For instance, some of the first published transcriptional profiling studies aimed at assigning gene functions to the yeast-to-hyphal switch, while other studies looked at the transcriptional response to various antifungal drugs or at the response when *C. albicans* enters into contact with the host [139,140,141,142].

Another technique relying on forward genetics is transposon mutagenesis. Generally, there are two ways this technique can be applied to probe gene functions in *C. albicans*. The first one relies on the concept of haploinsufficiency, which describes the phenomenon that lowering the dosage of a gene from two copies to one copy in a diploid organism results in a detectable phenotype [115]. The first report making use of haploinsufficiency by transposon mutagenesis in *C. albicans* aimed at linking genes to the yeast-to-hyphae switch. In order to do this, Uhl et al. mutagenized a genomic library of *C. albicans in vitro* by using the Tn7 transposon containing the uracil 3 (*URA3)* selectable marker [143]. The authors then transformed *C. albicans* with the resulting constructs and obtained 18 000 independent mutants, of which 146 were linked to a filamentation-defect phenotype. Other groups have used a similar strategy making use of haploinsufficiency. For instance, Shen et al. constructed another transposon-based library and identified the *C. albicans* pescadillo homolog, which is required for normal hyphal-to-yeast morphogenesis and yeast proliferation, while other groups have used haploinsufficiency coupled to chemical genetics to probe either the mechanism of action of drugs or to identify new drug targets in *C. albicans* [144,145,146].

The second approach making use of transposon mutagenesis is based on the *UAU1* technique. The advantage of this method compared to haploinsufficiency is that it inactivates both copies of a given gene. The *UAU1* cassette was developed in the Mitchell laboratory and consists of three main parts: a non-functional *ura3Δ3'*, the gene encoding for arginine 4 (*ARG4)*, and a non-functional *ura3Δ5'* containing 530 bp of

homology with *ura3Δ3'* [147]. To apply this approach, the *UAU1* cassette is first transformed into an *arg4/ura3* auxotrophic background, and *ARG4+* heterozygotes are selected. Next, after growth to allow mitotic recombination these transformants are replica plated on media lacking arginine and uracil, thus selecting for prototrophic *ARG4+/URA3+* colonies. In these prototrophs, the expectation is that one allele is still inactivated by the initial *ARG4* construct, while the other allele is inactivated by a *URA3* sequence that was formed by homologous recombination between the two non-functional but overlapping *ura3* sequences. The presence of two copies of the initial transposon cassette is essential to allow the formation of both an *URA3* and an *ARG4* gene; duplication of the transposon cassette prior to this mitotic event that generates the *URA3* gene is likely to result from either gene conversion, mitotic cross-over, chromosome duplication or chromosome loss followed by duplication [135]. Using the *UAU1* system as a marker, Davis and colleagues have added Tn7 transposon sequences on either side of the *UAU1* construct and mutagenized *in vitro* the genome of *C. albicans*. This resulted in a collection of plasmids carrying the *UAU1*:Tn7 marker flanked by *C. albicans* specific genomic sequences. They then randomly selected about 200 of those plasmids, transformed *C. albicans* and screened for filamentous defects, which led to the identification of *MDS3*, a gene encoding a pH-responsive regulator [148]. Consequently, this strategy has been expanded to look at other biological processes, such as chlamydospore and biofilm formation, as well as response to antifungal drugs [149,150,151].

Overall, while *S. cerevisiae* has been a tremendous help in functional genetics for *C. albicans*, several reverse and forward genetics strategies have become available over the last few years to probe gene functions directly in the pathogen. In the course of my thesis, I have made use of two of these approaches to probe two processes that are important in the biology of *C. albicans*, namely drug resistance and virulence.

I.6. Rationale and objectives

Despite several classes of clinically approved antifungals, the mortality rate due to fungal infections remains high. For instance, mortality rates due to *Candida* infections reach up to 50% while those caused by *Aspergillus* infections are as high as 57% [152,153]. Another factor to consider is that treatment costs are increasing, mostly because of prolonged hospital stays. For example, annual treatment costs for fungal infections reach $2.6 billion in the US alone [154]. Therefore, one challenge that remains is to improve current therapy options. One way to do this is by improving the efficacy and safety of available drugs, for instance by chemical modifications. On the other hand, because drug resistance has been observed against every existing drug used in the clinic, another and maybe more promising way would be to identify novel targets with the hope to develop drugs that have a different mode of action compared to existing drugs. The challenge here is to find such targets. In the previous sections, I have summarized functional genomic tools to study gene functions in *C. albicans*. Now, I will apply some of these concepts; I will describe in chapter II one example how we can find novel drug targets based on the surrogate model *S. cerevisiae*. Following up on this, I will extrapolate these findings and test the predictions from *S. cerevisiae* directly in *C. albicans* (chapter III).

Besides this reverse genetic approach, the post-genomic era in *C. albicans* has yielded some important tools to probe gene functions directly in the pathogen. Because the yeast-to-hyphal switch is a *C. albicans*-specific process that has contributed to its reputation as a pathogen, and because relying on budding yeast as surrogate model poses obvious limitations when addressing functions such as virulence, I investigated one forward genetic approach to probe aspects of virulence directly in the pathogen. The aim here was to identify genes involved in the yeast-to-hyphal switch and test whether they are involved in virulence (chapter IV).

Finally, in chapter V, I will follow up on one of the hits that resulted from chapter IV. In particular, I will look at the Arp2/3 complex with the goal of better understanding the biological function of this actin nucleating machinery in terms of actin dynamics and endocytosis.

Chapter
II

II. Chemogenomic profiling predicts antifungal synergies

Mol Syst Biol. 2009;5:338. Epub 2009 Dec 22. || PMID: 20029371

Molecular Systems Biology 5; Article number 338; doi:10.1038/msb.2009.95
Citation: ***Molecular Systems Biology*** **5:338**

www.molecularsystemsbiology.com

molecular systems biology

Chemogenomic profiling predicts antifungal synergies

Gregor Jansen[1,7,*], Anna Y Lee[2,3,7], Elias Epp[4,5], Amélie Fredette[1], Jamie Surprenant[1], Doreen Harcus[4], Michelle Scott[2,8], Elaine Tan[1], Tamiko Nishimura[1], Malcolm Whiteway[4,5], Michael Hallett[2,3,6] and David Y Thomas[1]

[1] Department of Biochemistry, Faculty of Medicine, McGill University, Montréal, Québec, Canada, [2] McGill Centre for Bioinformatics, McGill University, Montréal, Québec, Canada, [3] School of Computer Science, McGill University, Montréal, Québec, Canada, [4] Genetics Group, Biotechnology Research Institute, National Research Council of Canada, Montréal, Québec, Canada, [5] Department of Biology, McGill University, Montréal, Québec, Canada and [6] Rosalind and Morris Goodman Cancer Centre, McGill University, Montréal, Québec, Canada
[7] These authors contributed equally to this work
[8] Present address: School of Life Sciences Research, University of Dundee, Scotland DD1 5EH, UK
* Corresponding author. Department of Biochemistry, Faculty of Medicine, McGill University, McIntyre Medical Sciences Building, 3655 Promenade Sir William Osler, Montréal, Québec, Canada H3G 1Y6. Tel.: +1 514 398 1341; Fax: +1 514 398 7384; E-mail: gregor.jansen@mcgill.ca

Received 8.1.09; accepted 28.10.09

Chemotherapies, HIV infections, and treatments to block organ transplant rejection are creating a population of immunocompromised individuals at serious risk of systemic fungal infections. Since single-agent therapies are susceptible to failure due to either inherent or acquired resistance, alternative therapeutic approaches such as multi-agent therapies are needed. We have developed a bioinformatics-driven approach that efficiently predicts compound synergy for such combinatorial therapies. The approach uses chemogenomic profiles in order to identify compound profiles that have a statistically significant degree of similarity to a fluconazole profile. The compounds identified were then experimentally verified to be synergistic with fluconazole and with each other, in both *Saccharomyces cerevisiae* and the fungal pathogen *Candida albicans*. Our method is therefore capable of accurately predicting compound synergy to aid the development of combinatorial antifungal therapies.
Molecular Systems Biology **5**: 338; published online 22 December 2009; doi:10.1038/msb.2009.95
Subject Categories: functional genomics; computational methods
Keywords: antifungal; chemical genomics; drug profiling; synergy predictor

Introduction

Drugs that act against individual molecular targets are often insufficient to combat fungal infections, multigenic diseases such as cancer, and multiple cell or tissue type diseases, including immune and inflammatory disorders (White *et al*, 1998; Sams-Dodd, 2005; Onyewu and Heitman, 2007; Zimmermann *et al*, 2007). Combinatorial therapies that impact multiple targets simultaneously are less prone to development of drug resistance, and increase therapeutic efficacy (Groll and Walsh, 2002; Zimmermann *et al*, 2007). One of the major benefits of combinatorial therapies is the potential for synergistic effects: that is, the overall therapeutic benefit of the drug combination is greater than the sum of the effects of the individual agents. In particular, synergies between the constituent compounds can provide broader pharmacological windows and reduced toxicity (Fitzgerald *et al*, 2006). These advantages have driven drug discovery efforts towards the search for multi-agent therapies (Borisy *et al*, 2003; Fitzgerald *et al*, 2006; Onyewu and Heitman, 2007; Zimmermann *et al*, 2007).

Despite the obvious benefits, there are many challenges associated with the identification of multi-agent therapies. A sensitive, but low-throughput test for synergy is the dose-matrix response assay; in its simplest form it tests serial dilutions of two compounds in all possible permutations. The results from this assay can be analysed with respect to different models for quantifying synergy. Each model defines a baseline efficacy level for the compounds, when used in combination at concentrations X and Y, describing the expected level if the compounds are not synergistic. The Loewe additivity model defines the baseline as the level that would be expected if a compound were in fact combined with itself (Loewe, 1953). The Bliss boosting model, an extension of the Bliss independence model (Bliss, 1939), defines the baseline level as $I_{\mathrm{Mult}}=I_X+I_Y-I_XI_Y$, where I_X and I_Y are the efficacy levels of the compounds in isolation at concentrations X and Y, respectively (Lehár *et al*, 2007). Alternatively, the potentiation model defines the baseline level as $I_{\mathrm{Pot}}=\max(I_X, I_Y)$ (Lehár *et al*, 2007). The utility of any of these models depends on the comprehensiveness of the dose-matrix response data.

Large-scale searches have demonstrated that high-throughput screens of thousands of compounds can be straightforward (Zhang *et al*, 2007), but usually these screens can only test a small fraction of the exponential number of chemical

combinations available. Moreover, simplified dose-matrix assays are commonly used by these approaches, but the simplification may result in a failure to test the compound concentrations at which synergies occur, and therefore result in reduced synergy detection. Several lines of research address these problems (Borisy *et al*, 2003; Zhang *et al*, 2007). Some efforts reduce the scale issue by screening only combinations that include a particular compound of interest (i.e. by fixing one component). Other approaches tackle challenges later in the therapy development pipeline using *in silico* approaches to predict how two compounds act on pathways to achieve additive or synergistic effects (Lehár *et al*, 2007).

Although improvements in the scale and sensitivity of synergy identification techniques promise a greater exploration of combinatorial chemical space, it is unlikely that experimental techniques will be sufficient to completely survey this vast space in a cost-effective and timely manner. Consequently, there is a clear need for an approach that winnows this space to a manageably large set of combinations that is enriched for synergistic combinations. The combinations in the set could then be rigorously tested experimentally. A suggested experimental approach to finding this set entails an iterative 'maximal damage' search (Ágoston *et al*, 2005; Lehár *et al*, 2008a). In each iteration of the search, the most effective combination from the previous iteration is tested with all other compounds separately to identify a combination that is more effective. However, this directed strategy starts with the most effective compound and will thus miss potentiating synergies between compounds that incur minimal damage separately. In contrast, an accurate *in silico* approach would alleviate this challenge of synergy identification by enabling comprehensive and efficient exploration of the combinatorial space. Such a strategy could employ data from single compound treatments to effectively predict which combinations are most likely to behave synergistically. There are several approaches in the literature, including that of Nelander *et al* (2008), that attempt to use data from perturbation screens and prior knowledge regarding the targets of compounds to model the effects of these compounds when they are used alone or in combination. This approach is currently limited to compounds with known targets, but such an approach could potentially be extended to predict synergistic compound pairs (Nelander *et al*, 2008).

The use of chemogenomic profiles offers promise for characterizing the global cellular response to an arbitrary compound, for predicting the mode of action of a compound, and for inferring the function of genes. Here we focus on chemogenomic profiles generated for *Saccharomyces cerevisiae* where each member of the yeast gene deletion library is grown in the presence of a particular compound, and the resultant growth fitness is recorded. Strains with reduced fitness in comparison with untreated or wild-type cells suggest that the loss of particular genes confers sensitivity to the compound. For example, a set of genes involved in multi-drug resistance was identified by finding commonalities between yeast chemogenomic profiles of a chemically diverse panel of compounds (Parsons *et al*, 2004; Hillenmeyer *et al*, 2008). It has also been established that similarity between chemogenomic profiles often implies a similarity in the mode of action of the corresponding compounds (Parsons *et al*, 2006). In other words, two compounds that induce sensitivity in many of the same gene deletion strains may target similar cellular pathways. Conversely, strains that behave similarly across a panel of compounds may indicate that the corresponding genes are functionally related (Haggarty *et al*, 2003; Lee *et al*, 2005; Brown *et al*, 2006). The ability of chemogenomic profiles to predict similarities in cellular response, mode of action, and gene function poses the question as to whether they can be used to also predict synergy. This aspect has not been investigated to date and would provide a simple approach to synergy prediction that does not require prior knowledge of the targets of compounds and extensive modelling of previous approaches (Nelander *et al*, 2008).

We introduce here a combined experimental and bioinformatics approach to identify antifungal synergies. In particular, for each compound of interest, we obtain a chemogenomic profile, which we define as a set of genes whose deletions confer sensitivity to a given compound. The next step is to computationally measure the similarity between pairs of profiles. We establish that compound pairs that have correspondingly similar profiles are more likely to be synergistic when compared with randomly chosen compounds. This approach exploits the fact that chemogenomic profiles make compounds instantly comparable *in silico*: whereas exhaustive screening of only pairwise combinations already necessitates a quadratic number of dose-matrix assays, the computational method requires only a linear number of chemogenomic profiles and a small number of subsequent validation assays relative to the total number of possible combinations. Our approach is thus a practical way to comprehensively search the vast chemical space for synergistic compounds.

We validate this method by assessing the antifungal activity of compound combinations in *S. cerevisiae* and in the fungal pathogen *Candida albicans*. Infections by *Candida species* are an increasing problem, especially in patients who are immunocompromised (Groll and Walsh, 2002). We show that our approach successfully predicts antifungal synergies that occur in *S. cerevisiae* and *C. albicans*.

Results

Our goal was the identification of compound pairs that exhibit antifungal synergy. There are two types of antifungal synergy: the constituent compounds act synergistically to kill fungal cells (cytotoxic synergy) or arrest growth only (fungistatic synergy). Although a combination may be fungistatic against one fungal species, it might exhibit more potent synergy against others. Therefore, it may be useful to further investigate whether combinations that are fungistatic against particular fungal species can be developed into antifungal therapies against other fungal species.

The collection and generation of chemogenomic profiles

S. cerevisiae, with its accessible genetic resources, was used as the model for fungal pathogens. The first step in our method was to collect from the literature the results of ~1300

genome-wide, sensitivity and lethality screens generated with a broad range of compounds (Supplementary Table SI). This set forms our chemogenomic profile collection (Figure 1A). Although the screens were conducted differently (e.g. with diploids versus haploids; competitive versus non-competitive growth), the results of each screen permit the identification of a set of strains that are hypersensitive to the compound, which in turn define a set of hypersensitive genes. We focus on this hypersensitive gene set format of a chemogenomic profile in our analyses.

Fluconazole, a widely used fungistatic drug with favourable pharmacokinetic and toxicological properties (Grant and Clissold, 1990), would be an ideal constituent compound of a combinatorial antifungal therapy. We thus generated a *de novo* profile for fluconazole using the yeast haploid deletion strain collection (Winzeler *et al*, 1999). As a control, we used the hypomorphic strain for the essential gene *ERG11* (Schuldiner *et al*, 2005; Breslow *et al*, 2008). Fluconazole directly targets Erg11p and thus specifically inhibits its enzymatic activity in the biosynthetic pathway for ergosterol, an essential sterol in yeast (White *et al*, 1998). As expected, fluconazole was lethal to the *erg11* strain since inhibition of the already limited cellular amount of Erg11p likely decreased its activity to fatal levels. Although previous studies have identified strains that are sensitive to fluconazole (Parsons *et al*, 2004), we re-screened the drug to focus on deletions that are lethal in the presence of fluconazole. The results define a set of genes that we call FCZ-Fungicidal (Supplementary Table SII). We next validated the profile by determining the minimum inhibitory concentration (MIC) and minimum fungicidal concentration (MFC) for each strain (Figure 1B and Supplementary Table SIII). These values represent dosages where FCZ-Fungicidal strains are unable to recover after exposure to fluconazole, unlike wild-type cells.

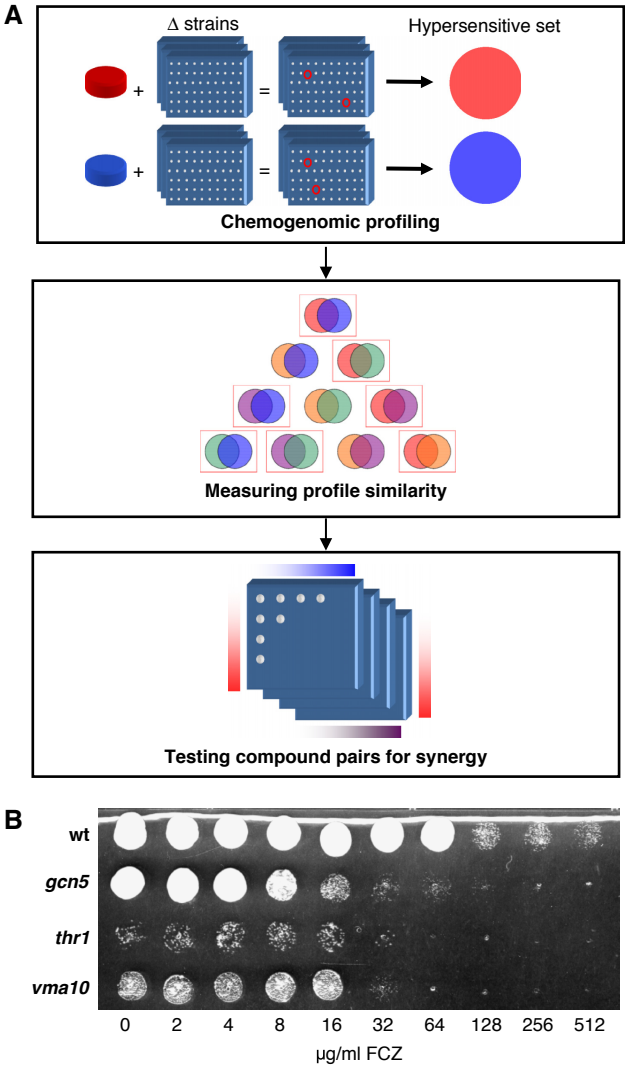

Figure 1 A method for identifying synergistic compounds with antifungal activity. (**A**) A schematic illustrating the steps of the method. (**B**) Validation of the first step: recovery after fluconazole treatment for defining the chemogenomic profile of the drug. Strains were treated with increasing amounts of fluconazole (0–128 μg/ml) for 24 h before spotting aliquots on YPD and incubating at 30°C for 2 days.

To exclude the possibility that any secondary mutations present in the deletion strains were responsible for the FCZ-Fungicidal phenotype, we complemented the FCZ-Fungicidal strains with plasmid-borne copies of their respective deleted genes to demonstrate reversibility of the phenotype. The presence of the overexpressed gene enabled the transformants to survive lethal concentrations of fluconazole above their MFCs (data not shown) without conferring resistance to fluconazole beyond levels observed for the wild type. Therefore, the complementation results confirm, for every FCZ-Fungicidal strain, that the gene deletion is responsible for the FCZ-Fungicidal phenotype.

Components of the FCZ-Fungicidal set

Of the 4997 deletion strains screened, 21 were unable to recover after exposure to fluconazole, in addition to the *erg11* hypomorphic strain (Supplementary Table SII). Members of the SAGA histone acetyltransferase complex and genes with general RNA polymerase-II transcription factor activity (e.g. members of the mediator complex) are significantly over-represented in the FCZ-Fungicidal set (adjusted $P=3.7\times10^{-6}$ and 0.01, respectively; see Materials and methods). Members of the vacuolar membrane H^+-ATPase complex and cytoskeleton genes are also over-represented in the set (adjusted $P=3.7\times10^{-6}$ and 0.03, respectively; see Materials and methods). Taken together, genes involved with transcriptional regulation, vacuole function, and cell structure are significantly associated with sensitivity to fluconazole.

Prediction of synergistic compounds

We assessed whether any given compound pair with a high level of similarity between its chemogenomic profiles is likely to exhibit antifungal synergy. A gold standard set of positive and negative examples of antifungal synergy was assembled for this purpose (Supplementary Table SIV). Specifically, the positive and negative examples are synergistic compound pairs curated from the literature and pairs that we showed are not synergistic in *S. cerevisiae* using a dose-matrix response assay (see Materials and methods; Supplementary Table SV), respectively. Moreover, the gold standard set is limited to

compound pairs where each constituent compound is associated with at least one chemogenomic profile in our collection. Although it would be interesting to investigate the potential differences in the accuracy of a synergy predictor built exclusively from either diploid- or haploid-based profiles, there are too few gold standard examples that are associated with both types of profiles to enable such a comparison (i.e. four positive examples). Similarly, there are too few examples to compare the accuracy of predictors built exclusively from either profiles generated from competitive or non-competitive growth assays (the literature contains only one positive example). Therefore, the gold standard set, together with our complete chemogenomic profile collection, was used to evaluate three different pairwise measures of chemogenomic profile similarity for their ability to predict antifungal synergy.

Previous studies suggest that the vast majority of compound pairs do not exhibit antifungal synergy. For example, Borisy *et al* (2003) tested 560 reference-listed compounds (i.e. known to have some bioactivity) in pairwise combination with fluconazole using a dose-matrix proliferation assay using fluconazole-resistant *C. albicans*. They described one synergistic combination, although they also confirmed 20 combinations as potentially synergistic because each of these combinations shows an effect that is greater than the baseline level defined by the highest single-agent model, that is, the larger of the effects produced by the constituent agents when they are applied singly. Overall, their results suggest that 0.2–3.6% of the tested combinations exhibit antifungal synergy (and the limited number of antifungal synergies reported in the literature in general suggests that synergy is even rarer in other chemical libraries). The scarcity of synergy would suggest that the evaluation of a synergy predictor should place great emphasis on the identification of true synergies.

It is standard practice to evaluate a predictor by estimating its receiver-operating characteristic (ROC) curve. However, applying this type of evaluation to a synergy predictor would equally emphasize the identification of true synergies and false positives. Furthermore, the estimated rarity of antifungal synergy implies that a ROC curve would be estimated with a very small fraction of all negative examples of synergy in the chemical space covered by our chemogenomic profile collection. That is, only 30 out of the estimated ~175 000 negative examples are known in our study, where the total number of negative examples is based on the estimated frequency of antifungal synergy, 3.6% (Borisy *et al*, 2003). A ROC curve estimated with the small negative gold standard set would likely hide the utility of the synergy predictor simply because our sample of negative examples is not sufficiently representative of the complete negative set. Therefore, instead of estimating ROC curves, we evaluated each synergy predictor by estimating to what degree its predictions are enriched for true synergies. That is, we computed a prediction score for every positive and negative example in our gold standard set and estimated to what degree the subset predicted to be synergistic is enriched with positive examples (with a hypergeometric test). This type of evaluation places greater value on the identification of true synergies as desired. We also estimated the true synergy enrichment of predictions made using random permutations of our chemogenomic profile collection (see Materials and methods). The enrichment estimates from the permutations establish a baseline enrichment distribution. The significance of the true synergy enrichment from the observed data was computed relative to this baseline distribution. Significant enrichment would suggest that testing a set of compound pairs that are predicted to be synergistic via profile similarity is expected to yield significantly more true synergies than testing an equal number of randomly selected compound pairs.

The first measure of chemogenomic profile similarity that we assessed quantifies the significance of the overlap between two hypersensitive gene sets (see the example in Figure 2A). In particular, when x genes are observed in both hypersensitive gene sets, the measure is the probability of obtaining x or more genes in the overlap by chance (i.e. a P-value from a hypergeometric distribution). With this gene-based profile similarity measure, a compound pair is predicted to be synergistic if its P-value is less than or equal to a given

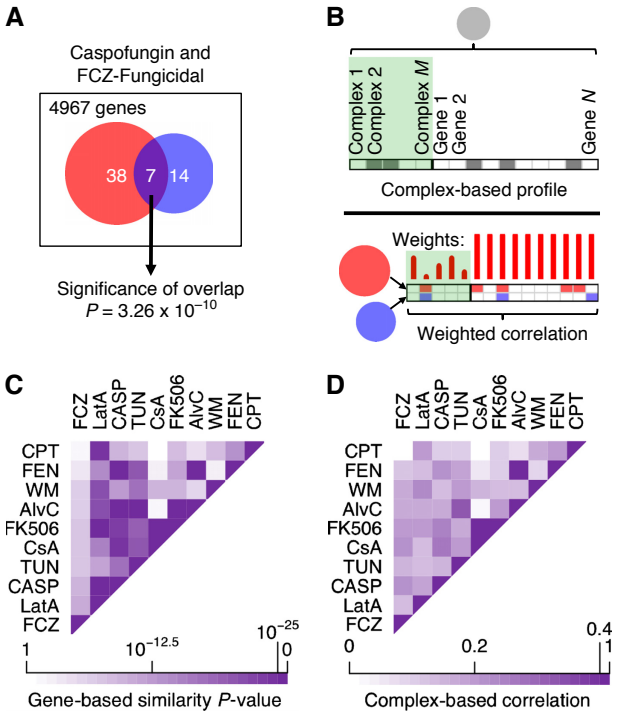

Figure 2 The measures of chemogenomic profile similarity and antifungal synergy predictions based on these measures. (**A**) An example of how the gene-based measure quantifies profile similarity with the hypergeometric test. (**B**) The complex-based measure. This measure compares complex-based profiles derived from hypersensitive gene sets. The similarity between the complex-based profiles is measured with weighted Pearson correlation. A protein complex is weighted less if it has many subunits, and all genes that are not annotated to any complex (i.e. non-complex genes) are assigned maximal weight. (**C**) A heatmap of the similarity values of select compound pairs, using the gene-based measure. The intensity of purple for a pair corresponds to the degree of similarity. All compounds in the heatmap are predicted as synergistic with fluconazole (using a threshold of $P \leqslant 10^{-6.5}$), except for camptothecin (included for contrast). (**D**) As in panel C, except that the similarity values were computed using the complex-based measure. AlvC, alverine citrate; CASP, caspofungin; CsA, cyclosporine-A; FCZ, fluconazole; FEN, fenpropimorph; LatA, latrunculin-A; TUN, tunicamycin; WM, wortmannin.

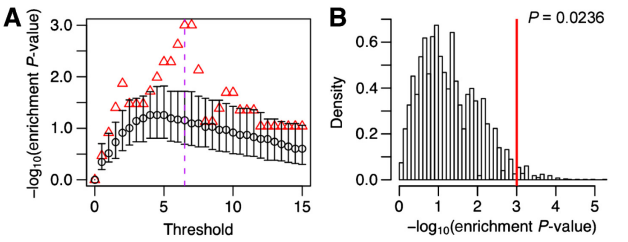

Figure 3 Statistical evaluation of the gene-based chemogenomic profile similarity measure as a predictor of antifungal synergy. The evaluation is based on the enrichment of the predictions with true positives/synergies, and higher values in this figure indicate greater enrichment. Baseline enrichment values were estimated using random permutations of the data (n=5000 permutations, see Materials and methods). The significance of the enrichment estimated from the observed data is computed relative to the baseline enrichment values. (**A**) The true synergy enrichment estimated from observed and randomly permuted data, at different similarity thresholds. The x-axis shows the $-\log_{10}$ transformation of the threshold values. The triangles indicate the enrichment values estimated from the observed data, at different thresholds. For each threshold, the median (o) and interquartile range (whiskers) of the enrichment values computed from the different permutations are also shown. (**B**) The significance of the true synergy enrichment associated with the predictor used with a threshold of $10^{-6.5}$, relative to the permutation distribution of the baseline enrichment. The red line indicates the enrichment estimated from the observed data and its P-value of significance is also shown. The threshold of $10^{-6.5}$ results in the most significant enrichment and is therefore considered the optimal profile similarity threshold for defining the synergy predictions.

threshold. We evaluated this profile similarity measure as a synergy predictor at different thresholds (Figure 3A). The predictions defined by the threshold $P \leqslant 10^{-6.5}$ exhibit a true synergy enrichment that represents a significant improvement over the expected baseline level (P=0.0236; see Figure 3B). Furthermore, this threshold produces the most significant improvement and is thus optimal for defining synergy predictions. Taken together, these results suggest that chemogenomic profile similarity predicts antifungal synergy.

We also assessed a chemogenomic profile similarity measure that accounts for additional commonality that is observable by viewing the profiles at the level of protein complexes (Figure 2B). That is, although one subunit of a protein complex may be associated with sensitivity to one compound and a different subunit associated with a second compound, it is nonetheless interesting that the same complex is associated with sensitivity to either compound. Each profile was converted into a complex-based profile defined by a list of 0 s and 1 s indicating absence or presence (respectively) of each complex, and also each non-complex gene, in the hypersensitive gene set. The similarity between two such profiles was measured via weighted Pearson correlation. A protein complex with many subunits is weighted less because it is less rare for that complex, via any one of its subunits, to be included in any given hypersensitive gene set. As with the gene-based profile similarity measure, a compound pair is predicted to be synergistic if the similarity of the corresponding profiles is greater than or equal to an optimal threshold. The enrichment of the predictions with true synergies is more significant for the complex-based measure than for the gene-based measure, relative to the expected baseline levels (P=0.0092 and 0.0378, respectively; see Supplementary Figure S1A). Taken together, these results suggest that the complex-based profile similarity measure can predict synergy more effectively than the simpler gene-based measure.

Lastly, we assessed a profile similarity measure that exploits the detailed quantitative data available for a subset of our chemogenomic profile collection. Namely, for some profiles each gene is associated with a $\log_2$ratio that reflects the growth of untreated versus chemically treated cells of the relevant deletion strain (Parsons *et al*, 2006; Hillenmeyer *et al*, 2008; Hoon *et al*, 2008). We thus considered the correlation across these $\log_2$ratios as a measure of profile similarity. Again, a compound pair is predicted to be synergistic if the similarity of the corresponding profiles is greater than or equal to an optimal threshold. Unlike measures of profile similarity based on hypersensitive gene sets, enrichment of the predictions with true synergies is not significant for the $\log_2$ratio-based measure, relative to the expected baseline level (P=0.3109; see Supplementary Figure S1A). Therefore, we focus on the gene-based profile similarity measure as a predictor of synergy (using the threshold $P \leqslant 10^{-6.5}$) due to its simplicity and significant enrichment of its predictions with true synergies (Figure 1A).

Consistent with the evidence that antifungal synergy is rare, the majority of compound pairs in the chemical space covered by our chemogenomic profile collection are not predicted to be synergistic (see the x-axis of Supplementary Figure S2A). In addition, the estimated accuracy of the predictor (=0.745) is significantly above the expected baseline level (P=0.018; see Supplementary Figure S2B), despite the fact that the estimate is likely based on a small fraction of all negative examples. If instead we over-estimate and assume that all compound pairs in our chemical space are negative examples (i.e. ∼182 000 instead of the estimated ∼175 000 examples, where the total number of negative examples is based on the estimated frequency of antifungal synergy, 3.6%; Borisy *et al*, 2003), our estimates would be based on a more representative set of negative examples (see Supplementary Figure S2A for the ROC curve). At the selected threshold, the estimated true positive rate is ∼67% and, using the overlarge negative set, the estimated false positive rate and accuracy are ∼5 and ∼95%, respectively. Furthermore, the level at which the predictions are enriched with true synergies would increase if the number of negative examples in the gold standard set were to increase and if all new examples were predicted as true negatives (Supplementary Figure S2C). Taken together, we have shown statistically that the predictor is surprisingly accurate and the estimate of its accuracy will increase as the community develops a more representative gold standard set. Therefore, we have shown that our predictor is useful for efficient identification of antifungal synergies.

The next step in the synergy identification method for our fluconazole example requires measuring the similarity between the FCZ-Fungicidal profile and each member of the chemogenomic profile collection. The FCZ-Fungicidal profile is significantly similar to 10 profiles ($P \leqslant 10^{-6.5}$) and these other profiles are associated with eight different compounds (Supplementary Table SVI). Consequently, eight compounds are predicted to be synergistic with fluconazole through the FCZ-Fungicidal profile.

Validation of predicted synergies in *S. cerevisiae*

Of the eight compounds predicted to be synergistic with fluconazole through the FCZ-Fungicidal profile, seven were tested for fungistatic and cytotoxic synergy with fluconazole in *S. cerevisiae*: latrunculin-A, caspofungin, tunicamycin, cyclosporine-A, FK506, alverine citrate, and wortmannin. Fenpropimorph is predicted to be synergistic with fluconazole through a different fluconazole profile (P=9.20 × 10^{-45}). Therefore, we also included fenpropimorph in our synergy tests. In total, eight predicted fluconazole combinations were experimentally tested for synergy.

We experimentally examined each compound combination using a dose-matrix response assay that measures the growth of treated cells. The results were used to quantify growth arrest synergy using the Loewe additivity model (Loewe, 1953; Barchiesi *et al*, 1998) (see Materials and methods; Supplementary Table SV). The dose-matrix response data were also fitted to Bliss boosting and potentiation models of synergy (Lehár *et al*, 2007) (see Materials and methods; Supplementary Table SVII). There is partial agreement between the results from the Loewe additivity model and the other models. However, we chose to identify synergies relative to the additive compound-with-itself baseline since it is the most conservative of the tested models. Each dose matrix of treated cells was also spotted on YPD to examine recovery of the cells post treatment (Figure 4). Absence of visible colonies after 24 h suggests that the treatment has some cytotoxic effects. Synergy in terms of this cytotoxic phenotype was also quantified with the Loewe additivity model (see Materials and methods). The cytotoxicity of compound combinations at particular concentrations was confirmed by a large reduction in the number of colony-forming units of treated versus untreated cells (data not shown). Compound combinations that exhibit growth arrest but not cytotoxic synergy are referred to as exhibiting fungistatic synergy. Figure 4C and D show examples of fungistatic and cytotoxic synergy (respectively) in *S. cerevisiae*.

Five compounds were validated as synergistic with fluconazole, including fenpropimorph (Supplementary Figure S3A and Table SV). Furthermore, we noticed that many of the compounds predicted to be synergistic with fluconazole are also predicted to be synergistic with each other (Figure 2C). The same observation can be made based on predictions with the complex-based profile similarity measure (Figure 2D). We thus extended our validation efforts to include 10 pairings of the predicted fluconazole partners. These pairings include two that are not predicted to be synergistic: cyclosporine-A + fenpropimorph and fenpropimorph + wortmannin. Of the 18 experimentally tested combinations in total, 11 showed a synergistic relationship with six and five demonstrated fungistatic and cytotoxic effects, respectively (Table I and Supplementary Figure S3 and Table SV). The two synergies involving fenpropimorph listed above are false negatives, although they are consistent with the observation that compounds that are synergistic with fluconazole tend to be synergistic with each other. Taken together, the results indicate a validation success rate of 56% in *S. cerevisiae*.

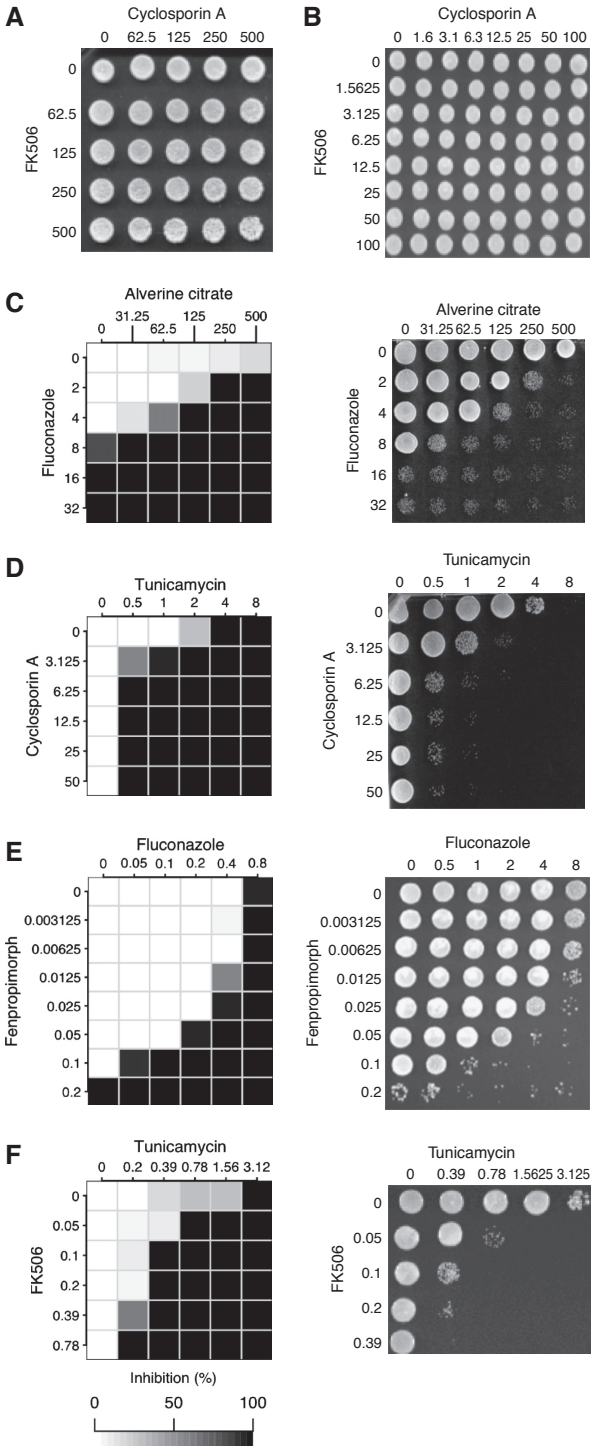

Figure 4 Dose-matrix responses to compound pairs that exhibit antifungal synergy. (C–F) Growth inhibition levels of cells grown in the presence of the compounds are shown on the left. The recovery of cells post treatment is shown on the right. (**A**, **B**) Recovery of cells treated with a compound pair that is not synergistic in *S. cerevisiae* and *C. albicans*, respectively. (**C**, **D**) Compound pairs that exhibit fungistatic and fungicidal synergy in *S. cerevisiae*, respectively. (**E**, **F**) Compound pairs that exhibit fungistatic and fungicidal synergy in *C. albicans*, respectively.

Validation of predicted synergies in *C. albicans*

We sought to identify synergies in *C. albicans* that establish potential multi-agent therapies, after validating our approach in the model *S. cerevisiae*. Four compound pairs that we identified as synergistic in *S. cerevisiae* are already described in the literature as synergistic in *Candida* species, suggesting that

our approach may successfully identify synergies in *C. albicans* (Table I). Using the dose-matrix response assay, the 18 combinations tested in *S. cerevisiae* were tested in *C. albicans* resulting in the identification of 10 synergistic combinations in the fungal pathogen, nine of which are cytotoxic (see Figure 4E and F for examples of fungistatic and cytotoxic synergy, respectively, and see Supplementary Figure S4 for all synergies identified in *C. albicans*). As before, we used the Loewe additivity model to quantify synergy (Supplementary Table SVIII), although we also fitted the dose-matrix response data to other synergy models (Supplementary Table SIX). Table I lists the complete set of synergistic compound pairs that we identified. We showed that eight synergistic combinations identified in *S. cerevisiae* are also synergistic in *C. albicans*, and we identified two additional synergies in the fungal pathogen that could not be identified in *S. cerevisiae* (caspofungin + fluconazole and fluconazole + latrunculin-A). Taken together, the validation success rate for the predictor of antifungal synergy is 69%. This implies that our method identifies true synergies at a rate that is ~20-fold better than the estimated rate for testing randomly selected compound pairs.

Table I Compound pairs that exhibit antifungal synergy

Compound pair	*S. cerevisiae*	*C. albicans*
AlvC + FCZ	Fungistatic	Cytotoxic
CASP + FCZ	—	Cytotoxic
CsA + FEN[a]	Fungistatic	Cytotoxic
CsA + FCZ[a]	Cytotoxic	Cytotoxic
CsA + TUN	Cytotoxic	Cytotoxic
FEN + FK506[a]	Fungistatic	—
FEN + FCZ	Fungistatic	Fungistatic
FEN + WM	Cytotoxic	—
FK506 + FCZ[a]	Fungistatic	Cytotoxic
FK506 + TUN	Cytotoxic	Cytotoxic
FK506 + WM	Cytotoxic	—
FCZ + LatA	—	Cytotoxic
FCZ + WM	Cytotoxic	Cytotoxic

AlvC, alverine citrate; CASP, caspofungin; CsA, cyclosporine-A; FCZ, fluconazole; FEN, fenpropimorph; LatA, latrunculin-A; TUN, tunicamycin; WM, wortmannin.
[a]Previously shown to be synergistic.

Finally, we tested one of the novel synergistic combinations in fluconazole-resistant clinical isolates of *C. albicans*. These strains acquired fluconazole resistance by mutations that either lead to upregulation of the target of fluconazole (*ERG11*, strain S2; Dunkel *et al*, 2008), or increased the expression of a multi-drug efflux pump (*MDR1*, strain G5; Morschhauser *et al*, 2007). We chose to test fluconazole (FDA-approved) in combination with wortmannin, analogues of which are in phase-I clinical trials (Noble *et al*, 2004). Even when applied at concentrations ~1000-fold higher than the MIC in corresponding wild-type strains, fluconazole has no readily detectable effect on cell growth in the clinical isolates. However, the combination of fluconazole and wortmannin exhibits a strong cytotoxic effect (Figure 5), suggesting potential clinical relevance.

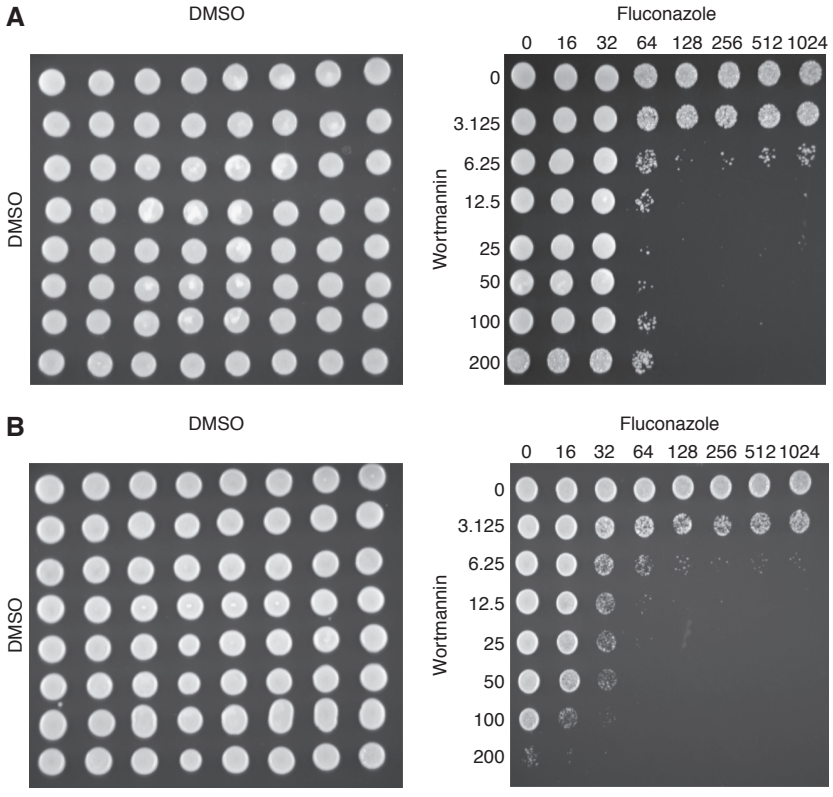

Figure 5 The dose-matrix recovery from treatment with fluconazole and wortmannin, a compound pair exhibiting antifungal synergy in (**A**) the multidrug-resistant clinical *C. albicans* isolate G5 and (**B**) the fluconazole-resistant clinical *C. albicans* isolate S2. Solvent controls are shown on the left.

A comparison of predictors dependent on haploid- and/or diploid-based profiles

After adding our novel synergistic compound pairs to the gold standard set of antifungal synergies, we revisited the question of whether the type of chemogenomic profiles used by the synergy predictor influences the enrichment of its predictions with true synergies. We therefore measured the significance of the enrichment associated with predictors dependent on haploid-based profiles only, diploid-based profiles only, and both haploid- and diploid-based profiles. However, this comparison could only be made using profiles generated from a competitive growth assay (i.e. the assay can use haploids or diploids) since there is an insufficient number of gold standard examples to also make the comparison in the context of profiles generated from a non-competitive growth assay. Although augmenting the gold standard set with validated synergies from this study may bias the enrichment values, all three predictors were subjected to the same bias since they were all evaluated with the same gold standard set, and here we are only interested in comparing the predictors relative to each other. As before, optimal prediction thresholds were selected for each of the three variants of the synergy predictor in the comparison. Our results suggest that the variant that exclusively uses haploid-based profiles produces predictions that are enriched with true synergies most significantly relative to the expected baseline enrichment level, followed by the variant that uses both haploid- and diploid-based profiles and the variant that exclusively uses diploid-based profiles (P=0.0372, 0.0572, and 0.0794, respectively; see Supplementary Figure S1B). However, our collection of haploid-based profiles contains data for only 20 compounds. Therefore, it is currently best to use all types of chemogenomic profiles with our approach for better coverage of chemical space, and thus, for enabling potential identification of more synergistic combinations.

Our results show that chemogenomic profile similarity predicts antifungal synergy. The similarity values for all pairings of the chemogenomic profiles in our collection are contained in Supplementary Table SX. These data can be used immediately to identify compound pairs that are likely to exhibit antifungal synergy, and thus should stimulate the search for effective combinatorial therapies.

Discussion

We have developed a bioinformatics-driven approach using chemogenomic profiles to predict compound pairs that exhibit antifungal synergy. First, we collected sensitivity-based chemogenomic profiles from the literature and generated a profile in *S. cerevisiae* for the widely used fungistatic drug fluconazole. We then showed statistical evidence supporting the use of our gene-based measure of profile similarity for predicting synergistic compound pairs. Our predictions of synergistic compound pairs validated with a high success rate. Overall, the results confirm that chemogenomic profile similarity can predict antifungal synergies.

Chemogenomic profiles can be generated in several ways. As more profiles of different type become available, it would be interesting to further investigate the relative utility of each type for the prediction of synergy. Our collection includes profiles based on competitive or non-competitive growth of diploids or haploids. Despite the heterogeneity of our collection, we used it in its entirety for better coverage of chemical space when predicting antifungal synergies. For example, had we limited the chemogenomic profile collection to haploid-based profiles, the cytotoxic synergy involving latrunculin-A would not have been predicted because a haploid-based profile was not generated for this compound. Despite the expected differences in the profiles simply due to the different ways in which they were generated, our approach was able to identify synergies based on the similarity between profiles generated with different methods (e.g. the FCZ-Fungicidal profile derived from non-competitive growth of haploids and the latrunculin-A profile derived from competitive growth of diploids). Therefore, different types of profiles may lead to false negatives; however, our approach generates predictions that are enriched with true antifungal synergies more significantly than what is expected by chance.

A chemogenomic profile encodes the genes involved in resistance to a particular compound (Lee *et al*, 2005; Parsons *et al*, 2006). If the profiles of two compounds are similar, there is likely some underlying drug-resistance machinery to which both apply stress. Cells treated with both compounds concurrently may not be able to mount an effective response to the challenge, and the compounds thus exhibit antifungal synergy. Previous studies have identified drug-resistance machinery (Parsons *et al*, 2004). Interestingly, the FCZ-Fungicidal set (Supplementary Table SII) includes the pleiotropic drug pump *PDR5*, genes that regulate the transcription of this pump as members of the SAGA and mediator complexes (Gao *et al*, 2004), and genes with vacuolar functionality. In short, the FCZ-Fungicidal set includes genes that have previously been associated with drug resistance. Our method, therefore, exploits the drug-response machinery identified by chemogenomic profiling to predict synergy.

The FCZ-Fungicidal set also includes genes associated with the cytoskeleton or cell wall, two of which (*BEM2*, *SLT2*) are synthetically lethal with the target of fluconazole, *ERG11* (Parsons *et al*, 2004). It is possible that these genes become vital for maintaining the structural integrity of the cell to compensate for the instability that may result from reduced ergosterol production. This is a possible explanation for why these genes are associated with resistance to fluconazole (i.e. if the genes are deleted, cells are hypersensitive to the drug). By similar reasoning, we would expect these genes to be associated with resistance to latrunculin-A, a compound that disrupts the actin cytoskeleton (Ayscough *et al*, 1997). Indeed, the hypersensitive gene set of latrunculin-A overlaps significantly with the FCZ-Fungicidal set, and the overlap includes genes associated with the cell wall or cytoskeleton (Supplementary Table SVI). Latrunculin-A was thus predicted as synergistic with fluconazole and this synergy was subsequently shown in *C. albicans*. Therefore, the FCZ-Fungicidal genes provide mechanisms to generate synergy.

Previous work suggests that compounds with similar chemogenomic profiles have similar modes of action (Parsons *et al*, 2004). However, in both *S. cerevisiae* and *C. albicans* we identified synergy between fluconazole and cyclosporine-A, which target ergosterol biosynthesis (White *et al*, 1998) and

calcineurin (Wang and Heitman, 2005), respectively. While fluconazole and cyclosporine-A profiles have distinguishing features (as expected due to the distinct targets of the compounds), our method uses a statistic that recognizes the profile similarities as significant, given what is possible by chance. That is, five genes in the overlap of the hypersensitive gene sets is in fact highly significant given that there are ~5000 possible genes for each set (with ~20 genes). As a predictor, our gene-based measure of profile similarity is thus useful for identifying synergies that might be unexpected given what is already known about the participating compounds.

The results establish that our method predicts synergy well in *S. cerevisiae*. It can also predict synergy in *C. albicans* based on chemogenomic profiles in *S. cerevisiae*. Despite differences in regulatory circuitry that have been observed between the fungal species (Martchenko *et al*, 2007; Hogues *et al*, 2008; Tuch *et al*, 2008), the majority of the synergies identified in *C. albicans* were transferred directly from *S. cerevisiae*. This suggests that the predicted synergies could be tested in *C. albicans* immediately, without first testing the predicted combinations in *S. cerevisiae* to filter out unlikely candidates. We have, therefore, shown that our method effectively uses *S. cerevisiae* resources to identify antifungal synergies in *C. albicans*. Furthermore, our method predicts synergies previously shown in other fungal pathogens (see Supplementary Table SIV for references) and it would thus be interesting to further investigate whether our method can predict broad-spectrum antifungal combinations that exhibit synergy.

We also statistically evaluated an alternative profile similarity measure, based on the correlation of $\log_2$ratios that quantify the growth of untreated versus treated cells, as a predictor of antifungal synergy. We found that this measure predicts synergy markedly worse than the validated gene-based measure (Supplementary Figure S1A). Interestingly, the gene-based measure compares $\log_2$ratio profiles by first converting them into hypersensitive gene sets. This suggests that the quantitative profile data that are useful for predicting synergy are effectively summarized by a hypersensitive gene set.

Our method for predicting antifungal synergy clearly requires chemogenomic profiles for compounds. Although construction of a chemogenomic profile for a compound is a significant task, the profile would be a beneficial resource in general because it is a multi-valued description of the bioactivity of a compound and can be used in all future studies. In fact, the number of published chemogenomic profiles is increasing (Lehár *et al*, 2008b) and as a result, the scope of our synergy prediction method is expanding.

Moreover, an alternative profile similarity measure was defined to enable analysis at the protein complex level. Statistical evaluation of this measure as a predictor of antifungal synergy (using the gold standard set) suggests that the measure actually predicts synergy better than the validated gene-based approach (Supplementary Figure S1A), although this may be an artefact of the small size of the gold standard set. Nevertheless, in combination with a variant of the complex-based measure, it may therefore be feasible to predict synergy using chemogenomic profiles built solely from strains pertaining to key members of protein complexes, thereby reducing the scale of the screening task. This would represent another important advance in our methodology.

In addition, our method is efficient because it is capable of reducing a huge set of all possible compound pairs down to a set of manageable size for thorough synergy testing in fungi and indeed may be applied to other organisms. Our results show that compounds that are synergistic with fluconazole tend to be synergistic with each other, suggesting that our method is also able to identify compound synergy clusters. Overall, the net gain from our method is greater compared with that from traditional screens since costs are reduced and sensitivity is increased.

Importantly, our method identified novel drug relationships, including cytotoxic synergy between fluconazole and wortmannin in *S. cerevisiae*, *C. albicans* and drug-resistant clinical isolates of *C. albicans*. Fluconazole is an FDA-approved drug and wortmannin analogues are in phase-I clinical trials (Noble *et al*, 2004). The method has thus uncovered a new synergistic combination that can be pursued as a viable therapy.

Combinatorial therapies have been widely used in different medical scenarios (Keith *et al*, 2005; Zimmermann *et al*, 2007). However, to discover new combinations using the vast number of compounds available (>10 million compounds available—http//www.emolecules.com), screening strategies must be adapted to address the scale of the discovery task. We have developed a powerful tool for rapid synergy discovery that represents a promising step towards realizing the potential of combinatorial therapies. We have validated this approach with antifungal combinations and pointed out a potential path to attack the persisting problem of drug-resistant *C. albicans* strains in the clinic. It would thus be interesting to investigate whether our approach can be used to streamline the combinatorial therapy development process in other therapeutic situations.

Materials and methods

Strains and media

The *S. cerevisiae* haploid strain BY4741 (*MAT***a***his3*Δ*1 leu2*Δ*0 met15*Δ*0 ura3*Δ*0*) and the complete yeast deletion array collection in the BY4741 background were obtained from the American Type Culture Collection. *S. cerevisiae* was cultured in rich media (YPD), synthetic complete media (SC), or synthetic drop-out media (SD-ura); for solid media 2% agar was added. The *C. albicans* wild-type strain SC5314, as well as the fluconazole- and multi-drug-resistant strains S2 (Dunkel *et al*, 2008) and G5 (Morschhauser *et al*, 2007), respectively, were cultured in YPDU media (YPD supplemented with 50 mg/l of uridine); for solid media 2% agar was added. Amiodarone, benomyl, camptothecin, carboplatin, fenpropimorph, FK506, fluconazole, mycophenolic acid, myriocin, tunicamycin, and wortmannin were dissolved in DMSO; chlorpromazine, desipramine, doxycycline, MMS, and nystatin were dissolved in water; and cyclosporine-A was dissolved in ethanol. Fluconazole was a gift from Pfizer Limited (Sandwich, Kent, UK), caspofungin was a gift from Merck Frosst Limited (Kirkland, Québec, Canada) and all other compounds were purchased from Sigma.

Library screen to generate the lethality-based chemogenomic profile for fluconazole

Ninety-six-well plates containing the American Type Culture Collection *S. cerevisiae* deletion strains were replicated with a 96-pin replicator (Boekel) to single-well Omnitray plates (Nalgene Nunc) containing YPD agar and geneticin (200 μg/ml), and, simultaneously, to plates containing YPD agar and fluconazole (85 μg/ml). The plates were incubated at 30°C for 48 h. Following incubation, cells on the YPD

control and fluconazole plates were replicated to fresh YPD plates (without fluconazole) and incubated at 30°C for 48 h. Plates were scored for deletion strains that were unable to grow after exposure to fluconazole. Strains that fit this criterion were subsequently retested in MIC and recovery assays (see below). The deletion strains that were unable to recover from fluconazole at concentrations that in contrast did not affect wild-type cells, were assigned a score of 1 in the chemogenomic profile and all other strains were assigned 0. Moreover, genes associated with the deletion strains with score 1 define our hypersensitive gene set for fluconazole (i.e. the FCZ-Fungicidal set).

MIC assays, recovery assays, and compound synergy tests in *S. cerevisiae* and *C. albicans*

Antifungal sensitivity testing was performed with a modified version of the CLSI (formerly NCCLS) procedure (NCCLS. Reference Method for Broth Antifungal Susceptibility Testing of Yeasts: Approved Standard-Second Edition. NCCLS document M27-A2). Briefly, overnight cultures of the wild-type and deletion strains were diluted to an OD_{600} of 0.0005 for *S. cerevisiae* and OD_{600} 0.001 for *C. albicans*. Volumes of 50 µl of culture were inoculated into 96-well flat-bottom plates containing 50 µl of SC media for *S. cerevisiae* and YPD media for *C. albicans* with increasing concentrations of compound (in twofold serial dilutions). The cultures were grown without shaking at 30°C for 24 h and OD_{600} measurements were taken with a Tecan Safire microplate monochromator reader (Tecan, Austria, GmbH). The MIC was determined by the first well with a growth reduction of at least 95% in the presence of a compound as compared with untreated cells. Cells were then spotted (2 µl) onto YPD plates and incubated at 30°C for 48 h to assess the extent to which cells recover from the treatments. The MFC of a given strain was determined from these recovery assays (Supplementary Tables SV and SVII).

Compound synergy interactions were assessed by growth in a dose-matrix titration assay. Volumes of 50 µl of each compound were twofold serially diluted in SC media for *S. cerevisiae* and YPD media for *C. albicans*, and dispensed into 96-well flat-bottom plates, either across columns of the plates (compound-A) or down rows of the plates (compound-B). Wells were then inoculated with 50 µl of wild-type yeast prepared as in the MIC assay. Plates were incubated at 30°C without shaking and OD_{600} measurements were taken after 24 h. MICs were determined for the compounds alone and in combination by the first well, with $\geqslant$95% decrease in absorbance relative to the control. The growth arrest synergy of a compound pair was quantified with respect to the Loewe additivity model (Loewe, 1953) through the fractional inhibitory concentration index ($FICI_{growthArrest}$)=($MIC_{A\ in\ combo}/MIC_{A\ alone}$) + ($MIC_{B\ in\ combo}/MIC_{B\ alone}$). A compound pair is classified as synergistic if its FICI is $\leqslant$0.5, the standard threshold (Loewe, 1953; Barchiesi *et al*, 1998). Cells were also spotted (2 µl) onto fresh YPD plates and incubated at 30°C for 24 h to test for cytotoxic synergy. The minimum cytotoxic concentration (MCC) was defined for a compound alone and in combination as the lowest concentration that did not result in visible colonies on the plate. Cytotoxicity was confirmed by measuring colony-forming units (CFUs) after compound treatment. Cells were treated with both compounds at their MCCs, then plated on YPD plates and CFUs were counted after 48 h incubation at 30°C. The cytotoxic synergy of a compound pair was quantified as $FICI_{cytotoxic}$=($MCC_{A\ in\ combo}/MCC_{A\ alone}$) + ($MCC_{B\ in\ combo}/MCC_{B\ alone}$). A compound pair was classified as exhibiting fungistatic synergy if we identified the pair as synergistic with respect to the growth arrest phenotype only.

Complementation assay

To demonstrate that fluconazole sensitivity was dependent on particular gene deletion and not on acquired secondary mutations, the deletion strains were transformed with plasmids carrying their respective deleted genes expressed from the galactose-inducible *GAL1* promoter (Gelperin *et al*, 2005; Jansen *et al*, 2005). The transformants were incubated in two sequential overnight cultures. Cells were diluted and treated with fluconazole as described above and then incubated at 30°C for 24 h. After incubation, 2 µl of cultures were spotted onto fresh YPD plates, incubated at 30°C for 2 days, and scored for growth. The complementation test was performed under both inducing (SC: 4% galactose) and non-inducing (SC: 2% glucose) conditions.

The chemogenomic profile collection

We collected the results of compound sensitivity screens described in the literature. Different screens used different schemes to score each deletion strain based on its observed level of sensitivity to a given compound (and the complete set of strain scores defines the chemogenomic profile of the compound). For each chemogenomic profile, we identified strains that were scored as moderately to highly sensitive to the compound by noting the strains with scores that surpass the threshold specified in Supplementary Table SI. The genes associated with these strains define the hypersensitive gene set of the compound.

Annotations of the FCZ-Fungicidal genes

Descriptions of the FCZ-Fungicidal genes were downloaded from the Saccharomyces Genome Database (SGD; ftp://ftp.yeastgenome.org/yeast/). Gene Ontology (GO)-based gene annotations (Ashburner *et al*, 2000) were used to test whether particular biological processes, molecular functions, and cellular components are significantly over-represented in the FCZ-Fungicidal gene set. For each GO gene set, a *P*-value was obtained from a hypogeometric test performed within the scope of the set of genes associated with strains that were used in the FCZ-Fungicidal screen. The *P*-values were adjusted for multiple comparisons using the Benjamini and Hochberg method (Benjamini and Hochberg, 1995).

The gold standard set

A gold standard set of positive and negative examples of antifungal synergy was assembled to evaluate the synergy predictors (Supplementary Table SIV). Specifically, the 21 positive examples are synergistic compound pairs curated from the literature. The 30 negative examples are pairs that we showed are not synergistic in *S. cerevisiae* using a dose-matrix response assay (Supplementary Table SV).

The measures of chemogenomic profile similarity

Consider profiles A and B and their associated hypersensitive gene sets G_A and G_B, respectively. Let U_A and U_B represent the sets of all genes associated with strains that were screened to generate profiles A and B, respectively. U_A and U_B may differ if, for example, one screen involved essential genes (through heterozygous strains) and the other did not. We define $U=U_A \cap U_B$ as the scope of the statistical test that measures the similarity between profiles A and B, and therefore compute $G_A'=G_A \cap U$ and $G_B'=G_B \cap U$.

The gene-based profile similarity measure compares the hypersensitive gene sets associated with the profiles. The measure is defined as the *P*-value obtained from a hypergeometric test that quantifies the significance of $|G_A' \cap G_B'|$ (i.e. the probability of obtaining an equal or larger number by chance), given $|G_A'|$, $|G_B'|$ and $|U|$.

The complex-based profile similarity measure compares hypersensitive gene sets that have been transformed into complex-based profiles (Figure 2B). Mappings of genes to GO-defined protein complexes were downloaded from SGD. Let C_i represent the set of genes associated with complex i. The GO hierarchy subdivides some complexes into its constituent domains. In these cases, we treat each domain as a separate complex, and the genes associated with the domains are removed from the gene set of the parent complex (to avoid redundancy). For protein complex i, we compute $C_i'=C_i \cap U$. If $G' \cap C_i' \neq \varnothing$, we say that complex i is present in G', else it is absent. We generate a complex-based profile $\mathbf{x}_A$, defined as a vector of 0 s and 1s indicating absence or presence (respectively) of each complex, and also each non-complex gene, in G_A'. Similarly, $\mathbf{x}_B$ was generated with G_B'. The similarity between $\mathbf{x}_A$ and $\mathbf{x}_B$ is measured via weighted

Pearson correlation. Each non-complex gene is assigned a full weight of 1 and complex i is assigned a weight equal to $1/|C_i'|$. That is, a protein complex with many subunits is weighted less because it is less rare (and thus less significant) for that complex, via any one of its subunits, to be present in any given G'.

The $\log_2$ratio-based profile similarity measure compares profiles that have $\log_2$ratio sensitivity scores. The $\log_2$ratios quantify the growth of untreated cells versus treated cells. We define $\mathbf{y_A}$ as the vector of $\log_2$ratios of profile A, with one value specified for each gene in U. Similarly, we define $\mathbf{y_B}$ for profile B, retaining the same gene order that is used in $\mathbf{y}_A$. The similarity between $\mathbf{y_A}$ and $\mathbf{y_B}$ is measured with Pearson correlation.

Synergy prediction

Our chemogenomic profile collection may contain several different profiles associated with a single compound. For example, these profiles may have been generated with different assays and/or different concentrations of the compound. For compounds A and B, every profile for A is compared to every profile for B. The similarity value for the compound pair is defined as the best similarity value obtained from all the pairwise profile comparisons. For the gene-based profile similarity measure, the best is the lowest P-value. If the similarity value of a compound pair is less than or equal to some threshold, the pair is predicted to be synergistic. For the complex-based and $\log_2$ratio-based measures, the best similarity value is the highest correlation value. For these measures, a compound pair is predicted to be synergistic if its similarity value is greater than or equal to some threshold.

For the comparison of the three profile similarity measures as predictors of synergy (Supplementary Figure S1A), a reduced gold standard set was used to evaluate each predictor (16 and 24 positive and negative examples, respectively). Each compound pair in the reduced set is associated with $\log_2$ratio profiles since the $\log_2$ratio-based measure requires these types of profiles (see Supplementary information).

Similarly, for comparison of the gene-based measure predictors dependent on haploid-based profiles only, diploid-based profiles only, and both types of profiles (Supplementary Figure S1B), a different gold standard set was used to evaluate these predictors (10 and 16 positive and negative examples, respectively). Each compound pair in the set is associated with both haploid-based and diploid-based profiles, and all the profiles were generated from a competitive growth assay. To avoid an extremely small number of positive examples, the set includes synergies validated in this study (see Supplementary information). Even so, there is insufficient number of gold standard examples to also make the comparison in the context of profiles generated from a non-competitive growth assay.

We evaluated each variant of the synergy predictor based on the significance of enrichment of its predictions with true positives/synergies, relative to the expected baseline level (see section Permutation analysis below). The optimal profile similarity threshold for defining the predictions of each variant is therefore the threshold that results in the most significant enrichment.

Permutation analysis

The chemogenomic profile labels were permuted 5000 times in order to estimate the baseline levels of different statistics, for each variant of the synergy predictor. For each type of profile (the type of each profile is specified in Supplementary Table SI), the labels were randomly permuted among all profiles of that type. This preserves any systematic differences between profiles of different type. However, we excluded permutations where at least one profile label is assigned to a profile corresponding to the same compound. For example, this could potentially occur when there are multiple profiles generated with different concentrations of the same compound. Additional restrictions were applied, depending on the type of analysis. For comparison between the three profile similarity measures, permutations were only performed across $\log_2$ratio profiles. For comparison of predictors dependent on haploid-based profiles only, diploid-based profiles only, and both types of profiles, permutations were only performed across profiles generated from a competitive growth assay. In addition, permutations were performed only across haploid- and diploid-based profiles for predictors exclusively dependent on haploid- and diploid-based profiles, respectively.

With each permutation, synergy predictions were made using a given variant of the predictor at different thresholds. We computed a statistic quantifying the enrichment of the predictions (defined by the optimal threshold) with true synergies. That is, the P-value obtained from a hypergeometric test that equals the probability of obtaining an equal or larger number of positive examples predicted to be synergistic by chance, given the numbers of positive examples, negative examples, and predicted synergies in the given gold standard set. For the final predictor, the predictions were also used to compute the accuracy at the optimal threshold.

For each statistic z (e.g. the enrichment P-value), a permutation distribution of the baseline value was obtained by collecting the computed values from all 5000 permutations. Moreover, the significance of the value computed with the observed/real data (z_{obs}) relative to the expected baseline value was quantified as $P=(x+1)/(n+1)$, where x is the number of permutations with a z value better than or equal to z_{obs} and n=5000, the number of permutations in this case (Moore *et al*, 2009).

Fitting to other models of synergy

For each compound pair that was experimentally tested for synergy, Bliss boosting and potentiation models of synergy were fit to the dose-matrix response data (Lehár *et al*, 2007). First, the OD_{600} values were used to compute a corresponding matrix of % inhibition values (I) relative to untreated cells. Model fits to the inhibition data were then obtained as previously described (Lehár *et al*, 2007). The sum-of-squared fit errors $(SS)=\Sigma(I_{observed}-I_{fit})^2$ was computed for each model. The best fit model was defined as the first consistent model, with the Bliss boosting model considered before the potentiation model because it is less complex. We define consistent as $|SS-SS_{min}|<SS_{min}$, where SS_{min} is the minimum SS of the two models.

A Bliss boosting surface is defined by $I_{Bliss}=I_X+I_Y+(\beta-E_{min})[(I_XI_Y)/(E_XE_Y)]$, where I_{Bliss} is the Bliss boosting inhibition level when both compounds are used in combination, with the first and second compounds used at concentrations X and Y, respectively. I_X and I_Y are the inhibition levels when the first and second compounds are used alone at concentrations X and Y, respectively. E_X and E_Y are the maximum inhibition levels achievable by the first and second compounds, respectively, and $E_{min}=\min(E_X, E_Y)$; β is the fitted parameter and it represents the amount of boosting above $\max(E_X, E_Y)$. Reference values of β indicate cancelling, suppressive, masking, multiplicative, and saturating levels of Bliss boosting. The selected Bliss boosting level of a compound pair is defined as the first consistent level (in the order shown above), where consistent is defined as $|\Delta\beta-\Delta\beta_{min}|<\Delta\beta_{min}$, with $\Delta\beta=|\beta-\beta_{ref}|$ for some reference level β_{ref}, and β_{min} is the minimum $\Delta\beta$ across all reference levels.

A potentiation model surface is defined by $I_{Potent}=\max(I_X(C), I_Y)$, where $I_X(C)$ is the inhibition level when the potentiated compound is used alone, at a shifted concentration C. We have that $C=X[1+(Y/Y_{pot})^{|p|}]^{sign(p)}$, where Y_{pot} and p are fitted parameters, representing the concentration of the potentiated compound above which potentiation occurs and the potentiation slope, respectively (Lehár *et al*, 2007). $P=0$, $P>0$, and $P<0$ indicate no potentiation, synergy, and antagonism, respectively. For each compound pair, the inhibition matrix was fitted to this model twice: the first time assuming that the first compound is potentiated, and the second time assuming that the second compound is potentiated. Of the two fits, we report the one with the lower SS (Supplementary Tables SVII and SIX).

All computational analyses were performed in the R statistical software framework (R Development Core Team, 2007).

Supplementary information

Supplementary information is available at the *Molecular Systems Biology* website (www.nature.com/msb).

Acknowledgements

We thank Dr Robert Annan for comments and suggestions regarding the writing of the paper. We thank Dr Charles Boone for providing additional chemogenomic profile data that were generated by Parsons *et al* (2006). This is National Research Council of Canada publication NRC 495413. This work was supported by the Natural Sciences and Engineering Research Council of Canada, and the Canadian Institutes of Health Research (scholarship to AYL and grants to MW, MH, and DYT).

Conflict of interest

The authors declare that they have no conflict of interest.

References

Ágoston V, Csermely P, Pongor S (2005) Multiple weak hits confuse complex systems: a transcriptional regulatory network as an example. *Phys Rev E Stat Nonlin Soft Matter Phys* **71:** 051909

Ashburner M, Ball CA, Blake JA, Botstein D, Butler H, Cherry JM, Davis AP, Dolinski K, Dwight SS, Eppig JT, Harris MA, Hill DP, Issel-Tarver L, Kasarskis A, Lewis S, Matese JC, Richardson JE, Ringwald M, Rubin GM, Sherlock G (2000) Gene ontology: tool for the unification of biology. The Gene Ontology Consortium. *Nat Genet* **25:** 25–29

Ayscough KR, Stryker J, Pokala N, Sanders M, Crews P, Drubin DG (1997) High rates of actin filament turnover in budding yeast and roles for actin in establishment and maintenance of cell polarity revealed using the actin inhibitor latrunculin-A. *J Cell Biol* **137:** 399–416

Barchiesi F, Di Francesco LF, Compagnucci P, Arzeni D, Giacometti A, Scalise G (1998) *In-vitro* interaction of terbinafine with amphotericin B, fluconazole and itraconazole against clinical isolates of *Candida albicans*. *J Antimicrob Chemother* **41:** 59–65

Benjamini Y, Hochberg Y (1995) Controlling the false discovery rate: a practical and powerful approach to multiple testing. *J R Stat Soc B* **57:** 289–300

Bliss C (1939) The toxicity of poisons applied jointly. *Ann Appl Biol* **26:** 585–615

Borisy AA, Elliott PJ, Hurst NW, Lee MS, Lehar J, Price ER, Serbedzija G, Zimmermann GR, Foley MA, Stockwell BR, Keith CT (2003) Systematic discovery of multicomponent therapeutics. *Proc Natl Acad Sci USA* **100:** 7977–7982

Breslow DK, Cameron DM, Collins SR, Schuldiner M, Stewart-Ornstein J, Newman HW, Braun S, Madhani HD, Krogan NJ, Weissman JS (2008) A comprehensive strategy enabling high-resolution functional analysis of the yeast genome. *Nat Methods* **5:** 711–718

Brown JA, Sherlock G, Myers CL, Burrows NM, Deng C, Wu HI, McCann KE, Troyanskaya OG, Brown JM (2006) Global analysis of gene function in yeast by quantitative phenotypic profiling. *Mol Syst Biol* **2:** 2006 0001

Cowen LE, Nantel A, Whiteway MS, Thomas DY, Tessier DC, Kohn LM, Anderson JB (2002) Population genomics of drug resistance in *Candida albicans*. *Proc Natl Acad Sci USA* **99:** 9284–9289

Dunkel N, Liu TT, Barker KS, Homayouni R, Morschhauser J, Rogers PD (2008) A gain-of-function mutation in the transcription factor Upc2p causes upregulation of ergosterol biosynthesis genes and increased fluconazole resistance in a clinical *Candida albicans* isolate. *Eukaryot Cell* **7:** 1180–1190

Fitzgerald JB, Schoeberl B, Nielsen UB, Sorger PK (2006) Systems biology and combination therapy in the quest for clinical efficacy. *Nat Chem Biol* **2:** 458–466

Gao C, Wang L, Milgrom E, Shen WCW (2004) On the mechanism of constitutive Pdr1 activator-mediated PDR5 transcription in *Saccharomyces cerevisiae*: evidence for enhanced recruitment of coactivators and altered nucleosome structures. *J Biol Chem* **279:** 42677–42686

Gelperin DM, White MA, Wilkinson ML, Kon Y, Kung LA, Wise KJ, Lopez-Hoyo N, Jiang L, Piccirillo S, Yu H, Gerstein M, Dumont ME, Phizicky EM, Snyder M, Grayhack EJ (2005) Biochemical and genetic analysis of the yeast proteome with a movable ORF collection. *Genes Dev* **19:** 2816–2826

Grant SM, Clissold SP (1990) Fluconazole. A review of its pharmacodynamic and pharmacokinetic properties, and therapeutic potential in superficial and systemic mycoses. *Drugs* **39:** 877–916

Groll AH, Walsh TJ (2002) Antifungal chemotherapy: advances and perspectives. *Swiss Med Wkly* **132:** 303–311

Haggarty SJ, Clemons PA, Schrieber SL (2003) Chemical genomic profiling of biological networks using graph theory and combinations of small molecule perturbations. *J Am Chem Soc* **125:** 10543–10545

Hillenmeyer ME, Fung E, Wildenhain J, Pierce SE, Hoon S, Lee W, Proctor M, St Onge RP, Tyers M, Koller D, Altman RB, Davis RW, Nislow C, Giaever G (2008) The chemical genomic portrait of yeast: uncovering a phenotype for all genes. *Science* **320:** 362–365

Hogues H, Lavoie H, Sellam A, Mangos M, Roemer T, Purisima E, Nantel A, Whiteway M (2008) Transcription factor substitution during the evolution of fungal ribosome regulation. *Mol Cell* **29:** 552–562

Hoon S, Smith AM, Wallace IM, Suresh S, Miranda M, Fung E, Proctor M, Shokat KM, Zhang C, Davis RW, Giaever G, St Onge RP, Nislow C (2008) An integrated platform of genomic assays reveals small-molecule bioactivities. *Nat Chem Biol* **4:** 498–506

Jansen G, Wu C, Schade B, Thomas DY, Whiteway M (2005) Drag&Drop cloning in yeast. *Gene* **344:** 43–51

Keith CT, Borisy AA, Stockwell BR (2005) Multicomponent therapeutics for networked systems. *Nat Rev Drug Discov* **4:** 71–78

Lee W, St Onge RP, Proctor M, Flaherty P, Jordan MI, Arkin AP, Davis RW, Nislow C, Giaever G (2005) Genome-wide requirements for resistance to functionally distinct DNA-damaging agents. *PLoS Genet* **1:** e24

Lehár J, Krueger A, Zimmermann G, Borisy A (2008a) High-order combination effects and biological robustness. *Mol Syst Biol* **4:** 215

Lehár J, Stockwell BR, Giaever G, Nislow C (2008b) Combination chemical genetics. *Nat Chem Biol* **4:** 674–681

Lehár J, Zimmermann GR, Krueger AS, Molnar RA, Ledell JT, Heilbut AM, Short III GF, Giusti LC, Nolan GP, Magid OA, Lee MS, Borisy AA, Stockwell BR, Keith CT (2007) Chemical combination effects predict connectivity in biological systems. *Mol Syst Biol* **3:** 80

Loewe S (1953) The problem of synergism and antagonism of combined drugs. *Arzneimittelforschung* **3:** 285–290

Martchenko M, Levitin A, Hogues H, Nantel A, Whiteway M (2007) Transcriptional rewiring of fungal galactose-metabolism circuitry. *Curr Biol* **17:** 1007–1013

Moore D, McCabe G, Craig B (2009) Bootstrap methods and permutation tests. In *Introduction to the Practise of Statistics*, Burke S, Scanlan-Rohrer A, Byrd M (eds), Vol. 16, 6th edn, pp 11–60. New York: WH Freeman and Company

Morschhauser J, Barker KS, Liu TT, Bla BWJ, Homayouni R, Rogers PD (2007) The transcription factor Mrr1p controls expression of the MDR1 efflux pump and mediates multidrug resistance in *Candida albicans*. *PLoS Pathog* **3:** e164

Nelander S, Wang W, Nilsson B, She QB, Pratilas C, Rosen N, Gennemark P, Sander C (2008) Models from experiments: combinatorial drug perturbations of cancer cells. *Mol Syst Biol* **4:** 216

Noble ME, Endicott JA, Johnson LN (2004) Protein kinase inhibitors: insights into drug design from structure. *Science* **303:** 1800–1805

Onyewu C, Heitman J (2007) Unique applications of novel antifungal drug combinations. *Anti-Infect Agents Med Chem* **6:** 3–15

Parsons AB, Brost ReL, Ding H, Li Z, Zhang C, Sheikh B, Brown GW, Kane PM, Hughes TR, Boone C (2004) Integration of chemical-genetic and genetic interaction data links bioactive compounds to cellular target pathways. *Nat Biotechnol* **22:** 62–69

Parsons AB, Lopez A, Givoni IE, Williams DE, Gray CA, Porter J, Chua G, Sopko R, Brost RL, Ho C-H, Wang J, Ketela T, Brenner C, Brill JA, Fernandez GE, Lorenz TC, Payne GS, Ishihara S, Ohya Y, Andrews B *et al* (2006) Exploring the mode-of-action of bioactive compounds by chemical-genetic profiling in yeast. *Cell* **126:** 611–625

R Development Core Team (2007) *R: a Language and Environment for Statistical Computing*. Vienna, Austria: R Foundation for Statistical Computing. ISBN 3-9000051-07-0, URL www.R-project.org

Sams-Dodd F (2005) Target-based drug discovery: is something wrong? *Drug Discov Today* **10:** 139–147

Schuldiner M, Collins SR, Thompson NJ, Denic V, Bhamidipati A, Punna T, Ihmels J, Andrews B, Boone C, Greenblatt JF, Weissman JS, Krogan NJ (2005) Exploration of the function and organization of the yeast early secretory pathway through an epistatic miniarray profile. *Cell* **123:** 507–519

Tuch BB, Galgoczy DJ, Hernday AD, Li H, Johnson AD (2008) The evolution of combinatorial gene regulation in fungi. *PLoS Biol* **6:** e38

Wang P, Heitman J (2005) The cyclophilins. *Genome Biol* **6:** 226

White TC, Marr KA, Bowden RA (1998) Clinical, cellular, and molecular factors that contribute to antifungal drug resistance. *Clin Microbiol Rev* **11:** 382–402

Winzeler EA, Shoemaker DD, Astromoff A, Liang H, Anderson K, Andre B, Bangham R, Benito R, Boeke JD, Bussey H, Chu AM, Connelly C, Davis K, Dietrich F, Dow SW, Bakkoury ME, Foury F, Friend SH, Gentalen E, Giaever G *et al* (1999) Functional characterization of the *S. cerevisiae* genome by gene deletion and parallel analysis. *Science* **285:** 901–906

Zhang L, Yan K, Zhang Y, Huang R, Bian J, Zheng C, Sun H, Chen Z, Sun N, An R, Min F, Zhao W, Zhuo Y, You J, Song Y, Yu Z, Liu Z, Yang K, Gao H, Dai H *et al* (2007) High-throughput synergy screening identifies microbial metabolites as combination agents for the treatment of fungal infections. *Proc Natl Acad Sci USA* **104:** 4606–4611

Zimmermann GR, Lehar J, Keith CT (2007) Multi-target therapeutics: when the whole is greater than the sum of the parts. *Drug Discov Today* **12:** 34–42

Chapter
III

The previous chapter described a chemical genetic screen in *S. cerevisiae* that aimed at identifying genes that become essential for the survival in the presence of FCZ, a fungistatic drug that normally doesn't kill fungal cells. This screen resulted in 22 mutants that could not survive in the presence of the drug. Now, I am using this information as a prediction and ask how many of the homologous genes in *C. albicans* are also linked to this phenotype. To this end, I constructed *C. albicans* mutants to test the prediction from budding yeast. This work together with extensive analysis of one mutant in particular, *age3*, is described in the following section.

III. Reverse genetics in *Candida albicans* predicts ARF cycling is essential for drug resistance and virulence

PLoS Pathog. 2010 Feb 5;6(2):e1000753. || PMID: 20140196

Reverse Genetics in *Candida albicans* Predicts ARF Cycling Is Essential for Drug Resistance and Virulence

Elias Epp[1,2], Ghyslaine Vanier[3], Doreen Harcus[1], Anna Y. Lee[4], Gregor Jansen[5], Michael Hallett[4], Don C. Sheppard[3], David Y. Thomas[5], Carol A. Munro[7], Alaka Mullick[1,6], Malcolm Whiteway[1,2]*

1 Biotechnology Research Institute, National Research Council of Canada, Montréal, Québec, Canada, **2** Department of Biology, McGill University, Montréal, Québec, Canada, **3** Department of Microbiology and Immunology, McGill University, Montréal, Québec, Canada, **4** McGill Centre for Bioinformatics, McGill University, Montréal, Québec, Canada, **5** Department of Biochemistry, McGill University, Montréal, Québec, Canada, **6** Département de Microbiologie et Immunologie, l'Université de Montréal, Montréal, Québec, Canada, **7** School of Medical Sciences, University of Aberdeen, Aberdeen, United Kingdom

Abstract

Candida albicans, the major fungal pathogen of humans, causes life-threatening infections in immunocompromised individuals. Due to limited available therapy options, this can frequently lead to therapy failure and emergence of drug resistance. To improve current treatment strategies, we have combined comprehensive chemical-genomic screening in *Saccharomyces cerevisiae* and validation in *C. albicans* with the goal of identifying compounds that can couple with the fungistatic drug fluconazole to make it fungicidal. Among the genes identified in the yeast screen, we found that only *AGE3*, which codes for an ADP-ribosylation factor GTPase activating effector protein, abrogates fluconazole tolerance in *C. albicans*. The *age3* mutant was more sensitive to other sterols and cell wall inhibitors, including caspofungin. The deletion of *AGE3* in drug resistant clinical isolates and in constitutively active calcineurin signaling mutants restored fluconazole sensitivity. We confirmed chemically the *AGE3*-dependent drug sensitivity by showing a potent fungicidal synergy between fluconazole and brefeldin A (an inhibitor of the guanine nucleotide exchange factor for ADP ribosylation factors) in wild type *C. albicans* as well as in drug resistant clinical isolates. Addition of calcineurin inhibitors to the fluconazole/brefeldin A combination only initially improved pathogen killing. Brefeldin A synergized with different drugs in non-*albicans Candida* species as well as *Aspergillus fumigatus*. Microarray studies showed that core transcriptional responses to two different drug classes are not significantly altered in *age3* mutants. The therapeutic potential of inhibiting ARF activities was demonstrated by *in vivo* studies that showed *age3* mutants are avirulent in wild type mice, attenuated in virulence in immunocompromised mice and that fluconazole treatment was significantly more efficacious when ARF signaling was genetically compromised. This work describes a new, widely conserved, broad-spectrum mechanism involved in fungal drug resistance and virulence and offers a potential route for single or improved combination therapies.

Citation: Epp E, Vanier G, Harcus D, Lee AY, Jansen G, et al. (2010) Reverse Genetics in *Candida albicans* Predicts ARF Cycling Is Essential for Drug Resistance and Virulence. PLoS Pathog 6(2): e1000753. doi:10.1371/journal.ppat.1000753

Editor: Aaron P. Mitchell, Carnegie Mellon University, United States of America

Received October 22, 2009; **Accepted** January 6, 2010; **Published** February 5, 2010

Funding: This work was supported by a NSERC grant (322252-05) to D.Y.T., M.H., M.W. and a CIHR team grant in fungal pathogenesis (CTP-79843) to D.Y.T., A.M., M.W. The funders had no role in study design, data collection and analysis, decision to publish, or preparation of the manuscript.

Competing Interests: The authors have declared that no competing interests exist.

* E-mail: malcolm.whiteway@cnrc-nrc.gc.ca

Introduction

Invasive fungal infections pose a serious health risk to hospitalized patients worldwide. Particularly affected are immunocompromised individuals with cancer or AIDS, people undergoing organ and hematopoietic stem cell transplantation (HSCT), and those receiving immunosuppressive therapy or implantable prosthetic devices [1,2]. The growing population of these at-risk groups is reflected in an increase in invasive fungal infection over the last three decades [3]. Annual treatment costs for fungal therapies reach $2.6 billion in the US alone [4]. Despite available therapy options mortality rates approaching 30–50% (*Candida* species) and 30–80% (*Aspergillus* species) remain high [5,6].

Candida and *Aspergillus* species together account for ~70% of all invasive fungal infections, with *Candida albicans* and *Aspergillus fumigatus* predominating [7,8,9]. Currently, three classes of antifungal drugs are suitable for treatment of systemic infections caused by these fungi: polyenes (most notably amphotericin B) and azoles (e.g. fluconazole, FCZ) have been applied for decades, while the echinocandins (e.g. caspofungin, CF) represent a new class of antifungal that has entered treatment regimes over the past 10 years [10,11]. While these therapy options can be effective, they also exhibit several shortcomings. First, current antifungals target a very limited number of biological processes. The majority of available drugs target ergosterol (polyenes) or inhibit lanosterol 14α-demethylase (azoles), resulting in the accumulation of toxic sterol intermediates that disrupt membrane integrity and lead to membrane stress. Because ergosterol, the major sterol in fungal cell membranes, is analogous to the mammalian lipid cholesterol, this strategy, particularly when amphotericin B is applied, can be problematic due to host toxicity [10]. Another complication of current antifungal strategies is that available drugs each possess a different spectrum of antifungal activities. For instance, azoles are typically fungistatic against pathogenic yeasts such as *Candida* species, but fungicidal against molds (*Aspergillus* species). CF, on the other hand, is fungicidal against yeasts and fungistatic against molds [12]. Finally, and most importantly, the small number of treatment options available has resulted in widespread drug

Author Summary

Candida albicans is a fungus that normally resides as part of the microflora in the human gut. *Candida* species can cause superficial infections like thrush in the healthy human population and life-threatening invasive infections in immunocompromised patients. Fungal infections are often treated with azole drugs, but due to the fungistatic nature of these agents, *C. albicans* can develop drug resistance, leading to therapy failure. To improve the action of azoles and convert them into fungicidal drugs, we first systematically analyzed the genetic requirements for tolerance to one such azole drug, fluconazole. We show, both genetically and pharmacologically, that components of the ARF cycling machinery are critical in mediating both azole and echinocandin tolerance in *C. albicans* as well as several other pathogenic *Candida* species and in the pathogenic mold *Aspergillus fumigatus*. We highlight the importance of ARF cycling in drug resistance by showing that genetic compromise of ARF functions overrides common drug resistance mechanisms in clinical samples and other key regulators of azole/echinocandin tolerance. We validated the therapeutic potential of ARF cycling in two mouse models and provide evidence that drug treatment is more efficacious when ARF activities are genetically compromised. Our study demonstrates a new mechanism involved in two important aspects of the biology of human fungal pathogens and provides a potential route for improved antifungal therapies.

resistance in pathogenic species. For each of the three major classes of antifungals (polyenes, azoles, echinocandins) isolation of drug-resistant clinical strains has been reported [11,12,13]; azole-resistant *Candida*, in particular, is now common among isolates from HIV-positive patients [14]. Developing new antifungal strategies, therefore, remains a pressing need.

One approach to satisfy this need is through combination antifungal therapy, where two (or more) agents combined are significantly more efficacious compared to either agent alone. This approach has recently been validated in a randomized, placebo-controlled trial, where approved antifungals were combined with immune regulatory agents [15]. Results from this study suggested that combining ergosterol inhibitors with a recombinant human monoclonal antibody against heat-shock 90 protein (HSP90) showed increased therapeutic benefits compared to monotherapy against *Candida* infection. Although the precise mechanisms involved remain elusive [16], extensive experiments have further established the benefits of such combinatorial approaches. For instance, a potent synergy resulted when inhibitors of HSP90 (geldanamycin, radicicol) or inhibitors of HSP90's key client protein, calcineurin (cyclosporin A (CsA), FK506) were combined either with azoles or echinocandins against *C. albicans* [10,16,17,18,19,20,21]. Similarly, pharmacological compromise of HSP90/calcineurin-signaling enhanced the efficaciousness of echinocandin treatment against *A. fumigatus in vitro* as well as in insect and mouse infection models [16,17]. Although these examples clearly demonstrate the potential for combination antifungal therapy, human host toxicity associated with inhibition of HSP90 or suppression of the human immune system by CsA/FK506 currently precludes the use of such inhibitors in the clinic [16,22]. While a non-immunosuppressive FK506 analogue (L-685, 818) has been identified, proprietary restrictions have currently prevented further testing [22]. Therefore, identification of new antifungal targets for optimal fungal killing remains a priority.

One of the challenges of finding new antifungal targets in *C. albicans* is the lack of sophisticated screening technologies often employed with, for example, *Saccharomyces cerevisiae*. Various large-scale chemical-genomic drug screening methods are now well established in *S. cerevisiae*, and have been effective for elucidating drug targets or revealing insights into the modes of action of bioactive compounds [23,24,25,26,27]. Similar approaches have only recently been applied directly to fungal pathogens [28]. Using *S. cerevisiae* as a model, we previously performed chemical-genomics to systematically analyze the genetic requirements to survive FCZ treatment [29]. In that work, we identified 22 genes that become essential for *S. cerevisiae* survival in the presence of FCZ.

Here, we expanded that work with the aim of identifying synergistic drug interactions that render FCZ fungicidal in *C. albicans*. To this end, we validated the *S. cerevisiae* FCZ-cidal gene set [29] in *C. albicans*. From 22 predicted genes, we found that only one gene, *AGE3*, mediated FCZ tolerance in the pathogen. We further show that both genetic and pharmacological compromise of ARF (ADP ribosylation factor) activities, a process that depends on Age3p, creates sensitivity to all three classes of antifungals used in clinics (polyenes, azoles, echinocandins), overrides clinical drug resistance and the calcineurin pathway, synergizes with fungistatic drugs against the two major pathogenic fungal species (*C. albicans* and *A. fumigatus*) and modifies fungal virulence in two established mouse models of candidiasis. Given that drug treatment in mice was significantly more efficacious when ARF activity was genetically compromised, this demonstrates that targeting ARF signaling has potential for antifungal therapies.

Results

Age3p mediates azole tolerance and sensitivity to cell wall inhibitors in *C. albicans*

To identify genes that become essential for survival in the presence of FCZ, we previously screened the non-essential *S. cerevisiae* knock-out collection (about 4900 strains) and identified 22 mutants that showed a robust FCZ-cidal phenotype [29]. BLAST searches identified *C. albicans* homologs for 21 of those *S. cerevisiae* genes. *YDR532c* appears to be the only gene that lacks a clear *C. albicans* homolog (Table S1). Recreating knockout or transposon insertion mutations of the 21 candidate genes in *C. albicans*, we found that four mutants (*bem2*, *sac6*, *srb8* and *ssn3*) showed FCZ sensitivity comparable to WT (Table S2, Figure S1). Twelve *C. albicans* mutants (57%) showed increased FCZ sensitivity, but all of these mutants could still resume growth when incubated for extended time in the presence of FCZ. Four genes (*GCN5*, *NGG1*, *ERG11* and *NUP84*) were linked to a slightly resistant FCZ phenotype. Only one mutant, *age3* (*ORF19.3683*), showed the FCZ sensitive phenotype predicted from the yeast screen. We therefore focused further investigation on *AGE3*.

We validated the FCZ sensitivity of *age3* cells by three different assays. When tested in a minimal inhibitory concentration (MIC) assay, the *age3* mutant initially showed similar drug sensitivity as WT and revertant strains at 24 hours. Since FCZ on its own is fungistatic, however, WT cells demonstrated robust growth above the initial MIC point after prolonged incubation (72 hours), a feature referred to as tolerance [19]. In contrast, *age3* cells did not resume growth above the 24 hours MIC point, indicating that *age3* mutants lost tolerance to FCZ (Figure 1A, Table S2). These results were confirmed visually by growth on solid rich media in the presence of FCZ (Figure 1B). We further characterized the FCZ sensitivity of *age3* cells by time-kill curves. Under FCZ treatment, the number of viable *age3* cells slightly decreased over time, while growth of WT cells in the presence of FCZ continued (Figure 1C).

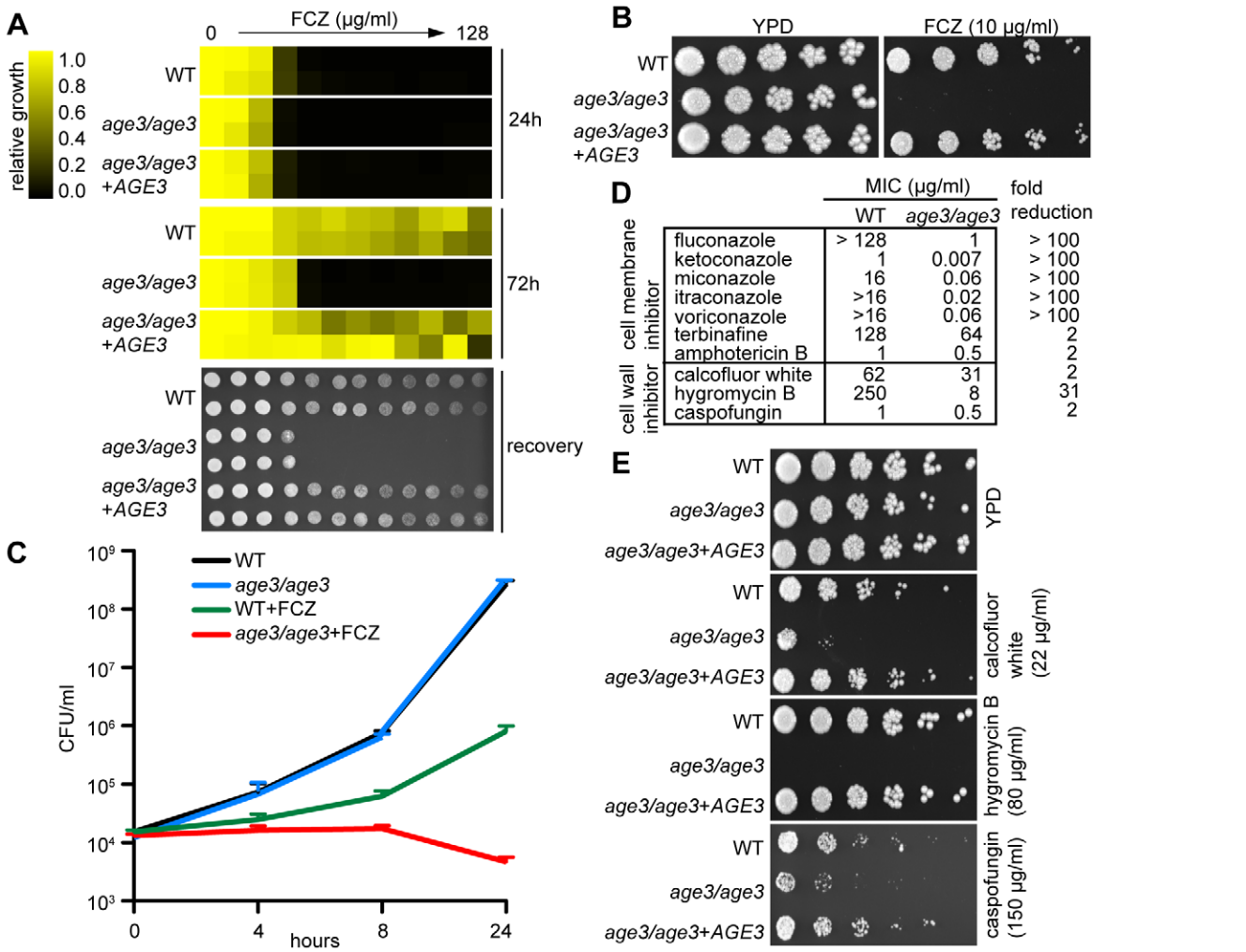

Figure 1. Age3p plays a major role in azole tolerance in *C. albicans*. (A) Minimal Inhibitory Concentration (MIC) assay in rich YPD media showing that *age3* cells are initially almost equally sensitive to FCZ compared to WT and revertant strains (24 hours reading, top), but fail to grow above this MIC threshold after prolonged incubation (72 hours reading, middle). MIC assays with two-fold serially diluted drug concentrations were done in duplicate and optical densities were normalized to drug-free control wells (see color bar). After 72 hours of incubation, 2 μl of each well of the MIC assay was spotted on fresh YPD media to assess the extent to which cells recover from the drug treatments (bottom). YPD recovery plates were incubated for 24 hours at 30°C. (B) FCZ sensitivity assayed on solid YPD media. No *age3* colonies grew on YPD plates containing 24 hours-supra-MIC concentrations of FCZ. Overnight cultures were adjusted to OD_{600} of 0.1, and then serially diluted four-fold, before 2 μl were spotted on plates. Plates were incubated for 48 hours at 30°C. (C) Time-kill curves in YPD media confirming that knocking out *AGE3* abrogates tolerance to FCZ. The number of viable *age3* cells decreases slightly over time, while growth of WT cells in the presence of FCZ still occurs. FCZ was used at 10 μg/ml. Shown is the average of two independent experiments plus SD values. Note that *age3* cells grow as efficiently as WT cells in the absence of drugs. (D) MIC assays in YPD media shows that *age3* mutants are extremely sensitive to numerous azoles after 48 hours and mildly more sensitive to non-azole ergosterol inhibitors (terbinafine, amphotericin B) as well as cell wall inhibitors when compared to WT cells. Fold reduction represents the ratio of the MIC value for WT over the MIC value of the *age3* mutant. (E) *age3* cells show differential sensitivity to different cell wall inhibitors on YPD media plates. The assay was done as described in (B).
doi:10.1371/journal.ppat.1000753.g001

We then tested the *age3* mutant against a variety of antifungals to gauge the specificity of the mutation. We included various compounds, including second-generation azoles (voriconazole), non-azole ergosterol inhibitors (terbinafine) and other membrane-targeting drugs (amphotericin B). We found that *age3* cells showed a generalized increased sensitivity to these compounds (Figure 1D). Among all cell-membrane drugs tested, the azoles caused by far the most significant enhancement in sensitivity in the *age3* mutant.

In order to determine the effect of deleting *AGE3* on the integrity of the cell wall, we tested the *age3* mutant for sensitivity to a variety of cell wall perturbing agents and other agents whose effect have been linked to altered cell wall and glycosylation. The *age3* mutant was slightly more sensitive to the β-1,3 glucan synthase inhibitor CF. Similarly, *age3* cells were slightly more sensitive to calcofluor white, a phenotype that is usually associated with altered chitin structures along the cell wall [30]. More remarkably, *age3* cells were extremely sensitive to hygromycin B, a phenotype usually seen in glycosylation mutants [31,32] (Figure 1D, 1E). No change in sensitivity was observed in the presence of other agents such as caffeine, cycloheximide, menadione, nocodazole, rapamycin, 5-FC and wortmannin (data not shown). Together, these data suggest that while *AGE3* plays a major role during membrane stress in *C. albicans*, its influence on the integrity of the cell wall remains somewhat less clear (see discussion).

Deleting *AGE3* overrides clinical drug resistance and the calcineurin pathway

Among the most commonly encountered resistance mechanisms in drug treated clinical *C. albicans* isolates are over-expression of drug pumps or alterations in sterol biosynthesis [13,33,34]. To test whether such common mechanisms of drug resistance are still effective in the absence of *AGE3*, we deleted *AGE3* in two FCZ-resistant clinical strains. The strain F5 carries a mutation in the transcription factor *MRR1*, which leads to constitutive over-expression of drug pumps. The strain S2 carries a mutation in the transcription factor *UPC2*, which causes up-regulation of ergosterol biosynthesis genes [35,36]. Figure 2A shows that deleting *AGE3* in strains F5 and S2 restored FCZ sensitivity even below WT levels, suggesting that loss of *AGE3* abrogates FCZ-resistance in these clinical isolates.

Because *age3* mutants lost tolerance to FCZ and because the calcineurin pathway is known to mediate FCZ-tolerance in WT as well as drug resistant clinical isolates [10,19], we tested whether constitutive calcineurin signaling could reverse the *AGE3*-dependent FCZ sensitivity. The calcineurin pathway can be activated by addition of extracellular $CaCl_2$ [19]. *C. albicans* WT became resistant to FCZ after only 24 hours of growth in the presence of extracellular $CaCl_2$, while this rescue was not observed in the absence of *AGE3* (Figure 2B). To further verify this observation, we deleted *AGE3* in a constitutively active calcineurin signaling mutant (DSY2146) that is resistant to FCZ even in the absence of extracellular $CaCl_2$ [19]. Deleting *AGE3* in this constitutively active calcineurin mutant restored FCZ sensitivity both in the absence and in the presence of extracellular $CaCl_2$ (Figure 2B). These results suggest that constitutive calcineurin signaling does not rescue the *age3*-dependent FCZ sensitivity. The results also support an argument that *AGE3* and calcineurin-dependent processes could be linked (see discussion).

Pharmacological compromise of ARF cycling converts FCZ into a fungicidal drug in *C. albicans*

Given *AGE3*'s role in sensitivity to various drugs and its implication in clinically relevant processes such as drug resistance, targeting either *AGE3* or its biological process seemed a plausible avenue for combination therapies to render FCZ fungicidal. The *S. cerevisiae* homolog of *C. albicans AGE3* is *GCS1*, which encodes an ARF GAP (ADP-Ribosylation Factor GTPase Activating Protein) [37]. ARFs are small G-proteins of the Ras GTPase superfamily that cycle between an active GTP-bound and an inactive GDP-bound state. ARF guanine nucleotide cycling, and hence function, is regulated by GAPs and GEFs (guanine nucleotide exchange factors) [38]. ARFs are involved in a variety of processes including vesicle trafficking (Golgi-to-ER retrograde vesicle trafficking, trans Golgi network-endosomal transport, transport from the Golgi to the membrane) and actin cytoskeleton organization [39,40,41,42]. Brefeldin A (BFA), a metabolite from the fungus *Penicillium decumbens*, is a noncompetitive inhibitor of ARF activity. Protein crystal structures showed that BFA binds to a ternary complex of ARF-GDP-GEF, thus stabilizing this otherwise transient protein-protein interaction [43,44,45,46,47,48]. Given that ARF cycling is a well-established target of BFA, we reasoned that BFA might be

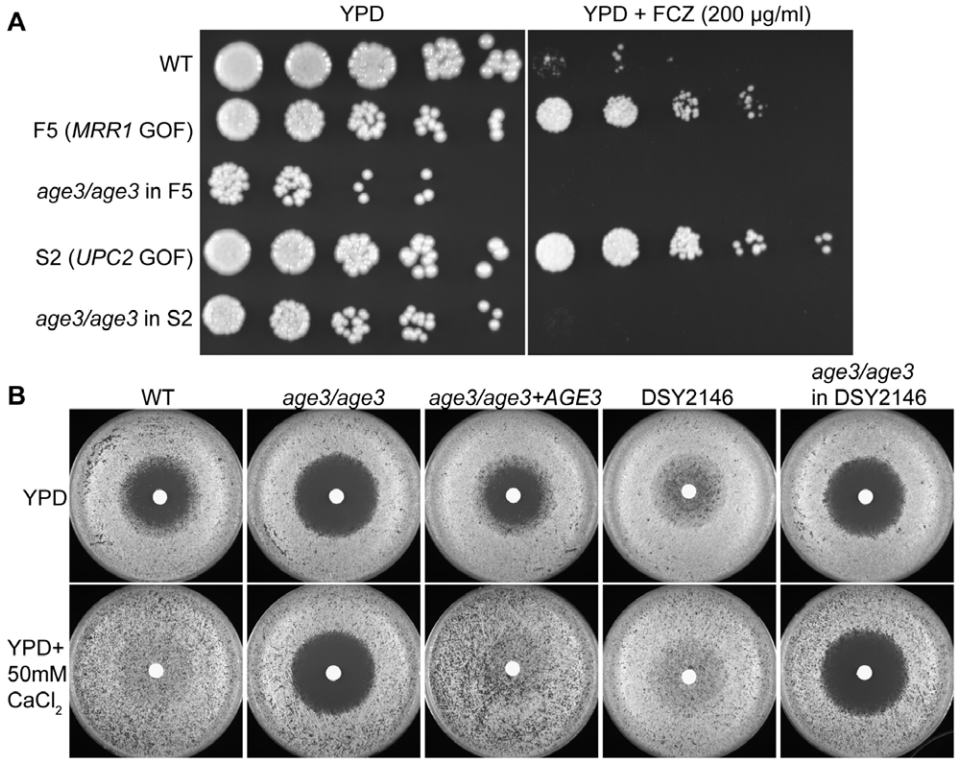

Figure 2. Deleting *AGE3* overrides clinical drug resistance and the calcineurin pathway. (A) When *AGE3* is knocked out in drug resistant clinical isolates F5 and S2, FCZ sensitivity is restored even below WT levels on solid YPD media. The assay was performed and analyzed as described in Figure 1B except plates were photographed after 24 hours. GOF = gain of function. (B) Calcineurin signaling stimulated either by extracellular $CaCl_2$ or by a constitutively active mutation in strain DSY2146 leads to FCZ resistance. *age3* mutants do not respond to extracellular $CaCl_2$, while knocking out *AGE3* in strain DSY2146 restored FCZ sensitivity. Disc diffusion assays were done by plating 2×10^5 cells on YPD plates followed by applying discs containing 50 mg of FCZ to the surface of agar. Plates were incubated for 24 hours at 30°C.
doi:10.1371/journal.ppat.1000753.g002

an ideal drug to synergize with FCZ in WT *C. albicans* by chemically mimicking the *age3*-dependent FCZ sensitivity. As illustrated by time-kill curves in Figure 3A, combining FCZ with BFA resulted in a potent fungicidal synergy in WT *C. albicans*, while either drug alone had only minor effects on cell growth. To compare the BFA/FCZ synergy to a well-established fungicidal synergy, we repeated the time-kill curves with CsA in combination with FCZ. CsA/FCZ co-treatment resulted in a similarly strong synthetic phenotype after 24 hours. This observation corroborates previous findings that calcineurin inhibition plus FCZ results in a potent fungicidal combination as assayed at 24 hours of drug treatment [19]. A triple drug combination of FCZ/BFA/CsA was significantly more efficacious than either FCZ/CsA or FCZ/BFA alone at 24 hours. However, when monitored for more than 24 hours, conditions that have not previously been reported [19], cells treated with FCZ/CsA could recover and resume growth, while cells treated with FCZ/BFA or FCZ/BFA/CsA could not resume growth above the detection limit (≈10 cells/ml). At 72 hours, drug combinations of either FCZ/BFA or FCZ/BFA/CsA appeared equally efficacious with no evidence of growth, while cells treated with FCZ/CsA continued to proliferate. Similar results were obtained when another calcineurin inhibitor, FK506, was combined with FCZ. These results suggest that while the combination of calcineurin inhibitors and an azole is initially efficient in pathogen killing, over prolonged drug treatment, combining ARF inhibitors with azoles is more efficacious.

A dose-matrix titration assay measuring growth of treated cells confirmed the synergy between FCZ/BFA (Figure 3B, Table S3).

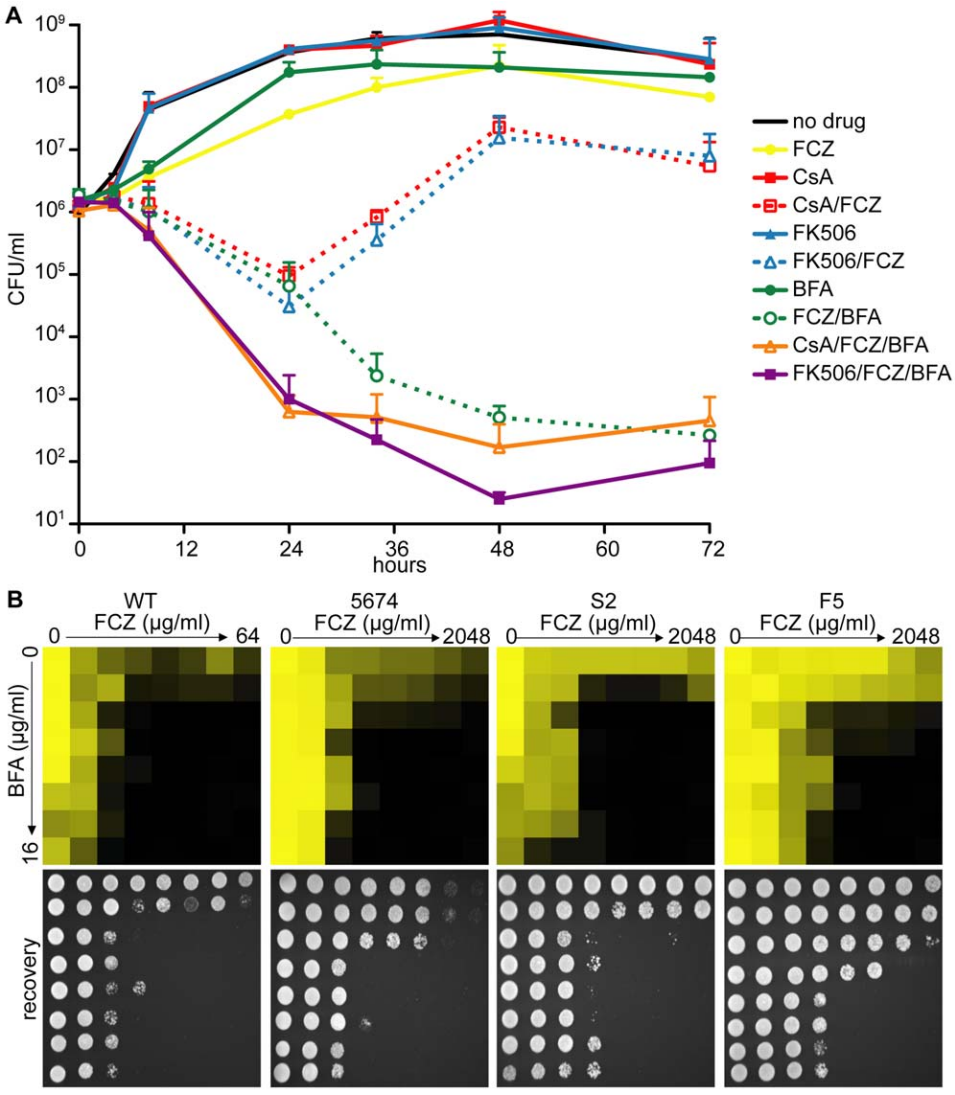

Figure 3. Pharmacological inhibition of ARF cycling results in a potent, fungicidal synergy in combination with FCZ in *C. albicans*. (A) Time-kill curves demonstrating that, while combining FCZ and BFA was initially equally efficacious in pathogen killing compared to combining FCZ and calcineurin inhibitors (FK506 or CsA), extended drug exposure only remained efficacious in pairwise BFA/FCZ combinations. Triple drug combinations of BFA/FCZ/calcineurin inhibitors were only initially (24 hours) more efficacious, but at 72 hours appeared equally efficacious compared to BFA/FCZ. The assay was done in YPD media. Drugs were used at 10 μg/ml for FCZ, 15 μg/ml for BFA, 1 μg/ml for CsA and 1 μg/ml for FK506. (B) Dose-matrix titration assay confirming the FCZ/BFA synergy in WT and drug resistant clinical isolates 5674, S2 and F5 in rich YPD media (top). Dose-matrix titration plates were incubated for 72 hours after which aliquots of each well were spotted on fresh YPD recovery plates (bottom). No-growth of recovery plates confirmed fungal cell death of the drug synergy. Recovery plates were incubated for 24 hours. Dose-matrix titration assays were analyzed as described for MIC assays in Figure 1A.
doi:10.1371/journal.ppat.1000753.g003

We also tested whether the FCZ/BFA synergy is still effective in *C. albicans* drug resistant clinical isolates and found that, although considerably higher concentrations of FCZ were needed, there was synergy in isolates F5 and S2 as well as in isolate 5674, which carries a gain-of-function mutation in *TAC1*, a transcriptional activator of *CDR* drug efflux pump genes [49]. Thus, genetic compromise of ARF cycling by deleting *AGE3* abrogated FCZ tolerance, while pharmacological compromise of ARF cycling by adding BFA converted the fungistatic drug FCZ into a fungicidal agent in WT and FCZ-resistant *C. albicans* clinical isolates. Together, this suggests that the process of ARF cycling becomes essential during cell membrane stress in this pathogen.

Combining ARF inhibition with other drugs across fungal species

Importantly, genetic or pharmacological compromise of ARF cycling did not appear to significantly affect the cells' initial response to FCZ (Figure 1A, 3B, Table S2). Instead, ARF cycling inhibition seems to act on tolerance. To test whether the effect of BFA on tolerance is observed in combination with other azole drugs, we tested miconazole (MICO) and ketoconazole (KETO) in combination with BFA, because MICO and KETO alone did show a tolerance effect (Figure 4A). When tested in a dose-matrix titration format, BFA synergized with MICO and KETO against WT *C. albicans*, independently of which media were used (Figure 4A, Figure S2).

Although CF is generally considered fungicidal in *C. albicans*, we tested whether BFA would synergize with CF. Recent reports showed that *C. albicans* can start to grow at supra MIC concentrations of CF, an outcome referred to as the paradoxical or trailing growth effect [50,51]. BFA did synergize with CF against WT *C. albicans* in a dose matrix titration assay at supra MIC concentrations of CF (Figure 4B). Together, these results indicate that genetic and pharmacological compromise of ARF cycling influences not only cell membrane stress, but also cell wall stress.

To examine whether BFA's inhibition of azole tolerance is conserved across other pathogenic *Candida* species, we tested BFA/drug interactions in *C. tropicalis*, *C. parapsilosis*, *C. glabrata* and *C. krusei*. Together, these species account for ~30–40% of all *Candida* isolates causing invasive infections; furthermore, *C. glabrata* and *C. krusei* are notoriously difficult to treat with FCZ [7,8,12]. *C. tropicalis*, *C. parapsilosis* and *C. glabrata* showed tolerance in the presence of FCZ, MICO and KETO (Figure 5A); these azoles synergized with BFA in dose-matrix titration assays with these fungi. FCZ also synergized with BFA in the non-pathogenic yeast *S. cerevisiae* (data not shown). On the other hand, *C. krusei* did not show an obvious tolerance effect (i.e. >2 fold variations between 24 hours and 72 hours MIC readings), which could explain why BFA did not synergize with azoles in this pathogen (Figure 5B).

To further investigate ARF cycling inhibition as a mechanism of abrogating drug tolerance in non-*Candida* human fungal pathogens, we asked whether BFA would synergize with FCZ or CF against *A. fumigatus*. Consistent with the idea that ARF cycling inhibition acts primarily on tolerance, a disc diffusion assay in *A. fumigatus* demonstrated that BFA synergized with CF, a drug that is generally fungistatic in *A. fumigatus* (Figure 6). CF treatment created an inhibition zone against *A. fumigatus* where cells could still grow within that zone due to the fungistatic nature of CF. In contrast, when BFA was combined with CF, not only was the size of that inhibition zone increased, but growth within that zone was also remarkably reduced. A MIC assay in defined synthetic media independently confirmed that CF synergized with BFA against *A. fumigatus* (Table S3). On the other hand, we found that BFA did not synergize with FCZ, a drug that is considered fungicidal in *A. fumigatus* (data not shown) [12]. In general, pharmacological compromise of ARF cycling in *A. fumigatus* was not as efficacious as in *Candida* species, possibly because BFA on its own had a more pronounced impact on growth of *A. fumigatus* compared to *Candida* species (Figure 6, Table S3). Taken together, these results show that

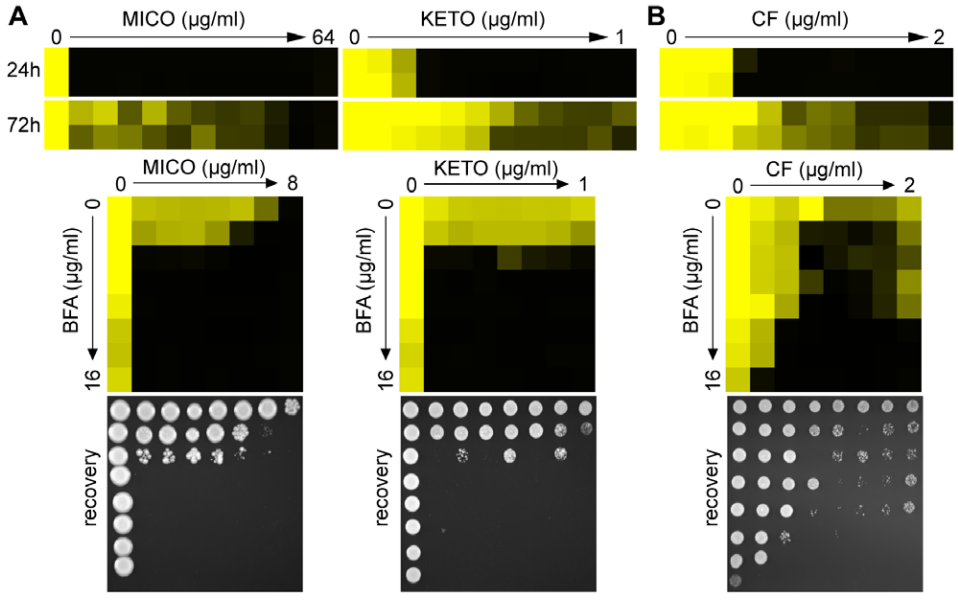

Figure 4. Pharmacological compromise of ARF cycling synergizes with various azoles as well as the cell wall inhibitor CF. (A) MIC assays in YPD media demonstrated that WT *C. albicans* shows tolerance to MICO and KETO (top, compare 24 hours to 72 hours MIC readings). Combining BFA with either MICO or KETO resulted in a similarly potent fungicidal combination compared to BFA/FCZ (bottom). (B) CF showed trailing growth in rich YPD media (top) and synergized with BFA in a dose-matrix titration assay (bottom) against WT *C. albicans*. MIC and dose-matrix titration assays were performed and analyzed as described in Figure 1A and 3B, respectively.
doi:10.1371/journal.ppat.1000753.g004

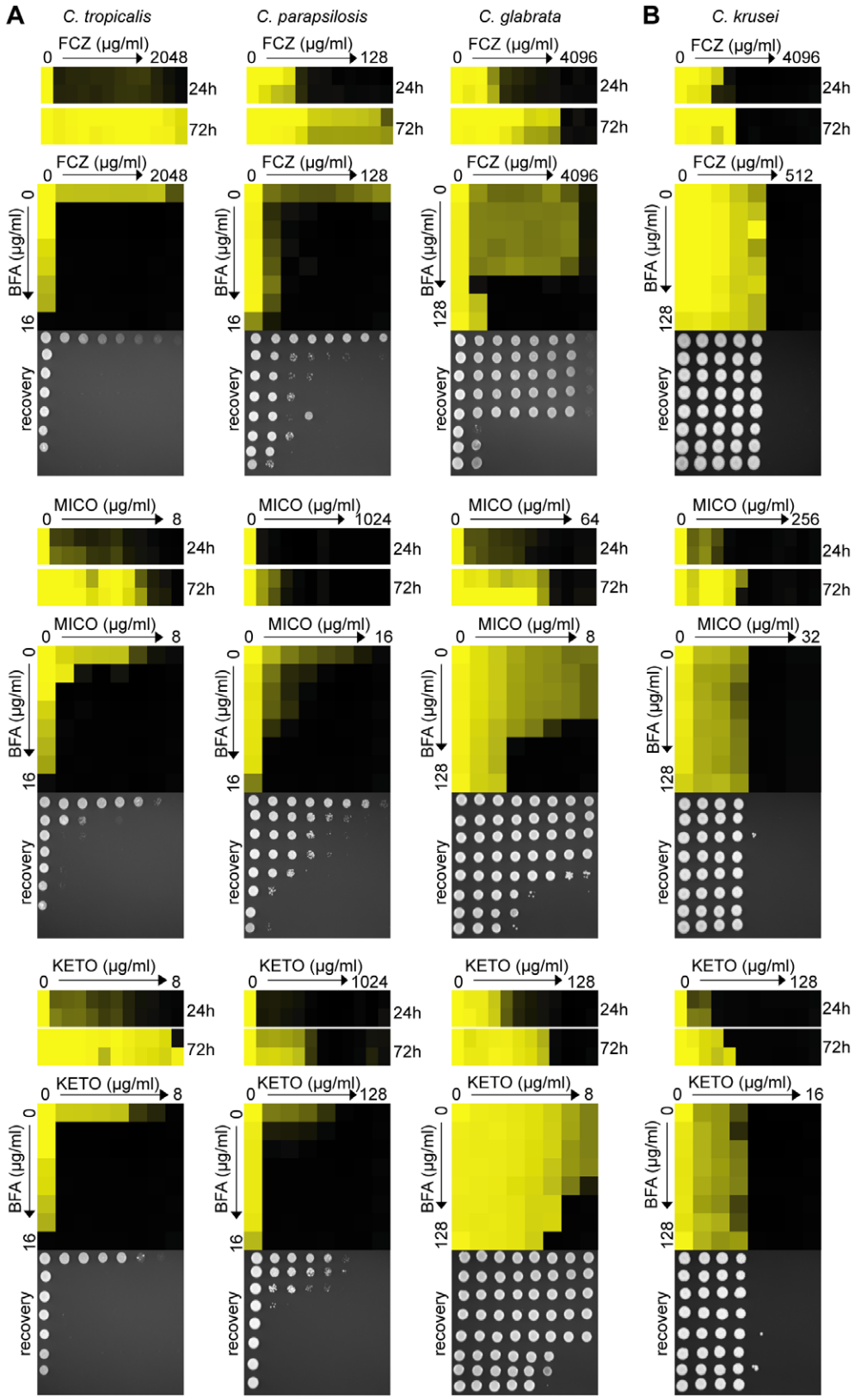

Figure 5. BFA synergizes with different azoles in pathogenic non-*albicans Candida* species. (A) When treated with FCZ, MICO or KETO, *C. tropicalis*, *C. parapsilosis* and *C. glabrata* isolates showed prominent growth above the initial MIC reading after extended incubation (24 hours vs. 72 hours). Dose-matrix titration assays confirming that BFA synergized with the three azoles in all three species. (B) No obvious tolerance effect was observed in *C. krusei* to any azoles tested and no synergy was observed when BFA was combined with these azoles. MIC and dose-matrix titration assays were performed and analyzed as described in Figure 1A and 3B.
doi:10.1371/journal.ppat.1000753.g005

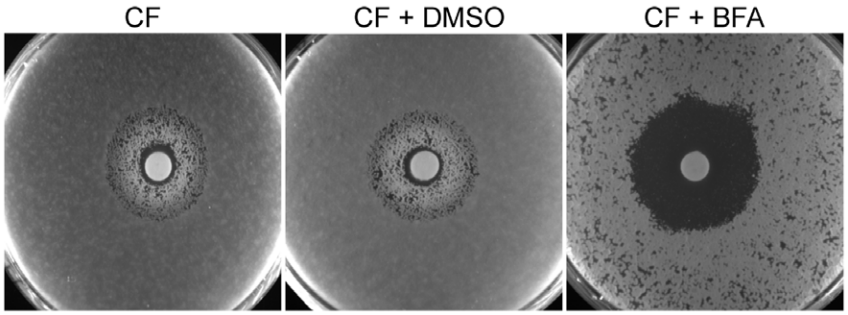

Figure 6. BFA synergism with the fungistatic cell wall inhibitor CF in *A. fumigatus*. BFA/CF interaction in an *A. fumigatus* disk diffusion assay on half-strength YPD media. CF alone creates an inhibition zone that still allows fungal growth. Combining CF and BFA abrogated growth within that zone. Discs containing 160 μg CF were applied after 10^5 conidia were plated on plates containing water only, vehicle control (DMSO) or BFA (16 μg/ml), as indicated. Plates were incubated for 48 hours.
doi:10.1371/journal.ppat.1000753.g006

ARF cycling inhibition can couple with different fungistatic drugs in many pathogenic fungi to generate potentially fungicidal activity.

Core transcriptional responses to FCZ and CF treatment are not significantly affected in the absence of *AGE3*

Analysis of transcriptional regulation has frequently been used to elucidate which cellular processes are linked to drug sensitivity or drug resistance in *C. albicans* [35,52,53]. We therefore performed microarray studies to test how transcriptional regulation is altered in *age3* mutants. We first compared WT to *age3* cells in the absence of drugs and found that 23 genes were differentially regulated when *AGE3* was absent (Table S4). Among those 23 genes were five GPI-anchored cell wall proteins (*ECM331*, *PGA13*, *CRH11*, *SAP9*, *PGA26*) and two genes with phospholipase activity (*FGR22* and *PI-PLC*). Because none of these genes have been linked to FCZ tolerance, it is currently unclear how they might influence the *age3*-dependent drug phenotypes.

We next analyzed the transcriptional response to FCZ. A typical transcriptional signature to FCZ is upregulation of ergosterol genes, presumably to compensate for depletion of these membrane lipids [54,55]. This core response to FCZ was not changed in the absence of *AGE3*. All ergosterol genes that became significantly upregulated in FCZ-treated WT cells were similarly upregulated in FCZ-treated *age3* cells (Table S5). Besides this core response to FCZ, clustering analysis of genes that were significantly regulated (>2 fold expression change and p-value <0.05) further confirmed that the overall transcriptional response to FCZ was very similar in WT and *age3* cells (Figure S3A, Table S6).

A similar lack of *AGE3*-dependent transcriptional consequences could be observed in microarray experiments when the cell wall inhibitor CF was used. Clustering analysis revealed that CF-treated WT cells and CF-treated *age3* cells showed an almost identical transcriptional response, with a significant overlap (p-value 4.8×10^{-194}) of differentially regulated genes (Figure S3B, Tables S7, S8). This overlap of 168 genes showed further statistically significant similarity (p-value 1.8×10^{-7}) when compared to core *C. albicans* CF-responsive genes previously identified in two independent studies [52,56]. Therefore, the core transcriptional response to CF in *C. albicans* seems not to depend on *AGE3*. In summary, these microarray experiments suggest that deleting *AGE3* does not cause major transcriptional changes in the presence of two different drug classes and further indicates that post-transcriptional processes might play a more dominant role in terms of ARF cycling-dependent drug phenotypes.

The *age3* mutant is avirulent in WT mice

To evaluate whether *AGE3* is a good drug target *in vivo*, we first injected *age3* mutant cells into WT B6 mice, and found that *age3* cells are avirulent in this mouse model. While 100% of mice infected with WT *C. albicans* became moribund within 11 days post-infection, none of the *age3* mutant strain infected mice became moribund during the same time frame (Figure 7A). To test whether mice infected with *age3* cells had cleared the infection, we sacrificed half of the mutant group on day 11 to analyze kidney fungal burden (Figure 7B). On average, kidney fungal load was significantly reduced (p-value <0.01, Mann Whitney test) in the *age3* group compared to moribund WT-infected mice. We continued with the other half of *age3* mutant-infected mice until the end of the experiment (day 21), but again found that none of the *age3*-infected mice became moribund. Comparing fungal load from these mice showed that three mice had cleared the infection, while two mice had a fungal load that was comparable to WT-infected mice. On average, however, there were significantly fewer *age3* cells recovered from the host compared to moribund mice infected with WT *C. albicans* (p-value <0.02, Figure 7B).

One key virulence factor in *C. albicans* pathogenicity is hyphal formation [57]. Because Arnold Bito and coworkers (Lettner T., Zeidler U., Gimona M., Breitenbach M., Bito A., manuscript submitted, personal communication from A. Bito) have observed some hyphal formation defects on solid media as well as defects in invasive growth in *age3* mutants, we collected kidneys for histological examination on day 11 from both WT-infected and *age3*-infected mice. No obvious difference was found between kidney sections recovered from WT or from *age3*-infected mice (Figure 7C). In all kidney sections examined, *age3* cells could be observed as elongated hyphal structures. Therefore, it remains unclear why *age3*-infected mice with a high fungal burden did not show any clinical signs, but might indicate that additional virulence factors are affected in *age3* mutants.

Genetic inhibition of ARF cycling results in attenuated virulence in an immunocompromised mouse model of disseminated candidiasis and FCZ treatment is significantly more efficacious when ARF activity is genetically compromised

To help evaluate the therapeutic potential of FCZ treatment of *age3* mutant-infected mice, we required a mouse model where *age3* cells retain at least partial virulence. Cells of the *C. albicans* strains

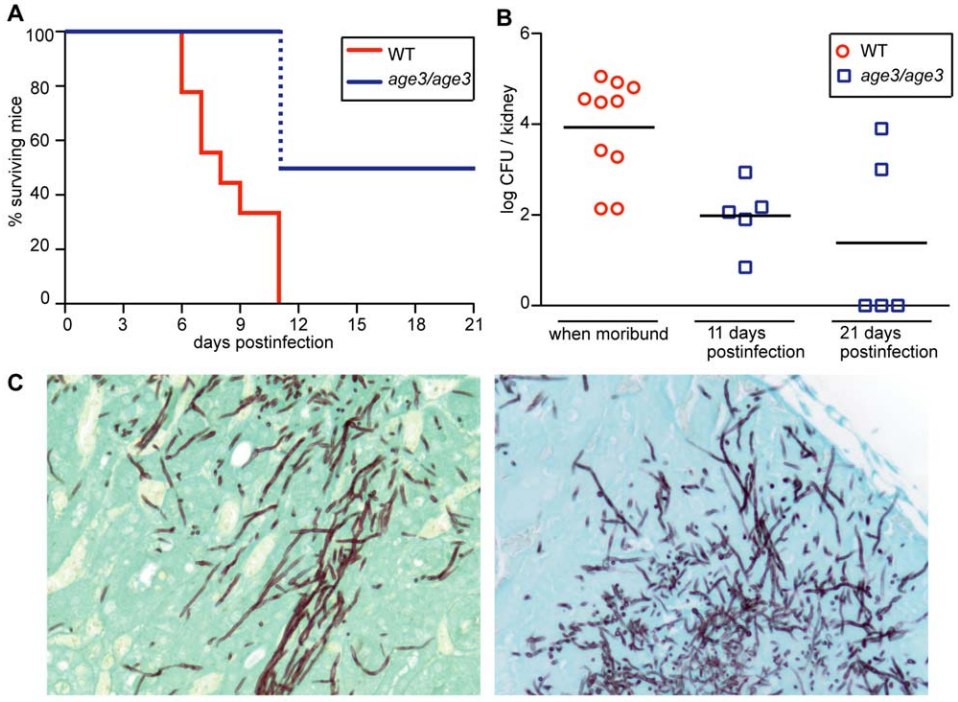

Figure 7. Genetic compromise of ARF cycling in *C. albicans* results in avirulence in a WT mouse model of disseminated disease. (A) *C. albicans* WT-infected mice become gradually moribund up to day 11, while mice infected with *age3* mutants did not show any clinical signs until the end of the experiment on day 21. The dotted blue line indicates that half of the *age3* mutant-infected mice were sacrificed to compare fungal load. Those mice were not moribund. (B) On average, fungal load of WT-infected mice, when moribund, is significantly higher compared to mutant fungal burden taken at indicated times. (C) Kidney section of WT-infected mice (left) showing fungal hyphal formation, which is also seen in mutant-infected kidneys (right). Kidneys were collected on day 11 for histological examination. Ten mice were used per experimental group and monitored according to approved standards.
doi:10.1371/journal.ppat.1000753.g007

WT, *age3* mutant and *age3* revertant were therefore injected in an immunocompromised C5-deficient A/J mouse model [58]. In this very sensitive animal system, *C. albicans* WT and revertant-infected A/J mice became rapidly moribund after 20 to 24 hours, while *age3* mutant-infected A/J mice survived significantly longer, with a median survival of two days (p-value <0.02, Log-rank test) (Figure 8A). However, comparing fungal burden indicated that mice infected with *C. albicans age3* cells accumulated a significantly higher fungal load when moribund (p-value <0.02), with hyphal formation still observed in the *age3* mutant-infected mice (Figure 8B, data not shown).

To test whether genetic compromise of ARF activity holds therapeutic potential, we repeated this experiment and injected WT, *age3* and the revertant strains in A/J mice to compare survival lengths after two days of FCZ therapy. FCZ administration extended survival of all three groups (p-value <0.001), but was significantly more efficacious in the mutant-infected mice, extending median survival time more than 10-fold compared to 7.5-fold median survival time extension for both the WT and revertant groups (p-value <0.01 for posthoc comparison between *age3* mutant group with and without FCZ, versus p-value >0.05 posthoc comparison between WT with and without FCZ or p-value >0.05 for posthoc comparison between revertant with and without FCZ, Dunnett's Multiple Comparison) (Figure 8C). In summary, we conclude from these *in vivo* experiments that genetic compromise of ARF cycling results in avirulence in WT mice, significant attenuation in virulence in an immunocompromised mouse model and further suggests that FCZ treatment in A/J mice is more efficacious when ARF cycling is genetically compromised.

Discussion

Identifying new drug targets is an important step in the challenging task of developing new antifungal therapies, which are urgently needed due to the emergence of drug resistance to every class of antifungals currently in clinical use [11,59]. Using a comprehensive reverse-genetics screen, we identified Age3p and the process of ARF cycling as potential new drug targets. We further established a widely conserved, potent fungicidal chemical synergy between the ARF cycling inhibitor BFA and several fungistatic drugs, and, through two murine infection models, validated the potential of ARF cycling as an antifungal target.

To render FCZ fungicidal through combination with other drugs, we applied a large-scale chemical-genomic approach in *S. cerevisiae* and found 22 FCZ-cidal genes (Table S1) [29]. The *S. cerevisiae* screen proved to have predictive power in that 12 of the 22 genes (57%) identified in *S. cerevisiae* were validated in *C. albicans* with an increased FCZ sensitivity (Figure S1, Table S2). Among those genes, only *CDR1* and *ADA2* have previously been linked to FCZ sensitivity in *C. albicans* [52,60]. On the other hand, our screen linked four genes to FCZ resistance in the pathogen (*NUP84*, *ERG11*, *GCN5* and *NGG1*). One of those genes, *ERG11*, has previously been linked to FCZ resistance in *C. albicans* [61]. Of note, Sanglard and coworkers have shown that the *C. albicans erg11* mutant was sensitive to a variety of drugs, including BFA [61]. Two other *C. albicans* genes that have been linked to FCZ resistance in our screen (*GCN5* and *NGG1*) are part of the SAGA, a conserved transcriptional co-activator [62]. Our data therefore expand the known events of transcriptional rewiring between *S. cerevisiae* and *C. albicans* in regards of drug resistance [63,64], as

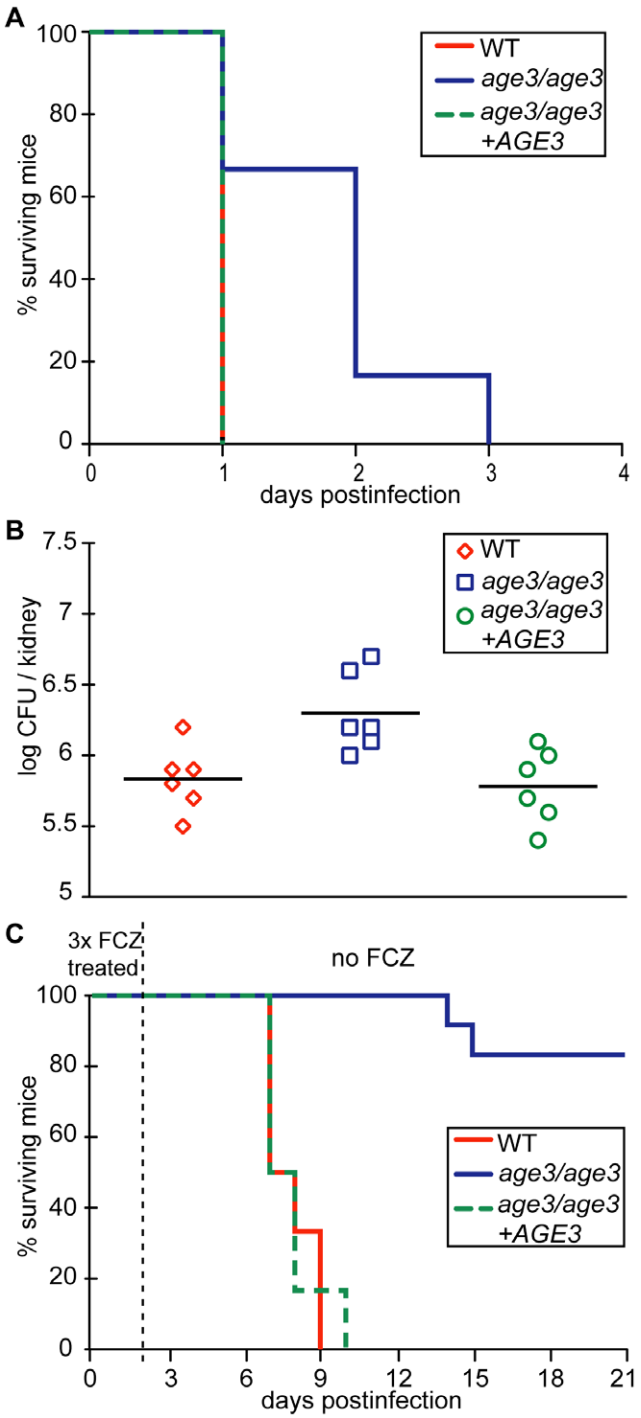

Figure 8. *age3* mutants are attenuated in virulence in A/J mice and FCZ treatment significantly extends survival of *age3*-infected A/J mice. (A) *age3* mutant-infected mice survive significantly longer with a median survival of two days versus one day for WT and revertant-infected mice. Six mice were used per experimental group. (B) Fungal kidney burden was examined from moribund mice and was significantly higher in *age3* mutant recovered cells compared to WT or revertant control groups. (C) A short FCZ therapy (4.5 mg/kg intraperitoneally once immediately after fungal infection, once on day one and once on day two post fungal infection) is significantly more efficacious when ARF cycling is genetically compromised as only the majority (83%) of mutant-infected mice survive until the end of the experiment (day 21). Six mice were used for WT and revertant groups and 12 mice for the *age3* mutant group.
doi:10.1371/journal.ppat.1000753.g008

another subunit of the SAGA complex, Ada2p, has been linked to increased drug sensitivity in our screen as well as in two previous studies [52,60]. The observation that different subunits of the same transcriptional co-activator complex regulate the opposing phenotypes of drug sensitivity or drug resistance illustrates the extreme adaptability and flexibility of transcriptional regulatory networks in fungi.

Given that diverse essential processes exhibit significantly different regulation in *S. cerevisiae* and *C. albicans* [65,66,67], reorganization of transcriptional regulation might in general account for *C. albicans* mutants that showed different drug phenotypes compared to the yeast prediction. Despite these considerations, budding yeast genetics remains a convenient and powerful approach to predict phenotypes in pathogenic fungal species, at least until similar sophisticated screening techniques become available in the pathogen itself.

An alternative speculation why the success rate of our screen was not higher is that the gene encoding *ERG11*, the target of FCZ in both species, is essential only in *S. cerevisiae* [29,61]. Thus, there may be redundant mechanisms for sterol biosynthesis in *C. albicans*, a suggestion that is further supported by the observation that another ergosterol biosynthesis gene, *ERG24*, is essential in *S. cerevisiae*, but not in *C. albicans* [68].

Chemical compromise of ARF cycling appeared far more potent than genetic compromise. When *age3* mutants were treated with FCZ, the number of viable cells was reduced in time-kill curve experiments by less than one log value, whereas combining FCZ with BFA reduced the number of viable WT cells more than one log value over the same time (Figure 1C, Figure 3A). Similarly, chemical compromise appeared more potent than genetic compromise in terms of synergy with CF. The *age3* mutant was only 2-fold more sensitive to CF than WT. On the other hand, combining BFA with CF resulted in a 32-fold reduction in sensitivity to CF in WT cells (Figure 1D and 1E, Figure 4B). These differences likely reflect that, while chemical interference with ARF function inhibits potentially all ARF GEFs, genetic inactivation was restricted to one ARF GAP (*AGE3*). Thus, it remains possible that some aspects of ARF signaling continue to function in the absence of *AGE3* under drug conditions, a suggestion that is supported by work in yeast that demonstrated that several ARF GAPs provide redundant functions [39,40].

The finding that both genetic and pharmacological blockage of ARF function result in increased azole sensitivity suggests that, among the multiple cellular roles described for the yeast homologue of *AGE3*, defects in proper ARF cycling and, therefore, defects in intracellular vesicle trafficking are responsible for drug phenotypes. One hypothesis to explain how incorrect vesicle trafficking could result in *age3*-dependent drug sensitivity is mislocalization of drug pumps. However, *CDR1* and *MDR1*, two major drug pumps in *C. albicans* appear not be involved, as Arnold Bito and coworkers (Lettner T., Zeidler U., Gimona M., Breitenbach M., Bito A., manuscript submitted, personal communication from A. Bito) observed that *CDR1* and *MDR1* pumps are correctly localized to the plasma membrane in *age3* mutants. They further established that *CDR1* drug pump activity was not affected in the absence of *AGE3*.

Another plausible explanation that could account for the azole sensitivity of *age3* mutants is defects in the biosynthesis of ergosterol or problems in transporting this membrane lipid to the cell membrane. Our microarray experiments provided evidence that the target pathway of azoles is not affected transcriptionally in the presence or the absence of FCZ (Figure S3A, Tables S5 and S6). We further found that the amount of ergosterol is similar in the plasma membrane of *age3* mutants compared to WT (our

unpublished data). These findings together with epistasis experiments showing that deletion of *AGE3* restored azole sensitivity in different clinical isolates, suggest that the azole sensitivity of *age3* cells is unlikely to depend on established mechanisms.

Finally, in support of the vesicle transport hypothesis is the observation that while *age3* cells showed slightly increased sensitivity to different cell wall perturbing agents (CF and calcofluor white), the most impressive effect besides azoles was observed when *age3* cells were treated with hygromycin B (Figure 1D). Hygromycin B sensitivity is usually linked to glycosylation defects [31,32]. Therefore, it remains possible that some glycosylated proteins, including GPI-anchored proteins that normally reside in the cell wall, are not properly localized in *age3* cells. How precisely defects in vesicle trafficking influence the observed drug phenotypes and whether drug sensitivity is caused by a general aspect of the secretory pathway or of a particular cell membrane or wall protein remains to be determined.

Drug resistance and virulence are two important biological aspects of pathogenic fungal species. While different fungal drug resistance mechanisms are now well understood [69,70], various virulence-related attributes have been described that help *Candida* to cause infections [57,59,71]. Whereas genes critically involved either in drug resistance or virulence are attractive drug targets [59], an undeniably better option is targeting genes that are involved in both processes. The broad-range sensitivity to azoles and an echinocandin together with *in vivo* data showing that *age3* mutants are avirulent in WT and exhibit significantly attenuated virulence even in an immunocompromised mouse model, indicates that Age3p and the process of ARF cycling is one such option. We further explored the therapeutic potential of ARF cycling inhibition by demonstrating that, in A/J mice, FCZ treatment was significantly more efficacious when ARF activity was genetically compromised.

One of our major problems was to reproduce the potent *in vitro* synergy of FCZ/BFA in animal models as we observed that a FCZ/BFA combination failed to rescue A/J mice infected with WT *C. albicans* (data not shown). One reason why the *in vitro* synergy failed to translate to *in vivo* conditions could be that BFA has low bioavailability characteristics [72] and efforts to chemically improve these unfavorable properties have not been successful so far [73,74]. The ability of BFA to induce apoptosis in cancer cells has stimulated an interest for developing BFA as an anti-cancer therapeutic agent [75,76,77,78,79,80]. Increasing evidence also shows that a variety of small G protein signaling pathways of the Ras superfamily, like RHO, RAS and ARF, have been linked to tumorigenesis [81,82,83]. Thus, despite being evolutionarily conserved, targeting ARF activities could be beneficial not only for antifungal, but also for cancer therapies. Clearly, one future challenge lies in finding fungal-specific ARF activity inhibitors that retain favorable bioavailability *in vivo*, a challenge that can now be approached cost- and time-effectively through virtual screening with both mammalian and yeast crystal structures of different ARF cycling proteins at hand [43,44,45,46,47,48,84,85].

The *age3* mutant lost tolerance to FCZ (Figure 1). This phenomenon of losing tolerance under membrane stress is not unique to ARF cycling. Previous work established that when HSP90 or calcineurin is genetically or pharmacologically inhibited in different fungal species, cells show a similar loss of tolerance and are not able to survive membrane stress [17,18,22,86]. Additional phenotypes that calcineurin inhibition shares with ARF inhibition include synergism with azoles and echinocandins as well as reduced virulence in the bloodstream of the host [17,19,87]. These overlapping phenotypes, together with our epistasis experiments that showed that deleting *AGE3* overrides constitutive calcineurin signaling, provide some arguments that ARF cycling and HSP90/calcineurin-dependent processes could be coupled. Although overlapping functions cannot be excluded, several lines of evidence support the current model that ARF and HSP90/calcineurin inhibition constitute two distinct mechanisms contributing to drug tolerance. First, a triple combination of azole/calcineurin/ARF inhibition is more efficacious than either pairwise combination at 24 hours. Second, consistent with previous observations that long term azole resistance evolves towards HSP90/calcineurin-independency [20], cells treated with calcineurin inhibitors plus FCZ recover after prolonged incubation, while BFA/FCZ treated cells do not. Finally, if ARF cycling is in fact coupled to HSP90/calcineurin signaling, then we might expect *age3* mutants to copy other HSP90/calcineurin phenotypes besides the demonstrated reduced virulence and drug sensitivity. One explanation, for instance, why calcineurin mutants are avirulent is that they do not survive in the presence of FBS or Ca^{2+} ions present in host serum [19,88]. We found, however, that *age3* mutants can survive FBS and Ca^{2+} stresses (data not shown).

More work is therefore required to elucidate how ARF G protein signaling relates to HSP90/calcineurin and other signaling pathways that share ARF-related phenotypes. With four ARF proteins, six ARF GAPs and seven ARF GEFs identified in yeast so far [89], this provides a rich resource for further investigations into which aspects of vesicle transport and ARF G protein signaling are responsible for two important aspects of the biology of pathogenic fungal species.

Materials and Methods

Strains, plasmids, primers and culture conditions

All strains, primers and plasmids used in this study are described in supplementary Table S9, S10 and S11, respectively. *C. albicans* mutants were constructed either with the UAU1-transposon insertion strategy [90] or by deleting the coding sequence of genes (Table S9). For insertion and deletion mutant construction, at least two mutants independently derived from two distinct heterozygous mutants were analyzed in each case. With regards to the *AEG3* gene (*ORF19.3683*), we propose to use *AGE3* as standard name for the *C. albicans* homolog of *S. cerevisiae's GCS1*, because another gene (*ORF19.5059*) has already been named '*GCS1*' in the Candida literature [91]. For the *AGE3* deletion mutant, long 100-mer primers flanking up- and downstream sequences, respectively, of the coding sequence of *AGE3* were used to amplify marker cassettes pFA-*HIS1* and pFA-*ARG4* [92]. Transformation was carried out according to standard protocols [93] and selected on synthetic media (2% dextrose, 6.7% yeast nitrogen base without amino acids, 2% agar) containing the necessary auxotrophic supplements. Correct marker integration was PCR-verified as described [94]. As genetic manipulation in *C. albicans* can frequently lead to aneuploidy [95,96], we verified the absence of any chromosomal rearrangements by Comparative Genome Hybridization (CGH) and found that deletion mutants of *AGE3* were aneuploidy free (Figure S4). For constructing the *AGE3*-revertant strain, the SAT1 flipper cassette was used [97]. Briefly, the *AGE3* coding sequence including upstream and a short downstream flanking sequence was amplified with primers oEE242/oEE243, *Kpn*I/*Xho*I-digested and cloned into the *Kpn*I/*Xho*I-digested pSFS2A plasmid, resulting in plasmid pCaEE25, which was sequenced. A long downstream flanking sequence of *AGE3* was amplified with primers oEE237/oEE238, *Not*I/*Sac*II-digested and then cloned into the *Not*I/*Sac*II-digested plasmid pCaEE25, resulting in plasmid pCaEE27. Following *Kpn*I/*Sac*II double digestion of plasmid pCaEE27, this digestion was

transformed directly into the *age3* deletion strain. Selection was done on YPD plates containing 200 μg/ml nourseothricin, as described [67] and PCR-verified. Counterselection of the nourseothricin marker was done as described [67].

The nourseothricin marker cassette [97] was also used to delete *AGE3* in FCZ-resistant strains F5, S2 and DSY2146. Briefly, a long upstream coding sequence of *AGE3* was first amplified from pEE27 with primers oEE235/oEE236, *Kpn*1/*Xho*1 digested and then cloned into the *Kpn*1/*Xho*1 digested plasmid pEE27, therefore replacing the coding sequence of *AGE3*. The resulting plasmid was designated pEE43.

Candida strains were routinely cultured at 30°C in either rich YPD media (1% yeast extract, 2% peptone, 2% dextrose, supplemented with 50 μg/ml uridine) or RPMI-MOPS media (RPMI-1640, SIGMA, supplemented with 0.3 g/l L-glutamine, 50 mg/ml uridine, 2% glucose, pH adjusted with MOPS buffer to 7.0). Media plates were supplemented with 2% agar. *A. fumigatus* was cultured in half-strength YPD media (not enriched with uridine) or RPMI-MOPS media (not enriched with uridine). Media plates were supplemented with 1.5% agar.

Antifungal susceptibility testing

Because drug susceptibility results did not differ significantly between WT *C. albicans* strains SC5314 (isolate) and SN95 (a standard laboratory auxotrophic mutant used to construct deletion mutants) [98] (Table S2), WT usually refers to SN95 unless indicated otherwise. Drug stock solutions were prepared using ethanol/10% Tween 20 as solvent for FK506 (5 mg/ml), cyclosporin A (25 mg/ml), DMSO for fluconazole (300 mg/ml), miconazole (100 mg/ml), ketoconazole (16.6 mg/ml), itraconazole (10 mg/ml), amphotericin B (20 mg/ml), calcofluor white (50 mg/ml), brefeldin A (20 mM), hygromycin B (50 mg/ml), and water for caspofungin (10 mg/ml). All drugs were obtained from Sigma, except caspofungin (Merck), fluconazole and itraconazole (both from SpectrumChemical, Mfg Corp, USA). Once in solution, drugs were stored at −20°C. Initial antifungal sensitivity testing with all *C. albicans* FCZ-cidal candidates was done using a modified version of the CLSI (formerly NCCLS) procedure [99]. Briefly, 50 μl of drugs at two-fold the final concentration was serially diluted in flat-bottom 96-well tissue culture plates (Corning Inc., NY, USA) and combined with 50 μl of overnight *Candida* cultures adjusted to 1×10^4 cells/ml. MIC plates were incubated at 30°C without shaking and optical densities were read at indicated time points with a Tecan Safire plate reader. The MIC was determined by the first well with a growth reduction of >95% in terms of OD_{600} values in the presence of a compound compared to untreated control cells. Before the 72 hours OD_{600} readings, plates were carefully shaken, so that a representative aliquot of 2 μl of each well could be spotted on fresh YPD recovery plates to assess the extent to which cells recover from the drug treatments. Recovery plates were incubated at 30°C between 24 hours and 48 hours before being photographed. Drug susceptibilities of robust hits that resulted from this initial MIC testing were then confirmed on solid media plates containing FCZ, disc diffusion or time-kill curve assays, as described [19].

Dose-matrix titration assays were used to evaluate drug synergies. Briefly, dose-matrix titration assays were done as described for the MIC assays, except that the final volume was 150 μl; 50 μl of three-fold the final drug concentration of drug A was dispensed in two-fold serial dilution steps across seven columns of the plate, 50 μl of three-fold the final drug concentration of drug B was dispensed in two-fold serial dilution steps down seven rows of the plate; 50 μl of overnight *Candida* cultures adjusted to 1.5×10^4 cells/ml was dispensed in all drug containing wells plus one control well containing no drugs. Synergy of a compound pair was quantified with respect to the Loewe additivity model [100] via the fractional inhibitory concentration index (FIC index) = $(MIC_{A\ in\ combo}/MIC_{A\ alone}) + (MIC_{B\ in\ combo}/MIC_{B\ alone})$, where "$MIC_{A\ in\ combo}$" is the MIC of drug A in combination, "$MIC_{A\ alone}$" is the MIC of drug A alone, "$MIC_{B\ in\ combo}$" is the MIC of drug B in combination and "$MIC_{B\ alone}$" is the MIC of drug B alone, respectively. Compound pairs were classified as synergistic if its FIC index is ≤0.5, the standard threshold [100,101]. For calculation purposes of the FIC index, MIC values of >1, >2, >8, >16, >64, >128, >2048, >4096 were assumed to be 2, 4, 16, 32, 128, 256, 4096, 8192, respectively. MIC and dose-matrix titration results were visualized with TreeView version 1.6 (http://rana.lbl.gov/EisenSoftware.htm).

A. fumigatus disc diffusion assays were done as described [16], with the following modifications. Conidiation was induced on YPD plates incubated at 37°C for seven days. Conidia were then washed off the plates and suspended in PBS+0.1% Tween media before spreading 1×10^5 conidia on appropriate plates. Discs containing 6.4 μg caspofungin were applied and the plates were incubated at 35°C for 48 hours. *A. fumigatus* MIC assays were done exactly as described [102]. All MIC and dose-matrix titration assays with *Candida* and *Aspergillus* were independently performed on at least two different occasions.

Virulence studies

Virulence testing of *C. albicans* was done as previously described [58]. Briefly, 8- to 12-week old C57BL/6J or A/J mice (Jackson Laboratories, Bar Harbor, ME) were inoculated via the tail vein with 200 μl of a suspension containing 3×10^5 *C. albicans* in PBS. Mice were closely monitored over a period of maximally 21 days for clinical signs of disease such as lethargy, ruffled fur, or hunched back. Mice showing extreme lethargy were considered moribund and were euthanized. All experimental procedures involving animals were approved by the Biotechnology Research Institute Animal Care Committee, which operates under the guidelines of the Canadian Council of Animal Care. Statistical analysis of survival curves as well as fungal load was done with GraphPad Prism version 5.0b. For kidney sections, extracted organs were fixed in 10% formaldehyde (Sigma) and processed at the Histology Core Facility at McGill (http://cancercentre.mcgill.ca/) by staining thin slices of tissue sections with Grocot–Gomori methenamine silver to visualize fungal cells.

Microarray and CGH studies

Comparative Genome Hybridization (CGH) analysis was done as previously described [49] with the following modifications. Genomic DNA was extracted from a *C. albicans* culture grown to saturation with the Qiagen Genomic DNA Extraction kit according to manufacturer's instructions. DNA hybridization was done with the Advalytix SlideBooster for 16 hours at 42°C according to manufacturer's instructions.

For the fluconazole microarray experiment, overnight cultures of *C. albicans* cells were diluted to OD_{600} of 0.05 in fresh YPD media, grown to early logarithmic phase (OD_{600} 0.8) and split into two 50 ml cultures in 250 ml Erlenmayer flasks. One culture was fluconazole treated (600 mg/ml), while the other group received an equal amount of DMSO as control. Cultures were grown for one hour, spun down, the supernatant was removed and the cell pellet was nitrogen-flash frozen and stored at −80°C until further use. RNA was extracted according to the hot-phenol protocol [103]. For the caspofungin microarray experiment, logarithmically growing cells were treated with 125 ng/ml caspofungin for one hour, as previously described [52]. RNA was extracted with the

RNase easy kit (Qiagen), as described [67]. Probe labeling, hybridization and slide washing was done as described [104], except that the SlideBooster was used for hybridization. At least three biological replicates including dye swaps were used for each condition on double spotted ORF microarrays (6,394 intragenic 70-mer oligonucleotide probes) [104]. Scanning was done with a ScanArray Lite microarray scanner (Perkin Elmer). QuantArray was used to quantify fluorescence intensities and data analysis was carried out using Genespring v.7.3 (Agilent Technologies). To compare overlap of different gene lists as well as analyzing Gene Ontology enrichment, *p*-values were calculated using the hypergeometric distribution as described in the GO Term Finder Tool web site (http://www.candidagenome.org/cgi-bin/GO/goTermFinder). Gene lists can be found in Tables S4, S5, S6, S7 and S8.

Supporting Information

Figure S1 Phenotypes of the predicted FCZ-cidal genes in C. *albicans* as determined on rich media containing FCZ. Five-fold serial dilutions starting with an overnight culture diluted to OD_{600} of 0.1 was spotted (2 µl) on YPD or YPD + 2 µg/ml FCZ. Plates were incubated at 30°C for the time indicated.
Found at: doi:10.1371/journal.ppat.1000753.s001 (5.05 MB TIF)

Figure S2 BFA synergy with different azoles in synthetically defined RPMI media at 30°C. (A) Prior to synergy testing, *C. albicans* WT strain was tested for drug sensitivity, which was measured over time on day one (24 hours), day three (72 hours) and day six (144 hours), respectively. Data was analyzed as in Figure 1A. (B) Optical densities of dose-matrix titration assays were measured on day three (72 hours) or day six (144 hours), respectively. Additionally, spot assays were done on day six. Except for media, assays were performed and analyzed as in Figure 1A and 3B.
Found at: doi:10.1371/journal.ppat.1000753.s002 (2.15 MB TIF)

Figure S3 Core transcriptional responses to FCZ or CF are not significantly affected in the absence of *AGE3*. (A) Transcriptional analysis under FCZ treatment. Significantly regulated genes (>2 fold change, *p-value* <0.05) were selected when WT was treated with FCZ (WT+FCZ vs. WT) and combined with significantly regulated genes when *age3* cells were FCZ treated (*age3*+FCZ vs. *age3*) to build a cluster tree (top). The same gene list was used to visualize in the Venn diagram (bottom) a significant overlap of core FCZ-responsive genes. (B) Transcriptional analysis under CF treatment. Gene lists were selected in the same way as described for the FCZ treatment to build a cluster tree. The Venn diagram illustrates that there is a significant overlap of core CF responsive genes. Tables S4, S5, S6, S7 and S8 list exact transcript changes for all significantly regulated genes used in the FCZ and CF analysis.
Found at: doi:10.1371/journal.ppat.1000753.s003 (0.89 MB TIF)

Figure S4 No aneuploidies were detected in the *AGE3* deletion mutant by CGH analysis. Cy3 labeled genomic DNA from either *age3* mutants or strain BWP17 was hybridized to DNA microarrays with Cy5 labeled genomic DNA from the reference strain SC5314. Shown are plots of CGH (comparative genome hybridization) analyses, where the y-axis shows the log2 fluorescence ratio of the mutant strains versus SC5314 and the x-axis shows all chromosomes (1 to R). A single black rhombus represents the log2 fluorescence ratio plotted as a function of its position in the *C. albicans*' assembly 21. In this representation, a 1.5-fold increase in fluorescence ratio (i.e. 3 chromosome copies versus 2) equals a log2 ratio of ~0.58. (A) CGH shows the known loss of one end of chromosome 5 in strain BWP17. This strain is also auxotroph for *URA3*, *HIS1*, *ARG4*. (B) The prototrophic *age3* mutant does not have any chromosomal rearrangements as determined by CGH.
Found at: doi:10.1371/journal.ppat.1000753.s004 (7.62 MB TIF)

Table S1 The 22 FCZ-cidal genes in *S. cerevisiae* and the *C. albicans* homologs.
Found at: doi:10.1371/journal.ppat.1000753.s005 (0.04 MB XLS)

Table S2 Phenotypes of the predicted FCZ-cidal genes in *C. albicans* as determined by MIC assay in YPD media.
Found at: doi:10.1371/journal.ppat.1000753.s006 (0.04 MB XLS)

Table S3 Drug synergy interaction as determined by FIC index.
Found at: doi:10.1371/journal.ppat.1000753.s007 (0.04 MB XLS)

Table S4 The genes listed here were significantly regulated (>2 fold, p-value <0.05) in absence of *AGE3*.
Found at: doi:10.1371/journal.ppat.1000753.s008 (0.04 MB XLS)

Table S5 Fluconazole (FCZ) responsive genes as identified by microarray analysis.
Found at: doi:10.1371/journal.ppat.1000753.s009 (0.07 MB XLS)

Table S6 This list contains the same genes as Table S5, but the genes are colored here according to the Venn Diagram in Figure S3A (bottom).
Found at: doi:10.1371/journal.ppat.1000753.s010 (0.07 MB XLS)

Table S7 Caspofungin (CF) responsive genes as identified by microarray analysis.
Found at: doi:10.1371/journal.ppat.1000753.s011 (0.13 MB XLS)

Table S8 This list contains the same genes as Table S7, but the genes are colored here according to the Venn Diagram in Figure S3B (bottom).
Found at: doi:10.1371/journal.ppat.1000753.s012 (0.13 MB XLS)

Table S9 Strains used in this study.
Found at: doi:10.1371/journal.ppat.1000753.s013 (0.04 MB XLS)

Table S10 Primers used in this study.
Found at: doi:10.1371/journal.ppat.1000753.s014 (0.05 MB XLS)

Table S11 Plasmids used in this study.
Found at: doi:10.1371/journal.ppat.1000753.s015 (0.03 MB XLS)

Acknowledgments

We thank Robert Annan for critical reading of the manuscript. We are grateful to Arnold Bito for communicating data before publication. We thank Dominique Sanglard, Joachim Morschhaeuser, Martine Raymond, Aaron Mitchell and Frank Odds for providing strains and plasmids. Guylaine Lépine is acknowledged for helping with construction of mutant strains, Mario Mercier and Cynthia Helie for excellent technical assistance in animal handling and Kuensook Lee for help with antifungal drug testing. This is NRC publication number 50678.

Author Contributions

Conceived and designed the experiments: EE MW. Performed the experiments: EE GV CAM. Analyzed the data: EE. Contributed reagents/materials/analysis tools: DH AYL GJ MH DCS DYT CAM AM. Wrote the paper: EE.

References

1. Nucci M, Marr KA (2005) Emerging fungal diseases. Clin Infect Dis 41: 521–526.

2. Pappas PG, Kauffman CA, Andes D, Benjamin DK Jr, Calandra TF, et al. (2009) Clinical practice guidelines for the management of candidiasis: 2009

update by the Infectious Diseases Society of America. Clin Infect Dis 48: 503–535.
3. Pfaller MA, Diekema DJ (2007) Epidemiology of invasive candidiasis: a persistent public health problem. Clin Microbiol Rev 20: 133–163.
4. Wilson LS, Reyes CM, Stolpman M, Speckman J, Allen K, et al. (2002) The direct cost and incidence of systemic fungal infections. Value Health 5: 26–34.
5. Shao PL, Huang LM, Hsueh PR (2007) Recent advances and challenges in the treatment of invasive fungal infections. Int J Antimicrob Agents 30: 487–495.
6. Richardson M, Lass-Florl C (2008) Changing epidemiology of systemic fungal infections. Clin Microbiol Infect 14 Suppl 4: 5–24.
7. Pfaller Michael A, Pappas Peter G, Wingard John R (2006) Invasive Fungal Pathogens: Current Epidemiological Trends. Clinical Infectious Diseases 43: S3–S14.
8. Leroy O, Gangneux JP, Montravers P, Mira JP, Gouin F, et al. (2009) Epidemiology, management, and risk factors for death of invasive Candida infections in critical care: a multicenter, prospective, observational study in France (2005–2006). Crit Care Med 37: 1612–1618.
9. Pfaller MA, Diekema DJ (2004) Rare and emerging opportunistic fungal pathogens: concern for resistance beyond Candida albicans and Aspergillus fumigatus. J Clin Microbiol 42: 4419–4431.
10. Cowen L (2008) The evolution of fungal drug resistance: modulating the trajectory from genotype to phenotype. Nat Rev Micro 6: 187–198.
11. Chapman SW, Sullivan DC, Cleary JD (2008) In search of the holy grail of antifungal therapy. Trans Am Clin Climatol Assoc 119: 197–215; discussion 215–196.
12. Cowen LE, Steinbach WJ (2008) Stress, drugs, and evolution: the role of cellular signaling in fungal drug resistance. Eukaryot Cell 7: 747–764.
13. Cannon RD, Lamping E, Holmes AR, Niimi K, Baret PV, et al. (2009) Efflux-mediated antifungal drug resistance. Clin Microbiol Rev 22: 291–321, table of contents.
14. Traeder C, Kowoll S, Arasteh K (2008) Candida infection in HIV positive patients 1985–2007. Mycoses 51 Suppl 2: 58–61.
15. Pachl J, Svoboda P, Jacobs F, Vandewoude K, van der Hoven B, et al. (2006) A randomized, blinded, multicenter trial of lipid-associated amphotericin B alone versus in combination with an antibody-based inhibitor of heat shock protein 90 in patients with invasive candidiasis. Clin Infect Dis 42: 1404–1413.
16. Cowen LE, Singh SD, Kohler JR, Collins C, Zaas AK, et al. (2009) Harnessing Hsp90 function as a powerful, broadly effective therapeutic strategy for fungal infectious disease. Proc Natl Acad Sci U S A 106: 2818–2823.
17. Singh SD, Robbins N, Zaas AK, Schell WA, Perfect JR, et al. (2009) Hsp90 governs echinocandin resistance in the pathogenic yeast Candida albicans via calcineurin. PLoS Pathog 5: e1000532. doi:10.1371/journal.ppat.1000532.
18. Cruz MC, Goldstein AL, Blankenship JR, Del Poeta M, Davis D, et al. (2002) Calcineurin is essential for survival during membrane stress in Candida albicans. EMBO J 21: 546–559.
19. Sanglard D, Ischer F, Marchetti O, Entenza J, Bille J (2003) Calcineurin A of Candida albicans: involvement in antifungal tolerance, cell morphogenesis and virulence. Mol Microbiol 48: 959–976.
20. Cowen LE, Lindquist S (2005) Hsp90 potentiates the rapid evolution of new traits: drug resistance in diverse fungi. Science 309: 2185–2189.
21. Marchetti O, Entenza JM, Sanglard D, Bille J, Glauser MP, et al. (2000) Fluconazole plus cyclosporine: a fungicidal combination effective against experimental endocarditis due to Candida albicans. Antimicrob Agents Chemother 44: 2932–2938.
22. Steinbach WJ, Reedy JL, Cramer RA Jr, Perfect JR, Heitman J (2007) Harnessing calcineurin as a novel anti-infective agent against invasive fungal infections. Nat Rev Microbiol 5: 418–430.
23. Lopez A, Parsons AB, Nislow C, Giaever G, Boone C (2008) Chemical-genetic approaches for exploring the mode of action of natural products. Prog Drug Res 66: 237, 239–271.
24. Hoon S, Smith AM, Wallace IM, Suresh S, Miranda M, et al. (2008) An integrated platform of genomic assays reveals small-molecule bioactivities. Nat Chem Biol 4: 498–506.
25. Ho CH, Magtanong L, Barker SL, Gresham D, Nishimura S, et al. (2009) A molecular barcoded yeast ORF library enables mode-of-action analysis of bioactive compounds. Nat Biotechnol 27: 369–377.
26. Butcher RA, Bhullar BS, Perlstein EO, Marsischky G, LaBaer J, et al. (2006) Microarray-based method for monitoring yeast overexpression strains reveals small-molecule targets in TOR pathway. Nat Chem Biol 2: 103–109.
27. Giaever G, Flaherty P, Kumm J, Proctor M, Nislow C, et al. (2004) Chemogenomic profiling: identifying the functional interactions of small molecules in yeast. Proc Natl Acad Sci U S A 101: 793–798.
28. Xu D, Jiang B, Ketela T, Lemieux S, Veillette K, et al. (2007) Genome-wide fitness test and mechanism-of-action studies of inhibitory compounds in Candida albicans. PLoS Pathog 3: e92. doi:10.1371/journal.ppat.0030092.
29. Jansen G, Lee AY, Epp E, Fredette A, Surprenant J, et al. (2009) Chemogenomic profiling predicts antifungal synergies. Mol Syst Biol 5: 338.
30. Uccelletti D, Farina F, Morlupi A, Palleschi C (1999) Mutants of Kluyveromyces lactis with altered protein glycosylation are affected in cell wall morphogenesis. Res Microbiol 150: 5–12.
31. Dean N (1995) Yeast glycosylation mutants are sensitive to aminoglycosides. Proc Natl Acad Sci U S A 92: 1287–1291.
32. Dean N, Poster JB (1996) Molecular and phenotypic analysis of the S. cerevisiae MNN10 gene identifies a family of related glycosyltransferases. Glycobiology 6: 73–81.
33. Morschhauser J (2002) The genetic basis of fluconazole resistance development in Candida albicans. Biochim Biophys Acta 1587: 240–248.
34. Kanafani ZA, Perfect JR (2008) Antimicrobial resistance: resistance to antifungal agents: mechanisms and clinical impact. Clin Infect Dis 46: 120–128.
35. Morschhauser J, Barker KS, Liu TT, Bla BWJ, Homayouni R, et al. (2007) The transcription factor Mrr1p controls expression of the MDR1 efflux pump and mediates multidrug resistance in Candida albicans. PLoS Pathog 3: e164. doi: 10.1371/journal.ppat.0030164.
36. Dunkel N, Liu TT, Barker KS, Homayouni R, Morschhauser J, et al. (2008) A gain-of-function mutation in the transcription factor Upc2p causes upregulation of ergosterol biosynthesis genes and increased fluconazole resistance in a clinical Candida albicans isolate. Eukaryot Cell 7: 1180–1190.
37. Poon PP, Wang X, Rotman M, Huber I, Cukierman E, et al. (1996) Saccharomyces cerevisiae Gcs1 is an ADP-ribosylation factor GTPase-activating protein. Proc Natl Acad Sci U S A 93: 10074–10077.
38. Moss J, Vaughan M (1998) Molecules in the ARF orbit. J Biol Chem 273: 21431–21434.
39. Poon PP, Cassel D, Spang A, Rotman M, Pick E, et al. (1999) Retrograde transport from the yeast Golgi is mediated by two ARF GAP proteins with overlapping function. EMBO J 18: 555–564.
40. Poon PP, Nothwehr SF, Singer RA, Johnston GC (2001) The Gcs1 and Age2 ArfGAP proteins provide overlapping essential function for transport from the yeast trans-Golgi network. J Cell Biol 155: 1239–1250.
41. Myers KR, Casanova JE (2008) Regulation of actin cytoskeleton dynamics by Arf-family GTPases. Trends Cell Biol 18: 184–192.
42. Gillingham AK, Munro S (2007) The small G proteins of the Arf family and their regulators. Annu Rev Cell Dev Biol 23: 579–611.
43. Singleton VL, Bohonos N, Ullstrup AJ (1958) Decumbin, a new compound from a species of Penicillium. Nature 181: 1072–1073.
44. Renault L, Guibert B, Cherfils J (2003) Structural snapshots of the mechanism and inhibition of a guanine nucleotide exchange factor. Nature 426: 525–530.
45. Cherfils J, Menetrey J, Mathieu M, Le Bras G, Robineau S, et al. (1998) Structure of the Sec7 domain of the Arf exchange factor ARNO. Nature 392: 101–105.
46. Goldberg J (1998) Structural basis for activation of ARF GTPase: mechanisms of guanine nucleotide exchange and GTP-myristoyl switching. Cell 95: 237–248.
47. Sata M, Moss J, Vaughan M (1999) Structural basis for the inhibitory effect of brefeldin A on guanine nucleotide-exchange proteins for ADP-ribosylation factors. Proc Natl Acad Sci U S A 96: 2752–2757.
48. Mossessova E, Corpina RA, Goldberg J (2003) Crystal structure of ARF1*Sec7 complexed with Brefeldin A and its implications for the guanine nucleotide exchange mechanism. Mol Cell 12: 1403–1411.
49. Znaidi S, De Deken X, Weber S, Rigby T, Nantel A, et al. (2007) The zinc cluster transcription factor Tac1p regulates PDR16 expression in Candida albicans. Mol Microbiol 66: 440–452.
50. Stevens DA, Espiritu M, Parmar R (2004) Paradoxical effect of caspofungin: reduced activity against Candida albicans at high drug concentrations. Antimicrob Agents Chemother 48: 3407–3411.
51. Fleischhacker M, Radecke C, Schulz B, Ruhnke M (2008) Paradoxical growth effects of the echinocandins caspofungin and micafungin, but not of anidulafungin, on clinical isolates of Candida albicans and C. dubliniensis. Eur J Clin Microbiol Infect Dis 27: 127–131.
52. Bruno VM, Kalachikov S, Subaran R, Nobile CJ, Kyratsous C, et al. (2006) Control of the C. albicans cell wall damage response by transcriptional regulator Cas5. PLoS Pathog 2: e21. doi:10.1371/journal.ppat.0020021.
53. Karababa M, Valentino E, Pardini G, Coste AT, Bille J, et al. (2006) CRZ1, a target of the calcineurin pathway in Candida albicans. Molecular Microbiology 59: 1429–1451.
54. Lepak A, Nett J, Lincoln L, Marchillo K, Andes D (2006) Time course of microbiologic outcome and gene expression in Candida albicans during and following in vitro and in vivo exposure to fluconazole. Antimicrob Agents Chemother 50: 1311–1319.
55. Sellam A, Tebbji F, Nantel A (2009) Role of Ndt80p in sterol metabolism regulation and azole resistance in Candida albicans. Eukaryot Cell 8: 1174–1183.
56. Liu TT, Lee RE, Barker KS, Wei L, Homayouni R, et al. (2005) Genome-wide expression profiling of the response to azole, polyene, echinocandin, and pyrimidine antifungal agents in Candida albicans. Antimicrob Agents Chemother 49: 2226–2236.
57. Whiteway M, Bachewich C (2007) Morphogenesis in Candida albicans. Annu Rev Microbiol 61: 529–553.
58. Mullick A, Elias M, Picard S, Bourget L, Jovcevski O, et al. (2004) Dysregulated inflammatory response to Candida albicans in a C5-deficient mouse strain. Infect Immun 72: 5868–5876.
59. Gauwerky K, Borelli C, Korting HC (2009) Targeting virulence: a new paradigm for antifungals. Drug Discov Today 14: 214–222.
60. Sellam A, Askew C, Epp E, Lavoie H, Whiteway M, et al. (2009) Genome-wide mapping of the coactivator Ada2p yields insight into the functional roles of SAGA/ADA complex in Candida albicans. Mol Biol Cell 20: 2389–2400.

61. Sanglard D, Ischer F, Parkinson T, Falconer D, Bille J (2003) Candida albicans mutations in the ergosterol biosynthetic pathway and resistance to several antifungal agents. Antimicrob Agents Chemother 47: 2404–2412.
62. Timmers HT, Tora L (2005) SAGA unveiled. Trends Biochem Sci 30: 7–10.
63. Znaidi S, Weber S, Al-Abdin OZ, Bomme P, Saidane S, et al. (2008) Genomewide location analysis of Candida albicans Upc2p, a regulator of sterol metabolism and azole drug resistance. Eukaryot Cell 7: 836–847.
64. Liu TT, Znaidi S, Barker KS, Xu L, Homayouni R, et al. (2007) Genome-wide expression and location analyses of the Candida albicans Tac1p regulon. Eukaryot Cell 6: 2122–2138.
65. Tuch BB, Li H, Johnson AD (2008) Evolution of eukaryotic transcription circuits. Science 319: 1797–1799.
66. Hogues H, Lavoie H, Sellam A, Mangos M, Roemer T, et al. (2008) Transcription factor substitution during the evolution of fungal ribosome regulation. Mol Cell 29: 552–562.
67. Askew C, Sellam A, Epp E, Hogues H, Mullick A, et al. (2009) Transcriptional Regulation of Carbohydrate Metabolism in the Human Pathogen Candida albicans. PLoS Pathog 5: e1000612. doi:10.1371/journal.ppat.1000612.
68. Jia N, Arthington-Skaggs B, Lee W, Pierson CA, Lees ND, et al. (2002) Candida albicans sterol C-14 reductase, encoded by the ERG24 gene, as a potential antifungal target site. Antimicrob Agents Chemother 46: 947–957.
69. Sanglard D, Coste A, Ferrari S (2009) Antifungal drug resistance mechanisms in fungal pathogens from the perspective of transcriptional gene regulation. FEMS Yeast Res 9: 1029–1050.
70. Cowen L, Steinbach W (2008) Stress, Drugs, and Evolution: the Role of Cellular Signaling in Fungal Drug Resistance. Eukaryotic Cell 7: 747–764.
71. d'Enfert C (2009) Hidden killers: persistence of opportunistic fungal pathogens in the human host. Curr Opin Microbiol 12: 358–364.
72. Bruning A, Ishikawa T, Kneusel RE, Matern U, Lottspeich F, et al. (1992) Brefeldin A binds to glutathione S-transferase and is secreted as glutathione and cysteine conjugates by Chinese hamster ovary cells. J Biol Chem 267: 7726–7732.
73. Fox BM, Vroman JA, Fanwick PE, Cushman M (2001) Preparation and evaluation of sulfide derivatives of the antibiotic brefeldin a as potential prodrug candidates with enhanced aqueous solubilities. J Med Chem 44: 3915–3924.
74. Anadu NO, Davisson VJ, Cushman M (2006) Synthesis and anticancer activity of brefeldin A ester derivatives. J Med Chem 49: 3897–3905.
75. Shao RG, Shimizu T, Pommier Y (1996) Brefeldin A is a potent inducer of apoptosis in human cancer cells independently of p53. Exp Cell Res 227: 190–196.
76. Zhu J-W, Hori H, Nojiri H, Tsukuda T, Taira Z (1997) Synthesis and activity of brefeldin a analogs as inducers of cancer cell differentiation and apoptosis. Bioorganic & Medicinal Chemistry Letters 7: 139–144.
77. Zhu JW, Nagasawa H, Nagura F, Mohamad SB, Uto Y, et al. (2000) Elucidation of strict structural requirements of brefeldin A as an inducer of differentiation and apoptosis. Bioorg Med Chem 8: 455–463.
78. Nojiri H, Manya H, Isono H, Yamana H, Nojima S (1999) Induction of terminal differentiation and apoptosis in human colonic carcinoma cells by brefeldin A, a drug affecting ganglioside biosynthesis. FEBS Lett 453: 140–144.
79. Guo H, Tittle TV, Allen H, Maziarz RT (1998) Brefeldin A-mediated apoptosis requires the activation of caspases and is inhibited by Bcl-2. Exp Cell Res 245: 57–68.
80. Hacki J, Egger L, Monney L, Conus S, Rosse T, et al. (2000) Apoptotic crosstalk between the endoplasmic reticulum and mitochondria controlled by Bcl-2. Oncogene 19: 2286–2295.
81. Sahai E, Marshall CJ (2002) RHO-GTPases and cancer. Nat Rev Cancer 2: 133–142.
82. Downward J (2003) Targeting RAS signalling pathways in cancer therapy. Nat Rev Cancer 3: 11–22.
83. Sabe H, Onodera Y, Mazaki Y, Hashimoto S (2006) ArfGAP family proteins in cell adhesion, migration and tumor invasion. Curr Opin Cell Biol 18: 558–564.
84. Cherfils J, Chardin P (1999) GEFs: structural basis for their activation of small GTP-binding proteins. Trends Biochem Sci 24: 306–311.
85. Amor JC, Horton JR, Zhu X, Wang Y, Sullards C, et al. (2001) Structures of yeast ARF2 and ARL1: distinct roles for the N terminus in the structure and function of ARF family GTPases. J Biol Chem 276: 42477–42484.
86. Marchetti O, Moreillon P, Glauser MP, Bille J, Sanglard D (2000) Potent synergism of the combination of fluconazole and cyclosporine in Candida albicans. Antimicrob Agents Chemother 44: 2373–2381.
87. Bader T, Bodendorfer B, Schroppel K, Morschhauser J (2003) Calcineurin is essential for virulence in Candida albicans. Infect Immun 71: 5344–5354.
88. Blankenship JR, Heitman J (2005) Calcineurin is required for Candida albicans to survive calcium stress in serum. Infect Immun 73: 5767–5774.
89. (SGD project. The Saccharomyces Genome Database, www.yeastgenome.org (as of October 2009)).
90. Davis DA, Bruno VM, Loza L, Filler SG, Mitchell AP (2002) Candida albicans Mds3p, a conserved regulator of pH responses and virulence identified through insertional mutagenesis. Genetics 162: 1573–1581.
91. Arnaud MB, Costanzo MC, Skrzypek MS, Shah P, Binkley G, et al. (2007) Sequence resources at the Candida Genome Database. Nucleic Acids Res 35: D452–456.
92. Gola S, Martin R, Walther A, Dünkler A, Wendland J (2003) New modules for PCR-based gene targeting in Candida albicans: rapid and efficient gene targeting using 100 bp of flanking homology region. Yeast 20: 1339–1347.
93. Chen DC, Yang BC, Kuo TT (1992) One-step transformation of yeast in stationary phase. Curr Genet 21: 83–84.
94. Walther A, Wendland J (2008) PCR-based gene targeting in Candida albicans. Nat Protoc 3: 1414–1421.
95. Bouchonville K, Forche A, Tang KE, Selmecki A, Berman J (2009) Aneuploid chromosomes are highly unstable during DNA transformation of Candida albicans. Eukaryot Cell 8: 1554–1566.
96. Arbour M, Epp E, Hogues H, Sellam A, Lacroix C, et al. (2009) Widespread occurrence of chromosomal aneuploidy following the routine production of Candida albicans mutants. FEMS Yeast Res.
97. Reuss O, Vik A, Kolter R, Morschhäuser J (2004) The SAT1 flipper, an optimized tool for gene disruption in Candida albicans. Gene 341: 119–127.
98. Noble SM, Johnson AD (2005) Strains and Strategies for Large-Scale Gene Deletion Studies of the Diploid Human Fungal Pathogen Candida albicans. Eukaryotic Cell.
99. NCCLS. Reference Method for Broth Dilution Antifungal Susceptibility Testing of Yeasts; Approved Standard-Second Edition. NCCLS document M27-A2 [ISBN 1-56238-469-4]. NCCLS, 940 West Valley Road, Suite 1400, Wayne, Pennsylvania 19087-1898 USA, 2002.
100. Loewe S (1953) The problem of synergism and antagonism of combined drugs. Arzneimittelforschung 3: 285–290.
101. Barchiesi F, Di Francesco LF, Compagnucci P, Arzeni D, Giacometti A, et al. (1998) In-vitro interaction of terbinafine with amphotericin B, fluconazole and itraconazole against clinical isolates of Candida albicans. J Antimicrob Chemother 41: 59–65.
102. NCCLS. Reference Method for Broth Dilution Antifungal Susceptibility Testing of Filamentous Fungi; Approved Standard. NCCLS document M38-A [ISBN 1-56238-470-8]. NCCLS, 940 West Valley Road, Suite 1400, Wayne, Pennsylvania 19087-1898 USA, 2002.
103. Kohrer K, Domdey H (1991) Preparation of high molecular weight RNA. Methods Enzymol 194: 398–405.
104. Nantel A, Rigby T, Hogues H, Whiteway M (2006) Microarrays for studying pathogenicity in Candida albicans; Kavanaugh KH, ed. New Jersey: Wiley Press.

Chapter IV

IV. Tackling *C. albicans*-specific phenotypes

In chapters II and III, I presented a method based on reverse genetics that addressed the problem of drug resistance. Specifically, we showed that using *S. cerevisiae* as a model is a useful approach to identify new drug targets in *C. albicans*. We also demonstrated how this strategy can be used to make drug treatments more efficacious *in vitro*. Although in our case this approach proved to be successful, there are clear limitations. In particular the fact that only 1 out of 22 predicted phenotypes from budding yeast was confirmed in *C. albicans* represents a low efficiency of the surrogate model approach. I was therefore curious to investigate alternative approaches that would allow us to link a function to a gene directly in the pathogen. The *UAU1* method, which I introduced in chapter I.4.2, would be an ideal technique, because in theory it allows us to randomly create homozygous *C. albicans* mutants, which we could then test for a desired phenotype. As well, because we would perform functional genomics directly in *C. albicans*, we wouldn't rely on surrogate models to predict gene function. This is of particular importance when addressing processes that are absent in the model, like virulence, which is usually not observed in *S. cerevisiae*. I therefore decided to evaluate the *UAU1* technique on a genome-wide scale and look for genes that are involved in virulence. In order to do this, I focused on the yeast-to-hyphae switch, because mutants defective in this process are often avirulent.

I will now first summarize our current understanding of how the yeast-to-hyphae switch works. The following section (chapter IV.2.) will then describe the published results from our forward genetics screen. This screen will introduce *ARP2*, a gene that will take center stage in the following chapter (chapter V), where I expanded on observations presented in this chapter.

IV.1. Regulation of morphogenesis in *C. albicans*

IV.1.1. The yeast-to-hyphae switch

C. albicans grows in the yeast form under standard laboratory conditions (30°C, rich media). Phenotypically, yeast-grown *C. albicans* cells are almost indistinguishable from *S. cerevisiae* yeast cells; both are oblate and divide by budding, where mother and daughter cells separate after the budding process. Pseudohyphal and hyphal cells, on the other hand, are both considered filamentous forms of *C. albicans*. These two morphologies each have several unique features. Pseudohyphae are elongated cells that do not separate from the mother but grow unidirectionally and vary in length, from only slightly longer to several times the length of yeast cells. They can be identified by constrictions between cells, as well as by septa that form directly at the border with the mother cell, and by the feature that the width of the 'filaments' is not constant, being wider in the middle compared to the two ends. These three properties distinguish pseudohyphal from true hyphal cells. True hyphae have strictly parallel cell walls with no constrictions between cells, and the first septa forms a short distance away from the mother cell along the hyphal tube. Hyphal cells are also longer than pseudohyphae, usually many times the length of yeast cells, but they are thinner than pseudohyphae (2 μm versus 3 μm) (reviewed in [155]). Another difference between pseudohyphal and hyphal cells is that nuclear division occurs across the mother-bud neck in pseudohyphae and within the germ tube (the hyphal projection that forms in the first cell cycle before septation) in hyphal cells. Finally, a variety of environmental conditions can induce either pseudohyphal or hyphal morphological changes. For example, high phosphate concentrations of up to 600 mM, pH 6.0 together with elevated growth temperature of 35°C, or nitrogen limitation on solid medium can all induce pseudohyphal growth, while serum together with high temperature (37°C), N-acetylglucosamine, or neutral pH together with 37°C all favour hyphal growth. Other environmental stimuli that influence morphogenesis include gas (O_2 and CO_2), osmotic stress as well as quorum sensing molecules such as farnesol (reviewed in [156]).

IV.1.2. The cAMP-mediated PKA pathway

The variety of environmental signals that influence morphology are transmitted by several known signalling pathways to downstream transcription factors, which in turn activate morphology-specific genes [58,157]. The interplay between environmental stimuli, signal transduction pathways and transcription factors is complex. Two of the best-understood signal transduction pathways involved in morphogenesis are the cAMP-dependent PKA pathway and the MAP kinase signalling pathway [158]. Both of these pathways are connected via the small GTP-binding protein Ras1. The central role of Ras1 in terms of regulating morphology has been demonstrated early on by experiments that showed that when Ras1 was deleted, the cells were only able to grow as yeast, but unable to transition into hyphal cells [159]. Later on, different groups have contributed to the picture that a variety of mutants in the cAMP-mediated signalling pathway cause morphological defects [108,160,161,162,163]. For instance, when the adenylyl cyclase encoded by *CDC35* (synonym *CYR1*), which is directly activated by Ras1, was deleted, the cells were unable to form hyphae. Similar results were found in experiments where the downstream effector of Cdc35, the protein kinase A was deleted. In that experiment, Bockmuhl and colleagues showed that when one of the two genes encoding for the catalytic subunits of the protein kinase A, *TPK2*, was deleted and the other subunit, *TPK1*, repressed to very low-expression levels, the hyphal program was abolished, even under strong hyphal induction conditions (serum plus 37°C) [164].

The main effector of the cAMP-mediated PKA pathway is the transcription factor Efg1, which, dependent on environmental conditions, regulates hyphae-stimulating or repressing gene expression. Efg1 activity is modulated by association with other transcription factors, such as Czf1, Efh1 or Flo8 [165,166,167]. One important downstream effector of Efg1 is the transcription factor Tec1, which directly modulates hyphal-specific gene expression [168]. Tec1 activity, however, is influenced by yet another transcription factor, Cph2, which acts in an Efg1-independent way [169]. The target genes of the cAMP-mediated PKA pathway that are activated by Tec1 upon hyphal induction mostly encode for secreted or cell wall proteins. These so-called hyphae-specific genes have been identified on the basis of microarray studies and include the

following core set of genes: *ECE1*, *HWP1*, *HYR1*, *ALS1, ALS3, RBT1*, *RBT4*, *SAP5*, *SAP6*, *DDR48*, *SOD5* and *IHD2* [140,166,170,171].

IV.1.3. The MAPK and other pathways

Compared to the cAMP-mediated PKA pathway, the MAPK pathway plays a less significant role in morphological switching. Many mutants that have been constructed in this pathway show condition-dependent morphological defects, most of which are only minor. For instance, the serine/threonine kinase Ste20 (synonym Cst20), which is dependent on Ras1 signalling for activation, is defective in filamentation under nutrient-limiting conditions (Spider media), but still forms hyphae in serum [107,172]. Similar results were found for the gene encoding for the MAPKK Ste7, as well as for the gene encoding for the MAPK, Cek1 (synonym Erk1) [173]. The MAPK pathway converges on the transcription factor Cph1, which is one of the main effectors regulating the filamentous program in the MAPK pathway [174]. Cph1 regulates the expression of a few hyphae-specific genes in response to serum and high temperature (37°C), including the secreted protein Ece1, the transcription factor Tye7, the flavo-hemoglobin Yhb1, as well as Hwp1, which encodes for a hyphae-specific cell wall protein that is essential for adhesion to epithelial cells [175].

Another pathway involved in regulating morphogenesis includes a transcriptional repressor system, where Tup1 associates with the co-repressors Nrg1 and Rfg1 under conditions favouring yeast-growth to repress hyphae-specific genes [128,176,177]. Microarray studies have been used to elucidate to which degree each repressor influences hyphae-specific gene expression. For instance, about half of the genes that were significantly increased in the *rfg1* mutant were also de-repressed in *tup1* cells, and 95% of genes with increased expression in *nrg1* cells were also under the control of Tup1 [178]. Results of these and other studies suggest that Tup1 is the major transcriptional repressor as it has a significant number of genes exclusively under its control [158].

Yet another pathway regulating morphogenesis in *C. albicans* is the pH responsive pathway, which works mainly through Rim101. This transcription factor is activated at neutral pH by a cysteine protease, Rim13, by proteolytic cleavage at the C-terminus. Other factors influencing Rim101 activation include Rim8 and Rim20, as well as some predicted transmembrane proteins (Rim9, Rim21, Dfg16), and a number of subunits of the ESCRT complex [179,180]. Rim101 can both positively and negatively influence transcription, for example by activating Phr1 and repressing Phr2, two almost functionally redundant cell wall glycosidases that are important for adaptation to either neutral or acidic conditions in the host [181,182]. Upon activation, Rim101 also represses Nrg1, which leads to de-repression of some hyphae-specific genes [183].

Finally, recent studies have shown that a number of other pathways are involved in morphogenesis, for example the protein kinase C pathway [167,184], the high osmolarity glycerol pathway [158], as well as the calcineurin pathway [185]. These and other pathways regulate morphogenesis in *C. albicans* in either a condition-dependent manner or by directly influencing the cAMP-PKA pathway.

Taken together, the numerous environmental signals effecting morphogenesis in *C. albicans* are transmitted by a variety of signalling pathways to regulate hyphae-specific gene expression. The main pathway regulating the yeast-to-hyphal switch is the cAMP-mediated PKA pathway, because mutants in this pathway are unable to form hyphae under many experimental conditions, including strong hyphal induction signals.

IV.1.4. Evidence linking morphology to virulence

One of the first experimental evidences that the yeast-to-hyphal switch is important for the pathogenicity in *C. albicans* was published in 1997 [106]. In that work, the authors demonstrated that a *C. albicans* mutant strain lacking Cph1 and Efg1 is locked in the yeast growth phase and avirulent in a mouse model of disease. Since that landmark publication, around 130 *C. albicans* mutants have been constructed and tested for virulence. Strikingly, the huge majority (93%) of those mutants that showed defects in

morphology (116 mutants) were also affected in virulence (108 mutants), thus supporting the initial observation that the yeast-to-hyphal switch is a good preliminary measure to assess pathogenicity [186]. A recent study has now looked at the link between morphology and virulence in more detail and has come to the conclusion that the two traits are not as intimately linked as previously assumed [186]. In that study, Noble and colleagues created a set of 674 homozygous deletion mutants (the largest deletion mutant set publicly available), and tested them for various defects, including morphology and virulence. They found that among 103 mutants that showed virulence defects, 48 (or 47%) had no obvious morphological defect, thus challenging the paradigm that virulence strictly depends on the ability to switch between the yeast and hyphal forms. Noble and colleagues explain the discrepancy between their study and previous studies in part by the fact that previous studies have primarily used *URA3* as marker to construct deletion mutants. The disadvantage of using *URA3* as marker is that inadequate *URA3* expression influences both virulence and morphology, so that differential marker activity depending on chromosomal position could easily confound proper analysis of these phenotypes [187]. In addition, many of the mutants previously tested for virulence are in major signalling pathways, such as the cAMP-mediated PKA or MAPK pathway, which can lead to morphology-independent defects involved in pathogenesis [187]. Another reason for this discrepancy could be that previous studies have not taken into account that genetic manipulation of *C. albicans* can frequently lead to aneuploidy, which can also influence virulence [188,189].

Despite this shift in the paradigm, the ability to switch between the yeast and hyphal form can still be regarded as a valuable prediction for pathogenicity, as evidenced by *in vitro* studies that have shown that filamentation is important for evasion from host immune cells, such as phagocytes and blood vessels [190,191]. In those studies, the authors demonstrated that the hyphal morphology of *C. albicans* resulted in rupture of the host cells, thus leading to release of the pathogen. Given the link of these *in vitro* observations between hyphal morphology and penetration of host cells, one current view is that hyphae are important during early stages of infection when *C. albicans* penetrates tissues, while yeast cells are more important during later stages of infection to rapidly disseminate within the host.

Having provided an overview of how morphology is regulated with a strong emphasis on the yeast-to-hyphae transition, I am now going to present our published work where I used forward genomic tools to tackle this switch in *C. albicans*. The goal here was to find genes regulating morphology.

IV.2. Forward genetics in *Candida albicans* that reveals the Arp2/3 complex is required for hyphal formation, but not endocytosis

Originally published in:
Mol Microbiol. 2010 Mar;75(5):1182-98. Epub 2010 Feb 4. || PMID: 20141603

Molecular Microbiology (2010) 75(5), 1182–1198 ■
doi:10.1111/j.1365-2958.2009.07038.x
First published online 5 February 2010

Forward genetics in *Candida albicans* that reveals the Arp2/3 complex is required for hyphal formation, but not endocytosis

Elias Epp,[1,2] Andrea Walther,[3] Guylaine Lépine,[4] Zully Leon,[1] Alaka Mullick,[1] Martine Raymond,[4] Jürgen Wendland[3] and Malcolm Whiteway[1,2]*

[1]*Biotechnology Research Institute, National Research Council of Canada, Montréal, QC H4P 2R2, Canada.*
[2]*Department of Biology, McGill University, Montréal, QC H3A 1B1, Canada.*
[3]*Yeast Biology, Carlsberg Laboratory, Gamle Carlsberg Vej 10, Valby Copenhagen, Denmark.*
[4]*Institut de Recherche en Immunologie et en Cancérologie (IRIC), Université de Montréal, Montréal, QC H3C 3J7, Canada.*

Summary

Candida albicans **is a diploid fungal pathogen lacking a defined complete sexual cycle, and thus has been refractory to standard forward genetic analysis. Instead, transcription profiling and reverse genetic strategies based on *Saccharomyces cerevisiae* have typically been used to link genes to functions. To overcome restrictions inherent in such indirect approaches, we have investigated a forward genetic mutagenesis strategy based on the UAU1 technology. We screened 4700 random insertion mutants for defects in hyphal development and linked two new genes (*ARP2* and *VPS52*) to hyphal growth. Deleting *ARP2* abolished hyphal formation, generated round and swollen yeast phase cells, disrupted cortical actin patches and blocked virulence in mice. The mutants also showed a global lack of induction of hyphae-specific genes upon the yeast-to-hyphae switch. Surprisingly, both *arp2Δ/Δ* and *arp2Δ/Δarp3Δ/Δ* mutants were still able to endocytose FM4-64 and Lucifer Yellow, although as shown by time-lapse movies internalization of FM4-64 was somewhat delayed in mutant cells. Thus the non-essential role of the Arp2/3 complex discovered by forward genetic screening in *C. albicans* showed that uptake of membrane components from the plasma membrane to vacuolar structures is not dependent on this actin nucleating machinery.**

Accepted 21 December, 2009. *For correspondence. E-mail malcolm.whiteway@cnrc-nrc.gc.ca; Tel. (+1) 514 496 6146; Fax (+1) 514 496 6213.

Introduction

Candida albicans is among the leading causes of hospital-acquired mycosis with an estimated mortality rate of 38–49% (Pfaller and Diekema, 2007; Koh *et al.*, 2008; Leroy *et al.*, 2009). Although found as a normal commensal in the gastrointestinal tracts and mouths of 70% of the healthy human population, *C. albicans* can become life-threatening to the increasing population of immunocompromized individuals that result from conditions such as HIV infections and organ transplatation and from patients undergoing broad-spectrum-antibiotic or chemotherapy treatments (Ruhnke and Maschmeyer, 2002; Pfaller and Diekema, 2007). Identifying new genes involved in the virulence of this fungus remains a challenge, especially because genetic manipulation and functional characterization studies in *C. albicans* have been limited because of its diploidy, the absence of a true sexual cycle and the pathogen's use of a non-canonical genetic code that translates CUG into a serine instead of a leucine (Kurtz *et al.*, 1988).

The well-studied yeast *Saccharomyces cerevisiae* has frequently been used as a model to identify functions in *C. albicans*. For instance, our understanding of morphogenesis, signal transduction, mating and drug resistance in *S. cerevisiae* has led to successful gene discovery and subsequently to functional analysis in the fungal pathogen (Berman and Sudbery, 2002; Casamayor and Snyder, 2002; Schwartz and Madhani, 2004; Bennett and Johnson, 2005; Berman, 2006; Whiteway and Bachewich, 2007; Cowen, 2008). There are, however, evident limitations to using yeast to define *C. albicans* processes. For example, clear homologues of many *S. cerevisiae* proteins have not been identified in *C. albicans* (Weig *et al.*, 2004; Bennett and Johnson, 2005; Braun *et al.*, 2005). In other cases a homologue of a *S. cerevisiae* gene was identified in *C. albicans*, but no functional conservation could be observed (Nicholls *et al.*, 2004; Santos *et al.*, 2004). Moreover, determining function based on

homology can become particularly challenging in cases where the yeast model lacks the process under investigation.

One such example is hyphal morphogenesis in *C. albicans*. Although for many years researchers have relied on principles of bud emergence in *S. cerevisiae* in an attempt to understand hyphal formation of filamentous fungi such as *C. albicans*, several features of hyphal growth cannot be explained by extrapolating findings from the model yeast (Harris and Momany, 2004). Overall, this reversible yeast-to-hyphal switch has been intensively studied in the polymorphic fungus (Liu, 2001; Whiteway and Bachewich, 2007). Well-known environmental signals that trigger the morphological transition involve high temperature (37°C), serum, neutral pH, starvation, CO_2, adherence and *N*-acetylglucosamine (GlcNAc) (Gow, 1997; Sudbery *et al*., 2004). Multiple pathways, for instance the cAMP protein kinase, MAP kinase or the pH-responsive pathways then transmit these signals to activate expression of hyphal-specific genes (Biswas *et al*., 2007). The importance of the yeast-to-hyphae transition in *C. albicans* is highlighted by its implication in virulence; *C. albicans* mutants unable to switch between a yeast and hyphal growth mode are greatly reduced in virulence in mouse infection models (Lo *et al*., 1997; Laprade *et al*., 2002; Kumamoto and Vinces, 2005). It has been proposed that while the yeast form contributes to the dissemination of an infection in the host, the hyphal form facilitates penetrating tissue surfaces and escaping host cell internalization (Gow *et al*., 2002; Whiteway and Oberholzer, 2004).

With the goal of identifying new genes involved in the yeast-to-hyphae transition in *C. albicans*, we have used an unbiased approach for randomly generating homozygous null mutants directly in the pathogen. Screening 4700 random transposon insertion mutants identified two new genes, *ARP2* and *VPS52*, which are both required for hyphal formation. Surprisingly, in contrast to many other organisms, the highly conserved Arp2/3 complex was not essential for viability or endocytosis in *C. albicans*, while structural differences in actin organization support the importance of a functional cytoskeletal architecture in permitting morphological switching. These findings underline the potential for forward genetics in the pathogen itself to link functions to genes.

Results

Strategy for an in vivo *random forward mutagenesis screen in* C. albicans

The UAU1 marker cassette (Enloe *et al*., 2000) allows the selection of homozygosed mutants in the diploid organism *C. albicans*. This insertional mutagenesis strategy employs a single transformation in an *arg4/arg4*, *ura3/ura3* double auxotrophic background selecting initially for Arg^+/Ura^- colonies (genotype *orf::UAU1/ORF*), then allowing mitotic recombination to homozygose the insertion (genotype *orf::UAU1/orf::UAU1*), and following this with a second round of selection yielding Arg^+/Ura^+ segregants (genotype *orf::UAU1/orf::URA3*) that potentially carry a homozygous disruption at the site of the initial insertion. Mitchell *et al.* (Davis *et al*., 2002) have used this UAU1 marker cassette to randomly mutagenize *in vitro* the genome of *C. albicans*. This *in vitro* random mutagenesis resulted in a pool of plasmids each carrying the UAU1 marker cassette flanked by a specific *C. albicans* genomic DNA sequence. We used the entire pool, rather than a chosen set of characterized UAU1 plasmids, to randomly mutagenize the genome of *C. albicans in vivo*, and then screened the potentially homozygous *orf::UAU1/orf::URA3* inserts for a phenotype of interest.

To assess whether it is possible to extract a desired phenotype by using the entire UAU1 plasmid pool, we created a preliminary set of 300 *orf::UAU1/orf::URA3* random insertion mutants and screened for specific auxotrophic mutants. We found one mutant that was unable to grow on SD-Trp media (Fig. 1A). To map this mutation we performed inverse PCR (Ochman *et al*., 1988) and found the transposon insertion in *TRP1* (*ORF19.6096*), the phosphoribosylanthranilate isomerase gene. *TRP1* is an essential enzyme for tryptophan biosynthesis, and mutating this gene results in tryptophan auxotrophy (Ostrander and Gorman, 1994).

In an attempt to link genes to more challenging and less conserved phenotypes between fungal species, such as carbon source utilization (Martchenko *et al*., 2007a,b; Askew *et al*., 2009), we expanded the number of *orf::UAU1/ORF* insertions to about 5000. From these we obtained about 4700 (94%) that generated Arg^+Ura^+ segregants that represent potential *orf::UAU1/orf::URA3* derivatives. Among them we found one insertion mutant (*Tn-orf19.875*) that cannot grow on glycerol (Fig. 1B). A deletion mutant and revertant strain confirmed the link between growth defects on glycerol and this uncharacterized *C. albicans* gene that has no obvious homologues in budding and fission yeast (Arnaud *et al*., 2007). Thus, this preliminary screen for auxotrophs and mutants that can not grow on media containing glycerol as the sole carbon source showed that it is possible to directly link functions to a gene by using the whole pool of UAU1 plasmids.

Screening for random mutants involved in hyphal formation

In order to link genes to a phenotype that is absent *S. cerevisiae*, we phenotypically analysed the 4700 candidate homozygotes for hyphae formation defects. No con-

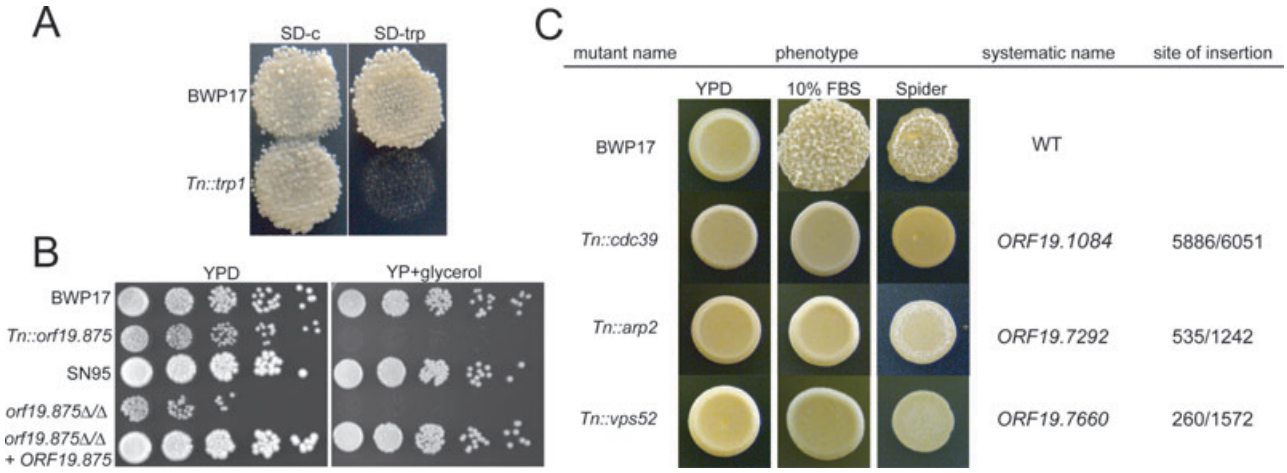

Fig. 1. Phenotypic hits resulting from forward genetics screening.
A. Screening for auxotrophs identified *TRP1*. The picture shows replica-plating of WT (BWP17) and an insertion in *TRP1* (*Tn::trp1*) on SD-complete (SD-c) versus SD-c minus tryptophan (SD-trp) media.
B. Screening for glycerol-sensitive mutants identified *ORF19.875*. An over night culture was adjusted to OD_{600} of 0.1 and then 10-fold serially diluted. Two microlitres was then spotted, and plates were incubated for 2 days before being photographed.
C. Examples of phenotypic hits involved in hyphal formation. Hyphae formation was assessed by spotting 10 μl of an over night culture diluted to OD_{600} 0.1 on different hyphae inducting media (10% FBS and Spider) or YPD media. Plates were incubated at 37°C for 2–3 days and photographed. Transposon insertions in *CDC39* (*Tn::cdc39*), *VPS52* (*Tn::vps52*) and *ARP2* (*Tn::arp2*) blocked wrinkle formation on the cell surface on all inducing media. The last column indicates the site of insertion, relative to the start codon, over the entire length of the ORF. See also Fig. S1 for morphology phenotypes associated with the remaining nine potential insertion mutant hits.

vincingly hyper-filamentous colonies were identified. By contrast, we isolated a total of 20 mutants with a strong and consistent hypo-filamentous phenotype and confirmed these phenotypes by retesting a single colony from each mutant. Mapping the 20 hits by inverse PCR showed that 11 insertions were directly in an ORF, while one insertion was mapped in the promoter of *ORF19.860*. In the remaining eight events we either could not map the insertion because of repeated sequences (six events) or they fell in an intergenic region (two events). Mutants that had a transposon insertion in an intergenic region were excluded from further analysis as it was unclear if the observed phenotype was linked to one of the genes adjacent to the transposon insertion. Figures 1C and S1 summarize hypo-filamentation phenotypes of the 11 ORF and one promoter insertion mutant hits as determined by plate assays. To distinguish between hypo-filamentation and non-filamenting phenotypes, we analysed the 11 ORF and one promoter hypo-filamentation insertion mutants under liquid hyphal inducing conditions [Yeast extract, peptone, dextrose (YPD) media + 10% fetal bovine serum (FBS) at 37°C for 3 h] and found that insertions in *CDC39, VPS52* and *ARP2* failed to form true hyphae in liquid.

VPS52 *and* ARP2 *deletion mutants do not form hyphae*

CDC39 was previously linked to a hypo-filamentation phenotype (Uhl *et al*., 2003), while *ARP2* and *VPS52* were newly identified mutants that could not form hyphae under liquid-inducing conditions. We validated these latter two transposon insertion hits by both verifying the absence of the WT band in each transposon mutant and constructing deletion mutants (Fig. S2). To confirm that *ARP2* and *VPS52* mutants are unable to form true hyphae, we re-analysed polarized morphogenesis under hyphal inducing conditions in liquid culture (Fig. 2). *Tn::arp2* (the transposon mutant for *ARP2*), *arp2Δ/Δ* (the deletion mutant for *ARP2*), *Tn::vps52* and *vps52Δ/Δ* did not form true hyphae, while BWP17 (WT strain for all transposon mutants) and SN95 (WT strain for all deletion mutants), both heterozygous mutants (*arp2/ARP2*, *vps52/VPS52*) as well as the *ARP2* and *VPS52* revertants (*arp2Δ/Δ + ARP2*, *vps52Δ/Δ + VPS52*) did.

To analyse polarized morphogenesis in more detail, we stained strains with calcofluor white (CFW) to assess what percentage of cells were growing as yeast, pseudohyphae or true hyphae (Fig. 2B). Cells that had the first septum/septin ring located in the growing bud tube and showed no constrictions at septal junctions were considered true hyphae (Sudbery *et al*., 2004). Under the conditions tested, more than 96% of the WT strain and both heterozygotes and revertants were growing as true hyphae. On the other hand, no true hyphal formation was observed in either *arp2Δ/Δ* or *vps52Δ/Δ* cells, while 60% of *arp2Δ/Δ* and 77% of *vps52Δ/Δ* cells were found to grow as pseudohyphae and 40% of *arp2Δ/Δ* and 23% of *vps52Δ/Δ* cells were still in the yeast state.

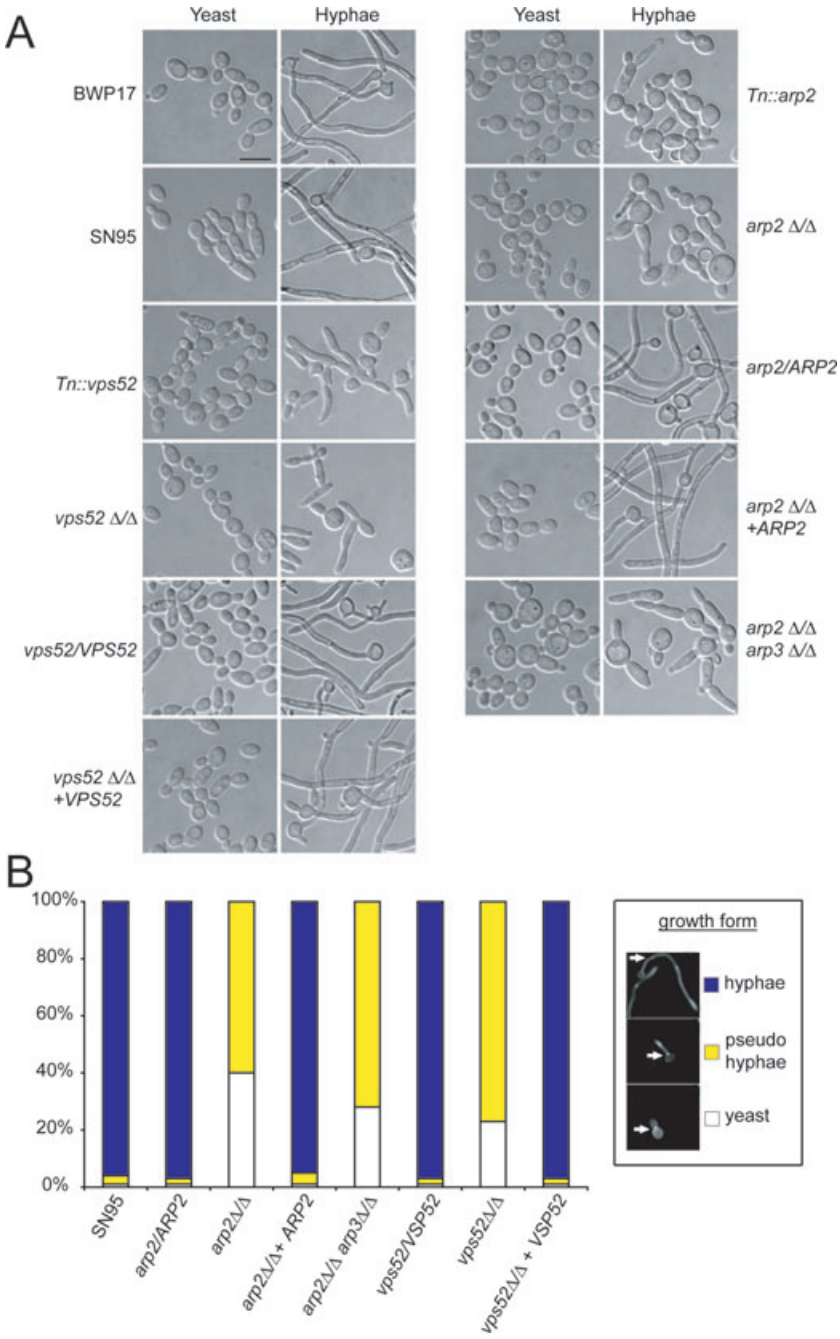

Fig. 2. *VSP52* and Arp2/3 complex mutants do not form hyphae.
A. Overnight cultures grown in YPD media were diluted 1:200 in YPD (yeast conditions) or YPD + 10% FBS (hyphae conditions) and placed for 3 h at either 30°C (yeast) or 37°C (hyphae). Both transposon and deletion mutants for *VSP52* and *ARP2* do not form hyphae under these conditions. Heterozygous mutants and revertants behaved like WT. An *arp2Δ/Δarp3Δ/Δ* double knockout showed identical behaviour compared with the *arp2Δ/Δ* single knockout. Bar = 10 μm.
B. Quantifying polarized morphogenesis. Hyphal induction was done as described for (A). While > 96% of WT, heterozygous and revertant strains formed true hyphae, the majority of *vps52Δ/Δ, arp2Δ/Δ* and *arp2Δ/Δarp3Δ/Δ* mutants did not form hyphae and grew as pseudohyphae instead. $n > 200$ for each strain.

Taken together, the hyphal-deficient transposon insertion phenotypes for *ARP2* and *VPS52* were confirmed by deletion mutants and by reverting phenotypes after reintroduction of the WT genes. Comparative genome hybridization analysis further showed that no aneuploidies were found in the *arp2Δ/Δ* or *vps52Δ/Δ* strains (Fig. S3). Because other *C. albicans* vacuolar protein sorting (VPS)-type mutants such as *vps11Δ/Δ*, *vps28Δ/Δ*, *vps32Δ/Δ* and the conditional *vps1Δ/VPS1-tetR* mutant showed hyphal formation defects similar to *vps52Δ/Δ* cells (Palmer *et al.*, 2003; Cornet *et al.*, 2005; Bernardo *et al.*, 2008), we decided to focus further investigation on the Arp2/3 complex.

C. albicans *Arp2/3 complex mutants show dramatic actin cytoskeleton defects, but are still able to endocytose*

ARP2 encodes one of seven evolutionary conserved subunits of the Arp2/3 complex, which nucleates actin filaments (F-actin) into branched networks (Machesky *et al.*, 1994; Welch *et al.*, 1997). Given its conserved association

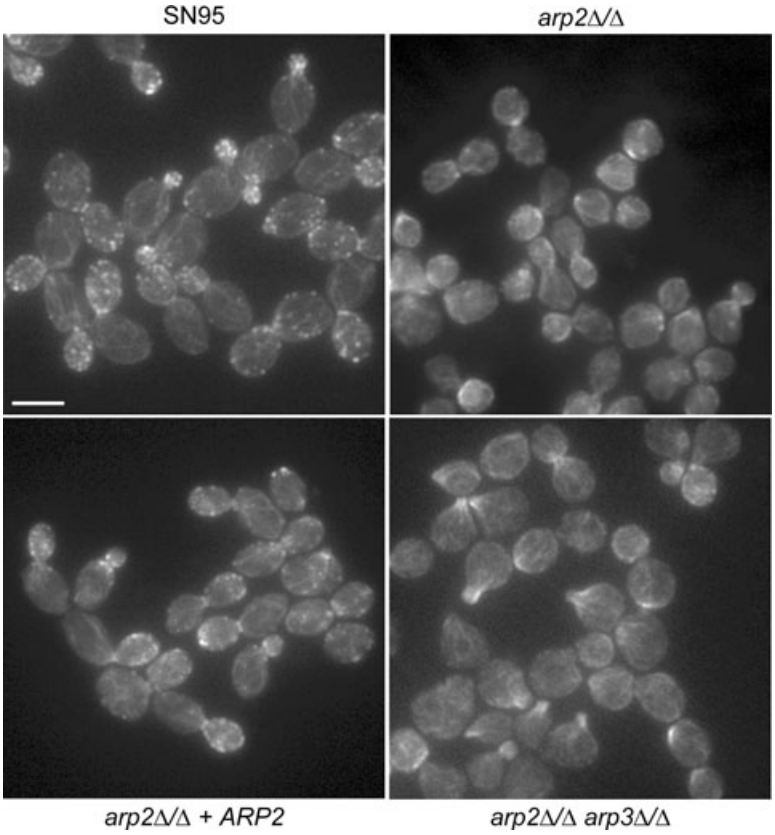

Fig. 3. Assaying actin cytoskeleton structures in Arp2/3 complex mutants. Rhodamine/phalloidin staining was used to visualize the actin cytoskeleton in logarithmically growing yeast cells. In WT (SN95) cells, actin patches localize to sites of polarized growth in most phases of the cell cycle. Independent of the cell cycle, distinctive actin patch structures were not observed in *arp2Δ/Δ* or *arp2Δ/Δarp3Δ/Δ* cells. Actin cables seemed unaffected in mutant cells. Bar = 5 μm.

with actin regulation, we asked how deletion of *ARP2* in *C. albicans* affects the actin cytoskeleton by staining logarithmically growing yeast cells with rhodamine/phalloidin (Fig. 3). In contrast to WT stained cells where actin patches are observed as bright dots localizing to sites of polarized growth, the *C. albicans arp2Δ/Δ* mutant did not show such distinct, bright actin patches. Instead, the most prominent actin structures that formed in *arp2Δ/Δ* cells were large filamentous aggregates similar to those observed in conditional *arp2* and *arp3* mutants of *S. cerevisiae* or in *bee1/las17* yeast mutants, which also lack actin patches (Li, 1997; Winter *et al.*, 1997; Martin *et al.*, 2005). On the other hand, other actin-based structures such as actin cables and cytokinetic rings were still observed in *arp2Δ/Δ* cells (Fig. 3). When only one copy of the *ARP2* gene was present (*arp2Δ/Δ* + *ARP2*), distinct actin patches were observed and hyphal formation was restored, but these patches appeared less frequent when compared with WT. A double KO mutant, where the two copies of both *ARP2* and *ARP3* were deleted (*arp2Δ/Δarp3Δ/Δ*), showed similar morphological phenotypes to the *arp2Δ/Δ* single mutant. These mutants also exhibited hyphal formation defects, cells clumping together when grown in logarithmic phase, and individual cells appearing phenotypically round and swollen with a wider bud neck as well as similar actin cytoskeleton defects (Figs 2 and 3).

Because assembly of actin filaments mediated by the Arp2/3 complex has been shown to be an essential part of endocytosis in a wide range of organisms (for reviews see: Goley and Welch, 2006; Kaksonen *et al.*, 2006; Galletta and Cooper, 2009), we stained *C. albicans* Arp2/3 complex mutants with the lipophilic dye FM4-64, which is commonly used to visualize membrane internalization and endocytotic delivery to the vacuole (Vida and Emr, 1995). Both *arp2Δ/Δ* and *arp2Δ/Δarp3Δ/Δ* mutants were clearly able to deliver FM4-64 to the vacuole as observed by the intracellular appearance of the dye after a 45 min chase period (Fig. 4A). In some Arp2/3 mutant cells, however, the vacuolar morphology appeared to be fragmented, which sometimes resulted in staining throughout the vacuole. While in WT cells typically one to three vacuoles were apparent, four or more smaller vacuoles could be observed in Arp2/3 complex mutant cells. This fragmented vacuolar morphology has also been described for *C. albicans wal1Δ/Δ* (*LAS17* in *S. cerevisiae*) mutants, an activator of the Arp2/3 complex (Walther and Wendland, 2004).

As some *S. cerevisiae* conditional Arp2/3 complex mutants were partially able to endocytose FM4-64, but not LY (Lucifer Yellow is a dye taken up by fluid phase endocytosis) (Riezman, 1985; Moreau *et al.*, 1996; 1997; Martin *et al.*, 2005; Daugherty and Goode, 2008), we assessed LY uptake in *C. albicans* Arp2/3 complex

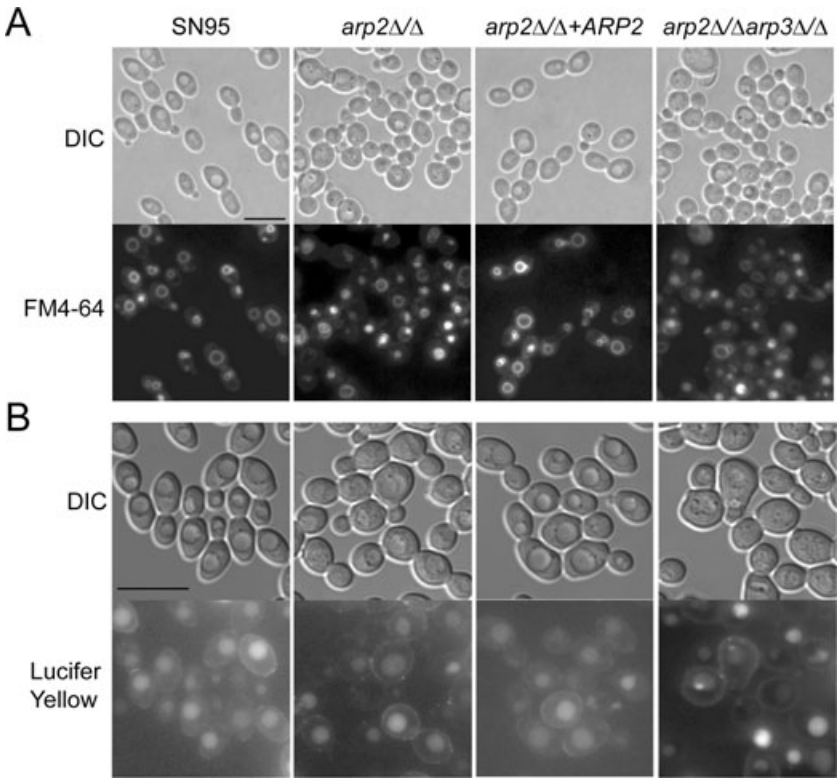

Fig. 4. Arp2/3 complex mutants can still endocytose FM4-64 and LY.
A. Cells in logarithmic phase were incubated for 5 min with 20 μM FM4-64, washed twice, chased for 45 min and visualized by epifluorescence microscopy. Under these conditions, the dye is endocytosed and reliably visualized by vacuolar membrane staining in WT (SN95) and mutant cells.
B. Logarithmically growing cells were incubated with 4 mg ml^{-1} Lucifer Yellow (LY), incubated for 90 min, washed twice and visualized. LY is endocytosed in both WT and Arp2/3 complex mutants. Bars = 10 μm.

mutants. No difference in LY uptake was observed in Arp2/3 mutants when compared with WT after 90 min incubation (Fig. 4B).

To quantitatively assess endocytosis, we performed time-lapse microscopy and included a *C. albicans myo5Δ/Δ* mutant that has been shown to be endocytosis-defective (Oberholzer *et al*., 2004). Co-incubation of GFP-labelled WT *C. albicans* with either *arp2Δ/Δ, arp2Δ/Δarp3Δ/Δ* or *myo5Δ/Δ* cells confirmed that endocytosis still occurred in *arp2Δ/Δ* and *arp2Δ/Δarp3Δ/Δ* mutants, while *myo5Δ/Δ* cells did not endocytose FM4-64 within 3 h (see movies 1, 2, 3 and 4 as well as Fig. S4, which can be found in the *Supporting information*). However, vacuolar staining was somewhat delayed in *arp2Δ/Δ* and *arp2Δ/Δarp3Δ/Δ* cells; FM4-64 staining appeared after 20–30 min in WT cells, and it took between 70 and 80 min until the dye reached the vacuole in the *arp2Δ/Δ* and *arp2Δ/Δarp3Δ/Δ* mutants. In both *arp2Δ/Δ, arp2Δ/Δarp3Δ/Δ* and *myo5Δ/Δ* cells, the dye initially appeared as punctate-like dots apparently stuck in the plasma membrane. As dye-internalization occurred in *arp2Δ/Δ* and *arp2Δ/Δarp3Δ/Δ* cells over time, the bright dots at the membrane slowly faded at the same time as vacuolar staining began to emerge. In *myo5Δ/Δ* cells, on the other hand, bright dot-like structures remained at the cell membrane until the end of our observations with no distinct vacuolar structures appearing. Taken together, these results suggest the Arp2/3 complex plays a crucial role in actin cytoskeleton organization in *C. albicans*, and while clearly delayed in endocytosis, Arp2/3 complex mutants can still endocytose as assessed by FM4-64 or LY uptake.

Transcriptional analysis of Arp2/3 complex mutants

To gain insights into cellular processes affected by disrupting Arp2/3 complex functions, we performed transcriptional profiling under yeast growth conditions (YPD at 30°C for 3 h) or hyphal induction (YPD + 10% FBS at 37°C for 3 h) and compared transcriptional consequences of deleting *ARP2* to *MYO5* and *SLA2* microarray data sets (Oberholzer *et al*., 2006). *MYO5* is an Arp2/3 complex activator, while *SLA2* is an actin binding protein that couples actin to the vesicle coat during endocytosis (Robertson *et al*., 2009a). Both *sla2Δ/Δ* and *myo5Δ/Δ C. albicans* mutants suffer similar related complications, such as no hyphal formation, delocalized actin patches and endocytosis defects (Asleson *et al*., 2001; Oberholzer *et al*., 2002; 2004). Despite using different chip platforms and different WT strains, there was a good overall correlation of the *ARP2* microaray data set and the *MYO5* and *SLA2* data sets (compare 'HY Epp' and 'HY Oberholzer' in Fig. 5A, Table S1 shows numerical values for each correlation coefficient). When significantly regulated genes (more than twofold, $P < 0.05$) were compared, deleting *ARP2*, *MYO5* or *SLA2* resulted in similar cellular responses, although the overlap of regulated genes was

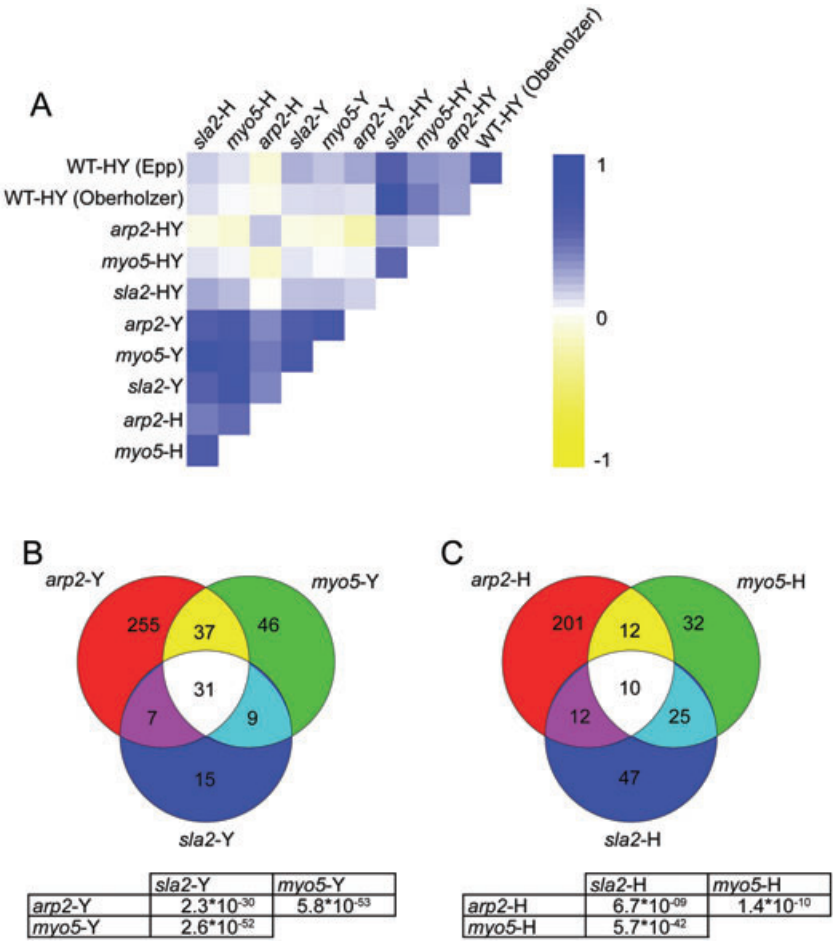

	sla2-Y	myo5-Y
arp2-Y	$2.3*10^{-30}$	$5.8*10^{-53}$
myo5-Y	$2.6*10^{-52}$	

	sla2-H	myo5-H
arp2-H	$6.7*10^{-09}$	$1.4*10^{-10}$
myo5-H	$5.7*10^{-42}$	

Fig. 5. Transcript similarities of the *ARP2* microaray data set and *MYO5/SLA2* data sets.
A. Pearson analysis showing the overall correlation of *ARP2* and *MYO5/SLA2* microarray data sets. Note that for this analysis no selection of significantly regulated genes was made. The conditions include comparing WT and mutant strains grown under hyphal growth conditions to the same strains grown under yeast growth conditions (HY) and comparing *arp2Δ/Δ*, *myo5Δ/Δ* and *sla2Δ/Δ* mutants against WT cells under yeast (Y) or hyphal (H) growth conditions. 'WT-HY (Epp)' and 'WT-HY (Oberholzer)' correspond our and the data set obtained by Oberholzer *et al.* respectively. A value of one (dark blue) corresponds to perfect correlation and –1 (dark yellow) to inverse correlation.
B and C. Venn diagrams showing that deleting *ARP2*, *MYO5* and *SLA2* resulted in similar transcriptional consequences when only significantly regulated genes were compared. *P*-values of overlap are given below the Venn diagram. B shows data from yeast form cells, C shows data from hyphal form cells.

much more significant under yeast compared with hyphal growth conditions (Fig. 5B and C). To further compare the transcriptional response of *arp2Δ/Δ* mutants upon hyphal induction, hyphae-specific genes, i.e. genes that are significantly regulated (more than twofold, $P < 0.05$) in our WT-HY comparison, were clustered in Fig. 6. Many of the genes in that list are known to become highly induced upon activation of the hyphal programme, for example *ECE1*, *ALS3*, *HYR1*, *SAP5*, *SAP6*, *HWP1*, *RBT8*, *IHD1*, *PST1*, *CIP1*, *DCK1* and *ORF19.1691* (Nantel *et al.*, 2002; Garcia-Sanchez *et al.*, 2005; Kadosh and Johnson, 2005) (Table S2). Deleting *ARP2* resulted in a global lack of hyphal-specific gene induction (arp2-H in Fig. 6). When arp2-Y was compared directly with arp2-H, this observation of improper hyphae-specific gene induction was confirmed as > 92% or 35 out of 38 of the most highly upregulated (more than fourfold) hyphae-specific genes were at least twofold less induced in the absence of *ARP2* and > 95% or 75 out of 79 of the remaining upregulated hyphae-specific genes were less induced in *arp2Δ/Δ* mutants compared WT cells (Fig. 6, Table S2). Deleting *myo5Δ/Δ* resulted in a comparable response in that some hyphae-specific genes are not properly induced (Oberholzer *et al.*, 2006). However, the lack of proper gene induction was much more pronounced in the absence of *ARP2* than in the absence of *MYO5* (compare arp2-H vs. myo5-H in Fig. 6, Table S3). Together, these results suggest that while the *ARP2* profile showed significant similarities to the *MYO5* and *SLA2* profiles under yeast growth conditions, there was less correlation under hyphal growth conditions possibly because of the pronounced lack of proper hyphal-specific gene induction in the absence of *ARP2*.

These observations suggest the failure in hyphal growth of Arp2/3 complex mutants could be a result of either impaired endocytosis, problems with the actin cytoskeleton, failure to activate hyphal-specific genes or some combination of these defects. If the hyphal defect was primarily due to failure to activate gene expression, derepressing hyphal-specific gene expression by deleting the *NRG1* repressor could potentially suppress the defect, as deletion of *NRG1* leads to constitutive filamentous growth even in the absence of any hyphal induction signals (Garcia-Sanchez *et al.*, 2005; Kadosh and Johnson, 2005). We created an *nrg1Δ/Δarp2Δ/Δ* mutant, which exhibited a doubling time more than twice as long as WT

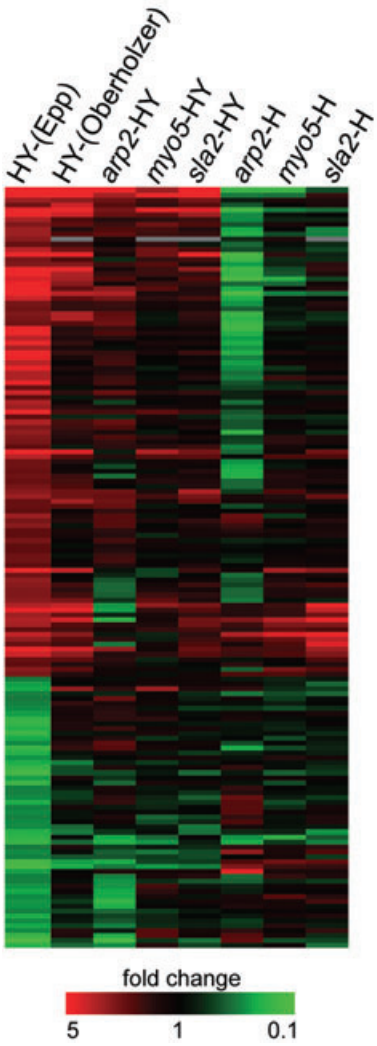

Fig. 6. Cluster tree of hyphae-specific genes. While the majority of hyphae-specific genes are not properly induced in the absence of *ARP2*, *MYO5* or *SLA2*, this lack of hyphal gene induction is most prominent in *arp2Δ/Δ* cells. Table S2 reports values used to create this cluster tree.

(Fig. S5). When grown under non-inducing conditions, *nrg1Δ/Δarp2Δ/Δ* cells showed the *arp2Δ/Δ* mutant morphology of round and swollen cells. When induced for hyphal growth, *nrg1Δ/Δarp2Δ/Δ* cells also exhibited the *arp2Δ/Δ* cell morphology and did not form hyphae even after extended overnight incubation times (Fig. 7). We also attempted to create a *tup1Δ/Δarp2Δ/Δ* mutant, but were not successful.

To determine if the hyphal-specific genes are derepressed in the *nrg1Δ/Δarp2Δ/Δ* mutant, we performed transcript profiling. We compared the *nrg1Δ/Δarp2Δ/Δ* mutant grown under hyphal conditions to the *arp2Δ/Δ* mutant grown under the same conditions (YPD + 10% serum, 37°C, 3 h) and found that a significant number of hyphal-specific genes that are normally induced when WT cells are undergoing the yeast-to-hyphae switch (WT-HY) showed greater expression in the *nrg1Δ/Δarp2Δ/Δ* mutant compared with *arp2Δ/Δ* cells (*P*-value 4.9×10^{-9}). When we examined the set of *NRG1*-dependent hyphal-specific genes previously identified (Kadosh and Johnson, 2005), we found that seven of 28 genes (*HYR1*, *SAP5*, *SAP4*, *KIP4*, *ORF19.6079*, *ALS3* and *UME6*) showed significantly increased expression (twofold or more) in *nrg1Δ/Δarp2Δ/Δ* cells compared with *arp2Δ/Δ* cells, while a further four genes (*IHD1*, *CBP1*, *ORF19.6705* and *ALS10*) showed moderately increased expression between 1.5- and 2-fold (Table S4). Thus, while deleting a transcriptional repressor of the filamentation programme leads to derepression of many hyphal genes, the entire regulated gene set is not derepressed; this presumably reflects the complex interplay that different transcriptional (co-)repressors exert on the yeast-to-hyphae transition (Garcia-Sanchez *et al.*, 2005; Kadosh and Johnson, 2005). We further found that despite the increased induction of some hyphal genes in the *nrg1Δ/Δarp2Δ/Δ* mutant, a few of those genes are not as highly induced as in WT cells (Table S4). One gene that was induced in both the '*nrg1Δ/Δarp2Δ/Δ* vs *arp2Δ/Δ*' and the '*nrg1Δ/Δarp2Δ/Δ* vs WT' comparisons is *UME6*, a recently identified key regu-

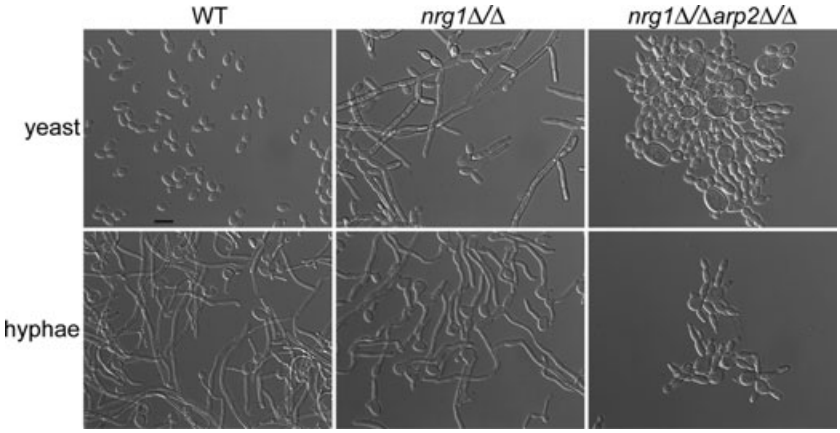

Fig. 7. The *nrg1Δ/Δarp2Δ/Δ* mutant phenocopies *arp2Δ/Δ* cell morphologies. Hyphal formation was assayed as described in Fig. 2A. Deletion of one transcriptional repressor for hyphal-specific genes, *NRG1*, leads to constitutive filamentous growth even in the absence of any hyphal signals (yeast). Deleting *NRG1* in the *arp2Δ/Δ* mutant (*nrg1Δ/Δarp2Δ/Δ*) did not restore filamentous growth even in the presence of hyphal signals (hyphae). Bar = 10 μm.

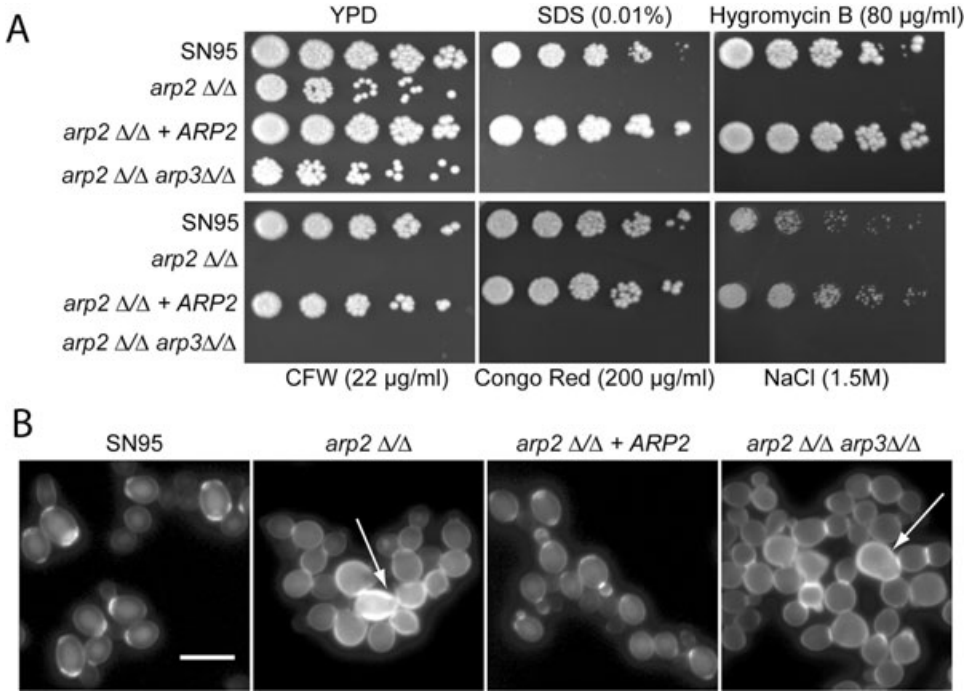

Fig. 8. Arp2/3 complex mutants show typical actin patch-associated phenotypes.
A. Plate spotting assays were done as described in Fig. 1 legend. Arp2/3 complex mutants show similar cell wall and cell membrane defects as well as salt sensitivity as previously described for *myo5Δ/Δ* mutants.
B. Arp2/3 complex mutants showed aberrant cell wall deposition, indicating defects in cell separation (arrows). See also movie 2 (*Supporting information*) with *arp2Δ/Δ* cells that show cell separation defects. Logarithmically growing cells were stained with CFW directly in YPD media for 5 min, washed and visualized. Bar = 10 µm.

lator of the hyphal programme (Banerjee *et al.*, 2008; Zeidler *et al.*, 2009). Interestingly, although constitutive overexpression of *UME6* in WT cells resulted in constitutive filamentous growth even in the absence of hyphae signals (Carlisle *et al.*, 2009), the increased expression level of *UME6* in the *nrg1Δ/Δarp2Δ/Δ* mutant is not sufficient to restore filamentation in the absence of a functional Arp2/3 complex. Thus despite partial derepression of the hyphal programme, hyphae do not form, making it likely other roles of the Arp2/3 complex, such as its function in actin patch formation and actin branching, are required for hyphal development.

Confirming 'actin-patch' phenotypes

Besides defects in filamentous growth, many phenotypes found in *myo5Δ/Δ* and *sla2Δ/Δ* mutants have been linked to the Arp2/3 complex and include cell membrane and cell wall defects as well as salt sensitivity (Oberholzer *et al.*, 2006). We tested whether these actin patch-associated phenotypes are also observed in Arp2/3 complex mutants. *arp2Δ/Δ* and *arp2Δ/Δarp3Δ/Δ* cells showed typical actin-patch phenotypes such as salt sensitivity as well as cell wall and cell membrane defects, illustrated by increased sensitivity to congo red, CFW, SDS and hygromycin B. Arp2/3 complex mutants also showed abnormal cell wall patterning with aberrant, relatively random chitin deposition (Fig. 8).

Transcriptional analysis also showed that many ergosterol genes (e.g. *ERG1*, *ERG5*, *ERG6*, *ERG10*, *ERG11*, *ERG27* and *ERG252*) were downregulated when *arp2Δ/Δ* cells were compared with WT cells in either yeast or hyphae condition (Table S5). We reasoned that Arp2/3 complex mutants might be more sensitive to drugs targeting this important component of fungal cell membranes. Figure 9 illustrates that both *arp2Δ/Δ* and *arp2Δ/Δarp3Δ/Δ* mutants showed increased sensitivity to the ergosterol targeting drug fluconazole, a phenotype that has also been described for *mob2Δ/Δ* cells, a key component of the RAM pathway that showed additional related actin-patch phenotypes (Song *et al.*, 2008). Taken together, many actin patch-associated phenotypes previously described for *myo5Δ/Δ*, *sla2Δ/Δ*, *wal1Δ/Δ* and *mob2Δ/Δ* cells could be confirmed with Arp2/3 complex mutants.

A functional Arp2/3 complex is required for virulence

Because the yeast-to-hyphae switch is one important virulence attribute, we tested the *arp2Δ/Δ* mutant for fungal replication in a complement-5 (C5)-deficient mouse model

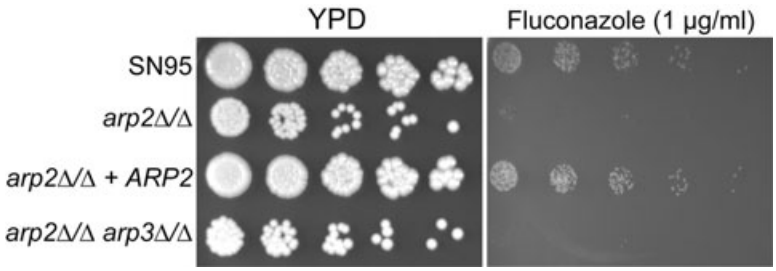

Fig. 9. Arp2/3 complex mutants show increased fluconazole sensitivity. *arp2Δ/Δ* and *arp2Δ/Δarp3Δ/Δ* mutants are more sensitive to the ergosterol targeting drug fluconazole compared with WT and revertant strains. Serial dilution and spotting was done as describe in Fig. 1 legend.

of disseminated candidiasis (Mullick *et al.*, 2004; 2006; Tuite *et al.*, 2005). Mice infected with the WT strain SN95 were moribund after 24 h post infection, while all mice infected with *arp2Δ/Δ* cells did not show any clinical signs such as lethargy, ruffled fur or hunched back even on day 4 post infection (Fig. 10A). This observation was confirmed by measuring fungal load from the kidney, the site of highest fungal replication in the A/J mouse model (Mullick *et al.*, 2004). WT-infected mice had a significantly higher fungal burden at 24 h post infection compared with the *arp2Δ/Δ*-infected mice sacrificed at the same time and at 4 days post infection hardly any fungal cells could be recovered from the kidneys of mice infected with *arp2Δ/Δ* mutants (Fig. 10B).

To gain further insights into the host–pathogen interaction and whether *arp2Δ/Δ* cells trigger a host response despite their reduced capacity to replicate in the A/J mice background, we biochemically analysed the host blood collected by heart puncture at 24 h post infection. We focused on two metabolic markers that typically show a specific response upon infection with *C. albicans* (Mullick *et al.*, 2006): levels of interleukin 6 (IL-6), a key inflammatory cytokine, and creatine kinase (CK), a cardiac protein, both of which become highly upregulated upon encounter with *C. albicans*. The blood from *arp2Δ/Δ* mutant-infected mice had significantly lower levels of IL-6 compared with WT-infected mice (Fig. 10C). Likewise, significantly lower amounts of CK were found in blood collected from mice infected with *arp2Δ/Δ* compared with the WT-infected mice (Fig. 10D). These results indicate that *arp2Δ/Δ* cells do not trigger a normal host response as determined by IL-6 and CK levels. Taken together, based on survival time, fungal burden and the biochemical analysis of the host blood, we conclude that *C. albicans arp2Δ/Δ* mutants are avirulent in this mouse model of infection.

Discussion

While the complete sequence of the *C. albicans* genome (assembly 20 became available in 2006), in combination with molecular tools such as epitope-tagging, inducible promoters, reporter genes, auxotrophic and dominant markers, has tremendously facilitated functional analysis in *C. albicans* (Care *et al.*, 1999; Reuss *et al.*, 2004; Nantel, 2006; Schaub *et al.*, 2006; Lavoie *et al.*, 2008), a comprehensive genome-wide collection of *C. albicans* mutants is not available, although clearly desirable for functional genomics. The inherent difficulty of genetic manipulation in *C. albicans* has resulted in only a few large-scale mutagenesis efforts capable of directly linking a gene to a cellular function (Roemer *et al.*, 2003; Uhl *et al.*, 2003; Nobile and Mitchell, 2005; Bruno *et al.*, 2006; Shen *et al.*, 2008). Here, we have investigated a forward genetics approach in *C. albicans*. Screening of 4700 insertion mutants showed that *VPS52* and *ARP2* are essential for the yeast-to-hyphae transition, demonstrating that this approach can successfully link genes to a phenotype of interest in *C. albicans*.

Advantages of forward genetics in C. albicans

Given that mutating any of the seven Arp2/3 complex subunits resulted in severe growth defects or lethality in *S. cerevisiae*, *Schizosaccharomyces pombe*, *Drosophila melanogaster* and *Caenorhbditis elegans* (Lees-Miller *et al.*, 1992; Schwob and Martin, 1992; Balasubramanian *et al.*, 1996; Mccollum *et al.*, 1996; Winter *et al.*, 1997; 1999; Hudson and Cooley, 2002; Zallen *et al.*, 2002; Sawa *et al.*, 2003), we were surprised that in *C. albicans* loss of two Arp2/3 complex subunits does not severely compromise viability (Fig. S5). Using reverse genetics by relying on other yeast models might have led to incorrect assumptions that the Arp2/3 complex is essential in *C. albicans* and therefore it might have escaped functional characterization. Functional analysis based on alternate models would also have proven challenging in linking *ORF19.875*, an uncharacterized gene in *C. albicans* with no obvious homologues in *S. cerevisiae* or *S. pombe* (Arnaud *et al.*, 2007), to a glycerol growth defect phenotype (Fig. 1B). These two examples demonstrate the utility of unbiased large-scale mutagenesis directly in *C. albicans*.

Limitations of forward genetics in C. albicans

Why did only two new robust filamentation phenotypes result out of 4700 potentially homozygosed *orf::UAU1/orf::URA3* mutants? First, only about 50% of the insertions were directly in an ORF or in a putative promoter

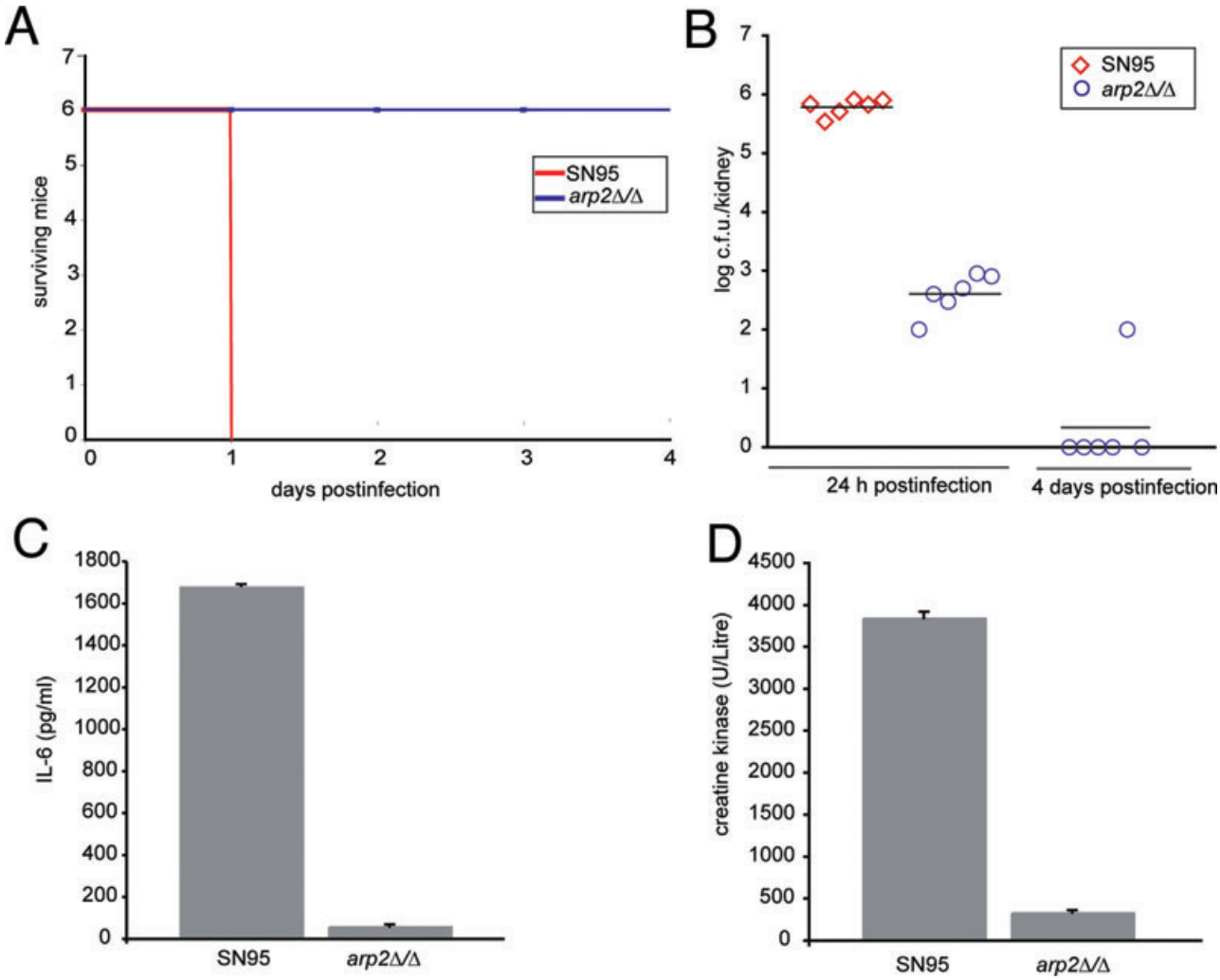

Fig. 10. The Arp2/3 complex is required for virulence in an A/J mouse model. Six mice were infected per group via tail vein with 3×10^5 *C. albicans* cells.
A. 100% of mice infected with WT *C. albicans* were moribund at 24 h post infection, while all mice infected with *arp2Δ/Δ* cells showed no clinical signs at the end of the experiment on day 4. Survival was closely monitored according to approved protocols.
B. Kidney fungal burden was determined at 24 h post infection. Mice infected with *arp2Δ/Δ* cells showed significantly lower fungal load compared with mice infected with WT cells (student *t*-test, $P < 1 \times 10^{-9}$). In an independent experiment, fungal load was collected at 4 days post infection from *arp2Δ/Δ*-infected mice. Bars represent means.
C. and D. IL-6 and CK levels were determined from blood collected at 24 h post infection. The IL-6 and CK levels for mice infected with *arp2Δ/Δ* cells were significantly lower compared with WT-infected mice ($P < 1 \times 10^{-5}$). Error bars indicate the standard errors of the means.

region (see *Supporting information*). For our analysis, we restricted in-depth characterization and deletion mutant construction of *orf::UAU1/orf::URA3* mutants to ORF insertions, because these showed the most consistent and pronounced phenotypes. Second, many insertion mutants were aneuploid, consistent with previous findings when directed UAU1 plasmids were used (Enloe *et al.*, 2000), or showed major chromosomal rearrangements on chromosomes other than where the initial UAU1 marker had inserted (Figs S2 and S3). Finally, we cannot exclude multiple insertions per transformant, which might explain why we could not map some insertions. As well, insertions into repeated regions can be difficult to map. For instance, we had several interesting phenotypes mapped to genes of the TLO (TeLOmere-associated gene) family, but because these genes are known to contain 80% or more similarity (van het Hoog *et al.*, 2007) we could not conveniently map the insertions to a single gene.

Taken together, based on random selection and verification of the WT band, we speculate that out of the 4700 potentially homozygosed *orf::UAU1/orf::URA3* mutants, about 5% or 200 would be simple homozygous gene insertion mutants with no aneuploidy at the site of insertion. This would make the overall isolation rate of hyphal defects close to one in 100 genes inactivated.

Exploiting the non-essential function of the Arp2/3 complex in C. albicans

The actin cytoskeleton plays a crucial role in cell polarity across most eukaryotes and hyphal growth in several fungal species in particular (Pruyne and Bretscher, 2000; Steinberg, 2007). In *C. albicans*, for instance, the importance of actin cytoskeleton structure and dynamics to morphogenesis was shown by experiments where *C. albicans* cells treated with Cytochalasin A, an actin monomer sequestering drug, led to hyphal formation defects while preserving other cellular growth processes (Akashi *et al.*, 1994). Subsequent work demonstrated a link between actin cytoskeleton stability and hyphae-specific gene expression, observations that corroborate our findings in that disrupting the Arp2/3 complex prevented morphological switching and that many hyphal-specific genes are not properly induced. This is consistent with the idea that besides a complex transcriptional regulatory system the actin cytoskeleton itself could influence hyphal gene activation (Hazan and Liu, 2002; Wolyniak and Sundstrom, 2007), potentially through cAMP signalling (Zou *et al.*, 2009). However, our data also show that partial derepression of the hyphal programme does not restore hyphae formation in the absence of a functional Arp2/3 complex, suggesting that in Arp2/3 complex mutants, additional factors are involved.

Several actin-patch phenotypes previously described for *C. albicans myo5Δ/Δ*, *wal1Δ/Δ*, *sla2Δ/Δ* or RAM pathway mutants could be confirmed with *arp2Δ/Δ* and *arp2Δ/Δarp3Δ/Δ* mutants. While a link between the Arp2/3 complex and the two Arp2/3 complex activators, *WAL1* and *MYO5*, or *SLA2*, an actin binding protein, are more obvious, it remains speculative how the RAM pathway could influence actin dynamics in general and the Arp2/3 complex in particular. Of all phenotypes displayed by Arp2/3 complex mutants, the most surprising was the ability to endocytose as it is now widely accepted that actin patches are the major sites of endocytosis from yeast to mammals (Kaksonen *et al.*, 2006; Moseley and Goode, 2006; Smythe and Ayscough, 2006; Galletta and Cooper, 2009). In general, although delayed, *arp2Δ/Δ* and *arp2Δ/Δarp3Δ/Δ* cells were clearly able to endocytose LY and FM4-64, which was not the case for the Arp2/3 complex activator Myo5p (compare movie 2 with movie 3, *Supporting information*), suggesting that in *myo5Δ/Δ* cells Arp2/3 complex-independent, *MYO5*-dependent pathways exist that contribute to plasma membrane component uptake. Together with our microarray studies that showed that the degree of similarity of the transcriptional response of *arp2Δ/Δ* and *myo5Δ/Δ* mutants was condition-dependent, this supports previous conclusions (Oberholzer *et al.*, 2006) that some *myo5Δ/Δ* phenotypes are Arp2/3 complex-independent.

The process of endocytosis can be divided into four phases (Robertson *et al.*, 2009a). During the earliest phase, assembly of the endocytic coat complex takes place and involves cargo recruitment, initial membrane curvature to facilitate the invagination process, as well as recruitment of proteins that will trigger actin polarization. This initial process seems unaffected in Arp2/3 complex mutants as bright FM4-64 dots still accumulate at the plasma membrane prior to membrane internalization in both WT and *arp2Δ/Δ* and *arp2Δ/Δarp3Δ/Δ* deletion mutants. These observations are consistent with the model that this first step of endocytosis is actin-independent (Robertson *et al.*, 2009a). During the second step of endocytosis, WT cells invaginate the FM4-64-loaded vesicles, while in Arp2/3 complex mutants a distinct invagination was not observed, again in good agreement with current models in that Arp2/3 complex-mediated actin polymerization is a central driving force during this step of membrane invagination. Instead, in *arp2Δ/Δ* and *arp2Δ/Δarp3Δ/Δ* mutants bright distinct dots appeared to be stuck in the membrane with little movement within the membrane and no appearance of invagination even after 3 h. Finally, during later steps of endocytosis, vesicle scission and movement away from the plasma membrane was readily detected in WT cells showing internalization of rapidly moving vesicles with subsequent dye accumulation in the vacuole. While although vacuolar dye accumulation was observed somewhat delayed and appeared overall weaker in Arp2/3 complex mutants, vacuolar accumulation of FM4-64 gradually occurred concomitantly with fading of the plasma membrane staining. Curiously, this vacuolar staining appeared independent of vesicle movement, as no clear, distinct vesicles emanating from the plasma membrane could be detected. This observation is lending support to recent reports in *S. cerevisiae* that Arp2/3-independent routes for actin-driven polymerization could be involved in endocytosis (Robertson *et al.*, 2009b), an idea that is particularly attractive in more distantly related eukaryotes like red algae where BLAST searches did not detect Arp2/3 complex subunits (Galletta and Cooper, 2009).

While more work is needed to refine the interplay of various endocytotic machinery components and the Arp2/3 complex in order to explore their spatiotemporal involvement in processes such as endocytosis or filamentous growth in *C. albicans*, the Arp2/3 complex mutants in this molecularly manipulatible model organism provide a powerful tool to probe this process in greater depth.

Experimental procedures

Strains, plasmids, primers and media

Strains, plasmids and primers (oligonucleotides) used in this study are listed in Tables S6–S8. YPD media consisted of

1% yeast extract, 2% peptone, 2% dextrose and 2% agar supplemented with 50 mg l^{-1} of uridine. YPD + 10% FBS and Spider media (1% Difco nutrient broth, 1% mannitol, 0.2% K_2HPO_4, 1.35% agar, pH 7.2), two media known to potently induce hyphal formation, were used for the hyphae screen (Liu *et al.*, 1994; Uhl *et al.*, 2003). SD media contained 2% dextrose, 6.7% yeast nitrogen base without amino acids, 2% agar and was supplemented with the appropriate amino acids.

In vivo *random mutagenesis and mapping the mutation*

The *Escherichia coli*-based UAU1 plasmid pool (Davis *et al.*, 2002) was first amplified on Luria broth (LB) plates supplemented with 50 μg ml^{-1} kanamycin and 50 μg ml^{-1} ampicillin at 37°C for 2 days followed by a 2 h liquid incubation at 37°C. For each transformation round into *C. albicans*, roughly 5 μg of a maxi-kit (Quiagen) extracted plasmid mix was *Not*I-digested and transformed (Chen *et al.*, 1992) into BWP17 (relevant genotype: *ura3/ura3 his1/his1 arg4/arg4*) (Wilson *et al.*, 1999). The *orf::UAU1/ORF* heterozygotes were selected on SD-Arg + Uri plates, patched on YPD media, grown at 30°C for 1–2 days and serially replica-plated up to eight times onto SD-Arg-Ura plates selecting for *orf::UAU1/orf::URA3* homozygotes. Generally, ~94% of the *orf::UAU1/ORF* heterozygotes gave rise to one or more *orf::UAU1/orf::URA3* homozygote colonies when replica-plated to SD-Arg-Ura plates from YPD plates compared with ~30% of heterozygotes that generated homozygotes when replica-plating the transformation plates directly to SD-Arg-Ura plates. For phenotypic analysis, potential *orf::UAU1/orf::URA3* insertion mutants were screened for a desired phenotype and simultaneously for Arg^+/Ura^+ prototrophy. If a desired phenotype was detected, a single colony of that mutant was selected, retested for growth on SD-Arg and SD-Ura media to verify segregation of the markers and at the same time retested for robustness of the desired phenotype. Only when each colony of this second testing showed a consistent phenotype, i.e. growth on SD-Arg, SD-Ura media together with a stable phenotype, was the insertion mapped. If the insertion was mapped directly in an ORF and no WT band was found by PCR analysis, a deletion mutant was constructed of this gene.

To map the transposon insertions inverse PCR was performed (Ochman *et al.*, 1988). For all mutants where we used inverse PCR or PCR to verify the absence of a WT band in *orf::UAU1/orf::URA3* mutants, a single colony was isolated and genomic DNA was extracted. Briefly, 20 μg of extracted DNA (Rose *et al.*, 1990) was purified using an ice-cold 2.5 M NH_4AcO solution (Maniatis *et al.*, 1982). *Mbo*I (New England Biolabs, NEB) was added at 2 U μg^{-1} of DNA and incubated at 37 C for 2 h. After enzyme inactivation and dilution of the DNA, T4 DNA ligase (NEB) was added to circularize the fragments that were then PCR-amplified with Taq polymerase (NEB) and oligonucleotides (primers) oEE5/oEE6. PCR products were sequenced with primers oEE9 and oEE23 at the Genome Sequencing Centre at McGill (http://www.genomequebecplatforms.com/mcgill). Sequences obtained after inverse PCR were mapped using the BLAST tools on the CDG homepage (http://www.candidagenome.org/).

Deletion mutant construction and phenotypic analysis

Strain SN95 (Noble and Johnson, 2005) was used for deletion mutant constructions. For each deletion mutant, at least two homozygotes derived from two different heterozygotes were constructed. One hundred-mer or 120-mer oligos flanking the coding sequence of genes *ARP2* or *VPS52* were used to amplify the Arginine and Histidine auxotrophic marker cassettes (Wilson *et al.*, 1999) for sequential disruption of both alleles. For the *arp2Δ/Δarp3Δ/Δ* double mutant, a fusion PCR approach and strain SN148 were used (Noble and Johnson, 2005). Correct integration of the marker cassettes and the absence of the WT gene were verified for each mutant by standard PCR analysis (Schaub *et al.*, 2006) (Fig. S2). In order to reintegrate the WT gene in each mutant at the WT locus, the nourseothricin marker was used (Reuss *et al.*, 2004). Briefly, the WT gene was amplified with primers oEE166/oEE228, oEE174/oEE232, oEE170/oEE229 for genes *ARP2, VPS52* and *ORF19.875*, respectively, and cloned into the *Kpn*I/*Xho*I-digested pSFS2A plasmid (Reuss *et al.*, 2004). The resulting plasmids, designated pEE22, pEE18 and pEE23, were sequenced. Downstream flanking sequences for *ARP2, VPS52* and *ORF19.875* were amplified with primers oEE167/oEE169, oEE233/oEE234 and oEE230/oEE231 and cloned into the *Not*I/*Sac*II-digested plasmids pEE22, pEE18 and pEE23 respectively. This resulted in plasmids pEE33, pEE20 and pEE30, which were then *Kpn*I/*Sac*II-digested and directly transformed into the corresponding deletion mutant. Selection was done on 200 μg ml^{-1} of nourseothricin, and correct integration was verified by PCR analysis. Finally, before revertant phenotypes were compared with mutant and WT phenotypes, the nourseothricin marker cassette was looped out by incubating the revertants for 6 h in YP media supplemented with 2% maltose. Loop out of the SAT1 flipper cassette was confirmed by nourseothricin sensitivity, Histidine or Arginine auxotrophy and finally by PCR analysis (not shown).

The *nrg1Δ/Δarp2Δ/Δ* mutant was created in the *nrg1Δ/Δ* deletion strain (Murad *et al.*, 2001). Briefly, the upstream flanking sequence of *ARP2* was first amplified with primers oEE166/oEE382 and cloned into the *Kpn*I/*Not*I-digested plasmid pEE33, which resulted in plasmid pEE59. This plasmid was then used to sequentially delete both alleles of the *ARP2* gene in the *nrg1Δ/Δ* mutant.

Microscopy and time-lapse

For microscopic analysis, an upright Leitz Aristoplan or an inverted Leica DMIRE2 microscope with a 100× immersion oil objective, and a 10× projection lense was used. Characterization of Arp2/3 complex mutant phenotypes was done as previously described for CFW, rhodamine/phalloidin and FM4-64 staining in (Vida and Emr, 1995; Oberholzer *et al.*, 2002) and LY visualization in (Baggett *et al.*, 2003).

Time-lapse movies (*Supporting information*) were performed with *TEF1*-GFP labelled WT cells that were co-incubated with mutant cells in a one-to-one ratio. Cells were grown to exponential phase and washed with SD media. Agar slides were prepared as follows: 0.75 ml of half strength YPD media was mixed with 0.75 ml of 3.4% Agarose (pre-heated) after which 1 μl of FM4-64 (200 μg ml^{-1}, in dimethylsulphoxide) was added. A total of 100 μl of this mixture was

then transferred to the deep well slides and covered with a coverslip without sealing. After the medium had solidified, the coverslip was removed; 1 μl of mixed WT/mutant culture was applied and covered with a fresh coverslip on top. Differential interference contrast (DIC) and GFP images were taken prior to time-lapse microscopy to distinguish between WT and mutant cells (Fig. S4). Time-lapse image acquisition started 5 min after application of the cells and was followed for 3 h with one image per minute. Images were taken with a Zeiss Axio Imager M1 microscope with a Photometrics Coolsnap HQ camera. Image acquisition and movie file assembly was performed with Metamorph 7 software (Molecular Devices).

Comparative genome hybridization and microarray studies

Comparative genome hybridization analysis was done as previously described (Znaidi *et al*., 2007) with the following modifications. Genomic DNA was extracted from a *C. albicans* culture grown to saturation with the Qiagen Genomic DNA Extraction kit according to manufacturer's instructions. DNA hybridization was done with the Advalytix SlideBooster for 16 h at 42°C according to manufacturer's instructions.

For the transcriptional profiling experiment, total RNA was extracted using the RNeasy Mini kit (Qiagen). Total RNA quantification was measured by nanodrop (ND-1000 spectrophotometer, NanoDrop Technologies). The quality of the mRNA was verified with a RNA lab-on-chip assay using a 2100 expert mRNA nano BIO analyser (Agilent). cDNA labelling, DNA microarray hybridization, washing and scanning was adapted from a standardized protocol (Nantel *et al*., 2006). Each condition was covered by a minimum of three DNA microarrays, and results were analysed using GeneSpring software (Silicon Genetics, Redwood City, CA). In order to compare significantly overlapping gene lists, the *P*-value was calculated using hypergeometric distribution as described in the GO Term Finder Tool web site (http://www.candidagenome.org/cgi-bin/GO/goTermFinder). Gene lists can be found in Tables S2–S5. The entire data set for all microarray experiments has also been deposited at GEO under the accession number GSE19583. (http://www.ncbi.nlm.nih.gov/geo). For calculating the Pearson correlation, GraphPad Prism 5 was used.

Virulence studies

Virulence testing of *C. albicans*, including survival experiments, tissue fungal burden counting and biochemical analysis of the host blood, was done as previously described (Mullick *et al*., 2004; 2006). Briefly, 8- to 12-week-old A/J mice (Jackson Laboratories, Bar Harbor, ME) were inoculated via the tail vein with 200 μl of a suspension containing 3×10^5 *C. albicans* in PBS. Three male and three female mice were used for each experimental group. Mice were closely monitored over a period of maximal 4 days for clinical signs of disease such as lethargy, ruffled fur or hunched back. Mice showing extreme lethargy were considered moribund and were euthanized. All experimental procedures involving animals were approved by the Biotechnology Research Institute Animal Care Committee, which operates under the guidelines of the Canadian Council of Animal Care.

Acknowledgements

We thank Aaron P. Mitchell for providing the UAU1 plasmid library, Cynthia Hélie and Mario Mercier for excellent technical assistance in animal handling, Jean-Sébastien Deneault and André Nantel for help with microarray studies and Lichun Liang (a summer student from John Abbott College, Montréal) for help in screening random *orf::UAU1/orf::URA3* mutants. This work was supported by a CIHR team grant in fungal pathogenesis to A.M., M.R. and M.W. (CTP-79843). This is NRC publication number 49596.

References

Akashi, T., Kanbe, T., and Tanaka, K. (1994) The role of the cytoskeleton in the polarized growth of the germ tube in *Candida albicans*. *Microbiology* **140:** 271–280.

Arnaud, M.B., Costanzo, M.C., Skrzypek, M.S., Shah, P., Binkley, G., Lane, C., *et al.* (2007) Sequence resources at the Candida Genome Database. *Nucleic Acids Res* **35:** D452–D456.

Askew, C., Sellam, A., Epp, E., Hogues, H., Mullick, A., Nantel, A., and Whiteway, M. (2009) Transcriptional regulation of carbohydrate metabolism in the human pathogen *Candida albicans*. *PLoS Pathog* **5:** e1000612.

Asleson, C.M., Bensen, E.S., Gale, C.A., Melms, A.S., Kurischko, C., and Berman, J. (2001) *Candida albicans* INT1-induced filamentation in *Saccharomyces cerevisiae* depends on Sla2p. *Mol Cell Biol* **21:** 1272–1284.

Baggett, J.J., Shaw, J.D., Sciambi, C.J., Watson, H.A., and Wendland, B. (2003) Fluorescent labeling of yeast. *Curr Protoc Cell Biol* **Chapter 4:** Unit 4, 13.

Balasubramanian, M.K., Feoktistova, A., McCollum, D., and Gould, K.L. (1996) Fission yeast Sop2p: a novel and evolutionarily conserved protein that interacts with Arp3p and modulates profilin function. *EMBO J* **15:** 6426–6437.

Banerjee, M., Thompson, D.S., Lazzell, A., Carlisle, P.L., Pierce, C., Monteagudo, C., *et al.* (2008) UME6, a novel filament-specific regulator of *Candida albicans* hyphal extension and virulence. *Mol Biol Cell* **19:** 1354–1365.

Bennett, R.J., and Johnson, A.D. (2005) Mating in *Candida albicans* and the search for a sexual cycle. *Annu Rev Microbiol* **59:** 233–255.

Berman, J. (2006) Morphogenesis and cell cycle progression in *Candida albicans*. *Curr Opin Microbiol* **9:** 595–601.

Berman, J., and Sudbery, P.E. (2002) *Candida albicans*: a molecular revolution built on lessons from budding yeast. *Nat Rev Genet* **3:** 918–930.

Bernardo, S.M., Khalique, Z., Kot, J., Jones, J.K., and Lee, S.A. (2008) *Candida albicans* VPS1 contributes to protease secretion, filamentation, and biofilm formation. *Fungal Genet Biol Mycopathologia* **167:** 55–63.

Biswas, S., Van Dijck, P., and Datta, A. (2007) Environmental sensing and signal transduction pathways regulating morphopathogenic determinants of *Candida albicans*. *Microbiol Mol Biol Rev* **71:** 348–376.

Braun, B.R., van Het Hoog, M., d'Enfert, C., Martchenko, M., Dungan, J., Kuo, A., *et al.* (2005) A human-curated annotation of the *Candida albicans* genome. *PLoS Genet* **1:** 36–57.

Bruno, V.M., Kalachikov, S., Subaran, R., Nobile, C.J., Kyrat-

sous, C., and Mitchell, A.P. (2006) Control of the *C. albicans* cell wall damage response by transcriptional regulator Cas5. *PLoS Pathog* **2:** e21.
Care, R.S., Trevethick, J., Binley, K.M., and Sudbery, P.E. (1999) The MET3 promoter: a new tool for *Candida albicans* molecular genetics. *Mol Microbiol* **34:** 792–798.
Carlisle, P.L., Banerjee, M., Lazzell, A., Monteagudo, C., Lopez-Ribot, J.L., and Kadosh, D. (2009) Expression levels of a filament-specific transcriptional regulator are sufficient to determine *Candida albicans* morphology and virulence. *Proc Natl Acad Sci USA* **106:** 599–604.
Casamayor, A., and Snyder, M. (2002) Bud-site selection and cell polarity in budding yeast. *Curr Opin Microbiol* **5:** 179–186.
Chen, D.C., Yang, B.C., and Kuo, T.T. (1992) One-step transformation of yeast in stationary phase. *Curr Genet* **21:** 83–84.
Cornet, M., Bidard, F., Schwarz, P., Da Costa, G., Blanchin-Roland, S., Dromer, F., and Gaillardin, C. (2005) Deletions of endocytic components VPS28 and VPS32 affect growth at alkaline pH and virulence through both RIM101-dependent and RIM101-independent pathways in *Candida albicans*. *Infect Immun* **73:** 7977–7987.
Cowen, L. (2008) The evolution of fungal drug resistance: modulating the trajectory from genotype to phenotype. *Nat Rev Microbiol* **6:** 187–198.
Daugherty, K.M., and Goode, B.L. (2008) Functional surfaces on the p35/ARPC2 subunit of Arp2/3 complex required for cell growth, actin nucleation, and endocytosis. *J Biol Chem* **283:** 16950–16959.
Davis, D.A., Bruno, V.M., Loza, L., Filler, S.G., and Mitchell, A.P. (2002) *Candida albicans* Mds3p, a conserved regulator of pH responses and virulence identified through insertional mutagenesis. *Genet* **162:** 1573–1581.
Enloe, B., Diamond, A., and Mitchell, A.P. (2000) A single-transformation gene function test in diploid *Candida albicans*. *J Bacteriol* **182:** 5730–5736.
Galletta, B.J., and Cooper, J.A. (2009) Actin and endocytosis: mechanisms and phylogeny. *Curr Opin Cell Biol* **21:** 20–27.
Garcia-Sanchez, S., Mavor, A.L., Russell, C.L., Argimon, S., Dennison, P., Enjalbert, B., and Brown, A.J. (2005) Global roles of Ssn6 in Tup1- and Nrg1-dependent gene regulation in the fungal pathogen, *Candida albicans*. *Mol Biol Cell* **16:** 2913–2925.
Goley, E.D., and Welch, M.D. (2006) The ARP2/3 complex: an actin nucleator comes of age. *Nat Rev Mol Cell Biol* **7:** 713–726.
Gow, N.A. (1997) Germ tube growth of *Candida albicans*. *Curr Top Med Mycol* **8:** 43–55.
Gow, N.A., Brown, A.J., and Odds, F.C. (2002) Fungal morphogenesis and host invasion. *Curr Opin Microbiol* **5:** 366–371.
Harris, S.D., and Momany, M. (2004) Polarity in filamentous fungi: moving beyond the yeast paradigm. *Fungal Genet Biol* **41:** 391–400.
Hazan, I., and Liu, H. (2002) Hyphal tip-associated localization of Cdc42 is F-actin dependent in *Candida albicans*. *Eukaryot Cell* **1:** 856–864.
van het Hoog, M., Rast, T.J., Martchenko, M., Grindle, S., Dignard, D., Hogues, H., *et al.* (2007) Assembly of the *Candida albicans* genome into sixteen supercontigs aligned on the eight chromosomes. *Genome Biol* **8:** R52.
Hudson, A.M., and Cooley, L. (2002) A subset of dynamic actin rearrangements in Drosophila requires the Arp2/3 complex. *J Cell Biol* **156:** 677–687.
Kadosh, D., and Johnson, A.D. (2005) Induction of the *Candida albicans* filamentous growth program by relief of transcriptional repression: a genome-wide analysis. *Mol Biol Cell* **16:** 2903–2912.
Kaksonen, M., Toret, C.P., and Drubin, D.G. (2006) Harnessing actin dynamics for clathrin-mediated endocytosis. *Nat Rev Mol Cell Biol* **7:** 404–414.
Koh, A.Y., Köhler, J.R., Coggshall, K.T., Van Rooijen, N., and Pier, G.B. (2008) Mucosal damage and neutropenia are required for *Candida albicans* dissemination. *PLoS Pathog* **4:** e35.
Kumamoto, C.A., and Vinces, M.D. (2005) Contributions of hyphae and hypha-co-regulated genes to *Candida albicans* virulence. *Cell Microbiol* **7:** 1546–1554.
Kurtz, M.B., Kirsch, D.R., and Kelly, R. (1988) The molecular genetics of *Candida albicans*. *Microbiol Sci* **5:** 58–63.
Laprade, L., Boyartchuk, V.L., Dietrich, W.F., and Winston, F. (2002) Spt3 plays opposite roles in filamentous growth in *Saccharomyces cerevisiae* and *Candida albicans* and is required for *C. albicans* virulence. *Genet* **161:** 509–519.
Lavoie, H., Sellam, A., Askew, C., Nantel, A., and Whiteway, M. (2008) A toolbox for epitope-tagging and genome-wide location analysis in *Candida albicans*. *BMC Genomics* **9:** 578.
Lees-Miller, J.P., Henry, G., and Helfman, D.M. (1992) Identification of act2, an essential gene in the fission yeast *Schizosaccharomyces pombe* that encodes a protein related to actin. *Proc Natl Acad Sci USA* **89:** 80–83.
Leroy, O., Gangneux, J.P., Montravers, P., Mira, J.P., Gouin, F., Sollet, J.P., *et al.* (2009) Epidemiology, management, and risk factors for death of invasive Candida infections in critical care: a multicenter, prospective, observational study in France (2005–2006). *Crit Care Med* **37:** 1612–1618.
Li, R. (1997) Bee1, a yeast protein with homology to Wiscott-Aldrich syndrome protein, is critical for the assembly of cortical actin cytoskeleton. *J Cell Biol* **136:** 649–658.
Liu, H. (2001) Transcriptional control of dimorphism in *Candida albicans*. *Curr Opin Microbiol* **4:** 728–735.
Liu, H., Kohler, J., and Fink, G.R. (1994) Suppression of hyphal formation in *Candida albicans* by mutation of a STE12 homolog. *Science* **266:** 1723–1726.
Lo, H.J., Köhler, J.R., DiDomenico, B., Loebenberg, D., Cacciapuoti, A., and Fink, G.R. (1997) Nonfilamentous *C. albicans* mutants are avirulent. *Cell* **90:** 939–949.
McCollum, D., Feoktistova, A., Morphew, M., Balasubramanian, M., and Gould, K.L. (1996) The *Schizosaccharomyces pombe* actin-related protein, Arp3, is a component of the cortical actin cytoskeleton and interacts with profilin. *EMBO J* **15:** 6438–6446.
Machesky, L.M., Atkinson, S.J., Ampe, C., Vandekerckhove, J., and Pollard, T.D. (1994) Purification of a cortical complex containing two unconventional actins from Acanthamoeba by affinity chromatography on profilin-agarose. *J Cell Biol* **127:** 107–115.
Maniatis, T., Fritsch, E.F., and Sambrook, J. (1982) *Molecular*

Cloning: A Laboratory Manual. New York: Cold Spring Harbor Laboratory Press, Cold Spring Harbor Laboratory, New York.

Martchenko, M., Levitin, A., Hogues, H., Nantel, A., and Whiteway, M. (2007a) Transcriptional rewiring of fungal galactose-metabolism circuitry. *Curr Biol* **17:** 1007–1013.

Martchenko, M., Levitin, A., and Whiteway, M. (2007b) Transcriptional activation domains of the *Candida albicans* Gcn4p and Gal4p homologs. *Eukaryot Cell* **6:** 291–301.

Martin, A.C., Xu, X.P., Rouiller, I., Kaksonen, M., Sun, Y., Belmont, L., *et al.* (2005) Effects of Arp2 and Arp3 nucleotide-binding pocket mutations on Arp2/3 complex function. *J Cell Biol* **168:** 315–328.

Moreau, V., Madania, A., Martin, R.P., and Winson, B. (1996) The *Saccharomyces cerevisiae* actin-related protein Arp2 is involved in the actin cytoskeleton. *J Cell Biol* **134:** 117–132.

Moreau, V., Galan, J.M., Devilliers, G., Haguenauer-Tsapis, R., and Winsor, B. (1997) The yeast actin-related protein Arp2p is required for the internalization step of endocytosis. *Mol Biol Cell* **8:** 1361–1375.

Moseley, J.B., and Goode, B.L. (2006) The yeast actin cytoskeleton: from cellular function to biochemical mechanism. *Microbiol Mol Biol Rev* **70:** 605–645.

Mullick, A., Elias, M., Picard, S., Bourget, L., Jovcevski, O., Gauthier, S., *et al.* (2004) Dysregulated inflammatory response to *Candida albicans* in a C5-deficient mouse strain. *Infect Immun* **72:** 5868–5876.

Mullick, A., Leon, Z., Min-Oo, G., Berghout, J., Lo, R., Daniels, E., and Gros, P. (2006) Cardiac failure in C5-deficient A/J mice after *Candida albicans* infection. *Infect Immun* **74:** 4439–4451.

Murad, A.M., Leng, P., Straffon, M., Wishart, J., Macaskill, S., MacCallum, D., *et al.* (2001) NRG1 represses yeast-hypha morphogenesis and hypha-specific gene expression in *Candida albicans*. *EMBO J* **20:** 4742–4752.

Nantel, A. (2006) The long hard road to a completed *Candida albicans* genome. *Fungal Genet Biol* **43:** 311–315.

Nantel, A., Dignard, D., Bachewich, C., Harcus, D., Marcil, A., Bouin, A.P., *et al.* (2002) Transcription profiling of *Candida albicans* cells undergoing the yeast-to-hyphal transition. *Mol Biol Cell* **13:** 3452–3465.

Nantel, A., Rigby, T., Hogues, H., and Whiteway, M. (2006) Microarrays for Studying Pathogenicity in *Candida albicans*. In *Medical Mycology: Cellular and Molecular Techniques*. Kavanaugh, K. (ed.). New York, NJ: Wiley Press.

Nicholls, S., Straffon, M., Enjalbert, B., Nantel, A., Macaskill, S., Whiteway, M., and Brown, A.J. (2004) Msn2- and Msn4-like transcription factors play no obvious roles in the stress responses of the fungal pathogen *Candida albicans*. *Eukaryot Cell* **3:** 1111–1123.

Nobile, C.J., and Mitchell, A.P. (2005) Regulation of cell-surface genes and biofilm formation by the *C. albicans* transcription factor Bcr1p. *Curr Biol* **15:** 1150–1155.

Noble, S.M., and Johnson, A.D. (2005) Strains and strategies for large-scale gene deletion studies of the diploid human fungal pathogen *Candida albicans*. *Eukaryot Cell* **4:** 298–309.

Oberholzer, U., Marcil, A., Leberer, E., Thomas, D.Y., and Whiteway, M. (2002) Myosin I is required for hypha formation in *Candida albicans*. *Eukaryot Cell* **1:** 213–228.

Oberholzer, U., Iouk, T.L., Thomas, D.Y., and Whiteway, M. (2004) Functional characterization of myosin I tail regions in *Candida albicans*. *Eukaryot Cell* **3:** 1272–1286.

Oberholzer, U., Nantel, A., Berman, J., and Whiteway, M. (2006) Transcript profiles of *Candida albicans* cortical actin patch mutants reflect their cellular defects: contribution of the Hog1p and Mkc1p signaling pathways. *Eukaryot Cell* **5:** 1252–1265.

Ochman, H., Gerber, A.S., and Hartl, D.L. (1988) Genetic applications of an inverse polymerase chain reaction. *Genet* **120:** 621–623.

Ostrander, D.B., and Gorman, J.A. (1994) Characterization of the *Candida albicans* TRP1 gene and construction of a homozygous trp1 mutant by sequential co-transformation. *Gene* **148:** 179–185.

Palmer, G.E., Cashmore, A., and Sturtevant, J. (2003) *Candida albicans* VPS11 is required for vacuole biogenesis and germ tube formation. *Eukaryot Cell* **2:** 411–421.

Pfaller, M.A., and Diekema, D.J. (2007) Epidemiology of invasive candidiasis: a persistent public health problem. *Clin Microbiol Rev* **20:** 133–163.

Pruyne, D., and Bretscher, A. (2000) Polarization of cell growth in yeast. *J Cell Sci* **113:** 571–585.

Reuss, O., Vik, A., Kolter, R., and Morschhäuser, J. (2004) The SAT1 flipper, an optimized tool for gene disruption in *Candida albicans*. *Gene* **341:** 119–127.

Riezman, H. (1985) Endocytosis in yeast: several of the yeast secretory mutants are defective in endocytosis. *Cell* **40:** 1001–1009.

Robertson, A.S., Smythe, E., and Ayscough, K.R. (2009a) Functions of actin in endocytosis. *Cell Mol Life Sci* **66:** 2049–2065.

Robertson, A.S., Allwood, E.G., Smith, A.P., Gardiner, F.C., Costa, R., Winder, S.J., and Ayscough, K.R. (2009b) The WASP homologue Las17 activates the novel actin-regulatory activity of Ysc84 to promote endocytosis in yeast. *Mol Biol Cell* **20:** 1618–1628.

Roemer, T., Jiang, B., Davison, J., Ketela, T., Veillette, K., Breton, A., *et al.* (2003) Large-scale essential gene identification in *Candida albicans* and applications to antifungal drug discovery. *Mol Microbiol* **50:** 167–181.

Rose, M.D., Winston, F., and Hieter, P. (1990) *Methods in Yeast Genetics: A Laboratory Course Manual*. New York: Cold Spring Harbor Laboratory Press, Cold Spring Harbor, New York.

Ruhnke, M., and Maschmeyer, G. (2002) Management of mycoses in patients with hematologic disease and cancer – review of the literature. *Eur J Med Res* **7:** 227–235.

Santos, R., Buisson, N., Knight, S.A., Dancis, A., Camadro, J.M., and Lesuisse, E. (2004) *Candida albicans* lacking the frataxin homologue: a relevant yeast model for studying the role of frataxin. *Mol Microbiol* **54:** 507–519.

Sawa, M., Suetsugu, S., Sugimoto, A., Miki, H., Yamamoto, M., and Takenawa, T. (2003) Essential role of the *C. elegans* Arp2/3 complex in cell migration during ventral enclosure. *J Cell Sci* **116:** 1505–1518.

Schaub, Y., Dunkler, A., Walther, A., and Wendland, J. (2006) New pFA-cassettes for PCR-based gene manipulation in *Candida albicans*. *J Basic Microbiol* **46:** 416–429.

Schwartz, M.A., and Madhani, H.D. (2004) Principles of MAP kinase signaling specificity in *Saccharomyces cerevisiae*. *Annu Rev Genet* **38:** 725–748.
Schwob, E., and Martin, R.P. (1992) New yeast actin-like gene required late in the cell cycle. *Nature* **355:** 179–182.
Shen, J., Cowen, L.E., Griffin, A.M., Chan, L., and Köhler, J.R. (2008) The *Candida albicans* pescadillo homolog is required for normal hypha-to-yeast morphogenesis and yeast proliferation. *Proc Natl Acad Sci USA* **105:** 20918–20923.
Smythe, E., and Ayscough, K.R. (2006) Actin regulation in endocytosis. *J Cell Sci* **119:** 4589–4598.
Song, Y., Cheon, S.A., Lee, K.E., Lee, S.Y., Lee, B.K., Oh, D.B., *et al.* (2008) Role of the RAM network in cell polarity and hyphal morphogenesis in *Candida albicans*. *Mol Biol Cell* **19:** 5456–5477.
Steinberg, G. (2007) Hyphal growth: a tale of motors, lipids, and the Spitzenkorper. *Eukaryot Cell* **6:** 351–360.
Sudbery, P., Gow, N., and Berman, J. (2004) The distinct morphogenic states of *Candida albicans*. *Trends Microbiol* **12:** 317–324.
Tuite, A., Elias, M., Picard, S., Mullick, A., and Gros, P. (2005) Genetic control of susceptibility to *Candida albicans* in susceptible A/J and resistant C57BL/6J mice. *Genes Immun* **6:** 672–682.
Uhl, M.A., Biery, M., Craig, N., and Johnson, A.D. (2003) Haploinsufficiency-based large-scale forward genetic analysis of filamentous growth in the diploid human fungal pathogen *C. albicans*. *EMBO J* **22:** 2668–2678.
Vida, T.A., and Emr, S.D. (1995) A new vital stain for visualizing vacuolar membrane dynamics and endocytosis in yeast. *J Cell Biol* **128:** 779–792.
Walther, A., and Wendland, J. (2004) Polarized hyphal growth in *Candida albicans* requires the Wiskott-Aldrich Syndrome protein homolog Wal1p. *Eukaryot Cell* **3:** 471–482.
Weig, M., Jansch, L., Gross, U., De Koster, C.G., Klis, F.M., and De Groot, P.W. (2004) Systematic identification in silico of covalently bound cell wall proteins and analysis of protein-polysaccharide linkages of the human pathogen Candida glabrata. *Microbiology* **150:** 3129–3144.
Welch, M.D., Iwamatsu, A., and Mitchison, T.J. (1997) Actin polymerization is induced by Arp2/3 protein complex at the surface of Listeria monocytogenes. *Nature* **385:** 265–269.
Whiteway, M., and Oberholzer, U. (2004) Candida morphogenesis and host-pathogen interactions. *Curr Opin Microbiol* **7:** 350–357.
Whiteway, M., and Bachewich, C. (2007) Morphogenesis in *Candida albicans*. *Annu Rev Microbiol* **61:** 529–553.
Wilson, R.B., Davis, D., and Mitchell, A.P. (1999) Rapid hypothesis testing with *Candida albicans* through gene disruption with short homology regions. *J Bacteriol* **181:** 1868–1874.
Winter, D., Podtelejnikov, A.V., Mann, M., and Li, R. (1997) The complex containing actin-related proteins Arp2 and Arp3 is required for the motility and integrity of yeast actin patches. *Curr Biol* **7:** 519–529.
Winter, D.C., Choe, E.Y., and Li, R. (1999) Genetic dissection of the budding yeast Arp2/3 complex: a comparison of the in vivo and structural roles of individual subunits. *Proc Natl Acad Sci USA* **96:** 7288–7293.
Wolyniak, M.J., and Sundstrom, P. (2007) Role of actin cytoskeletal dynamics in activation of the cyclic AMP pathway and HWP1 gene expression in *Candida albicans*. *Eukaryot Cell* **6:** 1824–1840.
Zallen, J.A., Cohen, Y., Hudson, A.M., Cooley, L., Wieschaus, E., and Schejter, E.D. (2002) SCAR is a primary regulator of Arp2/3-dependent morphological events in Drosophila. *J Cell Biol* **156:** 689–701.
Zeidler, U., Lettner, T., Lassnig, C., Muller, M., Lajko, R., Hintner, H., *et al.* (2009) UME6 is a crucial downstream target of other transcriptional regulators of true hyphal development in *Candida albicans*. *FEMS Yeast Res* **9:** 126–142.
Znaidi, S., De Deken, X., Weber, S., Rigby, T., Nantel, A., and Raymond, M. (2007) The zinc cluster transcription factor Tac1p regulates PDR16 expression in *Candida albicans*. *Mol Microbiol* **66:** 440–452.
Zou, H., Fang, H.M., Zhu, Y., and Wang, Y. (2009) *Candida albicans* Cyr1, Cap1 and G-actin form a sensor/effector apparatus for activating cAMP synthesis in hyphal growth. *Mol Microbiol* doi: 10.1111/j.1365-2958.2009.06980.x.

Supporting information

Additional supporting information may be found in the online version of this article:

Please note: Wiley-Blackwell are not responsible for the content or functionality of any supporting materials supplied by the authors. Any queries (other than missing material) should be directed to the corresponding author for the article.

Chapter V

V. The advantage of not being essential – the Arp2/3 complex in *C. albicans*

In the previous chapter (chapter IV.2), I presented a forward genetic screen directly in *C. albicans* that aimed at identifying genes involved in the yeast-to-hyphae switch. From the resulting hits, I chose to focus on Arp2 and showed that the Arp2/3 complex is required for hyphal formation as well as virulence. I also provided evidence that this complex is not essential for bulk membrane and liquid phase endocytosis. This observation that the Arp2/3 complex is apparently not involved in endocytosis was surprising, because the accepted view is that Arp2/3-mediated actin nucleation at endocytic sites is necessary to provide the force to drive vesicle internalization. Given the unexpected results, I was curious to further investigate the role of the Arp2/3 complex in regards to endocytosis. Our main advantage compared to other model organisms is that the Arp2/3 complex is not essential for viability in *C. albicans*, which allows us to directly assess functional consequences of Arp2/3. This has previously been difficult in living cells, because Arp2/3 is essential in almost all model organisms [192].

I will now first provide an overview of the actin cytoskeleton with a strong focus on the Arp2/3 complex and the processes of actin nucleation and endocytosis. In the following section (chapter V.2.), I will then present in a first draft version our analysis of how components of the only known endocytotic pathway in fungal cells behave in the absence of Arp2/3. In the same section I will also provide an analysis of actin dynamics in the absence of this actin-nucleating machinery.

V.1. The actin cytoskeleton

Actin is a highly conserved protein that was present in a common ancestor living some 3 billion years ago [193]. Today, actin is estimated to be among the 5 most abundant proteins found in eukaryotes, often being the most abundant protein in a cell. In muscle cells, for example, actin together with myosin constitute more than 60% of all protein [194]. Actin participates in more protein-protein interactions than any other protein and is involved in a variety of cellular processes, ranging from regulating cell motility, cell shape, polarity, organelle transport, cytokinesis to the regulation of transcription [195]. Considering its abundance, it is surprising that actin was only discovered in the 1940s in muscle cells and in the late 1960s in non-muscle cells. Although researchers have discovered more than 100 actin-binding proteins (ABPs) since then, the inventory of proteins that bind actin monomers, cap actin filament ends, nucleate, cross-link, stabilize, sever or move along actin filaments is still not complete. The importance of actin and ABPs is highlighted by genetic defects in actin-related processes that cause a range of human diseases, including hereditary heart diseases (cardiomyopathies), hereditary fragility of red blood cells (e.g. hemolytic anemia), or muscular dystrophy [194]. Finally, human pathogens such as *Salmonella*, *Shigella*, *Listeria* or *Toxoplasma gondii* can either hijack or disrupt the actin cytoskeleton of the host during infection, while some pathogenic bacteria produce toxins that ADP-ribosylate actin, leading to cytoskeleton disorganization and cell death [196,197].

To provide an overview of the actin cytoskeleton, I will introduce in the next 3 sections the main actin structures found in fungal cells; actin filaments, cytokinetic rings and actin patches.

V.1.1. Actin filaments

Actin filaments (or F-actin) are polymeric structures that are made up of globular actin monomers (G-actin), and provide tracks for type V myosin-directed delivery of vesicles and organelles to the growing tip of fungal cells [198]. Most eukaryotic organisms have multiple actin genes; humans have six, amoebae like

Dyctostelium have 10, but fungi such as budding yeast or *C. albicans* have only one. The G-actin protein crystal structure has been solved in 1990, and more than 80 actin structures have been described since then [195,199]. Most structures have been obtained by either chemically or genetically mutating actin to prevent polymerization or as part of complexes with ABPs. Despite such diverse crystallization conditions, the actin structures are remarkably similar, with the 375-amino-acid polypeptide chain folding into two major α/β-domains that are stabilized by an adenine nucleotide lying between the domains. Actin binds adenosine triphosphate (ATP) with higher affinity than adenosine diphosphate (ADP), and the ATP-actin state is more stable compared to ADP-actin. This is an important property of actin as nucleotide hydrolysis is one of the main factors regulating the F-actin to G-actin transition; *in vitro* experiments have shown that G-actin joins the fast growing barbed (or +) end of the actin filament in the ATP state, while hydrolysis takes place in the middle of the filament followed by ADP-actin monomers dissociating faster from the pointed (or -) end of the filament [200]. The nomenclature of barbed and pointed ends arose due to the asymmetrical arrowhead pattern created by myosin binding along the actin filaments [194]. The process of actin polymerization/dissociation at the barbed and pointed end, respectively, has been termed treadmilling [201]. Actin treadmilling *in vitro* is rather slow and inefficient compared to *in vivo* treadmilling due to the formation of kinetically unfavorable actin dimers and trimeric 'nuclei' [202]. The reason why treadmilling is faster *in vivo* is because cells use nucleating factors that directly elongate actin filaments.

One such class of actin filament nucleators, the formins, is present in virtually all eukaryotes, with 15 formins present in humans [203]. Much of what we know about formins has come from studies in budding yeast, which has two genes encoding for formins, Bni1 and Bnr1 [204]. Disrupting both formins in *S. cerevisiae* or *C. albicans*, which also has two formins, is lethal, while disrupting only one formin leads to polarity defects [205,206]. For example, when Bni1 was deleted in *C. albicans*, the mutant cells appeared round and enlarged, with a widened bud neck and a random budding pattern, and although these mutants could still undergo the yeast-to-hyphal switch, the hyphal structures appeared markedly swollen [206]. The unifying feature of formins is the

presence of the 'formin homology' domains (FH1 and FH2). Through their FH2 domains, formins associate with the barbed end of a growing actin filament. The function of the FH2-domain is to 'embrace' the actin filament as a dimer, thus protecting it from other ABPs like capping proteins that would terminate actin elongation. The function of the FH1 domain is to recruit profilin-actin, which likely leads to increased local concentrations of G-actin that can then be directly delivered to the barbed end [202]. Recently, other actin filament nucleators have been identified in higher eukaryotes. Most of these nucleators have a tandem cluster of three or more G-actin binding motifs such as WASP homology 2 (WH2) domains. Examples of this class of actin filament nucleators include the mammalian Spire, cordon-bleu, JMY, adenomatous polyposis coli (APC) and members of the leiomodin family [207]. How exactly these regulators organize actin monomers to favor actin nucleation is currently not known.

Besides formins and other actin filament nucleators, there are several other classes of proteins that influence actin filament dynamics. For instance, capping proteins can bind to either barbed or pointed end of filaments, resulting in a blockage of filament elongation or dissociation. Other proteins, like cofilin, are important for replenishing the G-actin pool. Cofilin acts by first binding to sites on the ADP-actin filament, leading to destabilization and severing of the filament, which results in two un-capped ends that are available for actin subunit association or disassociation [208,209]. Finally, several proteins like tropomyosin or fimbrin bind to the sides of actin filaments, thus increasing the tensile strength of the filaments [210]. The complexity of actin dynamics, particularly elements of filament elongation and dissociation, has been visualized *in vivo* in several species, e.g. in human tissue culture cells, mice, plants and fungal cells [211,212,213,214].

V.1.2. The cytokinetic ring

Although a link between the actin cytoskeleton and cytokinesis has been observed in the mid 1970s [215,216,217], it was not until the late 1990s when we saw a revolution

in our understanding of how cytokinesis works [reviewed in: 218]. Genetic screens in budding and fission yeast have fundamentally contributed to this understanding by identifying the players involved [219]. Fission yeast has further been instrumental in understanding cytokinesis because it buds by 'fission', thus providing an advantage when visualizing this process compared to budding yeast. Also, technological advances such as the ease of manipulating the genome by GFP-tagging, analyzing quantitative protein behavior, as well as *in vitro* approaches such as TIRF microscopy of individual actin filaments or myosin motility assays, have further clarified the role of the involved proteins in fission yeast [218]. Two complementary but independent mechanisms of ring assembly have been proposed based on the work in *S. pombe*. Briefly, the first one ['search, capture, pull, and release' (SCPR)] starts with the anillin-like Mid1 that accumulates about 1 hour before mitosis at mid-cell, thus providing the spatial cue for ring placement [220,221]. Mid1 then recruits IQGAP Rng2, type II myosin Myo2, followed by Rng3, F-BAR protein Cdc15, formin Cdc12 and α-actinin Ain1. Subsequently, Rng3 ensures activation of the Myo2 motor activity, while Cdc15 and Cdc12 stimulate actin assembly. Cdc8 is then recruited and further promotes actin filament assembly while at the same time inhibiting cofilin-mediated actin severing and directing Myo2 activity, which collectively leads to actomyosin ring compaction. Finally, Ain1 crosslinks actin filaments to provide tensile strength [218].

The second mechanism of ring assembly (the 'leading cable model') stems from observations that cytokinesis and growth are still supported in the absence of Mid1 [222,223,224]. Normally, deleting Mid1 results in delayed formation of actomyosin rings, which are often displaced and disorganized and lead to cytokinesis failure [222,225]. However, *mid1*-related defects can be suppressed by delaying septum formation, which is regulated by the 'septation initiation network' (SIN). Mutations in the SIN network, therefore, act as suppressors of *mid1* ring formation defects by ensuring that septum formation only occurs after the actomyosin ring has had a chance to form. Rings fail to form in the absence of both Mid1 and SIN function, highlighting the essential role of the two overlapping ring assembly mechanisms [218].

V.1.3. The Arp2/3 complex

In the 1990s, scientists discovered a set of highly conserved proteins called actin-related proteins (Arp). Among the Arps we find the Arp2/3 complex, which is composed of seven subunits that in budding yeast are Arp2 and Arp3, which give the complex its name, as well as Arc15 (actin related protein complex), Arc18, Arc19, Arc35 and Arc40. The function of the Arp2/3 complex is to nucleate actin, but in contrast to all other known actin nucleators, Arp2/3 organizes actin into branched filaments resulting in a regular 70° y-branching pattern [226,227]. This actin branching property of Arp2/3 is central to its function *in vivo* and is referred to as autocatalytic branching or dendritic nucleation [228]. In the current understanding of the dendritic nucleation model, Arp2/3 binds to the sides of an existing filament and caps the pointed end of the branched filament. The barbed end of the branched filament, however, is not capped and free to grow. Although several crystal structures of Arp2/3 have been solved, none of them is in the active form, because Arp2 and Arp3 are spaced too far apart to mimic the first building block for the branched filament – the most likely configuration for promoting actin side branching [202]. Recent studies using electron tomography and computational protein-protein docking simulations have resulted in a refinement of the actin branch creation model [229,230,231] (Figure 1); Arpc2, the mammalian homolog to budding yeast Arc35, and Arpc4, Arc19 in budding yeast, first bind to the mother filament, resulting in conformational changes in both filament and Arp2/3 that are thought to increase branch-point stability. Upon binding to the mother filament, Arp2 and Arp3 are likely to reorient into a dimer, thus creating the first two subunits of the branched filament.

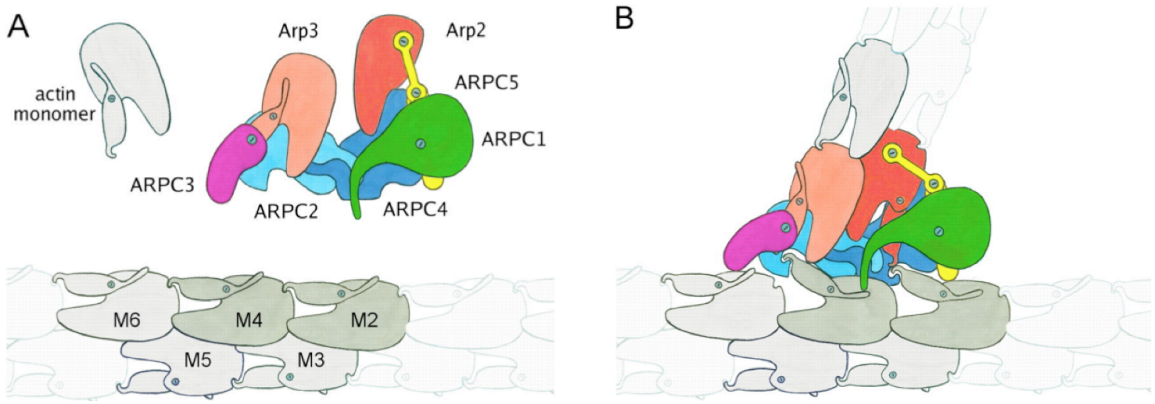

Figure A. Model of Arp2/3 binding to actin filament
(A) Schematic representation of the inactive Arp2/3 complex, actin monomer and actin filament. **(B)** Model of the branch junction. Upon binding of Arp2/3 to actin filament, the following steps are proposed to occur: (1) opening the nucleotide-binding clefts of mother filament subunits M2 and M4; (2) converting subunit M4 from a filament to a monomeric conformation; (3) converting Arp3 into filament conformation; (4) moving Arp2 tethered by ARPC5 next to Arp3 to form the first two subunits of the daughter filament; and (5) converting Arp2 into filament conformation. Reprint from [229] with permission from publisher. © 2008 Rockefeller University Press. Originally published in J. Cell Biol. doi: 10.1083/jcb.200709092.

The Arp2/3 complex on its own is not an efficient nucleator in mammalian cells and depends on several classes of nucleation-promoting factors (NPFs) [228]. Mammalian NPFs commonly activate Arp2/3 through their WCA domains, which are comprised of a WH2 domain that binds G-actin, an amphipathic connector region and an acidic peptide region that both bind Arp2/3. The current understanding is that binding Arp2/3 through the connector and acidic regions of the NPF triggers another conformational change that primes Arp2/3 for nucleation, while the WH2 region is responsible for delivering G-actin to the primed Arp2/3 complex. In budding yeast, there are 5 known NPFs, but in contrast to the mammalian Arp2/3 complex, in *S. cerevisiae* Arp2/3 can nucleate actin quite efficiently without NPFs [232], so maybe NPFs in budding yeast are more important for targeting Arp2/3 to sites of actin branch formation rather than activating it [233]. The five known NPFs in budding yeast include Las17 (a WAS, Wiskott–Aldrich syndrome protein), Myo3 and Myo5 (two type-I myosins), Pan1 [an Eps15 homology (EH) protein], and Abp1 (an actin filament–binding protein). Four of the 5 NPFs in budding yeast are also found in *C. albicans*; Las17, which is referred to as Wal1 in the pathogen [234], Pan1, Abp1 and Myo5. Myo3 is not present in *C. albicans* as it resulted after the whole-genome-duplication in *S. cerevisiae*, suggesting that Myo5

and Myo3 share functional redundancy in budding yeast.

V.1.3.1. Arp2/3 and endocytosis

The biological function of the Arp2/3 complex has been tightly linked to endocytosis, and we understand today that Arp2/3-mediated cortical actin patches are sites of endocytosis [192,235,236,237,238]. The first evidence linking actin to endocytosis came from a series of genetic screens in budding yeast that identified a number of endocytic mutants corresponding to actin-associated proteins [239,240,241,242,243]. It was also shown that receptor-mediated endocytosis, i.e. internalization of the [^{35}S]-labeled α-factor mating pheromone, as well as uptake of the fluid phase marker lucifer yellow (LY), was blocked in temperature sensitive actin mutants and that LY uptake was blocked in fimbrin (Sac6) and Arp2 or Arp3 point mutants [244,245]. Deletions in other actin-associated proteins like Arc35 or type I myosins, Myo3 and Myo5, also resulted in endocytotic defects [240,246]. Further studies have used chemical inhibition of the actin cytoskeleton. For instance, when *S. cerevisiae* cells were treated with Latrunculin-A (Lat-A), a drug that sequesters actin monomers, vesicle internalization was blocked [247,248,249], and when using jasplakinolide, a drug that stabilizes F-actin and causes it to accumulate as large F-actin clumps, uptake of LY was severely abrogated [250]. Immuno-electron microscopy further revealed that actin and actin-associated proteins localize to membrane invaginations [251]. Finally, technological advances such as two-color live cell microscopy have shown that endocytic and actin regulatory proteins colocalize in cortical actin patches and that endocytic cargos such as the lipid dye FM4-64 or fluorescent derivatives of the α-factor pheromone also colocalize with actin patches [252,253,254]. Collectively, these studies provide a substantial amount of evidence linking actin to endocytosis in budding yeast.

While it has been pointed out early on that actin, the Arp2/3 complex as well as many other proteins involved in budding yeast endocytosis have been conserved in mammals [255], some differences between budding yeast and mammalian endocytosis

have been noted. First, in contrast to yeast endocytosis where actin is absolutely required, actin's contribution to endocytosis in higher eukaryotes has remained controversial for many years [256]. Another difference is that clathrin adaptors like AP-2 that link cargo to the vesicle coat are central to endocytosis only in higher eukaryotes, but apparently dispensable in budding yeast. A third difference is that dynamins are crucial for vesicle scission in mammalian cells, but dynamin-related proteins play only a minor role in budding yeast [257,258]. More recent studies have now provided data that help explain some of those discrepancies. For instance, two large-scale screens have provided the first indication that the AP-2 and AP180/CALM adaptors may be important for cargo-specific uptake in budding yeast [259,260]. As well, recent studies have addressed the question why actin is essential for endocytosis in budding yeast, but not in mammalian cells. The answer to this might be that yeast cells have to overcome a turgor pressure that provides outward directed force on the plasma membrane. Aghamohammadzadeh and colleagues have shown that reducing the turgor pressure in *S. cerevisiae* by adding osmotic support to the growth medium allowed endocytosis in actin-bundling mutants or in cells treated with Lat-A [261]. Interestingly, clathrin-coated plaques that were recently found on the basal membrane of mammalian cells were shown to depend on actin for internalization, while clathrin-coated pits found in the same cells did not depend on actin for internalization [262]. It is therefore tempting to speculate that actin is required for internalization of plaques because of adhesive forces that anchor the basal membrane to the substrate [263]. Taken together, our current understanding is that many aspects of endocytosis are conserved from yeast to mammals despite some differences that remain.

The mechanism of how endocytosis works has been resolved in quite some detail and has been structured into different phases where protein modules perform specific functions. In budding yeast, for example, there are 3 phases, corresponding to endocytic site initiation, invagination and scission [192,236]. Five functional modules function during the 3 phases in a coordinated and sequential manner; the early module, the endocytic coat module, the WASP/myo module, the actin module and the vesicle scission module. In mammalian cells, on the other hand, there are 7 modules; the coat module, the NBAR domain module, the actin module, the dynamin/myosin/N-WASP

module, the GAK/post-scission module, the Rab5a module and the FBP17/CIP4 module [248,264,265]. For simplicity, I will briefly outline how the 5 modules in *S. cerevisiae* cooperate during the 3 phases of endocytosis (Figure 2).

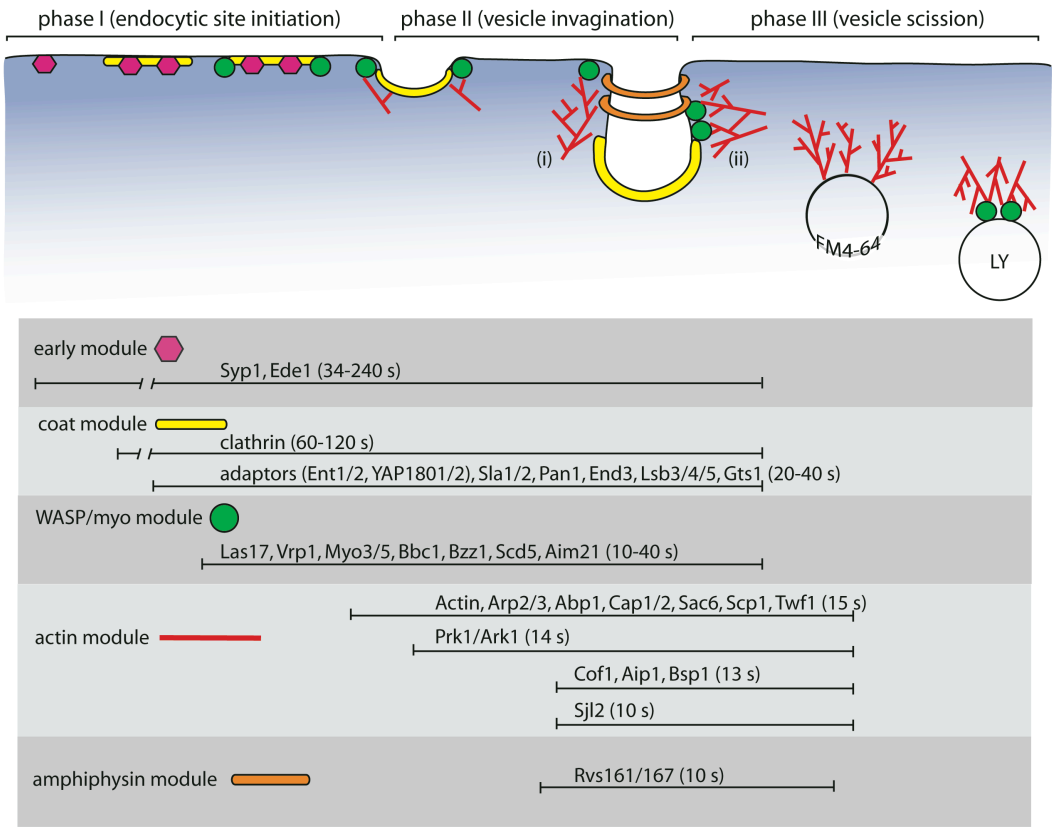

Figure B. Model of budding yeast endocytosis.
Five different protein modules cooperate during the 3 phases of endocytosis in *S. cerevisiae*. The top half of the figure represents an invaginating vesicle as it matures and the bottom half represents the lifetime (in seconds, bars not drawn to scale) of how long components of each module spend at sites of endocytic internalization. In this model, the early module first marks sites of endocytosis. Clathrin of the coat module arrives shortly after, followed by other coat module components like adapters (Ent1, Ent2, Yap1801, Yap1802) and Sla1, Sla2, Pan1 and End3. The WASP/myo module is recruited subsequently and prepares for actin nucleation. The actin module then arrives and nucleates actin to provide the force for vesicle invagination. Finally, the amphiphysins module arrives and is thought to pinch off the vesicle before cargo-loaded vesicles traffic to and fuse with endosomes. Note that two models of how actin nucleation drives invagination have been proposed: The growing barbed end of Arp2/3-driven actin nucleation can either push the vesicle away from the membrane [(i), and after scission FM4-64], or the growing barbed end could squeeze the invaginating tubule [(ii), and after scission LY]. This model has been redrawn based on several publications [192,235,238,265,266,267,268].

During the first phase, sites of endocytosis are marked by the early module, which

includes the F-BAR protein Syp1 and the adaptor-type protein Ede1 that both arrive 30 s to 210 s before initiation of actin nucleation [265]. Syp1 and Ede1 have roles in site formation (Ede1) or placement (Syp1). Later in phase I, the coat module arrives, and includes clathrin, adaptor proteins like the epsin homologues Ent1 and Ent2, as well as the AP180/CALM homologues (YAP1801/2). Following clathrin and adaptors, first Sla2 (a homologue of HIP1-R) and then a complex of three proteins, Pan1, End3 and Sla1, are recruited. Some of these proteins, like Ent1 or Sla2, contain ENTH or ANTH domains that are known to induce membrane curvature by interacting with phosphatidylinositol (4,5)-bisphosphate [PtdIns(4,5)P2] [236]. Other functions of the coat module include selection of cargo and preparation for actin nucleation. Las17, a component of the WASP-myo module, also arrives during phase I.

During phase II, other components of the WASP-myo module arrive, including Myo5 and Bbc1, an inhibitor of Las17. At about the same time, the actin module arrives and includes actin, Arp2/3, Abp1, Cap1, Cap2, Sac6, actin-regulating kinases Prk1/Ark1 and the phosphaditylinositol-4,5-bisphoshpate phosphatase Sjl2. This phase is the invagination step where Arp2/3-driven actin nucleation together with Myo5 motor activity promotes growth and extension of the membrane into the cell. Given the observation that all NPFs remain at the membrane, together with clever FRAP experiments on actin nucleation at the plasma membrane, it has been shown that Arp2/3-dependent actin nucleation occurs at the plasma membrane and not on the invaginating vesicle [252].

Finally, during the third phase of endocytosis scission occurs and the vesicle moves away from the membrane. This phase involves the scission module comprised of two amphiphysins (Rvs161 and Rvs167) that both have BAR domains important for membrane tabulation [269]. At about the same time as scission occurs, the coat complex is disassembled through both kinase and phosphatase activities. For instance, Prk1/Ark1 kinases directly phosphorylate coat components like Pan1 and Sla1, which leads to their disassembly, while Sjl2 dephosphorylates PtdIns(4,5)P2 to PtsIns 4-P, thus likely reducing the affinity of ENTH and ANTH containing proteins (Sla2, Ent1, Ent2) to the membrane [266]. Following scission and uncoating, the vesicles move along actin cables and fuse with endosomes. This process has been visualized with either FM4-64

containing vesicles or with fluorescently labeled α factor containing vesicles [253,254]. It has also been demonstrated that vesicles and endosomes move towards each other on actin cables, and that the speed of actin filament growth and endosome movement are very similar, suggesting that endocytotic vesicles move along actin cables as they are polymerized [253].

Taken together, there is substantial evidence that links the Arp2/3 complex to endocytosis and we understand in quite some detail how different protein modules cooperate during the 3 stages of endocytosis. Our previous observations that *arp2/3* mutants can still endocytose FM4-64 and LY in *C. albicans* were therefore surprising, and led to two important questions. First, which pathway was used to traffic cargo to the vacuole, and second, whether Arp2/3-independent actin dynamics were involved in endocytosis. In order to address these key points, we performed the following study.

V.2. Actin dynamics and endocytosis in the absence of Arp2/3 in *Candida albicans*

Elias Epp[1,2], Elena Nazarova[1], Lois M. Douglas[3], James B. Konopka[3], Jackie Vogel[1], Malcolm Whiteway[1,2]*

[1] Department of Biology, McGill University, Montreal, Quebec, Canada H3A 1B1
[2] Genetics Group, Biotechnology Research Institute, National Research Council of Canada, 6100 Royalmount Ave., Montreal, Quebec, Canada H4P 2R2
[3] Department of Molecular Genetics and Microbiology, Stony Brook University, Stony Brook, NY 11794-5222

Corresponding author:
Dr. Malcolm Whiteway
Genetics Group,
Biotechnology Research Institute,
National Research Council of Canada,
6100 Royalmount Ave.,
Montreal, Quebec,
Canada H4P 2R2
Tel: 001-514-496-6146
Fax: 001-514-496-6213
Email: malcolm.whiteway@cnrc-nrc.gc.ca

Abstract

The actin cytoskeleton plays a crucial role in many cellular processes, including various forms of cellular uptake. Clathrin mediated endocytosis (CME), one of the main routes for endocytosing a variety of cargos, is conserved across evolution and the only well-described endocytic pathway in fungal cells. Actin nucleation mediated by Arp2/3 provides the driving force needed during CME to successfully endocytose invaginating vesicles. Using a combination of spinning disc confocal, TIRF and electron microscopy coupled to quantitative motion analysis, we have compared the non-functional CME pathway of *Candida albicans* in the absence of the Arp2/3 complex to the pattern seen in wild type cells. While some components in this pathway are still correctly localized, all protein modules that act at different stages during CME become non-productive in the absence of Arp2/3. There are particularly severe consequences of loss of Arp2/3 function during the middle phase of the CME pathway, where components that normally localize with Arp2/3 fail to localize with either the coat or the scission machinery. We also present evidence for a parallel endocytic pathway that is Arp2/3-independent in this fungal pathogen. This Arp2/3-independent pathway is actin dependent and cargo specific as receptor mediated endocytosis was not functional without Arp2/3 activity, suggesting that, similar to mammalian systems, there is more than one endocytotic pathway in fungal cells. Finally, ultrastructural analysis of invaginating structures suggests that tubular-invaginations are longer, not shorter, in Arp2/3 mutants, implying that Arp2/3-mediated branched actin is involved in later stages of endocytosis when scission takes place.

Introduction

Clathrin-mediated endocytosis (CME) is a fundamental mechanism in living cells, important for capturing macromolecules from the extracellular environment as well as selectively recycling and internalizing membrane lipids and membrane-bound proteins [270,271]. Many of the molecular mechanisms involved in CME are conserved among eukaryotes and can be broken down into three main phases: (1) clustering of coat proteins and cargo molecules at the nascent endocytic site, (2) initial membrane deformation and inward membrane growth, and (3) vesicle scission and release into the cytoplasm [256]. More than 60 proteins have been identified that function during CME in *Saccharomyces cerevisiae* and many of them have been analyzed by multicolor live-cell fluorescent microscopy [248,252]. Such studies have shaped the picture of a highly coordinated process where 5 protein modules cooperate to drive vesicle development with individual factors temporally and spatially assembling and disassembling at endocytic sites [reviewed in: 192,235,236,237,238 and ,265]. A similar modular design of endocytosis has been described in the fission yeast *Schizosaccharomyces pombe* and recently in higher eukaryotes, where 7 protein modules function during CME [264,272,273].

In *S. cerevisiae*, the 5 functional modules that cooperate during the 3 phases of endocytosis are: (1) the early module, (2) the coat module, (3) the Wiskott-Aldrich syndrome protein (WASP)-myosin (WASP/Myo) module, (4) the actin module and (5) the scission (or amphiphysin) module. The early module is the first to arrive at the nascent endocytic site and consists of Syp1 (a F-BAR-related protein) and Ede1 (an Eps15 homology (EH)-domain protein) [265,274]. The coat module arrives next; first clathrin followed by other coat components like yeast epsins (Ent1, Ent2), Sla2 (a homologue of HIP1-R), Sla1 (a SH3 domain-containing protein), two EH-domain proteins (End3, Pan1), and YAP1801/2 (AP180/CALM homologues) [249,252]. The function of these early and coat modules include initial membrane bending and linking coat components to the actin cytoskeleton, respectively. The recruitment of these components is actin independent, but their disassembly or movement away from the membrane is actin dependent. The WASP/myo module arrives subsequently; this includes several Arp2/3 complex activators like Las17 (yeast WASp homologue) or type

I myosins (Myo3, Myo5). During this stage, Sla1 inhibits the actin polymerization function of Las17 until Vrp1 (yeast WIP homologue), Bbc1 and Bzz1 arrive to release Sla1's inhibition on Las17 [275]. The actin module is recruited next and includes actin, Arp2/3, Cap1, Cap2, Sac6, Abp1, actin-regulating kinases Prk1/Ark1, the phosphaditylinositol-4,5-bisphosphate phosphatase Sjl2 and others [248,266,268]. The actin module orchestrates the formation of actin patches, which have been shown to be sites of endocytosis [253,254]. The function of the Arp2/3-mediated branched actin network is thought to provide the force that together with type I myosin motor activity extends vesicle invagination [252,267]. As the nascent endocytic vesicle invaginates, facilitated by the dynamin-like protein Vps1, two amphiphysins (Rvs161, Rvs167) of the scission module are recruited and help release the vesicle, which then traffics along actin filaments to ultimately fuse with endosomes [253,254,257].

The majority of proteins involved in endocytosis regulate actin related processes at sites of clathrin coated pits [235,255], and consequently, the actin cytoskeleton has emerged as an essential element during endocytosis in fungal cells; it also plays a role during mammalian endocytosis [236,256]. Because of the essential nature of the actin cytoskeleton, however, studying its function in living cells and its contribution during CME has been challenging. To circumvent these limitations, studies in *S. cerevisiae* have made use of either conditional actin or Arp2/3 complex mutants or used chemical inhibition like Latrunculin-A (Lat-A), a drug that sequesters actin monomers, or jasplakinolide, a drug that stabilizes F-actin and causes it to accumulate as large F-actin clumps. In these cases, different forms of endocytosis have been severely abrogated or entirely inhibited [239,244,246,247,248,249,250,276]. These approaches, however, are limited in that conditional mutants don't completely reflect the effect of the gene's function as low protein levels might remain, while chemical inhibition of the actin cytoskeleton over longer periods is lethal to cells.

Conveniently, the human fungal pathogen *Candia albicans* is not significantly growth compromised in the absence of Arp2/3 function. The advantage here is that one can directly assess the prediction that Arp2/3-driven actin nucleation drives invagination, and test theoretical models that have predicted how initial actin-mediated curvature bending results in the recruitment of BAR domain proteins and lipid phosphatases to form a lipid

phase segregation, which generates a force that constricts the membrane and drives vesicle scission [277,278].

We have previously shown that although the Arp2/3 complex is not essential for survival in *C. albicans*, it is required for hyphal formation and virulence [279]. We also demonstrated that bulk membrane (FM4-64) and fluid phase (Lucifer Yellow, LY) endocytosis still occurred in *arp2/3* mutants, but it was unclear whether CME, the only well-described endocytic pathway in fungal cells, was still functional in *arp2/3* mutants. As well, given the essential link between actin and endocytosis in fungal cells [236], it remained unclear whether Arp2/3-independent actin dynamics were involved in endocytosis in *arp2/3* mutants. Here, we demonstrate that the CME pathway in WT *C. albicans* consists of the modular design similar to other fungal systems, but that this endocytic pathway is not functional in the absence of Arp2/3. As well, we show that receptor-mediated endocytosis is not functional in *arp2/3* mutants, while FM4-64-mediated uptake remains actin dependent in *arp2/3* cells, suggesting that similar to higher eukaryotes, there are more than one endocytotic route in fungal cells. Finally, EM analysis suggests that invaginating tubules are longer, not shorter, in *arp2/3* mutants, implying that the Arp2/3 complex is not involved in the initial formation of invaginations. Instead, the data suggest that Arp2/3-mediated actin structures could provide the force to squeeze together tubular invaginations and thereby assist other scission module components to help release the vesicle.

Results

Receptor-mediated endocytosis is not functional in the absence of Arp2/3

Given that cargos like bulk membrane (FM4-64) as well as a fluid phase marker (LY) were still internalized and correctly localized to the vacuole in *C. albicans arp2/3* mutants [279], we investigated whether these mutants showed any defects in receptor-mediated endocytosis. We used the GFP-labeled Ste2 pheromone receptor as a marker and assayed receptor uptake upon pheromone treatment. While the GFP-signal disappeared from the membrane in WT cells after 40 minutes of pheromone induction, in *arp2* mutants the signal remained at the membrane (Figure 1A). When we used a second inducible marker for receptor-mediated endocytosis, the methionine permease Mup1, we found the same results; no GFP-signal was detected at the plasma membrane in WT cells upon addition of methionine, but remained at the membrane in *arp2* cells (Figure 1B). To rule out that the strong vacuolar background staining observed in both the Ste2 and the Mup1 assays was not camouflaging any minor uptake in *arp2* cells, we developed the pH-sensitive GFP variant, pHluorin [280], for use in *C. albicans* and repeated the Mup1 assay. In WT cells the pHluorin signal disappeared completely after 60 minutes of incubation time, while Mup1 was still detected at the plasma membrane in *arp2* cells, even after extended overnight incubation periods (data not shown and see below).

Because a recent study has suggested that relieving the turgor pressure by providing osmotic support reduces the requirement for actin during endocytosis in *S. cerevisiae* [261], we grew *arp2* cells in 1.5 M sorbitol media to test whether this can suppress receptor-mediated endocytotic defects in *arp2* cells. As well, based on a report showing that increased Rho1 activity suppresses receptor-mediated endocytotic defects in adaptor mutants (Ent1, Ent2, Yap1801 and Yap1802) [281], we investigated whether overexpressing Rho1 in *C. albicans arp2* cells would allow Mup1 endocytosis. While qPCR analysis showed that Rho1 was 8.5 fold overexpressed in *arp2* cells, no difference was observed in the presence of either this Rho1 overexpression, osmotic support, or combination of the two in terms of Mup1-pHluorin-endocytosis in *arp2* cells (Figure 1B). These results demonstrate the crucial function of Arp2/3 in receptor-mediated

endocytosis in *C. albicans* and suggest a cargo-specific function for Arp2/3-independent endocytosis.

A modular architecture of CME in *C. albicans*

In order to gain insights into how cargo-specific endocytosis works in the absence of Arp2/3 in *C. albicans*, we tested the functionality of the only well-described endocytotic pathway in fungal cells, the clathrin-mediated pathway. To do this, we GFP-tagged proteins involved in every stage of this pathway and recorded their dynamic behavior by both high-speed spinning-disk confocal and total internal reflection fluorescence (TIRF) microscopy. GFP tags were inserted at the C-terminus of proteins; the fusion gene constructs were under the control of their endogenous promoters, and represented the only functional gene copy in the cell. All these GFP-tagged strains showed growth rates and morphologies comparable to both their respective parent strain, indicating that the GFP constructs didn't significantly interfere with functionality (Table S1). A summary of patch dynamics from all components tested in the clathrin-mediated pathway is provided as movie 1 (movies can be accessed online as described at the beginning of the material and method section).

We tracked the position of the GFP-tagged proteins over time and applied several forms of quantitative motion analysis to assess the affect of disrupting Arp2/3 function. We first expressed patch dynamics as mean square displacement (MSD) over time (Figure 2). This analysis showed that initial patch dynamics were similar in WT and *arp2* mutants for many components. For example, Syp1 of the early module showed similar dynamics in WT and *arp2* cells during the first 60 seconds of patch tracking (Figure 2A), but while Syp1 frequently disappeared in WT cells, Syp1 remained at the cell membrane in *arp2* mutants. In order to better express such additional quantitative tracking data, we complemented the MSD plots with 3 other analytical elements of patch dynamics. We determined the percentage of cells that left the origin, measured the average track displacement length and established the average track duration (Figure 3)(see material and methods for details). For instance, 86% of Syp1 patches in WT cells left the origin, i.e. disappeared in this case, while no Syp1 patch disappeared in *arp2* cells. The average

track displacement length, i.e. the distance between first to last spot detection, was comparable with 0.08 μm in WT and 0.04 μm in *arp2* cells. Finally, the track duration was on average 101 seconds in WT and 120 seconds (the maximum length of observation) in *arp2* cells. This analysis demonstrates that the early module component Syp1 is correctly recruited to the cell membrane in *arp2* cells, but that its turnover is dependent on a functional Arp2/3 complex.

A similar conclusion can be drawn for the coat module (Sla2, Pan2, End3) as well as the Myo/WASP module (Myo5, Vrp1, Wal1); all coat and Myo/Wasp components correctly localized to the plasma membrane, but remained static and didn't disappear in *arp2* cells. In WT cells, coat components typically showed an initial stationary phase followed by a mobile phase when patches moved away from the membrane. The average track durations varied and ranged from 66 s (Sla2) to 36 s (Pan1) and 63 s (End3), while the average track displacement length as well as the percentage of patches leaving the origin was similar for all three coat components, with around 0.20 to 0.30 μm displacement length and at least 97% of patches leaving the origin. The Myo/WASP module was characterized by a relatively short stationary phase followed by patch disappearance. Average track duration for Myo/WASP components varied between 13 s (Myo5 and Vrp1) and 31 s (Wal1), while all three components showed similar average track displacement length and percentage of cells leaving the origin, which were around 0.08 μm and 100%, respectively. Clearly, loosing Arp2/3 complex function has a profound impact on these early modules of the clathrin mediated pathway. Remarkably, when *arp2* cells carrying GFP coupled to clathrin light chain (Clc1) were analyzed, we found that clathrin existed in two populations. The first population remained static at the membrane and in most cases didn't disappear, suggesting that clathrin that participates in clathrin-mediated endocytosis at the stage of the vesicle internalization was non-functional. The second clathrin population appeared intracellular and retained dynamics similar to WT cells, indicating that clathrin-supported intra-organelle trafficking was still functional. TIRF microscopy confirmed these observations; clathrin close to the membrane disappeared in WT cells when imaged over 6 minutes, while during the same time frame clathrin remained static in *arp2* cells (movie 2).

The actin module (e.g. Sac6, Abp1, Cap1, Cap2) in *arp2* mutants still retained some properties of patch dynamics, but importantly, this behavior was unproductive. In WT cells, Sac6, Abp1, Cap1 and Cap2 were associated with an initial stationary phase, which was followed by a rapid phase of patches moving away from the membrane. Average track duration and average track displacement length for Cap2, Cap1, Sac6 and Abp1 was 11 s, 13 s, 16 s, and 20 s, and 0.38 μm, 0.41 μm, 0.45 μm and 0.49 μm, respectively. All observed patches left the origin. Imaging actin patches in *arp2* cells was more difficult as the same patch often seemed to drift in and out of the focal plane. Consequently, it was unclear whether patches actually internalized or whether they showed increased lateral movement along the membrane. We therefore analyzed patch behavior of actin module components in *arp2* mutants by recording 20 z stacks at 200 nm intervals over time. Analyzing dynamics from these movies demonstrated that while more than 70% of patches move at least 100 nm away from the origin, these patches don't disappear and turnaround, but instead are detected during the entire length of observation (120 seconds). The average displacement length was 0.27 μm, 0.20 μm, 0.43 μm and 0.29 μm for Cap2, Cap1, Sac6 and Abp1, respectively. The number of patches was remarkably reduced in *arp2* cells with usually 20 or less Cap2, Cap1, Sac6 or Abp1 signals present, suggesting that these signals are accumulated remains of non-functional Arp2/3 patches. Frequently, the signal appeared associated with actin filament-like structures. In the absence of Arp2/3, Cap1 was also often associated with the cytokinetic ring, an observation that might be explained by the fact that in WT cells cytokinetic rings are often decorated by bright Arp2/3 spots and therefore masked from detection.

Analyzing patch dynamics for Prk1 and Sjl2 was not possible in *arp2* mutants as Prk1 was not clearly localized to any structure and Sjl2 appeared associated with filamentous-like structures. In WT cells, Sjl2 and Prk1 had average track durations of 10 s and 15 s, respectively. Average track displacement was 0.38 μm for Sjl2 and 0.41 μm for Prk1. All Sjl2 and Prk1 spots left the origin.

Together, these data suggest that Arp2/3 is instrumental for the proper orchestration and spatial and temporal regulation of actin module components.

Finally, the scission module (e.g. Rvs167) was the only component that retained functionality in *arp2* cells. However, the efficiency of Rvs167 turnaround was significantly reduced. In WT cells, Rvs167 spots showed average track durations of 5 s, average displacement length of 0.15 μm and all observed Rvs167 signals disappeared from the origin. In *arp2* cells, only 14.6 % of Rvs167 spots disappeared from the origin with the remaining 85.4% spots staying stationary at the membrane. The few spots that disappeared showed WT-like tracking durations, but on average the track duration for all Rvs167 spots was 111 s and the average track displacement length was 0.08 μm in *arp2* cells. These results indicate that although Rvs167 dynamics is clearly impeded without Arp2/3, it is the only protein studied that retains aspects of all elements of functionality. Overall, the analysis of the clathrin-mediated pathway in absence of *arp2* demonstrated that this pathway is heavily affected, with most components loosing their functionality. This suggest that cargo uptake in *arp2/3* mutants follows a second, clathrin-independent pathway.

Actin dynamics in the absence of Arp2/3

In order to gain insights how Arp2/3-independent endocytosis works, and in particular whether this is an active process, we assessed the importance of the actin cytoskeleton and whether Arp2/3-independent elements of actin dynamics are required for endocytosis in *C. albicans*. In order to visualize the actin cytoskeleton in live cells, we first developed the LIFEACT probe coupled to GFP. LIFEACT consists of the first 51 amino acids of the *S. cerevisiae* Abp140, which is sufficient for actin binding [211]. LIFEACT-GFP didn't appear to affect growth as hyphae formation was not influenced in WT cells and sensitivity to Cytochalasin A (CA), a drug that binds barbed-ends of actin filaments [282,283], was the same compared to control cells (data not shown).

LIFEACT-GFP expressed in WT cells labeled actin patches and cables, while in *arp2* mutants no actin patches were observed and detection of cables was easier, probably facilitated by the absence of bright actin patches. In general, two populations of actin cable structures were observed in both WT and *arp2* cells; long cables that elongated and

depolymerized and shorter, fast moving cables that didn't appear to grow or shrink. The first actin cable population was observed in small and mid-size budded cells, corresponding to the G1/S phase of the cell division cycle, where actin cables originated at the bud neck and elongated towards the mother cell along the polarity axis. These actin cables depolymerized in the same direction, i.e. cable depolymerization began at the bud neck and proceeded towards the mother cell. In larger budded cells during the G2/M phase, cables also grew into the daughter cell starting from the bud neck. Actin depolymerization started again at the bud neck and proceeded towards the daughter. The rate of actin polymerization for long actin cables was similar in WT and *arp2* mutants; 0.20 ± 0.07 μm/s for WT and 0.22 ± 0.04 μm/s in *arp2* cells. Besides these long cables that usually span from the bud neck to the distal side of either the mother or daughter cell, a second population of actin cables was observed. These were typically short, they originated from different places and moved almost twice as fast as polymerization of long cables; 0.47 ± 0.13 μm/s for WT and 0.49 ± 0.12 μm/s for *arp2* cells (Figure 3, movie 3). Similar actin cable dynamics were previously observed in budding yeast [284].

One noticeable difference in actin cytoskeleton organization between WT and *arp2* mutants was that in mutant cells the actin cytoskeleton appeared less oriented and often disorganized. Cables were frequently aligned perpendicularly to the polarity axis. A second difference is that in *arp2* cells, more cables were visible. As well, in some cases the cables originating from the bud neck didn't grow until the cable reached the distal side, but remained disconnected from the cortex (data not shown).

Together, these data demonstrate that while actin cable dynamics are not significantly affected in *arp2* mutants, the Arp2/3 complex plays a role in spatially organizing different elements of the actin cytoskeleton including actin cables.

FM4-64 uptake is actin dependent in *arp2* mutants

We next used the LIFEACT-GFP probe to investigate whether Arp2/3-independent actin structures were involved in FM4-64 uptake in *arp2* mutants. To this end, we blocked actin dynamics by adding 10 μg/ml of CA. While this drug treatment completely

abolished all fluorescent signals in *arp2* mutants after 3 minutes, WT cells carrying LIFEACT-GFP were more resistant to this drug and showed non-motile actin patches at the membrane (Figure 5A). Because we were not able to completely block the LIFEACT signal in WT cells even at higher drug concentrations (data not shown), we performed the following experiments with *arp2* cells only. After actin dynamics was blocked for 3 minutes in *arp2* cells, we grew the cells in the presence of FM4-64 for 5 minutes, washed non-adherent dye away and chased dye internalization over 20 minutes while CA was still present. After 30 minutes we inhibited endocytosis by adding sodium azide and sodium fluoride and imaged immediately. This procedure showed that whereas 95% of controls cells treated with DMSO had FM4-64 internalization and a clear vacuolar staining, none of the CA treated cells showed dye uptake. In most cases, the dye appeared evenly distributed at the cell membrane and only occasionally did we observe the dye as concentrated punctae at the membrane. To rule out that cells are dead after 30 minutes of CA treatment as well as showing that this drug treatment is reversible and doesn't impede actin dynamics once the drug is washed away, we did two control experiments. First, *arp2* cells were assessed for viability after 30 minutes in the presence of CA and found to be as viable as when treated with DMSO (Figure 5B, bottom). Second, CA was washed away after 30 minutes and recovery of actin dynamics was assessed at 4, 8 and 24 hours after washing the drug away. This showed that at 4 and 8 hours only a few cells (2 % and 11%) showed actin dynamics and that at 24 hours the majority of cells (> 90%) had regained actin dynamics.

Together, these data demonstrate that *arp2* mutants endocytose FM4-64 in an actin dependent manner, suggesting that dye uptake is an active process in *arp2* cells.

Invaginating tubules are longer in *arp2/3* mutants compared to WT

To test whether the force generated by Arp2/3-mediated actin nucleation is needed for vesicle formation during endocytosis, we examined endocytic vesicles by analyzing cells at the ultrastructural level with transmission electron microscopy (TEM). Electron micrographs of log-phase cells grown in YPD media showed that invaginating tubules are

on average 121 and 117 nm long in WT and Arp2 revertant cells, respectively (Figure 6A). This observations stands in good agreement with studies in *S. cerevisiae* that showed that invaginating tubules can reach up to 180 nm in length and 50 nm in diameter in WT cells [285]. Surprisingly, in *arp2* and *arp2/arp3* mutants invaginations still formed and were on average longer compared to WT cells, ranging from 179 to 202 nm in *arp2* and *arp2/arp3* mutants, respectively. In addition, invaginating tubules appeared uniformly tubular in WT and revertant cells, but in mutant cells some tubules were inflated close to the membrane with diameters exceeding 100 nm (Figure 6B). In these cases, the cell wall appeared to be growing into the tubules, an observation that we never encountered with WT or revertant cells, which showed invaginations that typically have diameters of maximum 100 nm.

These data suggest that Arp2/3 is not required for initial membrane invagination, but that maintaining a uniform tubular structure is dependent on an actin meshwork nucleated by Arp2/3.

Discussion

The study of actin related processes in living cells is often challenged by the essential function of actin and its associated proteins, particularly when investigating gene functions in a deletion background. Here, we harnessed the non-essential function of Arp2/3 in *C. albicans* and addressed two key questions. First, given that previous results showed that FM4-64 and LY endocytosis takes place in *arp2* and *arp2/arp3* mutants [279], it remained unclear whether Arp2/3-independent endocytosis relied on the only well-described endocytic pathway in fungal cells, clathrin-mediated endocytosis, or whether Arp2/3-independent endocytosis used a different route. Second, given the substantial evidence that links actin to endocytosis in fungal cells, it was unclear whether Arp2/3-independent actin dynamics were involved in endocytosis in *arp2/3* mutants.

Evidence for clathrin-independent endocytosis in *C. albicans*

To answer these questions, we used confocal spinning disc and TIRF live cell imaging to analyze the dynamic behavior of components at every stage of the clathrin-mediated endocytic pathway. This analysis showed that in WT cells, overall protein dynamics were similar to those of other fungal systems. For example, Syp1 of the early module and clathrin of the coat module remained the longest at the membrane before disappearing. Other coat components like Sla2, Pan1 or End3 displayed variable length stays before invaginating. Myo5, Vrp1 and Wal1 of the Myo/WASP module left the membrane rather quickly, but didn't appear to invaginate. The actin module (e.g. Sac6, Cap1, Cap2, Abp1, Prk1, Sjl2) was characterized by an initially stationary phase, which was followed by rapid movement and invagination, while Rvs167 of the scission module showed similar characteristics, but didn't invaginate. These observations agree well with how clathrin-mediated endocytosis functions in both budding and fission yeast [235,272,273].

When analyzed in the *arp2* deletion background, all components showed drastically different patterns from the control. Components of the early, coat and Myo/WASP module remained stationary at the cell membrane and didn't disappear, demonstrating

that recruitment to the plasma membrane is Arp2/3-indpedenet, but recycling and movement away from the membrane critically depends on Arp2/3 function. The actin module was also heavily affected in *arp2* cells. The number of patches was remarkably reduced to only a few signals, and while most actin module components retained some dynamics, this movement was unproductive as patch internalization was not observed. The critical role of the actin module during clathrin-mediated endocytosis is further demonstrated by mislocalization of Prk1 and Sjl2. Both the actin-regulating kinases Prk1 and the phosphaditylinositol-4,5-bisphosphate phosphatase Sjl2 were not localized in distinct patch structures. Instead, Sjl2 appeared as filament-like structures and Prk1 signals were not associated with any clear pattern. Finally, Rvs167 of the scission module was the only protein that retained partial functionality in *arp2* cells, as in ~14 % of cases Rvs167 showed characteristics similar to WT. Because other components of the scission module like Rvs161 were not localized in *arp2* cells (data not shown), this suggests that scission module function is also heavily affected.

Besides this analysis that demonstrated that all components examined of the clathrin-mediated pathway lost either their dynamic behavior or productivity, several additional arguments support the idea of clathrin-independent endocytosis in *C. albicans*. For instance, clathrin exists as two populations in *arp2* cells. The first clathrin population is trapped at the membrane and remains static without clear evidence of recycling or turn around, while the second population appears intracellular and is very dynamic, similar to the situation in WT cells. This second clathrin population is likely involved in intracellular trafficking events and plays essential roles, as deleting clathrin in *C. albicans* results in lethality (Figure S1). If clathrin is involved in Arp2/3-independent endocytosis, then clathrin function doesn't seem necessary at the stage of membrane internalization.

Another argument for clathrin-independent endocytosis in *arp2/3* mutants is that cargo such as FM4-64 or LY is correctly localized to the vacuole, but not other organelles. This suggests that delivery from the membrane to the target destination is an active process and follows a controlled pathway. In agreement with this, we show that one such active process for FM4-64 uptake in *arp2* cells depends on the actin cytoskeleton. Inhibiting actin dynamics with CA completely abolished uptake of FM4-64 in *arp2* cells. How precisely Arp2/3-independent actin dynamics are involved in this process, how cargo

passes the plasma membrane barrier and how the dye is trafficked to the vacuole remains to be investigated. Time-lapse movies of FM4-64 uptake suggest that vesicles are not involved [279], or if they are, then they might be too faint or small to be detected with current imaging techniques.

Lastly, similar to mammalian cells where clathrin-independent endocytosis is cargo-specific [270], we found that receptor-mediated endocytosis was not functional without Arp2/3 in *C. albicans*. Both the pheromone receptor Ste2 and the methionine permease Mup1 were still present at the membrane in *arp2* cells after endocytic stimulation. A solid structure in the form of a receptor might need more energy to be internalized and therefore depend on both clathrin-supported vesicles as well as Arp2/3-mediated force generation.

Together, these observations demonstrate that Arp2/3-independent endocytosis doesn't rely on the clathrin-mediated endocytic pathway, is cargo specific and actin dependent, suggesting that besides CME there are additional endocytic pathways in *C. albicans*.

Arp2/3 function during endocytosis

Several decades of electron and live cell microscopy together with genetic and biochemical studies have provided substantial evidence that Arp2/3 functions during endocytosis [192,235,236,237,238]. Our studies corroborate this view, as a functional clathrin-mediated endocytic pathway strictly depends on Arp2/3-nucleated actin polymerization. The reason why CME is not functional and vesicle fission doesn't occur in *arp2/3* mutants is likely a result of different modules not being properly assembled at sites of endocytosis. Rvs161 and Rvs167 of the scission module, for example, were heavily affected with Rvs161 loosing any capacity to localize to the plasma membrane in *arp2* mutants. Prk1 and Sjl2 localization also strictly depended on Arp2/3 in *C. albicans*. This is similar to budding yeast, where a functional actin cytoskeleton is necessary for correct Prk1 and Sjl2 localization [286,287,288], which in the case of Prk1 could directly depends on Arp2 and Arc40, two physical interaction partners of the Arp2/3 complex [289,290]. Compared to other actin module components like capping or actin filament

crosslinking proteins such as Cap1, Cap2, Sac6 and Abp1, Prk1 and Sjl2 are not directly involved in actin filament regulation. Both Prk1 and Sjl2 are implicated in patch disassembly, Prk1 by phosphorylating coat components including Pan1 [291,292,293], and Sjl2 by dephosphorylating PtdIns(4,5)P2 to PtsIns 4-P, thus reducing the affinity of certain coat components for vesicle membranes [287,294]. Without these two disassembly routes, modules during early stages of endocytosis are not properly recycled, thus providing an explanation why components of the early, coat and Myo/WASP module are trapped at the plasma membrane in *C. albicans arp2* mutants [294]. These observations also suggest that besides force generation, Arp2/3-mediated branched actin provides spatial and temporal clues and therefore could serve as scaffold to orchestrate different proteins during the highly coordinated process of endocytosis.

One important step during clathrin-mediated endocytosis in budding yeast is the mechanochemical feedback between membrane curvature and biochemical pathways that cooperate to drive endocytosis [278,295]. In this theoretical model, which quantitatively recapitulates key features of budding yeast endocytosis and vesicle formation, coat proteins first deform the membrane, thus creating shallow dome-shaped invaginations. Actin then drives the invagination deeper into the cytoplasm leading to tubule formation. The resulting membrane curvature corresponds to the preferred curvature for BAR domain proteins (BDP), which subsequently bind and further promote tubule extension through their curvature sculpting activity. This leads to an even higher degree of tubule curvature and allows PIP_2 phosphatases like Sjl2 to access PIP_2 at places where BDP is not protecting PIP_2 from phosphatase activity. This spatial restriction of phosphatase activity leads to a lipid phase segregation, which provides an interfacial force to squeeze the neck. Squeezing of the neck in turn increases the local curvature, which feeds back to more phosphatase activity until enough force is generated to pinch off the vesicle [278,295].

Our data agree with this model in that localization of PIP_2 phosphatases, for instance Sjl2, to sites of endocytosis is critical for vesicle release. In the absence of *arp2*, Sjl2 is not localized to the plasma membrane and fission does not take place. The data presented here also agree well with previous results that have shown that Arp2/3-mediated actin

branches together with type I myosin motor activity provide the force for vesicle internalization during CME [252,267]. Surprisingly, our results indicate that Arp2/3 is not required for membrane invagination *per se*. Electron microcopy data showed that invaginating structures are on average longer in *arp2* and *arp2/arp3* mutants compared to WT cells and that such structures in some cases lost their tubular shape at the neck close to the membrane. These data suggest that the Arp2/3-nucleated actin meshwork is not primarily involved in creating tubular shapes of invaginating structures, but instead indicate that Arp2/3 is required at later stages of endocytosis just before scission takes place. Based on these observations, we propose a mechanism in *C. albicans* that uses the force generated by Arp2/3 to squeeze tubular membranes together to help release vesicles, instead of using this force for tubule creation or elongation [238,296]. In that model, if scission doesn't take place, invaginating tubules continue to grow, maybe through the cell wall that pushes material into the tubules, which leads to wider invaginations at the base close to the membrane.

The cooperative interaction between lipid-phase segregation, Arp2/3-driven force generation as well as dynamin-assisted vesicle tabulation is further illustrated in that both *arp2/3* mutants of *C. albicans* as well as *sjl1sjl2* and *vps1* mutants in budding yeast show invaginating structures that are at least as long as in the respective WT cells [257,297]. Therefore, lipid phase segregation, dynamin-mediated tubulation or Arp2/3-branched actin alone is not sufficient to allow vesicle fission to occur, but highlights the complex interplay of different players to drive clathrin-mediated endocytosis.

Materials and Methods

Movies are accessible at the following webpages (if the link doesn't work when clicking on it in the PDF version, copy and paste it manually in the address bar of the web browser. Movies can best be viewed with the QuickTime player):

movie 1 (legends to movies and figures are listed below, starting on page 111)
http://dl.dropbox.com/u/13736754/movie 1.mov

movie 2:
http://dl.dropbox.com/u/13736754/Movie 2.mov

movie 3:
http://dl.dropbox.com/u/13736754/movie 3.mov

Strains and media

All strains are derived from SN148 [298], and are listed in table S1 together with primers used in this study, which are listed in table S2. Table S1 and S2 can be accessed at the following webpage:

http://dl.dropbox.com/u/13736754/table S1 and S2.xlsx

Strain construction followed standard transformation protocols, using homologous recombination for genomic marker integration, and selection on synthetic media (s. below) that contained the necessary auxotrophic supplements, as described [299]. Correct marker insertion was verified by diagnostic PCR [300]. In order to have sufficient auxotrophic markers available for subsequent experiments, we first constructed strain CaEE341, which served as the *arp2* deletion background throughout this study. CaEE341 was created by deleting the first *ARP2* allele as described [279], using *LEU2* from

Candida maltose as a marker [301]. The second *ARP2* allele was deleted with the nourseothricin-based approach, using pSFS2A as described [299]. Briefly, 485 bp of upstream homologous sequence to *ARP2* was amplified with primers oEE166/oEE382 and cloned in pEE33 [279] between *Kpn1/Xho1* sites. This resulted in plasmid pEE59, which was digested with *Kpn1*/*SacII* prior to transformation.

In order to create strains with FP fusion constructs, 120-mer oligos were used to amplify CaGFPγ [302] or TagRFP-T cassettes and inserted at the 3' end of the respective open reading frame (ORF). For all GFP-tagged strains that we used for quantitative motion analysis, the second allele was disrupted, thus leaving only the GFP-tagged version in the genome. These GFP-tagged strains didn't show any significant defects in terms of growth rate or morphology, and all GFP-tagged strains created in the WT background formed hyphae (data not shown). For colocalization studies using GFP and RFP, we used *ABP1* as a marker to establish spatio-temporal relationships among components in the clathrin-mediated pathway. To do this, *ABP1*-TagRFP-T was inserted, while the second *ABP1* allele was still present in those strains.

In order to fuse *STE2* to GFP, we used plasmid pADH-STE2-GFP [303]. *STE2* pheromone receptor internalization was carried out by adding 30 μg/ml of a synthetic 13-amino-acid version of the α-factor mating pheromone dissolved in 50% methanol (1 mg/ml). Cells were imaged after 40 minutes of pheromone addition.

Strains were routinely grown in standard YPD media (1% yeast extract, 2% peptone, 2% dextrose, supplemented with 50 mg/ml uridine), synthetic complete (SC) media (2% dextrose, 6.7% yeast nitrogen base without amino acids, 1.5% of a complete amino acid mix, supplemented with 50 mg/ml of each uridine, histidine, leucine and arginine), or SC-met media, which is identical to SC media except that SC-met media lacked methionine and was adjusted to pH 5.5. Mup1 internalization was induced by adding 20 μl/ml of methionine to cells grown over night in SC-met media. Because *arp2* cells grew poorly in SC-met media, we incubated *arp2* mutants carrying Mup1-GFP or Mup1-pHluorin in YPD over night, then diluted cells into fresh SC or SC-met media before imaging. Sorbitol was added for 45 minutes in strain CaEE720. For experiments involving cytochalasin A (CA), the drug was dissolved to 1 mg/ml in DMSO and stored

at -20°C. Cells were grown in SC media for all CA experiments. The FM4-64 uptake was done as previously described in SC media [279], except that endocytosis was blocked by the addition of sodium azide and sodium fluoride (final concentration 10 mM).

Plasmids

Plasmid pFA-TagRFP-T-URA3 (pEE101) for use in *C. albicans* was constructed in the following way. The TagRFP-T sequence [304] was first codon-optimized for *C. albicans* by changing all CUG codons to TTG, which is the most frequently used *Candida* codon for leucine [305], and then synthesized by GeneScript Inc. This resulted in plasmid pUC57-TagRFP-T. Primers oEE613/oEE614B were used to amplify the TagRFP-T sequence and clone into plasmid pFA-GFP-URA3 [301] between *Pst1*/*Asc1*, thereby replacing GFP with TagRFP-T and conserving the S1-GFP and S2 annealing sites used for plasmid amplification in the pFA-modules [301].

The LIFEACT-GFP plasmid (pEE113) was constructed by amplifying the CaGFPγ sequence [302] with primers oEE653/oEE663 and cloned between *Pst1*/*Spe1* sites in pFA-GFP-URA3 [301]. Primer oEE653 contains the first 51 amino acids from the *S. cerevisiae ABP140*, which is sufficient for actin binding [211]. Primers oEE653 and oEE663 also contain 100 bp of homology to up- and downstream regions of Act1, which are used to insert pEE113 at the actin locus. Prior to transformation, pEE113 was digested with *Pst1*/*Spe1*.

The pH-sensitive GFP variant, pHluorin, was created based on the superecliptic pHluorin sequence [306]. In order to do this, the QuickChange Multi Site-Directed Mutagenesis kit (Agilent Technologies) was used to exchange the following sites in CaGFPγ [302]: S147D, N149Q, S202F, Q204T, A206T, Q80R, T167I, S175G, using primers oEE622/oEE623 and oEE680/oEE681/oEE682. This resulted in plasmid pCaEE114.

Overexpression of *RHO1* was achieved using the actin promoter from pACT1 [307] fused to the Rho1 coding sequence, resulting in plasmid pACT1-RHO1 where the Rho1 sequence was amplified with primers oEE705/oEE723 and inserted between the

HindIII/*XmaI* sites. pACT1-RHO1 was digested with *StuI* and inserted at the *RPS1* locus. Rho1 overexpression was confirmed by real-time quantitative PCR as described [120], using as reference the coding sequence for constitutively expressed *C. albicans* snoRNAs (primers pAsCaSnoR46F1 and pAsCaSnoR46R1) [120]. All plasmids created in this study were verified by sequencing.

Fluorescence microscopy

Cells were grown to log phase in SC or SC-met media, gently concentrated and applied on pre-cleaned slides, which were covered with coverslips. Slide cleaning was done as described [308]. Cells were grown at 30° for widefield microscopy and at room temperature for confocal microscopy. For widefield microscopy, an inverted Leica DMIRE2 microscope with a 100x immersion oil objective and a 10x projection lens was used. Images were acquired using OpenLab (version 5.5.0). For confocal microscopy, image data was collected using a customized WaveFX spinning disk confocal microscope (Quorum Technologies) built on a Leica DM6000 inverted body, with a 100X 1.46 NA plan-apochromat objective, piezo stage (ASI) and DAQ control board, laser merge module (Spectral), 493 and 561 nm solid state lasers (Coherent) and a water cooled bt-EMCCD camera with photon counting enabled (Hamamatsu). MetaMorph (version 7.7.3.0.) was used for image acquisition. Data was collected in two ways, either in one medial focal plane with 50 to 200 ms exposure time at intervals of 50 ms to 1 second for a duration of 2 to 6 minutes, or as stacks (200 nm z steps in 20 focal planes) with a capture time of ~2.5 sec/stack and intervals of ~2.5 to 3 seconds for 2 to 6 minutes. Strains carrying the LIFEACT probe were imaged using MetaMorph's stream function for time and stack. Between 20 and 120 tracks were analyzed for every component of the clathrin-mediated pathway.

TIRF microscopy was done using a Zeiss Axiovert Z1 microscope chassis, 100x 1.45 NA Plan-apo-chromat objective lens, and the Zeiss TIRF III slider. Diode-pumped solid-state lasers (Cobolt Jive, Cobolt Calypso) were coupled to fiber-optic cables in free space and introduced into the Zeiss slider. Images were recorded using an Andor iXon+ DV-897

EMCCD camera and MetaMorph software.

Image analysis

Quantitative motion analysis of patch dynamics was done using Imaris x64 (version 7.2.3) developed by Bitplane AG. Briefly, the spot detection algorithm in Imaris was used to measure spot dynamics over time by setting the estimated diameter to 0.35 μm with background subtraction selected. The quality attribute in the filter type setting was manually used to set signal threshold in order to distinguish background from patch signals. The autoregressive motion algorithm was used with parameters set between 0.5 and 0.1 micrometer for Max Distance and the Max Gap Size option was set between 1 and 3. All tracks created this way were visually inspected and had to satisfy the following criteria: (1) the patch was initially present at the cell cortex, (2) the patch was clearly distinguishable from other patches, i.e. didn't merge with another patch, and (3) the entire lifetime from patch appearance to disappearance was recorded. The last criterion didn't apply to *arp2* cells, as patches often didn't disappear. Statistics in the form of mean square displacement (MSD), track duration as well as track displacement length were exported into Excel, which was used to create graphs. MSD plots for WT cells were truncated when 50% of the patches have disappeared, thus representing the median lifetime, or in the case of *arp2* cells, MSD plots represent the first 70 seconds of analysis. Cells leaving origin was defined as signals that either moved more than 100 nm from where they were first detected (applied for the actin module) or signals that disappeared (applied for the early, coat, Myo/WASP and scission modules).

Electron microscopy

Samples used for transmission electron microcopy (TEM) were processed according to standard techniques as described [303]. Briefly, samples were fixed with 3% electron microscopy (EM) grade glutaraldehyde in 1x sodium cacodylate buffer (pH 7.4) at room temperature. After fixation, samples were washed in buffer and resuspended in an

aqueous 4% permanganate solution, washed, stained with uranyl acetate, dehydrated through a graded series of ethyl alcohol and embedded in Epon resin. Ultrathin sections of 80 nm were cut with a Reichert-Jung (Heidelberg, Germany) UltracutE ultramicrotome, placed on formvar-coated slot copper grids and viewed with a FEI Tecnai12 BioTwinG2 electron microscope (Eindhoven, The Netherlands). Digital images were acquired with an AMT XR-60 CCD Digital Camera System. The TEM analyses were carried out at Stony Brook University at the Microscopy Imaging Center.

Acknowledgements

We thank Judith Lacoste from the McGill CIAN facility for assisting with confocal microscopy, Aleksandrs Spurmanis and Claire Brown from the McGill Imaging Facility for advice on image analysis, and Cory Glowinski from Bitplane AG for advice on using Imaris. We also thank Susanne Bechstedt, Michal Wieczorek and Gary Brouhard from McGill University for assisting with TIRF microscopy, and Andrea Walther and Jürgen Wendland from Carlsberg Laboratory for sharing reagents. This work was supported by CIHR grant MOP42516 to M.W. E.E. was supported by a CIHR Systems Biology Scholarship through McGill University and the Carpenter Fellowship from McGill Biology Department.

Figure 1. Receptor-mediated endocytosis is not functional without Arp2/3

(A) Internalization of the Ste2 pheromone receptor was assayed after 40 minutes incubation in the presence of α-factor pheromone. This results in dominant vacuolar accumulation of Ste2-GFP in WT cells with some signals visible as vesicles trafficking *en route* to the vacuole. In *arp2* cells, no strong vacuolar signal or moving vesicles were observed. **(B)** Mup1 internalization was stimulated by the addition of methionine. Mup1-GFP signal disappeared in WT cells at the plasma membrane, but was still visible in *arp2* cells (right). When Mup1 was coupled to the pH-sensitive GFP variant, pHluorin, the Mup1-pHluorin signal almost completely disappeared in WT cells upon addition of methionine, while Mup1-pHluorin was still observed in *arp2* cells that carried a Rho1 overexpression and were treated with sorbitol (left). Bar = 10 μm.

Figure 2. The clathrin-mediated pathway is heavily affected in *arp2* cells

Dynamics of GFP-tagged components at every stage of the clathrin-mediated pathway were recorded in live cells by spinning disc confocal microscopy and quantitatively analyzed. Recorded displacement data of individual patches were aligned at the start of their lifetime and then averaged. MSD plots for WT cells were truncated at the time when 50% of spots have disappeared, corresponding to the median lifetime. For mutant cells, MSD plots represent the first 70 seconds of recording. Components of the early **(A)**, coat **(B),** Myo/WASP **(C)**, actin **(D)** and scission **(E)** module show dynamic behavior in WT cells. In *arp2* cells, early, coat and Myo/WASP components lost dynamics and remained static at the plasma membrane, while some actin module as well as scission module components retained partial dynamics in *arp2* mutants. Prk1 and Sjl2 didn't localize to any clear patch structures and dynamics could therefore not be quantitatively analyzed. WT is in blue, *arp2* cells in red. MSD plots correspond to mean ± SEM.

Figure 3. Arp2/3 is required for productive functioning of the clathrin-mediated pathway

Live cell imaging data were analyzed for three additional quantitative elements to demonstrate that the clathrin-mediated pathway becomes non-productive without Arp2/3. **(A)** Percent of patches leaving the origin was defined in two ways; patches that

disappeared (applied for the early, coat, Myo/WASP and scission modules) and patches that moved more than 100 nm from sites of first detection (applied for the actin module). In a few cases, Pan1 and End3 patches disappeared in *arp2* cells, which likely corresponds to patches moving out of the focal plane. **(B)** Track displacement length measures the distance between first and last patch detection. **(C)** Track duration refers to how long a patch was observed over a two-minute period. In the case of clathrin, movies were acquired for 6 minutes. All graphs correspond to mean ± SD.

Figure 4. Actin dynamics are not affected without Arp2/3 function

LIFEACT-GFP was used to visualize actin dynamics and showed that the rate of actin filament elongation was not affected in *arp2* cells. Two populations of actin filaments observed in WT and *arp2* cells are illustrated by arrowheads (first image in the time series) and arrows (subsequent images).

Figure 5. FM4-64 endocytosis is actin dependent in *arp2* mutants

(A) Top; schematic representation of the experimental setup. Cells were treated with 10 μg/ml CA or DMSO for 3 minutes, at which time LIFEACT-GFP signals were assessed. Only *arp2* cells completely lost LIFEACT-GFP signals (left). In a second experiment, *arp2* cells were treated with 10 μg/ml CA for 3 minutes, FM4-64 was added at 20 μg/ml for 5 minutes, unbound dye was washed away and cells were chased for another 20 minutes to allow dye internalization. During this 30 minutes procedure, either DMSO or CA was present in the corresponding solutions. Endocytosis was blocked after 30 minutes by adding sodium azide and sodium fluoride and *arp2* cells were assessed for endocytic capacity (right). **(B)** Two control experiments demonstrating that treating *arp2* cells for 30 minutes with CA doesn't significantly reduce viability (left), and blocking actin dynamics with CA is reversible with cells recovering almost completely after 24 hours of washing CA away (right). The bottom represents the schematic setup of the experiment in B. All experiments were done with *arp2* mutants, expect the left figure in part A.

Figure 6. Invaginating tubules form independently of the Arp2/3 complex

(A) Transmission electron microscopy showed that on average invaginating tubules are significantly longer in WT and revertant strains compared to *arp2* and *arp2/arp3* mutants. Statistical significance was assessed using the students' t-test. **(B)** Invaginating diameters at the membrane does not exceed 100 nm in WT and revertant cells, while in *arp2* and *arp2/arp3* mutants invagination diameters were larger than 100 nm in up to 28% (*arp2*) or 24% (*arp2/arp3*) of cases. **(C)** Examples of invaginating tubules. Bar equals 100 nm.

Figure S1. Clathrin is essential for survival in *C. albicans*

Conditional mutants of clathrin heavy chain (*chc1/tetO-CHC1*) or light chain (*clc1/tetO-CLC1*) were created using a tetracycline-regulatable cassette (tetO) [309]. Cells were grown for 4 days on SC media, which allows growth, or on SC media containing 100 μg/ml of tetracycline, which turns off the respective promoter. Growth of *clc1/tetO-CLC1* was severely affected on repressing conditions and no single colony of *chc1/tetO-CHC1* was observed. Two independently derived isolates were tested for *clc1/tetO-CLC1*.

Movie 1. Summary of dynamic behavior of GFP-tagged components in the clathrin-mediated pathway. Images were acquired by spinning disc confocal microscopy for at least two minutes in one single medial focal plane. Components in the pathway are grouped into modules.

Movie 2. Clathrin remains static at the plasma membrane in *arp2* cells. WT and *arp2* cells carrying Clc1-GFP were imaged by TIRF microscopy for 6 minutes. In WT cells, clathrin frequently appears and disappears from the membrane, while in *arp2* cells, most clathrin signals remained static at the membrane.

Movie 3. Actin dynamics in the absence of Arp2/3. LIFEACT coupled to GFP was used to visualize actin dynamics in living cells. Spinning disc confocal images acquired over 4 minutes in one single medial focal plane show two populations of actin both in WT and *arp2* cells. See figure 4 and description in the text for details.

Figure 1. Receptor-mediated endocytosis is not functional without Arp2/3

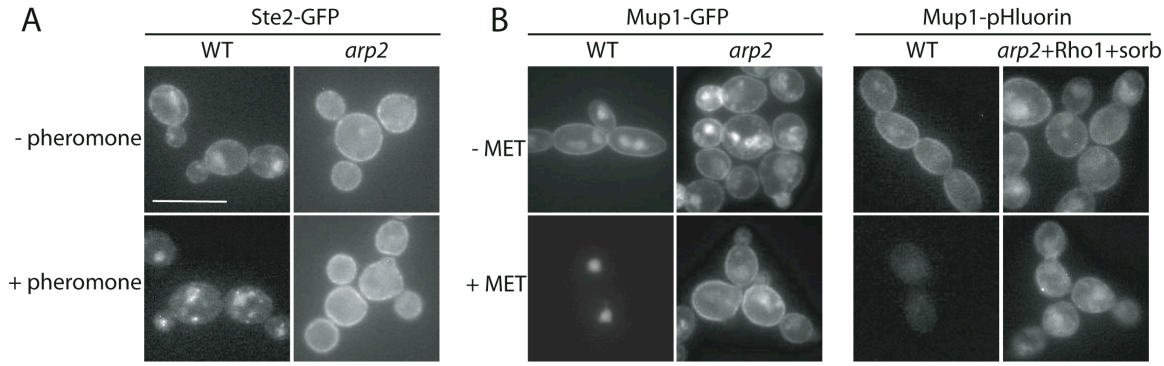

Figure 2. The clathrin-mediated pathway is heavily affected in *arp2* cells

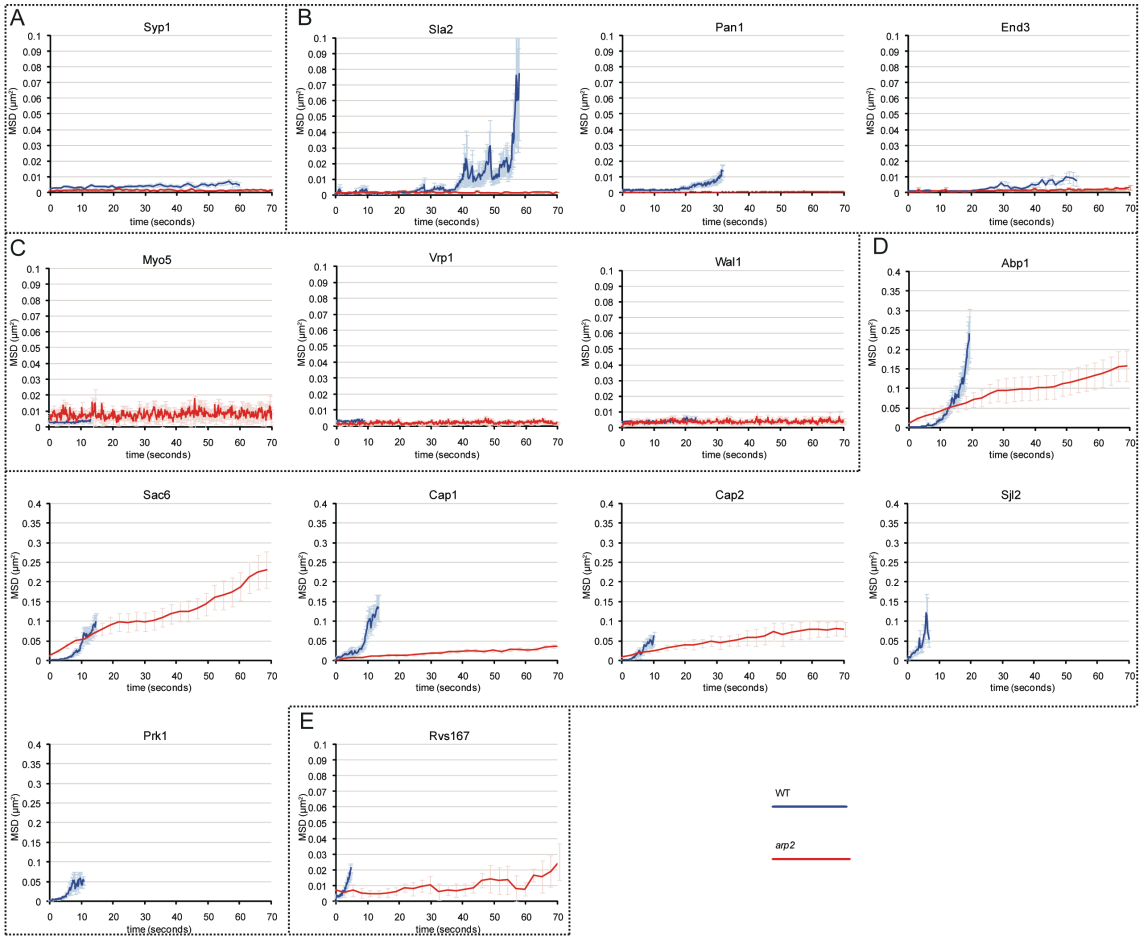

Figure 3. Arp2/3 is required for productive functioning of the clathrin-mediated pathway

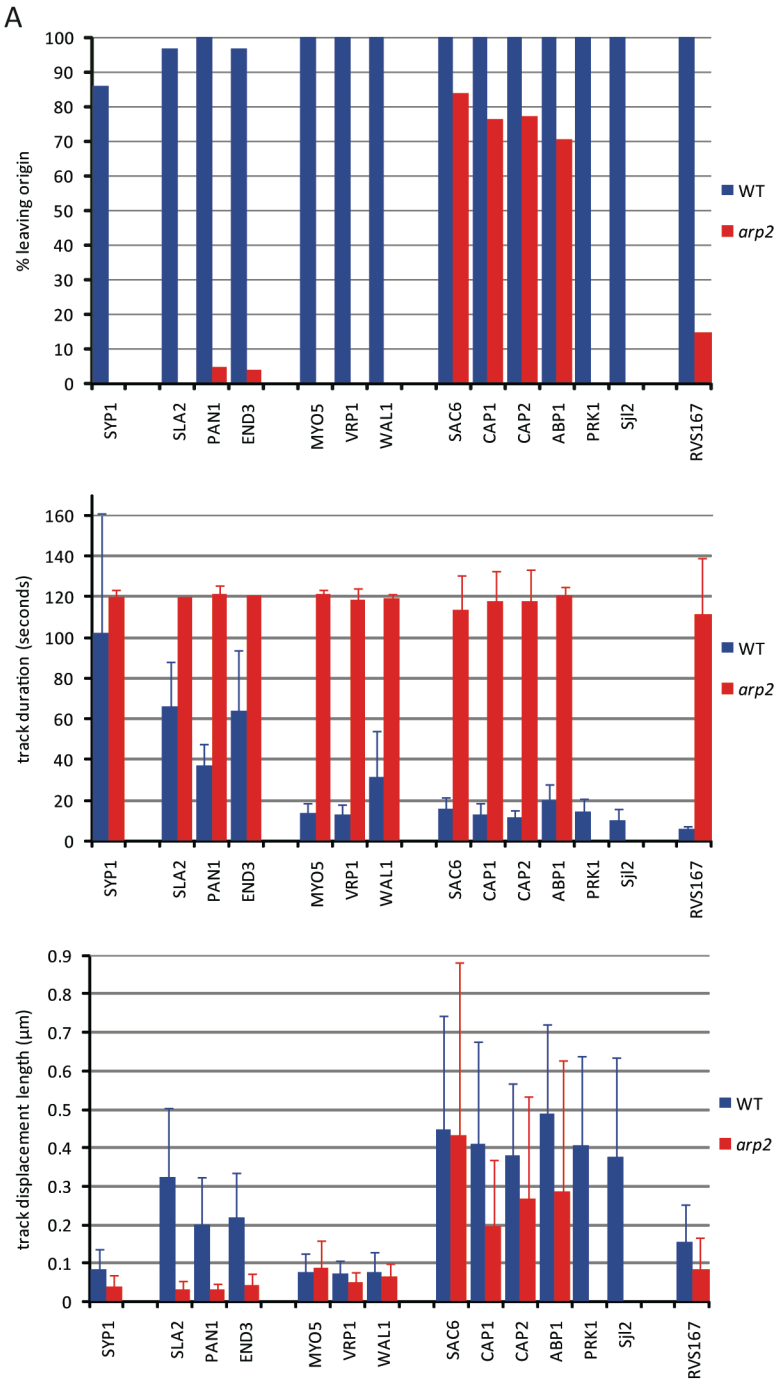

Figure 4. Actin filament elongation rate is not affected by the absence of Arp2/3 function

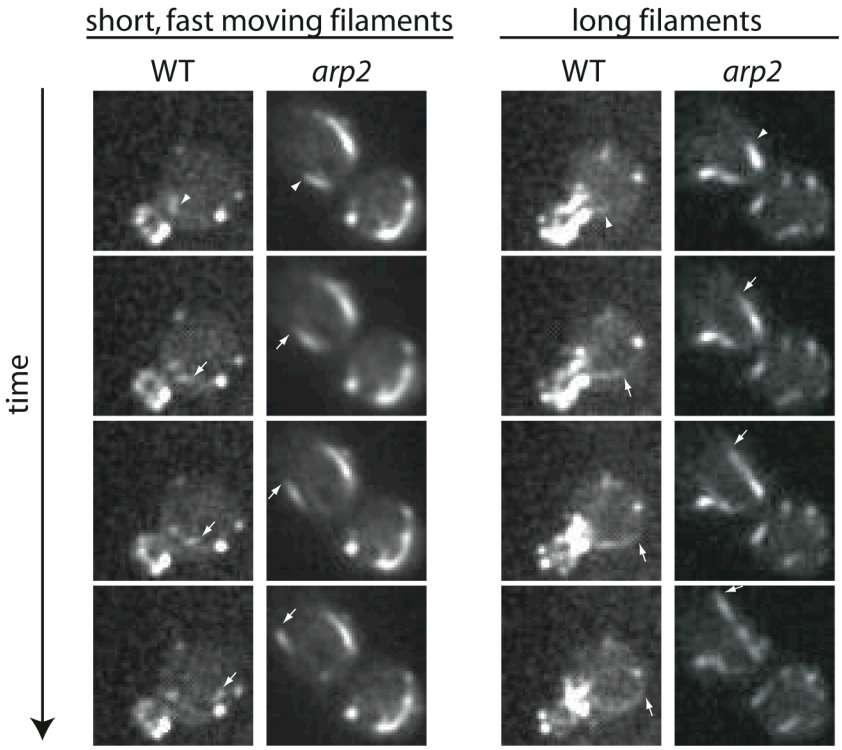

Figure 5. FM4-64 endocytosis is actin dependent in *arp2* mutants

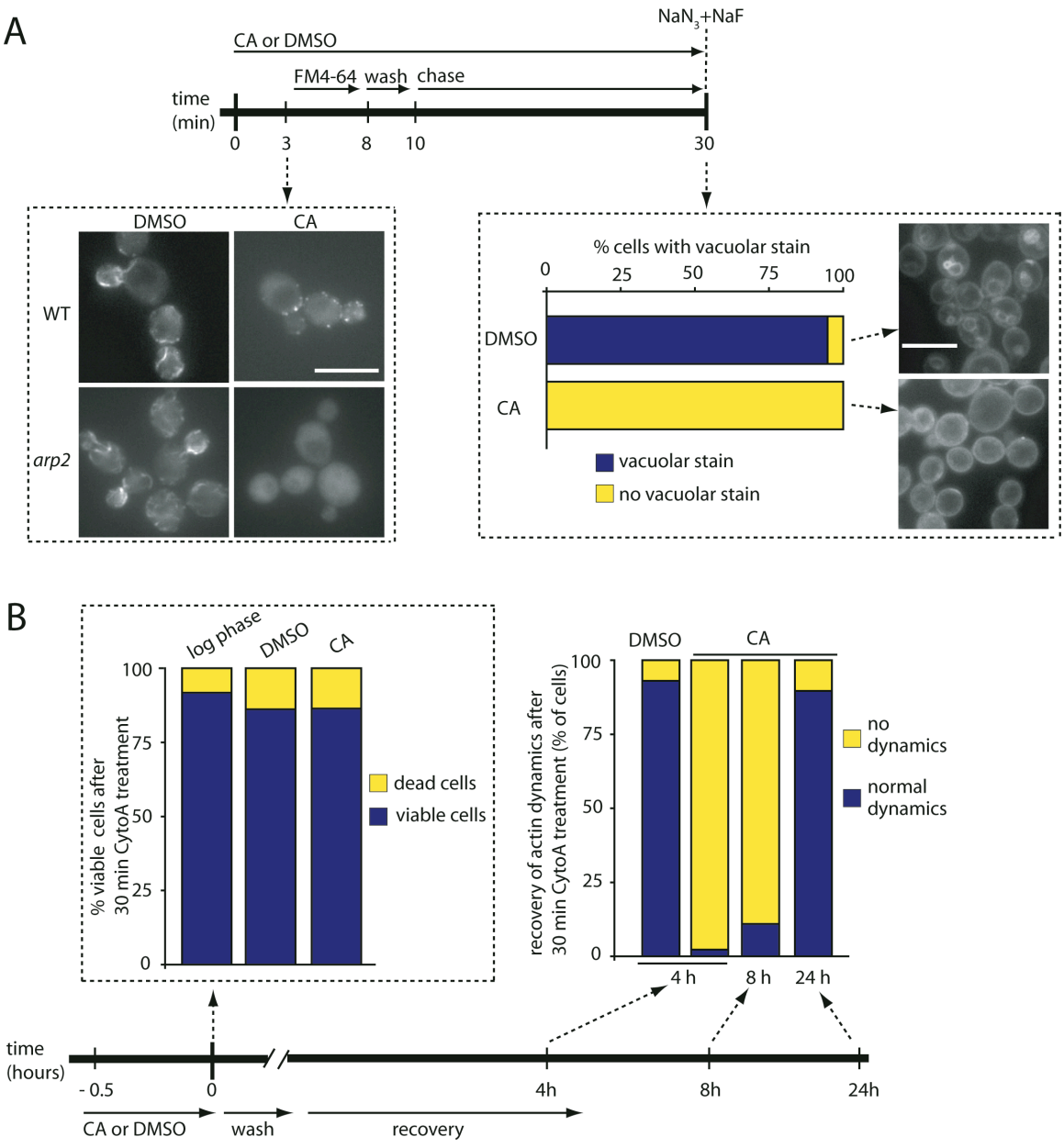

Figure 6. Invaginating tubules form independently of Arp2/3

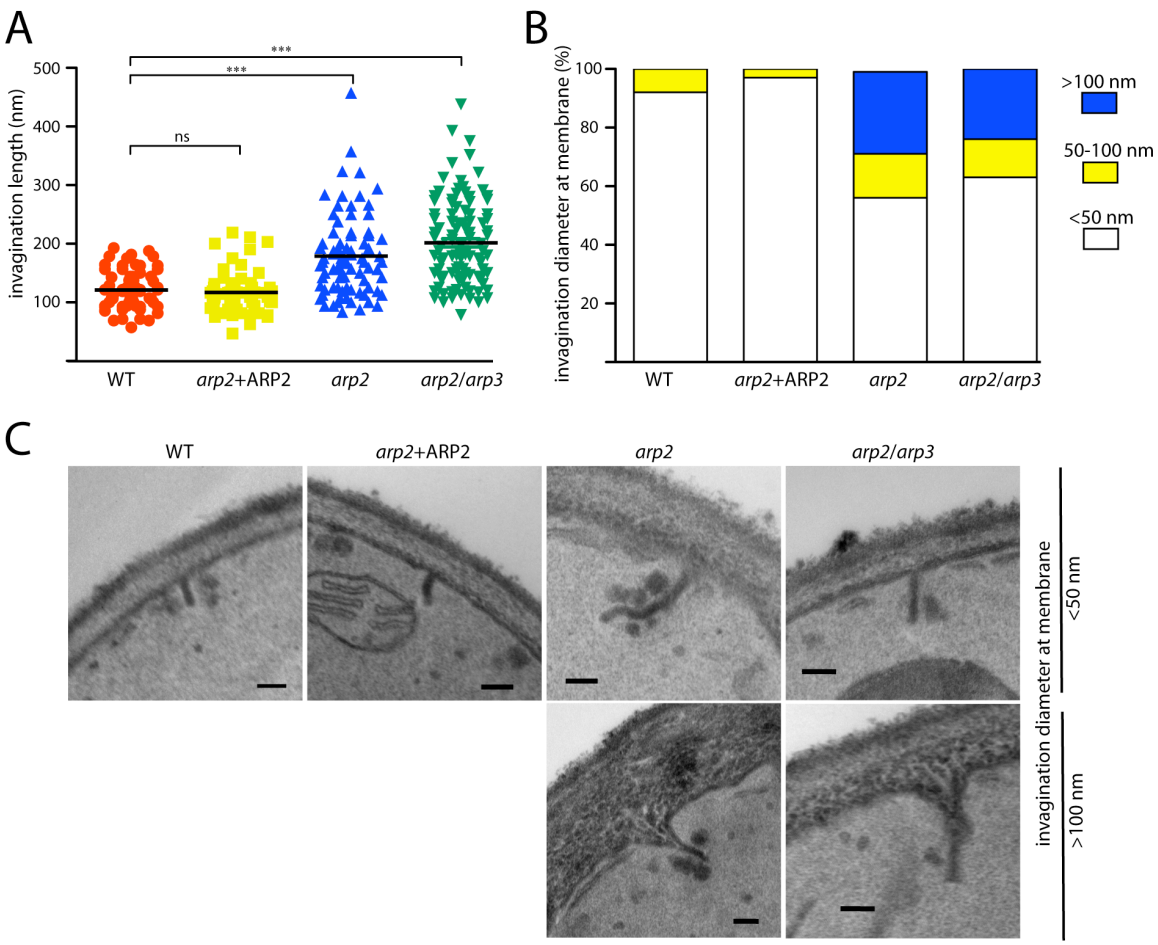

Figure S1. Clathrin is essential for survival in *C. albicans*

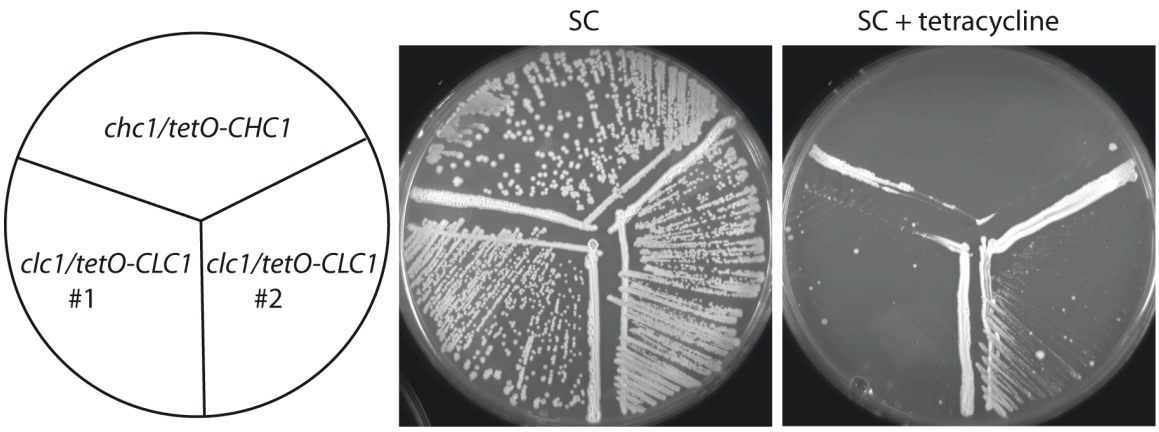

Chapter VI

VI. Conclusions

The excitement and beauty of large-scale genetic screens is that the hits are hard to predict. Consequently, although such screens often reveal anticipated results and thereby confirm what we know, some of the genes are surprising and therefore could reorient the direction for future research. In this thesis, I have presented two genome wide screens looking at two important features that contribute to the reputation of *C. albicans* as a human fungal pathogen, drug resistance and morphology. The first screen addressed drug resistance with the aim of identifying new drug targets and was based on the surrogate model *S. cerevisiae*, while the second screen focused on morphology directly in *C. albicans*, aiming at identifying genes involved in virulence. Both screens confirmed previous results, but more importantly, the two screens have each revealed some unexpected hits that were exciting to investigate further. In this last, partly philosophical chapter of the thesis, I will reflect on some of our main findings and provide my views of the significance of those results.

VI.1. *Candida albicans* – good or bad?

When scientists talk about *C. albicans* they often refer to it as 'the human fungal pathogen *Candida albicans*'. This has probably to do with the hope that pointing out how this organism affects society and human health in grant proposals increases chances of getting funding for a basic research program. On the other side, criminalizing this fungus as notoriously bad reflects only one side of the coin. While we have a good idea in which cases *C. albicans* becomes problematic (s. chapter I.1), our knowledge what *C. albicans* does in healthy individuals remains poorly understood. Why do we have *C. albicans* as a

commensal to start with, what is its biological role in healthy individuals? The fact that evolution has not selected against a commensal relationship between *C. albicans* and the human host provides a strong argument that there must be some benefit of keeping this fungus around. But what might these benefits be? Answering this question is very challenging and might not result in a complete answer anytime soon, because the 'perfect' experiment that could address this issue faces ethical restrictions. This experiment would rely on healthy human volunteers that have naturally established a commensal relationship with *C. albicans*. The goal of such an experiment would be to compare the overall health, blood pressure, weight, microbial flora etc. of these subjects at the beginning of the experiment and after *C. albicans* has been eliminated, for instance by chemical treatment. Of course, such treatments would have to impact only the fungus, but not other microorganisms or even host cells.

Fortunately, the creative scientist, driven by curiosity and a thirst for knowledge, has quickly adapted to such ethical limitations and substituted the human host with ethically less challenging models in mice and rats [310,311], as well as non-mammalian vertebrate (zebrafish, *Danio rerio*) [312] and invertebrate models (*Caenorhabditis elegans*, *Drosophila melanogaster, Galleria mellonella*) [313,314,315]. Using a variety of these models, some common principles have emerged as to what *C. albicans* does in the host. One of those emerging views is that there is extensive crosstalk between microbes. For instance, bacteria can physically associate with fungal cells [316,317], form biofilms on fungal hyphae [318], or form mixed bacterial-fungal biofilms on host surfaces [319]. Secreted molecules that often mediate quorum-sensing in single-species communities have also been shown to influence polymicrobial communities; for example bacterial quorum-sensing molecules can influence morphology in *C. albicans* or even kill the fungus [320,321,322,323,324]. Similarly, *C. albicans* can influence bacterial behavior through secreted factors like farnesol and other, yet unknown factors that result in altered bacterial swarming motility and biofilm formation [324,325,326]. Farnesol has also been demonstrated to reduce the production of the virulence factor pyocyanin in *Pseudomonas spp.* [325], inhibit the viability of *Acinetobacter baumannii* (a bacterium causing ventilator-associated pneumonia) [313], and increase the susceptibility of *Escherichia coli* and *Staphylococcus aureus* to antibacterials [327,328].

There is also extensive crosstalk between microbes and the immune system. For example, scientists have shown that challenging mice with *C. albicans* and/or pseudomonal lysates resulted in different immune responses [329]. Exposure of mice to *C. albicans* lysates led to mucus production and an increase in T helper 2 (T_H2) cell cytokines, whereas exposure to pseudomonal lysates didn't lead to mucus production and produced T_H1 helper cytokines. Given such examples of extensive crosstalk between microbes and the immune system, we can speculate that humans maintain such a rich microbial population including *C. albicans* in order to keep the immune system stimulated and in shape. The 'hygiene hypothesis', for instance, supports this view, as a more hygienic environment in which there is less microbial stimulation could lead to increased risks to atopic diseases like asthma, eczema or hay fever [330,331,332,333]

Taken together, as we are beginning to understand the complex crosstalk between different microbes and the immune system, it is becoming evident that eliminating *C. albicans* from healthy individuals could be dangerous, but also illustrates how limited our knowledge is in regards to what *C. albicans* does as a commensal.

VI.2. The "Holy Grail" of antifungal drug therapy

Despite some possible advantages that *C. albicans* offers its human host, there are situations when therapeutic interventions are required to limit fungal growth. As outlined in chapter I.2, several therapy options exist. Unfortunately, most of the currently used clinical drugs show either a limited antifungal spectrum or considerable side effects to the host. Moreover, existing drugs face limitations in that at least one resistance mechanism has been described for all 5 classes of existing drugs (see chapter I.3). This is a significant problem that results in increased mortality and treatment-related economic costs. Another significant complication is that by inhibiting growth of a targeted microbe, benign members of the human microbiome could also be affected. Clearly, current therapies only insufficiently address these issues and therefore new therapeutic approaches are needed.

The first step to do this could be identifying new drug targets. We reasoned that

a genetic screen could do that job. Since genomic tools are not as advanced in *C. albicans* as they are in other fungi like *S. cerevisiae* or *S. pombe* (s. chapter I.4), we decided to rely on budding yeast and its collection of deletion mutants. That library contains single knockout strains for every non-essential gene. Using this tool, we started with the idea that any budding yeast mutant that cannot survive a treatment with the normally fungistatic drug FCZ reveals a new drug target. If one then finds a drug that targets the deleted gene in this mutant and combines the new drug with FCZ, the combination would be expected to mimic the lethal drug-mutant phenotype and result in lethality against WT cells.

Our published work in chapter II summarized this screen, which resulted in 22 *S. cerevisiae* mutants that cannot survive a FCZ treatment. The next step on the long road towards a new drug therapy was then to knock out the homologous genes in *C. albicans*, and test those mutants for FCZ sensitivity. Surprisingly, although many of the 22 *C. albicans* mutants showed increased sensitivity to FCZ, only one mutant mirrored a robust FCZ fungicidal phenotype as predicted from *S. cerevisiae*. This hit, *AGE3*, which encodes for an ADP-ribosylation factor GTPase activating effector protein (ARF GAP), was a surprise in that it couldn't be linked to any known drug resistance mechanisms like drug pumps or the ergosterol pathway and therefore represented a new drug target [334]. Excited about this result, I looked for drugs that would directly target *AGE3*. Because I couldn't find such a drug based on extensive literature reviews, I reasoned that any drug that inhibits the process *AGE3* is involved in could potentially suffice. Fortunately, BFA is such a drug. When I combined FCZ with BFA, I recorded one of the most exciting results that I obtained during my graduate student experience; the FCZ/BFA combination resulted in a potent fungicidal synergy not only in *C. albicans* WT cells, but also against various drug resistant clinical isolates and other non-*albicans* fungal pathogens (s. chapter III). These *in vitro* results clearly demonstrate the potency and wide applicability of the FCZ/BFA combination. Encouraged by these positive outcomes, I next wanted to know whether FCZ/BFA would work *in vivo*. Although our *in vivo* results confirmed that *AGE3* is a good drug target, the FCZ/BFA combination didn't improve survival of mice challenged with *C. albicans* WT cells. One speculation for this outcome is that the host system rapidly eliminates BFA and thus the FCZ/BFA combination isn't acting long

enough to kill fungal cells. This view is supported by pharmacodynamic studies demonstrating that BFA is eliminated within minutes after administration, potentially through the host glutathione S-transferase system [335,336].

Together, our published reverse genetic strategy successfully led to the identification of a new drug target, but also highlighted that BFA is not an ideal candidate for *in vivo* use.

How could we improve the FCZ/BFA synergy? The FCZ/BFA combination satisfied one of two criteria that would qualify for the title 'Holy Grail of antifungal therapy'. The first criterion is that the therapy must attack a process that is essential for fungal survival (the FCZ/BFA combination did that), and the second criterion is that the treatment must be safe and doesn't attack the host (BFA is not safe for human use). In an attempt to satisfy the second criterion, one could replace BFA with a fungal specific drug that doesn't influence the mammalian ARF cycling process. This approach could be challenging, however, because *AGE3* and other proteins that are tightly linked to *AGE3*'s function like ARFs or ARF GEFs, are highly conserved. An alternative approach towards the Holy Grail therapy could be to elucidate why *AGE3* is important for drug resistance by identifying the downstream effector protein that mediates the drug phenotype, and then target that protein for combination therapy. This strategy might also be challenging because *AGE3* is not involved in a single process. Simply speaking, *AGE3*'s role relates to vesicle transport between the ER-Golgi, Golgi-membrane as well as from the membrane to endosomes [337,338,339]. Therefore, the reason why *age3* mutants are drug sensitive might be related to more than one protein that are either not trafficking correctly through the secretion pathway or are not properly recycled from the plasma membrane.

Yet another route towards the Holy Grail could be to go back to *S. cerevisiae* and perform a suppressor screen by asking which gene, when overexpressed, suppresses *age3*'s drug sensitivity. Such a screen might reveal fungal specific drug targets, but is also limited in case there is more than one gene responsible for *AGE3*'s drug phenotype.

Finally, given that this initial drug identification screen failed at the stage of translating promising *in vitro* results to the mouse model, setting up a new drug program

could begin directly at this critical stage. Several *in vivo C. albicans* infection models have been developed that would allow high throughput screening for drug synergies, for example by incubating *C. elegans* with *C. albicans* and than asking which drug combination eliminates the fungus but still allows the worm to live [340].

VI.3. Forward genetics and the hunt for new virulence genes

Finding the "Holy Grail" of antifungal drug therapy represents one way to get a grip on fungal infections. Another route towards improved therapy options is by first understanding the biology behind the infection. In other words, what makes a fungus pathogenic and what are the virulence factors? Morphological adaptation to environmental signals is such a virulence attribute of *C. albicans* (s. chapter IV.1). As demonstrated above, surrogate models can provide useful information for a process under investigation in the target organism, but this strategy is limited when looking at morphology, as true hyphal formation is not observed in *S. cerevisiae*. I was therefore curious to investigate genetic approaches that would allow screening for genes that are involved in the yeast-to-hyphae switch directly in the pathogen. This would ideally be done with a deletion library that represents single-knock out mutants of every non-essential gene. Unfortunately, such a resource is not available in *C. albicans*, but would clearly be desirable. To maximize chances of identifying new genes involved in regulating morphology, any alternative screening technique would have to meet the following three criteria; the screen should be on a genome-wide scale, it should be unbiased and should result in complete gene inactivation.

The *UAU1* technique (s. chapter I.4.2) satisfies these 3 criteria. I therefore selected this approach and created about 5000 mutants and screened them for different phenotypes (s. our published original research in chapter IV.2). As proof-of-concept, I was first interested in finding auxotrophic mutants and identified a *trp1* mutant. I then screened for mutants that result in FCZ sensitivity, but was unable to recover any robust hits (data not shown). At the same time, I was looking for mutants that are deficient in the yeast-to-hyphal transition. This identified two genes or processes that have previously

been linked to hyphal development (*CDC39* and *VPS52*) [143,341], as well as one gene that has not been linked to morphology in *C. albicans*, *ARP2*. Deletion mutants of *ARP2*, *ARP3* as well as a double *arp2/arp3* mutant were unable to form hyphae under all conditions tested and the *arp2* mutant was avirulent in a mouse systemic infection model. Taken together, this forward genetic screen successfully identified new genes involved in the yeast-to-hyphal switch and virulence.

Why is the yeast-to-hyphal switch critical for virulence? One current view is that while the yeast form contributes to the dissemination in the host, the hyphal form plays a role during organ colonization, facilitates tissue penetration and escape after host cell internalization [131,342]. Both the yeast and the hyphal form of *C. albicans* are important for virulence as mutants locked in either morphology become avirulent [343]. This suggests that elements of both growth forms are contributing cooperatively to virulence. Curiously, in contrast to *C. albicans*, where the filamentous form is induced once the fungus enters in contact with the host, most other pathogenic dimorphic fungi exist as non-pathogenic hyphal forms in the environment and transition into the pathogenic yeast form when in contact with the host. For example, *Histoplasma capsulatum* naturally grows in the filamentous form in the soil, but after humans have inhaled conidia (aerosolized spores), *H. capsulatum* transitions into the pathogenic yeast form, maybe to hide from host immune cells such as neutrophils, monocytes and macrophages [344]. Locking *H. capsulatum* in the hyphal from prevents virulence [345]. Other dimorphic fungi of the ascomycete phylum like *Blastomyces dermatitidis*, *Coccidioides immitis*, *Paracoccidioides brasiliensis*, *Sporothrix schenkii* and *Penicillium marnefiii* similarly exist as non-pathogenic filamentous forms in the soil and transition into the pathogenic yeast form when inhaled by humans and other mammalian hosts. Other fungi like *Cryptococcus spp.* require the filamentous form for production of spores that are either directly inhaled by humans or first germinate to from yeast-like cells, which can also be inhaled and cause disease [346]. Finally, the dimorphic plant pathogen *Ustilago maydis* from the basidiomycota phylum can grow as yeast, but successful plant infection requires the filamentous form [347]. Yet other plant and human fungal pathogens like *A. fumigatus* are strictly filamentous, but are still able to subvert host defenses and cause

disease.

Together, these examples illustrate that there is no universal rule, for example that yeast are pathogenic and hyphae are not, but instead exemplify the variety of mechanisms that fungi use to succeed as pathogens and thus support the idea that strategies for fungal pathogenesis have evolved repeatedly and independently throughout the fungal kingdom [343].

Another question in the field regarding *C. albicans* morphology is whether pseudohyphae are an intermediate state between yeast and hyphae or whether pseudohyphae represent a distinct morphological form [348]. This question has been addressed in a recent study that used regulated expression of a transcription factor, *UME6*, which regulates the yeast to hyphal switch [349]. In the absence of any hyphal inducting cues, *C. albicans* cells grew as yeast when *UME6* expression was not induced and as hyphae when *UME6* expression was induced. Intermediate expression levels resulted in a third state – pseudohyphae. Increasing *UME6* expression from the pseudohyphae state gave rise to a mix of pseudohyphae and hyphae. When cells were first allowed to grow as hyphae and *UME6* expression was then turned off, pseudohyphae formed within 3h and yeast cells were observed at 7h. Thus, the filamentous program can reversibly be invoked in a gradual fashion, providing evidence that pseudohyphae are an intermediate morphological form in *C. albicans* [348]. Despite these data, some observations remain that are not consistent with this simplified model of pseudohyphae being an intermediate state [155]. For example, differences in terms of the mechanism of polarized growth, cell cycle organization as well as hydrolysis of the primary septum after cytokinesis all suggest that pseudohyphae are more similar to yeast than hyphal cells [350]. As well, yeast and pseudohyphae possess a structure termed polarisome (a protein complex at the growing bud tip responsible for nucleating filamentous actin needed for delivering secretory vesicles to the tip), while hyphal cells have a polarisome and a spitzenkörper (a structure located near the growing hyphal tip that is rich in secretory vesicles) [351]. Therefore, while argument exist that support both sides of pseudohyphae being an intermediate vs transient state, additional experiments are required to settle this debate.

VI.4. The beauty and the beast of genetic screening

The finding that *ARP2* was not required for survival in *C. albicans* was surprising, as the Arp2/3 complex performs functions that are highly essential for survival in many organisms (s. chapter V). If it had not been through forward genetic screening, we might not have gained this knowledge in *C. albicans*. Thus, one beauty of forward genetic screening is that we ended up with a gene that is surprisingly not essential and now provides the advantage of studying related functions in a viable deletion mutant. The flipside, or the 'beast' of this result, is that we face the daunting question 'why is Arp2/3 not essential in *C. albicans?*'

Stepping back and looking at the evidence of essentiality in one model fungus, *S. cerevisiae*, it turns out that viable Arp2/3 complex mutants exist, but that almost all of these mutants show severe growth defects [352]. Six of the seven subunits have been successfully deleted, *ARC40* being the only 'truly' essential gene in that study [352]. Tetrad analysis of diploid strains carrying a disruption of one of the 7 subunits revealed that the frequency of viable spores varied between mutants and was 11%, 16%, 0%, 2.5%, 52%, 88%, or 11% for *ARP2*, *ARP3*, *ARC40*, *ARC35*, *ARC19*, *ARC18*, and *ARC15* respectively. Most viable mutants grew poorly with doubling times of 7-9h compared to 2-3h for WT or *arc18* mutants. The question of essentiality is difficult to answer by these initial studies, but in the best case suggest that deletion of most Arp2/3 complex subunits results in serious growth defects while *ARC18* might have Arp2/3-unrelated functions. Later on, other scientists independently attempted to reconstruct Arp2/3 mutants, but were not successful even when using the same strain background as the first study had used [353]. Today, the general perception in the field is that Arp2/3 performs functions that are essential for survival in *S. cerevisiae*.

Arp2/3 mutants in *C. albicans* show some morphological and cell wall related

phenotypes, but grow relatively well with doubling times only slightly increased from around 110 min for WT to about 130 min in *arp2* or *arp3* mutants (s. chapter IV.2). So why is Arp2/3 so dispensable in *C. albicans*? One way to answer this is by realizing that Arp2/3's essentiality is condition dependent. When grown in an artificial environment in the lab, this fungus doesn't need Arp2/3 for survival, but when grown in its natural habitat in the host, Arp2/3 becomes essential. Therefore, the identification of *arp2* mutants in our forward genetics screen might have been favored by using the right conditions to allow growth without Arp2/3's function. A similar conclusion has been drawn by Winter and colleagues who first published a report that showed that *ARP3* is essential in budding yeast, but 2 years later the same authors reported that they had obtained viable *arp3* cells [352,354]. They explain this difference by media conditions, where slight caramelization of the sugar results in cells death, whereas no caramelization of the media allowed isolation of viable spores.

While defects in the yeast-to-hyphae transition might explain why *C. albicans arp2/3* mutants are avirulent and therefore why Arp2/3 is essential *in vivo*, it is more difficult to speculate why Arp2/3 is not essential *in vitro*. Genome-wide transcriptional profiling showed that *arp2* mutants have significantly elevated expression of many actin related genes, such as actin bundling proteins Abp1 and Sac6 as well as other proteins involved in actin regulation (e.g. type I myosin Myo5, cofilin, the amphiphysin Rvs161, and other regulators of morphology such as Rga2, a GAP for the polarity-establishment protein Cdc42). This suggests that *arp2* cells might compensate for defect in Arp2/3 functions by using other parts of the actin cytoskeleton like actin filaments to perform processes essential for survival.

Why is Arp2/3 not needed for endocytosis? Our studies showed that in *C. albicans arp2/3* mutants could still endocytose bulk-membrane lipids (FM4-64) and a fluid marker (LY) (s. chapter IV.2). These initial observations were unexpected because live cell imaging has demonstrated that actin patches are sites of endocytosis and that these patches are being simultaneously internalized together with cargos like FM4-64 or fluorescently labeled α-factor pheromone in *S. cerevisiae* [252,253]. This has led to the

model of how clathrin-mediated endocytosis works, resulting in a pathway where different protein modules cooperate to drive vesicle internalization (s. Figure 2). Given that the clathrin-mediated endocytic (CME) pathway is the only well described endocytic route in fungal cells, I decided to investigate the CME pathway in *C. albicans* and test its functionality in *arp2/3* mutants (s. chapter V.2). To do this, I analyzed the behavior of every stage of the CME pathway by live cell fluorescent microcopy of GFP-tagged proteins and quantitative motion analysis. This analysis showed that in *C. albicans* WT cells the CME pathway has a similar structure compared to other fungal species. All proteins examined had spatio-temporal behavior that was predicted from other systems, thus demonstrating that the CME pathway is conserved in *C. albicans*. In *arp2* mutants, on the other hand, every component examined had major defects. Collectively, these data show that the clathrin-mediated pathway is non-functional in the absence of Arp2/3 and therefore suggest alternative endocytotic routes exist in *C. albicans* (s. chapter V.2).

How does Arp2/3-independent endocytosis work? There are several arguments that suggest that Arp2/3-independent endocytosis is an active process; First, chemical inhibition of actin dynamics abrogated FM4-64 uptake in *arp2* cells, and second, FM4-64 is selectively localized only to the vacuolar membranes, but not other organelles. We can speculate that if the FM4-64 cargo traffics by vesicles, then these structures might be either too small or too faint to be visualized by our microscopy techniques. Alternatively, we can think of mechanisms that help the cargo cross the plasma membrane, for example with the help of flippases. Once across the membrane, the cargo might fuse directly with the vacuole. This is supported by live cell imaging data showing that vacuoles are very mobile in *C. albicans* and often appear to be in close proximity to the plasma membrane (s. movies in chapter IV.2, available at: http://onlinelibrary.wiley.com/doi/10.1111/j.1365-2958.2009.07038.x/suppinfo). If flippases are involved in Arp2/3-independent endocytosis, maybe such a mechanism has evolved in the pathogen in order to survive drug treatments. Jia and colleagues have shown that flippases like Rta2 are involved in drug resistance [355,356]. The authors showed that deleting Rta2 resulted in increased azole susceptibility, while overexpression of Rta2 in a strain that lacks all three major drug pumps, *CDR1*, *CDR2* and *MDR1*,

conferred azole resistance. They also showed that export rate of some sphingolipids was decreased in *rta2* mutants. The notion that *C. albicans* has adapted mechanisms that evolved to overcome drug resistance, is also supported by the observation that drug pumps like *CDR1* and *CDR2* are involved in translocation of a second major lipid found in eukaryotic membranes, phospholipids [357]. Although it is not clear how lipids are transported across the plasma membrane or how the fluid phase marker LY is endocytosed in *arp2/3* mutants of *C. albicans*, it remains possible that this fungus adapted mechanisms initially involved in drug resistance to endocytose or exocytose defective lipids or cell wall components in an Arp2/3-independent fashion.

Together, while our studies have provided evidence for CME-independent endocytic pathways in fungal cells, how exactly this process works and whether this mechanism is *C. albicans* specific, remains an interesting area of future research. I could suggest that our initial studies can contribute to the start of a mini-scientific-revolution similar to the situation when scientists discovered that in mammalian systems, endocytosis does not need clathrin, which led to the identification of many clathrin-independent endocytic pathways.

VII. Appendix

During the course of my PhD work, I have contributed to several publications as a co-author. However, because the topics of those publications were not directly aligned with the main themes of my thesis, I consider mentioning the 5 co-authored publications in the appendix as appropriate. My contribution to these papers was that I performed all *in vivo* mouse studies, where we injected different *C. albicans* strains directly into the blood stream of either WT mice (B6) or immunocompromised A/J mice. The goal of these studies was to evaluate the pathogenicity of various *C. albicans* mutants that other lab members had created. Finally, in one publication (chapter VII.2.), I contributed by thoroughly evaluating two different methods that can be used to assess whether genetic manipulation of *C. albicans* mutants has resulted in unintended chromosomal rearrangements associated with aneuploidy. The five publications are listed below.

Finally, although evaluations for Faculty 1000 Biology (F1000) are not considered publications of original research, they are nevertheless a contribution to the scientific community. As an associate F1000 member, I have identified and evaluated some of the most significant articles in our field and explained their importance. Links to the 6 F1000 evaluations are given below (chapter VII.6).

VII.1. Genome-wide mapping of the coactivator Ada2p yields insight into the functional roles of SAGA/ADA complex in *Candida albicans*

Originally published in:
Mol Biol Cell. 2009 May;20(9):2389-400. Epub 2009 Mar 11. || PMID: 19279142

Molecular Biology of the Cell
Vol. 20, 2389–2400, May 1, 2009

Genome-wide Mapping of the Coactivator Ada2p Yields Insight into the Functional Roles of SAGA/ADA Complex in *Candida albicans*

Adnane Sellam,*† Christopher Askew,*‡ Elias Epp,*‡ Hugo Lavoie,*‡ Malcolm Whiteway,*‡ and André Nantel*†

*Biotechnology Research Institute, National Research Council of Canada, Montréal, QC, H4P 2R2, Canada; and Departments of †Anatomy and Cell Biology and ‡Biology, McGill University, Montréal, QC, H3A 1B1, Canada

Submitted November 4, 2008; Revised January 21, 2009; Accepted March 3, 2009
Monitoring Editor: Charles Boone

The SAGA/ADA coactivator complex, which regulates numerous cellular processes by coordinating histone acetylation, is widely conserved throughout eukaryotes, and analysis of the *Candida albicans* genome identifies the components of this complex in the fungal pathogen. We investigated the multiple functions of SAGA/ADA in *C. albicans* by determining the genome-wide occupancy of Ada2p using chromatin immunoprecipitation (ChIP). Ada2p is recruited to 200 promoters upstream of genes involved in different stress-response functions and metabolic processes. Phenotypic and transcriptomic analysis of *ada2* mutant showed that Ada2p is required for the responses to oxidative stress, as well as to treatments with tunicamycin and fluconazole. Ada2p recruitment to the promoters of oxidative resistance genes is mediated by the transcription factor Cap1p, and coactivator function were also established for Gal4p, which recruits Ada2p to the promoters of glycolysis and pyruvate metabolism genes. Cooccupancy of Ada2p and the drug resistance regulator Mrr1p on the promoters of core resistance genes characterizing drug resistance in clinical strains was also demonstrated. Ada2p recruitment to the promoters of these genes were shown to be completely dependent on Mrr1p. Furthermore, *ADA2* deletion causes a decrease in H3K9 acetylation levels of target genes, thus illustrating its importance for histone acetyl transferase activity.

INTRODUCTION

Candida albicans is a major cause of morbidity and mortality in bloodstream infections. This pathogen can also colonize various biomaterials and readily forms dense biofilms that are resistant to most antifungal agents. Because of the challenges of drug resistance (Kontoyiannis and Lewis, 2002), extensive efforts are underway to identify new drug targets for therapeutic intervention. Despite the large number of studies undertaken on the genetic determinism of *C. albicans* pathogenesis, transcriptional regulation involving chromatin remodeling in this potentially virulent commensal remains largely unknown.

In eukaryotic cells, remodeling of chromatin structure is a critical factor in the control of gene expression because nucleosomes create an inherent physical obstacle for the binding of transacting factors, such as transcription factors (TFs) and RNA polymerases. Histone proteins function as building blocks to package eukaryotic DNA into repeating nucleosomal units that can be organized into highly condensed chromatin fibers (Kornberg and Lorch, 1999). Histone tails protruding beyond the nucleosome core are subjected to many posttranslational modifications, such as acetylation, methylation, phosphorylation, and ubiquitination, all of which can affect chromatin structure and thus regulation of gene expression (Grant, 2001). The Spt-Ada-Gcn5-acetyltransferase (SAGA) coactivator complex regulates numerous cellular processes through coordination of histone posttranslational modifications (Baker and Grant, 2007). Histone acetylation mediated by the SAGA complex through the histone acetyl transferase (HAT) Gcn5p has been widely studied. SAGA is targeted specifically to inducible gene promoters primarily through direct interaction with acidic activator domains of TFs, such as Gal4p and Gcn4p (Baker and Grant, 2007). In the budding yeast *Saccharomyces cerevisiae*, SAGA modulates the expression of ~10% of the measurable genome. The SAGA-dominated genes are strongly enriched in stress-responsive genes involved in challenges such as heat, oxidative agents, acidity, DNA damage, carbon or nitrogen starvation, and unfolded proteins (Daniel and Grant, 2007). Other investigations showed that transcriptional activation of some processes such as amino acid, phosphate, and galactose metabolism were completely dependant on chromatin remodeling mediated by SAGA (Berger *et al.,* 1992). Although best known for its role in regulating transcriptional activation, SAGA is also required for optimal transcription elongation, mRNA export, and DNA repair (Huisinga and Pugh, 2004).

The Ada1-5 proteins (Alteration/deficiency in activation) are components of SAGA and are encoded by genes that,

This article was published online ahead of print in *MBC in Press* (http://www.molbiolcell.org/cgi/doi/10.1091/mbc.E08–11–1093) on March 11, 2009.

Address correspondence to: André Nantel (andre.nantel@cnrc-nrc.gc.ca).

Abbreviations used: ChIP-CHIP, chromatin immunoprecipitation–ChIP mircoarray; HAT, histone acetyl transferase; SAGA, Spt-Ada-Gcn5-acetyltransferase; TF, transcription factor.

Table 1. *Candida albicans* strains used in the study

Strain	Genotype	Reference
SC5314	Clinical isolate	Gillum et al. (1984)
BWP17	ura3D::limm434/ura3D::limm434 his1::hisG/his1::hisG arg4::hisG/arg4::hisG	Wilson et al. (1999)
DAY286	ura3::imm434/ura3::imm434 his1::hisG/his1::hisG arg4::hisG-ARG4-URA3/arg4::hisG	Davis et al. (2002)
VIC1057[a]	ada2Δ::ARG4/ada2Δ::URA3 his1::hisG/his1::hisG	Bruno et al. (2006)
VIC1145[a]	ada2Δ::ARG4/ada2Δ::URA3 pHIS1::his1::hisG/his1::hisG	Bruno et al. (2006)
VIC1197[a]	ada2Δ::ARG4/ada2Δ::URA3 pADA2::HIS1::his1::hisG/his1::hisG	Bruno et al. (2006)
CJD20[b]	ura3Δ::limm434/ura3Δ::limm434 his1::hisG/his1::hisG arg4::hisG/arg4::hisG cap1::hisG-URA3-hisG/cap1::hisG	Alarco and Raymond (1999)
CMM3[a]	gal4Δ::ARG4/gal4Δ::HIS1 his1::hisG/his1::hisG	Martchenko et al. (2007)
AS-20[a]	ADA2/ADA2-TAP-URA3	
AS-21[a]	gal4Δ::ARG4/gal4Δ::HIS1 his1::hisG/his1::hisG ADA2/ADA2-TAP-URA3	This study
AS-22[b]	cap1::hisG-URA3-hisG/cap1::hisG ADA2/ADA2-TAP-URA3	This study
AS-23[a]	MRR1/MRR1-TAP-URA3	This study
MRR1M4B[c]	mrr1Δ::FRT/mrr1Δ::FRT	Morschhauser et al. (2007)
AS-24[c]	mrr1Δ::FRT/mrr1Δ::FRTADA2/ADA2-TAP-SAT1	This study

[a] Strains derived from BWP17 and have the genotype *ura3Δ::λimm434/ura3Δ::λimm434 arg4::hisG/arg4::hisG his1::hisG/his1::hisG.*

[b] Strain derived from CAI4 and have the genotype *ura3::imm434/ura3::imm434.*

[c] Strain derived from the clinical strain SC5314.

when inactivated, alleviate the toxicity of the chimeric activator GAL4-VPS16 in *S. cerevisiae* (Barrios *et al.*, 2007). Furthermore, it was demonstrated (Marcus *et al.*, 1994) that the Ada2/Ada3/Gcn5 complex is sufficient for robust histone and nucleosomal HAT activity. Gcn5p interacts with Ada2p in vivo and in vitro, thus establishing a physical and genetic link between these transcriptional components (Marcus *et al.*, 1994). Moreover, biochemical studies have shown that Ada2p interacts directly with the activation domains of Gcn4p and Gal4p, and indirectly with the TATA-binding protein (TBP), arguing that Ada2p may mediate interactions between the acidic activator domains of TFs and the basal transcriptional machinery component TFIID (Barlev *et al.*, 1995; Bhaumik and Green, 2001; Larschan and Winston, 2001).

The first evidence in *C. albicans* of a role for chromatin remodeling was the report (Klar *et al.*, 2001) that treating cells with the deacetylase inhibitor trichostatin A or deletion of the deacetylase-encoding genes *HDA1* or *RPD3* caused increases in the frequency of white-opaque switching. A recent study undertaken in *C. albicans* has also shown that Ada2p is required for the cell wall damage response, most probably by acting in combination with a variety of other regulators (Bruno *et al.*, 2006). However, up to now there has been little information about the biological processes controlled by the *C. albicans* SAGA/ADA coactivator complex.

In this study we have begun to elucidate the multiple functions of SAGA/ADA coactivator complex in *C. albicans*. Using chromatin immunoprecipitation (ChIP) coupled with microarray analysis (ChIP–CHIP), we have established the promoter occupancy of the SAGA/ADA component Ada2p. Our results yield insight into the role of Ada2p in drug, oxidative stress, and unfolded protein responses (UPRs) as well as virulence. We also investigated the importance of Ada2p recruitment by the transcription factors Cap1p and Gal4p to the promoters of oxidative stress responsive and glycolysis genes, respectively. Interestingly, we showed that Ada2p was involved in fluconazole tolerance, and its cooccupancy with the drug resistance regulator Mrr1p on the promoters of core resistance genes characterizing drug resistance in *MDR1*-overexpressing clinical strains was demonstrated. Likewise, we have shown that an *ada2* deletion causes a clear decrease of histone acetylation in vivo. These data demonstrate the role of Ada2p in chromatin remodeling through histone acetylation in addition to its function as a specific transcriptional coactivator recruited by TFs to their target promoters.

MATERIALS AND METHODS

C. albicans Strain Construction, Plasmids, and Media

Strains used in this study are listed in Table 1. Cell growth, transformation, and DNA preparation were carried out using standard yeast procedures. Cells were grown at 30°C in YPD media (1% yeast extract, 2% peptone, 2% dextrose). *ADA2* and *MRR1* were tandem affinity purification (TAP)-tagged in vivo with a TAP-*URA3* PCR product containing 100-bp homology up- and downstream of each open reading frame (ORF) as described by Lavoie *et al.* (2008). Transformants were selected on YPD −ura plates and correct integration of the TAP-tag was checked by PCR and sequencing. For Ada2-TAP ChIP in *mrr1* mutant, the TAP-tagging was performed using pFA-TAP-SAT1 plasmid to generate a cassette that contains a dominant nourseothricin resistance marker (SAT1). pFA-TAP-SAT1 was generated as follows: the *SAT1* gene was amplified by PCR from the previously published plasmid (Reuss *et al.*, 2004) using primers SAT1F and SAT1R. Subcloning of the *C. albicans SAT1* marker was done by ligation of AscI-PmeI PCR fragments in AscI-PmeI–digested pFA-TAP-URA3.

ADA2-TAP expressed in BWP17 strain was fully functional based on complementation of the oxidative stress sensitivity phenotype. Deleting the nontagged allele in the ADA2-TAP strain revealed that this strain has a comparable sensitivity to the single knockout strain and even to the parental strain. The same procedure was used to demonstrate the functionality of MRR1-TAP using the fluconazole sensitivity phenotype.

Drug Susceptibility Tests

Stock solutions were prepared using ethanol as the solvent for menadione (200 mM) and DMSO for fluconazole (100 mg/ml). Growth inhibition by menadione was assessed using a serial dilution inhibition test as described by Bruno *et al.* (2006). Fluconazole susceptibility was quantified using a microtiter plate liquid assay. The data are presented as the percent of relative growth of the cells in fluconazole-containing medium compared with the growth of the same strain in fluconazole-free medium. The values represent the means ± SDs of three independent experiments performed in triplicate.

Whole-Genome Location Profiling by ChIP-CHIP and ChIP-Real Time Quantitative PCR

ChIP experiments were performed as described previously with some modifications (Guillemette *et al.*, 2005). Briefly, cells were grown to an optical density at 600 nm of 2 in 40 ml of YPD. We followed the ChIP protocol

available at http://www.ircm.qc.ca/microsites/francoisrobert/en/317.html with the following modifications: chromatin was sonicated to an average 300 bp, and 700 μl of whole-cell extract (WCE) was incubated with IgG Sepharose beads (Amersham, Piscataway, NJ). Immunoprecipitated DNA was used for either whole-genome location profiling or gene-specific real time quantitative PCR analysis. For whole-genome location profiling, tagged ChIPs were labeled with Cy5 dye, and untagged (mock) ChIPs were labeled with Cy3 dye. Microarrays containing 11,817 70-mer oligonucleotide probes were cohybridized with tagged immunoprecipitated (Cy5-labeled) and mock-immunoprecipitated (untagged strain; Cy3-labeled) DNA samples. Microarray hybridization, washing, and scanning were performed as described (Nantel *et al.*, 2006). Prehybridization and hybridization solutions consisted of DIG Easy Hyb solution (Roche Diagnostics, Mannheim, Germany) with 0.45% salmon sperm DNA and 0.45% yeast tRNA. Slides were washed once in 1.0% SSC, 0.2% SDS at 42°C for 10 min; twice in 0.1% SSC, 0.2% SDS at 42°C for 10 min; and once in 0.1% SCC at 24°C for 5 min, followed by four rinses in 0.1% SSC. ChIPs were air dried before being scanned using a ScanArray Lite microarray scanner (PerkinElmer, Waltham, MA). QuantArray was used to quantify fluorescence intensities. Data handling and analysis were carried out using Genespring v.7.3 (Agilent Technologies, Palo Alto, CA). The significance cutoff was determined using the distribution of log-ratios for each factor. It was set at 2 SDs from the mean of log-transformed fold enrichments. Values shown are an average of two biological replicates derived from independently isolated transformants of tagged and mock constructs.

Quantitative real-time PCR (qPCR) was performed using the Corbett Rotor-Gene RG-3000A (Corbett Research, Sydney, Australia) with SYBR Green fluorescence (Qiagen, Chatsworth, CA). qPCR was performed using 1 ng of TAP-ChIPed DNA or total genomic DNA extracted from WCE. Cycling was for 15 min at 95°C, followed by 45 cycles of 95°C for 10 s, 58°C for 15 s, and 72°C for 15 s. All samples were tested in triplicate and means were used for further calculations. Fold-enrichments of tested promoter sequences were estimated by using the coding sequence of the *C. albicans ACT1* ORF as a reference. *ACT1* was chosen as a reference since no IP enrichment was detected for *ACT1* ORF in the ADA2-TAP strain relative to the control strain BWP17. Fold-enrichment of the tested promoter sequences was estimated using the comparative ΔΔCt method as described by Guillemette *et al.* (2005). Primer sequences used for this analysis are summarized in Supplemental Table S1.

Histone acetylation was assessed by ChIP-qPCR as described above using anti-acetyl-Histone H3 (Lys9; 06-942, Upstate Biotechnology, Lake Placid, NY) and anti-acetyl-Histone H4 (06-598, Upstate Biotechnology) antibodies.

Expression Analysis by qPCR

For fluconazole, tunicamycin, and menadione treatments, cultures were inoculated from a fresh colony and grown overnight in YPD at 30°C. Cultures were then diluted to an OD600 of 0.1 in 100 ml of fresh YPD and grown at the same initial temperature until an OD600 of 0.8. The culture was divided in two volumes of 50 ml; one sample was maintained as the control, and the other treated with compounds cited above. *Candida* cells were exposed to 10 μg/ml fluconazole and 4.73 μM tuncamycin for 1 h and to 0.2 mM menadione for 30 min. Cells were then centrifuged 2 min at 3500 rpm, the supernatants were removed, and the samples were quick-frozen and stored at −80°C.

cDNA was synthesized from 2 μg of total RNA using the reverse-transcription system (50 mm Tris-HCl, 75 mm KCl, 10 mm dithiothreitol (DTT), 3 mm $MgCl_2$, 400 nm oligo$(dT)_{15}$, 1 μm random octamers, 0.5 mm dNTPs, and 200 U Superscript III reverse transcriptase; Invitrogen, Carlsbad, CA). The total volume was adjusted to 20 μl, and the mixture was then incubated for 60 min at 42°C. Aliquots of the resulting first-strand cDNA were used for real-time PCR amplification experiments. Real-time PCRs were performed as described for ChIP-qPCR.

The *HAC1* splicing rate in tunicamycin-challenged cells was evaluated by quantifying specifically the *HAC1* spliced mRNA (sHAC1) by qPCR using the primer pair HAC1F1 and HAC1R1. The primer HAC1R1 was designed to overlap the contiguous exons generated after the excision of the unconventional intron (Wimalasena *et al.*, 2008). The results were normalized using Ct values obtained for *ACT1*. The splicing rate in the *ada2* mutant was determined by comparing sHAC1 levels using the wild type (wt) as a reference.

Virulence Studies

Virulence testing of *C. albicans* was done as previously described (Mullick *et al.*, 2004). Briefly, 8- to 12-wk old C57BL/6J mice (Jackson Laboratories, Bar Harbor, ME) were inoculated via the tail vein with 200 μl of a suspension containing 3×10^5 *C. albicans* in PBS. Five male mice were used for each experimental group. Mice were closely monitored over a period of 21 d for clinical signs of disease such as lethargy, ruffled fur, or hunched back. Mice showing extreme lethargy were considered moribund and were killed. All experimental procedures involving animals were approved by the Biotechnology Research Institute Animal Care Committee, which operated under the guidelines of the Canadian Council of Animal Care.

RESULTS

Ada2p Binds 200 Gene Promoters Associated with Specific Functional Categories

BlastP analysis revealed that, in *C. albicans*, the same SAGA/ADA core components were present as in *S. cerevisiae* (Table 2). Functional domain conservation of the core components GCN5/ADA2/ADA3 was also verified and showed a high degree of similarity (data not shown). In the present study we focused on a core component of the SAGA/ADA complex: Ada2p, which was shown to be crucial for histone acetylation in *S. cerevisiae* (Marcus *et al.*, 1994; Barrios *et al.*, 2007).

We set out to investigate the genomic occupancy of Ada2p using ChIP-CHIP. Cells expressing a TAP-tagged version of Ada2p were lysed and sonicated, and the DNA-Ada2p-TAP was purified. Cross-linking was reversed, and the purified DNA was amplified by ligation-mediated PCR, labeled with Cy5, and hybridized to a microarray containing 5423 intergenic and 6394 intragenic 70-mer oligonucleotide probes. As a control, DNA that was precipitated from BWP17 cells was labeled with the Cy3 fluorochrome. All experiments were repeated twice from samples cross-linked separately. Using a cutoff of two SDs above the mean of log ratios (giving a 1.44-fold enrichment cutoff), Ada2p was found to associate with 200 of the 11,817 probes in our microarray layout (Figure 1A and Supplemental Table S2). To assess the reliability of the ChIP-CHIP method, the immunoprecipitated DNA from two other independent ChIP experiments was quantified using qPCR. A total of 18 promoters were selected and a set of three pairs of PCR primers per promoter were designed to amplify 0 to −200-bp, −200- to −400-bp, and −400- to −600-bp regions upstream the ATG. The result obtained for the 18 selected promoters confirmed binding of Ada2p to the promoters identified by ChIP-CHIP (Figure 1B). The peak intensity of enrichment was most commonly observed in the 0 to −400-bp region.

To gain further insight into the biological function of Ada2p, Gene Ontology (GO) biological process categories were assigned to the 200 genes near Ada2p-occupied loci. For these analyses, all GO categories of genes having an enrichment $p < 0.01$ were selected. Functional categories of Ada2p target genes are summarized in Figure 1C. This analysis revealed a significant enrichment in genes related to metabolic process such as glycolysis (p = 5.49e-17), pyruvate metabolism (p = 1.08e-07), and protein biosynthesis (p = 4.08e-05). Functional categories belonging to stress response were significantly represented in our set. These include genes connected to oxidative stress (p = 7.69e-05) and drug response (p = 1.56e-05), as well as protein folding (p = 3.95e-08). Ada2p was found to occupy cell wall gene promoters (p = 5.06e-07) consisting essentially of GPI (glycosylphosphatidylinositol)-anchored proteins. Interestingly, Ada2p was recruited to promoters of proteasome regulatory genes (p = 3.65e-03) including the gene encoding the transcription factor Rpn4p. Categories such as lipid metabolism (p = 2.23e-01), amino acid metabolism (p = 5.34e-02), DNA replication (p = 8.08 e-02), early secretion pathway (p = 8.3e-01), vacuolar acidification (p = 1.23e-01), and chromatin maintenance (p = 4.01e-01) did not meet the statistical cutoff criterion in this experiment. Ada2p was also found in the promoter of a large number of hypothetical genes (50 genes).

ADA2 Depletion Affects Histone Acetylation In Vivo

In the budding yeast *S. cerevisiae*, the HAT catalytic subunit of the SAGA coactivator complex, Gcn5p, was shown to preferentially acetylate multiple lysine residues on the N-

Table 2. *Candida albicans* homologs of the *Saccharomyces cerevisiae* SAGA/ADA coactivator complexes

S. cerevisiae protein	Systematic name	*C. albicans* homologs	E value	Function in *S. cerevisiae*
HAT				
Gcn5 (Ada4)	YGR252W	orf19.705	6.1e-153	Histone acetyltransferase
Ada				
Ada1	YPL254W	orf19.307	8.9e-37	Transcription coactivators required for nucleosomal acetylation by Gcn5
Ada2	YDR448W	orf19.2331	7.1e-127	
Ada3	YDR176W	orf19.3023	2.6e-49	
Spt				
Spt3	YDR392W	orf19.7622	6.0e-91	TBP interaction, transcriptional repression
Spt8	YLR055C	orf19.4312	9.1e-87	
Spt7	YBR081C	orf19.7572	9.8e-144	Complex stability and maintenance
Spt20 (Ada5)	YOL148C	orf19.422	1.2e-28	
TAF				
TAF5	YBR198C	orf19.536	4.7e-176	Structural integrity of the complex and interaction with basal transcription machinery
TAF6	YGL112C	orf19.7454	6.8e-106	
TAF9	YMR236W	orf19.1111	3.8e-41	
TAF10	YDR167W	orf19.3242	8.1e-35	
TAF12	YDR145W	orf19.470	1.1e-46	
H2B deubiquitylation				
Ubp8	YMR223W	orf19.1767	4.8e-70	Deubiquitylation of H2BK123
Sgf11	YPL047W	orf19.7360	9.1e-08	Required for association of Ubp8 and Sus1 with SAGA
Sus1	YBR111W-A	orf19.6795	8.8e-10	mRNA export
Chd				
Chd1	YER164W	orf19.3035	0	Recognition of H3K4 methylation and potentiation of histone acetylation by GCN5
Rtg2	YGL252C	—	—	SLIK stability
Other				
Sgf29	YCL010C	orf19.7074	8.8e-58	Unknown
Tra1	YHR099W	orf19.139	0	Interaction with transcriptional activators

terminal tails of histones H3 and H2B (Suka *et al.*, 2001). Furthermore, Ada2p was found to be required for the Gcn5p nucleosomal HAT activity in vivo (Candau *et al.*, 1997). In light of this data, we sought to examine the role of Ada2p in HAT in *C. albicans* by assessing histone acetylation levels and by performing ChIP-qPCR using antibodies directed against acetylated histones H3K9 and H4 in wt and in *ada2* cells.

Acetylation levels of the entire ORF as well as 1 kbp upstream of the *GAL4* and *MDR1* genes were quantified relative to the acetylation level of the *ACT1* coding region (Figure 2). In wt cells, *GAL4* and *MDR1* showed increased H3K9-acetylation compared with the *ACT1* coding region. Notably, the H3K9-acetylation profiles of the two genes were different; although *GAL4* exhibits a peak in the −200-bp promoter region, *MDR1* H3K9-acetylation level peaked at the 3′-extremity of the ORF (Figure 2). In both genes, H3K9-acetylation was significantly decreased but not completely abolished in the *ada2*-deleted strain. For each gene, the wt H4-acetylation profiles were similar to those of H3K9; however, no significant differences were recorded in the *ada2* mutant (data not shown). Thus, these results suggest that Ada2p is required for a specific histone acetylation in vivo.

ada2 Mutant Strains Show Altered Sensitivity to Fluconazole and Oxidative Stress and Display Attenuated Virulence

Genes involved in the oxidative stress and drug responses were significantly overrepresented in Ada2p-bound promoters. This finding prompted us to assess if the inactivation of this regulator affects drug and oxidative stress sensitivity. As shown in Figure 3A, on YPD medium, wt and the *ada2* mutant, as well as the revertant strain, grew similarly. On YPD medium supplemented with 0.2 mM menadione, growth of *ada2* mutant cells was completely abolished, whereas the revertant was slightly inhibited and its sensitivity was found to be comparable to that of the parent strain. The same effect was observed with hydrogen peroxide (data not shown). The sensitivity of an *ada2* mutant strain in the presence of the azole drug fluconazole was evaluated using a liquid microdilution assay. The growth of the *ada2* strain was indeed moderately inhibited in the presence of fluconazole compared with the revertant and parental strains (Figure 3B). This result suggests that in addition to the crucial role in mediating oxidative stress resistance, Ada2p contributes to azole tolerance.

Sensitivity to oxidative stress inducers is often linked to a decrease in virulence. Because *ada2* was hypersensitive to menadione and hydrogen peroxide, we determined if this gene is required for *C. albicans* virulence. The *C. albicans* strains DAY286 (wt), an *ada2* mutant strain, and an *ada2* revertant were tested in a mouse systemic infection model by intravenous tail infection. As shown in Figure 3C, although 100% of the mice infected with the wt strain died within 12 d, only 20% of mice infected with the *ada2* mutant died in this period. The revertant strain showed an intermediate survival rate consistent with the reintroduction of one copy of Ada2p. This finding reveals that the *ada2* deletion causes attenuated virulence during systemic infection.

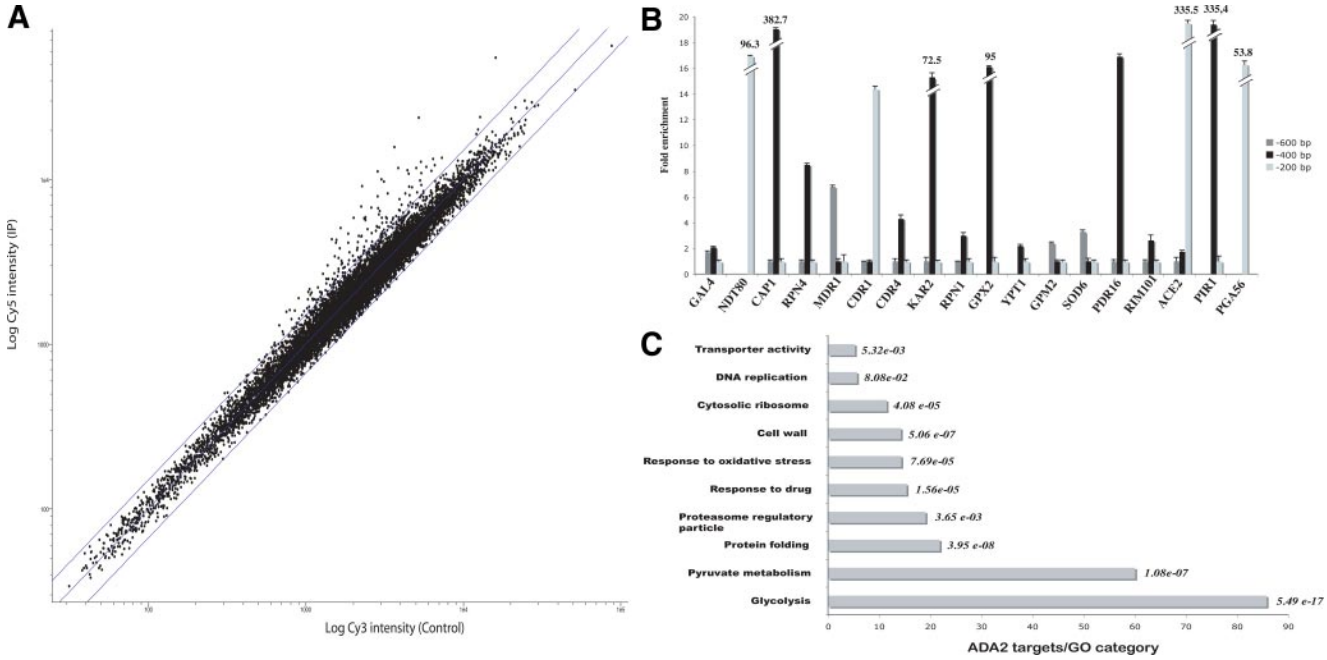

Figure 1. Genome-wide location of Ada2p. (A) Location analysis scatter plot. DNA fragments derived from ChIP were labeled with Cy5, compared with genomic DNA fragments from an untagged strain, and labeled with Cy3. Both samples were hybridized to a single array. Representative scatter plot for Ada2p includes lines representing the 2-SD cutoff (1.44-fold). (B) In vivo occupancy of Ada2p at various intergenic regions. TAP ChIP DNA was subjected to qPCR to validate ADA2 binding to 0 to −20-bp, −200- to −400-bp, and −400 to −600-bp promoter regions. SDs were based on data from two independent experiments. (C) GO biological process annotation of Ada2p bound promoters. The p value was calculated using hypergeometric distribution as described in the GO Term Finder Tool Web site (www.candidagenome.org/cgi-bin/GO/goTermFinder).

Ada2p Regulates the Expression of Drug, Oxidative Stress and Unfolded Protein–Responsive Genes

To assess whether hypersensitivity to oxidative stress, as well as Ada2p occupancy correlates with gene expression, RNA levels of oxidative stress–responsive genes was determined. We analyzed the expression level of the transcription factor *CAP1* as well as *CTA8* (homolog of *S. cerevisiae HSF1*), *SOD6*, *TRX1*, and the glutathione peroxidase *GPX2* in wt and the *ada2* mutant under normal growth conditions and after treatment with menadione. The data revealed that, for the wt, the transcript levels of the selected genes were noticeably increased when cells were challenged with menadi-

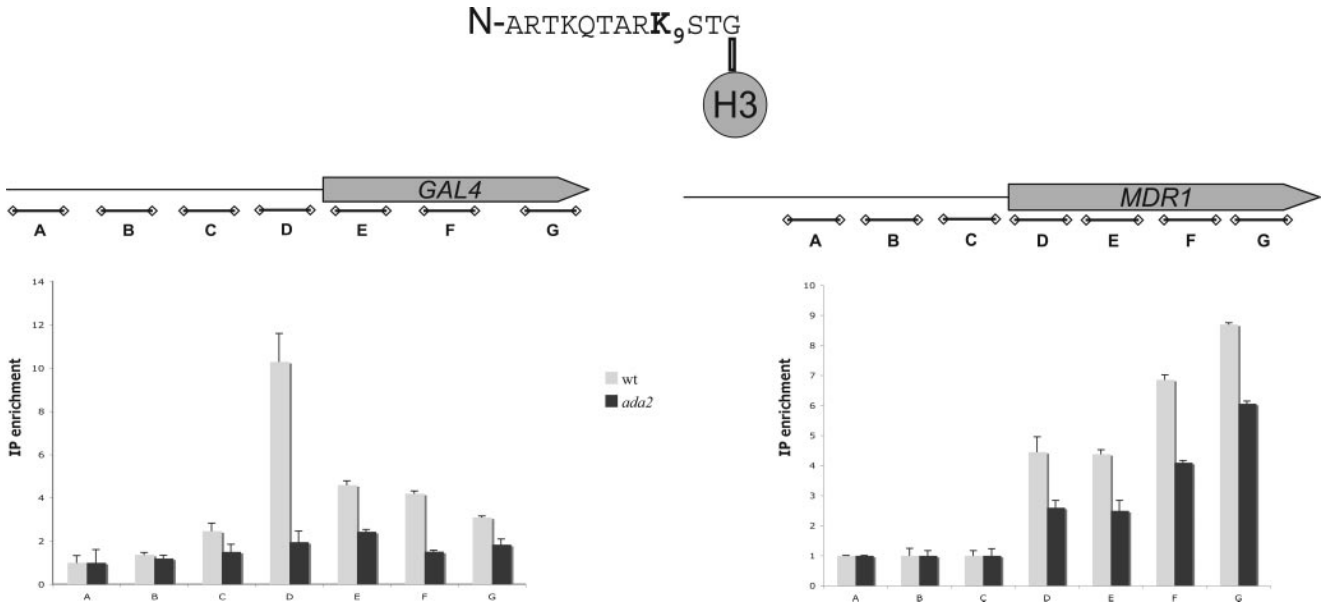

Figure 2. Ada2 deletion affects acetylation of H3K9 in vivo. Fine mapping of *GAL4* and *MDR1* H3K9 acetylation in the wt and *ada2* mutant using ChIP-qPCR. The IP enrichments represent the binding ratios that were all normalized to the *ACT1* ORF, which was set to 1.

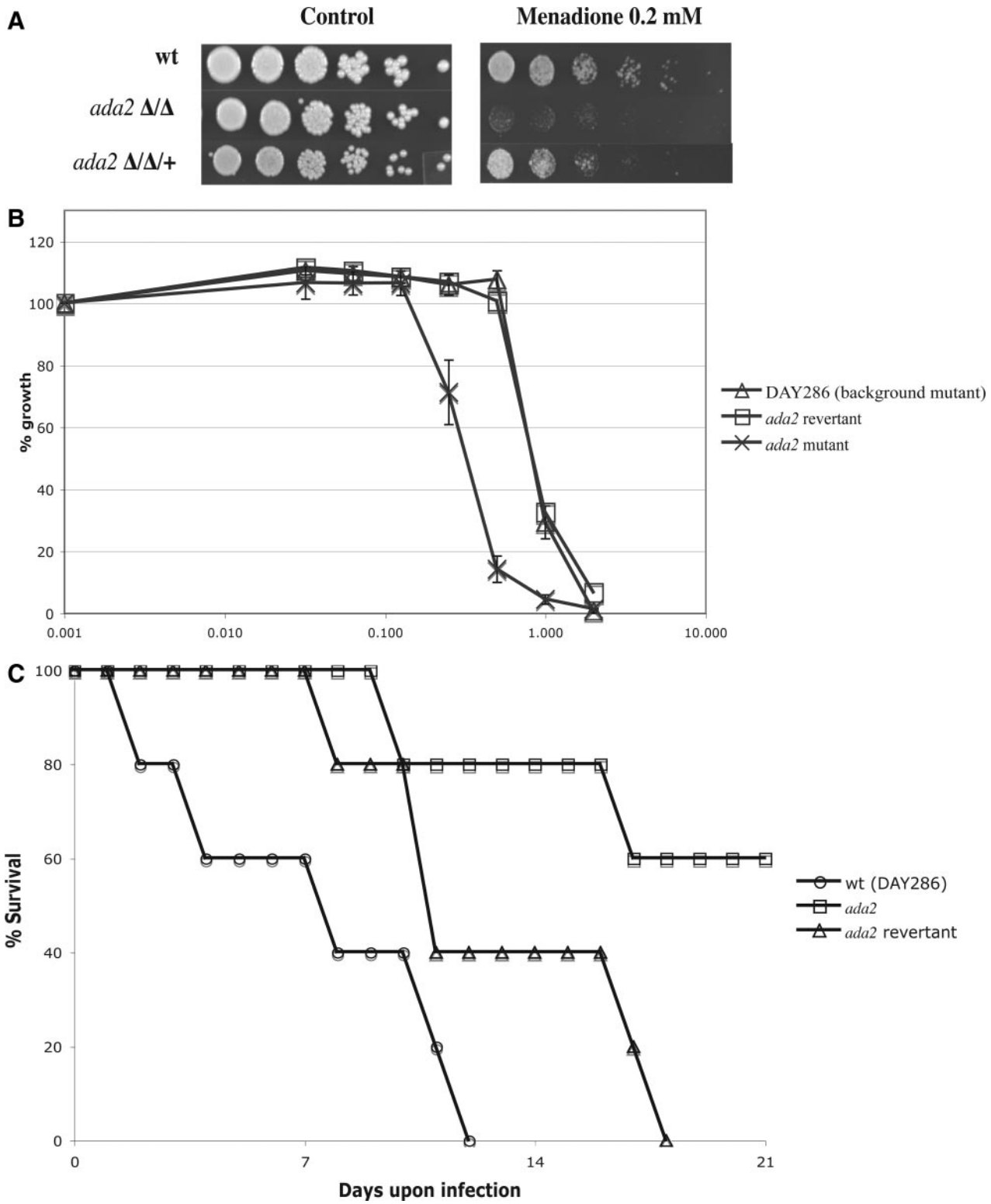

Figure 3. Phenotypic analysis of *ada2* mutant. (A) Absence of Ada2p causes hypersensitivity to menadione. Fivefold serial dilutions of wt, *ada2* mutant, and revertant strains were grown on YPD supplemented with menadione at 0.2 mM and grown at 30°C for 48 h. (B) Fluconazole sensitivity of *ada2* revealed using microtiter plate liquid assay. The data are presented as the percent relative growth of the cells in fluconazole-containing medium compared with the growth of the same strain in fluconazole-free medium. The values represent the means ± SDs of three independent experiments performed in duplicate. (C) Survival of mice infected with *C. albicans ada2* mutant (□), *ada2* revertant (△), and wt parental (○) strains. Mice were inoculated by tail vein injection, and survival was measured over a 21-d period. Average expression of oxidative stress–responsive genes is shown in wt and *ada2* cells 30 min after 0.2 mM menadione treatment. The reported values are the means ± SD of three independent experiments.

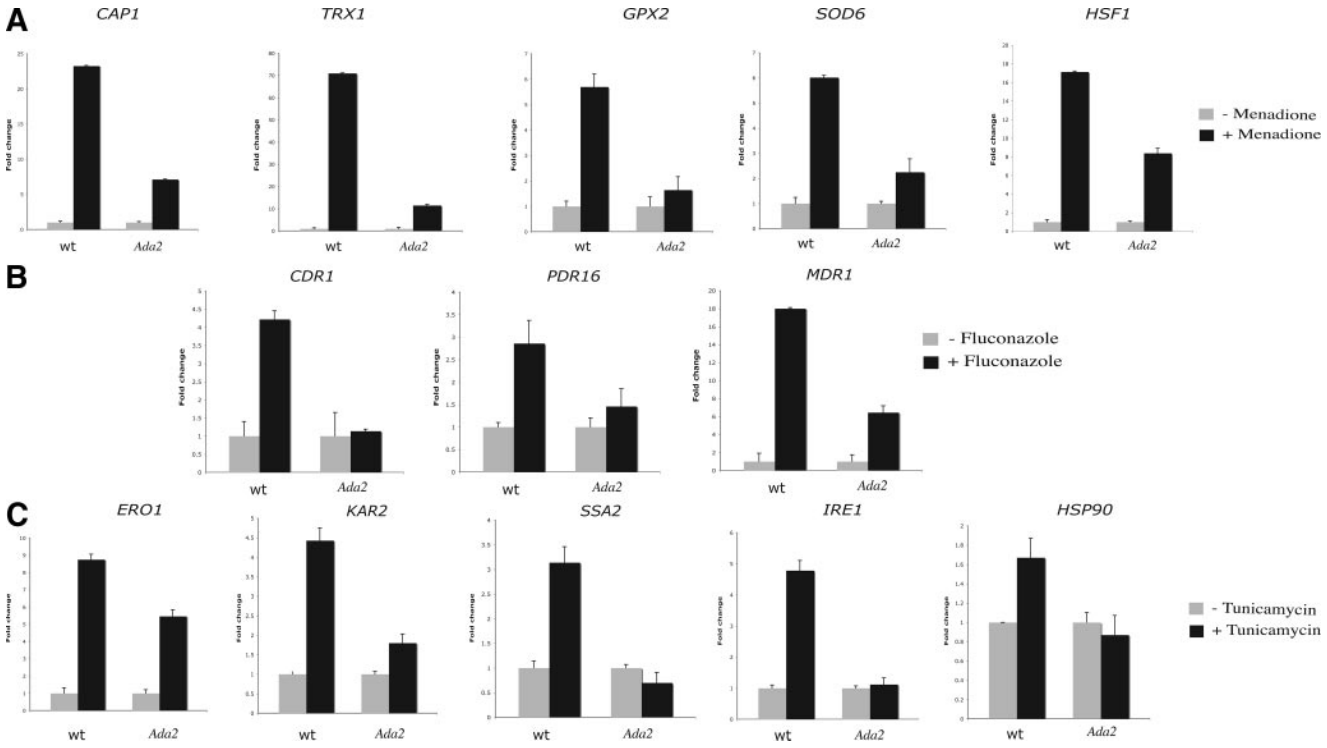

Figure 4. Ada2p regulates the expression of drug-, oxidative stress–, and UPR-responsive genes. Average expression of oxidative stress–(A), drug- (B), and UPR- responsive (C) genes is shown in wt and *ada2*. The reported values are the means ± SD of three independent experiments.

one (Figure 4A). This activation was significantly reduced but not fully abolished in the absence of Ada2p for all tested genes.

Furthermore, we sought to determine whether the Ada2p-dependent transcriptional inducibility of drug-responsive genes contributes to azole tolerance. To this end, transcript levels of the two drug transporters Cdr1p and Mdr1p, as well as the phosphatidylinositol transfer protein Pdr16p, were evaluated in the wt and in the *ada2* mutant under normal condition and after challenge with fluconazole. In the wt background, the expression of *CDR1*, *PDR16*, and *MDR1* was significantly induced, whereas in the *ada2* mutant the inducibility of those genes was impaired (Figure 4B). Although Ada2p was also seen to interact with the promoter of the transcription factor Ndt80p, known to be required for drug tolerance by regulating *CDR1* expression (Wang *et al.*, 2006a), no differential expression of the *NDT80* gene was noticed in the wt or in the *ada2* mutant in response to fluconazole (data not shown).

In the budding yeast *S. cerevisiae*, SAGA/ADA was shown to play an important role in mediating the UPR (Welihinda *et al.*, 1997, 2000). In our study, we found that Ada2p binding was significantly enriched for gene promoters whose products are involved in protein folding (Figure 1A). Indeed, promoters for several chaperones such as Hsp90p, Hsp104p, Hsp60p, and Hsp31p as well as the endoplasmic reticulum (ER)-resident chaperone Kar2p and the ER-thioloxidase Ero1p were bound by Ada2p. To investigate whether Ada2p is required for the activation of the UPR in *C. albicans*, expression of the chaperones *HSP90*, *SSA2*, and *KAR2* as well as *ERO1* was assessed in the wt and the *ada2* mutant treated or not with the UPR-inducing agent tunicamycin. Additionally, the expression level of *IRE1*, widely known to mediate the UPR in eukaryotes by regulating Hac1p synthesis through *HAC1* mRNA splicing, was also monitored. Noticeably, Ada2p bound to the *IRE1* promoter with a moderate enrichment ratio of 1.31, which was just below the defined cutoff. In the wt background, the transcript level of all selected genes was induced in tunicamycin-treated cells. In the *ada2* mutant, although tunicamycin inducibility of *KAR2* and *ERO1* was partially impaired, *SSA2*, *IRE1*, and *HSP90* up-regulation was completely abolished (Figure 4C). The effect of the *ada2* deletion on the splicing of *HAC1* mRNA was also evaluated using qRT-PCR as outlined in *Materials and Methods*. The Hac1p splicing rate was assessed in the presence of tunicamycin, and our results revealed a reduction of 26% of *HAC1* splicing in the *ada2* mutant compared with the wt (data not shown). Despite the apparent role of Ada2p in regulating UPR gene expression and *HAC1* splicing, there was no significant difference in sensitivity to tunicamycin or DTT between the *ada2* mutant and wt cells (data not shown).

Specific Recruitments of Ada2p by Gal4p, Cap1p, and Mrr1p Transcription Factors

Recruitment by Gal4p to Glycolysis and Pyruvate Metabolism Gene Promoters. In the budding yeast *S. cerevisiae*, recruitment of the SAGA complex to regulate *GAL* genes through Gal4p has been broadly investigated. Indeed, many studies have shown that the transcriptional activation of *GAL* genes was completely dependent on SAGA (Sterner *et al.*, 1999; Bhaumik and Green, 2001; Larschan and Winston, 2001). Although the sequence and synteny of the Leloir pathway genes are highly conserved between *S. cerevisiae* and *C. albicans*, the regulatory circuit controlling this metabolic process is completely different (Martchenko *et al.*, 2007). *GAL4* is not required for control of

Table 3. Ada2p promoter occupancies of glycolysis and pyruvate metabolism genes in the wt and *gal4* mutant

Orf19	Gene name	Description	Gal4p binding motif	Position	Binding ratio	
					wt	*gal4*
Glycolysis						
orf19.4941	*TYE7*	bHLH transcription factor	GCC $_{(N11)}$ GGC	−1214	2.11	0.91
orf19.3575	*CDC19*	Putative pyruvate kinase	CGG $_{(N11)}$ TCG	−263	2.14	0.91
orf19.3967	*PFK1*	Alpha subunit of phosphofructokinase	TCC $_{(N11)}$ GGG	−753	2.21	0.95
orf19.6540	*PFK2*	Beta subunit of phosphofructokinase	CCC $_{(N11)}$ GGC	−586	2.01	1.00
orf19.3997	*ADH1*	Alcohol dehydrogenase	CGG $_{(N11)}$ CCG	−613	2.04	1,03
orf19.3888	*PGI1*	Glucose-6-phosphate isomerase	TCC $_{(N11)}$ GGC	−508	1.84	0.96
orf19.6745	*TPI1*	Triose-phosphate isomerase	CGT $_{(N11)}$ CCG	-291	1.79	0.84
orf19.4617	*FBA1*	FBA1 Putative fructose-bisphosphate aldolase	GCC $_{(N11)}$ GGT	−397	1.78	1.1
orf19.5338	*GAL4*	Transcription factor with zinc cluster DNA-binding motif	CGA $_{(N11)}$ CCG	−710	1.5	1.04
orf19.1067	*GPM2*	Phosphoglycerate mutase	CGA $_{(N11)}$CCG	−268	1.55	1.15
orf19.6814	*TDH3*	Glyceraldehyde-3-phosphate dehydrogenase	ACC $_{(N11)}$ GGC	−303	1.65	1.08
orf19.395	*ENO1*	ENO1 Enolase (2-phospho-D-glycerate-hydrolyase)	GCC $_{(N11)}$ GGT	−308	2.6	1.03
orf19.903	*GPM1*	Phosphoglycerate mutase	AGG $_{(N11)}$ CCG	−268	2.55	1.13
orf19.3651	*PGK1*	Phosphoglycerate kinase	ACC $_{(N11)}$ GGC	−456	2.5	0.98
Pyruvate metabolism						
orf19.2877	*PDC11*	Pyruvate decarboxylase	GCC $_{(N11)}$ GGG	−324	1.95	0.89
orf19.5021	*PDX1*	Dihydrolipoamide dehydrogenase (E3)-binding protein of the mitochondrial pyruvate dehydrogenase (PDH) complex	GCC $_{(N11)}$ GGT	−164	2.02	1.15
orf19.3097	*PDA1*	E1 alpha subunit of the pyruvate dehydrogenase (PDH) complex	GCC $_{(N11)}$ GGT	−141	1.86	0.87
orf19.5294	*PDB1*	E1 beta subunit of the pyruvate dehydrogenase (PDH) complex	GCC $_{(N11)}$ GGT	−196	1.87	0.92
orf19.6561	*LAT1*	Dihydrolipoamide acetyltransferase component (E2) of pyruvate dehydrogenase complex	GCC $_{(N11)}$ GGT	−242	1.8	0.93
Translation and ribosome assembly						
orf19.2935	*RPL10*	Cytoplasmic ribosomal subunits	—	—	1.72	1.71
orf19.6265	*RPS22A*	Cytoplasmic ribosomal suunits	—	—	1.56	2.15

Occupancy of *RPL10* and *RPS22A* promoters is shown as a control. Detection of Gal4p motif was performed as described by Hogues *et al.* (2008).

the Leloir pathway genes but instead participates in the regulation of genes, representing 2% of *C. albicans* genome, which are involved in a diverse range of cellular process including glycolysis.

In our study glycolysis stood out as the most significantly enriched category for Ada2p binding. This prompted us to ask whether Ada2p is required for Gal4p to regulate glycolysis genes in *C. albicans*. To test this hypothesis, we performed genome-wide mapping of Ada2p in a *gal4* deletion mutant. Our result revealed clearly that the occupancy of all Ada2p-bound glycolysis promoters was dramatically reduced in the absence of *GAL4* (Table 3). Ada2p occupancy at promoters of genes encoding the pyruvate metabolism genes Pdc11p, Pda1p, Pdx1p, Lat1p, and Pdb1p was also lost in *gal4* background (Table 3). These data suggest that Ada2p is exclusively recruited by Gal4p to regulate genes from the glycolysis pathway and pyruvate metabolism.

Cap1p Recruitment to the Promoters of Oxidative Stress–responsive Genes. Because many promoters bound by Ada2p were found upstream of genes previously reported to be regulated by Cap1p, we compared the Ada2p occupancy data with the published transcription profiling undertaken on the *cap1* mutant treated with H_2O_2 (Wang *et al.*, 2006b). A significant overlap (p = 1.04e-13) was found between Cap1p-dependant genes and Ada2p bound promoters consisting of 15 common genes (Figure 5). When Ada2p binding cutoff was reduced to 1.2 the overlap was expanded to 27 genes (p = 1.8e-32). Based on these results, it is possible that Cap1p is recruited by Ada2p to its target promoter genes as part of the oxidative stress response. To test this hypothesis, we mapped, using ChIP, Ada2-TAP in vivo occupancy in a *cap1* mutant strain. The −1- and −200-bp promoter regions of the Cap1p-dependant genes *TTR1*, *GRP2*, *GPX2*, *YCF1*, *MDR1,* and *CIP1* were targeted for occupancy enrichment using qPCR. Our result demonstrates clearly that Ada2p promoter binding for all tested genes was decreased in the *cap1* mutant compared with the parental strain (Figure 5).

Mrr1p Recruitment to the Promoters of Genes Related to Fluconazole Clinical Resistance. Intriguingly, Ada2p was

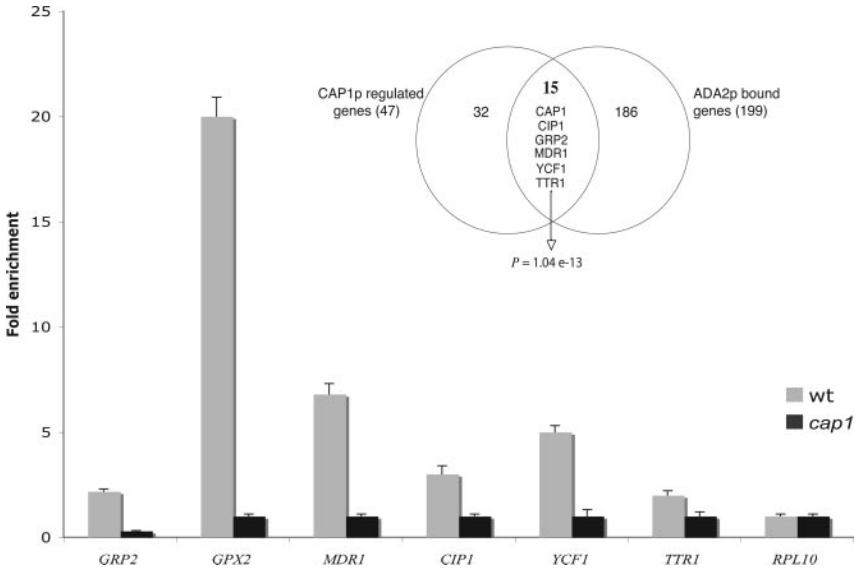

Figure 5. Cap1p recruits Ada2p to the promoter of oxidative stress–responsive genes. ChIP-qPCR occupancy analysis of Ada2p at the indicated promoter regions in the wt strain (▨) and *cap1* mutant (■). Error bars, SD of two biological replicates. Occupancy of *RPL10* promoters is shown as a control. Venn diagram depicting the overlap between Ada2p bound promoters and Cap1p-dependant genes is shown.

found to bind promoters of genes constitutively activated in azole-resistant clinical strains overexpressing Mdr1p (Karababa *et al.*, 2004). Recent work elucidated the mechanism controlling the overexpression of *MDR1* and multidrug resistance in those clinical isolates (Morschhauser *et al.*, 2007). Drug resistance was caused by a gain-of-function mutation in a zinc cluster transcription factor called Mrr1p. We identified a common core set of eight overexpressed genes, including *MDR1 (IFD5* and *IFD7* were not considered because they were removed from Assembly 21), which overlap with Ada2p-binding genes (Figure 6A). This finding suggests that Ada2p is recruited to the promoters of genes mediating azole resistance, most probably by its association with Mrr1p. To support this hypothesis we first used ChIP-qPCR to determine if Mrr1p binds to the *cis*-regulatory regions of these eight core genes mediating azole clinical resistance. As shown in Figure 6B, Mrr1p binding was significantly enriched for seven promoters among the eight resistance genes. The overlap with Ada2p-binding consisted of six resistance genes.

Taking into consideration the key role of Mrr1p as a master regulator of drug resistance, along with Ada2p cooccupancy of core resistance genes, Ada2p might function as a coactivator of Mrr1p. This was demonstrated by assessing Ada2-TAP in vivo occupancy in a *mrr1* mutant strain using ChIP-qPCR targeting the −1- and −200-bp promoter regions of the eight core resistance genes. Our result demonstrates clearly that Ada2p promoter binding for the six resistance genes cooccupied by both Ada2p and Mrr1p decreased in the *mrr1* mutant compared with the parental strain (Figure 6B).

DISCUSSION

The absence of a complete sexual cycle in *C. albicans*, in addition to its diploid nature, limits the use of classical genetic approaches to dissect mechanisms controlling its virulence. In the model yeast *S. cerevisiae* the usefulness of ChIP-CHIP has been demonstrated in several studies that revealed unexpected regulatory functions or features

A

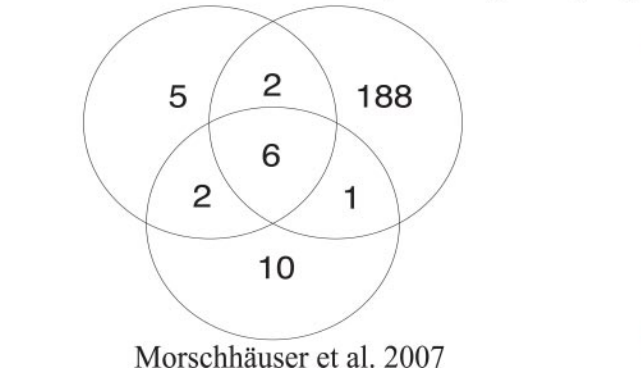

B

Gene name	Orf19 accession	Mrr1p binding[c]	Ada2p binding	ADA2 binding in *mrr1*[c]
IFD1	orf19.1048	9.3 ± 0.6	2.9	1.1 ± 0.1
IFD5	-- [(a)]	-	-	-
IFD7	orf19.629 [(b)]	-	-	-
CSH1	orf19.4477	6.3 ± 0.3	1.5	0.8 ± 0.2
HSP31	orf19.251	5.8 ± 0.4	3.3	0.9 ± 0.2
IPF5987	orf19.7306	8.5 ± 0.7	1.3	0.9 ± 0.1
GRP2	orf19.4309	5.2 ± 0.9	3	1.2 ± 0.1
MDR1	orf19.5604	4.3 ± 0.5	3.9	1.9 ± 0.4
OYE32	orf19.3131	1.4 ± 0.2	2.4	1 ± 0.2
GPX1	orf19.86	1.1 ± 0.4	1.1	0.9 ± 0.1
RPL10	orf19.2935	0.8 ± 0.1	1.7	2 ± 0.3

Figure 6. Mrr1p recruits Ada2p to the promoter of core genes related to fluconazole clinical resistance. (A) Relationship between Ada2p bound genes and the core genes associated with drug resistance of clinical strains overexpressing MDR1 as revealed by two independent profiling studies. (B) Ada2p and Mrr1p occupancy of the eight core resistance genes are listed in addition to *RPL10* used as a negative control. Primers were designed to amplify 200 base pairs upstream the ATG. [a] ORF not physically mapped; [b] ORF deleted from Assembly 20; [c] significantly enriched for seven promoters among the eight resistance genes.

(Harbison *et al.*, 2004; Pokholok *et al.*, 2006). Recently, ChIP-CHIP has been used in *C. albicans* to study TFs regulating drug resistance (Liu *et al.*, 2007; Znaidi *et al.*, 2008) and to describe the unexpected rewiring of transcriptional regulatory networks controlling the choice of mating type (Tsong *et al.*, 2006) or the expression of ribosomal protein genes (Hogues *et al.*, 2008). In our study, the use of this genomic tool allowed us to gain insights into the roles of Ada2p as a transcriptional regulator of many biological processes. Indeed, the functions of the promoter targets of Ada2p guided our experiments into its roles into the regulation of stress-dependent gene expression and azole sensitivity.

The finding that Ada2p occupies a broad range of *C. albicans* promoters suggests that this activator plays a global role in transcriptional regulation, as was already established for the SAGA/ADA coactivator complex in *S. cerevisiae*. This observation complements expression-profiling data that showed a wide variety of gene expression alterations in the *C. albicans ada2* mutant (Bruno *et al.*, 2006). These results, together with the fact that the deletion of *ADA2* leads to a significant decrease in H3K9 acetylation, imply that Ada2p is a general transcriptional regulator that operates through chromatin acetylation. This finding is consistent with the general model proposing that actively transcribed genes are correlated with increased histone acetylation mediated by enzymes with HAT activity (Roth *et al.*, 2001).

In eukaryotic cells, transcriptional coactivator complexes such as SAGA/ADA have been shown to facilitate the activity of sequence specific gene activators (TFs). This functional feature emphasizes that SAGA/ADA specificity is determined by the TF that recruits the coactivator complex to its target genes (Naar *et al.*, 2001). In the current study, the direct dependence of Ada2p recruitment on three TFs, Cap1p, Mrr1p, and Gal4p, was investigated. Ada2p occupancy of glycolysis as well as pyruvate metabolism gene promoters was almost completely lost in the *gal4* mutant (Table 3). This dependency was also demonstrated for Cap1p and Mrr1p directing Ada2p to the promoters of oxidative responsive and core resistance genes, respectively (Figures 5 and 6). This suggests the specific role of *C. albicans* Ada2p depending on the TFs Cap1p, Mrr1p and Gal4p and therefore uncovers the functional conservation of mechanism by which SAGA/ADA operates in this pathogen.

Identification of Ada2p target genes in *C. albicans* provided insights into different stress response categories controlled by this coactivator. In *S. cerevisiae*, SAGA was found to specifically effect the activation of genes that are commonly up-regulated in response to a variety of environmental stresses, such a heat, oxidation, acidity, DNA damage, starvation, and the presence of unfolded proteins (Huisinga and Pugh, 2004). These genes form what has been called the environmental stress response and are regulated by the TFs Msn2p and Msn4p (Gasch and Werner-Washburne, 2002). Even though the closest *C. albicans* homologues of *MSN2* and *MSN4* are not involved in modulating the response to global stress (Nicholls *et al.*, 2004), we nevertheless show that Ada2p binds the promoters of similar stress-response genes that are up-regulated after treatment with oxidative agents, heat, and inhibitors of protein folding (Figure 1C). Promoters of genes involved in vacuolar acidification (*RIM101*, *VMA7*, and *RBF1*), as well as DNA replication (*RNR1*, *RNR21*, *RNR22*, and *DLS1*), were also bound by Ada2p. Taking into consideration the high degree of functional similarity between SAGA/ADA in both *S. cerevisiae* and *C. albicans*, it seems likely that this complex is evolutionarily conserved and controls the general stress-response pathway in both species.

Because the genome-wide occupancy of Ada2p revealed association with specific functions in *C. albicans*, we evaluated the consequence of *ada2* deletion on different physiological responses. The sensitivity of *ada2* mutants was examined in different stress conditions such as heat (42 and 45°C), excess of unfolded protein (tunicamycin and DTT), pH (acid and alkaline), genotoxic agents (MMS and EMS), oxidative agents (H_2O_2 and menadione), and osmotic stress (NaCl). No obvious phenotypic aberrations were recorded except for the oxidative agents. The absence of apparent phenotypes could be explained by the presence of other redundant coactivator complexes that can be recruited as a substitute of SAGA/ADA. Indeed, this assumption is supported by the results of studies undertaken in *S. cerevisiae* that demonstrated overlapping functions between the TFIID and SAGA complexes (Lee *et al.*, 2000; Huisinga and Pugh, 2004). Thus, genes could depend equally on both complexes, and a promoter that is dominated by a particular complex could still use the other to a lesser degree. However it is important to note that Ada2p appears to be the major contributor to the response to oxidative stress in *C. albicans*. This implies that SAGA/ADA in *C. albicans* is the bona fide coactivator complex mediating oxidative tolerance. Consequently, our observation that *ada2* mutants are much less virulent in a systemic mouse infection model could be related to its high sensitivity to oxidative stress. This might result in reducing the protection of fungal cells against different ROS that are generated by phagocytes and dendritic cells (Urban *et al.*, 2006).

The mechanisms of antifungal resistance in *C. albicans* remain an area of intense scientific investigation (Cannon *et al.*, 2007). Interestingly, Ada2p binds the promoters of several drug transporters, namely *MDR1*, *CDR1*, *CDR4*, *QDR1*, *YCF1*, *FLU1*, *ORF19.4531*, and *ORF19.301* as well as the phosphatidylinositol transfer gene *PDR16*. A moderate increase in sensitivity to fluconazole was observed in cells lacking *ADA2* in addition to impaired inducibility of *MDR1*, *CDR,1* and *PDR16* after the addition of fluconazole. Thus, Ada2p plays a role in *C. albicans* azole tolerance, most probably by its recruitment as a coactivator by TFs that control the expression of at least *MDR1*, *CDR1*, and *PDR16*. Constitutive activation of the transcriptional regulators of efflux pumps such as Tac1p, Upc2p, or Mrr1p have been associated with clinical azole resistance in *C. albicans* (Coste *et al.*, 2007; Morschhauser *et al.*, 2007; Znaidi *et al.*, 2008), and those TFs could use Ada2p as a coactivator to activate their targets. The moderate phenotype of *ada2* mutants observed in the presence of fluconazole might be the consequence of the use of alternative transcriptional coactivators. Meanwhile, Ada2p was found to occupy promoters of core genes mediating azole resistance of clinical isolates overexpressing *MDR1*. Recently, the mechanism of this type of resistance has been shown to include a gain of function mutation in the TF Mrr1p, thus resulting in the overexpression of its target genes. In our work, we have shown that Mrr1p and Ada2p cooccupied six gene promoters among the eight core resistance genes, including *MDR1*. Ada2p occupancy of these genes was completely dependent on Mrr1p, demonstrating that Ada2p functions as a coactivator for Mrr1p. To investigate the role of Ada2p in mediating drug resistance in *C. albicans*, *ADA2* was deleted from a resistant clinical strain overexpressing *MDR1* (data not shown). No obvious alteration of fluconazole sensitivity was noticed. This can be explained again by the presence of redundant coactivator complexes that can be recruited by Mrr1p as a substitute for SAGA/ADA. However, we have also considered in the current study that the impaired inducibility of *CDR1* and

PDR16 in an *ada2* mutant could also be a cause of the reduced sensitivity toward fluconazole. The latter two resistance genes were shown to be under the control of Tac1p or Upc2p rather than Mrr1p (Liu *et al.*, 2007; Znaidi *et al.*, 2008). It is possible that these resistance regulators might share the recruitment of the coactivator Ada2p to their target genes.

Recent evidence describing the transcriptional rewiring of the Leloir pathway genes in *C. albicans* suggests that the *GAL* genes responsible for the breakdown of galactose are not under the control of the closest Gal4p homolog in this organism (Martchenko *et al.*, 2007). This TF was rather shown to be required for transcriptional activation of genes involved in glucose metabolism. Global location mapping of Gal4p binding demonstrates a significant enrichment at gene promoters involved in glycolysis as well as pyruvate metabolism (C. Askew and M. Whiteway, unpublished data). In the present study, we have demonstrated that Ada2p is recruited by Gal4p to regulate genes involved in glycolysis and pyruvate metabolism. Taking into consideration the complete dependency of transcriptional activation of *GAL* genes on SAGA/ADA in *S. cerevisiae*, our finding highlights the fact that even though *C. albicans* Gal4p has distinct functions, and even a different transcriptional activation domain, its intimate interaction with SAGA/ADA has been conserved in both organisms. This evidence further emphasizes the functional conservation of the SAGA/ADA coactivator complex in which Ada2p is a crucial constituent. Thus, it seems that transcriptional rewiring is not restricted to TF but also to their coactivators.

ACKNOWLEDGMENTS

We are grateful to Jean-Sébastien Deneault for technical help with microarrays and to Hervé Hogues for bioinformatics assistance. We thank Alaka Mullick for discussions and Mario Mercier, Cynthia Helie, and Zully Leon for excellent assistance in animal handling. This work was supported by grants from Canadian Institute for Health Research (CIHR) to M.W. and A.N. (MOP-84341 and MOP-42516). C.A. was supported by an Alexander Graham Bell CGS-NSERC scholarship and H.L. by a PhD CIHR fellowship. This is NRC manuscript 49600.

REFERENCES

Alarco, A. M., and Raymond, M. (1999). The bZip transcription factor Cap1p is involved in multidrug resistance and oxidative stress response in *Candida albicans*. J. Bacteriol. *181*, 700–708.

Baker, S. P., and Grant, P. A. (2007). The SAGA continues: expanding the cellular role of a transcriptional co-activator complex. Oncogene *26*, 5329–5340.

Barlev, N. A., Candau, R., Wang, L., Darpino, P., Silverman, N., and Berger, S. L. (1995). Characterization of physical interactions of the putative transcriptional adaptor, ADA2, with acidic activation domains and TATA-binding protein. J. Biol. Chem. *270*, 19337–19344.

Barrios, A., Selleck, W., Hnatkovich, B., Kramer, R., Sermwittayawong, D., and Tan, S. (2007). Expression and purification of recombinant yeast Ada2/Ada3/Gcn5 and Piccolo NuA4 histone acetyltransferase complexes. Methods *41*, 271–277.

Berger, S. L., Pina, B., Silverman, N., Marcus, G. A., Agapite, J., Regier, J. L., Triezenberg, S. J., and Guarente, L. (1992). Genetic isolation of ADA2, a potential transcriptional adaptor required for function of certain acidic activation domains. Cell *70*, 251–265.

Bhaumik, S. R., and Green, M. R. (2001). SAGA is an essential in vivo target of the yeast acidic activator Gal4p. Genes Dev. *15*, 1935–1945.

Bruno, V. M., Kalachikov, S., Subaran, R., Nobile, C. J., Kyratsous, C., and Mitchell, A. P. (2006). Control of the *C. albicans* cell wall damage response by transcriptional regulator Cas5. PLoS Pathog. *2*, e21.

Candau, R., Zhou, J. X., Allis, C. D., and Berger, S. L. (1997). Histone acetyltransferase activity and interaction with ADA2 are critical for GCN5 function in vivo. EMBO J. *16*, 555–565.

Cannon, R. D., Lamping, E., Holmes, A. R., Niimi, K., Tanabe, K., Niimi, M., and Monk, B. C. (2007). *Candida albicans* drug resistance another way to cope with stress. Microbiology *153*, 3211–3217.

Coste, A., Selmecki, A., Forche, A., Diogo, D., Bougnoux, M. E., d'Enfert, C., Berman, J., and Sanglard, D. (2007). Genotypic evolution of azole resistance mechanisms in sequential *Candida albicans* isolates. Eukaryot. Cell *6*, 1889–1904.

Daniel, J. A., and Grant, P. A. (2007). Multi-tasking on chromatin with the SAGA coactivator complexes. Mutat. Res. *618*, 135–148.

Davis, D. A., Bruno, V. M., Loza, L., Filler, S. G., and Mitchell, A. P. (2002). *Candida albicans* Mds3p, a conserved regulator of pH responses and virulence identified through insertional mutagenesis. Genetics *162*, 1573–1581.

Gasch, A. P., and Werner-Washburne, M. (2002). The genomics of yeast responses to environmental stress and starvation. Funct. Integr. Genomics *2*, 181–192.

Gillum, A. M., Tsay, E. Y., and Kirsch, D. R. (1984). Isolation of the *Candida albicans* gene for orotidine-5′-phosphate decarboxylase by complementation of *S. cerevisiae* ura3 and *E. coli* pyrF mutations. Mol. Gen. Genet. *198*, 179–182.

Grant, P. A. (2001). A tale of histone modifications. Genome Biol. *2*, REVIEWS0003.

Guillemette, B., Bataille, A. R., Gévry, N., Adam, M., Blanchette, M., Robert, F., and Gaudreau, L. (2005). Variant histone H2A.Z is globally localized to the promoters of inactive yeast genes and regulates nucleosome positioning. PLoS Biol. *3*, e384.

Harbison, C. T., *et al.* (2004). Transcriptional regulatory code of a eukaryotic genome. Nature *431*, 99–104.

Hogues, H., Lavoie, H., Sellam, A., Mangos, M., Roemer, T., Purisima, E., Nantel, A., and Whiteway, M. (2008). Transcription factor substitution during the evolution of fungal ribosome regulation. Mol. Cell *29*, 552–562.

Huisinga, K. L., and Pugh, B. F. (2004). A genome-wide housekeeping role for TFIID and a highly regulated stress-related role for SAGA in *Saccharomyces cerevisiae*. Mol. Cell *13*, 573–585.

Karababa, M., Coste, A. T., Rognon, B., Bille, J., and Sanglard, D. (2004). Comparison of gene expression profiles of *Candida albicans* azole-resistant clinical isolates and laboratory strains exposed to drugs inducing multidrug transporters. Antimicrob. Agents Chemother. *48*, 3064–3079.

Klar, A. J., Srikantha, T., and Soll, D. R. (2001). A histone deacetylation inhibitor and mutant promote colony-type switching of the human pathogen *Candida albicans*. Genetics *158*, 919–924.

Kontoyiannis, D. P., and Lewis, R. E. (2002). Antifungal drug resistance of pathogenic fungi. Lancet *359*, 1135–1144.

Kornberg, R. D., and Lorch, Y. (1999). Twenty-five years of the nucleosome, fundamental particle of the eukaryote chromosome. Cell *98*, 285–294.

Larschan, E., and Winston, F. (2001). The *S. cerevisiae* SAGA complex functions in vivo as a coactivator for transcriptional activation by Gal4. Genes Dev. *15*, 1946–1956.

Lavoie, H., Sellam, A., Askew, C., Nantel, A., and Whiteway, M. (2008). A toolbox for epitope-tagging and genome-wide location analysis in *Candida albicans*. BMC Genomics *9*, 578.

Lee, T. I., Causton, H. C., Holstege, F. C., Shen, W. C., Hannett, N., Jennings, E. G., Winston, F., Green, M. R., and Young, R. A. (2000). Redundant roles for the TFIID and SAGA complexes in global transcription. Nature *405*, 701–704.

Liu, T. T., Znaidi, S., Barker, K. S., Xu, L., Homayouni, R., Saidane, S., Morschhauser, J., Nantel, A., Raymond, M., and Rogers, P. D. (2007). Genome-wide expression and location analyses of the *Candida albicans* Tac1p regulon. Eukaryot. Cell *6*, 2122–2138.

Marcus, G. A., Silverman, N., Berger, S. L., Horiuchi, J., and Guarente, L. (1994). Functional similarity and physical association between GCN5 and ADA2, putative transcriptional adaptors. EMBO J. *13*, 4807–4815.

Martchenko, M., Levitin, A., Hogues, H., Nantel, A., and Whiteway, M. (2007). Transcriptional rewiring of fungal galactose-metabolism circuitry. Curr. Biol. *17*, 1007–1013.

Morschhauser, J., Barker, K. S., Liu, T. T., Bla, B.W.J., Homayouni, R., and Rogers, P. D. (2007). The transcription factor Mrr1p controls expression of the MDR1 efflux pump and mediates multidrug resistance in *Candida albicans*. PLoS Pathog. *3*, e164.

Mullick, A., Elias, M., Picard, S., Bourget, L., Jovcevski, O., Gauthier, S., Tuite, A., Harakidas, P., Bihun, C., Massie, B., and Gros, P. (2004). Dysregulated inflammatory response to *Candida albicans* in a C5-deficient mouse strain. Infect. Immun. *72*, 5868–5876.

Naar, A. M., Lemon, B. D., and Tjian, R. (2001). Transcriptional coactivator complexes. Annu. Rev. Biochem. *70*, 475–501.

Nantel, A., Rigby, T., Hogues, H., and Whiteway, M. (2006). Microarrays for studying pathology in *Candida albicans*. In: Medical Mycology: Cellular and Molecular Techniques, ed. K. Kavanaugh, Hoboken, NJ: Wiley Press, 181–209.

Nicholls, S., Straffon, M., Enjalbert, B., Nantel, A., Macaskill, S., Whiteway, M., and Brown, A. J. (2004). Msn2- and Msn4-like transcription factors play no obvious roles in the stress responses of the fungal pathogen *Candida albicans*. Eukaryot. Cell *3*, 1111–1123.

Pokholok, D. K., Zeitlinger, J., Hannett, N. M., Reynolds, D. B., and Young, R. A. (2006). Activated signal transduction kinases frequently occupy target genes. Science *313*, 533–536.

Reuss, O., Vik, A., Kolter, R., and Morschhauser, J. (2004). The SAT1 flipper, an optimized tool for gene disruption in *Candida albicans*. Gene *341*, 119–127.

Roth, S. Y., Denu, J. M., and Allis, C. D. (2001). Histone acetyltransferases. Annu. Rev. Biochem. *70*, 81–120.

Sterner, D. E., Grant, P. A., Roberts, S. M., Duggan, L. J., Belotserkovskaya, R., Pacella, L. A., Winston, F., Workman, J. L., and Berger, S. L. (1999). Functional organization of the yeast SAGA complex: distinct components involved in structural integrity, nucleosome acetylation, and TATA-binding protein interaction. Mol. Cell. Biol. *19*, 86–98.

Suka, N., Suka, Y., Carmen, A. A., Wu, J., and Grunstein, M. (2001). Highly specific antibodies determine histone acetylation site usage in yeast heterochromatin and euchromatin. Mol. Cell *8*, 473–479.

Tsong, A. E., Tuch, B. B., Li, H., and Johnson, A. D. (2006). Evolution of alternative transcriptional circuits with identical logic. Nature *443*, 415–420.

Urban, C. F., Lourido, S., and Zychlinsky, A. (2006). How do microbes evade neutrophil killing? Cell Microbiol. *8*, 1687–1696.

Wang, J. S., Yang, Y. L., Wu, C. J., Ouyang, K. J., Tseng, K. Y., Chen, C. G., Wang, H., and Lo, H. J. (2006a). The DNA-binding domain of CaNdt80p is required to activate CDR1 involved in drug resistance in *Candida albicans*. J. Med. Microbiol. *55*, 1403–1411.

Wang, Y., Cao, Y. Y., Jia, X. M., Cao, Y. B., Gao, P. H., Fu, X. P., Ying, K., Chen, W. S., and Jiang, Y. Y. (2006b). Cap1p is involved in multiple pathways of oxidative stress response in *Candida albicans*. Free Radic. Biol. Med. *40*, 1201–1209.

Welihinda, A. A., Tirasophon, W., Green, S. R., and Kaufman, R. J. (1997). Gene induction in response to unfolded protein in the endoplasmic reticulum is mediated through Ire1p kinase interaction with a transcriptional coactivator complex containing Ada5p. Proc. Natl. Acad. Sci. USA *94*, 4289–4294.

Welihinda, A. A., Tirasophon, W., and Kaufman, R. J. (2000). The transcriptional co-activator ADA5 is required for HAC1 mRNA processing in vivo. J. Biol. Chem. *275*, 3377–3381.

Wilson, R. B., Davis, D., and Mitchell, A. P. (1999). Rapid hypothesis testing with *Candida albicans* through gene disruption with short homology regions. J. Bacteriol. *181*, 1868–1874.

Wimalasena, T. T., Enjalbert, B., Guillemette, T., Plumridge, A., Budge, S., Yin, Z., Brown, A. J., and Archer, D. B. (2008). Impact of the unfolded protein response upon genome-wide expression patterns, and the role of Hac1 in the polarized growth, of *Candida albicans*. Fungal Genet Biol. *45*, 1235–1247.

Znaidi, S., Weber, S., Al-Abdin, O. Z., Bomme, P., Saidane, S., Drouin, S., Lemieux, S., De Deken, X., Robert, F., and Raymond, M. (2008). Genomewide location analysis of *Candida albicans* Upc2p, a regulator of sterol metabolism and azole drug resistance. Eukaryot. Cell *7*, 836–847.

VII.2. Widespread occurrence of chromosomal aneuploidy following the routine production of *Candida albicans* mutants

Originally published in:
FEMS Yeast Res. 2009 Oct;9(7):1070-7. Epub 2009 Aug 6. || PMID: 19732157

RESEARCH ARTICLE

Widespread occurrence of chromosomal aneuploidy following the routine production of *Candida albicans* mutants

Mélanie Arbour[1], Elias Epp[1,2], Hervé Hogues[1], Adnane Sellam[1,3], Celine Lacroix[1,3], Jason Rauceo[4], Aaron Mitchell[5], Malcolm Whiteway[1,2] & André Nantel[1,3]

[1]Biotechnology Research Institute, National Research Council of Canada, Montreal, QC, Canada; [2]Department of Biology, McGill University, Montreal, QC, Canada; [3]Department of Anatomy and Cell Biology, McGill University, Montreal, QC, Canada; [4]Department of Sciences, John Jay College of Criminal Justice, New York, NY, USA; and [5]Department of Biological Sciences, Carnegie Mellon University, Pittsburgh, PA, USA.

Correspondence: André Nantel, Biotechnology Research Institute, National Research Council of Canada, 6100 Royalmount Ave., Montreal, QC, Canada H4P 2R2. Tel.: +1 514 496 6370; fax: +1 514 496 9127; e-mail: andre.nantel@nrc-cnrc.gc.ca

Received 14 April 2009; revised 27 July 2009; accepted 4 August 2009.
Final version published online 1 September 2009.

DOI:10.1111/j.1567-1364.2009.00563.x

Editor: Frank Odds

Keywords
Candida albicans; aneuploidy; karyotype; chromosome structure; microarray.

Abstract

It has come to our attention that approximately 35% of > 100 published microarray datasets, where transcript levels were compared between two different strains, exhibit some form of chromosome-specific bias. While some of these arose from the use of strains whose aneuploidies were not known at the time, in a worrisome number of cases the recombinant strains have acquired additional aneuploidies that were not initially present in the parental strain. The aneuploidies often affected a different chromosome than the one harboring the insertion site. The affected strains originated from either CAI-4, RM1000, BWP17 or SN95 and were produced through a variety of strategies. These observations suggest that aneuploidies frequently occur during the production of recombinant strains and have an effect on global transcript profiles outside of the afflicted chromosome(s), thus raising the possibility of unintended phenotypic consequences. Thus, we propose that all *Candida albicans* mutants and strains should be tested for aneuploidy before being used in further studies. To this end, we describe a new rapid testing method, based on a multiplex quantitative PCR assay, that produces eight bands of distinct sizes from either the left or right arms of each *C. albicans* chromosome.

Introduction

We wish to warn the *Candida albicans* research community that cases of aneuploidy in *C. albicans* laboratory strains, first identified by Chen *et al.* (2004) and reviewed extensively by Rustchenko (2007), are commonly exacerbated following routine genetic manipulations such as gene insertions and inactivations.

Candida albicans is an opportunistic fungal pathogen with a diploid genome and an incomplete sexual cycle. While its genome sequence was first released in 2000, published in 2004 (Jones *et al.*, 2004) and annotated in 2005 (Braun *et al.*, 2005), the lack of detailed physical and genetic maps have delayed the production of a final chromosomal assembly by several years (Nantel, 2006). Nevertheless, researchers using techniques such as pulse-field gel electrophoresis and contour-clamped homogeneous electrical field (CHEF) gels were already amassing a significant body of evidence demonstrating chromosomal instability in *C. albicans* under laboratory conditions (Rustchenko, 2007). For example, cells whose sole source of carbon was L-sorbose tended to lose a copy of chromosome 5 (Chr 5) while growth in D-arabinose promoted Chr 6 trisomy (Rustchenko *et al.*, 1994; Kabir *et al.*, 2005). Chen *et al.* (2004) observed the loss of one copy of Chr 1 in strains exposed to 5-fluoroorotic acid. They also demonstrated that the commonly used laboratory strains CAI-4 and SGY-243 carried an extra copy of Chr 1 and that this triploidy had a negative effect on virulence. Comparative genome hybridization (CGH) studies conducted by Selmecki *et al.* (2005) identified an additional, albeit unstable, Chr 2 aneuploidy in CAI4 as well as a heterozygous deletion in the right arm of Chr 5 in RM1000 and its derivative BWP17. The recent release of the *C. albicans* genome assembly by van het Hoog *et al.* (2007) has permitted more detailed studies including the identification of a Chr 5 isochromosome linked to azole

resistance (Coste *et al*., 2006; Selmecki *et al*., 2006). Finally, it was suggested by Ahmad *et al*. (2008) that different stock of the same *C. albicans* laboratory strain may harbor different types of chromosomal aberrations. All of these results suggest that the *C. albicans* genome has enough plasticity to support a wide variety of different chromosomal aneuploidies and that changes in chromosome copy numbers often arise as a response to stress.

Materials and methods

Analysis of microarray data

Candida albicans transcriptional profiling data were extracted from a variety of sources and visualized using the GENESPRING GX v7.3 (Agilent Technologies) physical view. Alternatively, fluorescence data on target genes were sorted in Microsoft Excel according to their chromosomal map coordinates and visualized on a scatter plot.

CGHs

Candida albicans genomic DNA was isolated from a saturated overnight culture with the Qiagen Genomic DNA Extraction kit and labeled with either Cy3 or Cy5 dyes with the Bioprime CGH Labeling (Invitrogen). Unincorporated nucleotides were removed with Qiagen PCR columns and the labeled probes were then hybridized as described to DNA microarrays spotted with 6354 70mer oligonucleotide probes representing most of the genes identified in Genome Assembly 19 (Nantel *et al*., 2006). Normalization and data analysis were performed in GENESPRING GX v7.3 (Agilent Technologies). When used to validate suspected aneuploidies, most GCH experiments needed to be performed only once. Because our microarray probes are randomly distributed, it is impossible for noise, dye bias or probe localization artifacts to produce a fluorescence ratio bias that is specific only to certain chromosomes. Thus, even a very weak change in median fluorescence ratio becomes very obvious when viewed in this chromosomal context.

Multiplex PCR

The genomic DNA was purified by the Yeast Smash & Grab DNA miniprep method as described by Rose *et al*. (1990). For multiplex PCR, we used the Qiagen multiplex PCR kit. PCR reaction mixtures (total volume, 50 μL) contained 1 × Qiagen multiplex PCR master mix, 0.125 μM equimolar primers mixture (either A or B, see Table 1) and 1–50 ng of purified genomic DNA (the specific amount must be evaluated by each individual lab). Thermal cycling was carried out in a Thermocycler 9600 (Perkin-Elmer) with a denaturation step of 95 °C for 15 min, 23 cycles with 30 s denaturation at 94 °C, 30 s annealing at 57 °C, 45 s elongation at 72 °C and the last elongation step at 72 °C for 7 min. When performed to validate an already known aneuploidy, the PCR assays needed to be performed only once to validate the results. When used for screening, replicate experiments on several individual colonies are advisable.

Agilent 2100 Bioanalyzer microcapillary electrophoresis

Following amplification, 1 μL of the PCR reaction was loaded into the well of a Bioanalyzer chip prepared according to manufacturer's protocol for the DNA 7500 Lab Chips (Agilent Technologies). The aneuploidy of the mutant DNA was determined by the relative ratio of the peak height of the mutant and wild-type (SC5314) DNA fragments in the chromatogram. The ratio for each chromosome was then divided by the median of the ratio for all chromosomes. Alternatively, the elution profile graphics were scaled and overlapped in an image processing software such as ABODE PHOTOSHOP.

Results

Following the completion of the *C. albicans* genome assembly (van het Hoog *et al*., 2007), we noticed that some of our transcriptional profiles exhibited chromosome-specific bias. Thus, we extended this analysis to > 100 published and unpublished microarray experiments where two different strains, usually a mutant and its wild-type parent, were directly compared. As reported in Table 2, we observed cases of chromosomal bias in 22 out of 59 *C. albicans* strains (36.2%). For example, in Fig. 1, we can clearly see that the transcriptional profiles obtained by comparing a *Δmkc1* recombinant strain (Oberholzer *et al*., 2006) to the SC5314 control strain show an enrichment in overexpressed genes that are located in Chr 1, 2, 5, 6 and 7 while the genes in Chr 3, 4 and R tend to be repressed. While the actual fold-change can be minor, the bias can be easily detected, as long as the probes are spotted in a random position on the microarray slides so that experimental noise and most changes in transcript abundance are evenly distributed. The second example, taken from Tsong *et al*. (2003), is especially interesting because we can see both up- and downregulated chromosome bias; the general repression of Chr 2 genes is due to the use of the Chr 2 trisomic CAI4 strain as a control, while the increase in the fluorescence ratios of genes in Chr 6 is the probable result of a chromosome duplication event during the generation of this strain.

This analysis was conducted with transcriptional profiling data and not from CGH experiments, where genomic DNA from two strains is differently labeled and hybridized to microarrays. CGH on some strains has confirmed that the changes in transcript profiles are indeed the result of changes in gene copy number although it is difficult to

Table 1. Primer sequences used in the multiplex PCR aneuploidy detection assay

	Primer set A (left arm)			Primer set B (right arm)		
Chr	Sequences	Positions	Amplicon lengths	Sequences	Positions	Amplicon lengths
1	Ca21Chr1_A_L acttgtacggctggaaaaact	21272	301	Ca21Chr1_B_L caactgccaaactagttccaa	3155855	305
	Ca21Chr1_A_R gccaagtatgagagggttgat	21572		Ca21Chr1_B_R tgttggtgttttaccgtgttt	3156159	
2	Ca21Chr2_A_L cgagttaaactttcggtttcc	15481	383	Ca21Chr2_B_L tccttctggcccttctaagta	2213805	375
	Ca21Chr2_A_R attgagggattgaacaaggag	15863		Ca21Chr2_B_R aagagtgagcttgttctgggt	2214179	
3	Ca21Chr3_A_L atgctcctgtaatacgctcct	38238	478	Ca21Chr3_B_L catgttttagttggtcgatgg	1779058	471
	Ca21Chr3_A_R gctcacacaatccaaccatag	38715		Ca21Chr3_B_R gtaaccgacaaactccatgtg	1779528	
4	Ca21Chr4_A_L cacagagatgacagaacaccc	6565	588	Ca21Chr4_B_L gatttgcggtggtttatttttt	1614471	593
	Ca21Chr4_A_R cttgatccccaccatagactt	7152		Ca21Chr4_B_R aaactagtctaccctgccgaa	1615063	
5	Ca21Chr5_A_L tgacaacattggagatggtct	28726	472	Ca21Chr5_B_L cggtcatgtatttgattacgg	1163697	741
	Ca21Chr5_A_R agatttcgaatcacgcttttt	29467		Ca21Chr5_B_R tatctgcagacgactacccag	1164437	
6	Ca21Chr6_A_L acatcatcctgtaacgccata	13849	925	Ca21Chr6_B_L tgcgtctagatacaacaaggc	1014943	917
	Ca21Chr6_A_R caggtcaactcaacttccaga	14773		Ca21Chr6_B_R acttggcatcaacttccttct	1015859	
7	Ca21Chr7_A_L gtcattccgaatctcaaacct	4219	1153	Ca21Chr7_B_L aagtatgcaatttctttgggg	931287	1151
	Ca21Chr7_A_R tgaaaagtgcaggagaatcac	5371		Ca21Chr7_B_R tcctcagcctgtttgtagttg	932437	
R	Ca21ChrR_A_L ccaatataccccaatccaaac	18490	1430	Ca21ChrR_B_L atttggtagaagatcgatggg	2287349	1438
	Ca21ChrR_A_R aaagacttgttccacctcacc	19919		Ca21ChrR_B_R aagacaacaacgaagatgctg	2288786	

determine precisely whether we are dealing with chromosome duplication, chromosome loss or some other type of karyotype rearrangement. In some cases, we noticed that individual transformed colonies can carry different aneuploidies. For example, Fig. 2 shows CGH data from two individual colonies of a strain, produced at the NRC-BRI, that express an HA-tagged version of the Rfg1p transcription factor. While both clones had the extra copy of Chr 2 normally found in the parental CAI4 strain, one of the clones also had an additional copy of Chr 1. Whether the extra Chr 1 arose from an independent duplication event or from a mixed population of Chr 2 and Chr 1/2 triploids in our CAI4 stocks has not been determined. Nevertheless, it should be noted that we failed to detect any Chr 1 bias in CGH experiments comparing our CAI4 and SC5314 stocks. Another case of colony-specific aneuploidy occurred during the production of Δ*fun31* mutants at Columbia University. As illustrated in Fig. 3a, transcriptional profiling on three independently isolated strains revealed that two of them seem to be missing a copy of Chr R (or have an extra copy of Chr 1–7). This experiment is also used to illustrate that a chromosomal aneuploidy can also affect gene expression patterns in the nonamplified chromosomes. A mutant vs. wild-type comparison of the transcriptional profiles of genes located on the nonaneuploid Chr 1–7 showed that the two strains with the Chr R aneuploidies were more similar to each other than to the strain with the correct number of chromosome copies (Fig. 3b and c). These observations, along with those produced by Selmecki *et al.* (2006), thus confirm that changes in the copy number of certain genes can result in compensatory changes in the expression profiles of other genes located outside of the afflicted chromosomes.

In light of these results, we developed a multiplex PCR assay that can rapidly detect cases of chromosomal aneuploidy, the formation of isochromosomes or the loss of chromosome ends. Each assay consists of eight pairs of primers that are specific for unique regions near the left or the right arm of each chromosome (see Table 1). As

Table 2. Identification of unexpected aneuploidies in microarray profiles

Mutation	Function	Gene locations	Aneuploidy	Mode of production (reference if different from array data)	Reference for array data
D9-330	Antifungal resistance	N/A	Isochromosome 5* directed evolution	Cowen *et al*. (2002)	
D11-330	Antifungal resistance	N/A	Gain of Chr 7*	Directed evolution	Cowen *et al*. (2002)
D12-165	Antifungal resistance	N/A	Gain of Chr 7*	Directed evolution	Cowen *et al*. (2002)
D12-330	Antifungal resistance	N/A	Gain of Chr 4*	Directed evolution	Cowen *et al*. (2002)
Δ*efg1/cph1*	Transcription factors	Chr R and Chr 1	Gain of Chr 7‡	Ura-blaster (Lo *et al*., 1997)	Nantel *et al*. (2002)
35/65 profiles	Combinations of MTL transcriptional regulators in White and Opaque cells	Various	Mixed cell population, some with gain of either Chr 6 or 7. Use of CAI4 as control also caused Chr 2 bias in 33 of the comparisons	PCR disruption cassettes	Tsong *et al*. (2003)
Δ*cdc35*	Adenylate Cyclase	Chr 7	Gain of Chr 2‡	Ura-blaster (Rocha *et al*., 2001)	Harcus *et al*. (2004)
Δ*ssn6*	Transcription factor	Chr 3	Gain of Chr 7	Ura-blaster	Garcia-Sanchez *et al*. (2005)
Δ*mkc1*	MAP kinase	Chr R	Loss of Chr 3, 4 and R	PCR disruption Cassette	Oberholzer *et al*. (2006)
Δ*sst2*	GTPase activator	Chr 5	Gain of Chr 6	PCR disruption Cassette	Dignard & Whiteway (2006)
Δ*tac1*	Transcription factor	Chr 5	Loss of Chr 5†	MPA^R-flipping	Znaidi *et al*. (2007)
TAC1 replacements	Transcription factor	Chr 5	Gain of Chr 5 and/or 7†	MPA^R-flipping	Znaidi *et al*. (2007)
Δ*cph1*	Transcription factor	Chr 1	Gain of Chr 6 and 7‡	Ura-blaster (Lo *et al*., 1997)	Huang *et al*. (2008)
Δ*ras1*	Small GTPase	Chr 2	Gain of Chr 4 and loss of Chr 5–6	hph-URA3-hph disruption cassette (Feng et al., 1999)	B. Hube, GSE11490
Δ*ste4*	G® subunit	Chr 2	Loss of Chr 1-3	Ura-blaster	
Δ*rds2*	Transcription factor	Chr R	Loss of Chr 1	Ura-blaster	B. Turcotte (unpublished data)
Δ*fun31*	Ser/Thr protein kinase	Chr 3	Loss of Chr R	PCR disruption Cassette	J. Rauceo and A. Mitchell (unpublished data)
Δ*vma22*	Membrane protein	Chr R	Loss of right arm of Chr R†	PCR disruption Cassette	E. Epp and M. Whiteway (unpublished data)
Δ*nrg1*	Transcription factor	Chr 7	Gain of Chr 2 and 4†‡	Ura-blaster (Murad et al., 2001)	C. Lacroix and A. Nantel (unpublished data)
HA-Rfg1	Tagged transcription factor	Chr 1	Gain of Chr 1 and/or Chr 2†‡	Insertion in *Rps1* site	C. Lacroix and A. Nantel (unpublished data)
Nrg1-HA	Tagged transcription factor	Chr 1	Gain of Chr 2†‡	Insertion in *Rps1* site	C. Lacroix and A. Nantel (unpublished data)

Note that the 'loss' of a chromosome might also be indicative of duplication of the remaining chromosomes or the presence of a trisomic chromosome in the control strain.

Following a review of available data, profiles for the following mutants did not seem to exhibit obvious aneuploidies: Δace2, Δ*ada2*, Δ*als2*, Δ*als4*, Δ*bcr1*, Δ*bub2*, Δ*cdc5*, Δ*cdc53*, Δ*cdr1* Δ*cdr2*, Δ*cek1*, Δ*cka2*, Δ*crz1*, Δ*cph1* Δ*efg1*, Δ*cst20*, Δ*dfg16*, Δ*efg1*, Δ*efg1* Δ*efh1*, Δ*efh1*, Δ*gal4*, Δ*gcn2*, Δ*gcn4*, Δ*hog1*, Δ*hst7*, Δ*msn4* Δ*mnl1*, Δ*myo5*, Δ*myo5* Δ*hog1*, Δ*myo5* Δ*mkc1*, Δ*myo5*Δ*SH3*ΔA, Δ*rfg1*, Δ*rim101*, Δ*rlm1*, Δ*sit4*, Δ*sla2*, Δ*ssr1*, Δ*tup1*, D8-330, N4-330.

*Observation validated by CGH (Selmecki *et al*., 2006; A. Selmecki, L.E. Cowen and J. Berman, unpublished data).

†Observation validated by CGH in our lab.

‡Observation validated by the PCR assay.

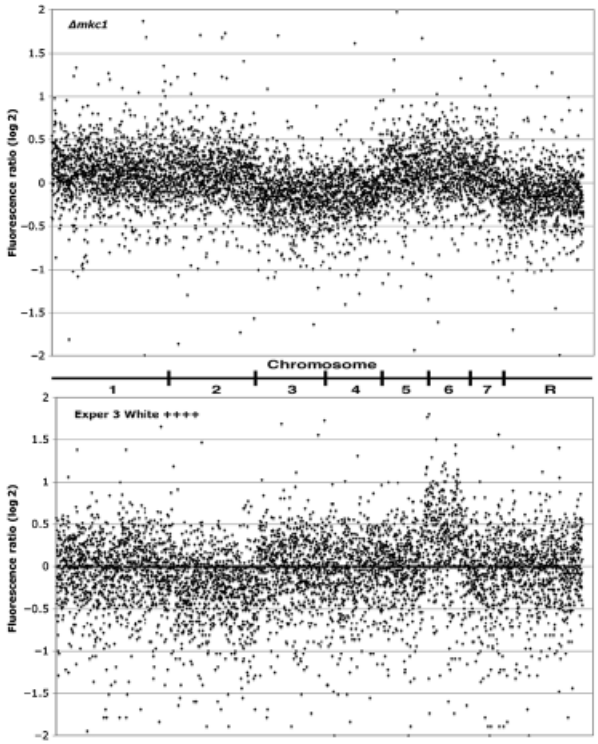

Fig. 1. Example of chromosomal bias in published transcriptional profiles. Each spot represents fluorescence ratio data (log 2) from genes that were ordered according to their position on the eight *Candida albicans* chromosomes. The top panel represents a comparison between a Δ*mkc1* strain and its *CAI4* parental strain (Oberholzer *et al.*, 2006). The bottom panel shows the profile obtained from a comparison between a 'white' morphology strain expressing the α1, α2, a1 and a2 *MTL* transcriptional regulators and its *CAI4* parental strain at 23 °C (Tsong *et al.*, 2003).

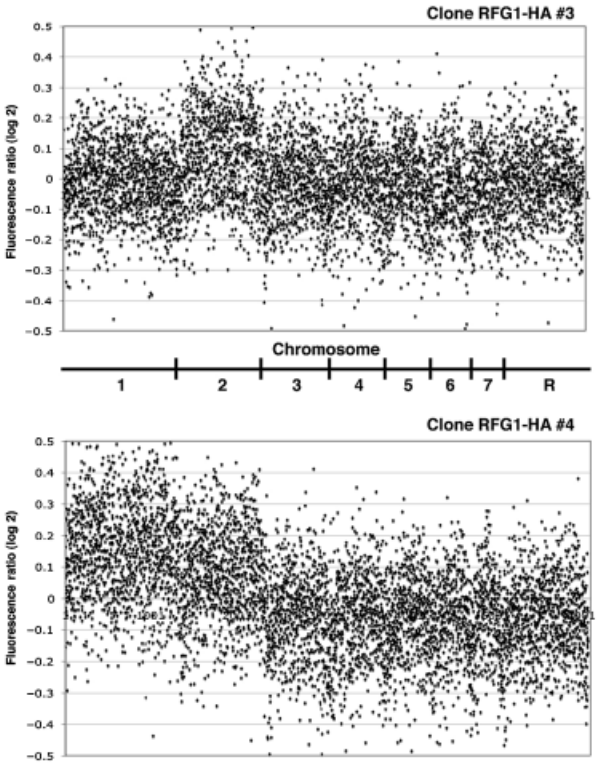

Fig. 2. Example of different aneuploidies from two distinct colonies. These graphs represent the fluorescence ratios (log 2) from individual probes in a CGH comparing one of two colonies expressing the HA-Rfg1p transcription factor with a CAI4-pCaEXP empty-vector control strain that had previously been confirmed to have two copies of each chromosome. While the fold change in CGH should be expected to be at least 1.5-fold for a triploid vs. diploid comparison, we note that the QUANTARRAY software used to quantify our microarrays tends to underestimate fluorescence ratios.

illustrated in Fig. 4, the resulting PCR reactions produce eight amplicons of different sizes, one from each chromosome arm. The production of quantitative data requires some optimization specific for each lab and PCR machine, usually by varying the amount of template genomic DNA or the number of amplification cycles. For quantification purposes, we use an Agilent Bioanalyzer, a very precise capillary electrophoresis instrument that produces reproducible results in a very short amount of time. Identification of aneuploidies can be performed either by directly comparing the elution profiles (Fig. 4a) or by measuring normalized peak heights (Fig. 4b). In the examples shown in Fig. 4a, we can easily detect the extra Chr 2 and Chr 4 in the Δ*nrg1* strain as well as the small deletion in the right arm of the BWP17 Chr 5. In Fig. 4b, we can discern the extra Chr 1 and Chr 6 in strain DkCa169 that were observed by Legrand *et al.* (2008) as well as the additional Chr 5 and Chr 7 described by Znaidi *et al.* (2007) in the *TAC1/tac1* Δ::FRT SZY20 strain. We choose these strains because they represent examples of aneuploidies in seven out of the eight chromosomes, while BWP17 is an example of a deletion that only affects one arm.

Discussion

We present evidence that the routine genetic manipulation of *C. albicans* often results in the acquisition of unwanted chromosomal aneuploidies. We have observed chromosome duplications in any one of eight chromosomes of *C. albicans*, with recombinant derivatives originating from either the CAI-4, RM1000, BWP17 or SN95 strains, and with strains produced by a variety of techniques including long-term treatment with Fluconazole, Ura-blaster-mediated gene deletion, the insertion of disruption cassettes produced by PCR, MPA^R-flipping or the insertion of genes encoding tagged transcription factors at the *Rps1* site. Almost all the cases of chromosomal bias affected a different chromosome(s) than the actual site of the recombinant modification, which is to be expected because same-chromosome aberrations would have been easily detected as part of the regular Southern blotting controls that often follow strain production. Ever since we became aware of this problem, aneuploidy testing has been routinely applied in our lab and

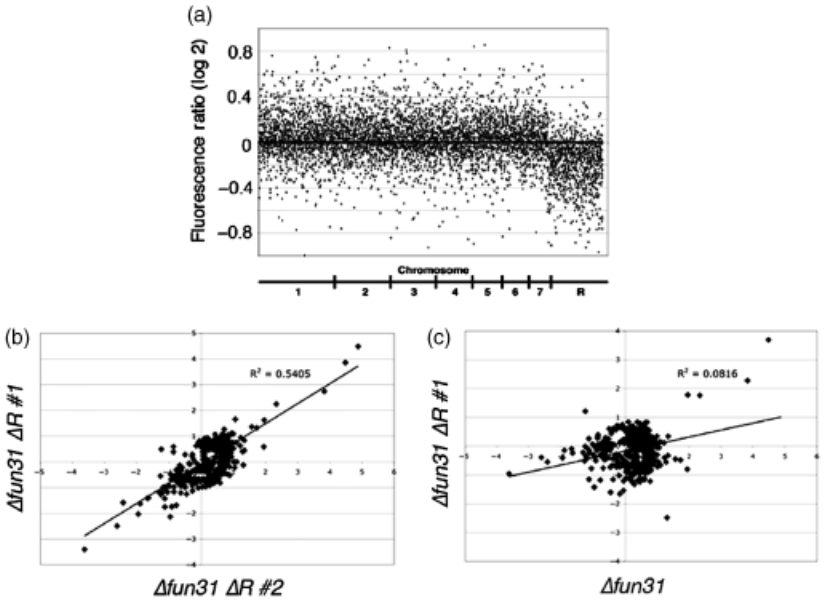

Fig. 3. Aneuploidies can affect transcriptional profiles outside of the afflicted chromosomes. (a) Fluorescence intensities in a transcriptional profiling experiment of one of three Δ*fun31* mutants compared with a DAY185 control strain. Downregulation of Chr R genes is apparent. (b and c) Scatter plots showing the similarity of transcriptional profiles between the genes outside of Chr R in a comparison of two individual Δ*fun31* mutants lacking a copy of Chr R (b), or a Δ*fun31* mutant lacking a Chr R, when compared with a control strain without the Δ*fun31* mutation and an equal number of chromosomes. Spots represent the fluorescence ratios of 486 genes in Chr 1–7 that had a 1.5-fold change or more in at least one experiment. R^2 values represent the similarities in the profiles between the two strains and indicate that the aneuploid strains produce profiles that are more similar to each other.

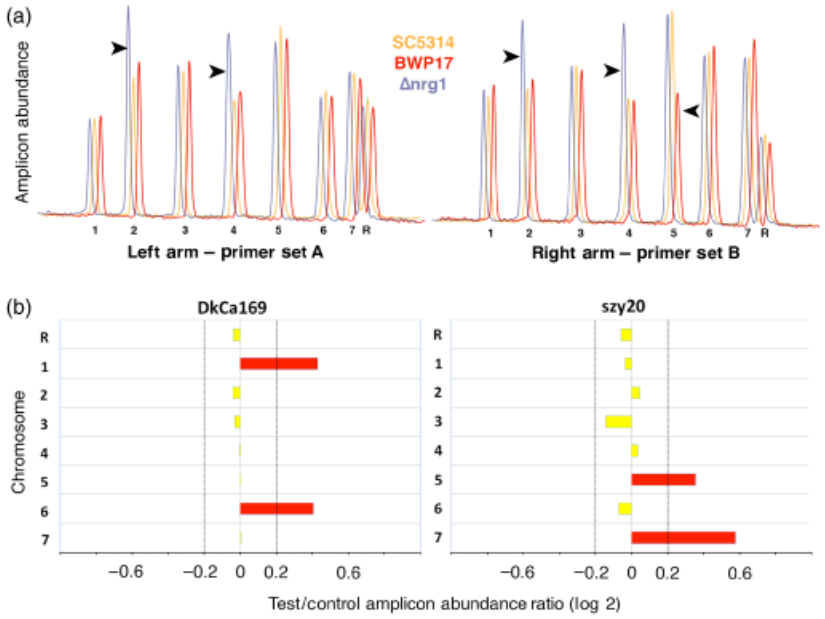

Fig. 4. Aneuploidy detection with a multiplex PCR assay. (a) Bioanalyzer profiles of multiplex PCR reactions using primer set A (left panel) or primer set B (right panel). We used as templates genomic DNA from either a validated SC5314 control strain, a Δ*nrg1* strain (with extra copies of Chr 2 and 4) or the BWP17 strain carrying a heterozygous deletion on the right arm of Chr 5. Images of the profiles were scaled to similar sizes, thus allowing the identification of amplicons with a different abundance (arrowheads). In (b), the multiplex PCR assay was conducted with primer set A on genomic DNA from strains SC5314, DkCa169 (Legrand *et al.*, 2008) and SZY20 (Znaidi *et al.*, 2007). Graphs represent the mutant/SC5314 ratio of the median normalized peak heights on the *X*-axis and each chromosome on the *Y*-axis. A $\log_2$ ratio above 0.2 (in red) was considered to be significant and indicative of aneuploidy for these chromosomes.

we have developed a rapid multiplex PCR assay that can cheaply identify chromosomal aberrations in less than a day. Although not every laboratory is expected to have access to a Bioanalyzer or similar equipment, band quantification from a regular gel is possible if the experimenter is skillful enough to detect a 50% increase in band intensity. Alternatively, the primer sequences included therein could easily be adapted into a quantitative PCR (qPCR) assay. In our hands, the PCR assay works fairly well in the detection of simple aneuploidies that affect one or even two chromosomes. Results with multichromosomal aneuploidies are much more difficult to interpret precisely; we can tell that something is wrong but matching peak heights to the afflicted chromosome is not always possible because we can not normalize the data. Finally, it should be noted that none of our assays can currently detect loss of heterozygocity (LOH). It would not surprise us if rates of unwanted LOH turned out to be as abundant as aneuploidies.

The phenotypic consequences of these chromosomal aberrations are difficult to assess without a direct

comparison between an aneuploid and a nonaneuploid strain. The aneuploidy-dependent bias in transcriptional profiling data is generally very subtle, most notably because *C. albicans* is a diploid and an extra allele would thus increase gene dosage by 50%. Assuming an equivalent change in gene expression, this would only result in a 1.5-fold change in fluorescence ratio, which is the detection limit of most transcriptional profiling experiments. Consequently, we believe that most of the lists of significantly modulated genes are still valid. More worrisome and difficult to detect would be variations in gene expression patterns that would result from a change in transcription factor dosage, a phenomenon that was observed by Selmecki *et al.* (2006) with the Tac1p transcription factor.

In conclusions, based on our global microarray data analysis and general observations by the Montreal *Candida* research community, we believe that we are dealing with a fairly common phenomenon with a significant impact on *Candida* research. In light of these observations, we propose the following recommendations:

- The affected transcriptional profiles listed in Table 2 should not be used in global data analysis. The data currently in public databases, such as CGD and GEO, should be tagged appropriately.
- Important *Candida albicans* mutants and strains should be tested for aneuploidy, either by CHEF, CGH on DNA microarrays or by qPCR, before being used in subsequent experiments. For example, our lab recently produced 31 strains that express TAP-tagged transcription factors. These control experiments allowed us to eliminate six additional cases of aneuploidies (19%).
- During the production of *C. albicans* strains, multiple colonies should be isolated after every transformation to facilitate the isolation of a strain with the standard background karyotype.
- Finally, researchers should pay close attention to the culture stocks used for the construction of their recombinant strains. Ahmad *et al.* (2008) have identified CAF4-2 as a stable Ura$^-$ derivative while we have tested the SN76, SN95, SN152 and SN148 strains (Noble & Johnson, 2005) and have found them to be initially free of aneuploidies.

Acknowledgements

We thank Marco van het Hoog for assistance in bioinformatics, Alistair Brown and Martine Raymond for strains and Judith Berman for strain DKCa169 and for critically reading the manuscript. This research was funded by grant CTP79843 from the Canadian Institutes of Health Research (CIHR). This is NRC Publication number 50662.

Statement

References

Ahmad A, Kabir M, Kravets A, Andaluz E, Larriba G & Rustchenko E (2008) Chromosome instability and unusual features of some widely used strains of *Candida albicans*. *Yeast* **25**: 433–448.

Braun BR, van het Hoog M, d'Enfert C *et al.* (2005) A human-curated annotation of the *Candida albicans* genome. *PLoS Genet* **1**: 36–57.

Chen X, Magee BB, Dawson D, Magee PT & Kumamoto CA (2004) Chromosome 1 trisomy compromises the virulence of *Candida albicans*. *Mol Microbiol* **51**: 551–565.

Coste A, Turner V, Ischer F, Morschhauser J, Forche A, Selmecki A, Berman J, Bille J & Sanglard D (2006) A mutation in Tac1p, a transcription factor regulating CDR1 and CDR2, is coupled with loss of heterozygosity at chromosome 5 to mediate antifungal resistance in *Candida albicans*. *Genetics* **172**: 2139–2156.

Cowen LE, Nantel A, Whiteway MS, Thomas DY, Tessier DC, Kohn LM & Anderson JB (2002) Population genomics of drug resistance in *Candida albicans*. *P Natl Acad Sci USA* **99**: 9284–9289.

Dignard D & Whiteway M (2006) SST2, a regulator of G-protein signaling for the *Candida albicans* mating response pathway. *Eukaryot Cell* **5**: 192–202.

Garcia-Sanchez S, Mavor AL, Russell CL, Argimon S, Dennison P, Enjalbert B & Brown AJ (2005) Global roles of Ssn6 in Tup1- and Nrg1-dependent gene regulation in the fungal pathogen, *Candida albicans*. *Mol Biol Cell* **16**: 2913–2925.

Harcus D, Nantel A, Marcil A, Rigby T & Whiteway M (2004) Transcription profiling of cyclic AMP signaling in *Candida albicans*. *Mol Biol Cell* **15**: 4490–4499.

Huang H, Harcus D & Whiteway M (2008) Transcript profiling of a MAP kinase pathway in *C. albicans*. *Microbiol Res* **163**: 380–393.

Jones T, Federspiel NA, Chibana H *et al.* (2004) The diploid genome sequence of *Candida albicans*. *P Natl Acad Sci USA* **101**: 7329–7334.

Kabir MA, Ahmad A, Greenberg JR, Wang YK & Rustchenko E (2005) Loss and gain of chromosome 5 controls growth of *Candida albicans* on sorbose due to dispersed redundant negative regulators. *P Natl Acad Sci USA* **102**: 12147–12152.

Legrand M, Forche A, Selmecki A, Chan C, Kirkpatrick DT & Berman J (2008) Haplotype mapping of a diploid non-meiotic organism using existing and induced aneuploidies. *PLoS Genet* **4**: e1.

Lo HJ, Kohler JR, DiDomenico B, Loebenberg D, Cacciapuoti A & Fink GR (1997) Nonfilamentous *C. albicans* mutants are avirulent. *Cell* **90**: 939–949.

Nantel A (2006) The long hard road to a completed *Candida albicans* genome. *Fungal Genet Biol* **43**: 311–315.

Nantel A, Dignard D, Bachewich C *et al.* (2002) Transcription profiling of *Candida albicans* cells undergoing the yeast-to-hyphal transition. *Mol Biol Cell* **13**: 3452–3465.

Nantel A, Rigby T, Hogues H & Whiteway M (2006) Microarrays for studying pathogenicity in *Candida albicans*. *Medical Mycology: Cellular and Molecular Techniques* (Kavanagh K, ed), pp. 181–209. Wiley Press, Hoboken, NJ.

Noble SM & Johnson AD (2005) Strains and strategies for large-scale gene deletion studies of the diploid human fungal pathogen *Candida albicans*. *Eukaryot Cell* **4**: 298–309.

Oberholzer U, Nantel A, Berman J & Whiteway M (2006) Transcript profiles of *Candida albicans* cortical actin patch mutants reflect their cellular defects: contribution of the Hog1p and Mkc1p signaling pathways. *Eukaryot Cell* **5**: 1252–1265.

Rocha CR, Schroppel K, Harcus D, Marcil A, Dignard D, Taylor BN, Thomas DY, Whiteway M & Leberer E (2001) Signaling through adenylyl cyclase is essential for hyphal growth and virulence in the pathogenic fungus *Candida albicans*. *Mol Biol Cell* **12**: 3631–3643.

Rose MD, Winston F & Hierter P (1990) *Methods in Yeast Genetics: A Laboratory Course Manual.* Cold Spring Harbor Laboratory Press, New York, NY.

Rustchenko E (2007) Chromosome instability in *Candida albicans*. *FEMS Yeast Res* **7**: 2–11.

Rustchenko EP, Howard DH & Sherman F (1994) Chromosomal alterations of *Candida albicans* are associated with the gain and loss of assimilating functions. *J Bacteriol* **176**: 3231–3241.

Selmecki A, Bergmann S & Berman J (2005) Comparative genome hybridization reveals widespread aneuploidy in *Candida albicans* laboratory strains. *Mol Microbiol* **55**: 1553–1565.

Selmecki A, Forche A & Berman J (2006) Aneuploidy and isochromosome formation in drug-resistant *Candida albicans*. *Science* **313**: 367–370.

Tsong AE, Miller MG, Raisner RM & Johnson AD (2003) Evolution of a combinatorial transcriptional circuit: a case study in yeasts. *Cell* **115**: 389–399.

van het Hoog M, Rast TJ, Martchenko M *et al.* (2007) Assembly of the *Candida albicans* genome into sixteen supercontigs aligned on the eight chromosomes. *Genome Biol* **8**: R52.

Znaidi S, De Deken X, Weber S, Rigby T, Nantel A & Raymond M (2007) The zinc cluster transcription factor Tac1p regulates PDR16 expression in *Candida albicans*. *Mol microbiol* **66**: 440–452.

VII.3. Transcriptional regulation of carbohydrate metabolism in the human pathogen *Candida albicans*

PLoS Pathog. 2009 Oct;5(10):e1000612. Epub 2009 Oct 9. || PMID: 19816560

OPEN ACCESS Freely available online

PLoS PATHOGENS

Transcriptional Regulation of Carbohydrate Metabolism in the Human Pathogen *Candida albicans*

Christopher Askew[1,2], Adnane Sellam[1,3], Elias Epp[1,2], Hervé Hogues[1], Alaka Mullick[1,4], André Nantel[1,3], Malcolm Whiteway[1,2]*

1 Biotechnology Research Institute, National Research Council of Canada, Montréal, Québec, Canada, **2** Department of Biology, McGill University, Montréal, Québec, Canada, **3** Department of Anatomy and Cell Biology, McGill University, Montréal, Québec, Canada, **4** Département de Microbiologie et Immunologie, l'Université de Montréal, Montréal, Québec, Canada

Abstract

Glycolysis is a metabolic pathway that is central to the assimilation of carbon for either respiration or fermentation and therefore is critical for the growth of all organisms. Consequently, glycolytic transcriptional regulation is important for the metabolic flexibility of pathogens in their attempts to colonize diverse niches. We investigated the transcriptional control of carbohydrate metabolism in the human fungal pathogen *Candida albicans* and identified two factors, Tye7p and Gal4p, as key regulators of glycolysis. When respiration was inhibited or oxygen was limited, a *gal4tye7 C. albicans* strain showed a severe growth defect when cultured on glucose, fructose or mannose as carbon sources. The *gal4tye7* strain displayed attenuated virulence in both *Galleria* and mouse models as well, supporting the connection between pathogenicity and metabolism. Chromatin immunoprecipitation coupled with microarray analysis (ChIP-CHIP) and transcription profiling revealed that Tye7p bound the promoter sequences of the glycolytic genes and activated their expression during growth on either fermentable or non-fermentable carbon sources. Gal4p also bound the glycolytic promoter sequences and activated the genes although to a lesser extent than Tye7p. Intriguingly, binding and activation by Gal4p was carbon source-dependent and much stronger during growth on media containing fermentable sugars than on glycerol. Furthermore, Tye7p and Gal4p were responsible for the complete induction of the glycolytic genes under hypoxic growth conditions. Tye7p and Gal4p also regulated unique sets of carbohydrate metabolic genes; Tye7p bound and activated genes involved in trehalose, glycogen, and glycerol metabolism, while Gal4p regulated the pyruvate dehydrogenase complex. This suggests that Tye7p represents the key transcriptional regulator of carbohydrate metabolism in *C. albicans* and Gal4p provides a carbon source-dependent fine-tuning of gene expression while regulating the metabolic flux between respiration and fermentation pathways.

Citation: Askew C, Sellam A, Epp E, Hogues H, Mullick A, et al. (2009) Transcriptional Regulation of Carbohydrate Metabolism in the Human Pathogen *Candida albicans*. PLoS Pathog 5(10): e1000612. doi:10.1371/journal.ppat.1000612

Editor: Alex Andrianopoulos, University of Melbourne, Australia

Received July 1, 2009; **Accepted** September 10, 2009; **Published** October 9, 2009

Funding: This work was supported by grants from the Canadian Institute for Health Research (CIHR) to A.M., A.N., and M.W. (CTP-79843, MOP-84341, and MOP-42516). C.A. was supported by NSERC Alexander Graham Bell CGS and PGS Extension Scholarships. The funders had no role in study design, data collection and analysis, decision to publish, or preparation of the manuscript.

Competing Interests: The authors have declared that no competing interests exist.

* E-mail: malcolm.whiteway@cnrc-nrc.gc.ca

Introduction

In order to grow and thrive in a wide range of hosts, pathogens not only depend on certain virulence factors but also metabolic flexibility; therefore, they must be able to assimilate various carbon sources. Carbohydrates are the primary and preferred source of metabolic carbon for most organisms, and are used for generating energy and producing biomolecules. Most sugars are converted to glucose 6-phosphate or fructose 6-phosphate before entering the glycolytic pathway. Glycolysis is then responsible for converting these hexose phosphates into the key metabolite pyruvate while producing ATP and NADH (Figure 1). From there, cells carry out two major strategies of energy production: fermentation and respiration. Although both processes regenerate NAD+, respiration is significantly more energetically efficient than fermentation as it produces additional ATP through the tricarboxylic acid (TCA) cycle and oxidative phosphorylation. However, regardless of the mode of energy production, glycolysis is the central, common pathway for both processes. As glycolysis is critical for carbon assimilation, the pathway has been shown to be up-regulated during infections and important to the virulence in pathogenic bacteria, parasites, and fungi [1–6].

Since glycolysis is a central metabolic pathway, it is strictly regulated. While there are different levels of regulation of the process, transcriptional control is common to bacteria, fungi, plants, and animals. The glycolytic enzymes are transcriptionally regulated in response to environmental conditions such as oxygen levels, carbon source and availability, and to cellular demands such as metabolite concentrations and energy needs. However, in most species the regulators of glycolytic gene expression have not been identified, so our understanding of transcriptional control of glycolysis in eukaryotes is mainly based on the non-pathogenic yeast *Saccharomyces cerevisiae* (for review see [7]). In *S. cerevisiae*, the transcription regulators Gcr1p and Gcr2p are primarily responsible for activating the expression of the glycolytic genes [8,9]. Gcr1p binds to CT boxes (5′-CTTCC-3′) upstream of the glycolytic genes and Gcr2p acts as a co-activator by forming a complex with Gcr1p [10,11]. Deleting either gene decreases the

Author Summary

Pathogens must be able to assimilate the carbon sources in their environment to generate sufficient energy and metabolites to survive. Since glycolysis is a central metabolic pathway, it is important for this metabolic flexibility. The most commonly isolated agent in human fungal infections, *Candida albicans*, depends upon glycolysis for the progression of systemic disease. We investigated glycolytic transcriptional regulation in *C. albicans* and defined two key regulators of the pathway, Tye7p and Gal4p. We demonstrated that these factors are important for the fermentative growth of *C. albicans* both *in vitro* and *in vivo* and also regulate the input and output fluxes of glycolysis. The *gal4tye7* strain showed attenuated virulence in a *Galleria* and two mouse models, potentially due to the severe growth defect in oxygen-limiting environments. Gal4p and Tye7p represent fungal specific regulators involved in the pathogenicity of the organism that may be exploited in the development of antifungal treatments. Our study describes a fungal glycolytic transcriptional circuit that is fundamentally different from that of the model yeast *Saccharomyces cerevisiae*, providing further evidence that the transcriptional networks in *S. cerevisiae* need not be generally representative of the fungal kingdom.

expression levels of the glycolytic genes resulting in growth defects during culture on glucose [9,12]. However, the mutant strains display wild type growth rates on non-fermentable carbon sources [9,12]. The factor Tye7p (also referred to as Sgc1p) is another glycolysis-specific regulator in *S. cerevisiae*. Tye7p has been shown to be involved in the activation of several glycolytic genes, although not to the same extent as Gcr1p and Gcr2p [13]. This activation is independent of *GCR1* and the *tye7* strain displays no growth defects under any carbon source regime [13,14]. The transcription factors Rap1p, Abf1p, and Reb1p also have roles in activating the glycolytic genes, but these are global factors involved in many cellular processes [15–18].

Although the glycolytic circuit is well characterized in *S. cerevisiae*, most organisms to do not have *GCR1* or *GCR2* homologs [19]. Furthermore, it is well established that the *Saccharomyces*-lineage exhibits a unique dependence on the fermentation pathway: these yeasts mainly ferment sugars to ethanol instead of using respiration, even under aerobic conditions [20]. *S. cerevisiae* up-regulates glycolysis and represses the TCA cycle in the presence of glucose allowing this aerobic fermentation behavior to occur [21]. Only when no fermentable carbon sources are present, after the post-diauxic shift, will *S. cerevisiae* switch to the respiratory mode. This phenomenon is known as the Crabtree effect and is due to a glucose repression circuit that is largely regulated by the transcriptional repressors Mig1p and Rgt1p, the protein kinase Snf1p, and the protein complex SCF^{Grr1} [20]. This regulatory circuit is proposed to have developed from the adaptive potential derived from the whole-genome duplication that occurred after the divergence of *Saccharomyces* from *Kluyveromyces* [22,23]; the repression circuit is common to the *Saccharomyces*-lineage and many of the genes retained from the whole-genome duplication are involved in the lifestyle adaptation to aerobic ethanol production [24–26].

The facultative anaerobic lifestyle of Crabtree-positive *Saccharomyces* yeasts is in contrast to that of most other eukaryotes, which are either facultative or obligate aerobes and lack the glucose repression circuit. Under aerobic conditions, Crabtree-negative cells predominately oxidize pyruvate to carbon dioxide through the TCA cycle. In the absence of oxygen, most aerobic organisms are able to utilize the fermentation pathway to some extent to continue regenerating NAD+. This difference in metabolic flux is highlighted by transcription profiles of the aerobic fungi *Trichoderma reesei*, *Neurospora crassa*, and *Aspergillus oryzae*, which show little or no repression of the TCA cycle in glucose rich compared to glucose poor growth conditions, and therefore do not rely as heavily on the fermentation pathway as does *S. cerevisiae* [27–29].

The opportunistic human fungal pathogen *Candida albicans* is a facultative aerobe and thus metabolizes carbon sources in response to oxygen availability similar to that of a typical eukaryotic cell. *C. albicans* is responsible for various non life-threatening infections such as oral thrush and vaginitis but in extreme cases, especially in immunosuppressed individuals, it can cause potentially lethal systemic infections. In fact, *Candida* species are the most common isolated agent in fungal infections and the fourth leading cause of nosocomial bloodstream infections in the United States, with an attributable mortality rate of approximately 38–49% and treatment costs estimated to be $1.7 billion annually [30–33]. *C. albicans* accounts for more than half of all *Candida* infections [30,33], highlighting the importance of understanding the metabolism of this pathogen for the development of effective antifungal treatments.

Crabtree-negative organisms that lack *GCR1/2* homologs, such as *C. albicans*, must control transcription of glycolytic genes differently than does *S. cerevisiae*. In this study, we characterized two fungal-specific activators of the glycolytic pathway in *C. albicans*, Tye7p and Gal4p. Deleting both genes resulted in severe growth defects when the mutant cells were cultured on fermentable carbon sources when respiration was inhibited or oxygen was limited, and chromatin immunoprecipitation coupled with microarray analysis (ChIP-CHIP) and transcription profiling showed these factors bind to and regulate expression of the glycolytic pathway genes. Tye7p and Gal4p are also required for complete pathogenicity as the mutant strains showed attenuated virulence. This work therefore defines the key regulatory elements controlling glycolytic gene expression in a facultative aerobic pathogen.

Results

Deletion of *CaGAL4* and *CaTYE7* results in a severe growth defect on fermentable carbon sources when the respiration pathway is disrupted

We investigated possible transcriptional regulators of glycolytic gene expression in *C. albicans*. In the well-studied yeast *S. cerevisiae*, Gcr1p, Gcr2p, and Tye7p are key glycolysis-specific activators. Unlike Gcr1p and Gcr2p, which are limited to *Saccharomyces* and closely related yeasts, Tye7-like transcription factors can be found throughout the Saccharomycotina subphylum. Therefore, while there are no homologs of Gcr1p or Gcr2p in *C. albicans*, there is a CaTye7p. ScTye7p and CaTye7p share 87% amino acid similarity in the DNA binding basic-helix-loop-helix (bHLH) domain but only 33% in the activation domain. A recent investigation also implicated the CaGal4p transcription regulator in the expression of genes involved in glycolysis [34]; while Gal4p in *S. cerevisiae* is a well-characterized zinc cluster transcription factor that regulates galactose catabolism, it does not fulfill this role in *C. albicans*. ScGal4p and CaGal4p also share homology strictly in the DNA-binding domain. Due to the potential or observed involvement of these factors in aspects of carbohydrate metabolism, we tested the role of CaTye7p and CaGal4p in the control of glycolytic gene expression in *C. albicans*.

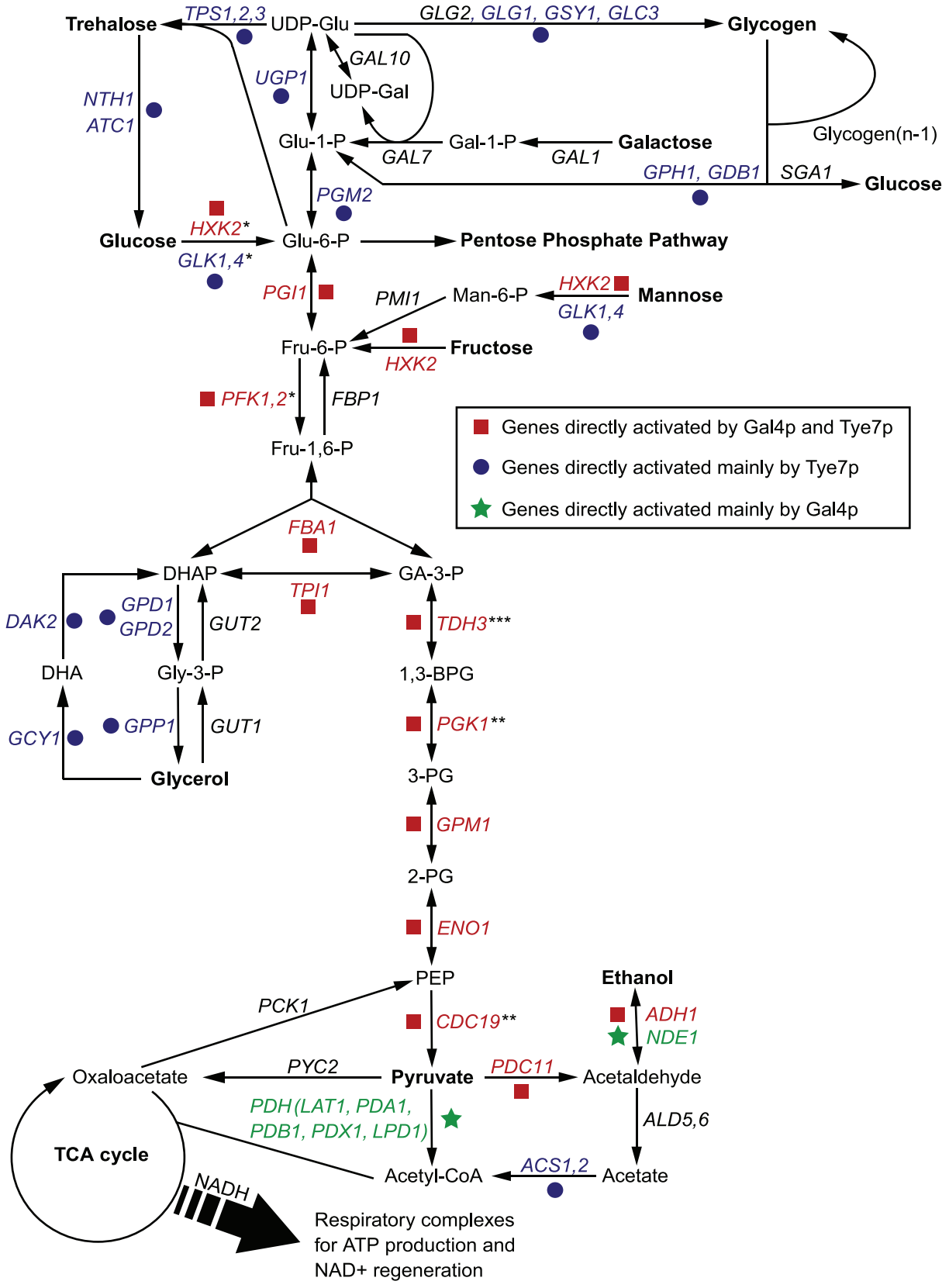

Figure 1. An overview of the central metabolic pathways in yeast. The enzyme names are for *C. albicans* but some have not been directly characterized and are annotated based on *S. cerevisiae* homology. Genes bound and activated by Gal4p and Tye7p are in red, genes bound and activated mainly by Tye7p are in blue, and genes bound and activated mainly by Gal4p are in green. Genes in black are not bound and activated by either factor. For simplicity, "*" represents reactions requiring ATP, "**" represents reactions producing ATP, and "***" represents reactions generating NADH. These symbols are given for reactions of the glycolytic pathway only.
doi:10.1371/journal.ppat.1000612.g001

We first constructed *tye7* and *gal4tye7* deletion strains to use in conjunction with our previously generated *gal4* strain [34]. We tested the ability of all strains to grow on the fermentable carbon sources glucose, fructose, mannose, and galactose, and the non-fermentable carbon source glycerol. On solid media, no growth defect was evident for any deletion strain regardless of the carbon source or concentration tested (Figure 2A). However, when the more sensitive liquid assay was used with glucose, galactose, and glycerol carbon sources, it was able to identify a minor growth defect for the *gal4tye7* strain with glucose media, as the doubling time was 147 min compared to that of the wild type of 123 min (Table 1 and Figure S1A). As *C. albicans* lacks the glucose repression mechanism that exists in *S. cerevisiae*, its respiration pathway is active under glucose growth conditions so it is not critically dependent on the glycolytic pathway. Although glycolysis is central to both the respiration and fermentation pathways, it is more important for fermentative metabolism since under these conditions the cell must rely exclusively on the ATP generated by glycolysis. As a result, glycolysis proceeds at a higher rate in fermenting cells [20].

To mimic the fermentative metabolism of *S. cerevisiae*, the mitochondrial inhibitor antimycin A was added to the solid media, and cells in liquid culture were grown without aeration. These changes disrupt the proton gradient and ultimately prevent the

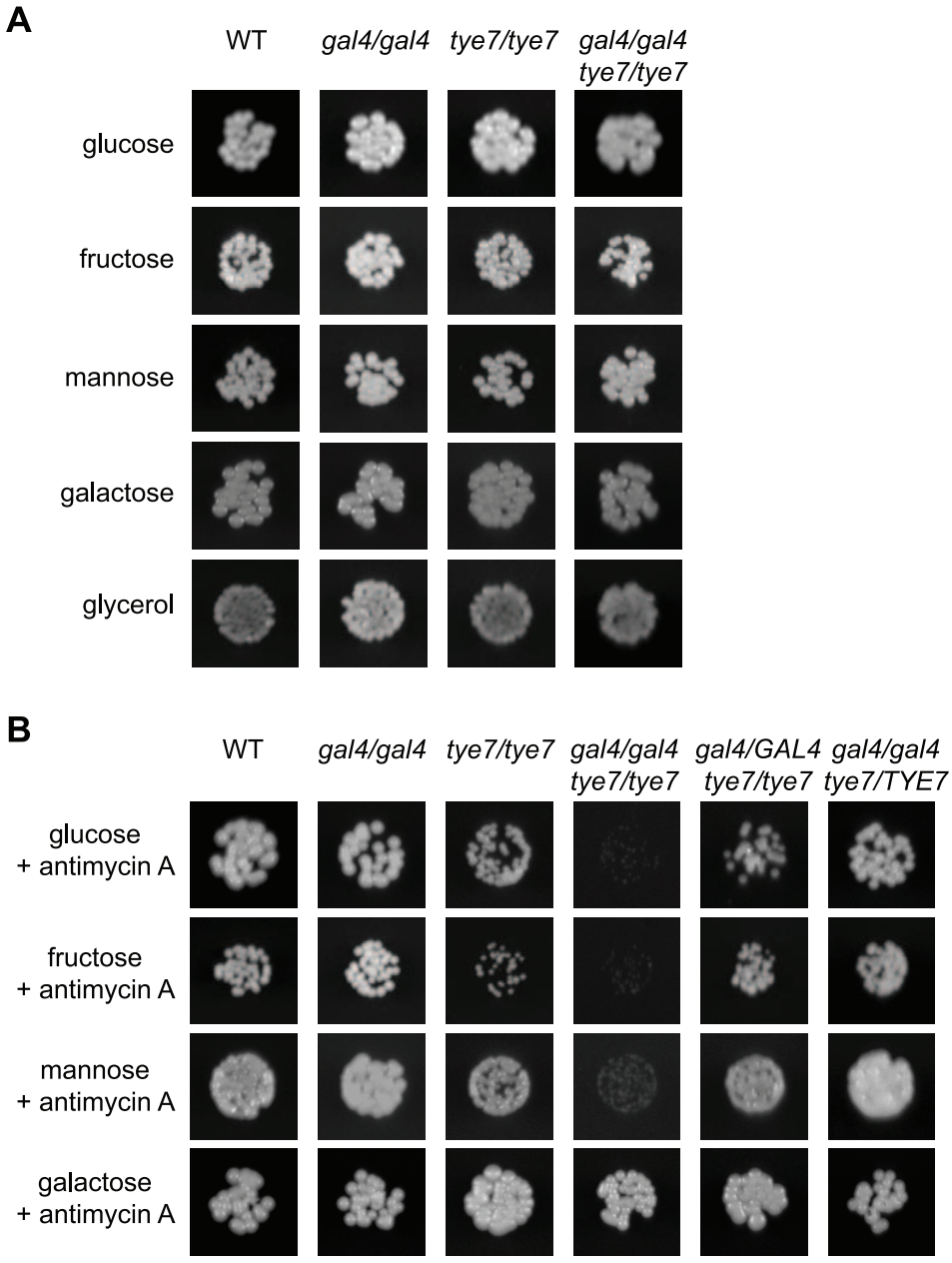

Figure 2. *GAL4* and *TYE7* are involved in fermentative growth with glucose, fructose or mannose as the sole carbon source. WT refers to strain CMM1. Cells were serially diluted and a representative dilution is displayed. Pictures were taken from plates where the carbon source was at 2% although the 0.2% plates gave similar results. (A) Solid media without antimycin A. Pictures were taken after 2–3 days of growth. (B) Solid media with antimycin A (2 μg/ml). Pictures were taken after 2–3 days of growth except for galactose (6 days).
doi:10.1371/journal.ppat.1000612.g002

Table 1. Doubling times under glucose growth conditions.

Strain	Aeration (min)	Static (min)
WT	123	139
tye7/tye7	121	155
gal4/gal4	116	132
gal4/gal4/tye7/tye7	147	210
gal4/GAL4/tye7/tye7	126	163
gal4/gal4/tye7/TYE7	129	138

Doubling times of the strains for the glucose growth curves in Figure S1. The natural log of the OD_{600} was plotted versus time and the best-fit line of the exponential phase was determined. The doubling time was equal to ln2/slope.
doi:10.1371/journal.ppat.1000612.t001

production of ATP by oxidative phosphorylation via the respiration pathway. When *C. albicans* was forced to use fermentation, a severe growth defect during culture on glucose, fructose or mannose media was evident for the double mutant strain (Figures 2B and S1B and Table 1). Therefore, it appears that both Gal4p and Tye7p are involved in fermentative growth with most fermentable carbon sources. The *tye7* strain showed a minor growth defect under these fermentative conditions while the *gal4* strain still grew at wild type levels, suggesting that Tye7p is a more important regulator of fermentative growth. This prediction was supported by the complemented strains, as reintroducing one copy of *TYE7* was sufficient to restore wild type growth rates to the double mutant strain, while one copy of *GAL4* resulted in only partial restoration (Figure S1B). Therefore, although both factors appear to be involved in regulating the fermentative growth pathway, Tye7p plays a more central role.

Galactose was unique among the fermentable carbon sources tested as no distinct phenotype was observed for the *gal4tye7* strain compared to the wild type under fermentative growth conditions (Figures 2B and S1B). This is likely due to the Kluyver effect, which is thought to be a result of insufficient sugar uptake, and prevents the growth on certain sugars in the absence of respiration [35]. The fermentative growth conditions used (growth without aeration and antimycin A at 2 μg/ml) do not completely inhibit respiration, which allowed the strains to grow, although very slowly, in galactose media. Most yeast hexose transporters are able to take up glucose, fructose, and mannose, while galactose uptake requires separate transporters. If galactose uptake is the limiting step, then any effect of *GAL4* or *TYE7* on the fermentation pathway will be minimized. Therefore, the lack of observed difference between the mutant strain and the wild type in Figures 2B and S1B is not because the *gal4tye7* strain grows well on galactose media when respiration is disrupted, but instead is a result of the comparably poor growth of the wild type strain (Table S1).

Location profiling reveals that Gal4p and Tye7p bind many carbohydrate metabolic promoter targets

To gain insight into why Gal4p and Tye7p are required for fermentative growth, we performed ChIP-CHIP to determine their binding targets. ChIP-CHIP of chromosomally TAP-tagged Gal4p and Tye7p was first performed during growth in glucose media since glucose is the primary carbon source that stimulates the glycolytic pathway. Two different microarray formats, single spot full-genome arrays and whole-genome tiling arrays, were used to provide different strategies for data analysis and for validation purposes. Gal4p bound 98 targets and Tye7p bound 271 targets with the single probe full-genome array (Tables S2 and S3), so Tye7p appears to function as a more global regulator. However, both gene sets were significantly enriched for glucose/carbohydrate metabolic processes and both factors bound essentially all the glycolytic genes. The Gene Ontology (GO) biological processes that were enriched in the bound-gene sets are displayed in Figure 3A. The results are similar between the two factors except, as is discussed below, Gal4p bound more targets involved in pyruvate metabolism. Although Tye7p bound a large number of targets, no GO process is enriched other than carbon metabolism.

The tiling array showed highly similar results but was able to identify a few additional targets including three glycolytic genes, *PFK26-2*, *GLK1*, and *GLK4*. Smoothed peak intensity curves of the tiling array binding events were created to estimate the largest fold enrichments and thus the most significant targets. For Gal4p, the 13 *bona fide* glycolytic pathway promoters are in the top 68 smoothed peak intensities while for Tye7p they are in the top 52 peaks (Tables S4 and S5). Therefore, the glycolytic promoters are among the most significant targets for both factors. As well, several genes involved in ethanol fermentation (*PDC11*, *ADH1*, and *NDE1*) are included in this group of targets. Therefore, the ChIP-CHIP data suggests that Gal4p and Tye7p are involved in the entire fermentation pathway from glucose to ethanol.

Although Gal4p and Tye7p bound many common targets, there were a significant number of individual binding events, some of which are related to carbohydrate metabolism (Figure 3B). The clearest example is that Gal4p bound the promoter sequences of the five genes encoding the pyruvate dehydrogenase complex (PDH) while Tye7p bound the promoter sequences of the three genes for the trehalose synthase complex. Tye7p also bound several genes involved in glycogen and glycerol metabolism. A summary of selected metabolic binding targets under glucose growth conditions is shown in Figure 4A and Table S6. Many of the Gal4p and Tye7p targets are linked to the glycolytic pathway suggesting that these factors also regulate the input and output fluxes of the pathway.

Both Gal4p and Tye7p activate genes required for fermentative growth

ChIP-CHIP is a whole-genome approach for determining binding locations of a transcription factor; however, it is insufficient to give a complete picture of a factor's biological function. As was observed with *GAL4*, the binding and transcription profiles can provide different insights. Therefore, to complement the ChIP-CHIP analysis, transcription profiling comparing wild type and mutant strains was performed under glucose growth conditions. The expression levels of selected carbohydrate metabolic genes is illustrated in Figure 4B and Table S7. As expected, not all targets bound by ChIP-CHIP showed differential expression and not all differentially regulated genes showed direct binding of the transcription factors; however, in general the most significantly bound targets were down-regulated in the absence of the factor. The glycolytic and fermentation genes were down-regulated in the *tye7* strain confirming Tye7p's role as an activator of fermentative metabolism. Gal4p is also involved in the activation of the glycolytic/fermentation genes because the expression levels of these genes were lower in the *gal4tye7* strain compared to the *tye7* strain. The involvement of Gal4p in the activation of glycolytic gene expression was masked in the *gal4* expression profiles, most likely because the absence of *GAL4* caused an up-regulation of *TYE7* [34]. Therefore, Tye7p appears able to significantly compensate for the loss of Gal4p, further supporting the idea that it plays a more central role in glycolytic gene regulation than does Gal4p.

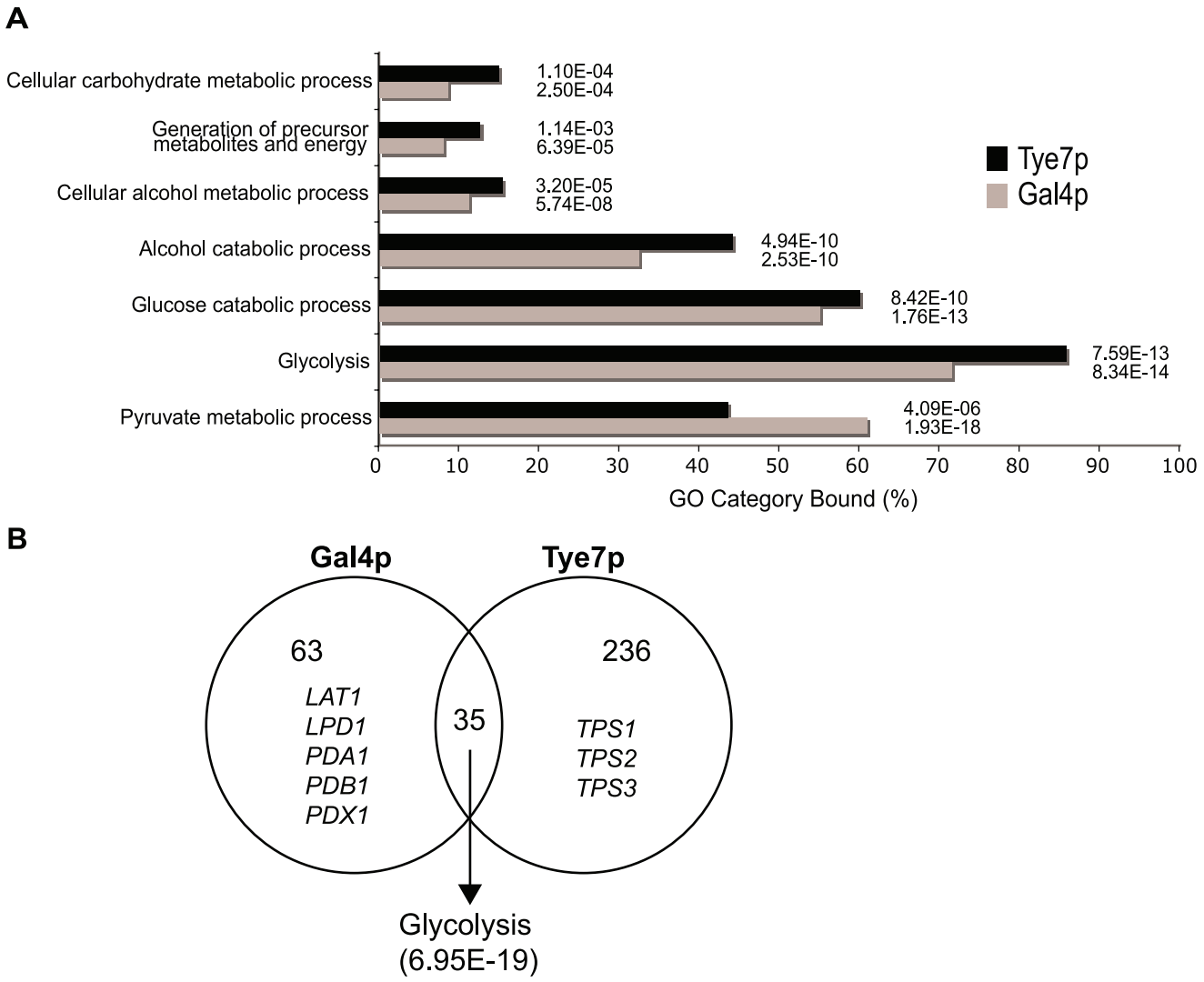

Figure 3. Gal4p and Tye7p bind many carbohydrate metabolic promoter targets under glucose growth conditions. (A) GO enrichment of YPD binding targets for Gal4p and Tye7p. Targets with a normalized fold enrichment >1.5 and a *P*-value<0.1 with the single spot full-genome microarray (98 and 271 genes for Gal4p and Tye7p, respectively) were analyzed with the CGD GO Term Finder (http://www.candidagenome.org/cgi-bin/GO/goTermFinder). The *P*-value of enrichment for each GO category is indicated. (B) Overlap of YPD binding targets from (A). The common targets are highly enriched for glycolysis genes. The Gal4p independent targets include the five components of the PDH while the Tye7p independent targets contain the three components of the trehalose synthase complex.
doi:10.1371/journal.ppat.1000612.g003

The ChIP-CHIP data showed that only Tye7p bound the genes involved in trehalose metabolism. Expression of the trehalose metabolic genes was down-regulated in the *tye7* strain but not further reduced in the *gal4tye7* strain indicating that Gal4p is not involved in their activation. Trehalose is a glucose disaccharide that has a role as a storage carbohydrate in yeast. Another important storage molecule in yeast is glycogen. Tye7p also bound several glycogen metabolic targets (*GPH1*, *GDB1*, *GLG1*, *GSY1*, and *GLC3*) that were subsequently down-regulated in the *tye7* strain and showed no influence of Gal4p in the *gal4tye7* strain. As well, Tye7p was the sole regulator of several glycerol metabolic targets (*DAK2*, *GCY1*, *GPP1*, *GPD1*, and *GPD2*). On the other hand, Gal4p activated the PDH genes with no influence from Tye7p. These genes were not down-regulated in the *tye7* strain (some were slightly up-regulated along with *GAL4*) but were reduced in the *gal4tye7* strain.

The down-regulated genes were analyzed for GO enrichment. As expected, all the categories were related to carbon metabolism. Generally, the two deletion strains had similar results with glycolysis (*tye7* *P*-value: 1.34E-18; *gal4tye7*: 1.44E-15) and cellular alcohol metabolic process (*tye7*: 4.48E-17; *gal4tye7*: 8.33E-16) being the most significantly enriched categories.

Tye7p regulates the cell's commitment to glycolysis

Tye7p directly activated many genes involved in trehalose and glycogen metabolism independently of Gal4p. As well, the genes encoding the glycolytic-committing enzyme phosphofructokinase (*PFK1* and *PFK2*) were among the top six most down-regulated genes in the *tye7* strain while the gluconeogenesis-specific gene *FBP1* was moderately down-regulated. Therefore, it appears that Tye7p regulates the flux between energy storage and energy production at the glucose-6-phosphate branch point (Figure 1). To support this claim, we investigated whether the levels of trehalose and glycogen were different in the *tye7* strain compared to the wild type. Since exponentially growing cells have low trehalose levels that rapidly

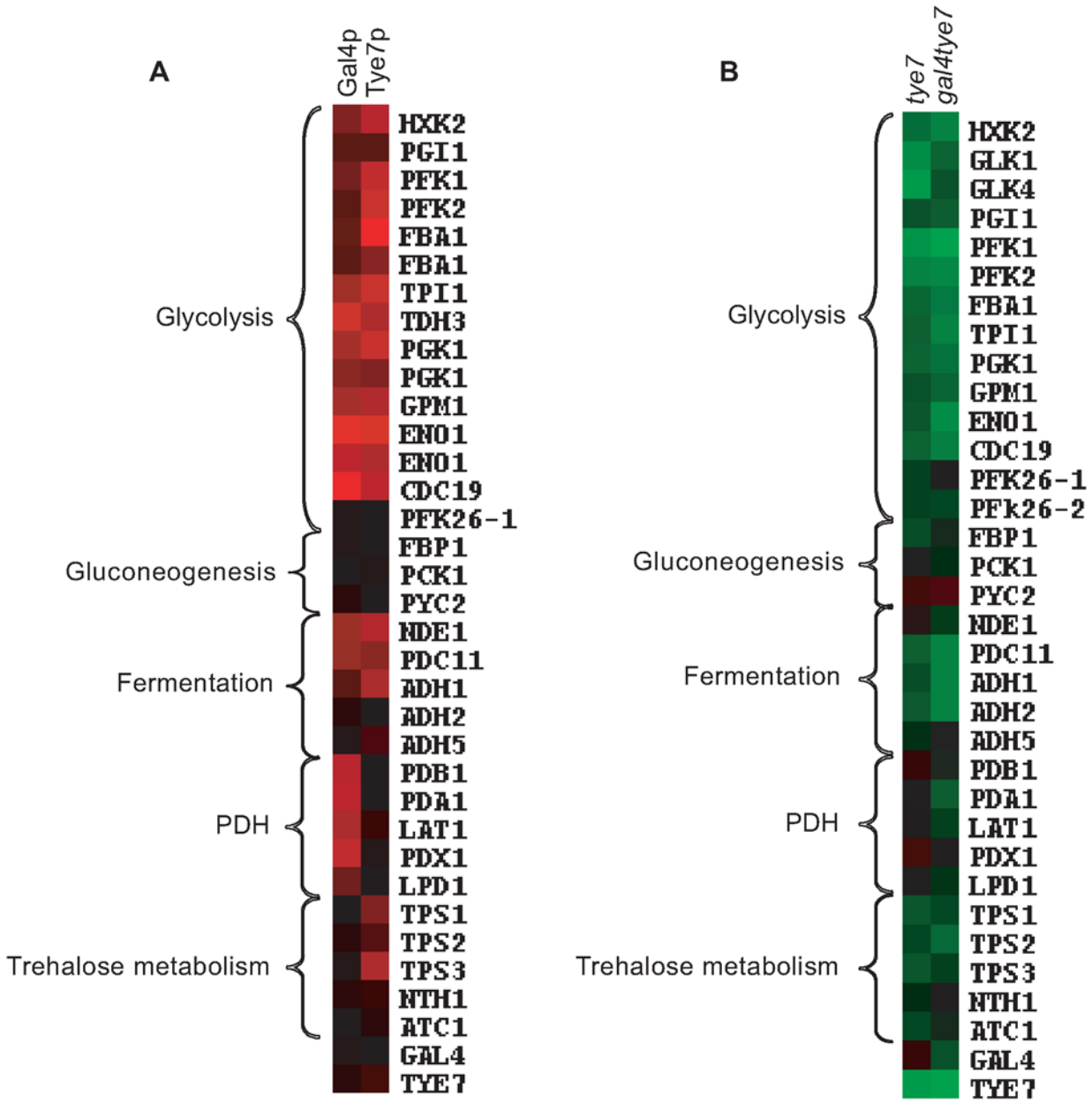

Figure 4. Gal4p and Tye7p bind to and regulate the expression of genes involved in the fermentation pathway under glucose growth conditions. Heat map displays of the ChIP-CHIP and expression profiles were created with the Cluster and TreeView programs (http://rana.lbl.gov/EisenSoftware.htm). (A) Tye7p and Gal4p ChIP-CHIP binding profiles of selected metabolic targets with the single spot full-genome microarray. Fold enrichments displayed represent the intergenic probe for the respective gene and enrichments <1.0 were adjusted to 1.0 for graphical purposes. Black represents no binding while red represents binding with the color brightness indicating the degree of enrichment. Binding to the glycolytic genes was so strong that binding to two neighboring probes was sometimes observed. In such cases, both values were included as these occurred in situations where a shared promoter region contained two probes but the tiling array confirmed the presence of a single binding site. The fold enrichments of these and other metabolic targets are given in Table S6. (B) Transcription profile of selected metabolic genes for the *tye7* and *gal4tye7* strains. Black represents no change in expression, green is down-regulated, and red is up-regulated with the color brightness indicating the degree of expression change. The expression levels of these and other metabolic genes are given in Table S7.
doi:10.1371/journal.ppat.1000612.g004

accumulate during stationary phase [36], trehalose amounts were determined from cells at both phases. We observed significantly increased levels of trehalose in the *tye7* strain for both stationary and logarithmic phase cells (Figure 5A). Additionally, iodine staining showed that the glycogen content in the *tye7* cells was higher than that of the wild type (Figure 5B). The higher storage carbohydrate levels correlate with the expression profile as *FBP1* and the majority of genes involved in trehalose and glycogen metabolism were down-regulated 2–3 fold while *PFK1* and *PFK2* were down-regulated approximately 6 and 9 fold, respectively. Therefore, the glucose-6-phosphate flux in the *tye7* strain would favor trehalose and glycogen synthesis. In contrast, the *gal4* strain showed wild type levels of both storage carbohydrates, suggesting that Tye7p alone regulates the cell's decision to commit to glycolysis or energy storage.

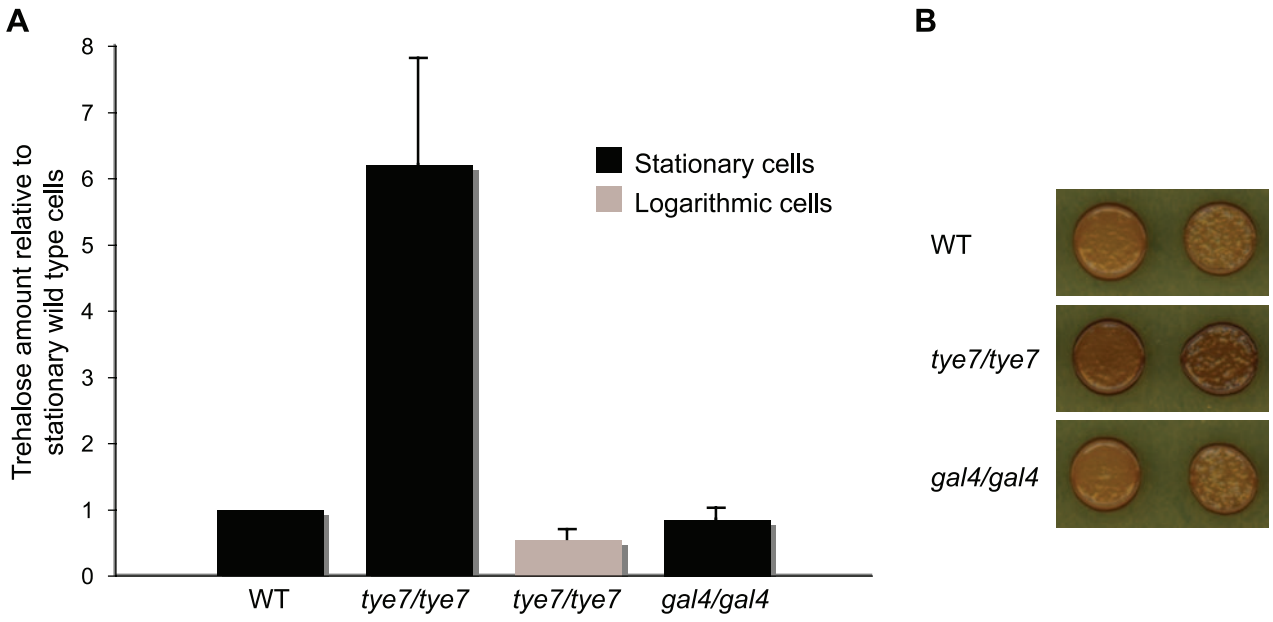

Figure 5. Deletion of *TYE7* results in higher trehalose and glycogen levels. (A) The trehalose content of wild type (BWP17), *tye7*, and *gal4* cells at both stationary and logarithmic phases were measured. Trehalose levels (nmol trehalose per mg cell protein) were reported relative to the wild type in stationary phase. Both wild type and *gal4* cells had no detectable trehalose levels in the logarithmic phase and were not included in the graph. (B) Wild type (BWP17), *tye7*, and *gal4* cells were exposed to iodine vapor to indicate the glycogen content as iodine vapor stains cells brown upon reacting with glycogen. The *tye7* cells stained a darker brown than the wild type indicating that there is more glycogen present.
doi:10.1371/journal.ppat.1000612.g005

Tye7p binds its targets independently of the carbon source while Gal4p displays differential binding

It is clear that Gal4p and Tye7p are important for fermentative growth when glucose, fructose or mannose is the carbon source. Although there was no phenotype during growth on galactose or glycerol, we investigated the effect of these carbon sources on binding to identify any differences (Dataset S1). Figure 6A illustrates the ChIP-CHIP results of selected carbohydrate metabolic targets during growth on galactose and glycerol media with the behavior during growth on glucose included as a comparison.

A striking trend was the difference in binding between Gal4p and Tye7p under the various carbon sources. Whereas the peak intensity of Gal4p binding changed based on the carbon source, the peak sizes of Tye7p binding were largely unaffected (Figure 7A). This pattern was consistent for the majority of targets resulting in a decrease in the overall number of Gal4p binding targets from glucose to galactose to glycerol and a similar overall number of binding sites for Tye7p with the different carbon sources (Figure S2). Therefore, Gal4p binds its few targets in a carbon source-dependent manner while Tye7p appears to be a more global regulator that binds its targets independently of the carbon source the cells are growing on. This difference in target binding dependent on the carbon source could be a direct result of the protein levels of the transcription factors. We compared protein levels during growth in YPD, YPGal, and YPGly media relative to YP media and observed that Gal4p is significantly induced by glucose while Tye7p has a more constitutive expression (Figure S3). These results further support the inference that Tye7p is the more central regulator of carbohydrate metabolism.

Another trend was that Gal4p showed stronger binding to the promoters of genes encoding the glycolytic pathway enzymes that acted in the later part of the pathway (from *TPI1* on) compared to the early part of the pathway, regardless of the carbon source of the growth medium (Figure 6A). In Figure 7A, *HXK2* binding is representative of early pathway genes and *PGK1* binding is representative of later pathway genes. Interestingly, this difference in binding within the pathway corresponds at the point where the six carbon glucose molecule has been converted to two three carbon products and also represents the separation between the initial ATP consuming steps and the later energy producing steps (Figure 1). Therefore, while Tye7p appears to be involved in committing the cell to glycolysis, Gal4p appears to focus on the later part of the pathway to promote energy production once the commitment is made.

CaTye7p and CaGal4p bind to distinct motifs

The binding distribution curves created with the tiling array were also used to predict the motif that CaGal4p and CaTye7p recognize by looking for sequences enriched around the binding sites of the top peak intensity targets. ScGal4p has a well established 5′-CGG(N_{11})CCG-3′ motif [37]. Analysis of the top CaGal4p binding targets revealed enrichment for this motif (Figure 7B). Since ScGal4p and CaGal4p have 86% sequence similarity in the DNA binding domain, it is reasonable to expect they would recognize a similar sequence. The binding distribution curves of *HXK2*, *PGK1*, and *PDA1* showed Gal4p motifs near the binding sites of CaGal4p (Figure 7A).

As previously mentioned, CaTye7p is a bHLH transcription factor. These type of factors are known to recognize the E-box sequence 5′-CANNTG-3′ [38]. The motif enriched among the top CaTye7p binding targets contains this bHLH signature (Figure 7B). The binding distribution curves of *HXK2*, *PGK1*, and *TPS3* showed Tye7p motifs near the binding sites of CaTye7p (Figure 7A).

Tye7p and Gal4p are carbon-source dependent activators

To gain further insight into how Gal4p and Tye7p regulate their targets in response to different carbon sources, transcription

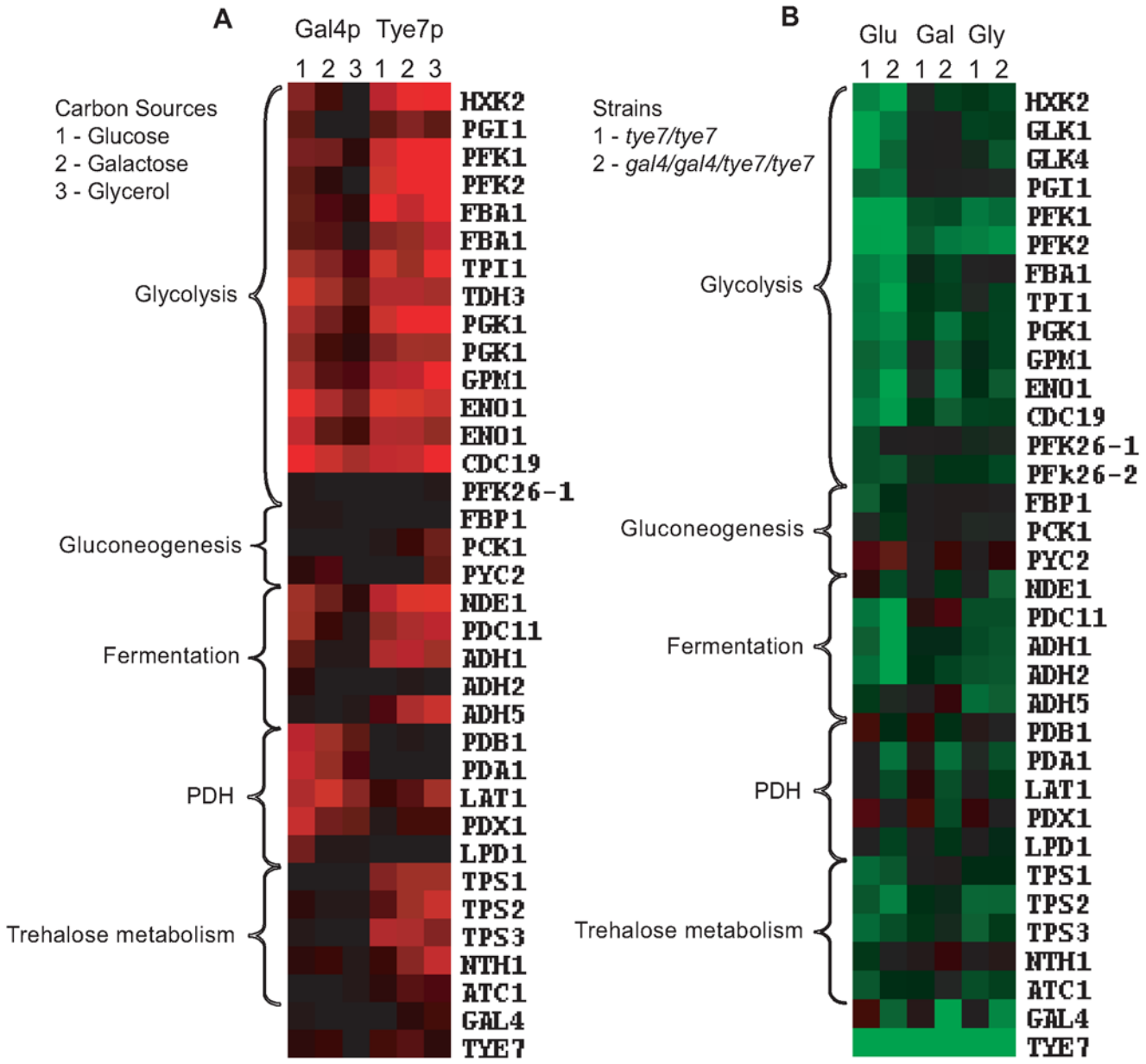

Figure 6. Comparison of ChIP-CHIP and expression profiles with glucose, galactose, and glycerol media. Heat map displays were created as described in Figure 4. (A) Tye7p and Gal4p ChIP-CHIP binding profiles of selected metabolic targets with the single probe full-genome microarray. The fold enrichments of these and other metabolic targets are given in Table S6. (B) Transcription profiles of selected metabolic genes for *tye7* (1) and *gal4tye7* (2) strains under glucose (Glu), galactose (Gal), and glycerol (Gly) carbon sources. The expression levels of these and other metabolic genes are given in Table S7.
doi:10.1371/journal.ppat.1000612.g006

profiles comparing wild type and deletion strains with galactose and glycerol as the sole carbon source were performed. Figure 6B illustrates the expression profiles of selected carbohydrate metabolic targets during growth on galactose and glycerol media with the behavior during growth on glucose included as a comparison (complete lists of down-regulated genes in Tables S8, S9, S10, S11, S12 and S13). The glycolytic genes were down-regulated in the *tye7* strain under galactose and glycerol growth conditions but not as significantly as with glucose-containing media. Gal4p strongly activated the glycolytic genes on glucose and galactose media but had only minimal effect when glycerol was the carbon source. This result correlates with the location profiling data as Gal4p displayed reduced binding under glycerol growth conditions. Tye7p and Gal4p's carbon-source dependent roles in glycolytic gene expression were validated by quantitative real-time PCR (qPCR) (Figure S4).

Gal4p and Tye7p are involved in glycolytic gene induction in hypoxic growth conditions

Pathogens must not only be adept at utilizing different carbon sources but must also be able to handle changes in oxygen levels. For *C. albicans*, this flexibility involves growth in oxygen rich environments such as the skin and oral mucosal layers and oxygen poor niches such as inner organs. Since serious systemic infections

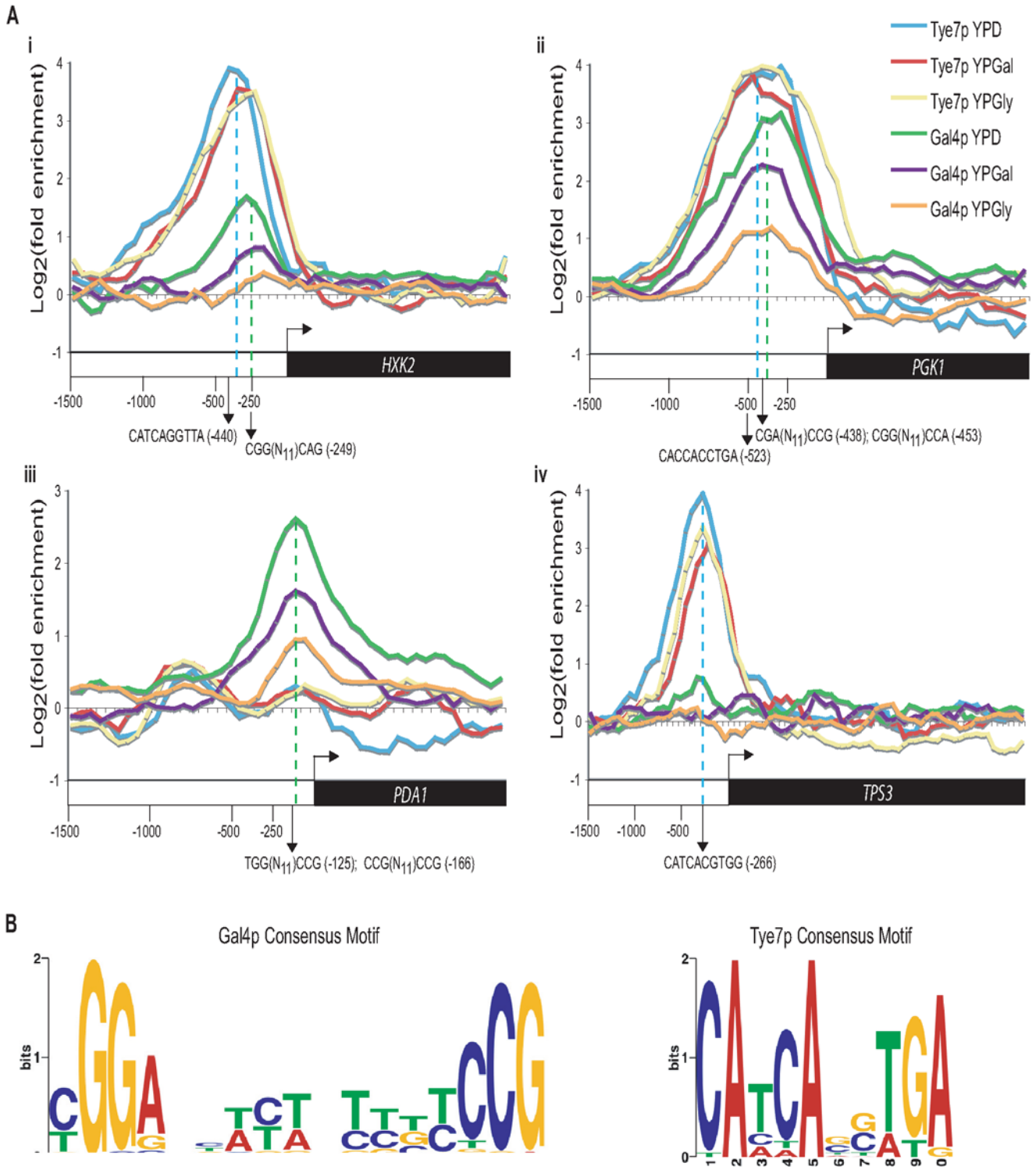

Figure 7. Gal4p displays carbon source-dependent binding while Tye7p binds its targets constitutively. (A) Binding of Gal4p and Tye7p to *HXK2* (i), *PGK1* (ii), *PDA1* (iii), and *TPS3* (iv) under glucose, galactose, and glycerol growth conditions with the tiling array. *HXK2* and *PGK1* represent common glycolytic targets while *PDA1* and *TPS3* represent Gal4p and Tye7p specific targets, respectively. The ORF and 1500 bp upstream region is shown. Values for each data point were determined by taking the mean fold enrichment of each probe and the surrounding four probes. The dashed blue and green lines represent the Tye7p and Gal4p binding sites, respectively (approximated over the three carbon sources). The consensus motifs and their positions are indicated for each factor. (B) Consensus motifs based on the top 30 peak intensities from the tiling array for Gal4p and Tye7p on glucose media. The sequence surrounding the peak point (covering 5 probes, 300 bp) for each target was sent to MEME (http://meme.sdsc.edu/meme4/) and the most significant motif (Gal4p: $E = 9.3E\text{-}24$; Tye7p: $E = 1.8E\text{-}15$) is reported.
doi:10.1371/journal.ppat.1000612.g007

are associated with these oxygen poor conditions and the glycolytic genes are known to be up-regulated in response to hypoxia in *C. albicans* [39], we tested the ability of our deletion strains to grow in oxygen-limiting environments. The *gal4* strain was unaffected but the *tye7* and *gal4tye7* strains displayed a severe growth defect (Figure 8A). This defect was observed not only at 30°C but also at 37°C, the human physiological temperature (Figure S5A). This is further validation for Gal4p and Tye7p's role in fermentative metabolism.

To confirm that Tye7p is responsible for the induction of the glycolytic genes under hypoxic conditions we repeated the expression profile under glucose growth conditions in the presence of nitrogen instead of oxygen (for complete lists see Tables S14 and S15). As observed under oxygen rich (normoxic) growth conditions, the glycolytic genes were down-regulated (Figure 8B and Table S7). However, there were some differences compared to the normoxia profile. First, some metabolic genes altered their expression to adjust to the low oxygen environment in the absence of the key glycolytic activator. These changes include the up-regulation of gluconeogenesis-specific genes, glycerol synthesis genes, pentose phosphate pathway genes, and the PDH genes, all of which were either down-regulated or not significantly regulated in the normoxia profile. The lack of a fully functional glycolytic pathway would result in gluconeogenesis stimulation, glycerol synthesis is an alternative to ethanol fermentation to regenerate NAD+, the pentose phosphate pathway is an alternative to glycolysis to generate reducing equivalents, and increasing PDH expression would promote respiration for any of the available pyruvate. Second, *GAL4* expression was significantly up-regulated (5.5 fold compared to 1.4 fold in normoxic conditions). This up-regulation also explains the increase in PDH expression and is likely why some glycolytic genes were not as significantly down-regulated. Third, the expression of many more genes was altered in the hypoxia profile, but many of these could be attributed to the significant growth defect of the *tye7* strain (doubling time was approximately 220 min compared to the wild type at around 110 min). We chose to just focus on the effect on metabolic gene expression as we had already established Tye7p as a metabolic regulator under normoxic conditions.

Based on the reduced growth rate of the *gal4tye7* strain compared to the *tye7* strain in low oxygen growth conditions, we assumed that Gal4p was also involved in the induction of the glycolytic genes. The expression profile with the *gal4tye7* strain was not done due to the severe growth defect. However, to confirm our hypothesis we transferred normoxia grown cultures to low oxygen conditions for 30 min and analyzed glycolytic gene expression by qPCR. The *gal4tye7* strain showed a significant further down-regulation compared to the *tye7* strain (Figure 8C).

To ensure our hypoxia experimental set-up was accurate and that the glycolytic genes were induced, we compared the wild type strain under hypoxic and normoxic conditions (Figure 8B and Table S7). Our results agreed well with previously published data [39] as glycolytic, fermentation, stress response, cell wall, fatty acid, iron metabolism, and hyphae-specific genes were up-regulated while TCA cycle, respiration, and ATP-synthesis genes were down-regulated (for complete lists see Tables S16 and S17).

Surprisingly, *TYE7* and *GAL4* expression appeared down-regulated in the wild type under hypoxia. Recently, it has been shown that the glycolytic genes can be rapidly induced under hypoxia before subsequently declining [40]. This dynamic expression is especially true for transcription factors that must be quickly up-regulated to activate their target genes but may become down-regulated once their target genes have reached their needed expression levels. Therefore, we measured the levels of *TYE7*, *GAL4*, and the glycolytic gene *CDC19* at four different time points following a shift to hypoxic growth conditions (Figure S6). We observed a rapid increase in *TYE7* and *GAL4* expression in the first 15 minutes followed by a sharp decline. In contrast, *CDC19* induction was longer and the decline less drastic. Thus, *TYE7* and *GAL4* are initially induced by hypoxia to activate the glycolytic genes before they are subsequently down-regulated.

Complete glycolytic activation by Gal4p and Tye7p is required for full virulence

Since metabolic flexibility and growth under low oxygen conditions are important for pathogens, we investigated the effect of deleting *GAL4* and *TYE7* on the virulence of *C. albicans*. We chose to first test all of our strains using the greater wax moth *Galleria mellonella* as a host model. Screening the virulence of *C. albicans* strains in *Galleria* has been shown to produce similar results to those measured through systemic infections with mice [41]. As controls, injections of PBS or UV/heat-killed BWP17 did not kill any *Galleria* over seven days, demonstrating that any death was attributable to viable *C. albicans* cells. The *gal4* strain showed a minor, but significant ($P = 0.008$, log-rank test) difference compared to the wild type, while both the *tye7* and *gal4tye7* strains showed very significant ($P < 0.0001$, log-rank test) attenuated virulence (Figure 9). These results correlate with the observed growth defects under hypoxic conditions. If the mutant strains grow slower than the wild type due to a lower oxygen environment inside the insect, the insect is able to survive for a longer period of time.

The double mutant strain was also tested in two mouse models, A/J and C57BL/6J, to support the result from the *Galleria* model and allow for further analysis. The A/J strain is C5 deficient and is highly sensitive to systemic infection with *C. albicans* while the C57BL/6J strain is C5 sufficient and therefore is less sensitive [42]. As with the *Galleria* model, the *gal4tye7* strain displayed significant attenuated virulence in both A/J ($P = 0.0009$, log-rank test) and C57BL/6J ($P = 0.0007$) mouse models (Figure 10A).

Fungal loads from different tissues were examined. For the A/J mice, two sets of six mice were injected with the *gal4tye7* strain. Fungal loads for the first set were determined 24 hours after injection, when the mice challenged with the wild type and revertant strains were euthanized due to moribundity. Fungal loads from the kidney, liver, and heart were significantly lower ($P = 0.002$, 0.002, and 0.009, respectively, Mann-Whitney test) in the *gal4tye7* infected mice compared to mice challenged with the wild type strain (Figure 10B and Table 2). The fungal load of the second set was determined when the *gal4tye7* infected mice became moribund. The fungal burden of this set showed comparable levels to the mice injected with the wild type strain (Figure 10B and Table 2). For the C57BL/6J mice, kidney fungal loads were determined following euthanization due to moribundity or survival until day 21. Five of the six C57BL/6J mice challenged with the *gal4tye7* strain survived until day 21 and four of them completely cleared the infection (Figure 10B).

Histological examination showed *in vivo* hyphae formation of the mutant strain in the kidney of A/J mice (Figure 10C) and confirmed the observations that the *gal4tye7* strain is able form hyphae in the presence of serum, N-acetylglucosamine, and spider media *in vitro* (data not shown). These results further support the hypothesis that the reduced virulence of the double mutant strain is attributed to a growth defect due to low oxygen environments in the host, which allows the organism to survive with the infection for a longer time and increases the chance the host's immune system is able to clear the infection.

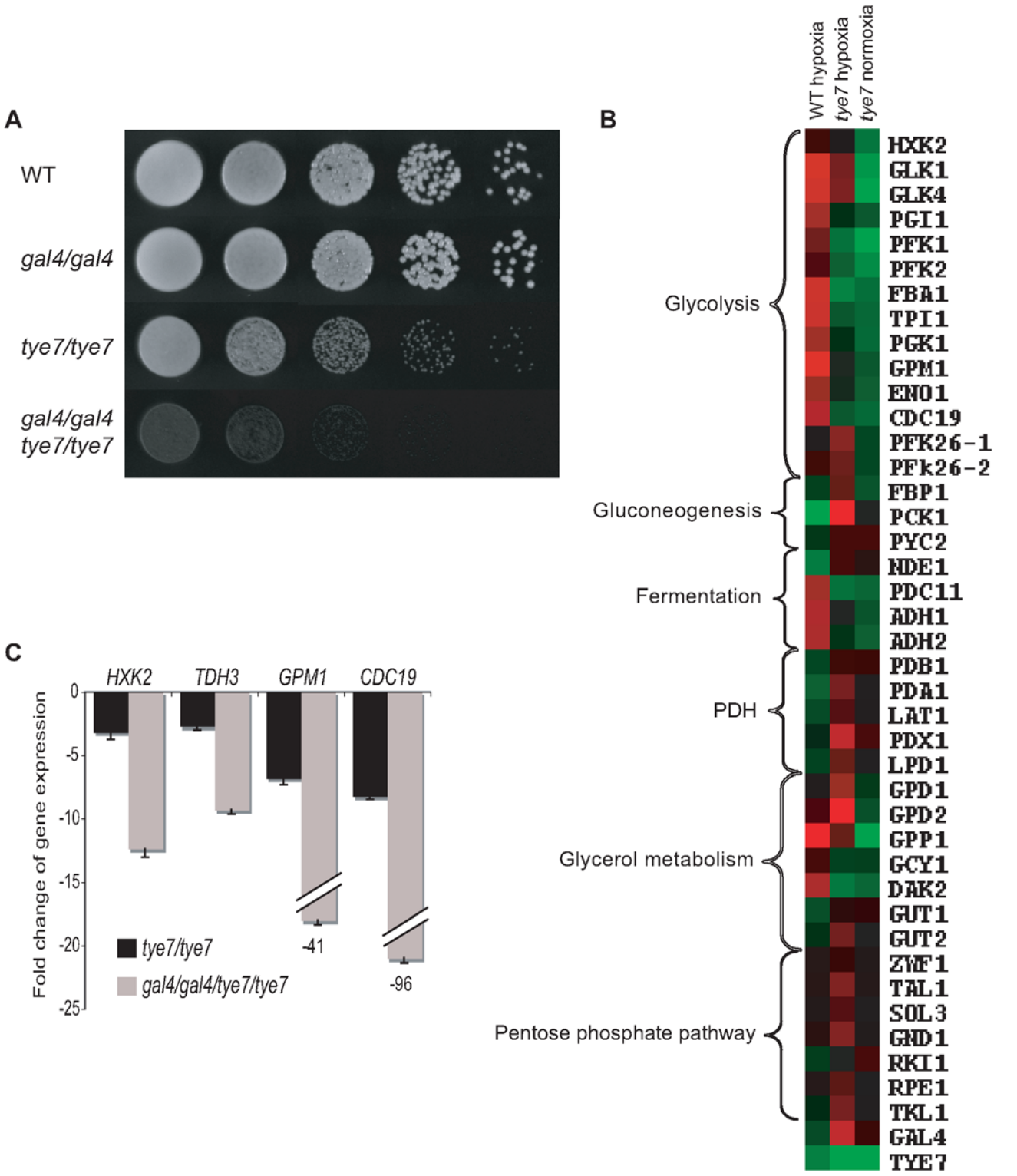

Figure 8. *TYE7* and *GAL4* are important for hypoxic growth and the induction of glycolytic genes in a low oxygen environment. (A) Cells were serially diluted, plated on YPD, and incubated in an anaerobic chamber at 30°C for 4 days. The chamber was flushed daily with nitrogen. Due to the space limitation of the chamber, the revertant strains were unable to be spotted on the same plate. A second experiment including the revertant strains was done on two separate plates to verify the results (Figure S5B). (B) Heat map displays were created as described in Figure 4. Transcription profiles of selected metabolic genes for (from left to right) BWP17 hypoxia relative to BWP17 normoxia, *tye7* hypoxia relative to BWP17 hypoxia, and *tye7* normoxia relative to BWP17 normoxia. The expression levels of these and other metabolic genes are given in Table S7. (C) The expression levels of several glycolytic genes were measured by qPCR in the *tye7* and *gal4tye7* strains relative to the wild type (BWP17) after 30 min of growth under hypoxic conditions. *ACT1* was used as the reference.
doi:10.1371/journal.ppat.1000612.g008

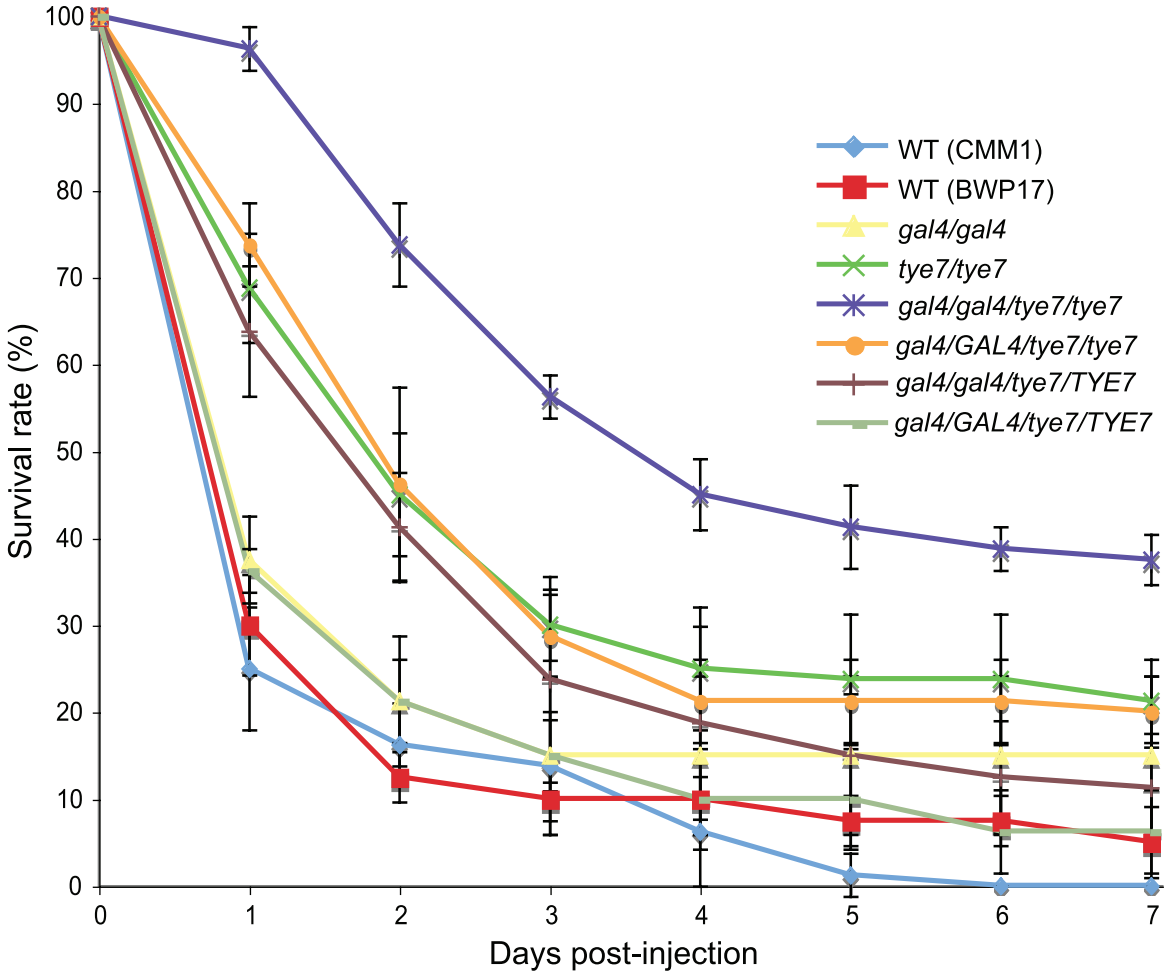

Figure 9. *GAL4* and *TYE7* are required for full virulence in a *Galleria* model. The survival curves for the indicated strains are shown. Each point represents the average daily survival rate based on four replicates of 20 insects. The BWP17 and CMM1 survival curves were not significantly different ($P>0.05$, log-rank test), demonstrating the limited effect of histidine and arginine auxotrophies.
doi:10.1371/journal.ppat.1000612.g009

Discussion

Although fungi generally have similarly designed metabolic pathways, their transcriptional regulation of these pathways can be quite different, as illustrated by the human fungal pathogen *C. albicans* and the non-pathogenic yeast *S. cerevisiae*. Crabtree-positive yeasts, such as *S. cerevisiae*, have developed a circuit that represses the respiration pathway and up-regulates the glycolytic/fermentation pathway in the presence of excess glucose even under aerobic conditions. In contrast, *C. albicans* is Crabtree-negative and prefers to completely oxidize carbohydrates through the respiration pathway in aerobic conditions, only relying on the fermentation pathway in the absence of oxygen. Furthermore, *C. albicans* up-regulates the glycolytic pathway in low oxygen conditions while *S. cerevisiae* does not [39]. These metabolic responses of *C. albicans* are similar to the majority of fungi and other eukaryotes. Therefore, it is important to extend our understanding of transcriptional control of carbohydrate metabolism beyond *S. cerevisiae* to other organisms.

Although the glycolytic transcriptional circuit has been studied in the yeast *Kluyveromyces lactis* [19,43], which lacks the glucose repression circuit, this organism is closely related to *S. cerevisiae* and its glycolytic genes are mainly regulated by orthologs of Gcr1p and Gcr2p. It appears that *K. lactis* is an intermediate between *S. cerevisiae* and the majority of aerobic fungi that do not contain *GCR1/2* homologs and therefore it is not a representative model of Crabtree-negative fungi. We characterized Tye7p and Gal4p, two transcriptional activators of the glycolytic pathway in *C. albicans*, which lacks *GCR1/2* homologs. Deleting both factors resulted in a severe growth defect during culture on several fermentable carbon sources (glucose, fructose, and mannose) when respiration was inhibited or oxygen was limited; the single mutant *gal4* strain showed no growth defects while the *tye7* strain displayed a slight growth defect under these conditions. All deletion strains grew at near wild type levels on a non-fermentable carbon source or with fermentable sources when the respiration pathway was not disrupted.

ChIP-CHIP and transcription profiling revealed that both Tye7p and Gal4p are directly involved in the activation of the entire glycolytic pathway. Tye7p bound all the glycolytic promoters in a carbon source-independent manner and the *tye7* strain showed a down-regulation of these genes that was most significant in glucose growth conditions. Gal4p binding to the promoter sequences of the glycolytic genes was affected by the carbon source with a decrease in binding from glucose to galactose to glycerol. Gal4p's role in the activation of these genes was also

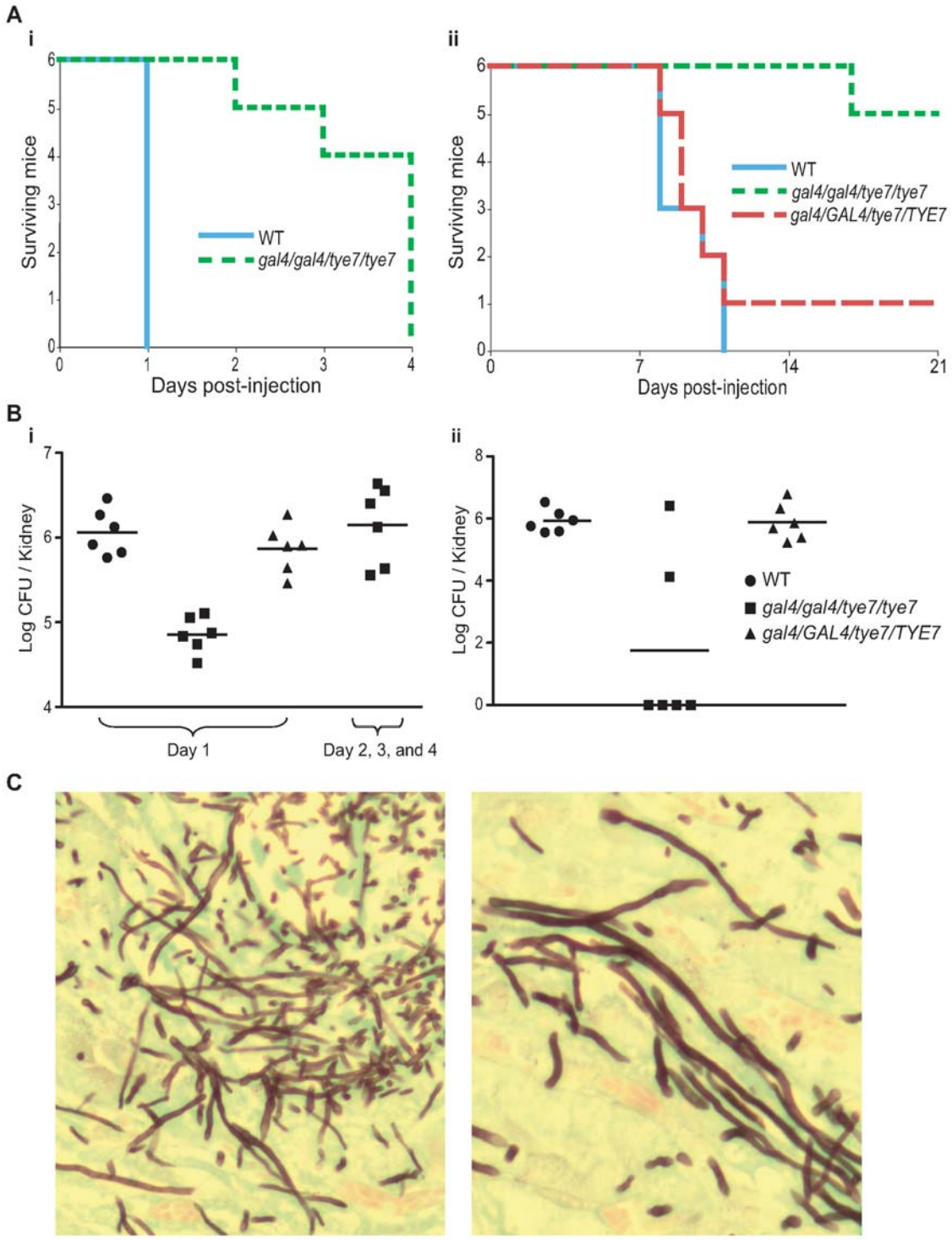

Figure 10. The *gal4tye7* strain shows attenuated virulence in both A/J and C57BL/6J mouse models. (A) A/J (i) and C57BL/6J (ii) mice were injected with either wild type (CAS8), *gal4/gal4/tye7/tye7* (CAS9), or *gal4/GAL4/tye7/TYE7* (CAS10) strains. A/J mice were monitored until considered moribund while C57BL/6J were monitored over a 21 day period. The revertant strain was omitted from the A/J graph since all six mice were euthanized on day 1 and would be masked by the wild type line. (B) (i) The kidney fungal load was determined 24 hours after injection for the A/J mice. Mice infected with the *gal4tye7* strain had approximately ten times less *C. albicans* cells than the mice challenged with either the wild type or revertant strains. Another fungal load of *gal4tye7* infected mice was determined upon moribundity and showed comparable levels to the mice injected with the wild type strain after 24 hours. (ii) The kidney fungal load was determined upon euthanization of C57BL/6J mice when moribundity was determined or mice survived until day 21. (C) Kidney sections of A/J infected mice were taken after euthanization and *C. albicans* cells were revealed with the Grocott-Gomori methenamine-silver stain. Pictures shown are from tissue infected with the *gal4tye7* strain indicating hyphal formation. There was no obvious difference compared to sections taken from kidneys infected with wild type or revertant strains (data not shown).
doi:10.1371/journal.ppat.1000612.g010

Table 2. Fungal loads of selected tissues from A/J infected mice.

Strain	Mean burden (log CFU/organ)					
	Day 1			Day 2, 3, and 4		
	Kidney	Liver	Heart	Kidney	Liver	Heart
WT	6.1±0.3	4.2±0.2	4.0±0.5	N/A	N/A	N/A
gal4/gal4/tye7/tye7	4.9±0.2	3.5±0.3	2.7±0.6	6.1±0.5	4.0±0.3	4.0±0.4
gal4/GAL4/tye7/TYE7	5.9±0.3	3.9±0.3	3.7±0.5	N/A	N/A	N/A

doi:10.1371/journal.ppat.1000612.t002

carbon source-dependent with the strongest effect during growth on glucose and galactose. Furthermore, transcription profiling and qPCR confirmed that both Tye7p and Gal4p are involved in the induction of the glycolytic genes under hypoxic growth conditions.

Gal4p and Tye7p also regulated metabolic processes linked to the glycolytic pathway. Some of these roles are common while some are independent of one another. Tye7p bound to and activated many genes involved in trehalose and glycogen metabolism without Gal4p's involvement. As well, Tye7p strongly activated the genes encoding phosphofructokinase, which catalyzes an irreversible glycolytic-committing reaction. We showed that deleting *TYE7* increases the levels of trehalose and glycogen, likely a result of the severely reduced glycolytic flux due to the extremely low expression of *PFK1* and *PFK2*. Deleting *GAL4* had no effect on the storage carbohydrate levels. Therefore, Tye7p has a role in determining whether glucose is stored or utilized for energy derivation, similar to Gcr1p in *S. cerevisiae* [44,45]. Coordinately regulating this flux ensures that the cell is committed either to storing energy or producing energy as to avoid futile cycling; therefore, it is logical that the key glycolytic activator also regulates trehalose and glycogen metabolism.

Another equilibrium that requires regulation is the flux between fermentation and respiration. This flux depends on the competition for pyruvate between pyruvate decarboxylase (PDC) and the pyruvate dehydrogenase complex (PDH) [46]. In *S. cerevisiae*, glucose induces PDC expression to promote fermentation while the PDH genes are unaffected and the TCA cycle is repressed [21]. In *A. oryzae* and *N. crassa*, both the PDC and PDH are induced by glucose and the TCA cycle is not repressed [28,29]. Increasing the transcription level of the PDH may be a mechanism employed by Crabtree-negative cells to allow the PDH to outcompete PDC, thereby increasing the respiratory capacity of the cell. Both Gal4p and Tye7p bound to and activated the genes involved in fermenting pyruvate to ethanol indicating that these factors regulate the entire fermentation process from glucose to ethanol. However, only Gal4p bound and activated the PDH genes suggesting that it plays an important role in the metabolic flux of the cell in directing respiration vs. fermentation modes. Consequently, Gal4p has an indirect effect on the TCA cycle. Although Gal4p did not bind the promoter sequences of the TCA cycle genes in the ChIP-CHIP profile (except *LSC1/2*), deleting *GAL4* subsequently results in the down-regulation of the PDH genes and ultimately several TCA cycle genes [34].

Therefore, although both Gal4p and Tye7p are key regulators of the glycolytic pathway, each has its own distinct role. Tye7p is the central transcriptional regulator of carbohydrate metabolism that provides a strong basal level of glycolytic expression while controlling the flux into the pathway and committing the cell to glycolysis. Gal4p is a carbon source-dependent regulator that fine-tunes gene expression based on the cells' need for the fermentation pathway. It assists Tye7p by increasing glycolytic gene expression during growth on fermentable carbon sources. In the presence of fermentable carbon sources Gal4p is able to significantly enhance the energy producing part of the glycolytic pathway and promote respiration by activating the PDH to meet the increased energy needs of the cell and minimize the dependence on fermentation. This assistance is not required with non-fermentable carbon sources as the glycolytic flux is lower since gluconeogenesis is stimulated and the cells grow at a slower rate with reduced energy needs.

The most common types of antifungal drugs for *C. albicans* infections, azoles, polyenes, and echinocandins, target cell membrane and cell wall integrity; however, targeting fungal metabolism could provide for future drug development. The importance of glycolysis to *C. albicans'* pathogenicity has been shown as deleting *CDC19* causes avirulence while a conditional mutant of *FBA1* results in attenuated virulence [3,4]. Since the components of metabolic pathways are generally highly conserved, orthologs exist in humans reducing interest in these functions as potential drug targets (i.e. *C. albicans CDC19* has approximately 50% amino acid identity with human pyruvate kinases). However, Gal4p and Tye7p are fungal-specific regulators and therefore represent potential antifungal targets. *GAL4* and *TYE7* were shown to be important for the virulence in a *Galleria* and two mouse models. This virulence effect is likely a result of a growth defect due to the low oxygen conditions that are present in invasive infections. The ability of two-thirds of the *gal4tye7* injected C57BL/6J mice to clear the infection highlights the real potential of Gal4p and Tye7p as drug targets. Although the double mutant strain did show significant attenuated virulence in all three host models, it was not avirulent. This is likely attributed to the metabolic flexibility of *C. albicans* and its ability to use alternative carbon sources. The importance of alternative carbon metabolism to *C. albicans'* pathogenicity has been previously demonstrated as deleting key enzymes of the glyoxylate cycle, gluconeogenesis, and ß-oxidation pathways reduces virulence [3,47,48].

It appears that Gal4p and Tye7p have altered their function throughout the evolution of fungi. We analyzed other genomes in the Saccharomycotina subphylum and observed a pattern relating the presence of *GCR1/2* homologs and the clustering of the Gal4p motif. Species that possess *GCR1/2* homologs have an enrichment of the Gal4p motif upstream of the *GAL* regulon genes while species lacking *GCR1/2* homologs have an enrichment of the Gal4p motif in the promoter regions of the glycolytic genes. Therefore, it appears that the rewiring of Gal4p coincides with the loss/gain of *GCR1/2*, and that Gal4p and Tye7p likely regulate glycolysis in the Saccharomycotina species lacking *GCR1/2* homologs. Intriguingly, this rewiring event also appears to coincide with changes in the galactose sensory network [49].

Along with the ribosomal transcriptional network [50,51], the transcriptional regulatory control of glycolysis represents an example of the plasticity of circuits throughout the evolution of fungi. The Rap1p ribosomal circuit and the Gcr1p/Gcr2p glycolytic circuit are unique to *S. cerevisiae* and closely related species, suggesting that the transcriptional networks of *S. cerevisiae* are not representative models of the fungal kingdom. However, there is a key distinction between these two rewiring events. While the regulatory components of the ribosomal network are different, the ultimate outcome is identical. On the other hand, carbon metabolism regulation is fundamentally different between *Saccharomyces* and other eukaryotes suggesting that the entire carbohydrate transcriptional network has undergone rewiring, not just the regulators. Thus, investigating the regulation of carbon metabo-

lism in Crabtree-negative organisms is important as little can be extrapolated based on *S. cerevisiae*. This study thus defines the key regulatory elements of glycolytic gene expression and provides insights into the mode of transcriptional regulation of carbohydrate metabolism in a typical eukaryotic cell and a human pathogen.

Materials and Methods

C. albicans strains and media

The *C. albicans* strains used in this study are listed in Table S18. Cells were generally grown at 30°C in media containing 1% yeast extract, 2% peptone, with either 2% dextrose (YPD), 2% galactose (YPGal), or 2% glycerol (YPGly). All media was supplemented with uridine (50 μg/ml).

Strain constructions

Plasmids and oligonucleotides used in this study are listed in Tables S19 and S20, respectively. Gal4p and Tye7p were tagged chromosomally with a TAP-*URA3* PCR product [52]. Transformations were carried out using standard procedures [53]. Correct integration of the TAP-tag was confirmed by PCR, and western blots were used to verify protein expression.

BWP17 was used for generating the *tye7* strain. CMM3 (*gal4*) [34] was used to generate the *gal4tye7* strain. The deletion and complementation strains were created using the *SAT1*-flipper cassette as described [54] with some modifications. The *tye7* disruption construct was created by cloning 500 bp flanking sequences of *TYE7* into the plasmid pSFS2A. The plasmid was linearized prior to transformation. Transformants were selected on YPD plates containing 200 μg/ml of nourseothricin and confirmed by PCR. Excision was performed by incubation at 30°C for 5 hours in YP media with 2% maltose before plating on YPD plates. Confirmation of excision events was done by PCR. The process was repeated for disruption of the second allele. Revertants of *tye7* and *gal4* were created using the *gal4tye7* strain. Complementation of *tye7* was carried out by reintroducing the ORF at its native locus by replacing the upstream flanking sequence in the *tye7* disruption cassette with the complete *TYE7* ORF. A complementation cassette that consisted of the complete *GAL4* ORF and a 500 bp downstream flanking sequence was constructed for reintroduction of *GAL4* at its native locus. We selected clones that replaced the *HIS1* deletion cassette and then restored histidine prototrophy by transformation with *Nru*I-digested pGEM-HIS1 [55].

CMM3 and CMM1 (wild type prototrophic equivalent of CMM3) [34] were also used in the phenotypic assays. In all assays BWP17 and CMM1 were used as control strains but they usually gave identical results so only one was generally shown. The exception was for the liquid growth curves as BWP17 plateaued at a lower OD_{600} than CMM1. In this case, the *tye7* strain was compared to BWP17 and normalized to CMM1 for graphical purposes.

As uridine auxotrophy affects virulence but can be restored by integration of *URA3* at the *RPS10* locus [56], for the mouse studies the CMM1, *gal4/gal4/tye7/tye7*, and *gal4/GAL4/tye7/TYE7* strains were made prototrophic by targeting the *URA3* marker to the *RPS10* locus through *Stu*I digestion of CIp10. Correct integration was confirmed by PCR and qPCR verified that only one copy of *URA3* was integrated.

Phenotypic assays

Serial spotting plate assays were carried out as described [57] except cells were washed twice with sterile water before plating. Cells were plated on synthetic complete media containing the carbon source at 0.2% or 2% and agarose at 2% to minimize carbon source impurities. Antimycin A (2 μg/ml) was added to inhibit respiration. For liquid assays, cells were grown to log phase in synthetic medium with 5% glycerol, washed twice with sterile water, and resuspended at an $OD_{600} = 0.1$ in synthetic media containing the carbon source at 2%. Cells were either grown at 30°C in flasks with shaking (aerobic conditions) or in microtiter plates without shaking (static conditions). Samples were done in triplicate and the average was used for analysis. For growth under hypoxic conditions, cells were spotted on YPD plates and incubated in an anaerobic chamber. The chamber was flushed daily with nitrogen to remove oxygen and any by-products.

ChIP-CHIP analysis

ChIP experiments were performed as previously described [52] with some modifications. Briefly, cells were grown to $OD_{600} = 2$ in 40 ml of YPD, YPGal, or YPGly. Tagged ChIPs were labeled with Cy5 dye and untagged (mock) ChIPs were labeled with Cy3 dye. Microarray hybridization and washing were performed as described [58]. Scanning was done with a ScanArray Lite microarray scanner (Perkin Elmer). QuantArray was used to quantify fluorescence intensities. Data handling and analysis were carried out using Genespring v.7.3 (Agilent Technologies). The significance cut-off was determined using the distribution of log-ratios for each factor. A minimum of three biological replicates were analyzed for each carbon source condition with hybridization to single spot full-genome (ORF and intergenic) microarrays containing 11,817 70-mer oligonucleotide probes [52]. For determining the number of targets and GO analysis with the single probe microarrays, the cut-off was a fold enrichment >1.5 and a t-test P-value<0.1.

One replicate of the ChIP-CHIP experiments for each carbon source condition was hybridized to a custom designed whole-genome tiling array for further analysis. Using the *C. albicans* Genome Assembly 21 [59] and the *MTL* alpha locus [60], we extracted a continuous series of 242,860 60 bp oligonucleotides each overlapping by 1 bp. We eliminated 2062 probes containing stretches of at least 13 A/T nucleotides. The remaining 240,798 probes were used to produce a whole-genome tiling array using the Agilent Technologies eArray service (https://earray.chem.agilent.com/erray/).

Tiling array data processing and peak detection

Lowess normalization of the intensity ratio of each of the 240,798 probes was done using an in-house software implementation. The signal along each chromosome was smoothed using a median filter ($n = 3$) followed by a Gaussian low-pass filter ($\sigma = 150$ bp). For peak localization, the smoothed signal was interpolated at 10 bp intervals using cubic-spline resampling. Peaks were reported in decreasing order of the smoothed intensities.

RNA extraction and transcription profiles

RNA was extracted with the RNeasy Kit (Qiagen) as per manufacturer's instructions. Briefly, cells were grown to $OD_{600} = 0.8$ in YPD, YPGal, or YPGly in aerated flasks (normoxia) and disrupted using acid washed glass beads. Transcriptional profiling was carried out as described [58] with 20 μg of RNA used for cDNA synthesis. A minimum of three biological replicates on double spotted ORF microarrays (6,394 intragenic 70-mer oligonucleotide probes) were used for analysis [58]. Scanning and analysis were carried out as described for ChIP-CHIP except scanning was performed at two different laser

PMTs to avoid saturated signals for a few highly expressed transcripts including several glycolytic genes. For GO analysis and the supplementary complete lists the cut-off was a difference in expression >1.5 or <0.67 and a t-test *P*-value<0.05.

Expression profiles under hypoxic conditions were performed as described above except bottles containing YPD media were flushed with nitrogen to remove oxygen. Two biological replicates were performed and statistical analysis was done as with normoxic conditions.

For qPCR analysis of glycolytic gene expression under hypoxic conditions, BWP17, *tye7*, and *gal4tye7* cultures were grown to $OD_{600} = 0.7$ in YPD in an aerated flask. The cultures were then transferred to bottles flushed with nitrogen and grown for an additional 30 min before the RNA was extracted as above and analyzed by qPCR.

For hypoxic induction kinetic analysis, BWP17 was grown to $OD_{600} = 0.8$ in YPD in an aerated flask. Half the culture was transferred to bottles flushed with nitrogen while the other half was left to grow in the aerated flask. At different time points the RNA was extracted and compared by qPCR.

qPCR analysis

For qPCR, cDNA was synthesized from 5 µg of total RNA using the reverse-transcription system (50 mM Tris-HCl, 75 mM KCl, 5 mM DTT, 3 mM $MgCl_2$, 400 nM oligo$(dT)_{15}$, 1 µM random octamers, 0.5 mM dNTPs, 200 units Superscript III reverse transcriptase; Invitrogen). The mixture was incubated for 60 min at 50°C. Aliquots were used for qPCR, which was performed using the Corbett Rotor-Gene RG3000A (Corbett Research) with SYBR Green fluorescence (Qiagen). Cycling was 10 min at 95°C followed by 40 cycles (95°C, 10 s; 58°C, 15 s; 72°C, 20 s). Samples were done in triplicate and means were used for calculations. Fold changes were estimated using the comparative ΔΔCt method as described [61] with the coding sequence of the *C. albicans ACT1* ORF as a reference.

Measuring trehalose and glycogen levels

Trehalose levels were measured as based on previous studies [62]. Briefly, cells were either grown to log phase ($OD_{600} = 2$) or grown for 40 hours to reach stationary phase, washed twice with cold water, and resuspended in water. Cells were lysed by incubating at 95°C for 30 min and the supernatant was used for enzymatic analysis. Reactions (50 µl of sample, 100 µl 270 mM citric acid buffer pH 5.7, and 0.15 U trehalase (Sigma)) were incubated at 37°C for 5 hours. Glucose amounts were assayed with the hexokinase glucose kit (Sigma) with endogenous glucose levels determined based on reactions without trehalase. A BCA protein assay (Pierce) was performed as per manufacturer's instructions. Relative trehalose levels were based on nmol trehalose per mg of cell protein. Three biological replicates were performed for each strain and condition. Glycogen levels were estimated using the iodine vapor method [63]. Cells were serially diluted, spotted on YPD plates, and incubated for 24 hours at 30°C. The cells were then exposed to iodine vapor for 5 minutes.

Measuring protein expression levels

To determine the protein expression of Gal4p and Tye7p under different carbon sources, overnight cultures in YPD were diluted to $OD_{600} = 0.4$ and grown for 2 hours in fresh YPD. Cells were washed twice with sterile water and resuspended in YP, YPD, YPGal, or YPGly media and grown for an additional 3 hours. The cells were then washed with TBS buffer and lysed using acid washed glass beads (same lysis buffer as ChIP-CHIP except for addition of a phosphatase inhibitor cocktail (Roche)). The protein extract was clarified by centrifugation and a BCA protein assay (Pierce) was performed as per manufacturer's instructions. Gal4p and Tye7p were separated on a 10% SDS gel and transferred to a PVDF membrane. A rabbit polyclonal antibody directed against the TAP-tag (Open Biosystems) was used (1:2000 dilution). A mouse anti-actin monoclonal antibody (1:500 dilution, Chemicon) was used to probe actin as a loading control. HRP-conjugated anti-rabbit and anti-mouse secondary antibodies (Santa Cruz) were used (1:10,000 dilution). The HRP signal was revealed using the Lumi-Light Western Blotting Substrate (Roche).

Virulence studies

For *Galleria mellonella* studies, overnight cultures were washed twice with PBS and resuspended in PBS at $OD_{600} = 8$. Larvae, in the final instar, weighing 180±10 mg were injected between the third pair prothoracic legs with 10 µl of suspension (8×10^5 cells). Infected larvae were incubated at 37°C in the dark with excess of a multigrain diet supplemented with glycerol and vitamins [64]. Four replicates, each consisting of 20 insects, were carried out with survival rates measured daily for a period of 7 days. Death was determined based on the lack of response to touch and the inability to right themselves. A BWP17 culture was irradiated with UV for 2 hours and incubated at 95°C for 1 hour before injection to confirm that viable *C. albicans* cells were responsible for death. Kaplan-Meier survival curves were created and compared with the log-rank test (GraphPad Prism 5).

Mouse studies were carried out as previously described [65]. Briefly, 8–12 week-old A/J and C57BL/6J mice (Jackson Laboratories, Bar Harbor, ME) were inoculated via the tail vein with 200 µl of a suspension containing 3×10^5 *C. albicans* in PBS. Six mice, three female and three male, were used for each experimental group except for the *gal4tye7* injected A/J set where six females and six males were used. Mice were closely monitored and those showing extreme lethargy were considered moribund and were euthanized. Target organs were removed aseptically and homogenized in PBS before plating on YPD plates containing chloramphenicol (34 µg/ml). The number of yeast colonies per organ was determined, log-transformed, and compared using the Mann-Whitney test (GraphPad Prism 5). Comparative genomic hybridization (CGH) analysis was performed on all strains prior to injection to verify that no aneuploidy arose as a result of any of the genetic manipulations. All experimental procedures involving mice were approved by the Biotechnology Research Institute Animal Care Committee, which operated under the guidelines of the Canadian Council of Animal Care.

Supporting Information

Figure S1 Liquid assays verify that *GAL4* and *TYE7* are involved in fermentative growth with glucose, fructose or mannose as the carbon source. WT refers to strain CMM1. (A) Growth curves where strains were grown with aeration. (B) Growth curves where strains were grown without aeration.
Found at: doi:10.1371/journal.ppat.1000612.s001 (1.30 MB PDF)

Figure S2 Overlap of binding targets for Gal4p and Tye7p under glucose, galactose, and glycerol growth conditions. Peaks common to all three carbon sources had peak intensities >2 fold in all three conditions with the tiling array data. A peak was considered to be unique to a carbon source (or sources) if the peak intensity in the condition (or conditions) was >2 fold and the peak intensities in the remaining carbon sources were <1.4 fold. This result confirms that for most targets Gal4p displays carbon-

source dependent binding while Tye7p binding is more constitutive.
Found at: doi:10.1371/journal.ppat.1000612.s002 (0.53 MB PDF)

Figure S3 Both Gal4p and Tye7p are induced by glucose but Tye7p has a higher constitutive expression. Protein expression levels of Gal4p and Tye7p under different carbon sources are presented. YP media with no additional carbon source was included to establish the basal level of expression. Actin was used as the loading control.
Found at: doi:10.1371/journal.ppat.1000612.s003 (0.24 MB PDF)

Figure S4 qPCR validation of transcription profile results under oxygen rich growth conditions. Expression levels for *HXK2* (A), *CDC19* (B), and *TDH3* (C) were determined in *tye7* and *gal4tye7* strains relative to the wild type (BWP17) under normoxic growth conditions. *ACT1* was used as the reference. *TDH3* was included since its expression was unchanged according to the transcription profiles despite being bound by Gal4p and Tye7p (Figure 6A); however, qPCR showed that *TDH3* is indeed activated by Gal4p and Tye7p. We later discovered that there was a spotting problem with the *TDH3* probe for the particular set of microarrays used and therefore we omitted the gene from the expression profile heat map displays in Figures 4B, 6B, and 8B.
Found at: doi:10.1371/journal.ppat.1000612.s004 (0.30 MB PDF)

Figure S5 *GAL4* and *TYE7* are important for hypoxic growth at both 30°C and 37°C. (A) Strains were serially diluted on YPD plates and incubated in an anaerobic jar at 37°C for 2 days. WT refers to strain CMM1. (B) Strains were serially diluted on two separate YPD plates and incubated in an anaerobic jar at 30°C for 4 days. One representative dilution is shown. The WT for the top row is CMM1 and the WT for the bottom row is BWP17. One copy of either *GAL4* or *TYE7* is able to restore the growth defect of the double mutant strain although the *GAL4* revertant does not grow at wild type levels since *TYE7* is still deleted.
Found at: doi:10.1371/journal.ppat.1000612.s005 (1.67 MB PDF)

Figure S6 *GAL4* and *TYE7* are initially induced by hypoxia. The expression levels of *GAL4*, *TYE7*, and *CDC19* were measured in BWP17 by qPCR at different time points following a shift from normoxic to hypoxic growth conditions. *ACT1* was used as the reference.
Found at: doi:10.1371/journal.ppat.1000612.s006 (0.57 MB PDF)

Table S1 Doubling times under fermentative growth conditions.
Found at: doi:10.1371/journal.ppat.1000612.s007 (0.02 MB XLS)

Table S2 Gal4p ChIP-CHIP targets with glucose as the carbon source.
Found at: doi:10.1371/journal.ppat.1000612.s008 (0.03 MB XLS)

Table S3 Tye7p ChIP-CHIP targets with glucose as the carbon source.
Found at: doi:10.1371/journal.ppat.1000612.s009 (0.05 MB XLS)

Table S4 Top Gal4p YPD binding peaks with tiling array.
Found at: doi:10.1371/journal.ppat.1000612.s010 (0.02 MB XLS)

Table S5 Top Tye7p YPD binding peaks with tiling array.
Found at: doi:10.1371/journal.ppat.1000612.s011 (0.02 MB XLS)

Table S6 ChIP-CHIP binding enrichments of selected metabolic genes under different carbon sources.
Found at: doi:10.1371/journal.ppat.1000612.s012 (0.03 MB XLS)

Table S7 Expression levels of selected metabolic genes for *tye7* and *gal4tye7* strains under different carbon sources and oxygen levels.
Found at: doi:10.1371/journal.ppat.1000612.s013 (0.03 MB XLS)

Table S8 Genes down-regulated in *tye7* strain in glucose growth conditions.
Found at: doi:10.1371/journal.ppat.1000612.s014 (0.03 MB XLS)

Table S9 Genes down-regulated in *gal4tye7* strain in glucose growth conditions.
Found at: doi:10.1371/journal.ppat.1000612.s015 (0.03 MB XLS)

Table S10 Genes down-regulated in *tye7* strain in galactose growth conditions.
Found at: doi:10.1371/journal.ppat.1000612.s016 (0.02 MB XLS)

Table S11 Genes down-regulated in *gal4tye7* strain in galactose growth conditions.
Found at: doi:10.1371/journal.ppat.1000612.s017 (0.04 MB XLS)

Table S12 Genes down-regulated in *tye7* strain in glycerol growth conditions.
Found at: doi:10.1371/journal.ppat.1000612.s018 (0.03 MB XLS)

Table S13 Genes down-regulated in *gal4tye7* strain in glycerol growth conditions.
Found at: doi:10.1371/journal.ppat.1000612.s019 (0.03 MB XLS)

Table S14 Genes down-regulated in *tye7* strain in glucose hypoxic growth conditions.
Found at: doi:10.1371/journal.ppat.1000612.s020 (0.07 MB XLS)

Table S15 Genes up-regulated in *tye7* strain in glucose hypoxic growth conditions.
Found at: doi:10.1371/journal.ppat.1000612.s021 (0.05 MB XLS)

Table S16 Genes down-regulated in BWP17 strain in glucose hypoxic growth conditions.
Found at: doi:10.1371/journal.ppat.1000612.s022 (0.04 MB XLS)

Table S17 Genes up-regulated in BWP17 strain in glucose hypoxic growth conditions.
Found at: doi:10.1371/journal.ppat.1000612.s023 (0.05 MB XLS)

Table S18 Strains used in this study.
Found at: doi:10.1371/journal.ppat.1000612.s024 (0.03 MB XLS)

Table S19 Plasmids used in this study.
Found at: doi:10.1371/journal.ppat.1000612.s025 (0.02 MB XLS)

Table S20 Primers used in this study.
Found at: doi:10.1371/journal.ppat.1000612.s026 (0.02 MB XLS)

Dataset S1 ChIP-CHIP normalized tiling array data. Columns correspond to (L to R) Tye7p YPD, YPGal, YPGly; Gal4p YPD, YPGal, YPGly. The start (>) and end (|) of each ORF is indicated. Values given for each probe are $\log_2$ (fold enrichment) with negative values indicating enrichment for Gal4p or Tye7p binding. Significant binding events are highlighted in green.
Found at: doi:10.1371/journal.ppat.1000612.s027 (3.52 MB ZIP)

Acknowledgments

We are grateful to Hugo Lavoie for assistance with the ChIP-CHIP protocol. Thanks also to members of the BRI Microarray Lab and the BRI Animal Facility, especially Jean-Sébastien Deneault, Mario Mercier, and Jessy Tremblay for technical assistance. Finally, thanks to Gary Dunphy and Jason Lapointe for providing the *Galleria* insects and media. This is National Research Council manuscript 50659.

Author Contributions

Conceived and designed the experiments: CA AS. Performed the experiments: CA EE. Analyzed the data: CA AS HH. Wrote the paper: CA. Supervised the project: AM AN MW.

References

1. Daily JP, Scanfeld D, Pochet N, Le Roch K, Plouffe D, et al. (2007) Distinct physiological states of Plasmodium falciparum in malaria-infected patients. Nature 450: 1091–1095.
2. Rosso ML, Chauvaux S, Dessein R, Laurans C, Frangeul L, et al. (2008) Growth of Yersinia pseudotuberculosis in human plasma: impacts on virulence and metabolic gene expression. BMC Microbiol 8: 211.
3. Barelle CJ, Priest CL, Maccallum DM, Gow NA, Odds FC, et al. (2006) Niche-specific regulation of central metabolic pathways in a fungal pathogen. Cell Microbiol 8: 961–971.
4. Rodaki A, Young T, Brown AJ (2006) Effects of depleting the essential central metabolic enzyme fructose-1,6-bisphosphate aldolase on the growth and viability of Candida albicans: implications for antifungal drug target discovery. Eukaryot Cell 5: 1371–1377.
5. Costa M, Borges CL, Bailao AM, Meirelles GV, Mendonca YA, et al. (2007) Transcriptome profiling of Paracoccidioides brasiliensis yeast-phase cells recovered from infected mice brings new insights into fungal response upon host interaction. Microbiology 153: 4194–4207.
6. Chaudhuri RR, Peters SE, Pleasance SJ, Northen H, Willers C, et al. (2009) Comprehensive identification of Salmonella enterica serovar typhimurium genes required for infection of BALB/c mice. PLoS Pathog 5: e1000529. 10.1371/journal.ppat.1000529.
7. Chambers A, Packham EA, Graham IR (1995) Control of glycolytic gene expression in the budding yeast (Saccharomyces cerevisiae). Curr Genet 29: 1–9.
8. Clifton D, Weinstock SB, Fraenkel DG (1978) Glycolysis mutants in Saccharomyces cerevisiae. Genetics 88: 1–11.
9. Uemura H, Fraenkel DG (1990) gcr2, a new mutation affecting glycolytic gene expression in Saccharomyces cerevisiae. Mol Cell Biol 10: 6389–6396.
10. Baker HV (1991) GCR1 of Saccharomyces cerevisiae encodes a DNA binding protein whose binding is abolished by mutations in the CTTCC sequence motif. Proc Natl Acad Sci U S A 88: 9443–9447.
11. Uemura H, Jigami Y (1992) Role of GCR2 in transcriptional activation of yeast glycolytic genes. Mol Cell Biol 12: 3834–3842.
12. Clifton D, Fraenkel DG (1981) The gcr (glycolysis regulation) mutation of Saccharomyces cerevisiae. J Biol Chem 256: 13074–13078.
13. Nishi K, Park CS, Pepper AE, Eichinger G, Innis MA, et al. (1995) The GCR1 requirement for yeast glycolytic gene expression is suppressed by dominant mutations in the SGC1 gene, which encodes a novel basic-helix-loop-helix protein. Mol Cell Biol 15: 2646–2653.
14. Sato T, Lopez MC, Sugioka S, Jigami Y, Baker HV, et al. (1999) The E-box DNA binding protein Sgc1p suppresses the gcr2 mutation, which is involved in transcriptional activation of glycolytic genes in Saccharomyces cerevisiae. FEBS Lett 463: 307–311.
15. Heinisch J, Vogelsang K, Hollenberg CP (1991) Transcriptional control of yeast phosphofructokinase gene expression. FEBS Lett 289: 77–82.
16. Scott EW, Baker HV (1993) Concerted action of the transcriptional activators REB1, RAP1, and GCR1 in the high-level expression of the glycolytic gene TPI. Mol Cell Biol 13: 543–550.
17. Drazinic CM, Smerage JB, Lopez MC, Baker HV (1996) Activation mechanism of the multifunctional transcription factor repressor-activator protein 1 (Rap1p). Mol Cell Biol 16: 3187–3196.
18. Brindle PK, Holland JP, Willett CE, Innis MA, Holland MJ (1990) Multiple factors bind the upstream activation sites of the yeast enolase genes ENO1 and ENO2: ABFI protein, like repressor activator protein RAP1, binds cis-acting sequences which modulate repression or activation of transcription. Mol Cell Biol 10: 4872–4885.
19. Neil H, Lemaire M, Wesolowski-Louvel M (2004) Regulation of glycolysis in Kluyveromyces lactis: role of KlGCR1 and KlGCR2 in glucose uptake and catabolism. Curr Genet 45: 129–139.
20. Johnston M (1999) Feasting, fasting and fermenting. Glucose sensing in yeast and other cells. Trends Genet 15: 29–33.
21. DeRisi JL, Iyer VR, Brown PO (1997) Exploring the metabolic and genetic control of gene expression on a genomic scale. Science 278: 680–686.
22. Wolfe KH, Shields DC (1997) Molecular evidence for an ancient duplication of the entire yeast genome. Nature 387: 708–713.
23. Kellis M, Birren BW, Lander ES (2004) Proof and evolutionary analysis of ancient genome duplication in the yeast Saccharomyces cerevisiae. Nature 428: 617–624.
24. Merico A, Sulo P, Piskur J, Compagno C (2007) Fermentative lifestyle in yeasts belonging to the Saccharomyces complex. FEBS J 274: 976–989.
25. Gordon JL, Byrne KP, Wolfe KH (2009) Additions, losses, and rearrangements on the evolutionary route from a reconstructed ancestor to the modern Saccharomyces cerevisiae genome. PLoS Genet 5: e1000485. 10.1371/journal.pgen.1000485.
26. Thomson JM, Gaucher EA, Burgan MF, De Kee DW, Li T, et al. (2005) Resurrecting ancestral alcohol dehydrogenases from yeast. Nat Genet 37: 630–635.
27. Chambergo FS, Bonaccorsi ED, Ferreira AJ, Ramos AS, Ferreira Junior JR, et al. (2002) Elucidation of the metabolic fate of glucose in the filamentous fungus Trichoderma reesei using expressed sequence tag (EST) analysis and cDNA microarrays. J Biol Chem 277: 13983–13988.
28. Xie X, Wilkinson HH, Correa A, Lewis ZA, Bell-Pedersen D, et al. (2004) Transcriptional response to glucose starvation and functional analysis of a glucose transporter of Neurospora crassa. Fungal Genet Biol 41: 1104–1119.
29. Maeda H, Sano M, Maruyama Y, Tanno T, Akao T, et al. (2004) Transcriptional analysis of genes for energy catabolism and hydrolytic enzymes in the filamentous fungus Aspergillus oryzae using cDNA microarrays and expressed sequence tags. Appl Microbiol Biotechnol 65: 74–83.
30. Wisplinghoff H, Bischoff T, Tallent SM, Seifert H, Wenzel RP, et al. (2004) Nosocomial bloodstream infections in US hospitals: analysis of 24,179 cases from a prospective nationwide surveillance study. Clin Infect Dis 39: 309–317.
31. Gudlaugsson O, Gillespie S, Lee K, Vande Berg J, Hu J, et al. (2003) Attributable mortality of nosocomial candidemia, revisited. Clin Infect Dis 37: 1172–1177.
32. Wilson LS, Reyes CM, Stolpman M, Speckman J, Allen K, et al. (2002) The direct cost and incidence of systemic fungal infections. Value Health 5: 26–34.
33. Leroy O, Gangneux JP, Montravers P, Mira JP, Gouin F, et al. (2009) Epidemiology, management, and risk factors for death of invasive Candida infections in critical care: a multicenter, prospective, observational study in France (2005–2006). Crit Care Med 37: 1612–1618.
34. Martchenko M, Levitin A, Hogues H, Nantel A, Whiteway M (2007) Transcriptional rewiring of fungal galactose-metabolism circuitry. Curr Biol 17: 1007–1013.
35. Goffrini P, Ferrero I, Donnini C (2002) Respiration-dependent utilization of sugars in yeasts: a determinant role for sugar transporters. J Bacteriol 184: 427–432.
36. Lillie SH, Pringle JR (1980) Reserve carbohydrate metabolism in Saccharomyces cerevisiae: responses to nutrient limitation. J Bacteriol 143: 1384–1394.
37. Marmorstein R, Carey M, Ptashne M, Harrison SC (1992) DNA recognition by GAL4: structure of a protein-DNA complex. Nature 356: 408–414.
38. Massari ME, Murre C (2000) Helix-loop-helix proteins: regulators of transcription in eucaryotic organisms. Mol Cell Biol 20: 429–440.
39. Setiadi ER, Doedt T, Cottier F, Noffz C, Ernst JF (2006) Transcriptional response of Candida albicans to hypoxia: linkage of oxygen sensing and Efg1p-regulatory networks. J Mol Biol 361: 399–411.
40. Stichternoth C, Ernst JF (2009) Hypoxic adaptation by Efg1 regulates biofilm formation by Candida albicans. Appl Environ Microbiol 75: 3663–3672.
41. Brennan M, Thomas DY, Whiteway M, Kavanagh K (2002) Correlation between virulence of Candida albicans mutants in mice and Galleria mellonella larvae. FEMS Immunol Med Microbiol 34: 153–157.
42. Ashman RB, Bolitho EM, Papadimitriou JM (1993) Patterns of resistance to Candida albicans in inbred mouse strains. Immunol Cell Biol 71 (Pt 3): 221–225.
43. Lemaire M, Guyon A, Betina S, Wesolowski-Louvel M (2002) Regulation of glycolysis by casein kinase I (Rag8p) in Kluyveromyces lactis involves a DNA-binding protein, Sck1p, a homologue of Sgc1p of Saccharomyces cerevisiae. Curr Genet 40: 355–364.
44. Turkel S (2002) The GCR1 gene function is essential for glycogen and trehalose metabolism in Saccharomyces cerevisiae. Folia Microbiol (Praha) 47: 663–666.
45. Seker T, Hamamci H (2003) Trehalose, glycogen and ethanol metabolism in the gcr1 mutant of Saccharomyces cerevisiae. Folia Microbiol (Praha) 48: 193–198.
46. Pronk JT, Yde Steensma H, Van Dijken JP (1996) Pyruvate metabolism in Saccharomyces cerevisiae. Yeast 12: 1607–1633.
47. Lorenz MC, Fink GR (2001) The glyoxylate cycle is required for fungal virulence. Nature 412: 83–86.
48. Ramirez MA, Lorenz MC (2007) Mutations in alternative carbon utilization pathways in Candida albicans attenuate virulence and confer pleiotropic phenotypes. Eukaryot Cell 6: 280–290.
49. Brown V, Sabina J, Johnston M (2009) Specialized sugar sensing in diverse fungi. Curr Biol 19: 436–441.
50. Tanay A, Regev A, Shamir R (2005) Conservation and evolvability in regulatory networks: the evolution of ribosomal regulation in yeast. Proc Natl Acad Sci U S A 102: 7203–7208.
51. Hogues H, Lavoie H, Sellam A, Mangos M, Roemer T, et al. (2008) Transcription factor substitution during the evolution of fungal ribosome regulation. Mol Cell 29: 552–562.
52. Lavoie H, Sellam A, Askew C, Nantel A, Whiteway M (2008) A toolbox for epitope-tagging and genome-wide location analysis in Candida albicans. BMC Genomics 9: 578.
53. Ausubel FM, Brent R, Kingston RE, Moore DD, Seidman JG, et al. (1992) Struhl K, ed. New York: John Wiley and Sons.
54. Reuss O, Vik A, Kolter R, Morschhauser J (2004) The SAT1 flipper, an optimized tool for gene disruption in Candida albicans. Gene 341: 119–127.
55. Wilson RB, Davis D, Mitchell AP (1999) Rapid hypothesis testing with Candida albicans through gene disruption with short homology regions. J Bacteriol 181: 1868–1874.
56. Brand A, MacCallum DM, Brown AJ, Gow NA, Odds FC (2004) Ectopic expression of URA3 can influence the virulence phenotypes and proteome of Candida albicans but can be overcome by targeted reintegration of URA3 at the RPS10 locus. Eukaryot Cell 3: 900–909.
57. Bruno VM, Kalachikov S, Subaran R, Nobile CJ, Kyratsous C, et al. (2006) Control of the C. albicans cell wall damage response by transcriptional regulator Cas5. PLoS Pathog 2: e21. doi:10.1371/journal.ppat.0020021.

58. Nantel A, Rigby T, Hogues H, Whiteway M (2006) Microarrays for studying pathology in Candida albicans; Kavanaugh K, ed. HobokenNJ: Wiley Press.
59. van het Hoog M, Rast TJ, Martchenko M, Grindle S, Dignard D, et al. (2007) Assembly of the Candida albicans genome into sixteen supercontigs aligned on the eight chromosomes. Genome Biol 8: R52.
60. Hull CM, Johnson AD (1999) Identification of a mating type-like locus in the asexual pathogenic yeast Candida albicans. Science 285: 1271–1275.
61. Guillemette T, Sellam A, Simoneau P (2004) Analysis of a nonribosomal peptide synthetase gene from Alternaria brassicae and flanking genomic sequences. Curr Genet 45: 214–224.
62. Benaroudj N, Lee DH, Goldberg AL (2001) Trehalose accumulation during cellular stress protects cells and cellular proteins from damage by oxygen radicals. J Biol Chem 276: 24261–24267.
63. Chester VE (1968) Heritable glycogen-storage deficiency in yeast and its induction by ultra-violet light. J Gen Microbiol 51: 49–56.
64. Dunphy GB, Oberholzer U, Whiteway M, Zakarian RJ, Boomer I (2003) Virulence of Candida albicans mutants toward larval Galleria mellonella (Insecta, Lepidoptera, Galleridae). Can J Microbiol 49: 514–524.
65. Mullick A, Elias M, Picard S, Bourget L, Jovcevski O, et al. (2004) Dysregulated inflammatory response to Candida albicans in a C5-deficient mouse strain. Infect Immun 72: 5868–5876.

VII.4. Role of transcription factor CaNdt80p in cell separation, hyphal growth, and virulence in *Candida albicans*

Originally published in:
Eukaryot Cell. 2010 Apr;9(4):634-44. Epub 2010 Jan 22. || PMID: 20097739

EUKARYOTIC CELL, Apr. 2010, p. 634–644 Vol. 9, No. 4
1535-9778/10/$12.00 doi:10.1128/EC.00325-09

Role of Transcription Factor CaNdt80p in Cell Separation, Hyphal Growth, and Virulence in *Candida albicans*▽†

Adnane Sellam,[1,2] Christopher Askew,[1,3] Elias Epp,[1,3] Faiza Tebbji,[1,4] Alaka Mullick,[1,5] Malcolm Whiteway,[1,3] and André Nantel[1,2]*

Biotechnology Research Institute, National Research Council of Canada, Montréal, Québec H4P 2R2, Canada[1]; Department of Anatomy and Cell Biology, McGill University, Montréal, Québec H3A 1B1, Canada[2]; Department of Biology, McGill University, Montréal, Québec H3A 1B1, Canada[3]; Institut de Recherche en Biologie Végétale, Université de Montréal, Montréal, Québec H1X 2B2, Canada[4]; and Département de Microbiologie et Immunologie, l'Université de Montréal, Montréal, Québec, Canada[5]

Received 3 November 2009/Accepted 15 January 2010

The NDT80/PhoG transcription factor family includes ScNdt80p, a key modulator of the progression of meiotic division in *Saccharomyces cerevisiae*. In *Candida albicans*, a member of this family, CaNdt80p, modulates azole sensitivity by controlling the expression of ergosterol biosynthesis genes. We previously demonstrated that CaNdt80p promoter targets, in addition to *ERG* genes, were significantly enriched in genes related to hyphal growth. Here, we report that CaNdt80p is indeed required for hyphal growth in response to different filament-inducing cues and for the proper expression of genes characterizing the filamentous transcriptional program. These include noteworthy genes encoding cell wall components, such as *HWP1*, *ECE1*, *RBT4*, and *ALS3*. We also show that CaNdt80p is essential for the completion of cell separation through the direct transcriptional regulation of genes encoding the chitinase Cht3p and the cell wall glucosidase Sun41p. Consistent with their hyphal defect, *ndt80* mutants are avirulent in a mouse model of systemic candidiasis. Interestingly, based on functional-domain organization, CaNdt80p seems to be a unique regulator characterizing fungi from the CTG clade within the subphylum Saccharomycotina. Therefore, this study revealed a new role of the novel member of the fungal NDT80 transcription factor family as a regulator of cell separation, hyphal growth, and virulence.

Candida albicans is an opportunistic pathogen responsible for various non-life-threatening infections, such as oral thrush and vaginitis, and accounts for more than half of all *Candida* infections (21, 40). This pathogen is also a major cause of morbidity and mortality in bloodstream infections, especially in immunosuppressed individuals. In addition, *C. albicans* can colonize various biomaterials and readily forms dense biofilms that are resistant to most antifungal agents. The ability of this fungus to switch from yeast to filamentous forms (true hyphae or pseuohyphae) is a crucial determinant for host invasion and thus virulence (1). Hyphal growth can be initiated by different environmental cues, such as temperature, pH, or nutrient availability (1). Consequently, morphological switching implies a complex interplay of various sensing and signal transduction pathways, as well as transcriptional regulatory networks stimulating or repressing hyphal formation. Deciphering the molecular mechanisms that underlie this morphological switch is currently of high interest. Despite the large number of studies in recent years, the molecular determinism of *C. albicans* morphogenesis is still not fully understood.

The NDT80/PhoG transcription factor (TF) family includes the DNA-binding meiosis-specific protein ScNdt80p, a key modulator of the progression of the meiotic divisions in the yeast *Saccharomyces cerevisiae* (15, 33). This family also includes VIB-1, which is a regulator of conidiation in *Neurospora crassa* (41) and shares a region of similarity to PhoG, a possible non-phosphate-repressible acid phosphatase in *Aspergillus nidulans* (23). Structural studies revealed that this family is related to the Ig-fold family of transcription factors, which includes the human TFs p53, NF-κB, STAT, and AML-Runt and the Rel subfamilies (20, 24). All of these Ig-fold proteins bind DNA in similar manners, using loops and other features at one end of the β-sandwich. In *C. albicans*, a member of this family, named CaNdt80p (orf19.2119), has recently been identified as a key modulator of azole sensitivity due to its participation in the control of ergosterol biosynthesis gene expression (36). Genome-wide occupancy using chromatin immunoprecipitation coupled with high-density tiling arrays showed that, in addition to *ERG* genes, this TF bound a large number of gene promoters with diverse biological functions, such as cell wall, hyphal growth, carbohydrate metabolism, and the mitotic cell cycle. Additionally, *de novo* motif analysis of CaNdt80p-bound promoters revealed that, as in *S. cerevisiae*, this regulator bound to the middle sporulation element, 5′-gNCRCAAAY-3′, in *C. albicans* (where the lowercase letter indicates a semiconserved residue, R indicates a purine, N indicates any nucleotide, and Y indicates either a thymine or a cytosine).

The finding that CaNdt80p occupies the promoter regions of 23% of *C. albicans* genes suggests that the TF might control other biological processes, in addition to drug sensitivity (6,

* Corresponding author. Mailing address: Biotechnology Research Institute, National Research Council of Canada, 6100 Royalmount Ave., Montreal, Quebec H4P 2R2, Canada. Phone: (514) 496-6370. Fax: (514) 496-9127. E-mail: andre.nantel@nrc-cnrc.gc.ca.

† Supplemental material for this article may be found at http://ec.asm.org/.

▽ Published ahead of print on 22 January 2010.

TABLE 1. *Candida albicans* strains used in the study

Strain	Genotype	Source or reference(s)
BWP17	*his1*/*his1 ura3*/*ura3 arg4*/*arg4*	13, 39
DAY286	*his1*/*his1 ura3*/*ura3 arg4*/*arg4*::*pARG4*::*URA3*	8
AS31	*ndt80*::*HIS1*/*ndt80*::*URA3 arg4*/*arg4*	36
AS32	*ndt80*::*HIS1*/*ndt80*::*HIS1 arg4*/*arg4*	36
AS33	*ndt80*::*HIS1*/*ndt80*::*HIS1 RP10*/*rp10*::*pCIp10-NDT80 arg4*/*arg4*	36
AS40	*ndt80*::*HIS1*/*ndt80*::*HIS1 RP10*/*rp10*::*pCIpACT1-CHT3 arg4*/*arg4*	This study
AS41	*ndt80*::*HIS1*/*ndt80*::*HIS1 RP10*/*rp10*::*pCIpACT1-SUN41 arg4*/*arg4*	This study

TABLE 2. Primers used in the study

Primer name	Primer sequence	Purpose
Cht3F1	CGACGCGTATGCTATACTTGTT AACTATATTTTC	CHT3 overexpression
Cht3R1	CTAGCTAGCATTATAGATAACC ACTGTACTTGGT	
Sun41F1	ATGAGATTTTCACAAGCTAC TGTT	SUN41 overexpression
Sun41R1	CTAGCTAGCATTATACAAGACA AAGTCAGCTTC	
qCht3F2	ACTACCTCCACAGCACCAAC	qPCR
qCht3R2	GTAGAAGTGGCAGGTTTAGTTG	
qSun41F2	TGTGAATGGGGTGTCAAGAA	qPCR
qSun41R2	AGCACCACCTCTCCAAGTGT	
qAct1 F1	GAAGCCCAATCCAAAAGA	qPCR
qAct1 R1	CTTCTGGAGCAACTCTCAATTC	
qAls3 F1	CGGTTGCGACTGCAAAGAC	qPCR
qAls3 R1	GACCAACCCAAAACAGCATTCC	
qHwp1 F1	CAGTTCCACTCATGCAACCATC	qPCR
qHwp1 R1	GCAATACCAATAATAGCAGC ACCG	
qYwp1 F1	CTG ATA TTC GTA ATG CTG GTA AAG TG	qPCR
qYwp1 R1	GGA GTT TCA CCC ATT AAT CTT CTT C	
qEce1 F1	CCGGCATCTCTTTTAACTGG	qPCR
qEce1 R1	GAGATGGCGTTCCAGATGTT	
qCax4 F1	TCAATTCATGGGATTTTTCG	qPCR
qCax4 R1	CCCCGTAATTAATCCAGCAA	
qNrg1 F1	TGCAACCCCAACAAACACTA	qPCR
qNrg1 R1	TGACGTTGTTGATATGATGCTG	
qTec1 F1	TGGTGCTTATTCACGTGTCC	qPCR
qTec1 R1	GTGGTGGTCATGCCAATAGT	
qRBT4 F1	CGATGCTGATGGTGGTAATG	qPCR
qRBT4 R1	TTGGTCATCTGAAGGGAAGC	

36). Since CaNdt80p targets were significantly enriched in genes related to hyphal growth, this prompted us to study its potential role in morphological switching and host invasion. In this study, we continued to elucidate the multiple functions of CaNdt80p in *C. albicans* by demonstrating its central role in regulating cell separation, hyphal differentiation, and virulence. Interestingly, based on its functional-domain organization, CaNdt80p seems to be a unique TF characterizing fungi from the CTG clade within the subphylum Saccharomycotina.

MATERIALS AND METHODS

***C. albicans* strains, plasmids, and media.** The strains used in this study are listed in Table 1. For general propagation and maintenance conditions, the strains were cultured at 30°C in yeast-peptone-dextrose (YPD) medium supplemented with uridine (2% Bacto peptone, 1% yeast extract, 2% dextrose, and 50 μg/ml uridine, with the addition of 2% agar for solid medium). Cell growth, transformation, and DNA preparation were carried out using standard yeast procedures. For filamentation assays, cells were grown at 37°C in YPD supplemented with either 10% fetal bovine serum (Invitrogen) or 2.5 mM *N*-acetyl-D-glucosamine (Sigma) or in M199 medium (Sigma) buffered with 150 mM HEPES to pH 8.0. For growth under hypoxic conditions, cells were spotted on YPS (2% Bacto peptone, 1% yeast extract, 2% sucrose, 2% agar) plates and incubated in an anaerobic chamber (Oxoid; HP0011A) at 37°C. The chamber was flushed daily with nitrogen to remove oxygen and any by-products.

Cell separation defects were assessed as described previously (11), except that more than 500 cells were counted for each strain.

To overexpress *CHT3* and *SUN41* in the null mutant *ndt80*, open reading frames (ORFs) of each gene were amplified from genomic DNA using the two sets of primers Cht3F1/Cht3R1 and Sun41F1/Sun41R1 (Table 2), respectively. The PCR fragments were digested with the restriction enzymes MluI and NheI and cloned in the same sites of the CIp-ACT1-CYC vector (2). The plasmid was sequenced to confirm the integrity of the genes. Plasmids CIp-ACT1-CHT3 and CIp-ACT1-SUN41 were digested with the StuI restriction enzyme and used to transform the *ndt80* mutant strain (AS32). The absence of aneuploidy was confirmed in the overexpressing mutants using comparative genome hybridization as described previously (36).

Gene expression profiling. For gene expression profiling under the yeast form, saturated overnight cultures of the wild type (wt) (BWP17) and *ndt80*/*ndt80* strain AS31 were diluted to a starting optical density at 600 nm (OD_{600}) of 0.1 in 50 ml fresh YPD and grown at 30°C to an OD_{600} of 0.8. Hyphae were induced by growing *Candida* cells in YPD plus 10% fetal bovine serum (FBS) at 37°C to an OD_{600} of 0.8. Cultures were harvested by centrifugation at 3,000 × *g* for 5 min, and the pellet was rapidly frozen in liquid nitrogen.

To extract RNA from cells, samples stored at −80°C were placed on ice, and RNeasy buffer RLT was added to the pellets at a buffer/pellet ratio of 10:1 (vol/vol). The pellet was allowed to thaw in the buffer while being vortexed briefly at high speed. The resuspended pellet was placed back on ice and divided into 1-ml aliquots in 2-ml screw cap microcentrifuge tubes containing 0.6 ml of 3-mm-diameter acid-washed glass beads. Samples were homogenized 5 times for 1 min each time at 4,200 rpm using a Beadbeater. The samples were placed on ice for 1 min after each homogenization step. After the homogenization, the Qiagen RNeasy protocol was followed as recommended. Total-RNA samples were eluted in RNase-free H_2O. The RNA quality and integrity were assessed using an Agilent 2100 bioanalyzer.

cDNA labelings and microarray hybridizations were performed as previously described (30). Briefly, 20 μg of total RNA was reverse transcribed using oligo$(dT)_{21}$ in the presence of Cy3- or Cy5-dCTP (Invitrogen) and Superscript III reverse transcriptase (Invitrogen). Thereafter, the template RNA was degraded by adding 2.5 units RNase H (USB) and 1 μg RNase A (Pharmacia), followed by incubation for 15 min at 37°C. The labeled cDNAs were purified with a QIAquick PCR Purification Kit (Qiagen). Prior to hybridization, Cy3/Cy5-labeled cDNA was quantified using a NanoDrop ND-1000 UV-VIS spectrophotometer (NanoDrop) to confirm dye incorporation. Prehybridization and hybridization solutions consisted of DIG Easy Hyb solution (Roche Diagnostics, Mannheim, Germany) with 0.45% salmon sperm DNA and 0.45% yeast tRNA. The hybridization was carried out at 42°C for 20 h in a SlideBooster Hyb chamber SB 800 (Advalytix, Brunnthal, Germany) with regular microagitation of the sample. The slides were washed once in 1.0% SSC (1× SSC is 0.15 M NaCl plus 0.015 M sodium citrate), 0.2% SDS at 42°C for 5 min; twice in 0.1% SSC, 0.2% SDS at 42°C for 5 min; and once in 0.1% SSC at 24°C for 5 min, followed by four rinses in 0.1% SSC. The chips were air dried before being scanned using a ScanArray Lite microarray scanner (Perkin Elmer). Microarray data were analyzed with GeneSpring GX v7.3 (Agilent Technologies), and genes with statistically significant changes in transcript abundance were identified using a Welch *t* test with a false-discovery rate (FDR) of less than 5%.

Expression analysis by qPCR. For quantitative real-time PCR (qPCR), cDNA was synthesized from 5 μg of total RNA using the Invitrogen reverse transcription system [50 mM Tris-HCl, 75 mM KCl, 5 mM dithiothreitol (DTT), 3 mM $MgCl_2$, 400 nM oligo$(dT)_{15}$, 20 ng random octamers, 0.5 mM deoxynucleotide triphosphates (dNTPs), 200 units Superscript III reverse transcriptase]. The mixture was incubated for 60 min at 50°C. The cDNAs were then treated with 2 U of RNase H (Promega) for 20 min at 37°C, followed by heat inactivation of the enzyme at 80°C for 10 min. Aliquots were used for qPCR, which was performed using the Mx3000P QPCR System (Agilent) with the QuantiTect SYBR green PCR master mix (Qiagen). Cycling was done for 10 min at 95°C, followed by 40 cycles of 95°C for 10 s, 58°C for 15 s, and 72°C for 15 s. Samples were done in triplicate, and means were used for calculations. Fold changes were estimated by using the coding sequence of the *C. albicans ACT1* ORF as a reference. Fold

enrichments of the tested coding sequences were estimated using the comparative $\Delta\Delta C_T$ method as described previously (14).

Virulence studies. Mouse studies were carried out as previously described (27). Briefly, 8- to 12-week-old B6 mice (Jackson Laboratories, Bar Harbor, ME) were inoculated via the tail vein with 200 μl of a suspension containing 3×10^5 *C. albicans* cells in phosphate-buffered saline (PBS). Six mice, three females and three males, were used for each experimental group. The mice were closely monitored, and those showing ruffled fur, hunched backs, and extreme lethargy were considered moribund and were euthanized. To determine fungal loads, the kidneys from each mouse were removed aseptically and homogenized in 5 ml of PBS before being plated on YPD plates containing chloramphenicol (34 μg/ml). The number of yeast colonies per kidney was determined and log transformed. All experimental procedures involving animals were approved by the Biotechnology Research Institute Animal Care Committee, which operated under the guidelines of the Canadian Council of Animal Care.

RESULTS

The Saccharomycotina CTG clade harbors two distinct paralogs of the NDT80/PhoG-like TF family. Screening the *C. albicans* genome allowed us to identify two putative proteins with a conserved NDT80/PhoG-like DNA-binding domain (DBD), corresponding to *orf19.2119* (CaNdt80p) and *orf 19.513*. Analysis of their DBDs at the amino acid level revealed that they both shared 55% similarity with the meiosis-specific transcription factor ScNdt80p of *S. cerevisiae*. Domain architecture analysis of the two *C. albicans* TFs showed that *orf19.513* had a domain organization similar to that of ScNdt80p, consisting of the DBD located in the N-terminal region followed by a putative activation domain in the C-terminal region (Fig. 1A). In contrast, *orf19.2119* exhibited a unique organization that was the opposite of that of orf19.513 and ScNdt80p (Fig. 1A).

Examination of ascomycete genomes using the BlastP program was performed in order to identify putative orthologs of the NDT80/PhoG TF. The results showed that all ascomycete fungi have a single putative Ndt80p displaying a domain organization similar to those of ScNdt80p and orf19.513. The sole exception was the monophyletic CTG clade within the Saccharomycotina, containing organisms that translate CTG as serine instead of leucine and that harbor an additional gene homolog with a domain organization similar to that of orf19.2119 (Fig. 1B).

Deletion of *CaNDT80* affects cell separation. By combining genome-wide location and transcriptional profiling, we have previously revealed a key role of CaNdt80p in modulating azole sensitivity through the regulation of the expression of ergosterol (*ERG*) biosynthesis genes (36). In addition to *ERG* gene promoters, Ndt80p was found to bind a large number of gene promoters, demonstrating that the regulator might operate in other biological processes. In order to further analyze other potential cellular functions controlled by CaNdt80p, we monitored the yeast growth morphology of cells missing both *ndt80* alleles when cultured in YPD at 30°C. As shown in Fig. 2A, microscopic observation revealed that *ndt80* cells showed altered cell morphology corresponding to a defect in cell separation, as well as abnormal cell size, compared to both wt and revertant strains. *ndt80* mutants consist of relatively swollen yeast cells forming chains connected by septa, as visualized by calcofluor white staining, along with a significant increase in the percentages of chains of cells with 3 or 4, 5 or 6, or more than 6 cells (Fig. 2B).

CaNdt80p is required for the transcriptional activation of cell separation genes. To gain insight into the underlying molecular mechanism leading to the cell separation defect, we examined transcriptional differences between wt and *ndt80* cells growing in YPD at 30°C using whole-genome microarrays. Using a statistical-significance analysis with an estimated false-discovery rate of 5%, in addition to a cutoff of 1.5-fold, we identified 111 genes that require CaNdt80p for their proper expression, including 68 upregulated genes and 43 downregulated genes (see Table S1 in the supplemental material).

Our previous genome-wide location study demonstrated that, under yeast-promoting growth conditions, CaNdt80p binds 1,446 gene promoters (36). By cross-referencing these data with the list of Ndt80p transcriptionally dependent genes, we were able to identify candidate CaNdt80p direct target promoters whose genes are transcriptionally regulated during the yeast growth phase (Fig. 3A). Gene expression analysis indicated that some CaNdt80p direct targets were activated (46 genes), whereas others were repressed (25 genes), in the *ndt80* mutant. This finding suggests that the TF functions as both an activator and a repressor of gene expression.

Interestingly, among the genes that the *ndt80* mutants failed to activate, we found the putative cell wall glycosidase gene *SUN41*, which is required for cell separation in *C. albicans* (11, 16). Additionally, we were interested in the Cht3p chitinase, which showed an average reduction in transcript abundance of 4.5-fold in *ndt80*/*ndt80* mutants, although these levels of repression were not consistent enough for it to pass the threshold of statistical significance in our 4 replicates. Both the *SUN41* and *CHT3* gene promoters are bound by CaNdt80p (Fig. 3B), and their inactivation leads to a cell separation defect similar to that observed in *ndt80* mutants. This suggests that CaNdt80p could directly control the expression of genes implicated in cell separation completion and that the cell separation defect in *ndt80* mutants is the consequence of *CHT3* and/or *SUN41* depletion.

The *ndt80* cell separation phenotype is suppressed by overexpression of *CHT3* or *SUN41*. In order to confirm that the cell separation defect observed in *ndt80* is related to the depletion of at least one of these two cell wall degradation genes, we sought to investigate if overexpression of either *CHT3* or *SUN41* could restore the wt phenotype in *ndt80* mutants. For this purpose, the *CHT3* and *SUN41* ORFs were placed under the control of the *CaACT1* promoter and expressed in the *ndt80* background. Overexpression of these two genes was confirmed using quantitative real-time PCR, and the results demonstrated that the expression levels of *CHT3* and *SUN41* were significantly augmented compared to the wt strain (Fig. 4A). We then quantified the cell separation defect by counting the cells per chain in the overexpression mutants. As shown in Fig. 4B, the *ndt80* cell separation phenotype was reverted by overexpressing either *CHT3* or *SUN41*. Indeed, cells were found predominantly as single cells or as mother-daughter cells in overexpression mutants, similar to what was observed in the wt and revertant strains. This supports the idea that the cell separation defect in *ndt80* cells can be attributed to the depletion of *CHT3* and *SUN41*.

CaNdt80p is essential for hyphal growth in response to different filament-inducing conditions. The *ndt80* mutants were also tested for the ability to form hyphae under different environmental conditions. Wt cells grown in liquid medium

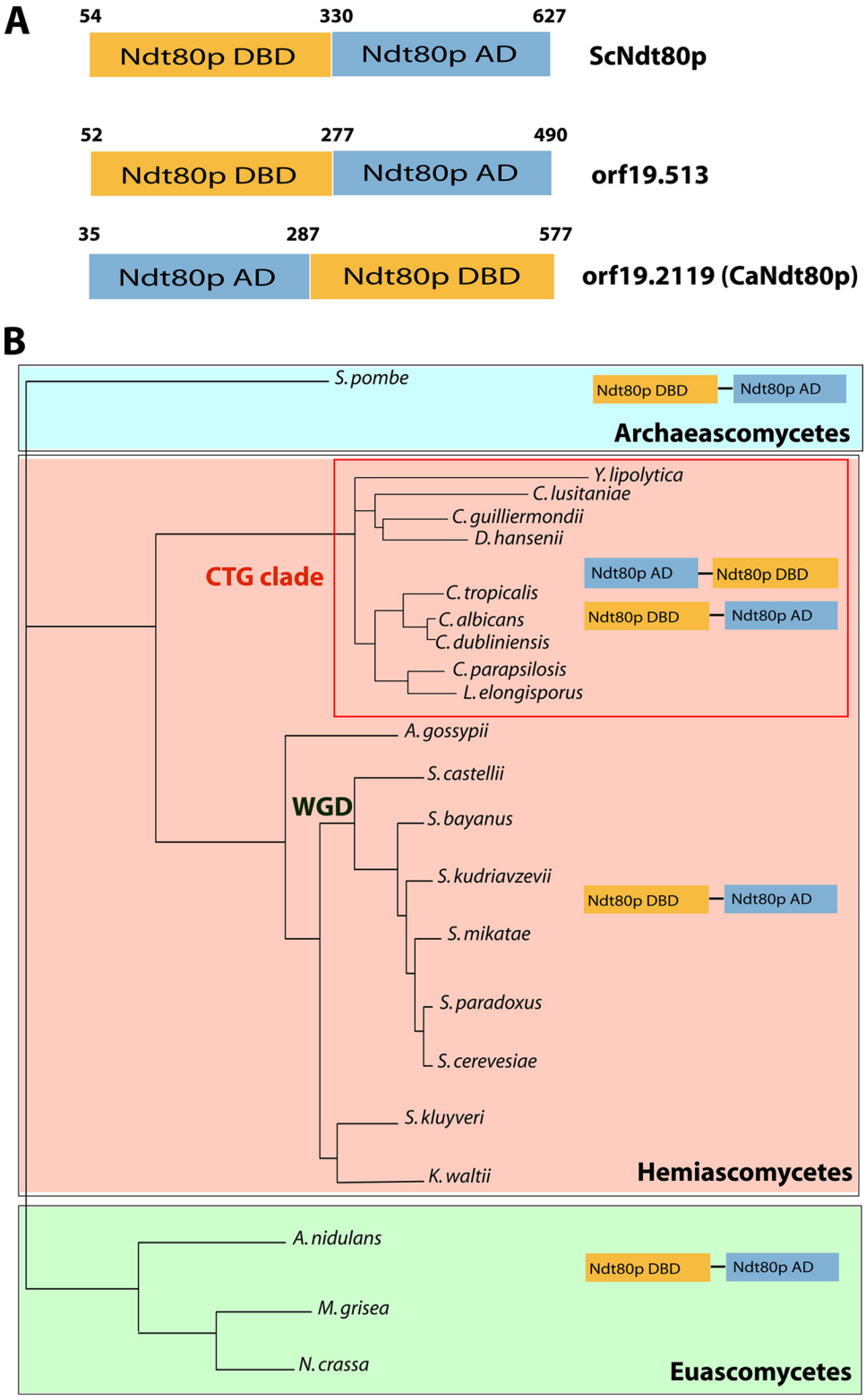

FIG. 1. The NDT80/PhoG transcription factor family across *Ascomycota.* (A) Functional-domain organizations of NDT80/PhoG family members in *Saccharomyces cerevisiae* and *Candida albicans.* Both the DNA-binding domain (Ndt80p DBD) and putative glutamine-rich activation domain (Ndt80p AD) are represented. (B) Structural organizations of NDT80/PhoG family members across different classes of ascomycetes. The topology of the tree was based on Fitzpatrick et al. (12). The CTG clade is highlighted by a red box. WGD identifies the clade containing species in which whole-genome duplication has occurred.

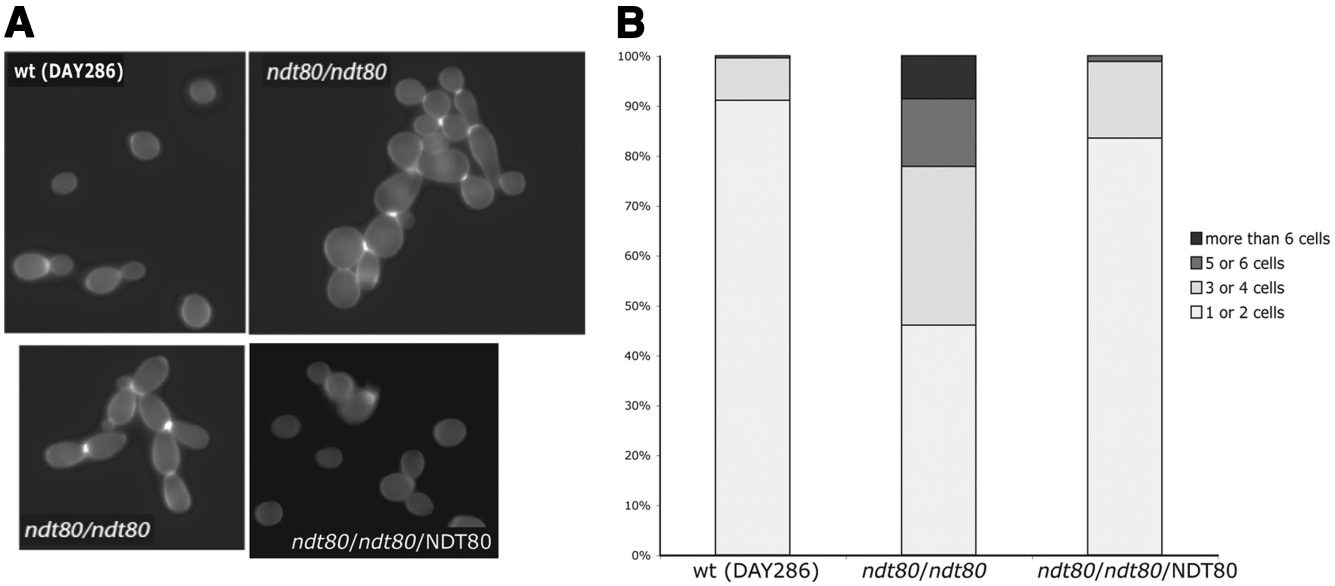

FIG. 2. Ndt80p is required for cell separation completion. (A) Images of wt (DAY286), *ndt80*/*ndt80* mutant (AS31), and revertant *ndt80*/*ndt80*/NDT80 (AS33) strains showing the cell separation defect. The cells were stained with calcofluor white. (B) Quantification of the cell separation defect. Shown are the percentages of chains of cells containing 1 or 2, 3 or 4, 5 or 6, or more than 6 cells.

containing serum or *N*-acetylglucosamine revealed vigorous filamentation (Fig. 5A and B). In contrast, the *ndt80* mutants differentiated into short and swollen elongated cells with a high frequency of lateral branches in the presence of the serum (Fig. 5A).

Similar results were obtained under hypoxic conditions and at pH 8. Indeed, while the wt and revertant strains showed abundant filamentation at the edges of colonies, *ndt80* developed smooth colonies with no mycelial growth even after prolonged incubation (Fig. 5C and D). This filamentation defect of *ndt80* mutants was

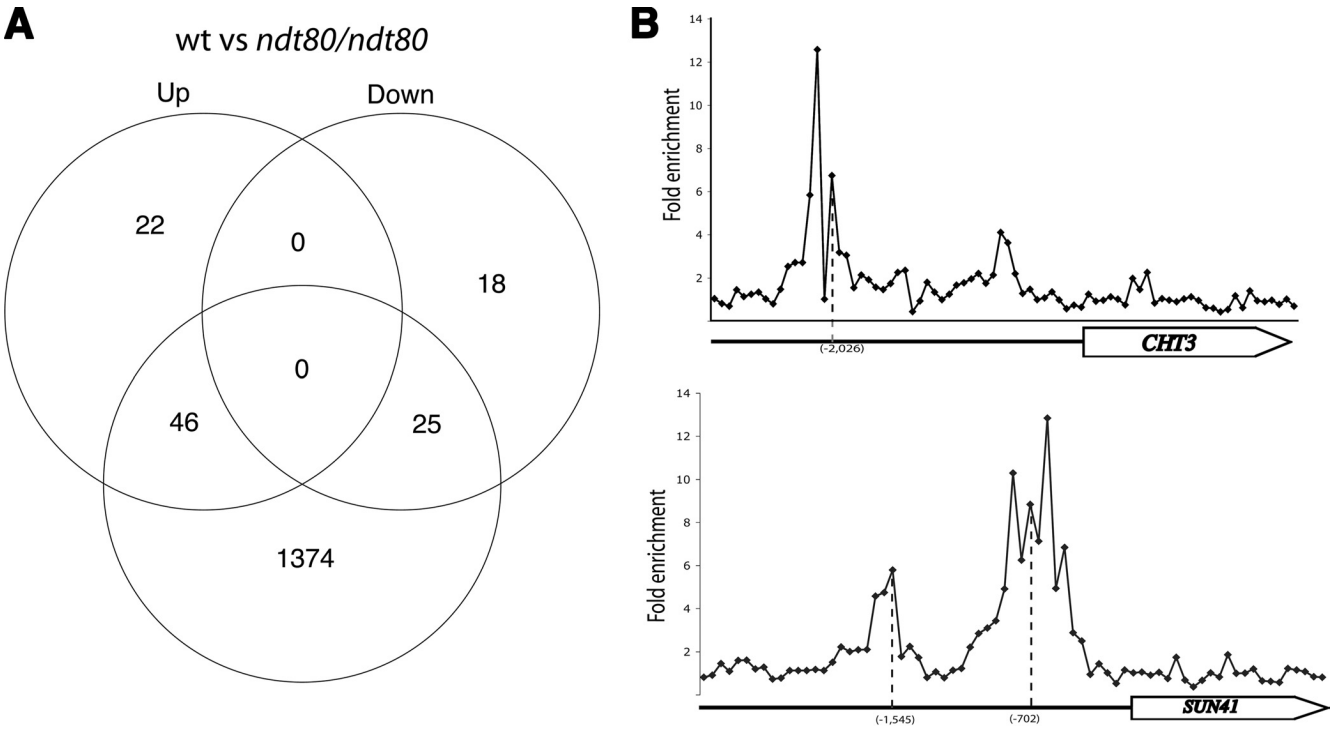

FIG. 3. Ndt80p directly regulates genes implicated in cell separation. (A) Relationship between Ndt80p-bound genes and genes showing altered expression in the *ndt80* mutant (AS31). (B) Ndt80p promoter occupancies of the endochitinase Cht3p and the glucosidase Sun41p as determined by Sellam et al. (36). The positions of the middle sporulation element motifs are shown.

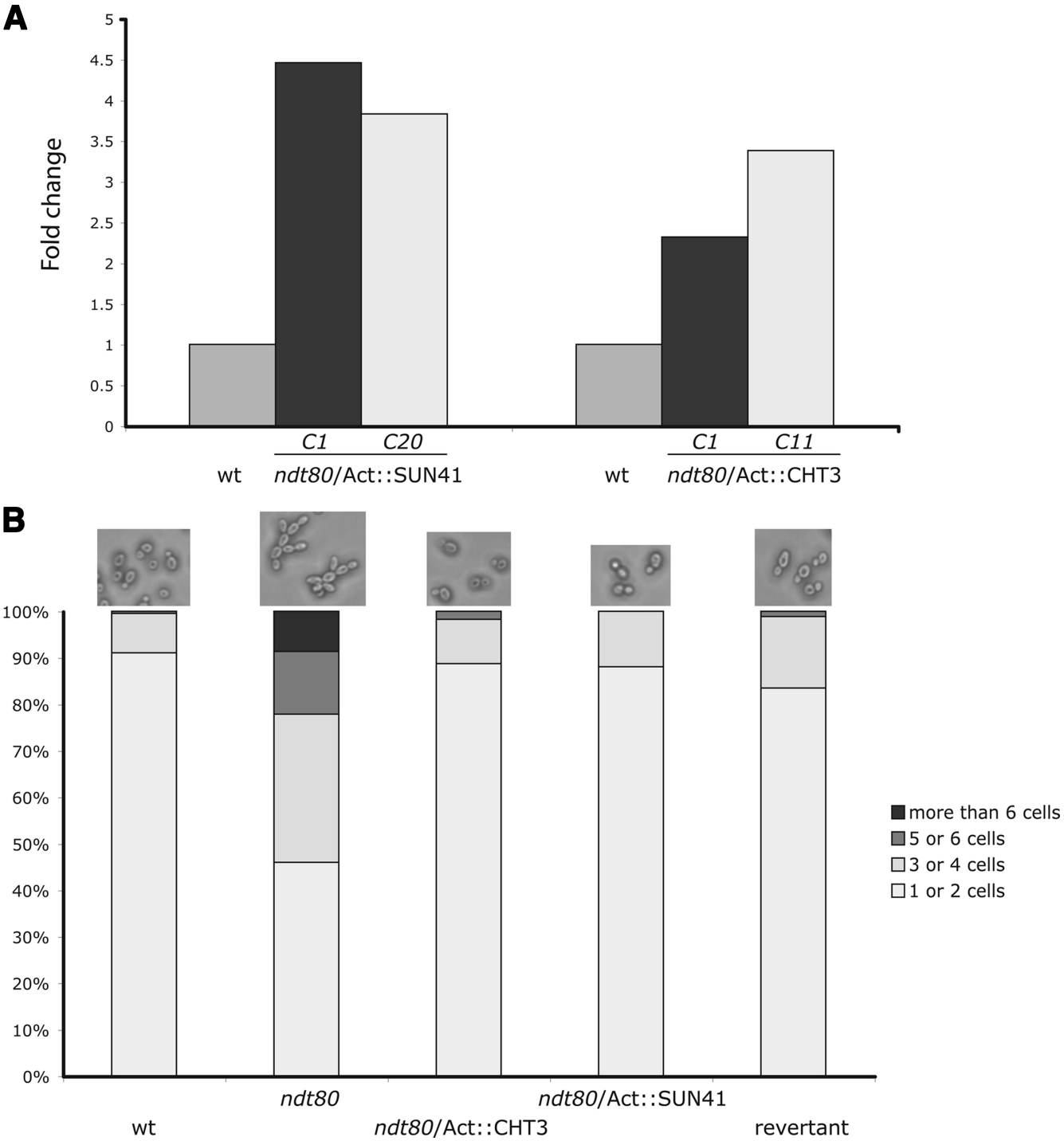

FIG. 4. The *ndt80* cell separation defect is reverted by the overexpression of *CHT3* or *SUN41*. (A) Average transcript levels of *CHT3* and *SUN41* in overexpression mutants relative to the wt strain (DAY286). For each gene, two clones (clones C1 and C20 for the *ndt80*/*Act*::SUN41 strain and clones C1 and C11 for the *ndt80*/Act::CHT3 strain) were evaluated. The reported values are the means of two independent experiments. (B) Evaluation of the percentages of chains of cells with 1 or 2, 3 or 4, 5 or 6, or more than 6 cells in overexpressing strains.

also observed under other filament-inducing conditions, namely, RPMI and spider media (data not shown).

CaNdt80p is required for the activation of hypha-specific genes. To gain insight into the role of CaNdt80p in mediating hyphal growth in *C. albicans*, we used microarrays to compare the transcriptomes of *ndt80* mutant and wt cells grown in the presence of serum at 37°C. Using a statistical-significance analysis with an estimated false-discovery rate of 5%, in addition to a stringent cutoff of 3-fold, we found that *ndt80* mutant cells had a severe gene expression defect, as they failed to fully

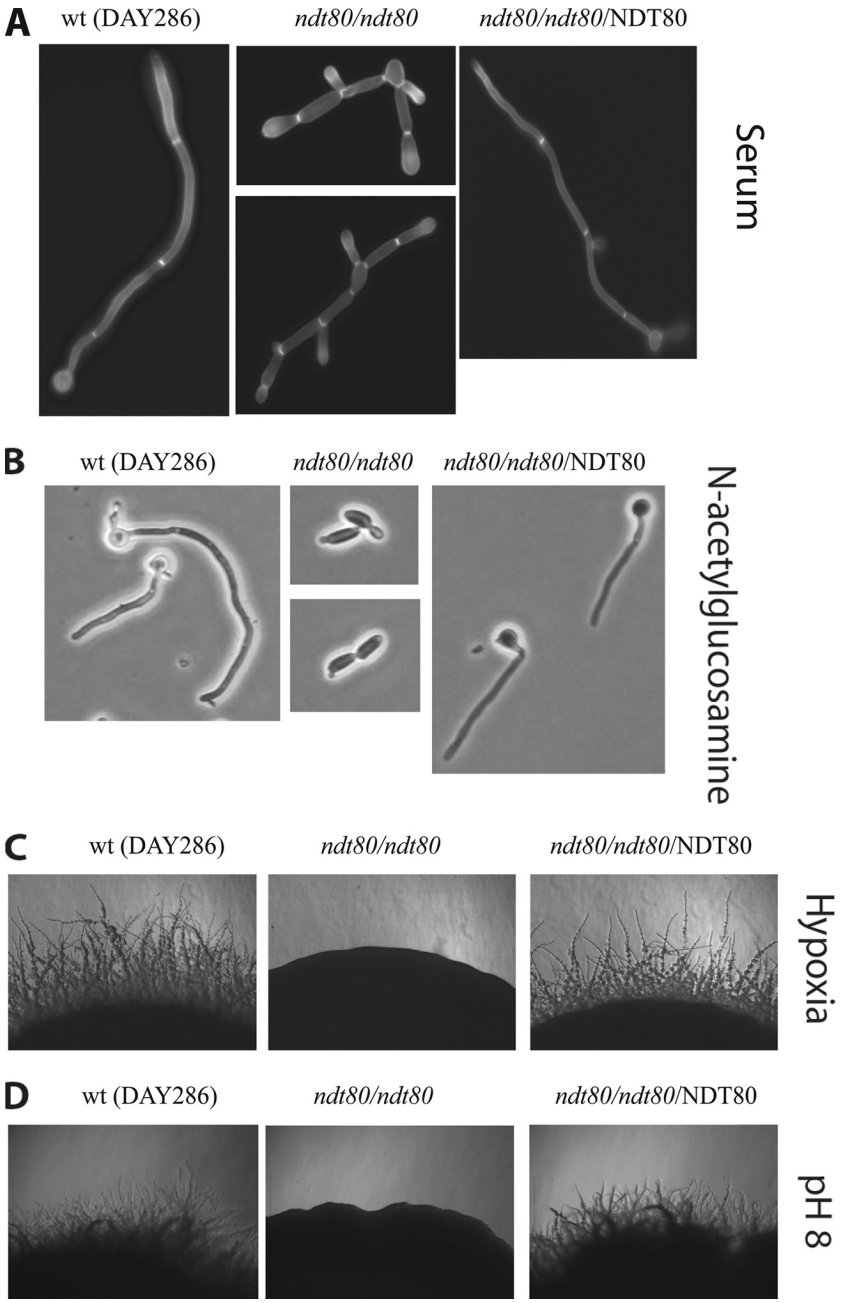

FIG. 5. CaNdt80p is essential for hyphal growth in response to different filament-inducing conditions. (A and B) Cell morphologies of wt (DAY286), *ndt80*/*ndt80* mutant (AS31), and revertant *ndt80*/*ndt80*/NDT80 (AS33) strains on liquid media supplemented with fetal bovine serum (A) or *N*-acetyl-D-glucosamine (B). (C and D) Colony morphologies of wt, *ndt80*, and revertant strains after 5 days of growth on solid media under hypoxic conditions (C) or in M199 medium at pH 8 (D).

activate 82 genes and to repress 41 genes (see Table S2 in the supplemental material). As illustrated in Fig. 6, the *ndt80* mutant was unable to upregulate genes that had been previously characterized as being activated during the yeast-to-hypha switch, including genes encoding cell wall components (*HWP1*, *ECE1*, *RBT4*, *ALS3*, *ALS10*, and *HYR1*) and a superoxide dismutase (*SOD5*), as well as two secreted aspartyl proteinases (*SAP4* and *SAP5*). Quantitative real-time PCR was used to confirm the expression defects of some of these genes specifying the yeast-to-hypha transition (Table 3).

Interestingly, activation of two TFs required for the positive regulation of hypha-specific genes, Ume6p and Tec1p, was found to be dependent on CaNdt80p. Additionally, *ndt80* mutants failed to downregulate genes repressed during hypha formation, including *YWP1*, *CAX4*, *MNN22*, *RHD1*, *RHD3*, *ALD5*, and the transcriptional repressor *NRG1* (Fig. 6). This clearly demonstrates that CaNdt80p is required for both the

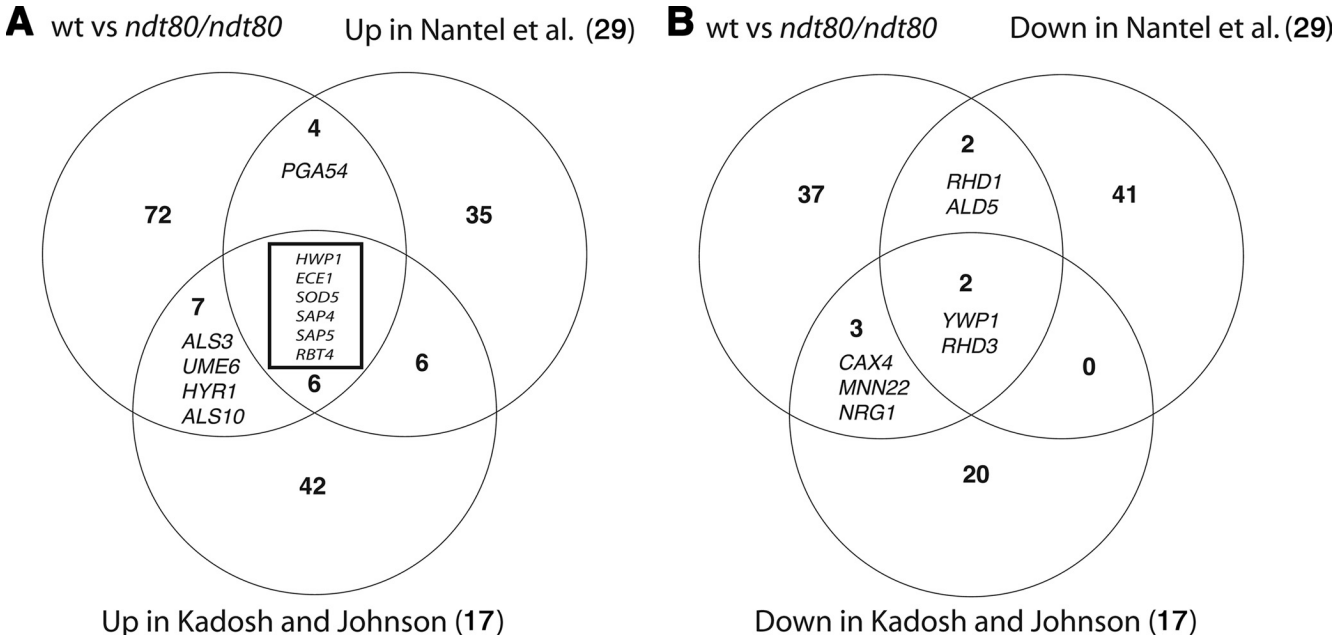

FIG. 6. CaNdt80p is required for the activation of hypha-specific genes. Shown are the overlaps between genes differentially regulated during the yeast-to-hypha switch as determined by Nantel et al. (29) and Kadosh et al. (17) and genes downregulated (A) or upregulated (B) in a wt-versus-*ndt80* comparison.

activation and the repression of genes characterizing the morphogenetic transcriptional program in *C. albicans*.

CaNdt80p is required for full virulence in a mouse model. The ability of *C. albicans* to switch from yeast to hyphae is critical for host invasion and virulence. Since *ndt80* mutants were unable to form hyphae in response to different filament-inducing conditions, we investigated if the TF is required for *C. albicans* virulence by using a mouse model. The *C. albicans* strain DAY286 (wt), an *ndt80* mutant strain, and a revertant were tested in a mouse model for systemic infection by intravenous injection in the tail vein. As shown in Fig. 7A, while 70% of the mice infected with the wt and revertant strains became moribund within 12 days postinfection, none of the *ndt80* strain-infected mice showed any clinical signs of advanced infection, such as ruffled fur, hunched back, or extreme lethargy, until the end of the experiment (day 21). Fungal loads from kidney tissues were also examined. As shown in Fig. 7B, the fungal loads were significantly lower in *ndt80* strain-infected mice than in mice challenged with the wt or revertant strain. Taken together, these findings demonstrate that Ndt80p is a critical determinant of *C. albicans* pathogenicity.

TABLE 3. qPCR analysis of genes identified as differentially expressed by microarray experiments in wt-versus-*ndt80* comparison under hypha-promoting conditions

Gene	ORF	Microarray[a]	qPCR[a,b]
ALS3	orf19.1816	0.03	5.08E−03 ± 0.0
HWP1	orf19.1321	0.08	8.73E−03 ± 0.0
ECE1	orf19.3374	0.03	2.16E−02 ± 0.2
YWP1	orf19.3618	30.59	867.06 ± 0.4
CAX4	orf19.3682	5.10	19.42 ± 3.2
NRG1	orf19.7150	3.87	7.16 ± 0.1
TEC1	orf19.5908	0.20	0.23 ± 0.1
RBT4	orf19.6202	0.02	0.34 ± 0.1

[a] Average fold change.
[b] Each value is the mean ± standard deviation of two independent experiments, each with three replicates.

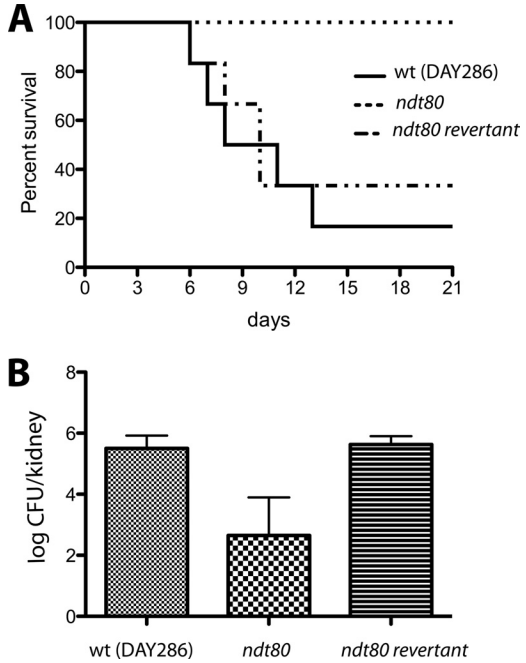

FIG. 7. Ndt80p is required for full virulence in a B6 mouse model. (A) Survival of mice infected with *ndt80* mutant, *ndt80* revertant, and wt parental strains. Mice were inoculated by tail vein injection, and survival was measured over a 21-day period. (B) The kidney fungal load was determined 7 days after injection. The error bars indicate standard deviations.

DISCUSSION

CaNdt80p is a novel transcriptional regulator unique to the Saccharomycotina CTG clade. In the present study, we have shown that CaNdt80p, encoded by orf19.2119, has a unique functional domain organization distinct from that of ScNdt80p. However, another member of the Ndt80/PhoG TF family, encoded by orf19.513, exists in *C. albicans*, and in addition to significant sequence similarity, this TF showed exactly the same domain organization as the meiosis-specific TF ScNdt80p. This suggests that orf19.513 is the "true" *C. albicans* ortholog of ScNdt80p. Nevertheless, we have decided to continue using the common name *CaNDT80* to define orf19.2119, as this gene has already been the subject of several publications by us and others and we have been unable to find any growth conditions that would result in the transcription of the *orf19.513* gene (results not shown).

The presence of an ScNdt80p-like TF in all ascomycetes suggests an important function of this regulator (Fig. 1B). Surprisingly, orf19.2119-like TFs were found exclusively in fungi belonging to the monophylic CTG clade of Saccharomycotina. In addition to *C. albicans*, this group contains a large number of closely related pathogenic yeasts, such as *Candida parapsilosis*, *Candida tropicalis*, *Candida lusitaniae*, and *Candida guilliermondii*. Recently, Butler et al. (3) revealed significant expansions of the cell wall, secreted aspartase, and transporter gene families in pathogenic species of the CTG clade, suggesting adaptations associated with pathogenesis. Such large-scale amplification of a gene family and its contributions to promoting virulence have also been attributed to other ascomycete and basidiomycete species (34, 37). Gene duplication and the expansion of multiple gene families are considered to be major forces in evolution by allowing functional innovation. These observations argue that the presence of two members of the Ndt80/PhoG TF family in *C. albicans*, with highly similar DBDs, is most likely the result of gene duplication events from a common ancestor. Taking into consideration the role of CaNdt80p in virulence, the appearance or the retention of this TF in the *Candida* clade could be related to its critical role in adaptation to its mammalian host environment.

CaNdt80p is a general transcriptional regulator acting as both an activator and a repressor. Using the global and unbiased approach of *c*hromatin *i*mmuno*p*recipitation (ChIP)-Chip assays, we have demonstrated that CaNdt80p occupies a large number of promoter regions representing 23% of *C. albicans* genes (36). In addition, we have clearly demonstrated that CaNdt80p is required for the modulation of different biological processes, such as cell separation, hyphal growth, virulence, and azole sensitivity. Taken together, these results suggest that CaNdt80p is a multifunctional general transcriptional regulator. Gene expression analysis indicated that some direct targets of CaNdt80p were upregulated whereas others were repressed in *ndt80* mutants. These findings suggest that this TF plays bifunctional roles as a repressor and an activator. Interestingly, in addition to structural and functional similarities between the CaNdt80p and p53 family members (20), p53 also has positive or negative effects on the activities of its target promoters (31).

Intriguingly, CaNdt80p was found to bind a large number of gene promoters that did not show any significant changes in gene expression under yeast-promoting conditions when the TF was absent. This phenomenon seems to be common in human TFs, where changing the level of a TF alters the expression levels of only 1 to 10% of its known target genes (10). It seems, therefore, that only a small proportion of the binding sites for a factor might be functional in a given cell type and that their functionality could be determined by cell-specific partners that need to be recruited for transcriptional activation or repression. Alternatively, TF networks may be fairly robust and able to compensate for a missing regulator. In our study, this can be illustrated by the example of the promoter region of *NRG1*, which exhibits significant Ndt80p binding in cells growing as yeasts. However, no *NRG1* transcript level alteration was observed in *ndt80* mutants grown under the same conditions. On the other hand, transcriptional profiling in the presence of serum revealed that the *ndt80* mutants failed to downregulate *NRG1* in response to serum. Assuming that Ndt80p binds to the *NRG1* promoter under hypha-promoting conditions, this suggests that the repression of this transcriptional repressor requires a hypha-specific partner.

Ndt80p is a new regulator of cell separation in *C. albicans*. In *S. cerevisiae*, cell separation occurs during the G_1 phase and is achieved by the degradation of septal components, composed essentially of chitin, which holds the mother and daughter cells together after cytokinesis (4, 9). Degradation of septal materials is accomplished by the endochitinase Cts1p, which is responsible for the lysis of the primary septum at the neck (19). In addition to chitinase, glucanases, such as Eng1p, Scw11p, and Sun4p, play a complementary role and are required for dissolution of the secondary septum and/or the surrounding cell wall materials holding the mother and daughter cells together (25, 42). In addition to the tight spatial regulation of hydrolytic enzymes, strict temporal regulation during the cell cycle is also required (42). In both *S. cerevesiae* and fission yeast, this is achieved by the transcription factor Ace2p, which activates the expression of the chitinase *CTS1* and other glucanases specifically in the G_1 phase (9). In *C. albicans*, deleting Ca*ACE2* results in a dramatic defect in cell separation, as well as attenuated virulence (18). Additionally, it was shown that CaAce2p is required for the transcriptional activation of the chitinase Cht3p and other glucanases, highlighting an evolutionarily conserved role of this TF in fungi (18, 26). Recent genome-wide investigations using DNA microarrays have revealed four successive waves of genes that are expressed periodically during the *C. albicans* cell cycle (7). Among these waves, *ACE2* was found to peak periodically during the G_2/M transition and to activate cell separation genes (*CHT3*, *DSE1*, *SCW4*, *SCW11*, and *ENG1*), which therefore are transcribed periodically at the M/G_1 transition. Interrogation of the Candida Cell Cycle database (http://www.bri.nrc.ca/candida/cycle/) for cycling transcripts revealed that *NDT80* was not considered a periodic gene; however, a slight peak was observed exactly at the G_2/M transition in synchrony with *ACE2*. Based on this observation, the cell separation role of Ndt80p might be cell cycle regulated, as it is for Ace2p.

In this work, we have reported a novel function of Ndt80p in controlling cell separation in *C. albicans* through direct transcriptional activation of genes encoding the endochitinase Cht3p and the β-glucanase Sun41p. It is therefore likely that cell separation completion in this pathogen is the result of contributions from both Ace2p and Ndt80p gene targets.

While both Ndt80p and Ace2p are required for cell separation during mitotic exit, the overlap between the targets of these two TFs consists of only two genes, *CHT3* and *SUN41* (26). Ndt80p was not found to be required for transcriptional activation of other Ace2p cell separation targets, such as *DSE1*, *DSE4*, and *SCW11*. Considering that Ndt80p was not found in the promoter region of *ACE2* (36) and is not required for its proper expression, in addition to the fact that *NDT80* expression was not altered in *ace2* mutants, the two TFs might operate independently in two distinct transcriptional regulatory networks to control cell separation.

Ndt80p plays a central role in hyphal development and virulence in *C. albicans*. In *C. albicans*, the role of transcriptional regulators of hyphal growth has been the subject of numerous investigations. In this work, we have enriched the repertoire of *C. albicans* filamentation TFs by demonstrating the critical function of CaNdt80p in hyphal development. In *C. albicans*, the yeast-to-hypha transition is triggered by various environmental stimuli, such as serum, neutral pH, high temperature, nutrient starvation, and CO_2 (1). Deletion of *CaNDT80* abolished the ability of *C. albicans* to undergo the yeast-to-hypha transition in response to a large set of hypha-inducing conditions. Since sensing of filamentation stimuli operates through a variety of distinct sensing/signalization pathways, Ndt80p is thus thought to act as a critical downstream effector promoting hypha formation in response to different signals conveyed by different upstream pathways.

Transcriptional profiling revealed that the hyphal defect of *ndt80* mutants was correlated with the inability to activate hypha-specific genes, such as *HWP1*, *ECE1*, *RBT4*, *ALS3*, *HYR1*, *SAP4*, and *SAP5*. Additionally, given the fact that Ndt80p can act as a repressor, the hyphal defect of the *ndt80* mutants could also be the consequence of the nonrepression of yeast-specific genes, such as *YWP1*, *CAX4*, *MNN22*, *RHD1*, *RHD3*, and *ALD5.* Based on our transcriptional-profiling data, the molecular basis of the hyphal defects of the *ndt80* mutants can be explained in three possible ways. (i) *ndt80* cells fail to repress the transcriptional repressor Nrg1p. Taking into account the critical role of Nrg1p in hypha-specific gene regulation (17), together with the occupancy of the *NRG1* promoter by Ndt80p (36), *C. albicans* filamentous growth mediated by CaNdt80p might be an outcome of the release of Nrg1p repression at hypha-specific gene promoters. (ii) *ndt80* cells fail to activate the expression of genes encoding the transcriptional activators Ume6p and Tec1p. In our previous study, the *UME6* and *TEC1* promoters were shown to be bound by Ndt80p, and we have shown here that *UME6* and *TEC1* activation in the presence of serum requires Ndt80p. Thus, CaNdt80p acts upstream of Ume6p and Tec1p, which, in turn, are implicated in activating the filamentation transcriptional program. (iii) *ndt80* cells fail to activate key hypha-specific genes. In addition to the indirect-regulation models, we cannot rule out the possibility that CaNdt80p directly activates part of the hypha transcriptional responses, since it was found to bind the promoters of many hypha-specific genes, such as *ECE1*, *ALS3*, *ALS1*, *HWP1*, *HYR1*, and *RBT4.*

The ability of *C. albicans* to undergo morphological switching is a critical pathogenicity determinant. In fact, hyphal differentiation facilitates the invasion of host tissues and also helps *C. albicans* to escape from phagocytosis (22, 35). The loss of virulence of *ndt80* mutants is most likely attributable to the key role of Ndt80p in controlling hyphal growth. However, the ability of this TF to activate other virulence-related functions, such as adhesion (*HWP1*, *ALS1*, *ALS3*, and *ALS10*) (5, 32, 38) or extracellular proteolytic activity (*SAP4* and *SAP5*) (28), cannot be ruled out.

ACKNOWLEDGMENTS

Thanks are due to members of the BRI Microarray Laboratory and the BRI Animal Facility, especially Khairul Islam, Jean-Sébastien Deneault, Mario Mercier, and Jessy Tremblay, for technical assistance.

This work was supported by grants from the Canadian Institute of Health Research (CIHR) to A.N. (MOP-42516). C.A. was supported by an Alexander Graham Bell CGS-NSERC scholarship.

This is NRC publication number 50681.

REFERENCES

1. **Biswas, S., P. Van Dijck, and A. Datta.** 2007. Environmental sensing and signal transduction pathways regulating morphopathogenic determinants of Candida albicans. Microbiol. Mol. Biol. Rev. **71:**348–376.
2. **Blackwell, C., C. L. Russell, S. Argimon, A. J. Brown, and J. D. Brown.** 2003. Protein A-tagging for purification of native macromolecular complexes from Candida albicans. Yeast **20:**1235–1241.
3. **Butler, G., M. D. Rasmussen, M. F. Lin, M. A. Santos, S. Sakthikumar, C. A. Munro, E. Rheinbay, M. Grabherr, A. Forche, J. L. Reedy, I. Agrafioti, M. B. Arnaud, S. Bates, A. J. Brown, S. Brunke, M. C. Costanzo, D. A. Fitzpatrick, P. W. de Groot, D. Harris, L. L. Hoyer, B. Hube, F. M. Klis, C. Kodira, N. Lennard, M. E. Logue, R. Martin, A. M. Neiman, E. Nikolaou, M. A. Quail, J. Quinn, M. C. Santos, F. F. Schmitzberger, G. Sherlock, P. Shah, K. A. Silverstein, M. S. Skrzypek, D. Soll, R. Staggs, I. Stansfield, M. P. Stumpf, P. E. Sudbery, T. Srikantha, Q. Zeng, J. Berman, M. Berriman, J. Heitman, N. A. Gow, M. C. Lorenz, B. W. Birren, M. Kellis, and C. A. Cuomo.** 2009. Evolution of pathogenicity and sexual reproduction in eight Candida genomes. Nature **459:**657–662.
4. **Cabib, E., R. Roberts, and B. Bowers.** 1982. Synthesis of the yeast cell wall and its regulation. Annu. Rev. Biochem. **51:**763–793.
5. **Chaffin, W. L.** 2008. Candida albicans cell wall proteins. Microbiol. Mol. Biol. Rev. **72:**495–544.
6. **Chen, C. G., Y. L. Yang, H. I. Shih, C. L. Su, and H. J. Lo.** 2004. CaNdt80 is involved in drug resistance in Candida albicans by regulating CDR1. Antimicrob. Agents Chemother. **48:**4505–4512.
7. **Cote, P., H. Hogues, and M. Whiteway.** 2009. Transcriptional analysis of the Candida albicans cell cycle. Mol. Biol. Cell **20:**3363–3373.
8. **Davis, D. A., V. M. Bruno, L. Loza, S. G. Filler, and A. P. Mitchell.** 2002. Candida albicans Mds3p, a conserved regulator of pH responses and virulence identified through insertional mutagenesis. Genetics **162:**1573–1581.
9. **Dohrmann, P. R., G. Butler, K. Tamai, S. Dorland, J. R. Greene, D. J. Thiele, and D. J. Stillman.** 1992. Parallel pathways of gene regulation: homologous regulators SWI5 and ACE2 differentially control transcription of HO and chitinase. Genes Dev. **6:**93–104.
10. **Farnham, P. J.** 2009. Insights from genomic profiling of transcription factors. Nat. Rev. Genet **10:**605–616.
11. **Firon, A., S. Aubert, I. Iraqui, S. Guadagnini, S. Goyard, M. C. Prevost, G. Janbon, and C. d'Enfert.** 2007. The SUN41 and SUN42 genes are essential for cell separation in Candida albicans. Mol. Microbiol. **66:**1256–1275.
12. **Fitzpatrick, D. A., M. E. Logue, J. E. Stajich, and G. Butler.** 2006. A fungal phylogeny based on 42 complete genomes derived from supertree and combined gene analysis. BMC Evol. Biol. **6:**99.
13. **Gillum, A. M., E. Y. Tsay, and D. R. Kirsch.** 1984. Isolation of the Candida albicans gene for orotidine-5′-phosphate decarboxylase by complementation of S. cerevisiae ura3 and E. coli pyrF mutations. Mol. Gen. Genet. **198:**179–182.
14. **Guillemette, T., A. Sellam, and P. Simoneau.** 2004. Analysis of a nonribosomal peptide synthetase gene from Alternaria brassicae and flanking genomic sequences. Curr. Genet. **45:**214–224.
15. **Hepworth, S. R., H. Friesen, and J. Segall.** 1998. NDT80 and the meiotic recombination checkpoint regulate expression of middle sporulation-specific genes in Saccharomyces cerevisiae. Mol. Cell. Biol. **18:**5750–5761.
16. **Hiller, E., S. Heine, H. Brunner, and S. Rupp.** 2007. Candida albicans Sun41p, a putative glycosidase, is involved in morphogenesis, cell wall biogenesis, and biofilm formation. Eukaryot. Cell **6:**2056–2065.
17. **Kadosh, D., and A. D. Johnson.** 2005. Induction of the Candida albicans filamentous growth program by relief of transcriptional repression: a genome-wide analysis. Mol. Biol. Cell **16:**2903–2912.
18. **Kelly, M. T., D. M. MacCallum, S. D. Clancy, F. C. Odds, A. J. Brown, and G. Butler.** 2004. The Candida albicans CaACE2 gene affects morphogenesis, adherence and virulence. Mol. Microbiol. **53:**969–983.
19. **Kuranda, M. J., and P. W. Robbins.** 1991. Chitinase is required for cell

separation during growth of Saccharomyces cerevisiae. J. Biol. Chem. **266:** 19758–19767.
20. **Lamoureux, J. S., D. Stuart, R. Tsang, C. Wu, and J. N. Glover.** 2002. Structure of the sporulation-specific transcription factor Ndt80 bound to DNA. EMBO J. **21:**5721–5732.
21. **Leroy, O., J. P. Gangneux, P. Montravers, J. P. Mira, F. Gouin, J. P. Sollet, J. Carlet, J. Reynes, M. Rosenheim, B. Regnier, and O. Lortholary.** 2009. Epidemiology, management, and risk factors for death of invasive Candida infections in critical care: a multicenter, prospective, observational study in France (2005–2006). Crit. Care Med. **37:**1612–1618.
22. **Lo, H. J., J. R. Kohler, B. DiDomenico, D. Loebenberg, A. Cacciapuoti, and G. R. Fink.** 1997. Nonfilamentous C. albicans mutants are avirulent. Cell **90:**939–949.
23. **MacRae, W. D., F. P. Buxton, S. Sibley, S. Garven, D. I. Gwynne, H. N. Arst, Jr., and R. W. Davies.** 1993. Characterization of an Aspergillus nidulans genomic DNA fragment conferring phosphate-non-repressible acid-phosphatase activity. Gene **130:**247–251.
24. **Montano, S. P., M. L. Cote, I. Fingerman, M. Pierce, A. K. Vershon, and M. M. Georgiadis.** 2002. Crystal structure of the DNA-binding domain from Ndt80, a transcriptional activator required for meiosis in yeast. Proc. Natl. Acad. Sci. U. S. A. **99:**14041–14046.
25. **Mouassite, M., N. Camougrand, E. Schwob, G. Demaison, M. Laclau, and M. Guerin.** 2000. The ′SUN′ family: yeast SUN4/SCW3 is involved in cell septation. Yeast **16:**905–919.
26. **Mulhern, S. M., M. E. Logue, and G. Butler.** 2006. Candida albicans transcription factor Ace2 regulates metabolism and is required for filamentation in hypoxic conditions. Eukaryot. Cell **5:**2001–2013.
27. **Mullick, A., M. Elias, S. Picard, L. Bourget, O. Jovcevski, S. Gauthier, A. Tuite, P. Harakidas, C. Bihun, B. Massie, and P. Gros.** 2004. Dysregulated inflammatory response to Candida albicans in a C5-deficient mouse strain. Infect. Immun. **72:**5868–5876.
28. **Naglik, J. R., S. J. Challacombe, and B. Hube.** 2003. Candida albicans secreted aspartyl proteinases in virulence and pathogenesis. Microbiol. Mol. Biol. Rev. **67:**400–428.
29. **Nantel, A., D. Dignard, C. Bachewich, D. Harcus, A. Marcil, A. P. Bouin, C. W. Sensen, H. Hogues, M. van het Hoog, P. Gordon, T. Rigby, F. Benoit, D. C. Tessier, D. Y. Thomas, and M. Whiteway.** 2002. Transcription profiling of Candida albicans cells undergoing the yeast-to-hyphal transition. Mol. Biol. Cell **13:**3452–3465.
30. **Nantel, A., T. Rigby, H. Hogues, and M. Whiteway.** 2006. Microarrays for studying pathogenicity in *Candida albicans*, p. 181–210. *In* K. Kavanagh (ed.), Medical mycology: cellular and molecular techniques. Wiley Press, Hoboken, NJ.
31. **Oren, M.** 2003. Decision making by p53: life, death and cancer. Cell Death Differ. **10:**431–442.
32. **Phan, Q. T., C. L. Myers, Y. Fu, D. C. Sheppard, M. R. Yeaman, W. H. Welch, A. S. Ibrahim, J. E. Edwards, Jr., and S. G. Filler.** 2007. Als3 is a Candida albicans invasin that binds to cadherins and induces endocytosis by host cells. PLoS Biol. **5:**e64.
33. **Pierce, M., K. R. Benjamin, S. P. Montano, M. M. Georgiadis, E. Winter, and A. K. Vershon.** 2003. Sum1 and Ndt80 proteins compete for binding to middle sporulation element sequences that control meiotic gene expression. Mol. Cell. Biol. **23:**4814–4825.
34. **Powell, A. J., G. C. Conant, D. E. Brown, I. Carbone, and R. A. Dean.** 2008. Altered patterns of gene duplication and differential gene gain and loss in fungal pathogens. BMC Genomics **9:**147.
35. **Rocha, C. R., K. Schroppel, D. Harcus, A. Marcil, D. Dignard, B. N. Taylor, D. Y. Thomas, M. Whiteway, and E. Leberer.** 2001. Signaling through adenylyl cyclase is essential for hyphal growth and virulence in the pathogenic fungus Candida albicans. Mol. Biol. Cell **12:**3631–3643.
36. **Sellam, A., F. Tebbji, and A. Nantel.** 2009. Role of Ndt80p in sterol metabolism regulation and azole resistance in Candida albicans. Eukaryot. Cell **8:**1174–1183.
37. **Soanes, D. M., I. Alam, M. Cornell, H. M. Wong, C. Hedeler, N. W. Paton, M. Rattray, S. J. Hubbard, S. G. Oliver, and N. J. Talbot.** 2008. Comparative genome analysis of filamentous fungi reveals gene family expansions associated with fungal pathogenesis. PLoS One **3:**e2300.
38. **Staab, J. F., S. D. Bradway, P. L. Fidel, and P. Sundstrom.** 1999. Adhesive and mammalian transglutaminase substrate properties of Candida albicans Hwp1. Science **283:**1535–1538.
39. **Wilson, R. B., D. Davis, and A. P. Mitchell.** 1999. Rapid hypothesis testing with Candida albicans through gene disruption with short homology regions. J. Bacteriol. **181:**1868–1874.
40. **Wisplinghoff, H., T. Bischoff, S. M. Tallent, H. Seifert, R. P. Wenzel, and M. B. Edmond.** 2004. Nosocomial bloodstream infections in US hospitals: analysis of 24,179 cases from a prospective nationwide surveillance study. Clin. Infect. Dis. **39:**309–317.
41. **Xiang, Q., and N. L. Glass.** 2002. Identification of vib-1, a locus involved in vegetative incompatibility mediated by het-c in Neurospora crassa. Genetics **162:**89–101.
42. **Yeong, F. M.** 2005. Severing all ties between mother and daughter: cell separation in budding yeast. Mol. Microbiol. **55:**1325–1331.

VII. 5. The zinc cluster transcription factor Ahr1p directs Mcm1p regulation of *Candida albicans* adhesion

Originally published in:
Mol Microbiol. 2011 Feb;79(4):940-53. Epub 2010 Dec 30. || PMID: 21299649

Molecular Microbiology (2011) 79(4), 940–953 ■
doi:10.1111/j.1365-2958.2010.07504.x
First published online 30 December 2010

The zinc cluster transcription factor Ahr1p directs Mcm1p regulation of *Candida albicans* adhesion

Christopher Askew,[1,2] Adnane Sellam,[1,3] Elias Epp,[1,2] Jaideep Mallick,[1] Hervé Hogues,[1] Alaka Mullick,[1,4] André Nantel[1,3] and Malcolm Whiteway[1,2]*

[1]*Biotechnology Research Institute, National Research Council of Canada, Montréal, Québec, Canada H4P 2R2.*
[2]*Department of Biology, McGill University, Montréal, Québec, Canada H3A 1B1.*
[3]*Department of Anatomy and Cell Biology, McGill University, Montréal, Québec, Canada H3A 1B1.*
[4]*Département de Microbiologie et Immunologie, l'Université de Montréal, Montréal, Québec, Canada H3T 1J4.*

Summary

Biofilm development by *Candida albicans* requires cell adhesion for the initial establishment of the biofilm and the continued stability after hyphal development occurs; however, the regulation of the process has not been fully established. Using chromatin immunoprecipitation coupled to microarray analysis (ChIP-chip) we have characterized a regulon containing the Mcm1p factor that is required for the initial surface adhesion during biofilm formation. In the yeast *Saccharomyces cerevisiae* several Mcm1p regulons have been characterized in which regulatory specificity is achieved through cofactors binding a sequence adjacent to the Mcm1p binding site. This new Mcm1p regulon in *C. albicans* also requires a cofactor, which we identify as the transcription factor Ahr1p. However, in contrast to the other yeast regulons, Ahr1p alone binds the target promoters, which include several key adhesion genes, and recruits Mcm1p to these sites. Through transcription profiling and qPCR analysis, we demonstrate that this Ahr1p–Mcm1p complex directly activates these adhesion genes. When the regulatory circuit was disrupted by deleting *AHR1*, the strain displayed reduced adherence to a polystyrene surface. We also demonstrate a role for the regulon in hyphal growth and in virulence. Our work thus establishes a new mechanism of Mcm1p-directed regulation distinct from those observed for other Mcm1p co-regulators.

Accepted 2 December, 2010. *For correspondence. E-mail malcolm.whiteway@cnrc-nrc.gc.ca; Tel. (+1) 514 496 6146; Fax (+1) 514 496 5143.

Introduction

Candida albicans is a commensal fungus inhabiting the skin, gastrointestinal and genitourinary tracts of warm-blooded animals such as humans. However, *C. albicans* is also an opportunistic pathogen that can colonize and invade host tissues causing potentially lethal systemic infections. In fact, *Candida* species are the most commonly isolated agent in human fungal infections with *C. albicans* accounting for more than half of these cases (Wisplinghoff *et al*., 2004; Leroy *et al*., 2009).

Part of the success of *C. albicans* as a pathogen is attributed to its development of biofilm structures that protect the fungus from host defence mechanisms and decrease its sensitivity to most antifungal drugs (Hawser and Douglas, 1995; Chandra *et al*., 2001; Ramage *et al*., 2002), although the precise mechanisms of this resistance are not well understood (Vediyappan *et al*., 2010). An initial step in biofilm formation is adherence of yeast cells to a surface. After a basal layer is established, the biofilm matures by developing hyphal filaments and producing an extracellular matrix. The result is a stable, dense mass of yeast, pseudohyphal and hyphal cells embedded within this matrix of carbohydrates and proteins. *C. albicans* is able to adhere to a variety of surfaces both *in vitro* and *in vivo*; these include implanted medical devices such as catheters and heart valves. Biofilm development on these devices is frequently linked with nosocomial infections (Douglas, 2003; Kojic and Darouiche, 2004) and the resistance of biofilms towards antifungals significantly complicates treatment. Often catheters must be removed to allow for effective antifungal therapy (Mermel *et al*., 2001) and thus the understanding of biofilm regulation is of significant medical interest.

Adhesion is critical for the development of the initial basal layer as well as the stability of the mature biofilm. The Agglutinin-Like Sequence (ALS) gene family of cell surface glycoproteins and the cell surface hyphal protein *HWP1* have a primary role in adhesion in *C. albicans*. Deletion of *ALS1*, *ALS2*, *ALS3* or *HWP1* has been shown

to disrupt biofilm formation (Zhao *et al*., 2005; 2006; Nobile *et al*., 2006a; Sellam *et al*., 2009a). With the exception of *ALS2*, these genes are known to be under the positive regulation of the transcription factor Bcr1p (Nobile and Mitchell, 2005). A *bcr1* deletion strain has a severe adhesion defect resulting in the formation of a rudimentary biofilm (Nobile and Mitchell, 2005; Nobile *et al*., 2006b). Outside of Bcr1p, little is known about the regulation of adhesion genes in *C. albicans*, although it is probable that any additional adhesion regulators will be *Candida*-specific transcription factors. *C. albicans* and the model yeast *Saccharomyces cerevisiae* diverged from a common ancestor approximately 235–841 million years ago (Heckman *et al*., 2001; Douzery *et al*., 2004), and unlike *C. albicans*, *S. cerevisiae* does not naturally form biofilms or have orthologues of the ALS gene family, *HWP1* or *BCR1*.

In general, transcription factors are bipartite in nature, possessing distinct DNA binding and activation domains. The requirement of a strong protein–DNA interaction constrains the flexibility of the DNA binding domain to evolve, resulting in several well-conserved domains that form the basis of transcription factor families. One of these families, the zinc cluster proteins, is characterized by a signature motif ($CX_2CX_6CX_{5-12}CX_2CX_{6-8}C$) containing six conserved cysteine residues that bind two zinc atoms (for review see MacPherson *et al*., 2006). This family of regulators is found exclusively in fungi. In *S. cerevisiae*, zinc cluster transcription factors are involved in regulating a broad range of cellular processes including primary and secondary metabolism, mitosis and meiosis, chromatin remodelling, stress response and multidrug resistance (MacPherson *et al*., 2006). Interestingly, while *S. cerevisiae* possesses 54 such factors, *C. albicans* contains 77 (Braun *et al*., 2005). Thus, there are many zinc cluster proteins in *C. albicans* with no obvious orthologues in *S. cerevisiae.* These factors represent regulators that are potentially involved in *Candida*-specific processes such as virulence, the white–opaque transition, hyphal growth and biofilm formation.

This study characterizes one of these *Candida*-specific zinc cluster factors encoded by *ORF19.7381*. Provisionally named *ZCF37* in the *Candida* Genome Database (CGD, http://www.candidagenome.org/), our findings demonstrate that Zcf37p is the DNA binding factor that recruits Mcm1p to target promoters that lack canonical Mcm1 binding sites, establishing a new mechanism of Mcm1p-directed regulation. This Zcf37p–Mcm1p complex plays an important role in adhesion by directly activating adhesion genes, and is also involved in hyphal growth and in virulence. As a result, we have named *ORF19.7381* as *AHR1* for Adhesion and Hyphal Regulator.

Results

Identification of a Candida*-specific zinc cluster transcription factor*

Candida albicans possesses many uncharacterized putative zinc cluster transcription factors. Our group recently characterized CaNdt80p, a transcription factor involved in regulating ergosterol biosynthesis, hyphal growth, cell separation and virulence (Sellam *et al*., 2009b; 2010). Interestingly, a putative zinc cluster transcription factor, *AHR1* (*ORF19.7381*), was significantly downregulated in the *ndt80* expression profile under hyphal-inducing conditions (Sellam *et al*., 2010), suggesting that Ahr1p might contribute to the inability of the *ndt80* deletion strain to form hyphae. As well, it was reported that an *ahr1* deletion strain exhibits morphological defects when cultured on Spider media at 30°C or on either YPD or Lee's media at 37°C (Homann *et al*., 2009).

Sequence analysis of *C. albicans* Ahr1p revealed putative orthologues only in the *Candida*-clade of the Saccharomycotina subphylum (data not shown), a pattern similar to that previously observed for CaNdt80p (Sellam *et al*., 2010). Searches directed outside of the *Candida*-clade showed homology strictly in the well-conserved zinc cluster DNA binding domain. Our lab and others have used the technique of chromatin immunoprecipitation coupled to microarray analysis (ChIP-chip) to characterize *C. albicans* transcription factors and provide insights into the evolution of its transcriptional networks (Borneman *et al*., 2007; Hogues *et al*., 2008; Tuch *et al*., 2008; Askew *et al*., 2009; Nobile *et al*., 2009; Lavoie *et al*., 2010). Therefore, we decided to perform ChIP-chip with Ahr1p as this factor represents a potential *Candida*-specific morphological regulator.

Location profiling reveals that Ahr1p binds the promoters of genes involved in biofilm formation

We performed two biological replicates of the ChIP-chip experiment under standard growth conditions (log phase in YPD media at 30°C) and hybridized half of each sample to our full-genome microarray that contains single-intergenic probes. The enriched targets of the two replicates were highly similar ($P = 4.82 \times 10^{-121}$) so one replicate was chosen to hybridize to a tiling array for detailed analysis. There were 275 sites with a smoothed-peak intensity greater than twofold. Assigning these peaks to particular genes (Table S1, see *Experimental procedures* for criteria) and taking into account multiple peaks in the same gene's promoter resulted in 182 gene targets. Gene ontology (GO) analysis of these targets revealed enrichment for biofilm formation, filamentous growth, adhesion, regulation of RNA metabolism and amino acid transport (Fig. 1A). While approximately 60%

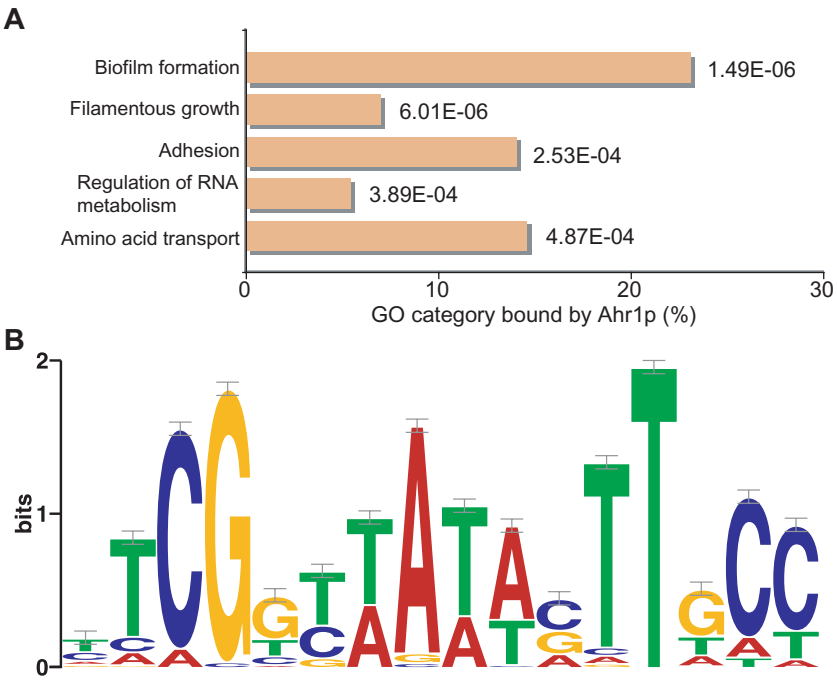

Fig. 1. Ahr1p binds many promoter targets involved in biofilm formation and recognizes a typical zinc cluster motif.
A. ChIP-chip of Ahr1p was performed and the 182 gene targets with a peak intensity greater than twofold were analysed for GO enrichment. GO categories with $P < 0.0005$ are displayed with the *P*-value indicated. Only the general categories of adhesion and filamentous growth are shown although more specific categories related to these processes were enriched but were omitted because of redundancy.
B. Consensus motif representing the binding site of Ahr1p based on the top peak intensity targets (> 5-fold enrichment). The sequence surrounding each peak point (covering five probes, 300 bp) was sent to MEME (http://meme.sdsc.edu/meme4_5_0/intro.html) and the most significant motif is reported.

of *C. albicans*' genes have an orthologue in *S. cerevisiae* (based on the latest CGD orthologue mapping, March 29, 2010, http://www.candidagenome.org), only 41% of Ahr1p targets (74 out of 182 genes) have a *S. cerevisiae* orthologue, suggesting that the factor is important for regulating *Candida*-specific processes.

Ahr1p recognizes a characteristic zinc cluster factor motif

The binding sites of Ahr1p were analysed for the presence of a motif. Zinc cluster factors commonly bind as dimers to a pair of CGG triplets organized as direct, indirect or inverted repeats that are separated by a sequence of variable length (MacPherson *et al*., 2006). *De novo* motif analysis by MEME of the top Ahr1p peak intensity targets (at least fivefold) showed a strong enrichment for one motif (*E*-value = 1.0×10^{-73}) (Fig. 1B). This sequence shows characteristics of a typical zinc cluster factor motif with CGG/GCC triplets separated by eight bases.

Ahr1p recruits Mcm1p to Ahr1p target sites

Intriguingly, the motif enriched in the Ahr1p ChIP-chip targets is identical to a motif previously reported for Mcm1p in *C. albicans* (Tuch *et al*., 2008). Mcm1p is a highly conserved fungal regulator with a MADS-box domain that functions as both a DNA binding and a dimerization domain. Mcm1p has been well studied in *S. cerevisiae* where it has been shown to be involved in modulating distinct regulons controlling the cell cycle, mating and arginine metabolism (for review see Messenguy and Dubois, 2003). Mcm1p functions as a combinatorial regulator; it requires different cofactors to achieve regulatory specificity, with the cofactor binding to a sequence adjacent to the Mcm1p binding site. ChIP-chip of Mcm1p in *C. albicans* showed that a subset of the targets (110 of the 761 total targets) had a non-canonical motif distinct from the standard MADS-box type motif [CC(A/T)$_6$GG] found at the other targets (Tuch *et al*., 2008). This binding pattern was unique to *C. albicans* as ChIP-chip of Mcm1p in *S. cerevisiae* and the dairy yeast *Kluyveromyces lactis* showed enrichment only for the canonical Mcm1p motif (Tuch *et al*., 2008). The *C. albicans*-specific non-canonical Mcm1p motif was the same one we discovered among the Ahr1p targets, and as seen with the Ahr1p sites, this subset of Mcm1p targets was enriched for genes involved in adhesion and biofilm formation (Tuch *et al*., 2008).

As the Mcm1p non-canonical motif has characteristics of a zinc cluster factor motif and it is unlikely Mcm1p recognizes two distinct motifs, we hypothesized that Ahr1p is responsible for binding to these non-canonical motif targets and directing Mcm1p to regulate gene expression. To test this hypothesis we performed ChIP-chip of Mcm1p in both a wild-type strain [Mcm1p(WT)] and a strain deleted for *AHR1* [Mcm1p(*ahr1*)]. We had previously performed ChIP-chip with Mcm1p to demonstrate the validity of our TAP-tag approach (Lavoie *et al*., 2008) compared with the Mcm1p antibody method employed by Tuch *et al*. (2008). However, we did not hybridize Mcm1p to a tiling array in that previous work so we repeated the

ChIP-chip experiment of Mcm1p in the wild-type strain. As a control, before hybridizing to the tiling array we hybridized half the sample to the single-intergenic-probe full-genome array. The enriched targets were highly similar to our previously published list ($P = 6.88 \times 10^{-182}$) (Lavoie *et al*., 2008). Two biological replicates of Mcm1p(*ahr1*) were performed and showed highly similar results with the single-intergenic-probe array ($P < 10^{-300}$). One replicate was chosen for hybridization to the tiling array.

Comparison of the Mcm1p(WT) and Ahr1p ChIP-chip targets with the tiling array revealed a strong overlap between the two experiments. All of the top 50 Ahr1p peak intensity sites were bound by Mcm1p(WT) (Table 1). Of the 182 gene targets of Ahr1p, 179 were bound by Mcm1p(WT) with a peak intensity greater than 1.5 with 146 having an enrichment of more than 2. Additionally, Mcm1p(WT) bound the promoters of 352 genes that were not Ahr1p targets (see Table S2 for complete gene targets).

Including the Mcm1p(*ahr1*) ChIP-chip results (see Table S3 for complete gene targets) in the analysis showed a clear interaction between Mcm1p and Ahr1p. Of the top 50 Ahr1p peak intensity targets, 48 were affected by the loss of *AHR1* with 42 having peak intensities less than twofold in Mcm1p(*ahr1*) (Table 1). Comparing Mcm1p(WT) vs. Mcm1p(*ahr1*), GO analysis revealed that the *P*-value of enrichment was reduced for the Ahr1p-related processes including biofilm formation (1.07×10^{-06} vs. 2.79×10^{-04}), filamentous growth (9.49×10^{-07} vs. 1.29×10^{-04}) and adhesion (1.53×10^{-06} vs. 2.54×10^{-03}) but increased for Ahr1p-independent processes such as arginine metabolism (2.12×10^{-04} vs. 4.47×10^{-07}).

We performed motif analysis with the highest peak intensity targets (at least fivefold). For Mcm1p(WT), MEME analysis showed enrichment of two motifs corresponding to the Mcm1p canonical motif (*E*-value = 3.7×10^{-110}) and non-canonical motif (*E*-value = 2.5×10^{-17}) (Fig. 2A) as previously reported (Tuch *et al*., 2008). For Mcm1p(*ahr1*), MEME analysis revealed only the canonical motif (*E*-value = 5.8×10^{-167}) with a higher enrichment in the data set compared with Mcm1p(WT) (Fig. 2A). Therefore, based on GO and motif analysis, Ahr1p is required for Mcm1p to recognize the non-canonical motif. Thus, from here on, the Mcm1p motif refers to the canonical motif for Mcm1p, and the Ahr1p motif refers to the non-canonical motif that represents Mcm1p binding directed by Ahr1p.

The Mcm1p targets can be divided into four groups. The first group (type 1) is the largest and represents Mcm1p targets that were unaffected by the loss of *AHR1* (Fig. 2Bi). Mcm1p binds these targets directly as the binding sites generally contained Mcm1p motifs and were not significantly bound by Ahr1p. The second group (type 2) consists of targets that were bound by Mcm1p(WT), but

Table 1. Mcm1p ChIP-chip fold enrichments of the top Ahr1p binding sites.

Gene name[a]	Ahr1p fold enrichment	Mcm1p(WT) fold enrichment	Mcm1p(*ahr1*) fold enrichment[b]
CTA4	20.67	12.67	–
RME1[c]	15.73	7.95	–
orf19.699	14.96	9.47	–
CAM1	13.03	7.37	–
SPO11/RCR1	12.53	11.17	–
orf19.7152	11.19	6.99	–
EFG1[c]	10.55	10.73	–
COG2/RFG1[c]	10.48	11.33	–
CDC8/SVL3	10.41	5.92	–
AHR1/orf19.7380[c]	10.36	7.95	–
N/A	10.09	7.24	–
CTN2	9.91	3.76	–
N/A	9.90	6.47	–
MDR1[d]	9.52	12.88	6.99
N/A	9.46	7.10	–
AHR1	9.15	10.55	2.04
GIT2	9.14	5.94	–
ALS1	9.07	7.06	–
orf19.6805[c]	9.00	6.69	–
ENA21	8.87	7.87	–
TEC1[c]	8.67	9.03	–
GCN4	8.48	3.88	–
orf19.2332/orf19.2333	7.98	5.62	–
N/A	7.87	7.12	–
orf19.7306	7.61	9.35	2.24
EMC9/orf19.1906	7.60	5.25	–
CSR1	7.45	6.85	–
orf19.251[d]	7.04	8.06	5.66
orf19.6996	7.03	6.48	–
orf19.4459	6.98	6.67	–
FCR1	6.95	5.46	–
NTA1/orf19.851	6.86	5.50	–
GAP4	6.75	4.30	–
APN2/orf19.1835	6.73	4.94	–
orf19.4531[d]	6.70	8.90	8.45
orf19.450[c]	6.66	6.95	–
SFK1[c]	6.40	6.52	–
PHM7/orf19.2169	6.37	10.38	–
AAF1[c]	6.35	5.44	–
PHO2[c]	6.16	4.73	–
N/A	6.16	4.08	–
orf19.2724	6.15	3.60	3.58
N/A	6.12	5.19	–
RPC31	6.08	4.93	–
CRZ2[c]	6.00	5.36	–
PYR2	5.91	2.84	–
SFK1[c]	5.78	5.70	3.02
FAA4[c]	5.73	5.92	3.64
SOD5/orf19.2059	5.59	3.18	–
GPX2	5.40	4.23	–

a. Peaks at the 3′ ends of adjacent genes could not be associated with a gene and are called N/A.
b. Fold enrichments < 2 are indicated with '–'.
c. Binding site is > 2 kb upstream of the gene's start codon.
d. Mcm1p canonical motif at binding site among Mcm1p(*ahr1*) targets with a fold enrichment > 2.

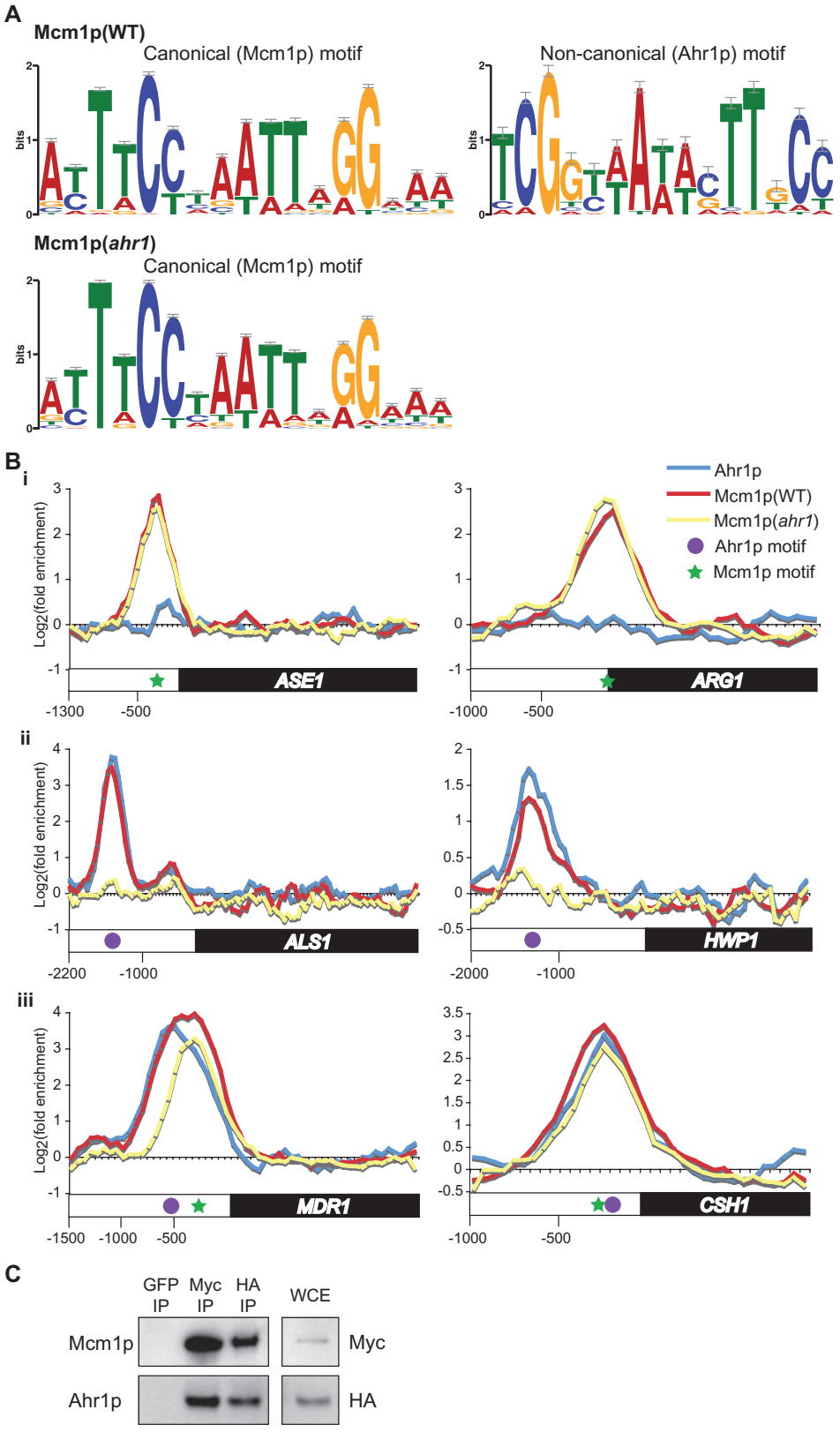
A
Mcm1p(WT)
Canonical (Mcm1p) motif
Non-canonical (Ahr1p) motif
Mcm1p(ahr1)
Canonical (Mcm1p) motif
bits
B
i
ii
iii
Ahr1p
Mcm1p(WT)
Mcm1p(ahr1)
Ahr1p motif
Mcm1p motif
Log2(fold enrichment)
ASE1
ARG1
ALS1
HWP1
MDR1
CSH1
C
GFP IP
Myc IP
HA IP
WCE
Mcm1p
Ahr1p
Myc
HA

Fig. 2. Ahr1p directs Mcm1p binding to the non-canonical motif.
A. Consensus motifs representing the binding sites of Mcm1p in a wild-type strain and an *ahr1* deletion strain based on ChIP-chip. The sequence surrounding (covering five probes, 300 bp) the top peak intensity targets (> 5-fold enrichment) was sent to MEME (http://meme.sdsc.edu/meme4_5_0/intro.html) and the most significant high-complexity motifs are reported.
B. ChIP-chip binding curves representing Ahr1p, Mcm1p(WT) and Mcm1p(*ahr1*) binding for type 1 (i), type 2 (ii) and type 3 (iii) Mcm1p targets. Data points for the curves were plotted at each probe position of 60 bp intervals. Values were determined by taking the mean fold enrichment of each probe and the surrounding four probes.
C. Immunoprecipitations with an Ahr1p HA-tagged and Mcm1p Myc-tagged strain were performed with cells grown in YPD media at 30°C. The top labels refer to the antibody used in the immunoprecipitation and the labels on the right refer to the primary antibody used to probe the membrane. The GFP antibody was used as a negative control and WCE represents the whole cell extract.

lost all binding in Mcm1p(*ahr1*) (Fig. 2Bii). These targets were strongly bound by Ahr1p and generally possessed the Ahr1p motif. Note in Fig. 2Bii how the Ahr1p and Mcm1p(WT) peaks overlap indicating a common binding site. Mcm1p binds this group of targets, which includes several adhesion genes and hyphal regulators involved in biofilm formation (*ALS1*, *ALS4*, *HWP1*, *EFG1* and *TEC1*), indirectly through Ahr1p. The third group (type 3) is the smallest and is characterized by a reduction but not complete loss of Mcm1p(*ahr1*) binding compared with Mcm1p(WT) (Fig. 2Biii). These targets were bound by Ahr1p but analysis of these promoter regions often revealed the presence of both the Mcm1p and Ahr1p motifs. As Mcm1p is able to bind these targets both directly and indirectly, loss of *AHR1* only disrupts the indirect interaction. In the case of *MDR1*, the Mcm1p(*ahr1*) peak is narrower than the Mcm1p(WT) peak and has shifted towards the Mcm1p motif demonstrating loss of the indirect interaction through Ahr1p while maintaining a direct interaction through the Mcm1p motif (Fig. 2Biii). The final group (type 4) represents targets with a higher peak intensity in Mcm1p(*ahr1*) compared with Mcm1p(WT) and is discussed later.

To confirm an interaction between Ahr1p and Mcm1p at the protein level, we performed immunoprecipitations using an Ahr1p HA-tagged and Mcm1p Myc-tagged strain. In an anti-HA antibody immunoprecipitation we were able to detect both Ahr1p and Mcm1p (Fig. 2C). As well, we were able to detect both proteins in an anti-Myc antibody immunoprecipitation. Therefore, Ahr1p and Mcm1p interact with each other, further supporting our conclusions that Ahr1p recruits Mcm1p to Ahr1p target promoters. Although it is impossible to accurately quantitate proteins during immunoprecipitations, essentially no Ahr1p was found in the extracts after co-immunoprecipitation with tagged Mcm1p, while considerable Mcm1p was detected remaining after the Ahr1p immunoprecipitation (data not shown). This result suggests that the majority of Ahr1p is complexed with Mcm1p while only a small fraction of Mcm1p is associated with Ahr1p, which correlates with the observation that Mcm1p forms several other protein complexes (Tuch *et al*., 2008).

The Ahr1p–Mcm1p complex directly activates the expression of adhesion genes

To gain insight into the role of the Ahr1p–Mcm1p complex, we focused on the effect of deleting *AHR1*. This approach was used as Mcm1p is recruited to virtually all of Ahr1p's targets but Mcm1p is also involved in other Ahr1p-independent regulons. Therefore, deleting *AHR1* selectively disrupts the Ahr1p–Mcm1p complex without interfering with the other Mcm1p regulatory circuits. Furthermore, *MCM1* is an essential gene (Rottmann *et al*., 2003) so deletion analysis is not possible.

We first performed an expression profile with an *ahr1* deletion strain (log phase in YPD media at 30°C) to complement the ChIP-chip profile and determine which genes the Ahr1p–Mcm1p complex directly controls. Comparing expression levels between the *ahr1* deletion strain and the wild type and using a 1.5-fold cut-off, 92 genes were expressed at lower levels in the mutant while 93 genes were expressed at higher levels (Tables S4 and S5). The most significantly downregulated genes showed a strong correlation with the Ahr1p ChIP-chip results and this suggests that Ahr1p functions mainly as a transcriptional activator. Of the top 15 genes with reduced expression in the *ahr1* strain, 13 were bound while only 3 of the top 15 upregulated genes were bound. Strikingly, four of the top nine downregulated genes are involved in adhesion (*ALS1*, *ALS2*, *ALS4* and *CSH1*).

The adhesion gene *HWP1* was not differentially expressed even though Ahr1p bound its promoter. However, *HWP1* is expressed at higher levels in biofilm cells compared with free-living yeast cells (Garcia-Sanchez *et al*., 2004). Therefore, we determined the expression levels of a set of adhesion genes in the *ahr1* strain compared with the wild type during the initial adhesion step in biofilm formation on polystyrene (Fig. 3). Under these conditions *HWP1* was downregulated in the *ahr1* strain, demonstrating that the Ahr1p–Mcm1p complex activates the gene during adhesion to polystyrene. We also measured *BCR1* expression to determine whether any changes in adhesion gene expression could be indirectly attributed to this factor but we observed no change (0.98 ± 0.16).

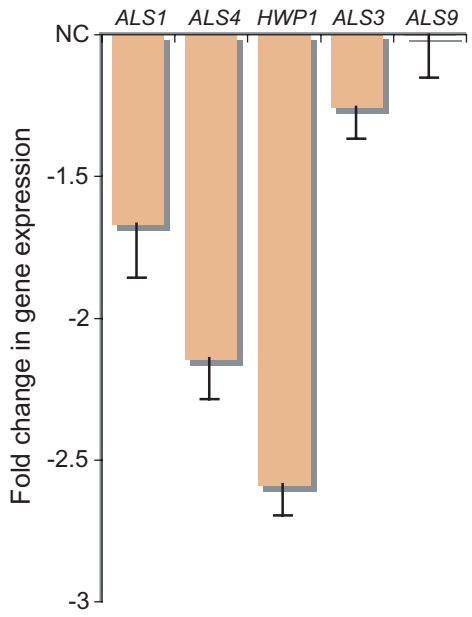

Fig. 3. The Ahr1p–Mcm1p complex activates *ALS1*, *ALS4* and *HWP1* under adhesion-promoting growth conditions. RNA was extracted after 2 h of adhesion to a polystyrene surface and mRNA expression of selected adhesion genes was determined by qPCR for the *ahr1* strain (CAS12) compared with the wild-type strain (CAS19). 'NC' indicates no change in gene expression. *ALS3* and *ALS9* were included as comparison references as neither Ahr1p nor Mcm1p bound their promoters and their expression was unchanged in the *ahr1* transcription profile.

Disrupting the Ahr1p–Mcm1p complex affects adhesion ability and hyphal growth

During analysis of the adhesion gene expression levels, we observed that after the 2 h incubation on polystyrene there was a clear reduction in the number of *ahr1* adhered cells compared with the wild type (Fig. 4A). This adhesion defect was also observed when silicone was used as the substrate (data not shown). For the polystyrene sample, a semi-quantitative XTT assay was performed to measure the metabolic activity of the cells and thus approximate the number of cells. The wells containing the *ahr1* cultures had about one-third of the metabolic activity of the wells containing the wild-type cultures (Fig. 4B). The *ahr1/AHR1*-TAP strain was included to demonstrate that the TAP-tag used for the ChIP-chip experiment did not interfere with the function of Ahr1p. The *ahr1* strain was still able to develop a biofilm with filamentation, although the density was reduced because of the initial adhesion defect (Fig. 4A). This result was reflected by the reduction in the biofilm dry mass (Fig. 4C).

Although we observed hyphal formation in the *ahr1* strain during biofilm development, we wanted to further investigate the role of the Ahr1p–Mcm1p complex in hyphal growth as our initial hypothesis was that Ahr1p was a morphological regulator and the ChIP-chip of Ahr1p was enriched for targets involved in filamentous growth. On solid media at 37°C with YPD, YPD and serum, or M199 pH 8, the *ahr1* colonies were unable to form wrinkles or filaments compared with the wild type (Fig. 5). In liquid media, the *ahr1* strain was still able to filament when induced with serum but the average hyphal length of the *ahr1* cells was significantly shorter ($P < 0.0001$, *t*-test) than either the wild-type or complemented strains (Table S6). Therefore, the Ahr1p–Mcm1p complex is involved in the regulation of adhesion and hyphal growth.

An ahr1 *strain has attenuated virulence in a systemic infection mouse model*

As the Ahr1p–Mcm1p complex was involved in regulating adhesion and showed defects in the yeast–hyphal switch, we tested whether deleting *AHR1* affects the virulence in a systemic infection C57BL/6J mouse model. However, because the *ahr1* mutant (CAS12) was constructed in a uracil auxotrophic background (BWP17), which can influence the interpretation of virulence results (Lay *et al.*, 1998), we created a new *ahr1* deletion strain (CaEE534) in the SN95 background. The SN95 strain does not have any influence on virulence as shown by different labs using various mouse models (Noble and Johnson, 2005; Epp *et al.*, 2010a). The SN95 *ahr1* deletion strain (CaEE534) showed filamentation and biofilm phenotypes similar to strain CAS12 (data not shown). In the C57BL/6J mouse model, the *ahr1* strain (CaEE534) displayed significant attenuated virulence compared with both the wild-type (SN95, $P = 0.0152$, log–rank test) and complemented strains (CaEE573, $P = 0.0032$) (Fig. 6A). We also observed that the *ahr1*-injected mice accumulated a significantly higher fungal burden at the time when the mice became moribund (Fig. 6B), suggesting that the mice can tolerate higher levels of the attenuated pathogen. Together, our data suggest that the Ahr1p–Mcm1p regulon is important for the full pathogenicity of *C. albicans*.

Discussion

The sequencing of multiple *Candida* species has allowed for a detailed comparative genomic analysis between the genomes of the Saccharomycotina subphylum (Butler *et al.*, 2009). A major goal of such an investigation is to identify the genomic basis for the phenotypic differences in pathogenicity. As the zinc finger transcription factor family is more abundant in *Candida* species compared with *Saccharomyces* species (Butler *et al.*, 2009), these transcription factors are ideal candidates for regulators of *Candida*-specific processes important for virulence including the yeast–hyphal transition and biofilm formation. By investigating the *Candida*-specific zinc cluster transcription factor Ahr1p in *C. albicans*, we were able to identify a new Mcm1p

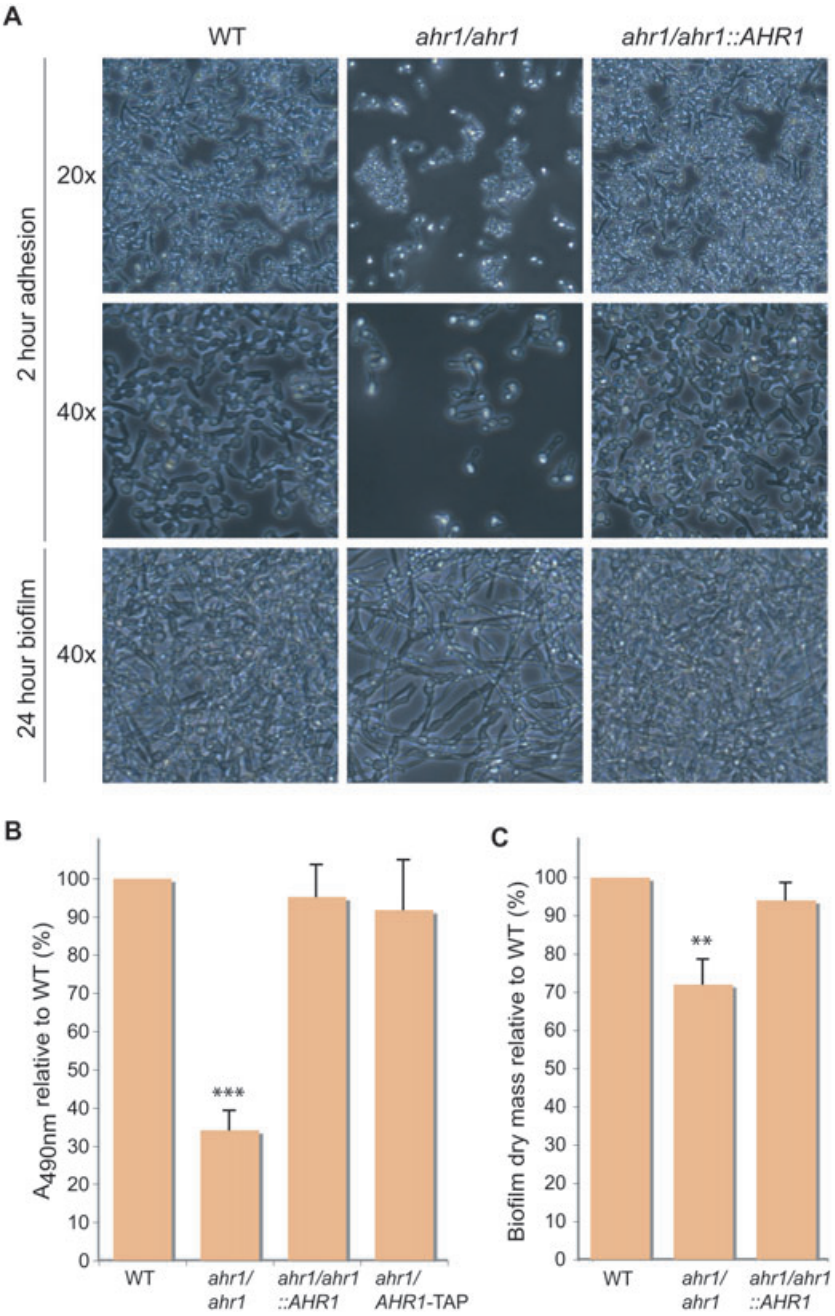

Fig. 4. Disrupting the Ahr1p–Mcm1p complex affects adherence to polystyrene and reduces biofilm density. Strains used were WT (CAS19), *ahr1/ahr1* (CAS12), *ahr1/ahr1::AHR1* (CAS13) and *ahr1/AHR1-TAP* (CAS15).
A. Overnight cultures were resuspended in RPMI media at OD_{600} = 1 and 100 µl was added to each well in a 96-well plate. After 2 h of rocking incubation at 37°C, the non-adherent cells were removed, the wells were washed with PBS, and pictures were taken at 20× (top panel) and 40× (middle panel) magnification. Fresh RPMI media was added, the plate was incubated with rocking for 24 h at 37°C to allow for biofilm development, and pictures were then taken at 40× magnification (bottom panel).
B. An XTT assay was performed after the 2 h adhesion step. Absorbencies were reported relative to the WT strain. The symbol '***' indicates a significant difference ($P < 0.0001$, *t*-test) compared with both wild-type and complemented strains.
C. Biofilm dry masses were determined after 24 h of development. Masses were reported relative to the WT strain. The symbol '**' indicates a significant difference ($P < 0.01$, *t*-test) compared with both wild-type and complemented strains.

co-regulator involved in virulence and virulence-related processes. Using ChIP-chip and co-immunoprecipitation, we established that Ahr1p binds its target promoters, including several adhesion genes, through a zinc cluster factor motif, and that it interacts with and recruits Mcm1p to these sites. Previously observed Mcm1p regulons required both Mcm1p and the cofactor to bind adjacently to the DNA. Therefore, our study not only established an interaction between Mcm1p and Ahr1p but also a new mechanism of Mcm1p-directed regulation.

This new mode of Mcm1p regulation appears to be a recent development; the Ahr1p motif is only found in *C. albicans* and the closely related *C. dubliniensis* as shown by promoter analysis of the Mcm1p non-canonical motif target orthologues across 32 fungal species (Tuch *et al*., 2008), although the complex may have evolved earlier and just recently moved to this set of targets. If the regulon is a recent development, it is possible that the mode of Ahr1p–Mcm1p regulation is still in a transitory state. Originally, Ahr1p and Mcm1p might have each

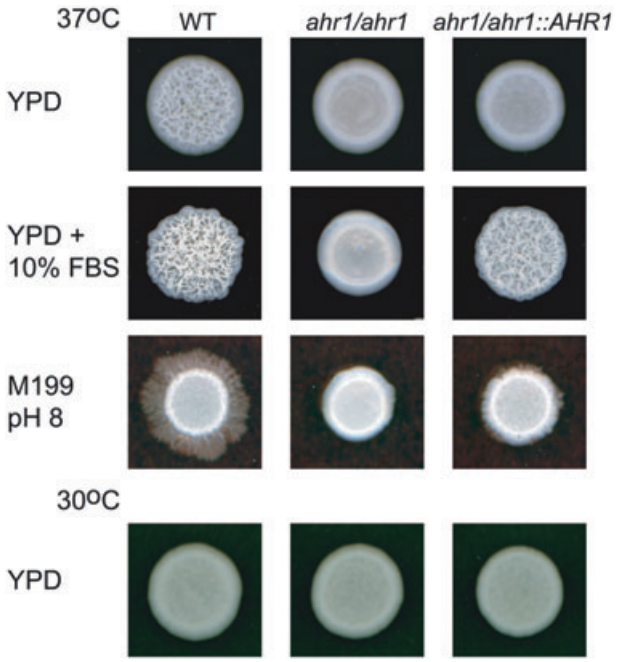

Fig. 5. The Ahr1p–Mcm1p complex controls the yeast–hyphal switch. Cells were serially diluted and a representative dilution is shown. Strains used were WT (CAS19), *ahr1/ahr1* (CAS12) and *ahr1/ahr1::AHR1* (CAS13). Pictures were taken after 4 days for M199 pH 8 and after 2 days for the other conditions. Although the *ahr1/ahr1::AHR1* strain did not revert the phenotype for YPD and M199 pH 8 at 37°C, three independently constructed heterozygous strains (CAS25) showed the same phenotype as the complemented strain (data not shown), indicating that *AHR1* shows haplo-insufficiency under some hyphal growth conditions.

bound DNA separately, similar to the situation observed with the other known yeast Mcm1p regulons (Messenguy and Dubois, 2003). Over time, Ahr1p and Mcm1p might then have evolved to interact at a protein level with DNA providing a scaffold for this to occur. Eventually, the two proteins developed a strong enough interaction that Mcm1p no longer needed to directly bind DNA. Without selective pressure acting on the Mcm1p motif at the Ahr1p–Mcm1p targets, it was lost for most of the targets, resulting in the type 2 targets that are completely dependent on Ahr1p DNA binding, while it was retained at a few sites, the current type 3 targets containing both Ahr1p and Mcm1p motifs. Alternatively, the type 2 targets might represent the ancestral mode of regulation developed by an initial protein–protein interaction between Mcm1p and Ahr1p. Over time, Mcm1p binding sites developed for a few targets allowing Mcm1p to directly interact with the DNA. In this scenario, the regulon is evolving towards type 3 targets and the standard mode of Mcm1p regulation.

Mcm1p type 2 targets demonstrate the potential of ChIP-chip to detect indirect protein–DNA interactions and falsely associate a motif with a transcription factor. Recent studies have developed methods that attempt to address this problem by distinguishing direct and indirect transcription factor binding events (Gordan *et al.*, 2009; Zhu *et al.*, 2009). It was found that 16% of the ChIP-chip data sets from *S. cerevisiae* correlated with indirect binding of the factor (Gordan *et al.*, 2009). The ability to determine whether a transcription factor is binding directly or indirectly is useful in predicting protein complexes, just as we showed in this study.

We further investigated the functional role of this newly formed Mcm1p complex in *C. albicans*. Our results established that the Ahr1p–Mcm1p complex is a direct activator of several key adhesion genes and that disrupting this complex by deleting *AHR1* resulted in reduced adherence of *C. albicans* cells to polystyrene

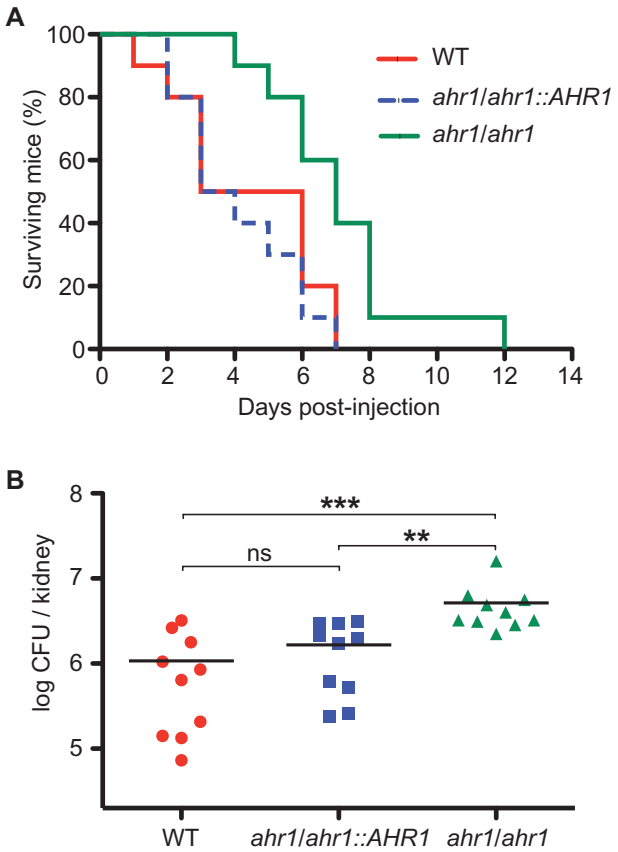

Fig. 6. An *ahr1* strain displays attenuated virulence in a C57BL/6J mouse model.
A. Survival curves of mice infected with WT (SN95), *ahr1/ahr1* (CaEE534) and *ahr1/ahr1::AHR1* (CaEE573) strains. Mice were monitored daily according to approved protocols.
B. Comparison of the kidney fungal load of mice infected with WT (SN95), *ahr1/ahr1* (CaEE534) and *ahr1/ahr1::AHR1* (CaEE573) strains. Kidney fungal burdens were assessed at the time of sacrifice when mice were determined to be moribund. Mutant-infected mice survived longer and accumulated a statistically significantly higher fungal burden compared with both WT and revertant-infected mice as indicated (***$P < 0.001$; **$P < 0.01$; ns $P > 0.05$).

and silicone surfaces. The *ahr1* strain was able to develop a biofilm, but with a reduced biomass. As well, the *ahr1* strain had defects in the yeast–hyphal switch under several different growth conditions. Although we analysed the *ahr1* strain in order to selectively disrupt the Ahr1p–Mcm1p complex, it should be noted that overexpression of *MCM1* has been shown to result in increased adhesion as well as defects in the yeast–hyphal transition (Rottmann *et al*., 2003).

Our results, combined with previous studies on Bcr1p, suggest that the Ahr1p–Mcm1p complex and Bcr1p regulate adhesion genes separately. Ahr1p or Mcm1p did not bind the promoter of Bcr1p and *BCR1* expression was not affected by deletion of *AHR1*. As well, *AHR1* expression was not affected by deletion of *BCR1* (Nobile and Mitchell, 2005). Furthermore, the Ahr1p–Mcm1p complex and Bcr1p have some different adhesion targets as Ahr1p–Mcm1p solely regulate *ALS4* while Bcr1p solely regulates *ALS3* (Nobile and Mitchell, 2005; Nobile *et al*., 2006b).

Disrupting the Ahr1p–Mcm1p interaction caused Mcm1p to bind new sites in which the peak intensity was greater in the *ahr1* mutant strain compared with the wild-type strain (type 4 targets). Analysis of this group of targets revealed that these sites are almost exclusively found near protein translation genes including most of the ribosomal protein encoding genes. Interestingly, many of the peaks were at the 3′ end of these genes so our peak analysis algorithm would either not associate the peak with a gene or assign the peak to a different gene. The peak intensity of the type 4 targets was generally just above the cut-off in the *ahr1* strain (2- to 2.5-fold) and often there was a weak signal in the wild-type strain. Generally, no Mcm1p motif was present. Therefore, it appears that Mcm1p very weakly associates with the translational machinery genes and disrupting the interaction with Ahr1p enhances this association.

Our study primarily focused on the role of the Ahr1p–Mcm1p complex in regulating adhesion; however, our results suggest additional roles for the regulon. As previously mentioned, there is a link between biofilm development and drug resistance. Mcm1p has been shown to regulate *MDR1*, which encodes a key drug transporter that is upregulated in many fluconazole-resistant strains, although it was concluded that elements upstream of the Mcm1p canonical motif were also required for *MDR1* activation (Riggle and Kumamoto, 2006). Our results demonstrated that Mcm1p binds to the *MDR1* promoter at its canonical motif independently of Ahr1p and is also recruited to a non-canonical motif by Ahr1p. This Ahr1p motif is upstream of the Mcm1p motif and is located in a region identified as containing a *cis*-acting sequence of *MDR1* (Harry *et al*., 2005; Hiller *et al*., 2006). As well, Cdr1p, another key drug transporter upregulated in fluconazole-resistant strains, is also a type 3 Mcm1p target. Although the *ahr1* strain shows no difference in sensitivity to fluconazole compared with the wild type (Homann *et al*., 2009), the role of the Ahr1p–Mcm1p complex in regulating drug transporters is an area of interest.

Links have also been established between biofilm formation and mating in *C. albicans*. Pheromone induces mating in opaque cells but promotes substrate adhesion and enhanced biofilm development in white cells (Daniels *et al*., 2006). Both white and opaque cell responses to pheromone involve the same receptors and MAP-kinase pathway but activate a different transcription factor (Yi *et al*., 2008). While Cph1p is the target of the opaque cell pheromone response pathway (Yi *et al*., 2008), Tec1p is the downstream target of the white cell pheromone response pathway (Sahni *et al*., 2010). Tuch *et al*. (2008) identified that the subset of non-canonical Mcm1p targets includes several regulators of the white–opaque switch and strongly overlaps with the binding targets of Wor1p. As Ahr1p recruits Mcm1p to the promoter regions of *TEC1* and the white–opaque regulators *WOR1*, *WOR2* and *EFG1,* the complex's role in this aspect of cell function is another area of interest.

Our study provides insight into a Mcm1p regulon controlled by a *Candida*-specific zinc cluster factor involved in the regulation of important pathogenic characteristics such as adhesion and the yeast–hyphal transition. The reduced virulence of the *ahr1* strain in a systemic infection mouse model further highlights the potential of zinc cluster proteins as antifungal drug targets. Zinc cluster proteins have a common structural domain, are fungal specific and regulate diverse cellular processes; therefore, the targeted disruption of the zinc cluster domain would certainly result in severe consequences to the cell. Continuing to characterize the zinc cluster family members unique to *C. albicans* will allow for more insight into the regulation of *Candida*-specific transcriptional networks that are critical for the virulence of this fungus.

Experimental procedures

C. albicans *strain construction and media*

The *C. albicans* strains used in this study are listed in Table S7. Unless otherwise stated, cells were grown at 30°C in media containing 1% yeast extract, 2% peptone, 2% dextrose (YPD) and supplemented with uridine (50 μg ml^{-1}).

Gene disruption of *AHR1* was done as described previously for *NDT80* (Sellam *et al*., 2009b) in a BWP17 background using *URA3* and *HIS1* PCR deletion cassettes, resulting in *ahr1* deletion strain CAS12. For an auxotrophic control, the plasmid CIp20 (Dennison *et al*., 2005) was digested with StuI and transformed into BWP17, resulting in strain CAS19. The *ahr1/ahr1::AHR1* complemented strain

(CAS13) was created using the *SAT1*-flipper cassette as previously done for *TYE7* and *GAL4* (Askew *et al*., 2009). The *AHR1* gene along with 500 bp upstream and downstream homology regions of *AHR1* were cloned into plasmid pSFS2A (Reuss *et al*., 2004), resulting in plasmid pCA4. We selected clones that replaced the *HIS1* deletion cassette and then restored histidine prototrophy by transformation with NruI-digested pGEM-*HIS1* (Wilson *et al*., 1999). As some filamentation phenotypes were not reverted, independent *AHR1/ahr1* heterozygous deletion strains (CAS25) were created with the *HIS1* PCR deletion cassette and then transformed with StuI-digested Clp10 (Murad *et al*., 2000). For ChIP-chip experiments, Ahr1p and Mcm1p were tagged chromosomally with a TAP-*URA3* PCR product (Lavoie *et al*., 2008) in either a BWP17 or *ahr1* background (strains CAS11, CAS23 and CAS24). For the *ahr1* strain (CAS12) background, the *URA3* marker from the deletion cassette was recycled using 5-fluoroorotic acid. To ensure that the TAP-tag did not interfere with the function of Ahr1p, the *HIS1* PCR deletion cassette was used to delete the untagged allele of strain CAS11, resulting in strain CAS15. For immunoprecipitations, Ahr1p was tagged with a HA-*HIS1* PCR product and Mcm1p was tagged with a MYC-*URA3* PCR product (Lavoie *et al*., 2008) in a SN76 background, resulting in strain CAS18. Correct integration for all tags was confirmed by PCR and Western blots were used to verify protein expression. For the mouse study, a new *ahr1* deletion strain (CaEE534) and complemented strain (CaEE573) were constructed in the SN95 background to eliminate any *URA3* positional effects (Lay *et al*., 1998). The nourseothricin marker was used as previously described (Epp *et al*., 2010b). Briefly, 300 bp of upstream and downstream homology regions of *AHR1* were cloned into plasmid pSFS2A (Reuss *et al*., 2004), resulting in plasmid pEE95, to sequentially delete both alleles of *AHR1*. Plasmid pCA4 was used to construct the revertant strain (CaEE573) as was done to create CAS13 in the BWP17 background.

ChIP-chip

ChIP-chip experiments were performed as previously described (Askew *et al*., 2009) with two biological replicates for each condition. Half of the labelled samples were hybridized to single spot full-genome (ORF and intergenic) microarrays containing 11 817 70-mer oligonucleotide probes (Lavoie *et al*., 2008). Targets with a fold enrichment > 1.5 were compared between the two replicates to ensure a high degree of overlap. The other half of one replicate was then chosen for hybridization to a custom designed whole-genome tiling array (Askew *et al*., 2009). Normalization and peak detection were performed as previously described (Askew *et al*., 2009). Peaks located within 2 kb upstream and 120 bp downstream (to account for location uncertainty of the tiling array) of a start codon were assigned to the gene and reported in Tables S1–S3 with ORFs annotated as 'dubious' or 'spurious' removed from the analysis. In the case of divergent promoters both genes were included provided the peak was within 2 kb of each gene's start codon. Genes with multiple peaks in the promoter were counted only once for GO analysis, which was performed as previously described (Lavoie *et al*., 2010).

Immunoprecipitations and Western blotting

An Ahr1p HA-tagged and Mcm1p Myc-tagged strain (CAS18) was grown to OD_{600} = 1.0 in YPD media at 30°C. Cells were harvested by centrifugation, washed with IP150 buffer [50 mM Tris-HCl (pH 7.4), 150 mM NaCl, 2 mM $MgCl_2$, 0.1% NP40], and lysed by vortexing with glass beads in IP150 buffer supplemented with a protease inhibitor cocktail tablet (Roche) and 1 mM phenylmethylsulfonyl fluoride (PMSF). The protein extract was clarified by centrifugation and incubated at 4°C with beads conjugated with anti-Myc mouse monoclonal antibody (9E10), anti-GFP rabbit polyclonal antibody (Santa Cruz) or anti-HA rabbit polyclonal antibody (Roche). Following incubation, beads were washed three times with IP150 buffer, boiled with SDS gel loading buffer and resolved in 4–20% gradient SDS polyacrylamide gels. The separated polypeptides were transferred onto a nitrocellulose membrane and analysed by Western blotting using anti-HA (3F10) or anti-Myc (9E10) monoclonal antibodies.

RNA extraction, transcription profiles and qPCR analysis

RNA extraction and transcription profiles were performed and analysed as previously described (Askew *et al*., 2009). Four biological replicates were done (YPD at 30°C) comparing the wild-type (BWP17) and *ahr1* deletion (CAS12) strains and gene lists were created using a fold change in expression > 1.5 or < 0.67 and a *t*-test *P*-value < 0.05.

Cells for qPCR analysis were prepared as described for the XTT adhesion assays below except 2 ml of OD_{600} = 0.5 cell suspension was added to each well in a six-well polystyrene plate (Nunclon). After a 2 h incubation at 37°C both adherent and non-adherent cells were collected with a cell scraper and the RNA was extracted. qPCR analysis was performed as previously described (Askew *et al.,* 2009) except with the Mx3005P QPCR System (Agilent). Samples were done in triplicate and four biological replicates were performed.

Adhesion and biofilm analysis

XTT assays were carried out as previously described (Ramage *et al*., 2001; Kelly *et al*., 2004). Briefly, overnight YPD cultures were washed twice with PBS and resuspended in RPMI 1640 (Gibco) supplemented with L-glutamine to OD_{600} = 1. Ninety-six-well polystyrene plates (Costar) were used and 100 µl of cells was added to each well. The plates were placed in a rocking incubator at 37°C for 2 h. The media and any non-adherent cells were removed and the wells were washed three times with PBS. After washing, 100 µl of a freshly prepared XTT-menadione solution (0.5 g l^{-1} XTT in PBS and 1 µM menadione in acetone) was added to sample and control wells. The plate was incubated in the dark for 2 h at 37°C and the colorimetric change resulting from XTT reduction was measured at 490 nm. Five biological replicates done in triplicate were performed.

Determination of biofilm dry mass was determined based on previous studies (Palanisamy *et al*., 2010) with 2 ml of OD_{600} = 0.5 cell suspension added to each well in a six-well polystyrene plate (Nunclon) for the 2 h adhesion step. After

washing with PBS, 2 ml of fresh media was added and the plate was incubated with rocking for an additional 24 h. Biofilms were collected and dried at 37°C for 48 h. Three biological replicates done in triplicate were performed.

Virulence study

The mouse study was carried out as previously described (Mullick *et al*., 2004). Briefly, 8- to 12-week-old C57BL/6J mice (Jackson Laboratories, Bar Harbor, ME, USA) were inoculated via the tail vein with 200 µl of a suspension containing 3×10^5 *C. albicans* in PBS. Ten mice, five female and five male, were used for each experimental group. Mice were closely monitored according to approved protocols and those mice showing extreme lethargy were considered moribund and were euthanized. Kaplan–Meier survival curves were created and compared with the log–rank test and the Kruskal–Wallis test was used to assess significance between fungal burdens (GraphPad Prism 5). The number of fungal cells per kidney was determined by removing kidneys aseptically and homogenizing in PBS before plating on YPD plates containing chloramphenicol (34 µg ml^{-1}). All experimental procedures involving mice were approved by the Biotechnology Research Institute Animal Care Committee, which operated under the guidelines of the Canadian Council of Animal Care.

Accession codes

Microarray data for ChIP-chip and transcription profiling experiments have been submitted to the NCBI Gene Expression Omnibus (GEO) under the Accession Number GSE25174 (http://www.ncbi.nlm.nih.gov/geo).

Acknowledgements

Thanks to members of the Whiteway Lab, BRI Microarray Lab, and BRI Animal Facility, especially Mario Mercier, Patricia Liscourt, Jessy Tremblay and Khairul Islam for technical assistance. This work was supported by grants from the Canadian Institute for Health Research (CIHR) to A.M., A.N. and M.W. (CTP-79843, MOP-84341 and MOP-42516). C.A. was supported by a NSERC PGS Extension Scholarship. This is National Research Council manuscript 53136.

References

Askew, C., Sellam, A., Epp, E., Hogues, H., Mullick, A., Nantel, A., and Whiteway, M. (2009) Transcriptional regulation of carbohydrate metabolism in the human pathogen *Candida albicans*. *PLoS Pathog* **5:** e1000612.

Borneman, A.R., Gianoulis, T.A., Zhang, Z.D., Yu, H., Rozowsky, J., Seringhaus, M.R., *et al*. (2007) Divergence of transcription factor binding sites across related yeast species. *Science* **317:** 815–819.

Braun, B.R., van Het Hoog, M., d'Enfert, C., Martchenko M., Dungan, J., Kuo, A., *et al*. (2005) A human-curated annotation of the *Candida albicans* genome. *PLoS Genet* **1:** 36–57.

Butler, G., Rasmussen, M.D., Lin, M.F., Santos, M.A., Sakthikumar, S., Munro, C.A., *et al*. (2009) Evolution of pathogenicity and sexual reproduction in eight Candida genomes. *Nature* **459:** 657–662.

Chandra, J., Mukherjee, P.K., Leidich, S.D., Faddoul, F.F., Hoyer, L.L., Douglas, L.J., and Ghannoum, M.A. (2001) Antifungal resistance of candidal biofilms formed on denture acrylic in vitro. *J Dent Res* **80:** 903–908.

Daniels, K.J., Srikantha, T., Lockhart, S.R., Pujol, C., and Soll, D.R. (2006) Opaque cells signal white cells to form biofilms in *Candida albicans*. *EMBO J* **25:** 2240–2252.

Dennison, P.M., Ramsdale, M., Manson, C.L., and Brown, A.J. (2005) Gene disruption in *Candida albicans* using a synthetic, codon-optimised Cre-loxP system. *Fungal Genet Biol* **42:** 737–748.

Douglas, L.J. (2003) Candida biofilms and their role in infection. *Trends Microbiol* **11:** 30–36.

Douzery, E.J., Snell, E.A., Bapteste, E., Delsuc, F., and Philippe, H. (2004) The timing of eukaryotic evolution: does a relaxed molecular clock reconcile proteins and fossils? *Proc Natl Acad Sci USA* **101:** 15386–15391.

Epp, E., Vanier, G., Harcus, D., Lee, A.Y., Jansen, G., Hallett, M., *et al*. (2010a) Reverse genetics in *Candida albicans* predicts ARF cycling is essential for drug resistance and virulence. *PLoS Pathog* **6:** e1000753.

Epp, E., Walther, A., Lepine, G., Leon, Z., Mullick, A., Raymond, M., *et al*. (2010b) Forward genetics in *Candida albicans* that reveals the Arp2/3 complex is required for hyphal formation, but not endocytosis. *Mol Microbiol* **75:** 1182–1198.

Garcia-Sanchez, S., Aubert, S., Iraqui, I., Janbon, G., Ghigo, J.M., and d'Enfert, C. (2004) *Candida albicans* biofilms: a developmental state associated with specific and stable gene expression patterns. *Eukaryot Cell* **3:** 536–545.

Gordan, R., Hartemink, A.J., and Bulyk, M.L. (2009) Distinguishing direct versus indirect transcription factor-DNA interactions. *Genome Res* **19:** 2090–2100.

Harry, J.B., Oliver, B.G., Song, J.L., Silver, P.M., Little, J.T., Choiniere, J., and White, T.C. (2005) Drug-induced regulation of the MDR1 promoter in *Candida albicans*. *Antimicrob Agents Chemother* **49:** 2785–2792.

Hawser, S.P., and Douglas, L.J. (1995) Resistance of *Candida albicans* biofilms to antifungal agents in vitro. *Antimicrob Agents Chemother* **39:** 2128–2131.

Heckman, D.S., Geiser, D.M., Eidell, B.R., Stauffer, R.L., Kardos, N.L., and Hedges, S.B. (2001) Molecular evidence for the early colonization of land by fungi and plants. *Science* **293:** 1129–1133.

Hiller, D., Stahl, S., and Morschhauser, J. (2006) Multiple cis-acting sequences mediate upregulation of the MDR1 efflux pump in a fluconazole-resistant clinical *Candida albicans* isolate. *Antimicrob Agents Chemother* **50:** 2300–2308.

Hogues, H., Lavoie, H., Sellam, A., Mangos, M., Roemer, T., Purisima, E., *et al*. (2008) Transcription factor substitution during the evolution of fungal ribosome regulation. *Mol Cell* **29:** 552–562.

Homann, O.R., Dea, J., Noble, S.M., and Johnson, A.D. (2009) A phenotypic profile of the *Candida albicans* regulatory network. *PLoS Genet* **5:** e1000783.

Kelly, M.T., MacCallum, D.M., Clancy, S.D., Odds, F.C., Brown, A.J., and Butler, G. (2004) The *Candida albicans*

CaACE2 gene affects morphogenesis, adherence and virulence. *Mol Microbiol* **53:** 969–983.
Kojic, E.M., and Darouiche, R.O. (2004) Candida infections of medical devices. *Clin Microbiol Rev* **17:** 255–267.
Lavoie, H., Sellam, A., Askew, C., Nantel, A., and Whiteway, M. (2008) A toolbox for epitope-tagging and genome-wide location analysis in *Candida albicans*. *BMC Genomics* **9:** 578.
Lavoie, H., Hogues, H., Mallick, J., Sellam, A., Nantel, A., and Whiteway, M. (2010) Evolutionary tinkering with conserved components of a transcriptional regulatory network. *PLoS Biol* **8:** e1000329.
Lay, J., Henry, L.K., Clifford, J., Koltin, Y., Bulawa, C.E., and Becker, J.M. (1998) Altered expression of selectable marker URA3 in gene-disrupted *Candida albicans* strains complicates interpretation of virulence studies. *Infect Immun* **66:** 5301–5306.
Leroy, O., Gangneux, J.P., Montravers, P., Mira, J.P., Gouin, F., Sollet, J.P., *et al*. (2009) Epidemiology, management, and risk factors for death of invasive Candida infections in critical care: a multicenter, prospective, observational study in France (2005–2006). *Crit Care Med* **37:** 1612–1618.
MacPherson, S., Larochelle, M., and Turcotte, B. (2006) A fungal family of transcriptional regulators: the zinc cluster proteins. *Microbiol Mol Biol Rev* **70:** 583–604.
Mermel, L.A., Farr, B.M., Sherertz, R.J., Raad, I.I., O'Grady, N., Harris, J.S., and Craven, D.E. (2001) Guidelines for the management of intravascular catheter-related infections. *Clin Infect Dis* **32:** 1249–1272.
Messenguy, F., and Dubois, E. (2003) Role of MADS box proteins and their cofactors in combinatorial control of gene expression and cell development. *Gene* **316:** 1–21.
Mullick, A., Elias, M., Picard, S., Bourget, L., Jovcevski, O., Gauthier, S., *et al*. (2004) Dysregulated inflammatory response to *Candida albicans* in a C5-deficient mouse strain. *Infect Immun* **72:** 5868–5876.
Murad, A.M., Lee, P.R., Broadbent, I.D., Barelle, C.J., and Brown, A.J. (2000) Clp10, an efficient and convenient integrating vector for *Candida albicans*. *Yeast* **16:** 325–327.
Nobile, C.J., and Mitchell, A.P. (2005) Regulation of cell-surface genes and biofilm formation by the C. albicans transcription factor Bcr1p. *Curr Biol* **15:** 1150–1155.
Nobile, C.J., Nett, J.E., Andes, D.R., and Mitchell, A.P. (2006a) Function of *Candida albicans* adhesin Hwp1 in biofilm formation. *Eukaryot Cell* **5:** 1604–1610.
Nobile, C.J., Andes, D.R., Nett, J.E., Smith, F.J., Yue, F., Phan, Q.T., *et al*. (2006b) Critical role of Bcr1-dependent adhesins in *C. albicans* biofilm formation in vitro and in vivo. *PLoS Pathog* **2:** e63.
Nobile, C.J., Nett, J.E., Hernday, A.D., Homann, O.R., Deneault, J.S., Nantel, A., *et al*. (2009) Biofilm matrix regulation by *Candida albicans* Zap1. *PLoS Biol* **7:** e1000133.
Noble, S.M., and Johnson, A.D. (2005) Strains and strategies for large-scale gene deletion studies of the diploid human fungal pathogen *Candida albicans*. *Eukaryot Cell* **4:** 298–309.
Palanisamy, S.K., Ramirez, M.A., Lorenz, M., and Lee, S.A. (2010) *Candida albicans* PEP12 is required for biofilm integrity and in vivo virulence. *Eukaryot Cell* **9:** 266–277.
Ramage, G., Vande Walle, K., Wickes, B.L., and Lopez-Ribot, J.L. (2001) Standardized method for in vitro antifungal susceptibility testing of *Candida albicans* biofilms. *Antimicrob Agents Chemother* **45:** 2475–2479.
Ramage, G., VandeWalle, K., Bachmann, S.P., Wickes, B.L., and Lopez-Ribot, J.L. (2002) In vitro pharmacodynamic properties of three antifungal agents against preformed *Candida albicans* biofilms determined by time-kill studies. *Antimicrob Agents Chemother* **46:** 3634–3636.
Reuss, O., Vik, A., Kolter, R., and Morschhauser, J. (2004) The SAT1 flipper, an optimized tool for gene disruption in *Candida albicans*. *Gene* **341:** 119–127.
Riggle, P.J., and Kumamoto, C.A. (2006) Transcriptional regulation of MDR1, encoding a drug efflux determinant, in fluconazole-resistant *Candida albicans* strains through an Mcm1p binding site. *Eukaryot Cell* **5:** 1957–1968.
Rottmann, M., Dieter, S., Brunner, H., and Rupp, S. (2003) A screen in Saccharomyces cerevisiae identified CaMCM1, an essential gene in *Candida albicans* crucial for morphogenesis. *Mol Microbiol* **47:** 943–959.
Sahni, N., Yi, S., Daniels, K.J., Huang, G., Srikantha, T., and Soll, D.R. (2010) Tec1 mediates the pheromone response of the white phenotype of *Candida albicans*: insights into the evolution of new signal transduction pathways. *PLoS Biol* **8:** e1000363.
Sellam, A., Al-Niemi, T., McInnerney, K., Brumfield, S., Nantel, A., and Suci, P.A. (2009a) A *Candida albicans* early stage biofilm detachment event in rich medium. *BMC Microbiol* **9:** 25.
Sellam, A., Tebbji, F., and Nantel, A. (2009b) Role of Ndt80p in sterol metabolism regulation and azole resistance in *Candida albicans*. *Eukaryot Cell* **8:** 1174–1183.
Sellam, A., Askew, C., Epp, E., Tebbji, F., Mullick, A., Whiteway, M., and Nantel, A. (2010) Role of the transcription factor CaNdt80p in cell separation, hyphal growth and virulence in *Candida albicans*. *Eukaryot Cell* **9:** 634–644.
Tuch, B.B., Galgoczy, D.J., Hernday, A.D., Li, H., and Johnson, A.D. (2008) The evolution of combinatorial gene regulation in fungi. *PLoS Biol* **6:** e38.
Vediyappan, G., Rossignol, T., and d'Enfert, C. (2010) Interaction of *Candida albicans* biofilms with antifungals: transcriptional response and binding of antifungals to beta-glucans. *Antimicrob Agents Chemother* **54:** 2096–2111.
Wilson, R.B., Davis, D., and Mitchell, A.P. (1999) Rapid hypothesis testing with *Candida albicans* through gene disruption with short homology regions. *J Bacteriol* **181:** 1868–1874.
Wisplinghoff, H., Bischoff, T., Tallent, S.M., Seifert, H., Wenzel, R.P., and Edmond, M.B. (2004) Nosocomial bloodstream infections in US hospitals: analysis of 24 179 cases from a prospective nationwide surveillance study. *Clin Infect Dis* **39:** 309–317.
Yi, S., Sahni, N., Daniels, K.J., Pujol, C., Srikantha, T., and Soll, D.R. (2008) The same receptor, G protein, and mitogen-activated protein kinase pathway activate different downstream regulators in the alternative white and opaque pheromone responses of *Candida albicans*. *Mol Biol Cell* **19:** 957–970.
Zhao, X., Oh, S.H., Yeater, K.M., and Hoyer, L.L. (2005) Analysis of the *Candida albicans* Als2p and Als4p adhesins

suggests the potential for compensatory function within the Als family. *Microbiology* **151:** 1619–1630.
Zhao, X., Daniels, K.J., Oh, S.H., Green, C.B., Yeater, K.M., Soll, D.R., and Hoyer, L.L. (2006) *Candida albicans* Als3p is required for wild-type biofilm formation on silicone elastomer surfaces. *Microbiology* **152:** 2287–2299.
Zhu, C., Byers, K.J., McCord, R.P., Shi, Z., Berger, M.F., Newburger, D.E., *et al.* (2009) High-resolution DNA-binding specificity analysis of yeast transcription factors. *Genome Res* **19:** 556–566.

Supporting Information

Additional supporting information may be found in the online version of this article.

Please note: Wiley-Blackwell are not responsible for the content or functionality of any supporting materials supplied by the authors. Any queries (other than missing material) should be directed to the corresponding author for the article.

VII.6. Faculty 1000 Biology evaluations

Epp E, Whiteway M: "This paper fills a gap of our understanding of how endocytosis works in yeast by..." Evaluation of: [Smaczynska-de Rooij II et al. A role for the dynamin-like protein Vps1 during endocytosis in yeast. J Cell Sci. 2010 Oct 15; 123(Pt 20):3496-506; doi: 10.1242/jcs.070508]. Faculty of 1000, 18 Jan 2011. http://www.F1000.com/7664956

Epp E, Whiteway M: "This paper confirms that the yeast dynamin-like protein *VPS1* is involved in the internalization step..." Evaluation of: [Nannapaneni S et al. The yeast dynamin-like protein Vps1:vps1 mutations perturb the internalization and the motility of endocytic vesicles and endosomes via disorganization of the actin cytoskeleton. Eur J Cell Biol. 2010 Jul; 89(7):499-508; doi: 10.1016/j.ejcb.2010.02.002]. Faculty of 1000, 18 Jan 2011. http://www.F1000.com/2629956

Epp E, Whiteway M: "In this paper by Wurtele et al. the authors show that modulation of the acetylation..." Evaluation of: [Wurtele H et al. Modulation of histone H3 lysine 56 acetylation as an antifungal therapeutic strategy. Nat Med. 2010 Jul; 16(7):774-80; doi: 10.1038/nm.2175]. Faculty of 1000, 13 Aug 2010. http://www.F1000.com/4770956

Epp E, Whiteway M: "Interestingly, the authors of this work have shown that *Candida albicans* pathogenesis has a requirement..." Evaluation of: [Lopes da Rosa J et al. Histone acetyltransferase Rtt109 is required for *Candida albicans* pathogenesis. Proc Natl Acad Sci U S A. 2010 Jan 26; 107(4):1594-9; doi: 10.1073/pnas.0912427107]. Faculty of 1000, 13 Aug 2010. http://www.F1000.com/4769957

Epp E, Whiteway M: "This interesting study enhances our understanding of how azole drugs act against fungal pathogens by..." Evaluation of: [Zhang YQ et al. Requirement for ergosterol in V-ATPase function underlies antifungal activity of azole drugs. PLoS Pathog. 2010; 6(6):e1000939; doi: 10.1371/journal.ppat.1000939]. Faculty of 1000, 11 Jun 2010. http://www.F1000.com/3540960

Epp E, Whiteway M: "This interesting paper provides a mechanism for how the actin cytoskeleton regulates morphogenesis in *Candida*..." Evaluation of: [Zou H et al. *Candida albicans* Cyr1, Cap1 and G-actin form a sensor/effector apparatus for activating cAMP synthesis in hyphal growth. Mol Microbiol. 2010 Feb; 75(3):579-91; doi: 10.1111/j.1365-2958.2009.06980.x]. Faculty of 1000, 18 Jan 2010. http://www.F1000.com/1480960

VIII. References

1. Reece JB, Urry LA, Cain ML, Wasserman SA, Minorsky PV, et al. (2011) Fungi. In: Reece JB, Urry LA, Cain ML, Wasserman SA, Minorsky PV et al., editors. Campbell Biology. San Francisco, CA: Pearson Benjamin Cummings. pp. 636-653.
2. Calderone RA (2002) Introdcution and Historical Perspectives. In: Calderone RA, editor. Candida and Candidiasis. Washington D.C.: ASM Press. pp. 3-13.
3. Winner HI, and R. Hurley (1954) Candida albicans. Boston, Mass.: Little, Brown and Company.
4. Wilson LS, Reyes CM, Stolpman M, Speckman J, Allen K, et al. (2002) The direct cost and incidence of systemic fungal infections. Value Health 5: 26-34.
5. Langenbeck B (1839) Auffinggung von Pilzen aus der Schleimhaut der Speiserohne einer Typhus-Leiche. Neue Not Geb Natur-u-Helik (Froriep) 12: 145-147.
6. Wilkinson JS (1849) Some remarks upon the development of epiphytes with the description of new vegetable formation found in connection with the human uterus. Lancet 2: 448.
7. Mayer L (1862) Die Pflanzlichen Parasiten der weiblichen Sexualorgane in ihrer praktischen Bedeutung. Mschr Geburtsch Frauenkrank 20: 2-16.
8. Robin CP (1853) Histoire naturelle des vegetaux. Parasites qui croissent sur l'homme et sur les animaux vivants. Balliere, Paris, France.
9. Berkhout CM (1923) De schimmelgeschlachten Monilia, Oidium, Oospora, en Torula. Dissertation, Utrecht, the Netherlands: University of Utrecht.
10. Whelan WL, Magee PT (1981) Natural heterozygosity in Candida albicans. J Bacteriol 145: 896-903.
11. Blaschke-Hellmessen R (1999) [Habitats for Candida in medical and hygienic respects]. Mycoses 42 Suppl 1: 22-29.
12. Schauer F, Hanschke R (1999) [Taxonomy and ecology of the genus Candida]. Mycoses 42 Suppl 1: 12-21.
13. Calderone RA (2002) Taxonomy and Biology of Candida. In: Calderone RA, editor. Candida and Candidiasis. Washington D.C.: ASM Press. pp. 15-27.
14. St-Germain G, Laverdiere M, Pelletier R, Rene P, Bourgault AM, et al. (2008) Epidemiology and antifungal susceptibility of bloodstream Candida isolates in Quebec: Report on 453 cases between 2003 and 2005. Can J Infect Dis Med Microbiol 19: 55-62.
15. Pfaller MA, Diekema DJ (2007) Epidemiology of invasive candidiasis: a persistent public health problem. Clin Microbiol Rev 20: 133-163.
16. Pfaller Michael A, Pappas Peter G, Wingard John R (2006) Invasive Fungal Pathogens: Current Epidemiological Trends. Clinical Infectious Diseases 43: S3-S14.
17. Greene CE, Chandler FW (2006) Candidiasis and Rhodotorulosis. In: Greene CE, editor. Infectious Diseases of the Dog and Cat, 3rd ed. Philadelphia:: Saunders Elsevier. pp. 627–633.
18. Russell C, Lay KM (1973) Natural history of Candida species and yeasts in the oral cavities of infants. Arch Oral Biol 18: 957-962.
19. Kumamoto CA, Pierce JV (2011) Immunosensing during colonization by Candida albicans: does it take a village to colonize the intestine? Trends Microbiol.
20. Ruhnke M, Maschmeyer G (2002) Management of mycoses in patients with hematologic disease and cancer -- review of the literature. European journal of medical research 7: 227-235.
21. Gudlaugsson O, Gillespie S, Lee K, Vande Berg J, Hu J, et al. (2003) Attributable mortality of nosocomial candidemia, revisited. Clin Infect Dis 37: 1172-1177.
22. Martin GS, Mannino DM, Eaton S, Moss M (2003) The epidemiology of sepsis in the United States from 1979 through 2000. N Engl J Med 348: 1546-1554.
23. Perfect JR, Casadevall A (2006) Fungal Molecular Pathogenesis: What Can It Do and Why Do We Need it? In: Heitman J, Filler SG, Edwards JE, Mitchell A, editors. Molecular principles of fungal pathogenesis. Washington D.C.: ASM Press. pp. 3-11.
24. Pfaller MA, Diekema DJ (2010) Epidemiology of invasive mycoses in North America. Crit Rev Microbiol 36: 1-53.
25. Wisplinghoff H, Bischoff T, Tallent SM, Seifert H, Wenzel RP, et al. (2004) Nosocomial bloodstream infections in US hospitals: analysis of 24,179 cases from a prospective nationwide surveillance study. Clin Infect Dis 39: 309-317.
26. Hazen EL, Brown R (1950) Two antifungal agents produced by a soil actinomycete. Science 112: 423.
27. O'Shaughnessy EM, Lyman CA, Walsh TJ (2009) Amphotericin B: Polyene Resistance Mechanisms. In: D.L. M, editor. Antimicrobial Drug Resistance. New York, NY: Humana Press. pp. 295-205.
28. Pound MW, Townsend ML, Dimondi V, Wilson D, Drew RH (2011) Overview of treatment options for invasive fungal infections. Med Mycol.
29. Sanglard D, White CT (2006) Molecular Principles of Antifungal Drug Resistance. In: Heitman J, Filler SG, Edwards JE, Mitchell A, editors. Molecular principles of fungal pathogenesis. Washington D.C.: ASM Press. pp. 197-212.
30. Brajtburg J, Bolard J (1996) Carrier effects on biological activity of amphotericin B. Clin Microbiol Rev 9: 512-531.
31. Vertut-Croquin A, Bolard J, Gary-Bobo CM (1985) Transfer of amphotericin B from gel state vesicles to mycoplasma cells: biphasic action on potassium transport and permeability. Antimicrob Agents Chemother 28: 167-171.
32. Gallis HA, Drew RH, Pickard WW (1990) Amphotericin B: 30 years of clinical experience. Rev Infect Dis 12: 308-329.
33. Goodwin SD, Cleary JD, Walawander CA, Taylor JW, Grasela TH, Jr. (1995) Pretreatment regimens for adverse events related to infusion of amphotericin B. Clinical infectious diseases : an official publication of the Infectious Diseases Society of America 20: 755-761.
34. Kuhn DM, George T, Chandra J, Mukherjee PK, Ghannoum MA (2002) Antifungal susceptibility of Candida biofilms: unique efficacy of amphotericin B lipid formulations and echinocandins. Antimicrob Agents Chemother 46: 1773-1780.
35. Chaudhuri NK, Montag BJ, Heidelberger C (1958) Studies on fluorinated pyrimidines. III. The metabolism of 5-fluorouracil-2-C14 and 5-fluoroorotic-2-C14 acid in vivo. Cancer Res 18: 318-328.

36. Perfect JR, Dismukes WE, Dromer F, Goldman DL, Graybill JR, et al. (2010) Clinical practice guidelines for the management of cryptococcal disease: 2010 update by the infectious diseases society of america. Clin Infect Dis 50: 291-322.
37. Pappas PG, Kauffman CA, Andes D, Benjamin DK, Jr., Calandra TF, et al. (2009) Clinical practice guidelines for the management of candidiasis: 2009 update by the Infectious Diseases Society of America. Clin Infect Dis 48: 503-535.
38. Mauceri AA, Cullen SI, Vandevelde AG, Johnson JE, 3rd (1974) Flucytosine. An effective oral treatment for chromomycosis. Arch Dermatol 109: 873-876.
39. Waldorf AR, Polak A (1983) Mechanisms of action of 5-fluorocytosine. Antimicrobial Agents and Chemotherapy 23: 79-85.
40. Diasio RB, Bennett JE, Myers CE (1978) Mode of action of 5-fluorocytosine. Biochemical pharmacology 27: 703-707.
41. Chandra J, Mohammad S, Ghannoum MA (2009) Flucytosine: Site of Action, Mechanism of Resistance and Use in Combination Therapy. In: Mayers DL, editor. Antimicrobial Drug Resistance. New York, NY: Humana Press. pp. 313-326.
42. Heeres J, Backx LJ, Mostmans JH, Van Cutsem J (1979) Antimycotic imidazoles. part 4. Synthesis and antifungal activity of ketoconazole, a new potent orally active broad-spectrum antifungal agent. Journal of medicinal chemistry 22: 1003-1005.
43. Chapman SW, Dismukes WE, Proia LA, Bradsher RW, Pappas PG, et al. (2008) Clinical practice guidelines for the management of blastomycosis: 2008 update by the Infectious Diseases Society of America. Clinical infectious diseases : an official publication of the Infectious Diseases Society of America 46: 1801-1812.
44. Maertens JA (2004) History of the development of azole derivatives. Clinical microbiology and infection : the official publication of the European Society of Clinical Microbiology and Infectious Diseases 10 Suppl 1: 1-10.
45. Sheehan DJ, Hitchcock CA, Sibley CM (1999) Current and emerging azole antifungal agents. Clinical Microbiology Reviews 12: 40-79.
46. Chapman SW, Sullivan DC, Cleary JD (2008) In search of the holy grail of antifungal therapy. Trans Am Clin Climatol Assoc 119: 197-215; discussion 215-196.
47. Lopez-Ribot JL, Patterson TF (2009) Fungal Drug Resistance: Azoles. In: Mayers DL, editor. Antimicrobial Drug Resistance. New York, NY: Humana Press. pp. 307-312.
48. Sanglard D, Odds FC (2002) Resistance of Candida species to antifungal agents: molecular mechanisms and clinical consequences. The Lancet infectious diseases 2: 73-85.
49. White TC, Marr KA, Bowden RA (1998) Clinical, cellular, and molecular factors that contribute to antifungal drug resistance. Clinical Microbiology Reviews 11: 382-402.
50. Cronin S, Chandrasekar PH (2010) Safety of triazole antifungal drugs in patients with cancer. The Journal of antimicrobial chemotherapy 65: 410-416.
51. Chen SC, Slavin MA, Sorrell TC (2011) Echinocandin antifungal drugs in fungal infections: a comparison. Drugs 71: 11-41.
52. Masurekar PS, Fountoulakis JM, Hallada TC, Sosa MS, Kaplan L (1992) Pneumocandins from Zalerion arboricola. II. Modification of product spectrum by mutation and medium manipulation. The Journal of antibiotics 45: 1867-1874.
53. Akins RA, Sobel JD (2009) Antifungal Targets, Mechanisms of Action, and Resistance in Candida albicans. In: Mayers DL, editor. Antimicrobial Drug Resistance. New York, NY: Humana Press. pp. 347-407.
54. Antachopoulos C, Meletiadis J, Sein T, Roilides E, Walsh TJ (2007) Concentration-dependent effects of caspofungin on the metabolic activity of Aspergillus species. Antimicrobial Agents and Chemotherapy 51: 881-887.
55. Kurtz MB, Heath IB, Marrinan J, Dreikorn S, Onishi J, et al. (1994) Morphological effects of lipopeptides against Aspergillus fumigatus correlate with activities against (1,3)-beta-D-glucan synthase. Antimicrobial Agents and Chemotherapy 38: 1480-1489.
56. Nakai T, Uno J, Ikeda F, Tawara S, Nishimura K, et al. (2003) In vitro antifungal activity of Micafungin (FK463) against dimorphic fungi: comparison of yeast-like and mycelial forms. Antimicrobial Agents and Chemotherapy 47: 1376-1381.
57. Liu TT, Lee RE, Barker KS, Wei L, Homayouni R, et al. (2005) Genome-wide expression profiling of the response to azole, polyene, echinocandin, and pyrimidine antifungal agents in Candida albicans. Antimicrob Agents Chemother 49: 2226-2236.
58. Whiteway M, Bachewich C (2007) Morphogenesis in Candida albicans. Annu Rev Microbiol 61: 529-553.
59. Hawser SP, Norris H, Jessup CJ, Ghannoum MA (1998) Comparison of a 2,3-bis(2-methoxy-4-nitro-5-sulfophenyl)-5-[(phenylamino)carbonyl]-2H-t etrazolium hydroxide (XTT) colorimetric method with the standardized National Committee for Clinical Laboratory Standards method of testing clinical yeast isolates for susceptibility to antifungal agents. Journal of clinical microbiology 36: 1450-1452.
60. Sewell DL, Pfaller MA, Barry AL (1994) Comparison of broth macrodilution, broth microdilution, and E test antifungal susceptibility tests for fluconazole. Journal of clinical microbiology 32: 2099-2102.
61. White TC, Pfaller MA, Rinaldi MG, Smith J, Redding SW (1997) Stable azole drug resistance associated with a substrain of Candida albicans from an HIV-infected patient. Oral diseases 3 Suppl 1: S102-109.
62. Marr KA, Lyons CN, Rustad TR, Bowden RA, White TC (1998) Rapid, transient fluconazole resistance in Candida albicans is associated with increased mRNA levels of CDR. Antimicrobial Agents and Chemotherapy 42: 2584-2589.
63. Sanglard D, Ischer F, Marchetti O, Entenza J, Bille J (2003) Calcineurin A of Candida albicans: involvement in antifungal tolerance, cell morphogenesis and virulence. Mol Microbiol 48: 959-976.
64. Marchetti O, Moreillon P, Glauser MP, Bille J, Sanglard D (2000) Potent synergism of the combination of fluconazole and cyclosporine in Candida albicans. Antimicrob Agents Chemother 44: 2373-2381.
65. Steinbach WJ, Reedy JL, Cramer RA, Jr., Perfect JR, Heitman J (2007) Harnessing calcineurin as a novel anti-infective agent against invasive fungal infections. Nat Rev Microbiol 5: 418-430.
66. Moore CB, Sayers N, Mosquera J, Slaven J, Denning DW (2000) Antifungal drug resistance in Aspergillus. The Journal of infection 41: 203-220.
67. Ellis D (2002) Amphotericin B: spectrum and resistance. The Journal of antimicrobial chemotherapy 49 Suppl 1: 7-10.
68. Sanglard D, Ischer F, Parkinson T, Falconer D, Bille J (2003) Candida albicans mutations in the ergosterol biosynthetic pathway and resistance to several antifungal agents. Antimicrob Agents Chemother 47: 2404-2412.
69. Polak A (1977) 5-Fluorocytosine--current status with special references to mode of action and drug resistance. Contributions to microbiology and immunology 4: 158-167.
70. Hope WW, Tabernero L, Denning DW, Anderson MJ (2004) Molecular mechanisms of primary resistance to flucytosine in Candida albicans. Antimicrobial Agents and Chemotherapy 48: 4377-4386.

71. Fasoli M, Kerridge D (1988) Isolation and characterization of fluoropyrimidine-resistant mutants in two Candida species. Annals of the New York Academy of Sciences 544: 260-263.
72. Sanglard D, Bille J (2002) Current understanding of the mode of action and resistance mechanism to conventional and emerging antifungal agents for treatment of Candida infections. In: Calderone RA, editor. Candida and Candidiasis. Washington D.C.: ASM Press. pp. 349-383.
73. Manoharlal R, Gaur NA, Panwar SL, Morschhauser J, Prasad R (2008) Transcriptional activation and increased mRNA stability contribute to overexpression of CDR1 in azole-resistant Candida albicans. Antimicrobial Agents and Chemotherapy 52: 1481-1492.
74. Znaidi S, De Deken X, Weber S, Rigby T, Nantel A, et al. (2007) The zinc cluster transcription factor Tac1p regulates PDR16 expression in Candida albicans. Molecular Microbiology 66: 440-452.
75. Coste A, Turner V, Ischer F, Morschhauser J, Forche A, et al. (2006) A mutation in Tac1p, a transcription factor regulating CDR1 and CDR2, is coupled with loss of heterozygosity at chromosome 5 to mediate antifungal resistance in Candida albicans. Genetics 172: 2139-2156.
76. Wirsching S, Michel S, Morschhauser J (2000) Targeted gene disruption in Candida albicans wild-type strains: the role of the MDR1 gene in fluconazole resistance of clinical Candida albicans isolates. Molecular Microbiology 36: 856-865.
77. Barchiesi F, Calabrese D, Sanglard D, Falconi Di Francesco L, Caselli F, et al. (2000) Experimental induction of fluconazole resistance in Candida tropicalis ATCC 750. Antimicrobial Agents and Chemotherapy 44: 1578-1584.
78. Pfaller MA, Messer SA, Boyken L, Rice C, Tendolkar S, et al. (2004) Cross-resistance between fluconazole and ravuconazole and the use of fluconazole as a surrogate marker to predict susceptibility and resistance to ravuconazole among 12,796 clinical isolates of Candida spp. Journal of clinical microbiology 42: 3137-3141.
79. Muller FM, Weig M, Peter J, Walsh TJ (2000) Azole cross-resistance to ketoconazole, fluconazole, itraconazole and voriconazole in clinical Candida albicans isolates from HIV-infected children with oropharyngeal candidosis. The Journal of antimicrobial chemotherapy 46: 338-340.
80. Akins RA (2005) An update on antifungal targets and mechanisms of resistance in Candida albicans. Medical mycology : official publication of the International Society for Human and Animal Mycology 43: 285-318.
81. Morschhauser J, Barker KS, Liu TT, Bla BWJ, Homayouni R, et al. (2007) The transcription factor Mrr1p controls expression of the MDR1 efflux pump and mediates multidrug resistance in Candida albicans. PLoS Pathogens 3: e164.
82. Franz R, Kelly SL, Lamb DC, Kelly DE, Ruhnke M, et al. (1998) Multiple molecular mechanisms contribute to a stepwise development of fluconazole resistance in clinical Candida albicans strains. Antimicrobial Agents and Chemotherapy 42: 3065-3072.
83. White TC (1997) The presence of an R467K amino acid substitution and loss of allelic variation correlate with an azole-resistant lanosterol 14alpha demethylase in Candida albicans. Antimicrobial Agents and Chemotherapy 41: 1488-1494.
84. Li X, Brown N, Chau AS, Lopez-Ribot JL, Ruesga MT, et al. (2004) Changes in susceptibility to posaconazole in clinical isolates of Candida albicans. The Journal of antimicrobial chemotherapy 53: 74-80.
85. Kelly SL, Lamb DC, Corran AJ, Baldwin BC, Kelly DE (1995) Mode of action and resistance to azole antifungals associated with the formation of 14 alpha-methylergosta-8,24(28)-dien-3 beta,6 alpha-diol. Biochemical and biophysical research communications 207: 910-915.
86. Welihinda AA, Beavis AD, Trumbly RJ (1994) Mutations in LIS1 (ERG6) gene confer increased sodium and lithium uptake in Saccharomyces cerevisiae. Biochimica et biophysica acta 1193: 107-117.
87. Miyazaki T, Miyazaki Y, Izumikawa K, Kakeya H, Miyakoshi S, et al. (2006) Fluconazole treatment is effective against a Candida albicans erg3/erg3 mutant in vivo despite in vitro resistance. Antimicrobial Agents and Chemotherapy 50: 580-586.
88. MacPherson S, Akache B, Weber S, De Deken X, Raymond M, et al. (2005) Candida albicans zinc cluster protein Upc2p confers resistance to antifungal drugs and is an activator of ergosterol biosynthetic genes. Antimicrobial Agents and Chemotherapy 49: 1745-1752.
89. Silver PM, Oliver BG, White TC (2004) Role of Candida albicans transcription factor Upc2p in drug resistance and sterol metabolism. Eukaryotic Cell 3: 1391-1397.
90. Dunkel N, Liu TT, Barker KS, Homayouni R, Morschhauser J, et al. (2008) A gain-of-function mutation in the transcription factor Upc2p causes upregulation of ergosterol biosynthesis genes and increased fluconazole resistance in a clinical Candida albicans isolate. Eukaryotic Cell 7: 1180-1190.
91. Znaidi S, Weber S, Al-Abdin OZ, Bomme P, Saidane S, et al. (2008) Genomewide location analysis of Candida albicans Upc2p, a regulator of sterol metabolism and azole drug resistance. Eukaryotic Cell 7: 836-847.
92. Balashov SV, Park S, Perlin DS (2006) Assessing resistance to the echinocandin antifungal drug caspofungin in Candida albicans by profiling mutations in FKS1. Antimicrobial Agents and Chemotherapy 50: 2058-2063.
93. Gardiner RE, Souteropoulos P, Park S, Perlin DS (2005) Characterization of Aspergillus fumigatus mutants with reduced susceptibility to caspofungin. Medical mycology : official publication of the International Society for Human and Animal Mycology 43 Suppl 1: S299-305.
94. Perlin DS (2007) Resistance to echinocandin-class antifungal drugs. Drug resistance updates : reviews and commentaries in antimicrobial and anticancer chemotherapy 10: 121-130.
95. Berman J, Sudbery PE (2002) Candida Albicans: a molecular revolution built on lessons from budding yeast. Nature reviews Genetics 3: 918-930.
96. Giaever G, Chu AM, Ni L, Connelly C, Riles L, et al. (2002) Functional profiling of the Saccharomyces cerevisiae genome. Nature 418: 387-391.
97. Goffeau A, Barrell BG, Bussey H, Davis RW, Dujon B, et al. (1996) Life with 6000 genes. Science 274: 546, 563-547.
98. Spellman PT, Sherlock G, Zhang MQ, Iyer VR, Anders K, et al. (1998) Comprehensive identification of cell cycle-regulated genes of the yeast Saccharomyces cerevisiae by microarray hybridization. Molecular biology of the cell 9: 3273-3297.
99. Gavin AC, Bosche M, Krause R, Grandi P, Marzioch M, et al. (2002) Functional organization of the yeast proteome by systematic analysis of protein complexes. Nature 415: 141-147.
100. Huh WK, Falvo JV, Gerke LC, Carroll AS, Howson RW, et al. (2003) Global analysis of protein localization in budding yeast. Nature 425: 686-691.

101. Uetz P, Giot L, Cagney G, Mansfield TA, Judson RS, et al. (2000) A comprehensive analysis of protein-protein interactions in Saccharomyces cerevisiae. Nature 403: 623-627.
102. Tong AH, Evangelista M, Parsons AB, Xu H, Bader GD, et al. (2001) Systematic genetic analysis with ordered arrays of yeast deletion mutants. Science 294: 2364-2368.
103. Tong AH, Lesage G, Bader GD, Ding H, Xu H, et al. (2004) Global mapping of the yeast genetic interaction network. Science 303: 808-813.
104. Gimeno CJ, Ljungdahl PO, Styles CA, Fink GR (1992) Unipolar cell divisions in the yeast S. cerevisiae lead to filamentous growth: regulation by starvation and RAS. Cell 68: 1077-1090.
105. Liu H, Styles CA, Fink GR (1993) Elements of the yeast pheromone response pathway required for filamentous growth of diploids. Science 262: 1741-1744.
106. Lo HJ, Kohler JR, DiDomenico B, Loebenberg D, Cacciapuoti A, et al. (1997) Nonfilamentous C. albicans mutants are avirulent. Cell 90: 939-949.
107. Kohler JR, Fink GR (1996) Candida albicans strains heterozygous and homozygous for mutations in mitogen-activated protein kinase signaling components have defects in hyphal development. Proceedings of the National Academy of Sciences of the United States of America 93: 13223-13228.
108. Rocha CR, Schroppel K, Harcus D, Marcil A, Dignard D, et al. (2001) Signaling through adenylyl cyclase is essential for hyphal growth and virulence in the pathogenic fungus Candida albicans. Molecular biology of the cell 12: 3631-3643.
109. Reynolds TB, Fink GR (2001) Bakers' yeast, a model for fungal biofilm formation. Science 291: 878-881.
110. Finkel JS, Mitchell AP (2011) Genetic control of Candida albicans biofilm development. Nature reviews Microbiology 9: 109-118.
111. Kakeya H, Miyazaki Y, Miyazaki H, Nyswaner K, Grimberg B, et al. (2000) Genetic analysis of azole resistance in the Darlington strain of Candida albicans. Antimicrobial agents and chemotherapy 44: 2985-2990.
112. Douglas CM, D'Ippolito JA, Shei GJ, Meinz M, Onishi J, et al. (1997) Identification of the FKS1 gene of Candida albicans as the essential target of 1,3-beta-D-glucan synthase inhibitors. Antimicrobial agents and chemotherapy 41: 2471-2479.
113. Douglas CM, Marrinan JA, Li W, Kurtz MB (1994) A Saccharomyces cerevisiae mutant with echinocandin-resistant 1,3-beta-D-glucan synthase. Journal of bacteriology 176: 5686-5696.
114. Anderson JB, Sirjusingh C, Parsons AB, Boone C, Wickens C, et al. (2003) Mode of selection and experimental evolution of antifungal drug resistance in Saccharomyces cerevisiae. Genetics 163: 1287-1298.
115. Ho CH, Piotrowski J, Dixon SJ, Baryshnikova A, Costanzo M, et al. (2011) Combining functional genomics and chemical biology to identify targets of bioactive compounds. Current opinion in chemical biology 15: 66-78.
116. Winzeler EA, Shoemaker DD, Astromoff A, Liang H, Anderson K, et al. (1999) Functional characterization of the S. cerevisiae genome by gene deletion and parallel analysis. Science 285: 901-906.
117. SGD "Saccharomyces Genome Database" http://www.yeastgenome.org/cache/genomeSnapshot.html (accessed 16. March 2011).
118. Arnaud M, Costanzo M, Inglis D, Skrzypek M, Binkley J, et al. "Candida Genome Database" http://www.candidagenome.org/cache/genomeSnapshot.html (accessed 16. March 2011).
119. Arnaud MB, Costanzo MC, Shah P, Skrzypek MS, Sherlock G (2009) Gene Ontology and the annotation of pathogen genomes: the case of Candida albicans. Trends in microbiology 17: 295-303.
120. Sellam A, Hogues H, Askew C, Tebbji F, van Het Hoog M, et al. (2010) Experimental annotation of the human pathogen Candida albicans coding and noncoding transcribed regions using high-resolution tiling arrays. Genome biology 11: R71.
121. Bruno VM, Wang Z, Marjani SL, Euskirchen GM, Martin J, et al. (2010) Comprehensive annotation of the transcriptome of the human fungal pathogen Candida albicans using RNA-seq. Genome research 20: 1451-1458.
122. Kabir MA, Hussain MA (2009) Human fungal pathogen Candida albicans in the postgenomic era: an overview. Expert review of anti-infective therapy 7: 121-134.
123. Scannell DR, Wolfe K (2004) Rewiring the transcriptional regulatory circuits of cells. Genome biology 5: 206.
124. van het Hoog M, Rast TJ, Martchenko M, Grindle S, Dignard D, et al. (2007) Assembly of the Candida albicans genome into sixteen supercontigs aligned on the eight chromosomes. Genome biology 8: R52.
125. Hogues H, Lavoie H, Sellam A, Mangos M, Roemer T, et al. (2008) Transcription factor substitution during the evolution of fungal ribosome regulation. Molecular cell 29: 552-562.
126. Tsong AE, Tuch BB, Li H, Johnson AD (2006) Evolution of alternative transcriptional circuits with identical logic. Nature 443: 415-420.
127. Ihmels J, Bergmann S, Gerami-Nejad M, Yanai I, McClellan M, et al. (2005) Rewiring of the yeast transcriptional network through the evolution of motif usage. Science 309: 938-940.
128. Kadosh D, Johnson AD (2001) Rfg1, a protein related to the Saccharomyces cerevisiae hypoxic regulator Rox1, controls filamentous growth and virulence in Candida albicans. Molecular and cellular biology 21: 2496-2505.
129. Forche A, Alby K, Schaefer D, Johnson AD, Berman J, et al. (2008) The parasexual cycle in Candida albicans provides an alternative pathway to meiosis for the formation of recombinant strains. PLoS biology 6: e110.
130. Santos MA, Tuite MF (1995) The CUG codon is decoded in vivo as serine and not leucine in Candida albicans. Nucleic acids research 23: 1481-1486.
131. Whiteway M, Bachewich C (2007) Morphogenesis in Candida albicans. Annual review of microbiology 61: 529-553.
132. Jones T, Federspiel NA, Chibana H, Dungan J, Kalman S, et al. (2004) The diploid genome sequence of Candida albicans. Proceedings of the National Academy of Sciences of the United States of America 101: 7329-7334.
133. Braun BR, van Het Hoog M, d'Enfert C, Martchenko M, Dungan J, et al. (2005) A human-curated annotation of the Candida albicans genome. PLoS genetics 1: 36-57.
134. Butler G, Rasmussen MD, Lin MF, Santos MA, Sakthikumar S, et al. (2009) Evolution of pathogenicity and sexual reproduction in eight Candida genomes. Nature 459: 657-662.
135. Firon A, d'Enfert C (2007) From Genes to Function: Systematic Approaches Used to Study Candida albicans and Candida glabrata Biology and Pathogenesis. In: d'Enfert C, Hube B, editors. Candida Comparative and Functional Genomics. Norfolk, UK: Caister Academic Press. pp. 195-216.

136. Lavoie H, Sellam A, Askew C, Nantel A, Whiteway M (2008) A toolbox for epitope-tagging and genome-wide location analysis in Candida albicans. BMC genomics 9: 578.
137. Garaizar J, Brena S, Bikandi J, Rementeria A, Ponton J (2006) Use of DNA microarray technology and gene expression profiles to investigate the pathogenesis, cell biology, antifungal susceptibility and diagnosis of Candida albicans. FEMS yeast research 6: 987-998.
138. Nantel A, Rigby T, Hogues H, Whiteway M (2006) Microarrays for studying pathology in Candida albicans. In: Kavanaugh K, editor. Medical Mycology: Cellular and Molecular Techniques: Wiley Press.
139. Murad AM, Leng P, Straffon M, Wishart J, Macaskill S, et al. (2001) NRG1 represses yeast-hypha morphogenesis and hypha-specific gene expression in Candida albicans. The EMBO journal 20: 4742-4752.
140. Nantel A, Dignard D, Bachewich C, Harcus D, Marcil A, et al. (2002) Transcription profiling of Candida albicans cells undergoing the yeast-to-hyphal transition. Molecular biology of the cell 13: 3452-3465.
141. Cheng S, Clancy CJ, Checkley MA, Handfield M, Hillman JD, et al. (2003) Identification of Candida albicans genes induced during thrush offers insight into pathogenesis. Molecular microbiology 48: 1275-1288.
142. Rogers PD, Barker KS (2002) Evaluation of differential gene expression in fluconazole-susceptible and -resistant isolates of Candida albicans by cDNA microarray analysis. Antimicrobial agents and chemotherapy 46: 3412-3417.
143. Uhl MA, Biery M, Craig N, Johnson AD (2003) Haploinsufficiency-based large-scale forward genetic analysis of filamentous growth in the diploid human fungal pathogen C.albicans. The EMBO journal 22: 2668-2678.
144. Xu D, Jiang B, Ketela T, Lemieux S, Veillette K, et al. (2007) Genome-wide fitness test and mechanism-of-action studies of inhibitory compounds in Candida albicans. PLoS Pathogens 3: e92.
145. Oh J, Fung E, Schlecht U, Davis RW, Giaever G, et al. (2010) Gene annotation and drug target discovery in Candida albicans with a tagged transposon mutant collection. PLoS Pathogens 6.
146. Shen J, Cowen LE, Griffin AM, Chan L, Kohler JR (2008) The Candida albicans pescadillo homolog is required for normal hypha-to-yeast morphogenesis and yeast proliferation. Proceedings of the National Academy of Sciences of the United States of America 105: 20918-20923.
147. Enloe B, Diamond A, Mitchell AP (2000) A single-transformation gene function test in diploid Candida albicans. Journal of bacteriology 182: 5730-5736.
148. Davis DA, Bruno VM, Loza L, Filler SG, Mitchell AP (2002) Candida albicans Mds3p, a conserved regulator of pH responses and virulence identified through insertional mutagenesis. Genetics 162: 1573-1581.
149. Nobile CJ, Bruno VM, Richard ML, Davis DA, Mitchell AP (2003) Genetic control of chlamydospore formation in Candida albicans. Microbiology 149: 3629-3637.
150. Richard ML, Nobile CJ, Bruno VM, Mitchell AP (2005) Candida albicans biofilm-defective mutants. Eukaryotic Cell 4: 1493-1502.
151. Bruno VM, Kalachikov S, Subaran R, Nobile CJ, Kyratsous C, et al. (2006) Control of the C. albicans cell wall damage response by transcriptional regulator Cas5. PLoS Pathogens 2: e21.
152. Shao PL, Huang LM, Hsueh PR (2007) Recent advances and challenges in the treatment of invasive fungal infections. International journal of antimicrobial agents 30: 487-495.
153. Baddley JW, Andes DR, Marr KA, Kontoyiannis DP, Alexander BD, et al. (2010) Factors associated with mortality in transplant patients with invasive aspergillosis. Clinical infectious diseases : an official publication of the Infectious Diseases Society of America 50: 1559-1567.
154. Wilson LS, Reyes CM, Stolpman M, Speckman J, Allen K, et al. (2002) The direct cost and incidence of systemic fungal infections. Value in health : the journal of the International Society for Pharmacoeconomics and Outcomes Research 5: 26-34.
155. Sudbery P, Gow N, Berman J (2004) The distinct morphogenic states of Candida albicans. Trends Microbiol 12: 317-324.
156. Cottier F, Muhlschlegel FA (2009) Sensing the environment: response of Candida albicans to the X factor. FEMS microbiology letters 295: 1-9.
157. Biswas S, Van Dijck P, Datta A (2007) Environmental sensing and signal transduction pathways regulating morphopathogenic determinants of Candida albicans. Microbiol Mol Biol Rev 71: 348-376.
158. Eckert SE, Sheth CC, Mühlschlegel FA (2007) Regulation of Morphogenesis in Candida species. In: d'Enfert C, Hube B, editors. Candida Comparative and Functional Genomics. Norfolk, UK: Caister Academic Press. pp. 263-291.
159. Leberer E, Harcus D, Dignard D, Johnson L, Ushinsky S, et al. (2001) Ras links cellular morphogenesis to virulence by regulation of the MAP kinase and cAMP signalling pathways in the pathogenic fungus Candida albicans. Molecular Microbiology 42: 673-687.
160. Bahn YS, Staab J, Sundstrom P (2003) Increased high-affinity phosphodiesterase PDE2 gene expression in germ tubes counteracts CAP1-dependent synthesis of cyclic AMP, limits hypha production and promotes virulence of Candida albicans. Molecular Microbiology 50: 391-409.
161. Cloutier M, Castilla R, Bolduc N, Zelada A, Martineau P, et al. (2003) The two isoforms of the cAMP-dependent protein kinase catalytic subunit are involved in the control of dimorphism in the human fungal pathogen Candida albicans. Fungal genetics and biology : FG & B 38: 133-141.
162. Jung WH, Stateva LI (2003) The cAMP phosphodiesterase encoded by CaPDE2 is required for hyphal development in Candida albicans. Microbiology 149: 2961-2976.
163. Maidan MM, De Rop L, Serneels J, Exler S, Rupp S, et al. (2005) The G protein-coupled receptor Gpr1 and the Galpha protein Gpa2 act through the cAMP-protein kinase A pathway to induce morphogenesis in Candida albicans. Molecular biology of the cell 16: 1971-1986.
164. Bockmuhl DP, Krishnamurthy S, Gerads M, Sonneborn A, Ernst JF (2001) Distinct and redundant roles of the two protein kinase A isoforms Tpk1p and Tpk2p in morphogenesis and growth of Candida albicans. Molecular Microbiology 42: 1243-1257.
165. Cao F, Lane S, Raniga PP, Lu Y, Zhou Z, et al. (2006) The Flo8 transcription factor is essential for hyphal development and virulence in Candida albicans. Molecular biology of the cell 17: 295-307.
166. Doedt T, Krishnamurthy S, Bockmuhl DP, Tebarth B, Stempel C, et al. (2004) APSES proteins regulate morphogenesis and metabolism in Candida albicans. Molecular biology of the cell 15: 3167-3180.

167. Kumamoto CA (2005) A contact-activated kinase signals Candida albicans invasive growth and biofilm development. Proceedings of the National Academy of Sciences of the United States of America 102: 5576-5581.
168. Schweizer A, Rupp S, Taylor BN, Rollinghoff M, Schroppel K (2000) The TEA/ATTS transcription factor CaTec1p regulates hyphal development and virulence in Candida albicans. Molecular Microbiology 38: 435-445.
169. Lane S, Birse C, Zhou S, Matson R, Liu H (2001) DNA array studies demonstrate convergent regulation of virulence factors by Cph1, Cph2, and Efg1 in Candida albicans. The Journal of biological chemistry 276: 48988-48996.
170. Lane S, Zhou S, Pan T, Dai Q, Liu H (2001) The basic helix-loop-helix transcription factor Cph2 regulates hyphal development in Candida albicans partly via TEC1. Molecular and cellular biology 21: 6418-6428.
171. Sohn K, Urban C, Brunner H, Rupp S (2003) EFG1 is a major regulator of cell wall dynamics in Candida albicans as revealed by DNA microarrays. Molecular Microbiology 47: 89-102.
172. Leberer E, Harcus D, Broadbent ID, Clark KL, Dignard D, et al. (1996) Signal transduction through homologs of the Ste20p and Ste7p protein kinases can trigger hyphal formation in the pathogenic fungus Candida albicans. Proceedings of the National Academy of Sciences of the United States of America 93: 13217-13222.
173. Csank C, Schroppel K, Leberer E, Harcus D, Mohamed O, et al. (1998) Roles of the Candida albicans mitogen-activated protein kinase homolog, Cek1p, in hyphal development and systemic candidiasis. Infection and immunity 66: 2713-2721.
174. Liu H, Kohler J, Fink GR (1994) Suppression of hyphal formation in Candida albicans by mutation of a STE12 homolog. Science 266: 1723-1726.
175. Staab JF, Bradway SD, Fidel PL, Sundstrom P (1999) Adhesive and mammalian transglutaminase substrate properties of Candida albicans Hwp1. Science 283: 1535-1538.
176. Garcia-Sanchez S, Mavor AL, Russell CL, Argimon S, Dennison P, et al. (2005) Global roles of Ssn6 in Tup1- and Nrg1-dependent gene regulation in the fungal pathogen, Candida albicans. Molecular biology of the cell 16: 2913-2925.
177. Murad AM, d'Enfert C, Gaillardin C, Tournu H, Tekaia F, et al. (2001) Transcript profiling in Candida albicans reveals new cellular functions for the transcriptional repressors CaTup1, CaMig1 and CaNrg1. Molecular Microbiology 42: 981-993.
178. Kadosh D, Johnson AD (2005) Induction of the Candida albicans filamentous growth program by relief of transcriptional repression: a genome-wide analysis. Molecular biology of the cell 16: 2903-2912.
179. Barwell KJ, Boysen JH, Xu W, Mitchell AP (2005) Relationship of DFG16 to the Rim101p pH response pathway in Saccharomyces cerevisiae and Candida albicans. Eukaryotic Cell 4: 890-899.
180. Penalva MA, Arst HN, Jr. (2002) Regulation of gene expression by ambient pH in filamentous fungi and yeasts. Microbiology and molecular biology reviews : MMBR 66: 426-446, table of contents.
181. Ramon AM, Fonzi WA (2003) Diverged binding specificity of Rim101p, the Candida albicans ortholog of PacC. Eukaryotic Cell 2: 718-728.
182. Muhlschlegel FA, Fonzi WA (1997) PHR2 of Candida albicans encodes a functional homolog of the pH-regulated gene PHR1 with an inverted pattern of pH-dependent expression. Molecular and cellular biology 17: 5960-5967.
183. Lotz H, Sohn K, Brunner H, Muhlschlegel FA, Rupp S (2004) RBR1, a novel pH-regulated cell wall gene of Candida albicans, is repressed by RIM101 and activated by NRG1. Eukaryotic Cell 3: 776-784.
184. Navarro-Garcia F, Eisman B, Fiuza SM, Nombela C, Pla J (2005) The MAP kinase Mkc1p is activated under different stress conditions in Candida albicans. Microbiology 151: 2737-2749.
185. Shapiro RS, Uppuluri P, Zaas AK, Collins C, Senn H, et al. (2009) Hsp90 orchestrates temperature-dependent Candida albicans morphogenesis via Ras1-PKA signaling. Current biology : CB 19: 621-629.
186. Noble SM, French S, Kohn LA, Chen V, Johnson AD (2010) Systematic screens of a Candida albicans homozygous deletion library decouple morphogenetic switching and pathogenicity. Nature genetics 42: 590-598.
187. Magee PT (2010) Fungal pathogenicity and morphological switches. Nature genetics 42: 560-561.
188. Chen X, Magee BB, Dawson D, Magee PT, Kumamoto CA (2004) Chromosome 1 trisomy compromises the virulence of Candida albicans. Molecular Microbiology 51: 551-565.
189. Arbour M, Epp E, Hogues H, Sellam A, Lacroix C, et al. (2009) Widespread occurrence of chromosomal aneuploidy following the routine production of Candida albicans mutants. FEMS yeast research.
190. Lorenz MC, Bender JA, Fink GR (2004) Transcriptional response of Candida albicans upon internalization by macrophages. Eukaryotic Cell 3: 1076-1087.
191. Phan QT, Belanger PH, Filler SG (2000) Role of hyphal formation in interactions of Candida albicans with endothelial cells. Infection and immunity 68: 3485-3490.
192. Galletta BJ, Cooper JA (2009) Actin and endocytosis: mechanisms and phylogeny. Current opinion in cell biology 21: 20-27.
193. Erickson HP (2007) Evolution of the cytoskeleton. BioEssays : news and reviews in molecular, cellular and developmental biology 29: 668-677.
194. Pollard TD, Earnshaw WC, Lippincott-Schwartz J (2008) Cell biology; Pollard TD, editor. Philadelphia: Saunders/Elsevier. chapter 33 p.
195. Dominguez R, Holmes KC (2011) Actin Structure and Function. Annu Rev Biophys 40:169–86.
196. Barth H, Stiles BG (2008) Binary actin-ADP-ribosylating toxins and their use as molecular Trojan horses for drug delivery into eukaryotic cells. Current medicinal chemistry 15: 459-469.
197. Gouin E, Welch MD, Cossart P (2005) Actin-based motility of intracellular pathogens. Current opinion in microbiology 8: 35-45.
198. Pruyne D, Bretscher A (2000) Polarization of cell growth in yeast. Journal of cell science 113 (Pt 4): 571-585.
199. Kabsch W, Mannherz HG, Suck D, Pai EF, Holmes KC (1990) Atomic structure of the actin:DNase I complex. Nature 347: 37-44.
200. Pollard TD (1986) Rate constants for the reactions of ATP- and ADP-actin with the ends of actin filaments. The Journal of cell biology 103: 2747-2754.
201. Wegner A, Isenberg G (1983) 12-fold difference between the critical monomer concentrations of the two ends of actin filaments in physiological salt conditions. Proceedings of the National Academy of Sciences of the United States of America 80: 4922-4925.
202. Campellone KG, Welch MD (2010) A nucleator arms race: cellular control of actin assembly. Nature reviews Molecular cell biology 11: 237-251.

203. Schonichen A, Geyer M (2010) Fifteen formins for an actin filament: a molecular view on the regulation of human formins. Biochimica et biophysica acta 1803: 152-163.
204. Chesarone MA, DuPage AG, Goode BL (2010) Unleashing formins to remodel the actin and microtubule cytoskeletons. Nature reviews Molecular cell biology 11: 62-74.
205. Vallen EA, Caviston J, Bi E (2000) Roles of Hof1p, Bni1p, Bnr1p, and myo1p in cytokinesis in Saccharomyces cerevisiae. Molecular biology of the cell 11: 593-611.
206. Li CR, Wang YM, De Zheng X, Liang HY, Tang JC, et al. (2005) The formin family protein CaBni1p has a role in cell polarity control during both yeast and hyphal growth in Candida albicans. Journal of cell science 118: 2637-2648.
207. Firat-Karalar EN, Welch MD (2011) New mechanisms and functions of actin nucleation. Current opinion in cell biology 23: 4-13.
208. McGough A, Pope B, Chiu W, Weeds A (1997) Cofilin changes the twist of F-actin: implications for actin filament dynamics and cellular function. The Journal of cell biology 138: 771-781.
209. Blanchoin L, Pollard TD (1999) Mechanism of interaction of Acanthamoeba actophorin (ADF/Cofilin) with actin filaments. The Journal of biological chemistry 274: 15538-15546.
210. Matsudaira P (1991) Modular organization of actin crosslinking proteins. Trends in biochemical sciences 16: 87-92.
211. Riedl J, Crevenna AH, Kessenbrock K, Yu JH, Neukirchen D, et al. (2008) Lifeact: a versatile marker to visualize F-actin. Nature methods 5: 605-607.
212. Era A, Tominaga M, Ebine K, Awai C, Saito C, et al. (2009) Application of Lifeact reveals F-actin dynamics in Arabidopsis thaliana and the liverwort, Marchantia polymorpha. Plant & cell physiology 50: 1041-1048.
213. Riedl J, Flynn KC, Raducanu A, Gartner F, Beck G, et al. (2010) Lifeact mice for studying F-actin dynamics. Nature methods 7: 168-169.
214. Berepiki A, Lichius A, Shoji JY, Tilsner J, Read ND (2010) F-actin dynamics in Neurospora crassa. Eukaryotic Cell 9: 547-557.
215. Fujiwara K, Pollard TD (1976) Fluorescent antibody localization of myosin in the cytoplasm, cleavage furrow, and mitotic spindle of human cells. The Journal of cell biology 71: 848-875.
216. Mabuchi I, Okuno M (1977) The effect of myosin antibody on the division of starfish blastomeres. The Journal of cell biology 74: 251-263.
217. Schroeder TE (1973) Actin in dividing cells: contractile ring filaments bind heavy meromyosin. Proceedings of the National Academy of Sciences of the United States of America 70: 1688-1692.
218. Kovar DR, Sirotkin V, Lord M (2011) Three's company: the fission yeast actin cytoskeleton. Trends in cell biology 21: 177-187.
219. Balasubramanian MK, Bi E, Glotzer M (2004) Comparative analysis of cytokinesis in budding yeast, fission yeast and animal cells. Current biology : CB 14: R806-818.
220. Vavylonis D, Wu JQ, Hao S, O'Shaughnessy B, Pollard TD (2008) Assembly mechanism of the contractile ring for cytokinesis by fission yeast. Science 319: 97-100.
221. Wu JQ, Sirotkin V, Kovar DR, Lord M, Beltzner CC, et al. (2006) Assembly of the cytokinetic contractile ring from a broad band of nodes in fission yeast. The Journal of cell biology 174: 391-402.
222. Chang F, Woollard A, Nurse P (1996) Isolation and characterization of fission yeast mutants defective in the assembly and placement of the contractile actin ring. Journal of cell science 109 (Pt 1): 131-142.
223. Hachet O, Simanis V (2008) Mid1p/anillin and the septation initiation network orchestrate contractile ring assembly for cytokinesis. Genes & development 22: 3205-3216.
224. Huang Y, Yan H, Balasubramanian MK (2008) Assembly of normal actomyosin rings in the absence of Mid1p and cortical nodes in fission yeast. The Journal of cell biology 183: 979-988.
225. Sohrmann M, Fankhauser C, Brodbeck C, Simanis V (1996) The dmf1/mid1 gene is essential for correct positioning of the division septum in fission yeast. Genes & development 10: 2707-2719.
226. Mullins RD, Heuser JA, Pollard TD (1998) The interaction of Arp2/3 complex with actin: nucleation, high affinity pointed end capping, and formation of branching networks of filaments. Proceedings of the National Academy of Sciences of the United States of America 95: 6181-6186.
227. Amann KJ, Pollard TD (2001) Direct real-time observation of actin filament branching mediated by Arp2/3 complex using total internal reflection fluorescence microscopy. Proceedings of the National Academy of Sciences of the United States of America 98: 15009-15013.
228. Goley ED, Welch MD (2006) The ARP2/3 complex: an actin nucleator comes of age. Nature reviews Molecular cell biology 7: 713-726.
229. Rouiller I, Xu XP, Amann KJ, Egile C, Nickell S, et al. (2008) The structural basis of actin filament branching by the Arp2/3 complex. The Journal of cell biology 180: 887-895.
230. Goley ED, Rammohan A, Znameroski EA, Firat-Karalar EN, Sept D, et al. (2010) An actin-filament-binding interface on the Arp2/3 complex is critical for nucleation and branch stability. Proceedings of the National Academy of Sciences of the United States of America 107: 8159-8164.
231. Beltzner CC, Pollard TD (2004) Identification of functionally important residues of Arp2/3 complex by analysis of homology models from diverse species. Journal of molecular biology 336: 551-565.
232. Wen KK, Rubenstein PA (2005) Acceleration of yeast actin polymerization by yeast Arp2/3 complex does not require an Arp2/3-activating protein. The Journal of biological chemistry 280: 24168-24174.
233. Galletta BJ, Chuang DY, Cooper JA (2008) Distinct roles for Arp2/3 regulators in actin assembly and endocytosis. PLoS biology 6: e1.
234. Walther A, Wendland J (2004) Polarized hyphal growth in Candida albicans requires the Wiskott-Aldrich Syndrome protein homolog Wal1p. Eukaryotic Cell 3: 471-482.
235. Kaksonen M, Toret CP, Drubin DG (2006) Harnessing actin dynamics for clathrin-mediated endocytosis. Nature reviews Molecular cell biology 7: 404-414.
236. Robertson AS, Smythe E, Ayscough KR (2009) Functions of actin in endocytosis. Cellular and molecular life sciences : CMLS 66: 2049-2065.
237. Girao H, Geli MI, Idrissi FZ (2008) Actin in the endocytic pathway: from yeast to mammals. FEBS letters 582: 2112-2119.

238. Galletta BJ, Mooren OL, Cooper JA (2010) Actin dynamics and endocytosis in yeast and mammals. Current opinion in biotechnology 21: 604-610.
239. Munn AL, Riezman H (1994) Endocytosis is required for the growth of vacuolar H(+)-ATPase-defective yeast: identification of six new END genes. The Journal of cell biology 127: 373-386.
240. Munn AL, Stevenson BJ, Geli MI, Riezman H (1995) end5, end6, and end7: mutations that cause actin delocalization and block the internalization step of endocytosis in Saccharomyces cerevisiae. Molecular biology of the cell 6: 1721-1742.
241. Raths S, Rohrer J, Crausaz F, Riezman H (1993) end3 and end4: two mutants defective in receptor-mediated and fluid-phase endocytosis in Saccharomyces cerevisiae. The Journal of cell biology 120: 55-65.
242. Wendland B, McCaffery JM, Xiao Q, Emr SD (1996) A novel fluorescence-activated cell sorter-based screen for yeast endocytosis mutants identifies a yeast homologue of mammalian eps15. The Journal of cell biology 135: 1485-1500.
243. Benedetti H, Raths S, Crausaz F, Riezman H (1994) The END3 gene encodes a protein that is required for the internalization step of endocytosis and for actin cytoskeleton organization in yeast. Molecular biology of the cell 5: 1023-1037.
244. Kubler E, Riezman H (1993) Actin and fimbrin are required for the internalization step of endocytosis in yeast. The EMBO journal 12: 2855-2862.
245. Martin AC, Xu XP, Rouiller I, Kaksonen M, Sun Y, et al. (2005) Effects of Arp2 and Arp3 nucleotide-binding pocket mutations on Arp2/3 complex function. The Journal of cell biology 168: 315-328.
246. Geli MI, Riezman H (1996) Role of type I myosins in receptor-mediated endocytosis in yeast. Science 272: 533-535.
247. Ayscough KR, Stryker J, Pokala N, Sanders M, Crews P, et al. (1997) High rates of actin filament turnover in budding yeast and roles for actin in establishment and maintenance of cell polarity revealed using the actin inhibitor latrunculin-A. The Journal of cell biology 137: 399-416.
248. Kaksonen M, Toret CP, Drubin DG (2005) A modular design for the clathrin- and actin-mediated endocytosis machinery. Cell 123: 305-320.
249. Newpher TM, Smith RP, Lemmon V, Lemmon SK (2005) In vivo dynamics of clathrin and its adaptor-dependent recruitment to the actin-based endocytic machinery in yeast. Developmental cell 9: 87-98.
250. Ayscough KR (2000) Endocytosis and the development of cell polarity in yeast require a dynamic F-actin cytoskeleton. Current biology : CB 10: 1587-1590.
251. Mulholland J, Preuss D, Moon A, Wong A, Drubin D, et al. (1994) Ultrastructure of the yeast actin cytoskeleton and its association with the plasma membrane. The Journal of cell biology 125: 381-391.
252. Kaksonen M, Sun Y, Drubin DG (2003) A pathway for association of receptors, adaptors, and actin during endocytic internalization. Cell 115: 475-487.
253. Toshima JY, Toshima J, Kaksonen M, Martin AC, King DS, et al. (2006) Spatial dynamics of receptor-mediated endocytic trafficking in budding yeast revealed by using fluorescent alpha-factor derivatives. Proceedings of the National Academy of Sciences of the United States of America 103: 5793-5798.
254. Huckaba TM, Gay AC, Pantalena LF, Yang HC, Pon LA (2004) Live cell imaging of the assembly, disassembly, and actin cable-dependent movement of endosomes and actin patches in the budding yeast, Saccharomyces cerevisiae. The Journal of cell biology 167: 519-530.
255. Engqvist-Goldstein AE, Drubin DG (2003) Actin assembly and endocytosis: from yeast to mammals. Annual review of cell and developmental biology 19: 287-332.
256. Conibear E (2010) Converging views of endocytosis in yeast and mammals. Current opinion in cell biology 22: 513-518.
257. Smaczynska-de R, II, Allwood EG, Aghamohammadzadeh S, Hettema EH, Goldberg MW, et al. (2010) A role for the dynamin-like protein Vps1 during endocytosis in yeast. Journal of cell science 123: 3496-3506.
258. Nannapaneni S, Wang D, Jain S, Schroeder B, Highfill C, et al. (2010) The yeast dynamin-like protein Vps1:vps1 mutations perturb the internalization and the motility of endocytic vesicles and endosomes via disorganization of the actin cytoskeleton. European journal of cell biology 89: 499-508.
259. Carroll SY, Stirling PC, Stimpson HE, Giesselmann E, Schmitt MJ, et al. (2009) A yeast killer toxin screen provides insights into a/b toxin entry, trafficking, and killing mechanisms. Developmental cell 17: 552-560.
260. Burston HE, Maldonado-Baez L, Davey M, Montpetit B, Schluter C, et al. (2009) Regulators of yeast endocytosis identified by systematic quantitative analysis. The Journal of cell biology 185: 1097-1110.
261. Aghamohammadzadeh S, Ayscough KR (2009) Differential requirements for actin during yeast and mammalian endocytosis. Nature cell biology 11: 1039-1042.
262. Saffarian S, Cocucci E, Kirchhausen T (2009) Distinct dynamics of endocytic clathrin-coated pits and coated plaques. PLoS biology 7: e1000191.
263. Traub LM (2009) Clathrin couture: fashioning distinctive membrane coats at the cell surface. PLoS biology 7: e1000192.
264. Taylor MJ, Perrais D, Merrifield CJ (2011) A high precision survey of the molecular dynamics of Mammalian clathrin-mediated endocytosis. PLoS biology 9: e1000604.
265. Stimpson HE, Toret CP, Cheng AT, Pauly BS, Drubin DG (2009) Early-arriving Syp1p and Ede1p function in endocytic site placement and formation in budding yeast. Molecular biology of the cell 20: 4640-4651.
266. Toret CP, Lee L, Sekiya-Kawasaki M, Drubin DG (2008) Multiple pathways regulate endocytic coat disassembly in Saccharomyces cerevisiae for optimal downstream trafficking. Traffic 9: 848-859.
267. Sun Y, Martin AC, Drubin DG (2006) Endocytic internalization in budding yeast requires coordinated actin nucleation and myosin motor activity. Developmental cell 11: 33-46.
268. Tonikian R, Xin X, Toret CP, Gfeller D, Landgraf C, et al. (2009) Bayesian modeling of the yeast SH3 domain interactome predicts spatiotemporal dynamics of endocytosis proteins. PLoS biology 7: e1000218.
269. Peter BJ, Kent HM, Mills IG, Vallis Y, Butler PJ, et al. (2004) BAR domains as sensors of membrane curvature: the amphiphysin BAR structure. Science 303: 495-499.
270. Doherty GJ, McMahon HT (2009) Mechanisms of endocytosis. Annual review of biochemistry 78: 857-902.
271. Kirchhausen T (2009) Imaging endocytic clathrin structures in living cells. Trends in cell biology 19: 596-605.
272. Sirotkin V, Beltzner CC, Marchand JB, Pollard TD (2005) Interactions of WASp, myosin-I, and verprolin with Arp2/3 complex during actin patch assembly in fission yeast. The Journal of cell biology 170: 637-648.

273. Sirotkin V, Berro J, Macmillan K, Zhao L, Pollard TD (2010) Quantitative analysis of the mechanism of endocytic actin patch assembly and disassembly in fission yeast. Molecular biology of the cell 21: 2894-2904.
274. Boettner DR, D'Agostino JL, Torres OT, Daugherty-Clarke K, Uygur A, et al. (2009) The F-BAR protein Syp1 negatively regulates WASp-Arp2/3 complex activity during endocytic patch formation. Current biology : CB 19: 1979-1987.
275. Rodal AA, Manning AL, Goode BL, Drubin DG (2003) Negative regulation of yeast WASp by two SH3 domain-containing proteins. Current biology : CB 13: 1000-1008.
276. Moreau V, Galan JM, Devilliers G, Haguenauer-Tsapis R, Winsor B (1997) The yeast actin-related protein Arp2p is required for the internalization step of endocytosis. Molecular biology of the cell 8: 1361-1375.
277. Liu J, Kaksonen M, Drubin DG, Oster G (2006) Endocytic vesicle scission by lipid phase boundary forces. Proceedings of the National Academy of Sciences of the United States of America 103: 10277-10282.
278. Liu J, Sun Y, Drubin DG, Oster GF (2009) The mechanochemistry of endocytosis. PLoS biology 7: e1000204.
279. Epp E, Walther A, Lepine G, Leon Z, Mullick A, et al. (2010) Forward genetics in Candida albicans that reveals the Arp2/3 complex is required for hyphal formation, but not endocytosis. Molecular microbiology 75: 1182-1198.
280. Miesenbock G, De Angelis DA, Rothman JE (1998) Visualizing secretion and synaptic transmission with pH-sensitive green fluorescent proteins. Nature 394: 192-195.
281. Prosser D, Drivas TG, Maldonado-Baez L, Wendland B (2010) The Small GTPase Rho1 Mediates Endocytosis through the Formin Bni1. Mol Biol Cell 21, 4299 (abstract number: 1247).
282. Cooper JA (1987) Effects of cytochalasin and phalloidin on actin. The Journal of cell biology 105: 1473-1478.
283. Akashi T, Kanbe T, Tanaka K (1994) The role of the cytoskeleton in the polarized growth of the germ tube in Candida albicans. Microbiology 140 (Pt 2): 271-280.
284. Yang HC, Pon LA (2002) Actin cable dynamics in budding yeast. Proceedings of the National Academy of Sciences of the United States of America 99: 751-756.
285. Idrissi FZ, Grotsch H, Fernandez-Golbano IM, Presciatto-Baschong C, Riezman H, et al. (2008) Distinct acto/myosin-I structures associate with endocytic profiles at the plasma membrane. The Journal of cell biology 180: 1219-1232.
286. Fazi B, Cope MJ, Douangamath A, Ferracuti S, Schirwitz K, et al. (2002) Unusual binding properties of the SH3 domain of the yeast actin-binding protein Abp1: structural and functional analysis. The Journal of biological chemistry 277: 5290-5298.
287. Stefan CJ, Padilla SM, Audhya A, Emr SD (2005) The phosphoinositide phosphatase Sjl2 is recruited to cortical actin patches in the control of vesicle formation and fission during endocytosis. Molecular and cellular biology 25: 2910-2923.
288. Cope MJ, Yang S, Shang C, Drubin DG (1999) Novel protein kinases Ark1p and Prk1p associate with and regulate the cortical actin cytoskeleton in budding yeast. The Journal of cell biology 144: 1203-1218.
289. Jin M, Cai M (2008) A novel function of Arp2p in mediating Prk1p-specific regulation of actin and endocytosis in yeast. Molecular biology of the cell 19: 297-307.
290. Tarassov K, Messier V, Landry CR, Radinovic S, Serna Molina MM, et al. (2008) An in vivo map of the yeast protein interactome. Science 320: 1465-1470.
291. Zeng G, Yu X, Cai M (2001) Regulation of yeast actin cytoskeleton-regulatory complex Pan1p/Sla1p/End3p by serine/threonine kinase Prk1p. Molecular biology of the cell 12: 3759-3772.
292. Zeng G, Cai M (1999) Regulation of the actin cytoskeleton organization in yeast by a novel serine/threonine kinase Prk1p. The Journal of cell biology 144: 71-82.
293. Toshima J, Toshima JY, Martin AC, Drubin DG (2005) Phosphoregulation of Arp2/3-dependent actin assembly during receptor-mediated endocytosis. Nature cell biology 7: 246-254.
294. Sun Y, Carroll S, Kaksonen M, Toshima JY, Drubin DG (2007) PtdIns(4,5)P2 turnover is required for multiple stages during clathrin- and actin-dependent endocytic internalization. The Journal of cell biology 177: 355-367.
295. Liu J, Sun Y, Oster GF, Drubin DG (2010) Mechanochemical crosstalk during endocytic vesicle formation. Current opinion in cell biology 22: 36-43.
296. Suetsugu S (2009) The direction of actin polymerization for vesicle fission suggested from membranes tubulated by the EFC/F-BAR domain protein FBP17. FEBS letters 583: 3401-3404.
297. Singer-Kruger B, Nemoto Y, Daniell L, Ferro-Novick S, De Camilli P (1998) Synaptojanin family members are implicated in endocytic membrane traffic in yeast. Journal of cell science 111 (Pt 22): 3347-3356.
298. Noble SM, Johnson AD (2005) Strains and strategies for large-scale gene deletion studies of the diploid human fungal pathogen Candida albicans. Eukaryotic Cell 4: 298-309.
299. Epp E, Vanier G, Harcus D, Lee AY, Jansen G, et al. (2010) Reverse genetics in Candida albicans predicts ARF cycling is essential for drug resistance and virulence. PLoS Pathogens 6: e1000753.
300. Walther A, Wendland J (2008) PCR-based gene targeting in Candida albicans. Nature protocols 3: 1414-1421.
301. Schaub Y, Dunkler A, Walther A, Wendland J (2006) New pFA-cassettes for PCR-based gene manipulation in Candida albicans. Journal of basic microbiology 46: 416-429.
302. Zhang C, Konopka JB (2010) A photostable green fluorescent protein variant for analysis of protein localization in Candida albicans. Eukaryotic Cell 9: 224-226.
303. Alvarez FJ, Douglas LM, Rosebrock A, Konopka JB (2008) The Sur7 protein regulates plasma membrane organization and prevents intracellular cell wall growth in Candida albicans. Molecular biology of the cell 19: 5214-5225.
304. Shaner NC, Lin MZ, McKeown MR, Steinbach PA, Hazelwood KL, et al. (2008) Improving the photostability of bright monomeric orange and red fluorescent proteins. Nature methods 5: 545-551.
305. Gerami-Nejad M, Dulmage K, Berman J (2009) Additional cassettes for epitope and fluorescent fusion proteins in Candida albicans. Yeast 26: 399-406.
306. Ng M, Roorda RD, Lima SQ, Zemelman BV, Morcillo P, et al. (2002) Transmission of olfactory information between three populations of neurons in the antennal lobe of the fly. Neuron 36: 463-474.
307. Nicholls S, Straffon M, Enjalbert B, Nantel A, Macaskill S, et al. (2004) Msn2- and Msn4-like transcription factors play no obvious roles in the stress responses of the fungal pathogen Candida albicans. Eukaryotic Cell 3: 1111-1123.
308. Rauch A, Nazarova E, Vogel J (2010) Analysis of microtubules in budding yeast. Methods in cell biology 97: 277-306.
309. Roemer T, Jiang B, Davison J, Ketela T, Veillette K, et al. (2003) Large-scale essential gene identification in Candida albicans and applications to antifungal drug discovery. Molecular microbiology 50: 167-181.

310. Peleg AY, Hogan DA, Mylonakis E (2010) Medically important bacterial-fungal interactions. Nature reviews Microbiology 8: 340-349.
311. Marchetti O, Entenza JM, Sanglard D, Bille J, Glauser MP, et al. (2000) Fluconazole plus cyclosporine: a fungicidal combination effective against experimental endocarditis due to Candida albicans. Antimicrobial agents and chemotherapy 44: 2932-2938.
312. Brothers K, Newman Z, Wheeler R (2011) Live imaging of disseminated candidiasis in zebrafish reveals role of phagocyte oxidase in limiting filamentous growth. Eukaryotic Cell doi:10.1128/EC.05005-11.
313. Peleg AY, Tampakakis E, Fuchs BB, Eliopoulos GM, Moellering RC, Jr., et al. (2008) Prokaryote-eukaryote interactions identified by using Caenorhabditis elegans. Proceedings of the National Academy of Sciences of the United States of America 105: 14585-14590.
314. Sibley CD, Duan K, Fischer C, Parkins MD, Storey DG, et al. (2008) Discerning the complexity of community interactions using a Drosophila model of polymicrobial infections. PLoS Pathogens 4: e1000184.
315. Brennan M, Thomas DY, Whiteway M, Kavanagh K (2002) Correlation between virulence of Candida albicans mutants in mice and Galleria mellonella larvae. FEMS immunology and medical microbiology 34: 153-157.
316. Holmes AR, Gopal PK, Jenkinson HF (1995) Adherence of Candida albicans to a cell surface polysaccharide receptor on Streptococcus gordonii. Infection and immunity 63: 1827-1834.
317. Ocana VS, Nader-Macias ME (2002) Vaginal lactobacilli: self- and co-aggregating ability. British journal of biomedical science 59: 183-190.
318. Hogan DA, Kolter R (2002) Pseudomonas-Candida interactions: an ecological role for virulence factors. Science 296: 2229-2232.
319. Adam B, Baillie GS, Douglas LJ (2002) Mixed species biofilms of Candida albicans and Staphylococcus epidermidis. Journal of medical microbiology 51: 344-349.
320. Boon C, Deng Y, Wang LH, He Y, Xu JL, et al. (2008) A novel DSF-like signal from Burkholderia cenocepacia interferes with Candida albicans morphological transition. The ISME journal 2: 27-36.
321. Hogan DA, Vik A, Kolter R (2004) A Pseudomonas aeruginosa quorum-sensing molecule influences Candida albicans morphology. Molecular microbiology 54: 1212-1223.
322. Wang LH, He Y, Gao Y, Wu JE, Dong YH, et al. (2004) A bacterial cell-cell communication signal with cross-kingdom structural analogues. Molecular microbiology 51: 903-912.
323. Kerr JR, Taylor GW, Rutman A, Hoiby N, Cole PJ, et al. (1999) Pseudomonas aeruginosa pyocyanin and 1-hydroxyphenazine inhibit fungal growth. Journal of clinical pathology 52: 385-387.
324. Gibson J, Sood A, Hogan DA (2009) Pseudomonas aeruginosa-Candida albicans interactions: localization and fungal toxicity of a phenazine derivative. Applied and environmental microbiology 75: 504-513.
325. Cugini C, Calfee MW, Farrow JM, 3rd, Morales DK, Pesci EC, et al. (2007) Farnesol, a common sesquiterpene, inhibits PQS production in Pseudomonas aeruginosa. Molecular microbiology 65: 896-906.
326. McAlester G, O'Gara F, Morrissey JP (2008) Signal-mediated interactions between Pseudomonas aeruginosa and Candida albicans. Journal of medical microbiology 57: 563-569.
327. Jabra-Rizk MA, Meiller TF, James CE, Shirtliff ME (2006) Effect of farnesol on Staphylococcus aureus biofilm formation and antimicrobial susceptibility. Antimicrobial agents and chemotherapy 50: 1463-1469.
328. Brehm-Stecher BF, Johnson EA (2003) Sensitization of Staphylococcus aureus and Escherichia coli to antibiotics by the sesquiterpenoids nerolidol, farnesol, bisabolol, and apritone. Antimicrobial agents and chemotherapy 47: 3357-3360.
329. Allard JB, Rinaldi L, Wargo MJ, Allen G, Akira S, et al. (2009) Th2 allergic immune response to inhaled fungal antigens is modulated by TLR-4-independent bacterial products. European journal of immunology 39: 776-788.
330. Braun-Fahrlander C, Riedler J, Herz U, Eder W, Waser M, et al. (2002) Environmental exposure to endotoxin and its relation to asthma in school-age children. The New England journal of medicine 347: 869-877.
331. Garn H, Renz H (2007) Epidemiological and immunological evidence for the hygiene hypothesis. Immunobiology 212: 441-452.
332. Bach JF (2002) The effect of infections on susceptibility to autoimmune and allergic diseases. The New England journal of medicine 347: 911-920.
333. Peleg AY, Hogan DA, Mylonakis E (2010) Medically important bacterial-fungal interactions. Nat Rev Microbiol 8: 340-349.
334. Lettner T, Zeidler U, Gimona M, Hauser M, Breitenbach M, et al. (2010) Candida albicans AGE3, the ortholog of the S. cerevisiae ARF-GAP-encoding gene GCS1, is required for hyphal growth and drug resistance. PloS one 5: e11993.
335. Bruning A, Ishikawa T, Kneusel RE, Matern U, Lottspeich F, et al. (1992) Brefeldin A binds to glutathione S-transferase and is secreted as glutathione and cysteine conjugates by Chinese hamster ovary cells. The Journal of biological chemistry 267: 7726-7732.
336. Phillips LR, Supko JG, Malspeis L (1993) Analysis of brefeldin A in plasma by gas chromatography with electron capture detection. Analytical biochemistry 211: 16-22.
337. Lippincott-Schwartz J, Yuan LC, Bonifacino JS, Klausner RD (1989) Rapid redistribution of Golgi proteins into the ER in cells treated with brefeldin A: evidence for membrane cycling from Golgi to ER. Cell 56: 801-813.
338. Fujiwara T, Oda K, Yokota S, Takatsuki A, Ikehara Y (1988) Brefeldin A causes disassembly of the Golgi complex and accumulation of secretory proteins in the endoplasmic reticulum. The Journal of biological chemistry 263: 18545-18552.
339. Low SH, Wong SH, Tang BL, Tan P, Subramaniam VN, et al. (1991) Inhibition by brefeldin A of protein secretion from the apical cell surface of Madin-Darby canine kidney cells. The Journal of biological chemistry 266: 17729-17732.
340. Ewbank JJ, Zugasti O (2011) C. elegans: model host and tool for antimicrobial drug discovery. Disease models & mechanisms.
341. Cornet M, Bidard F, Schwarz P, Da Costa G, Blanchin-Roland S, et al. (2005) Deletions of endocytic components VPS28 and VPS32 affect growth at alkaline pH and virulence through both RIM101-dependent and RIM101-independent pathways in Candida albicans. Infection and immunity 73: 7977-7987.
342. Gow NA, Brown AJ, Odds FC (2002) Fungal morphogenesis and host invasion. Current opinion in microbiology 5: 366-371.
343. Heitman J (2011) Microbial Pathogens in the Fungal Kingdom. Fungal biology reviews 25: 48-60.
344. Klein BS, Tebbets B (2007) Dimorphism and virulence in fungi. Current opinion in microbiology 10: 314-319.
345. Medoff G, Kobayashi GS, Painter A, Travis S (1987) Morphogenesis and pathogenicity of Histoplasma capsulatum. Infection and immunity 55: 1355-1358.

346. Kronstad JW, Attarian R, Cadieux B, Choi J, D'Souza CA, et al. (2011) Expanding fungal pathogenesis: Cryptococcus breaks out of the opportunistic box. Nature reviews Microbiology 9: 193-203.
347. Kamper J, Kahmann R, Bolker M, Ma LJ, Brefort T, et al. (2006) Insights from the genome of the biotrophic fungal plant pathogen Ustilago maydis. Nature 444: 97-101.
348. Bastidas RJ, Heitman J (2009) Trimorphic stepping stones pave the way to fungal virulence. Proceedings of the National Academy of Sciences of the United States of America 106: 351-352.
349. Carlisle PL, Banerjee M, Lazzell A, Monteagudo C, Lopez-Ribot JL, et al. (2009) Expression levels of a filament-specific transcriptional regulator are sufficient to determine Candida albicans morphology and virulence. Proceedings of the National Academy of Sciences of the United States of America 106: 599-604.
350. Kim J, Sudbery P (2011) Candida albicans, a major human fungal pathogen. Journal of microbiology 49: 171-177.
351. Crampin H, Finley K, Gerami-Nejad M, Court H, Gale C, et al. (2005) Candida albicans hyphae have a Spitzenkorper that is distinct from the polarisome found in yeast and pseudohyphae. Journal of cell science 118: 2935-2947.
352. Winter DC, Choe EY, Li R (1999) Genetic dissection of the budding yeast Arp2/3 complex: a comparison of the in vivo and structural roles of individual subunits. Proceedings of the National Academy of Sciences of the United States of America 96: 7288-7293.
353. Schaerer-Brodbeck C, Riezman H (2000) Saccharomyces cerevisiae Arc35p works through two genetically separable calmodulin functions to regulate the actin and tubulin cytoskeletons. Journal of cell science 113 (Pt 3): 521-532.
354. Winter D, Podtelejnikov AV, Mann M, Li R (1997) The complex containing actin-related proteins Arp2 and Arp3 is required for the motility and integrity of yeast actin patches. Current biology : CB 7: 519-529.
355. Jia XM, Wang Y, Jia Y, Gao PH, Xu YG, et al. (2009) RTA2 is involved in calcineurin-mediated azole resistance and sphingoid long-chain base release in Candida albicans. Cellular and molecular life sciences : CMLS 66: 122-134.
356. Jia XM, Ma ZP, Jia Y, Gao PH, Zhang JD, et al. (2008) RTA2, a novel gene involved in azole resistance in Candida albicans. Biochemical and biophysical research communications 373: 631-636.
357. Smriti, Krishnamurthy S, Dixit BL, Gupta CM, Milewski S, et al. (2002) ABC transporters Cdr1p, Cdr2p and Cdr3p of a human pathogen Candida albicans are general phospholipid translocators. Yeast 19: 303-318.